Thomas Foken

Micrometeorology

Second Edition

Springer

Micrometeorology

Thomas Foken

Micrometeorology

Second Edition

With 112 Figures

Springer

Thomas Foken
Bayreuth Center of Ecology and
    Environmental Research (BayCEER)
University of Bayreuth
Bayreuth
Germany

and

Bischberg
Germany

Preface

About 8 years after the first edition of this book was published, a revision and new edition was urgently needed. The book was carefully updated whereby new developments and especially new references were incorporated in the text. Because of didactical reasons I rearranged some parts of the text, e.g. the zero-plane displacement is now already introduced in Chap. 2. New topics are aspects of the atmospheric boundary layer, which are relevant for micrometeorological investigations, and some measurement methods like soil chamber measurements and some issues of local climate and land use changes. Contrary to some other monographs, the book has again a large number of historical and recent references to give the reader the opportunity to study the topics also with the original sources.

It was not my aim to transfer the book into a style where the German and Russian backgrounds of my teachers cannot be seen. On the other hand, I hope that the reader will find some references of interest. These are mainly references to German standards or historical sources. The book is addressed to graduate students, scientists, practical workers, and those who need knowledge of micrometeorology for applied or ecological studies. The main parts are written as a textbook, but also included are references to historical sources and recent research even though the final solutions are still under discussion. Throughout the book, the reader will find practical tips, especially in the chapters on experimental techniques where several such tips are given. The appendix should give the reader an overview of many important parameters and equations, which are not easily found in other books.

Fortunately, several monographs about the same topic were published in the last years. Upon a closer view, these books complement the topic in an excellent way. However, this book still is the most detailed when it comes to the micrometeorological and experimental part. These books are related to the atmospheric boundary layer (Kraus 2008; Vilà-Guerau de Arellano et al. 2015), basics of atmospheric turbulence (Wyngaard 2010), physical basics of micrometeorology (Monteith and Unsworth 2008), plant and soil processes (Hari et al. 2013; Moene and van Dam 2014; Monson and Baldocchi 2014) and general measurement techniques (Emeis 2010). Therefore, the reader has several monographs about micrometeorology and related disciplines with different form of presentation by their authors. This book is

nearly identical with the third edition of the German version of the book "Angewandte Meteorologie".

I am extremely thankful for the wonderful cooperation with Dr. Carmen Nappo, who edited my translation of the first edition into the English language in a way that keeps alive the style of a German or European book and also makes it easily readable. In the same way I thank Prof. Dr. Petra Klein, who edited all revised and newly added text in the second edition, and who also read and proposed edits to the whole book. Last but not least I thank my wife Ute, who gave me the opportunity and encouragement to do this time consuming work.

Bayreuth, Germany
Bischberg, Germany   Thomas Foken
October 2016

Preface of the First German Edition

Even though the beginning of modern micrometeorology was started 60–80 years ago in the German speaking countries, the division of meteorological phenomena according their scales in time and space is generally not used in Germany. Perhaps because the classic book by R. Geiger (1927) *The climate near the ground* focused on a phenomenological description of the processes at the ground surface, the word *micro* became associated with very small-scale processes. The development of micrometeorology combined with progress in turbulence theory started in the 1940s in the former Soviet Union, and continued e.g. in Australia and the USA. In these countries, *micrometeorology* is a well-established part of meteorology of processes near the ground surface occurring on scales some decameters in height and some kilometers in horizontal extension. In the Russian-speaking countries, *experimental meteorology* is more common than micrometeorology, but not connected to meteorological scales, and instead is used for all experiments. Because the area of investigation of micrometeorology is nearly identical with the area of human activity, it is obvious that applied meteorology and micrometeorology are connected; however, the latter is more theoretical and orientated toward basic research. That both fields are connected can be seen in the papers in the *Journal of Applied Meteorology*. In Germany, applied meteorology is well established in the environment-related conferences METTOOLS of the German Meteorological Society, but the necessary basics are found only with difficulty mostly in the English literature. While Flemming (1991) gave a generally intelligible introduction to parts of meteorology which are relevant for applied meteorology, the present book gives the basics of micrometeorology. It is therefore understandable that a book in German will provide not only quick and efficient access to information, but also encourage the use of the German scientific language. Furthermore, this book seeks to give the practical user directly applicable calculating and measuring methods and also provides the basics for further research.

This book has a long history. Over nearly 30 years spent mainly in experimental research in micrometeorology, it was always fascinating to the author, how measuring methods and the applications of measuring devices are directly dependent on

the state of the atmospheric turbulence and many influencing phenomena. This connection was first discussed in the book by Dobson et al. (1980). The present book is a modest attempt along these lines. It is nearly a didactically impossible task to combine always divided areas of science and yet show their interactions. Contrary to the classical micrometeorological approach of looking only at uniform ground surfaces covered with low vegetation, this book applies these concepts to heterogeneous terrain covered with tall vegetation. References are given to very recent research, but these results may change with future research. The progressive application of micrometeorological basics in ecology (Campbell and Norman 1998) makes this step necessary.

The sources of this book were lectures given in *Experimental Meteorology* at the Humboldt-University in Berlin, in *Micrometeorology* at the University of Potsdam, and since 1997 similar courses at the University of Bayreuth. The book would not be possible to write without my German and Russian teachers, my colleagues and co-workers, and master and Ph.D. students who supported me in many cases. Many publishing houses and companies very kindly supported the book with pictures or allowed their reproduction. Mr. Engelbrecht has drawn some new pictures. Special thanks are given to Prof. Dr. H.P. Schmid for his critical review of the German manuscript, and to Ute for her understanding support of the work and for finding weaknesses in the language of the manuscript.

Bayreuth, Germany   Thomas Foken
October 2002

References

Campbell GS and Norman JM (1998) Introduction to environmental biophysics. Springer, New York, 286 pp.

Dobson F, Hasse L and Davis R (eds) (1980) Air-Sea Interaction, Instruments and Methods. Plenum Press, New York, 679 pp.

Emeis S (2010) Measurement Methods in Atmospheric Sciences. Borntraeger Science Publishers, Stuttgart, 257 pp.

Flemming G (1991) Einführung in die Angewandte Meteorologie. Akademie-Verlag, Berlin, 168 pp.

Geiger R (1927) Das Klima der bodennahen Luftschicht. Friedr. Vieweg & Sohn, Braunschweig, 246 pp.

Hari P, Heliövaara K and Kulmala L (eds) (2013) Physical and Physiological Forest Ecology. Springer, Dordrecht, Heidelberg, New York, London, 534 pp.

Kraus H (2008) Grundlagen der Grenzschichtmeteorologie. Springer, Berlin, Heidelberg, 211 pp.

Moene AF and van Dam JC (2014) Transport in the Atmosphere-Vegetation-Soil Continuum. Cambridge University Press, Cambridge, 436 pp.

Monson R and Baldocchi D (2014) Terrestrial Biosphere-Atmosphere Fluxes. Cambridge University Press, New York, XXI, 487 pp.

Monteith JL and Unsworth MH (2008) Principles of Environmental Physics, 3rd edition. Elsevier, Academic Press, Amsterdam, Boston, 418 pp.

Vilà-Guerau de Arellano J, Van Heerwaarden CC, van Stratum BJH and van den Dries K (2015) Atmospheric Boundary Layer. Cambridge University Press, Cambridge, 265 pp.

Wyngaard JC (2010) Turbulence in the Atmosphere. Cambridge University Press, Cambridge, 393 pp.

Contents

Symbols

Symbols that are used only in single equations are not included in this list, but are explained in the text.

a	Albedo (–)
a	Absolute humidity (kg m^{-3})
a	Scalar (general) (*)
a_G	Molecular heat conductance coefficient in soil (W m^{-1} K^{-1})
a_T	Molecular heat conductance coefficient in air (W m^{-1} K^{-1})
A	Run off (mm)
A	Exchange (Austausch) coefficient (*)
A	Coefficient of the resistance law (–)
b	Accuracy (bias) (*)
b	Constant used for REA measurements (–)
b_{st}	Species−dependent constant according to Jarvis (W m^{-2})
B	Sublayer Stanton number (–)
B	Coefficient of the resistance law (–)
Bo	Bowen ratio (–)
c	Sound speed (m s^{-1})
c	Concentration (general) (*)
c	Comparability (*)
c_p	Specific heat at constant pressure (J kg^{-1} K^{-1})
c_v	Specific heat at constant volume (J kg^{-1} K^{-1})
c_x	Structure constant (general) (–)
C_D	Drag coefficient (–)
C_E	Dalton number (–)
C_G	Volumetric heat capacity (W s m^{-3} K^{-1})
C_H	Stanton number (–)
C_n^2	Refraction structure-function parameter (m$^{-2/3}$)
C_T^2	Temperature structure-function parameter (K m$^{-2/3}$)

$C_{x,y}$, Co	Cospectrum (general) (*)
d	Displacement height (m)
d	Measuring path (m)
D	Molecular diffusion constant (general) (*)
D	Structure function (general) (*)
Da_k	Kolmogorov–Damköhler number (–)
Da_t	Turbulent Damköhler number (–)
DOY	Day of the year: Jan. 1 = 1 (–)
e	Basis of the natural logarithm (–)
e	Water vapour pressure (hPa)
e'	Fluctuation of the water vapour pressure (hPa)
E	Water vapour pressure at saturation (hPa)
E	Power spectra (general) (*)
E_a	Ventilation term (hPa m s^{-1})
Eu	Euler number (–)
f	Function (general) (–)
f	Frequency (s^{-1})
f	Coriolis parameter (s^{-1})
f	Footprint function (*)
f_g	Cut frequency (s^{-1})
f_N	Nyquist frequency (s^{-1})
F	Flux (general) (*)
F	Power spectra (general) (*)
F_w	Ventilation flow (kg m^{-1} s^{-1})
F_χ	Flux of a scalar (*)
Fi	Inverse Froude number (–)
Fi_o	Inverse external Froude number (–)
g	Acceleration due to gravity (m s^{-2})
g_0	Constant gravity velocity (m s^{-2})
h	Height of a volume element (m)
h	Wave height (m)
H	Water depth (m)
I	Long-wave radiation (W m^{-2})
$I{\downarrow}$	Down-welling long-wave radiation (W m^{-2})
$I{\uparrow}$	Up-welling long-wave radiation (W m^{-2})
I^*	Long-wave net radiation (W m^{-2})
k	Wave number (m^{-1})
k	Absorption coefficient (m^{-1})
k	Reaction rate (*)
K	Turbulent diffusion coefficient (general) (m^{-2} s^{-1})
K_E	Turbulent diffusion coefficient of latent heat (m^{-2} s^{-1})
K_H	Turbulent diffusion coefficient of sensible heat (m^{-2} s^{-1})
K_m	Turbulent diffusion coefficient of momentum (m^{-2} s^{-1})
$K{\downarrow}$	Down-welling short-wave radiation (at surface), global radiation (W m^{-2})

$K\downarrow_{\text{extr}}$	Extra-terrestrial radiation (W m^{-2})
$K\uparrow$	Reflected short-wave radiation (at the ground surface) (W m^{-2})
l	Mixing length (m)
L	Obukhov length (m)
L	Characteristic length (m)
L	Distance constant (m)
L_{h}	Horizontal characteristic length (m)
L_{s}	Shearing parameter (m)
L_{z}	Vertical characteristic length (m)
LAI	Leaf area index (m^2 m^{-2})
m	Mixing ratio (kg kg^{-1})
n	Dimensionless frequency (–)
N	Precipitation (mm)
N	Brunt–Väisälä frequency (Hz)
N	Cloud cover (–)
N	Dissipation rate (general) (*)
Nu	Nusselt number (–)
Og	Ogive function (*)
p	Air pressure (hPa)
p_0	Air pressure at sea level (hPa)
p'	Pressure fluctuation (hPa)
P_{WKA}	Power of a wind power station (W)
PAR	Photosynthetically active radiation (µmol m^{-2} s^{-1})
Pr	Prandtl number (–)
Pr_{t}	Turbulent Prandtl number (–)
q	Specific humidity (kg kg^{-1})
q_{c}	Specific concentration (*)
q_{a}	Specific humidity near the ground (kg kg^{-1})
q_{e}	Conversion factor from specific humidity into water vapour pressure (kg kg^{-1} hPa^{-1})
q_{s}, q_{sat}	Specific humidity by saturation (kg kg^{-1})
q_*	Scale of the mixing ratio (kg kg^{-1})
Q	Source density (general) (*)
Q_{c}	Dry deposition (kg m^{-2} s^{-1})
Q_{E}	Latent heat flux (W m^{-2})
Q_{E}	Latent heat flux expressed as a water column (mm)
Q_{G}	Ground heat flux (W m^{-2})
Q_{H}	Sensible heat flux (W m^{-2})
Q_{HB}	Buoyancy flux (W m^{-2})
Q^*_{s}	Net radiation (W m^{-2})
Q_{η}	Source density of the η parameter (*)
r	Correlation coefficient (–)
r_{a}, r_{t}	Turbulent atmospheric resistance (s m^{-1})
r_{c}	Canopy resistance (s m^{-1})
r_{g}	Total resistance (s m^{-1})

r_{mt}	Molecular-turbulent resistance (s m^{-1})
r_{st}	Stomatal resistance (s m^{-1})
r_{si}	Stomatal resistance of a single leaf (s m^{-1})
R	Resistance (Ω)
R	Relative humidity (%)
R	Universal gas constant (mol kg^{-1} K^{-1})
R_{G}	Relative humidity near the surface (%)
R_{L}	Gas constant of dry air (J kg^{-1} K^{-1})
R_{s}	Relative humidity near the surface (%)
R_{W}	Gas constant of water vapour (J kg^{-1} K^{-1})
Re	Reynolds number (–)
Re_{s}	Roughness Reynolds number (–)
Rf	Flux Richardson number (–)
Ri	Richardson number, gradient Richardson number (–)
Ri_{B}	Bulk Richardson number (–)
Ri_{c}	Critical Richardson number (–)
Ro	Rossby number (–)
s	Precision (*)
s_{c}	Temperature dependence of specific humidity at saturation (kg kg^{-1} K^{-1})
S	Power spectra (general) (*)
S	Solar constant (W m^{-2})
Sc	Schmidt number (–)
Sc_{t}	Turbulent Schmidt number (–)
Sd	Duration of sunshine (h)
Sd_0	Astronomical maximal possible sunshine duration (h)
Sf	Radiation error (K)
t	Time (s)
t	Temperature (°C)
t'	Wet-bulb temperature (°C)
T	Transfer function (–)
T	Temperature, temperature difference (K)
T'	Fluctuation of the temperature (K)
T_*	Temperature scale (K)
T^+	Dimensionless temperature (–)
T_{K}	Transmission coefficient (–)
T_0	Surface temperature (K)
T_{p}	Wavelet coefficient (*)
T_{s}	Sonic temperature (K)
T_{v}	Virtual temperature (K)
u	Wind speed (general) (m s^{-1})
u	Longitudinal component of the wind velocity (m s^{-1})
u_{g}	Horizontal component of the geostrophic wind velocity (m s^{-1})
u_{10}	Wind velocity at 10 m height (m s^{-1})
u'	Fluctuation of the longitudinal component of the wind velocity (m s^{-1})

u_*	Friction velocity (m s^{-1})
v	Lateral component of the wind velocity (m s^{-1})
v_g	Lateral component of the geostrophic wind velocity (m s^{-1})
v'	Fluctuation of the lateral component of the wind velocity (m s^{-1})
v_D	Deposition velocity (m s^{-1})
V	Characteristic velocity (m s^{-1})
w	Vertical component of the wind velocity (m s^{-1})
w'	Fluctuation of the vertical component of the wind velocity (m s^{-1})
w_*	Deardorff (convective) velocity (m s^{-1})
w_0	Deadband for REA method (m s^{-1})
x	Fetch (m)
x	Horizontal direction (length) (m)
x, X	Measuring variable (general) (*)
y	Horizontal direction (length, perpendicular to x) (m)
y, Y	Measuring variable (general) (*)
z	Height (general, geometric) (m)
z_H	Height of a building (m)
z_i	Mixed-layer height (m)
z_m	Measuring height (m)
z_R	Reference height (m)
z_0	Roughness parameter, roughness height (m)
z_{0eff}	Effective roughness height (m)
z_{0E}	Roughness height for water vapour pressure (m)
z_{0T}	Roughness height for temperature (m)
z'	Height (aerodynamic) (m)
z^+	Dimensionless height (–)
z_*	Height of the roughness sublayer (m)
Z	Geopotential height (m)
Z	Equation of time (min)
α	Angle of inflow (°)
α_{pt}	Priestley–Taylor coefficient (–)
β	Kolmogorov constant (general) (–)
β	Obukhov–Corrsin constant (general) (–)
γ	Psychrometeric constant (hPa K^{-1}or kg kg^{-1} K^{-1})
γ	Factor in O'KEYPS equation (–)
Γ	Profile coefficient (m s^{-1})
Γ_d	Dry adiabatic temperature gradient (K m^{-1})
δ	Depth of the internal boundary layer (m)
δ	Depth of the molecular-turbulent (viscous) sublayer (m)
δ_{ij}	Kronecker symbol (–)
δ_T	Thickness of the thermal internal boundary layer (m)
δ_T	Thickness of the molecular temperature boundary layer (m)
δ_T^+	Dimensionless thickness of the molecular temperature boundary layer (−)
δ_w	Thickness of the mixing layer (m)

Δc	Concentration difference (*)
Δe	Water vapour pressure difference (hPa)
ΔP	Pressure difference (hPa)
ΔT	Temperature difference (K)
Δu	Wind velocity difference (m s^{-1})
Δz	Height difference (m)
ΔQ_S	Energy source or sink (W m^{-2})
ΔS_W	Water source or sink (mm)
Δ_z	Characteristic vertical gradient (*)
ε	Energy dissipation (m^2 s^{-3})
ε	Small measurement error (–)
ε_{IR}	Infrared emissivity (–)
ε_{ijk}	Levi-Civita symbol (epsilon tensor) (–)
ζ	Obukhov parameter (=z/L)
η	Measurement variable (*)
θ	Potential temperature (K)
θ_v	Virtual potential temperature (K)
κ	Von-Kármán constant (–)
λ	Heat of evaporation for water (J kg^{-1})
λ	Geographical longitude (°)
λ_F	Frontal area fraction calculated as the fraction of the frontal area of built-up elements relative to the total plan area (–)
λ_P	Plan area fraction calculated as the plan area occupied by built-up elements relative to the total plan area (–)
Λ	Local Obukhov length (m)
Λ_u	Eulerian turbulent length scale for the horizontal wind (m)
Λ_x	Ramp structure-parameter (m)
μ	Dynamic viscosity (kg m^{-1} s^{-1})
μ	Stability parameter of the atmospheric boundary layer (–)
v	Kinematic viscosity (m^2 s^{-1})
v_T	Thermal diffusion coefficient (m^2 s^{-1})
ξ	Scalar (general) (*)
ξ	Time delay (s)
ρ	Air density (kg m^{-3})
ρ'	Air density fluctuation (kg m^{-3})
ρ_c	Partial density (kg^2 kg^{-1} m^{-3})
σ_c	Standard deviation of the concentration (*)
σ_{cH}	Cloud cover for high cloud (–)
σ_{cL}	Cloud cover for low clouds (–)
σ_{cM}	Cloud cover for middle high clouds (–)
σ_{SB}	Stefan–Boltzmann constant (W m^{-2} K^{-4})
σ_u	Standard deviation of the longitudinal wind component (m s^{-1})
σ_v	Standard deviation of the lateral wind component (m s^{-1})
σ_w	Standard deviation of the vertical wind component (m s^{-1})
σ_T	Standard deviation of the temperature (K)

σ_θ	Standard deviation of the potential temperature (K)
σ_φ	Standard deviation of the wind direction (°)
τ	Dew point temperature (K)
τ	Shear stress (kg m^{-1} s^{-2})
τ	Time constant (s)
Φ	Geopotential (m^2 s^2)
φ	Geographical latitude (°)
φ_E	Universal function for latent heat flux (–)
φ_H	Universal function for sensible heat flux (–)
φ_m	Universal function for momentum exchange (–)
φ_T	Universal function for temperature structure function parameter (–)
φ_ε	Universal function for energy dissipation (–)
φ_*	Correction function for the roughness sublayer (–)
χ	Scalar (general) (*)
ψ	Integral of the universal function (–)
Ψ	Inclination of the sun (°)
ω	Circular frequency (–)
ω	Hour angle (°)
Ω	Angular velocity of the rotation of the Earth (s^{-1})

Indices

a	Air
w	Water

Remark

* Dimension according to the use of the parameter

Chapter 1
General Basics

This introductory chapter provides the basics for this book, and terms such as micrometeorology, atmospheric boundary layer, and meteorological scales are defined and presented in relation to the subject matter of this book. Besides an historical outline, the energy and water balance equations at the Earth's surface and the transport processes are discussed. The first chapter of the book focus on the micrometeorological basics, which are then expanded in the following theoretical and experimental chapters.

1.1 Micrometeorology

Meteorology is one of the oldest sciences in the world. It can be traced back to Aristotle (384–322 BCE), who wrote the four volumes of the book *Meteorology*. In ancient times, appearances in the air were called meteors. In the first half of the 20th century, the upper soil layers were considered part of meteorology (Hann and Süring 1939). Today meteorology is understood in a very general sense to be the science of the atmosphere (Glickman 2000; Dutton 2002; Kraus 2004), and includes also the mean states (climatology). Sometimes the definition of meteorology is very narrow, and only related to the physics of the atmosphere or weather prediction. To understand atmospheric processes, many other sciences such as physics, chemistry, biology and all geosciences are necessary, and it is not easy to find the boundaries of these disciplines. In a pragmatic way, meteorology is related only to processes that take place in situ in the atmosphere, while other sciences can investigate processes and reactions in the laboratory. This underlines the specific character of meteorology, i.e., a science that investigates an open system with a great number of atmospheric influences operating at all times but with changing intensity. Meteorology is subdivided into branches (Houghton 1985; Glickman 2000; Kraus 2004; Hupfer and Kuttler 2005). The main branches are theoretical meteorology,

observational meteorology, and applied meteorology. Applied meteorology includes weather prediction and climatology. Climatology must be seen in a much wider geosciences context. The subdivision is continued up to special areas of investigation such as maritime meteorology.

The applications of time and space scales became popular over the last 50 years, and subdivisions into macro-, meso- and micrometeorology were developed. Micrometeorology is not restricted to particular processes, but to the time and space scales of these processes (see Sect. 1.2). The significance of micrometeorology is in this limitation. The living environment of mankind is the main object of micrometeorological research. This is the atmospheric surface layer, the lowest 5–10% of the atmospheric boundary layer, which ranges in depth from about 0.5–2 km.

The surface layer is one of the main energy-exchange layers of the atmosphere, and accordingly the transformations of solar energy into other forms of energy are a main subject of micrometeorology. Furthermore, the surface layer is a source of friction, which causes a dramatic modification of the wind field and the exchange processes between the Earth's surface and the free troposphere. Due to the coupling of time and space scales in the atmosphere, the relevant time scale of micrometeorology is less than the diurnal cycle. A recent definition of micrometeorology is (Glickman 2000):

> Micrometeorology is a part of Meteorology that deals with observations and processes in the smaller scales of time and space, approximately smaller than 1 km and one day. Micrometeorological processes are limited to shallow layers with frictional influence (slightly larger phenomena such as convective thermals are not part of micrometeorology). Therefore, the subject of micrometeorology is the bottom of the atmospheric boundary layer, namely, the surface layer. Exchange processes of energy, gases, etc., between the atmosphere and the underlying surface (water, soil, plants) are important topics. Microclimatology describes the time-averaged (long-term) micrometeorological processes while the micrometeorologist is interested in their fluctuations.

If one examines the areas of investigation of applied meteorology (Fig. 1.1) it will be apparent that the main topics are related to microscale processes (Houghton 1985). Therefore, we see that micrometeorology gives the theoretical, experimental, and climatological basis for most of the applied parts of meteorology, which are related to the surface layer and the atmospheric boundary layer. Also, recent definitions such as environmental meteorology are related to micrometeorology. Applied meteorology often includes weather prediction and the study of air pollution.

The basics of micrometeorology come from hydrodynamics and in particular the dynamics of turbulent flow. An interesting overview about the history of the science of turbulence is given by Davidson et al. (2011). The following historical remarks are based on papers by Lumley and Yaglom (2001), Foken (2006), and Davidson

Applied Meteorology					
Hydro meteo-rology	Technical Meteorology			Biometeorology		
	Construc-tion Meteoro-logy	Traffic Mete-orology	Industrial Mete-orology	Agricultural Meteoro-logy	Forest Mete-orology	Human Biometeoro-logy
		Transport Mete-orology		Phenology		

Fig. 1.1 Classification of applied meteorology

et al. (2011). The origin may be dated to the year 1895, when Reynolds (1894) defined the averaging of turbulent processes, and described the equation of turbulent energy. Further steps were the mixing length approach by Taylor (1915) and Prandtl (1925), and the consideration of buoyancy effects by Richardson (1920). The every-day term 'turbulence element' is based on Barkov (1914), who found these in wind observations analyzed during a long stay in winter in the Antarctic ice shield. The actual term *micrometeorology* is dated to the determination of energy and matter exchange and the formulation of the *Austausch coefficient* by Schmidt (1925) in Vienna. At the same time in Munich, Geiger (1927) summarized microclimatological works in his famous book *The Climate near the Ground*, which is still in print (Geiger et al. 2009; Geiger 2013). The experimental and climatological application of these investigations of turbulent exchange processes were done mainly by Albrecht (1940) in Potsdam, who also wrote parts of the classical textbook by Kleinschmidt (1935) on meteorological instruments. Furthermore, Lettau (1939, translation into English 1944 in USA) investigated the turbulence near the surface and the atmospheric boundary layer in Leipzig and continued his investigation after the Second World War in the U.S.A. (Lettau and Davidson 1957). With the end of the Second World War, an era of more than 20 years of famous German-speaking micrometeorological scientists ended, but the word *Austausch coefficient* was maintained from that period on.

   The origin of modern turbulence research in micrometeorology was in the 1940s in Russia. Following the fundamental studies on isotropic turbulence and the turbulence spectra by Kármán and Howardt (1938) and Taylor (1938), Kolmogorov (1941a, b) gave theoretical reasons for the turbulence spectra. In 1943, Obukhov (published in 1946), found a scaling parameter that connects all near-surface turbulence processes. This paper (Obukhov 1971) was so important because of its relevance to micrometeorology, it was once again published by Businger and Yaglom (1971). A similar paper was published by Lettau (1949), but was not applied because it used a different scaling. Using what became known as *Monin-Obukhov*

similarity theory, Monin and Obukhov (1954) created the basics of the modern stability-dependent determination of the exchange process. At the same time, a direct method to measure turbulent fluxes was developed (Montgomery 1948; Obukhov 1951; Swinbank 1951), which has become known as the *eddy-covariance* method. This method became truly established only after the development of the sonic anemometer, for which the basic equations were given by Schotland (1955). Following the development of a sonic thermometer by Barrett and Suomi (1949), a vertical sonic anemometer with 1 m path length (Suomi 1957) was used in the O'Neill experiment in 1953 (Lettau and Davidson 1957). The design of today's anemometers was first developed by Bovscheverov and Voronov (1960), and later improved by Kaimal and Businger (1963) and Mitsuta (1966). These first anemometers used the phase shift method between the transmitted and the received signal or the difference in the travel time between the transmitter and receiver as the signal travels in both directions. Recent anemometers directly measure the travel times in both directions along each path (Hanafusa et al. 1982). Following the early work by Sheppard (1947), the surface stress was directly measured with a drag plate in Australia (Bradley 1968), and the sensible and latent heat fluxes were measured with highly sensitive modified classical sensors (Dyer et al. 1967).

The new theoretical concepts and sensor developments formed the basis for many famous experiments (see Appendix A.5). Among them were the many prominent Australian experiments for studying turbulent exchange processes (Garratt and Hicks 1990), and the so-called intercomparison experiments for turbulence sensors (Miyake et al. 1971; Tsvang et al. 1973; Dyer et al. 1982; Tsvang et al. 1985). Present day parameterizations are primarily based on the *KANSAS 1968* experiment (Izumi 1971; Kaimal and Wyngaard 1990). That experiment became the basis for the formulation of the universal functions (Businger et al. 1971) and the turbulence energy equation (Wyngaard et al. 1971), which were based on an earlier, not well-known paper by Obukhov (1960). Twenty years after the issue of the first textbook on micrometeorology by Sutton (1953), an important state-of-the-art summary of turbulent exchange between the lower atmosphere and the surface was given in 1973 at the *Workshop on Micrometeorology* (Haugen 1973).

After some criticism of the experimental design of the KANSAS experiment by Wieringa (1980), and the reply by Wyngaard et al. (1982), who recommended a repetition of the experiment, several micrometeorological experiments were conducted, including investigations of fundamental micrometeorological issues, for example the Swedish experiments at Lövsta (Högström 1990). Finally, the corrected universal functions by Högström (1988) comprise our most current knowledge.

At the end of the 1980s, the step to micrometeorological experiments in heterogeneous terrain became possible. At about the same time, similar experiments were conducted in the U.S.A. (FIFE, Sellers et al. 1988), in France (HAPEX, André et al. 1990) and in Russia (KUREX, Tsvang et al. 1991). These experiments were to become the bases of many further experiments (see Appendix A.5). A number of experiments, often equipped with an extensive suite of instruments, focused on

investigating particular atmospheric processes, such as turbulent fluxes in an heterogeneous landscape (LITFASS-2003, Beyrich and Mengelkamp 2006), energy exchange above ice and snow in the Arctic (SHEBA, 1997/98, Persson et al. 2002), stable stratification (CASES-99, Poulos et al. 2002), energy balance closure (EBEX-2000, Oncley et al. 2007), convective boundary layer processes (COPS 2007, Wulfmeyer et al. 2011), or boundary layer processes in the late afternoon (BLLAST 2011, Lothon et al. 2014).

During the last 40 years, significant progress has been made in the theoretical understanding of surface-layer processes and in the development of precision instruments. As a result, the number of available data sets has increased significantly, but scientific breakthroughs for a more realistic treatment of phenomena such as heterogeneous surfaces or stable boundary layers are still missing.

1.2   Atmospheric Scales

Contrary to other geophysical processes, meteorological processes have a clear time-space scaling (Beniston 1998). The reason for this is the spectral organization of atmospheric processes, where relevant wavelengths (extensions) are related to distinct durations in time (frequencies). The largest wavelengths are those of atmospheric circulation systems with 3–6 days duration and an extension of some thousands of kilometers (macro-turbulence, Rossby waves). The daily cycle is a prominent frequency. The time interval from minutes to seconds is characterized by exchange processes of energy and matter in the range of the so-called micro-turbulence, a main topic of micrometeorological investigations (see Sect. 1.4.3). The intermediate range, called meso-turbulence, is an area of relatively low energy (Etling 2008) that includes also local circulation systems. The principle of classification was formulated by Orlanski (1975), see Fig. 1.2. While atmospheric processes are strictly organized, the hydrological processes in soils and plant ecosystems have for the same time scales significantly smaller space scales. It is possible to define an "ecological gap" between single-plant or chamber measurements and the micrometeorological measurements, which are related to a footprint with a spatial dimension of about 50–100 m. For example, in the case of coupling hydrological or ecological with atmospheric models one must develop strategies to transfer the small-scale processes to the larger atmospheric space scale.

Different scale definitions in different scientific disciplines create problems in interdisciplinary communications. In addition, in climatology textbooks different scale concepts are discussed which are not easily comparable with the very clear meteorological scale concepts (see Sect. 7.1).

Because weather phenomena are classified according to space-time scales, the space-time scales of climate and weather prediction models must be classified in a similar way. For example, large-scale circulation models are assigned to the macro-β range. The classical weather forecast was formally related to the meso-α range,
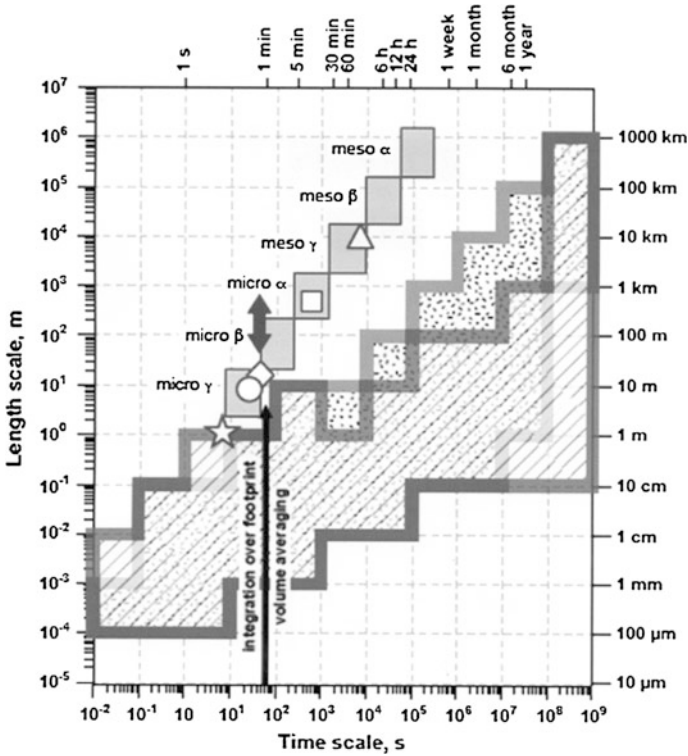
Fig. 1.2 Temporal and spatial scales of atmospheric (turbulent), biospheric (physiological) and soil processes. Atmospheric processes (Orlanski 1975) are *light grey* quadrats in the size of one scale (von micro γ bis meso α) shown. The scales of the plant processes, relevant for the energy and matter exchange with the atmosphere (Schoonmaker 1998) are shown as the speckled area and the soil processes (Blöschl and Sivapalan 1995; Vogel and Roth 2003) as hatched area (Foken et al. 2012, modified). Additionally, shown are (see following chapters): transport processes in tall forest canopies that comprise turbulent transport inside canopies (*star*), vertical advection inside canopies (*circle*), turbulent transport above canopies (*diamond*), coherent structures (*double arrow*), footprint averaged turbulent fluxes (*square*), and horizontal advection at the canopy top (*triangle*). Chemical reactions can be related to relevant scales by volume averaging (with kind permission of © Author(s) 2012. CC Attribution 3.0 License, All rights reserved)

but with today's high-resolution models they are related to the meso-β,γ scale. Micrometeorology is related to all micro-scales and also partly to the meso-γ scale.

This scaling principle is basic for measurements of atmospheric processes. For instance, to measure the spatial extension of a small low-pressure system, high-resolution (small scale) measurements are necessary, which are often not available in operational meteorological networks. The same is true for the movement of systems. The frequency of these measurements must be related to the velocity of the pressure system. This is valid for all scales, and phenomena can only be observed if the measurements are made on smaller space and time scales.

Therefore, the sampling theorem (see Sect. 6.1.2) is of prime importance for all meteorological measurements and scales. It is also possible to postulate a "technical sensing gap" between the typical range of the footprint (50–100 m) of meteorological measurements and the smallest size of grid cells of most of the conventional models or of polar circulating satellites (see Sect. 6.2).

1.3 Atmospheric Boundary Layer

The atmospheric boundary layer is the lowest part of the troposphere near the ground where the friction stress decreases with height. The wind velocity decreases significantly from its geostrophic value above the boundary layer to the wind near the surface, and the wind direction changes counter-clockwise up to 30–45° in the Northern hemisphere. In addition, thermal properties influence the boundary layer (Stull 1988; Kraus 2008). Frequently the synonym *planetary boundary layer* is used in theoretical meteorology, where the general regularities of the boundary layers of planetary atmospheres are investigated. Above the boundary layer, lays a mostly statically-stable layer (inversion) with intermittent turbulence. The exchange processes between the atmospheric boundary layer and the troposphere take place in the entrainment zone. The thickness of this layer is approximately 10% of the atmospheric boundary layer, which has a thickness of about 1–2 km over land and 0.5 km over the oceans. For strong stable stratification, its thickness can be about 10 m or less.

The daily cycle is highly variable (Stull 1988), see Fig. 1.3. After sunrise, the atmosphere is warmed by the turbulent heat flux from the ground surface, and the inversion layer formed during the night brakes up. The new layer is very turbulent, well mixed (mixed layer), and bounded above by an entrainment zone. Shortly before sunset, the stable (night time) boundary layer develops near the ground. This stable layer has the character of a surface inversion. Above this layer, remnants of the daytime mixed layer linger but turbulence, but turbulence is much weaker in this so called residual layer. It is capped by a free (capping) inversion—the upper border of the boundary layer (Seibert et al. 2000). After sunrise, the developing

Fig. 1.3 Daily cycle of the structure of the atmospheric boundary layer, EZ Entrainment zone (published with kind permission of © Prof. Roland Stull, Vancouver, All rights reserved)
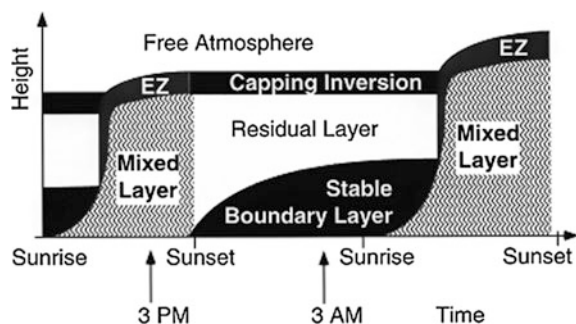
Height in m	Name		Exchange		Stability
1000	Upper layer (Ekman-layer)		Turbulent	No const. flux	Influence of stability
20	Turbulent layer	Surface layer (Prandtl-layer)		Flux constant with height	
	Roughness sublayer				
1	Dynamical sublayer				No influence of stability
0.01	Viscous sublayer		Molecular/turbulent		
0.001	Laminar boundary layer		Molecular		

Fig. 1.4 Structure of the atmospheric boundary layer

mixed layer quickly destroys the stable boundary layer and the residual layer. On cloudy days and in winter, when the solar radiation and the energy transport from the surface to the atmosphere are weak, the mixed-layer development will be damped, and characteristics of the previous day boundary layer may persist throughout the day. On days with strong solar radiation, the nocturnal boundary-layer structure quickly vanishes as convective cells develop at about 10 m above the ground over areas with strong sensible heat fluxes. These convective cells, have narrow areas of strong updrafts surrounded by broader regions of weaker downdrafts. According to model studies, these convective cells develop over areas which are larger than 200–500 m (e.g. Shen and Leclerc 1995).

In the upper part of the atmospheric boundary layer (upper layer or Ekman layer), the changes of the wind direction take place. The lowest 10% is called the surface or Prandtl layer (Fig. 1.4). It is also called the *constant flux layer* because of the assumption of constant fluxes with height within the layer. This offers the possibility to estimate, for example, the fluxes of sensible and latent heat in this layer while in the upper layers flux divergences dominate. The atmospheric boundary layer is turbulent to a large degree, and only within a few millimeters above the surface do the molecular exchange processes dominate. Because the turbulent processes are about 10^5-fold more effective than molecular processes and because of the assumption of a constant flux, the linear vertical gradients of properties very near the surface must be very large. For example, temperature gradients up to 10^3 Km^{-1} have been measured (Fig. 1.5). Between this molecular boundary layer (term used for scalars) or laminar boundary layer (term used for the flow field) and the turbulent layer, a viscous sublayer (buffer layer) exists with mixed exchange conditions and a thickness of about 1 cm. According to the

Fig. 1.5 Vertical temperature profile above a water surface with a molecular boundary layer, which has an linear temperature gradient (adapted from Foken et al. 1978 with kind permission of © Kluwer Academic Publisher B.V. Dordrecht 1978, All rights reserved)
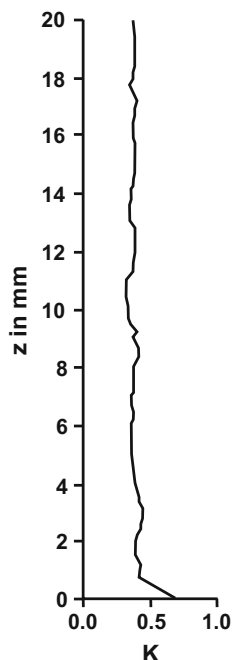
similarity theory of Monin and Obukhov (1954), a layer with a thickness of approximately 1 m (dynamical sublayer) is not influenced by the atmospheric stability—this layer is nearly neutral all of the time. Above tall vegetation or buildings, the constant flux layer assumption is no longer fulfilled due to the high friction and the surface layer must be divided into additional layers. Immediately above the canopy up to roughly twice of the canopy height, in the so-called mixing layer or roughness sublayer (Garratt 1978), turbulent mixing is increased. If the vegetation is not too high, a surface layer may develop above the mixing layer but its thickness is reduced. Within the canopy layer the constant flux assumption is also not fulfilled; for more details see Sects. 3.1.3 and 3.5.

All processes in the atmospheric boundary layer, mainly in the micrometeorological range near the ground surface (nearly neutral stratification), can be compared easily with measurements made in the laboratory (wind tunnels and water channels). Thus, the research of the hydrodynamics of boundary layers at a wall, for example by Prandtl, is applicable to atmospheric boundary layer research (Monin and Yaglom 1973, 1975; Schlichting and Gersten 2003; Oertel 2004). As will be shown in the following chapters, knowledge in micrometeorology is based to a large extent on hydrodynamic investigations. In the wind tunnel, many processes can be studied more easily than in nature. But, the reproduction of atmospheric processes in the wind tunnel also means a transformation of all the similarity

numbers (see Sect. 2.1.2). Therefore, non-neutral processes can be studied in the laboratory only if extremely large temperature or density gradients can be realized in the fluid channels.

1.4   Energy Balance at the Earth's Surface

The earth's surface is the main energy transfer area for atmospheric processes (Fig. 1.6). It is heated by the shortwave down-welling irradiation from the sun ($K\downarrow$), and only a part of this radiation is reflected back ($K\uparrow$). Furthermore, the surface absorbs longwave down-welling radiation due to longwave emission by clouds, particles and gases ($I\downarrow$). The absorbed energy is emitted only partly into the atmosphere as longwave up-welling radiation ($I\uparrow$). In the total balance, the earth's surface receives more radiation energy than is lost, i.e. the net radiation at the ground surface is positive ($-Q_s^*$, see Sect. 1.4.1). The surplus of supplied energy will be transported back to the atmosphere due to two turbulent energy fluxes (see Sect. 1.4.3), the sensible heat flux (Q_H) and the latent heat flux (Q_E, evaporation). Furthermore, energy is transported into the soil due to the ground heat flux (Q_G) (see Sect. 1.4.2) and will be stored by plants, buildings, etc. (ΔQ_S). The sensible heat flux is responsible for heating the atmosphere from the surface up to some 100 m during the day, except for days with strong convection. The energy balance at the earth's surface according to the law of energy conservation (see also Sect. 3.7) is:

$$-Q_s^* = Q_H + Q_E + Q_G + \Delta Q_s \tag{1.1}$$
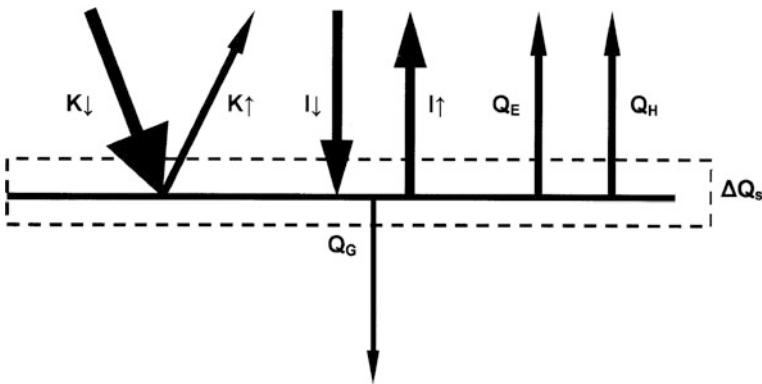
Fig. 1.6 Schematic diagram of the radiation and energy fluxes at the earth's surface. The net radiation according to Eq. (1.1) is the sum of the short-wave down-welling ($K\downarrow$) and reflected radiation ($K\uparrow$), and the long-wave radiation fluxes from the earth surface ($I\uparrow$) and from clouds, particles, and gases ($I\downarrow$). The energy balance is the sum of the net radiation, the sensible heat flux (Q_H), the latent heat flux (Q_E), and the ground heat flux (Q_G). In addition to the turbulent fluxes, the energy storage ΔQ_s in the air, in the plants, and in the soil are given

Supplement 1.1[1] **Energy and radiation fluxes in meteorology**

Energy and radiation-fluxes in meteorology are given in terms of densities. While the unit of energy is the Joule (J) and for power is Watt (W = J s^{-1}), the unit for the energy flux density is W m^{-2}. It appears that the energy flux density has *apparently* no relation to time, but the exact unit is J s^{-1} m^{-2}. To determine the energy that 1 m^2 gets during 1 h, multiply the energy flux density by 3600 s. Energy fluxes expressed as J m^{-2} are unusual in meteorology except daily sums which are given in MJ m^{-2} (Mega-Joules per square meter), and sometimes kWh (kilo-Watt-hours).

Energy balance values are defined as radiation and energy flux densities (Bird et al. 2007) given in the dimension Wm^{-2} (Supplement 1.1).The following convention will be applied:

Radiation and energy fluxes are positive if they transport energy away from the earth's surface (into the atmosphere or into the ground), otherwise they are negative. The sign of the number gives the direction of the flux.

The advantage of this convention is that the turbulent fluxes and the ground heat flux are positive at noon. This convention is not used in a uniform way in the literature, e.g. in macro-scale meteorology the opposite sign is used. Often, all upward directed fluxes are assumed as positive (Stull 1988). In this case, the ground heat flux has the opposite sign of that given above. In other textbooks, the global radiation and the turbulent fluxes are shown with a positive sign in the figures (Oke 1987; Arya 2001), which makes the figures easier to read but can be confusing. The applied convention is identical with the presentations by Garratt (1992), because $-Q_s^* > 0$. In the end, the choice of the convention is not important, but the energy balance Eq. (1.1) must be fulfilled.

The components of the energy balance are shown in schematic form in Fig. 1.7. Remarkable is the high variation of the sensible and latent heat flux in comparison to the net radiation, which is a result of wind velocity changes. In the case of changing cloudiness, all terms become highly variable. The same variations occur in the case of some micrometeorological processes, which will be discussed in the following chapters. The most important variances are a positive latent heat flux after sunset and a negative sensible heat flux that begins in the early afternoon (oasis effect). A negative latent heat flux (evaporation) is identical with dewfall. The long-term mean values of the earth's energy balance are given in Table 1.1. Even

---

[1]Supplements are short summaries from textbooks in meteorology and other sciences. These are included for an enhanced understanding of this book or for comparisons. For details, see the relevant textbooks.
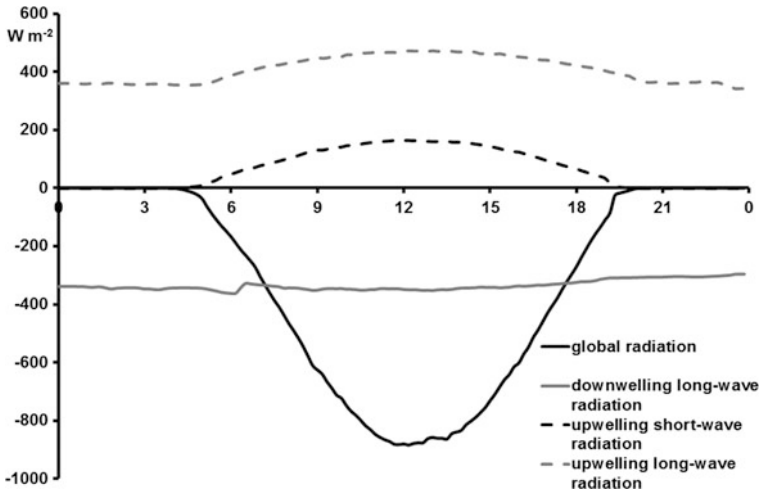
Fig. 1.7 Schematic of the daily cycle energy balance (May 24, 2012, Ecological-Botanical Garden of the University of Bayreuth, from Foken 2013 with kind permission from © Edition am Gutenbergplatz Leipzig 2013, All rights reserved)

Table 1.1 Radiation and energy fluxes in Wm^{-2} at the earth surface (Kiehl and Trenberth 1997, modified and updated)

Reference	$K{\downarrow}$ - $K{\uparrow}$-	$I{\uparrow}$-$I{\downarrow}$	Q_H	Q_E
Budyko (1974)[a]	−157	52	17	88
Henderson-Sellers and Robinson (1986)[a]	−171	68	24	79
Liou (1992)[a]	−151	51	21	79
Hartmann (1994)[a]	−171	72	17	82
Kiehl and Trenberth (1997)[a]	−168	66	24	78
Trenberth et al. (2009)[b]	−161	63	17	80
Wild et al. (2013)[c], uncertainty	−161 (−154 ⋯ −166)	56 (46 ⋯ 62)	20 (15 ⋯ 25)	84 (70 ⋯ 85)
Wild et al. (2015)[c], Land uncertainty	−136 (−132 ⋯ −143)	34 (27 ⋯ 39)	32 (25 ⋯ 36)	38 (34 ⋯ 45)
Wild et al. (2015)[c], Ocean uncertainty	−170 (−174 ⋯ −176)	53 (49 ⋯ 57)	16 (11 ⋯ 18)	100 (90 ⋯ 105)

[a]Irradiation at the upper boundary of the atmosphere 342 Wm^{-2}
[b]Irradiation at the upper boundary of the atmosphere 341 Wm^{-2}, 1 Wm^{-2} at the earth surface absorbed
[c]Irradiation at the upper boundary of the atmosphere 340 Wm^{-2}, 0.6 Wm^{-2} (uncertainty 0.2 …1.0 Wm^{-2}) at the earth surface absorbed

though the values of the radiation fluxes are high, the radiation balance is relatively low with a value of about 100 Wm^{-2}. Noticeable is the inaccuracy of the turbulent fluxes, which, among other factors, can be explained by the difficulties in measuring and evaluation these terms. The 1 K increase of the global mean temperature in the last century due to anthropogenic greenhouse gas emissions corresponds to an additional radiation energy of 2 Wm^{-2}. Therefore, changes in the radiation and energy fluxes, e.g. due to changes in land use, can have significant effects on the climate system.

1.4.1   Net Radiation at the Earth's Surface

The radiation in the atmosphere is divided into shortwave (solar) radiation and longwave (heat) radiation. Longwave radiation has wavelengths >3 µm (Supplement 1.2). The net radiation at the ground surface is given by:

$$Q_s^* = K\uparrow + K\downarrow + I\uparrow + I\downarrow \tag{1.2}$$

From Eq. (1.2) we see that the net radiation is the sum of the shortwave down-welling radiation mainly from the sun (global radiation), the longwave down-welling infrared (heat) radiation emitted by clouds, aerosols, and gases, the shortwave up-welling reflected (solar) radiation, and the longwave up-welling infrared (heat) radiation. The shortwave radiation can be divided into the diffuse radiation from the sky and direct solar radiation.

Table 1.1 gives the climatological-averages of the magnitudes of the components of the energy and radiation balance equation. These values are based on recent measurements of the mean solar incoming shortwave radiation at the upper boundary of the atmosphere (cross-section area of the earth πR^2, R: radius of the earth), i.e. $S = -1361\ Wm^{-2}$ (Kopp and Lean 2011) in energetic units or $-1.119\ Kms^{-1}$ in kinematic units (for conversion between these units, see Sect. 2. 3.1). Therefore, the daily average at the upper boundary layer of the atmosphere (surface of the globe $4\pi R^2$) is 340 Wm^{-2}. Figure 1.8 shows the typical daily cycle of the components of the net radiation. The ratio of reflected to the incoming shortwave radiation is called the albedo:

$$a = -\frac{K\uparrow}{K\downarrow} \tag{1.3}$$

In Table 1.2 the albedos for different surfaces are given.
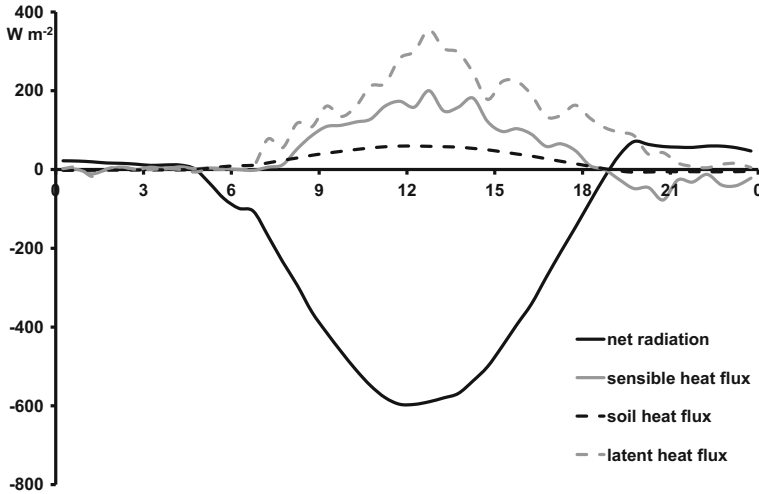
Fig. 1.8 Schematic of the diurnal cycle of the components of the net radiation (May 24, 2012, Ecological-Botanical Garden of the University of Bayreuth, from Foken 2013 with kind permission from © Edition am Gutenbergplatz Leipzig 2013, All rights reserved)

Table 1.2 Albedo of different surfaces (Geiger et al. 2009)

Surface	Albedo
Clean snow	0.75–0.98
Grey soil, dry	0.25–0.30
Grey soil, wet	0.10–0.12
White sand	0.34–0.40
Wheat	0.10–0.25
Grass	0.18–0.20
Oaks	0.18
Pine	0.14
Water, rough, solar angle 90°	0.13
Water, rough, solar angle 30°	0.024

The longwave radiation fluxes can be determined according to the Stefan-Boltzmann law:

$$I = \varepsilon_{IR}\, \sigma_{SB}\, T^4 \tag{1.4}$$

Supplement 1.2 Spectral classification of the radiation
   Spectral classification of short and long wave radiation (Wendisch and Yang 2012, modified)

Notation	Wave length in μm	Remarks
Ultraviolet radiation		
UV-C-range	0.010–0.280	Does not penetrate the atmosphere
UV-B-range	0.280–0.315	Does partly penetrate the atmosphere
UV-A-range	0.315–0.370	Penetrates the atmosphere
Visible radiation		
Violet	0.370–0.455	
Blue	0.455–0.492	
Green	0.492–0.576	
Yellow	0.576–0.597	
Orange	0.597–0.622	
Red	0.622–0.680	
Dark red	0.680–0.750	
Infrared radiation		
Near infrared (NIR)	0.750–2.0	
Infrared (IR)	2.0–1000.0	

where the infrared emissivities for different surfaces are given in Table 1.3, and $\sigma_{SB} = 5.67 \cdot 10^{-8}$ W m^{-2} K^{-4} is the Stefan-Boltzmann constant.

In general, the up-welling longwave radiation is greater than the down-welling longwave radiation, because the earth's surface is warmer than clouds, aerosols, and gases. It is only in the case of fog, that up-welling and down-welling radiation are equal. The down-welling radiation may be greater if clouds appear in a previously clear sky and the ground surface has cooled. Under clear sky without clouds and dry air, the radiation temperature is approximately −55 °C.

Meteorological data are usually measured in UTC (Universal Time Coordinated) or in local time; however, for radiation measurements the mean or, even better, the true local time is desirable. Then, the sun is at its zenith at 12:00 true local time.

Table 1.3 Infrared emissivity of different surfaces (Geiger et al. 2009)

Surface	Emissivity
Water	0.960
Fresh snow	0.986
Coniferous needles	0.971
Dry fine sand	0.949
Wet fine sand	0.962
Thick green grass	0.986

Appendix A.4 gives the necessary calculations and astronomical relations to determine true local time.

Measurements of global radiation are often available in meteorological networks, but other radiation components may be missing. Parameterizations of these missing components using available measurements can be helpful. However, it should be noted that such parameterizations are often based on climatological mean values, and are valid only for the places where they were developed. Their use for short-time measurements is invalid. Jiang et al. (2015) give an overview of how to calculate the net radiation only from data of the global radiation and some additional information.

The possibility to parameterize radiation fluxes using cloud observations was proposed by Burridge and Gadd (1977). For shortwave radiation fluxes, the transmissivity of the atmosphere is used:

$$T_K = (0.6 + 0.2 \ \sin \ \Psi)(1 - 0.4 \ \sigma_{c_H})(1 - 0.7 \ \sigma_{c_M})(1 - 0.4 \ \sigma_{c_L}) \qquad (1.5)$$

For solar elevation angles $\Psi = 90°$, the transmission coefficient, T_K, ranges from 0.8 to 0.086. σ_c is the cloud cover (0.0–1.0) of high clouds, c_H, of middle clouds, c_M, and c_L of low clouds, (see Supplement 1.3). Please note, that in meteorology the cloud cover is given in octas. (An octa is a fraction equal to one-eighth of the sky.) The incoming shortwave radiation can be calculated using the solar constant S:

$$K \downarrow = \begin{pmatrix} S\,T_K \ \sin \ \Psi, & \Psi \geq 0 \\ 0, & \Psi \leq 0 \end{pmatrix} \qquad (1.6)$$

Supplement 1.3 Cloud genera

The classification of clouds is made according their genera and typical height. In the middle latitudes, high clouds are at 5–13 km a.g.l.; middle high clouds at 2–7 km a.g.l., and low clouds at 0–2 km a.g.l. The cloud heights in Polar Regions are lower while in tropical regions clouds heights can be up to 18 km.

Cloud genera	Height	Description
Cirrus (Ci)	High	White, fibrously ice cloud
Cirrocumulus (Cc)	High	Small ice cloud, small fleecy cloud
Cirrostratus (Cs)	High	White stratified ice cloud, halo
Altocumulus (Ac)	Mean	Large fleecy cloud
Altostratus (As)	Mean	White-grey stratified cloud, ring
Nimbostratus (Ns)	Low	Dark rain/snow cloud
Stratocumulus (Sc)	Low	Grey un-uniform stratified cloud
Stratus (St)	Low	Grey uniform stratified cloud
Cumulus (Cu)	Low[a]–mean	Cumulus cloud
Cumulonimbus (Cb)	Low[a]–high	Thundercloud, anvil cloud

[a]in parameterizations classified as low clouds

The reflected shortwave radiation can be calculated according to Eq. (1.3) by using typical values of the albedo of the underlying surface (Table 1.2). The longwave radiation balance can be parameterized using the cloud cover:

$$I^* = I\uparrow + I\downarrow = \left(0.08\,\text{Kms}^{-1}\right)\left(1 - 0.1\,\sigma_{c_H} - 0.3\,\sigma_{c_M} - 0.6\,\sigma_{c_L}\right) \quad (1.7)$$

If the surface temperature is given, then the longwave up-welling radiation can be calculated using the Stefan-Boltzmann law, Eq. (1.4). The longwave down-welling radiation can be calculated using Eqs. (1.4) and (1.7).

More often, parameterizations use the duration of sunshine because it was measured for a long time in agricultural networks. Note that time series of sunshine durations are often inhomogeneous because the older Campbell-Stokes sunshine autograph was replaced by electronic methods. These parameterizations are based on climatological cloud structures and can be used only for monthly and annual averaged values, and in the region where the parameterization was developed. The parameterization is based on the well-known Ångström equation with sunshine duration, Sd:

$$K\downarrow = K\downarrow_{\text{extr}}[a + b(Sd/Sd_0)], \quad (1.8)$$

where constants a and b depend on the place of determination. For the German low lands, the constants are, for example, $a \sim 0.19$ and $b \sim 0.55$ (Wendling et al. 1997). The mean daily extraterrestrial incoming irradiation at the upper edge of the atmosphere can be calculated in Wm^{-2} according to:

$$K\downarrow_{\text{extr}} = 28.2[9.9 + 7.08\,\varsigma + 0.18(\varsigma - 1)(\varphi - 51°)] \quad (1.9)$$

This equation is given in a form such that for a geographical latitude of $\varphi = 51°$ no correction for the latitude is necessary. The theoretical sunshine duration is the time between sunrise and sunset and can be expressed in hours

$$Sd_0 = 12.3 + 4.3\,\varsigma + 0.167\,\varsigma\,(\varphi - 51), \quad (1.10)$$

with (DOY = day of the year)

$$\varsigma = \sin[DOY\,(2\pi/365) - 1.39]. \quad (1.11)$$

Because direct measurements of the radiation components are now available, parameterizations should only be used for calculations with historical data.

1.4.2   Ground Heat Flux and Ground Heat Storage

The ground surface (including plants and urban areas) is heated during the day by the incoming shortwave radiation. During the night, the surface cools due to longwave up-welling radiation, and is cooler than the air and the deeper soil layers. High

gradients of temperature are observed in layers only a few millimetres thick (see Sect. 1.3). The energy surplus according to the net radiation is compensated by the turbulent sensible and latent heat fluxes and the mainly molecular ground heat flux. For the generation of latent heat flux, an energy surplus at the ground surface is necessary, and water must be transported through the capillaries and pores of the soil. Energy for the evaporation can also be provided by the soil heat flux in the upper soil layer.

In meteorology, the soil and the ground heat fluxes are often described in a very simple way, e.g. the large differences in the scales in the atmosphere and the soil are often not taken into account. The heterogeneity of soil properties in the scale of 10^{-3}–10^{-2} m is ignored, and the soil is assumed to be nearly homogeneous for the given meteorological scale. For more detailed investigations, soil physics textbooks must be consulted. In the following, convective heat fluxes and latent heat fluxes in large pores are ignored, because these are measured as sensible and latent heat flux in the atmosphere.

The ground heat flux, Q_G, is based mainly on molecular heat transfer and is proportional to the temperature gradient times the thermal molecular conductivity a_G (Table 1.4):

$$Q_G = a_G \frac{\partial T}{\partial z} \tag{1.12}$$

This molecular heat transfer is so weak that during the day only the upper decimetres are heated. When considering the annual cycle of ground temperature, maximum temperature is at the surface during the summer, but 10–15 m below the surface during winter (Lehmann and Kalb 1993). On a summer day, the ground heat flux is about 50–100 Wm^{-2}. A simple but not reliable calculation (Liebethal and Foken 2007) is: $Q_G = -0.1 \ Q_s^*$ or $Q_G = 0.3 \ Q_H$ (Stull 1988).

The determination of the ground heat flux according to Eq. (1.12) is not practicable because the temperature profile must be extrapolated to the surface to determine the partial derivative there. This can be uncertain because of the high temperature gradients near the surface (Fig. 1.9) and the difficulties in the determining thermal heat conductivity.

Table 1.4 Thermal molecular conductivity a_G, volumetric heat capacity C_G, and molecular thermal diffusivity v_T for different soil and ground properties (Stull 1988)

Ground surface	a_G in W m^{-1} K^{-1}	C_G in 10^6 W s m^{-3} K^{-1}	v_T in 10^{-6} m^2 s^{-1}
Rocks (granite)	2.73	2.13	1.28
Moist sand (40%)	2.51	2.76	0.91
Dry sand	0.30	1.24	0.24
Sandy clay (15%)	0.92	2.42	0.38
Swamp (90% water)	0.89	3.89	0.23
Old snow	0.34	0.84	0.40
New snow	0.02	0.21	0.10
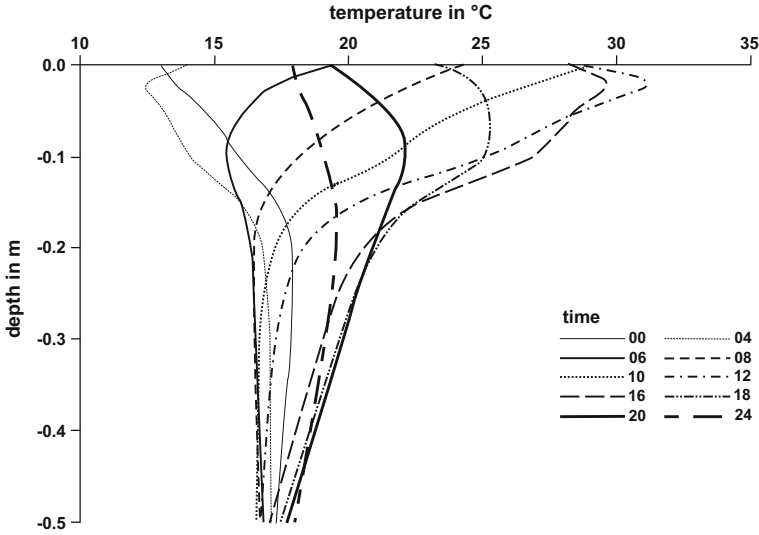
Fig. 1.9 Temperature profile in the upper soil layer on June 05, 1998, measured by the University of Bayreuth during the LITFASS-98 experiment (bare soil) at the boundary layer measuring field site of the Meteorological Observatory Lindenberg (high clouds from 12:00 to 14:00)

However, the ground heat flux at the surface can be estimated as the sum of the soil heat flux measured at some depth using soil heat flux-plates (see Sect. 6.2.6) and the heat storage in the layer between the surface and the plate:

$$Q_G(0) = Q_G(-z) + \int_{-z}^{0} \frac{\partial}{\partial t} C_G(z) T(z) dz \tag{1.13}$$

An optimal design for ground heat flux measurements was developed by Liebethal et al. (2005) using sensitivity analysis. According to their method, the soil heat-flux plate should be buried rather deeply (10–20 cm) with several temperature measurements made above it to calculate the heat storage. A similar accuracy can be achieved if only one temperature profile is measured to calculate both the soil heat flux according to Eq. (1.12) over the depth of 10–20 cm and the heat storage term above this layer and the surface.

The volumetric heat capacity $C_G = a_G/v_T$ (v_T is the molecular thermal diffusivity, Table 1.4), can be assumed constant with depth in the case of uniform soil moisture. A general measurement and calculation guide for the integral of the change of the soil temperature with time is not available. Most institutes have their own schemes, not all of which are optimal solutions. The simplest method is the measurement with an integrating temperature sensor of the mean temperature of the soil layer between the surface and the heat-flux plate. For the ground heat flux near the surface, it then follows that:

$$Q_G(0) = Q_G(-z) + \frac{C_G\,|\Delta z|\,\left[\overline{T(t_2)} - \overline{T(t_1)}\right]}{t_2 - t_1} \qquad (1.14)$$

The change of the soil temperature with the time can be determined from the vertical gradient of the soil heat flux and using of Eq. (1.12):

$$\frac{\partial T}{\partial t} = \frac{1}{C_G}\frac{\partial Q_G}{\partial z} = v_T \frac{\partial^2 T}{\partial z^2} \qquad (1.15)$$

The daily cycle of the soil temperature is to first-order a sine function (Fig. 1.10). Therefore, the surface temperature T_s can be calculated depending on a temperature T_M, which is not affected by the daily cycle, i.e.

$$T_s = T_M + A_s \sin\left[\left(\frac{2\pi}{P}\right)(t - t_M)\right], \qquad (1.16)$$

where A_s is the amplitude and P is the period of the wave of the surface temperature and t_M is the time required for $T_s = T_M$ (Arya 2001).

Multiple layers are used for the modelling of the ground heat flux. Because during the daily cycle only the upper soil layers are heated (Fig. 1.10), the two-layer model (force-restore method) developed by Blackadar (1976) is widely used. The ground heat flux can be calculated from two components, i.e., from the change of the temperature of the thin surface layer due to radiation and from the slow wave of the temperature difference between the surface layer and a deeper layer. The equation for the ground heat flux is (Stull 1988):
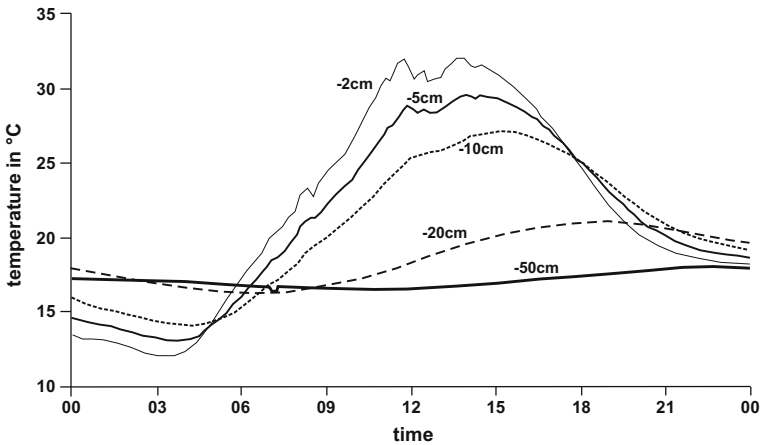

Fig. 1.10 Daily cycle of soil temperatures at different depth on June 05, 1998, measured by the University of Bayreuth during the LITFASS-98 experiment (bare soil) at the boundary layer measuring field site of the Meteorological Observatory Lindenberg (high clouds from 12:00 to 14:00)

$$Q_G = z_G C_G \frac{\partial T_G}{\partial t} + \left(2\pi \frac{z_G C_G}{P} \right)(T_G - T_M), \tag{1.17}$$

where, T_G is the temperature of the upper soil layer, T_M is the temperature of the deeper soil layer, P is the time of the day, and z_G is the thickness of the surface layer. According to Blackadar (1976), $2\pi/P$ is $3 \cdot 10^{-4}$ s^{-1} during the day, and $1 \cdot 10^{-4}$ s^{-1} at night (day: $T_a < T_G$, night: $T_a > T_G$, T_a: air temperature). The thickness of the upper soil layer depends on the depth of the daily temperature wave:

$$z_G = \sqrt{\frac{v_T P}{4\pi}} \tag{1.18}$$

This can be derived from Eq. (1.15) using Eq. (1.16), see Arya (2001). The force-restore method has the best results in comparison to other parameterization methods (Liebethal and Foken 2007).

1.4.3   Turbulent Fluxes

Contrary to the molecular heat exchange in the soil, heat exchange in the air due to turbulence is much more effective. This is because turbulent exchange occurs over scales of motions ranging from millimetres to kilometres. Turbulent elements can be thought of as air parcels with largely uniform thermodynamic characteristics. Small-scale turbulence elements join to form larger ones and so on. The largest eddies are atmospheric pressure systems. The heated turbulent elements transport their energy by their random motion. This process applies also for trace gases such as water vapour and kinetic energy. The larger turbulent elements receive their energy from the mean motion, and deliver the energy by a cascade process to smaller elements (Fig. 1.11). Small turbulent elements disappear by releasing energy in form of heat (energy dissipation). On average, the transformation of kinetic energy into heat is about 2 Wm^{-2}, which is very small and not considered in the energy balance equation. The reason for this very effective exchange process, which is about a factor of 10^5 greater than the molecular exchange, is the atmospheric turbulence.

Atmospheric turbulence is a specific feature of atmospheric flows with air parcels (turbulent elements or turbulent eddies that are much larger than molecules:) moving irregularly and randomly around a mean state. The length and time scales of these motions cover wide ranges from centimetres and seconds to thousands of kilometres and days.

injection
of energy

flux
of energy

dissipation
of energy
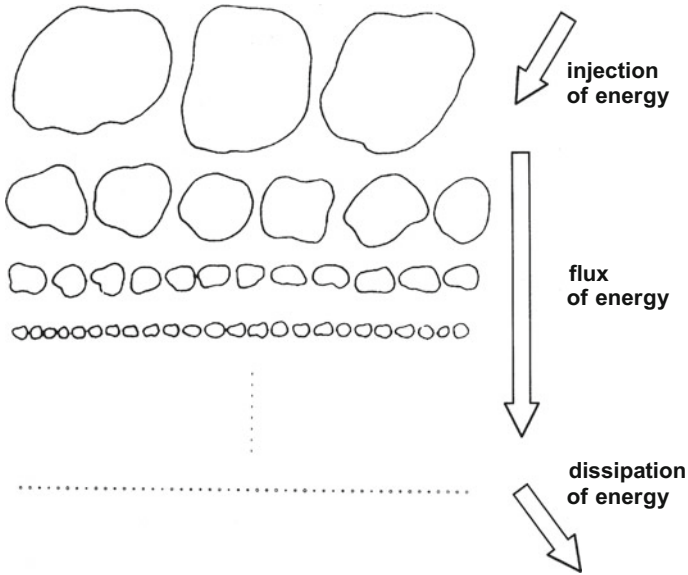
Fig. 1.11 Cascade process of turbulent elements (Frisch 1995), please note that the diminishing
of the sizes of the elements is continuous (With kind permission of © Cambridge University Press
Cambridge 1995, All rights reserved)

The characteristic distribution of turbulent elements (turbulent eddies) takes
place according their size and is represented by the turbulence spectrum:

The turbulence spectrum describes the energy distribution of turbulent ele-
ments (turbulent eddies) according to their wavelength or frequency.
Depending on the frequency, the distribution is classified as macro-, meso-
or micro turbulence.

The division of atmospheric turbulence occurs over three time ranges, i.e.
changes of high and low pressure systems within 3–6 days; the daily cycle of
meteorological elements, and the transport of energy, momentum, and trace gases at
frequencies ranging from 0.0001 to 10 Hz (Fig. 1.12). The transport of energy and
trace gases is the main issue of micrometeorology.

Of special importance, is the inertial sub-range, which is characterized by iso-
tropic turbulence and a constant decrease of the energy density with increasing
frequency. In the range from about 0.01–5 Hz, no dominant direction exists for the
motion of turbulent elements. The decrease of energy by the decay of larger
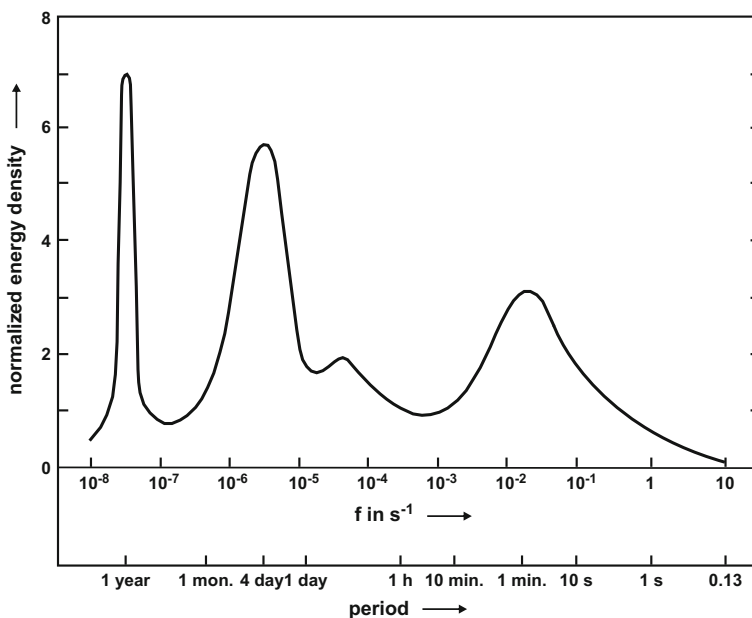
Fig. 1.12 Schematic plot of the turbulence spectra (adaptiert from Roedel and Wagner 2011 with kind permission of © Springer Verlag, Berlin Heidelberg 2000, All rights reserved); the range of frequencies $> 10^{-3}$ Hz is called micro-turbulence, macro-turbulence is from 10^{-6} to 10^{-5} Hz. Between 10^{-5} and 10^{-3} Hz is the range of low energy, the meso-turbulence, and the daily cycle

turbulent elements into smaller ones takes place in a well-defined way according to Kolmogorov's *-5/3-law* (Kolmogorov 1941b). This law predicts that the energy density decreases by five decades when the frequency increases by three decades. The inertial sub-range merges into the dissipation range at the *Kolmogorov's microscale*. The shape of the turbulence spectra depends on the meteorological parameters, the thermal stratification, the height above the ground surface, and the wind velocity (see Sect. 2.5).

A typical property of turbulence, especially in the inertial sub-range, is that turbulent elements change little as they move with the mean flow. Thus, at two neighbouring downwind measuring points the same turbulent structure can be observed at different times. This means that a high autocorrelation of the turbulent fluctuations exists. This is called *frozen turbulence* according to Taylor (1938).

Furthermore, the length scales of turbulent elements increase with the height above the ground surface. In an analogous way, the smallest turbulent elements with the highest frequencies are found near the ground surface. From these findings, it is reasonable to plot the turbulence spectra not as a function of frequency *f*, but as a dimensionless frequency, *n*, normalized with the wind speed *u* and the height *z*:
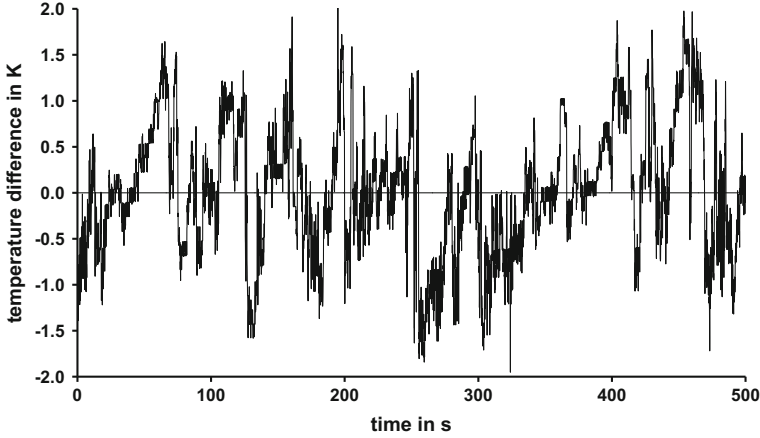
Fig. 1.13 Time series of the air temperature above a spruce forest (University of Bayreuth, Waldstein-Weidenbrunnen site), Aug. 19, 1999, 11:51–12:00 UTC, 500 s measuring period (Wichura et al. 2001)

$$n = f \frac{z}{\bar{u}} \qquad (1.19)$$

(In the English literature, one often sees n as the frequency and f as the dimensionless frequency.)

Turbulent elements can be easily seen, e.g., in plots of temperature time series with high time resolution. In Fig. 1.13, we see short-period disturbances with different intensities superposed onto longer-period (~ 60 s) disturbances. We also see that even significantly larger structures are present.

In analogy to the molecular transport equations (Eq. 1.12), the turbulent heat fluxes (sensible and latent) are often calculated using the vertical gradients of temperature T and specific humidity q (see Supplement 2.2), respectively. However, the molecular transfer coefficients must be replaced by the turbulent diffusion coefficients. The sensible heat flux, Q_H, describes the turbulent transport of heat from and to the earth's surface. The latent heat flux, Q_E, describes the vertical transport of water vapour and the heat required for evaporation at the ground surface. This heat will be deposited later in the atmosphere when condensation occurs, e.g. in clouds. The relevant equations are:

$$Q_H = -\rho\, c_p\, K_H \frac{\partial T}{\partial z}, \qquad (1.20)$$

$$Q_E = -\rho\, \lambda\, K_E \frac{\partial q}{\partial z} \qquad (1.21)$$

with the air density ρ, the specific heat for constant pressure c_p, and evaporation heat of water λ. The turbulent diffusion coefficients K_H and K_E are normally complicated functions of the wind speed, the stratification, and the properties of the underlying surface. Their evaluation is a special issue of micrometeorology. In Sect. 2.3, several possible calculations of the diffusion coefficients are discussed. Also common is the *Austausch coefficient* (Schmidt 1925), which is the product of the diffusion coefficient and the air density:

$$A = \rho K \tag{1.22}$$

A typical example of the daily cycle of the turbulent fluxes of two neighbouring surfaces, where one is bare soil and the other covered with barley, is shown in Fig. 1.14. It is obvious that during the night all fluxes have the opposite sign than during the day, and the absolute values are much smaller at night. After sunrise, the signs change and the turbulent fluxes increase rapidly. The time shift between the irradiation and the beginning of turbulence is only a few minutes (Foken et al. 2001). The time shift of the ground heat flux (not shown here) depends on the depth of the soil layer. The maximum of the turbulent fluxes on clear days occurs shortly after midday. Optimal conditions for evaporation are available on the vegetated site, i.e. high soil moisture and strong winds. The sensible heat flux may become negative 1–3 h before sunset, or sometimes shortly after noon, if the radiative fluxes cannot balance the latent heat flux. This phenomenon is called the "oasis effect", and is also found in temperate latitudes. The latent heat flux, on the other hand, remains large after sunset, until it changes its sign after midnight (dewfall). In contrary, an oasis effect is not prominent on the bare soil (Fig. 1.14), because it dries out during the day and not enough water is available for evaporation.
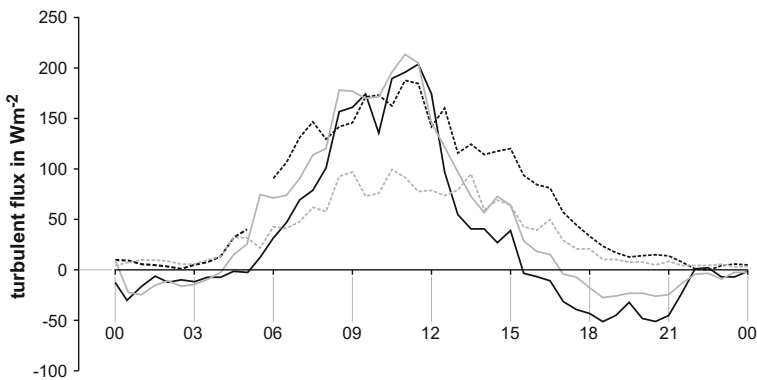
Fig. 1.14 Typical daily cycle of the sensible heat flux (*full line*) and the latent heat flux (*dashed line*) above a barley field (*black lines*) and bare soil (*grey lines*), both fields in a distance of 100 m on June 04, 2003 during the experiment LITFASS–2003

If the sum of all energy fluxes is plotted (Figs. 1.7 and 1.8) it becomes obvious that the energy balance according to Eq. (1.1) is typically not closed when measured data are analysed. This very complex problem is discussed in Sect. 3.7.

While over land in the temperate latitudes the sensible and latent heat fluxes are of the same order, over the ocean the evaporation is much greater. In some climate regions and under extreme weather conditions, significant deviations are possible (Table 1.1).

1.5   Water Balance Equation

The energy balance Eq. (1.1) is connected to the evaporation through the water balance equation:

$$0 = N - Q_E - A \pm \Delta S_W, \tag{1.23}$$

where N is the precipitation, A the runoff, and ΔS_W the sum of the water storage in the soil and ground water. Evaporation is often divided into the physically-caused part, the *evaporation*, which is dependent on the availability of water, the energy input, and the intensity of the turbulent exchange process; and the *transpiration* which is caused by plant-physiology, the water vapour saturation deficit, and the photosynthetic active radiation. The sum of both forms is called *evapotranspiration*. Evaporation occurs on the ground, on water surfaces, and on wetted plant surfaces. The latter is the evaporation of precipitation water held back at plant surfaces (interception). Micrometeorology plays an important role for the determination of evapotranspiration and the investigation of the water cycle (Table 1.5). Data show that the precipitation-evaporation cycle over the land is not as strongly coupled as they are over the ocean. This means that precipitation is mainly generated over regions where water evaporated.

The water balance equation is widely used in hydrological investigations. Thus, evaporation connects meteorology with hydrology. This field of investigations is often called hydrometeorology.

Table 1.5 Water cycle of the earth in 10^3 km^3 a^{-1} (Brutsaert 2005, modified and updated)

Reference	N	Q_E	N	Q_E	Transport
	Above land		*Above ocean*		*Ocean–land*
Budyko (1974)	109	63	412	455	46
Baumgartner and Reichel (1975)	112	72	386	426	40
Korzun (1978)	119	72	458	505	47
Houghton (2015)	111	71	385	425	40

References

Albrecht F (1940) Untersuchungen über den Wärmehaushalt der Erdoberfläche in verschiedenen Klimagebieten. Reichsamt Wetterdienst, Wiss Abh. Bd. VIII, Nr. 2:1–82.

André J-C, Bougeault P and Goutorbe J-P (1990) Regional estimates of heat and evaporation fluxes over non-homogeneous terrain, Examples from the HAPEX-MOBILHY programme. Boundary-Layer Meteorol. 50:77–108.

Arya SP (2001) Introduction to Micrometeorology. Academic Press, San Diego, 415 pp.

Barkov E (1914) Vorläufiger Bericht über die meteorologischen Beobachtungen der Deutschen Antarktisexpedition 1911–1912. Meteorol Z. 49:120–126.

Barrett EW and Suomi VE (1949) Preliminary report on temperature measurement by sonic means. J Meteorol. 6:273–276.

Baumgartner A and Reichel E (1975) The World Water Balance. Elsevier, Amsterdam, New York, 179 pp.

Beniston M (1998) From Turbulence to Climate. Springer, Berlin, Heidelberg, 328 pp.

Beyrich F and Mengelkamp H-T (2006) Evaporation over a heterogeneous land surface: EVA_GRIPS and the LITFASS-2003 experiment - an overview. Boundary-Layer Meteorol. 121:5–32.

Bird RB, Stewart WE and Lightfoot EN (2007) Transport Phenomena. John Wiley & Sons, Inc., New York, 905 pp.

Blackadar AK (1976) Modeling the nocturnal boundary layer. 4th Symposium on Atmospheric Turbulence, Diffusion and Air Pollution, Raylaigh, NC, Oct. 19–22, 1976. Am. Meteorol. Soc., pp. 46-49.

Blöschl G and Sivapalan M (1995) Scale issues in hydrological modelling - a review. Hydrol Processes. 9:251–290.

Bovscheverov VM and Voronov VP (1960) Akustitscheskii fljuger (Acoustic rotor). Izv AN SSSR, ser Geofiz. 6:882–885.

Bradley EF (1968) A shearing stress meter for micrometeorological studies. Quart J Roy Meteorol Soc. 94:380–387.

Brutsaert W (2005) Hydrology. Cambridge University Press, Cambridge, XII, 605 pp.

Budyko MI (1974) Climate and Life. Academic Press, New York, 508 pp.

Burridge DM and Gadd AJ (1977) The Meteorological Office operational 10-level numerical weather prediction model (December 1975). Meteorological Office Technical Notes. 34:39 pp.

Businger JA and Yaglom AM (1971) Introduction to Obukhov's paper "Turbulence in an atmosphere with a non-uniform temperature". Boundary-Layer Meteorol. 2:3–6.

Businger JA, Wyngaard JC, Izumi Y and Bradley EF (1971) Flux-profile relationships in the atmospheric surface layer. J Atmos Sci. 28:181–189.

Davidson PA, Kaneda Y, Moffatt K and Sreenivasan KR (eds) (2011) A Voyage through Turbulence. Cambridge University Press, Cambridge, 434 pp.

Dutton JA (2002) The Ceaseless Wind: An Introduction to the Theory of Atmospheric Motion. Dover Publications, Mineola, NY, 640 pp.

Dyer AJ, Hicks BB and King KM (1967) The Fluxatron - A revised approach to the measurement of eddy fluxes in the lower atmosphere. Journal Applied Meteorology. 6:408–413.

Dyer AJ, Garratt JR, Francey RJ, McIlroy IC, Bacon NE, Hyson P, Bradley EF, Denmead DT, Tsvang LR, Volkov JA, Kaprov BM, Elagina LG, Sahashi K, Monji N, Hanafusa T, Tsukamoto O, Frenzen P, Hicks BB, Wesely M, Miyake M and Shaw WJ (1982) An international turbulence comparison experiment (ITCE 1976). Boundary-Layer Meteorol. 24:181–209.

Etling D (2008) Theoretische Meteorologie. Springer, Berlin, Heidelberg, 376 pp.

Foken T, Kitajgorodskij SA and Kuznecov OA (1978) On the dynamics of the molecular temperature boundary layer above the sea. Boundary-Layer Meteorol. 15:289–300.

Foken T, Wichura B, Klemm O, Gerchau J, Winterhalter M and Weidinger T (2001) Micrometeorological conditions during the total solar eclipse of August 11,1999. Meteorol Z. 10:171–178.

Foken T (2006) 50 years of the Monin-Obukhov similarity theory. Boundary-Layer Meteorol. 119:431–447.

Foken T, Meixner FX, Falge E, Zetzsch C, Serafimovich A, Bargsten A, Behrendt T, Biermann T, Breuninger C, Dix S, Gerken T, Hunner M, Lehmann-Pape L, Hens K, Jocher G, Kesselmeier J, Lüers J, Mayer JC, Moravek A, Plake D, Riederer M, Rütz F, Scheibe M, Siebicke L, Sörgel M, Staudt K, Trebs I, Tsokankunku A, Welling M, Wolff V and Zhu Z (2012) Coupling processes and exchange of energy and reactive and non-reactive trace gases at a forest site – results of the EGER experiment. Atmos Chem Phys. 12:1923–1950.

Foken T (2013) Energieaustausch an der Erdoberfläche. Edition am Gutenbergplatz, Leipzig, 99 pp.

Frisch U (1995) Turbulence. Cambridge Univ. Press, Cambridge, 296 pp.

Garratt JR (1978) Flux profile relations above tall vegetation. Quart J Roy Meteorol Soc. 104:199–211.

Garratt JR and Hicks BB (1990) Micrometeorological and PBL experiments in Australia. Boundary-Layer Meteorol. 50:11–32.

Garratt JR (1992) The Atmospheric Boundary Layer. Cambridge University Press, Cambridge, 316 pp.

Geiger R (1927) Das Klima der bodennahen Luftschicht. Friedr. Vieweg & Sohn, Braunschweig, 246 pp.

Geiger R, Aron RH and Todhunter P (2009) The Climate near the Ground. Rowman & Littlefield, Lanham, XVIII, 623 pp.

Geiger R (2013) Das Klima der bodennahen Luftschicht. Springer Vieweg, Wiesbaden, 646 pp.

Glickman TS (ed) (2000) Glossary of Meteorology. Am. Meteorol. Soc., Boston, MA, 855 pp.

Hanafusa T, Fujitana T, Kobori Y and Mitsuta Y (1982) A new type sonic anemometer-thermometer for field operation. Papers Meteorol Geophys. 33:1–19.

Hann JF and Süring R (1939) Lehrbuch der Meteorologie. Verlag von Willibald Keller, Leipzig, 480 pp.

Hartmann DL (1994) Global Physical Climatology. Academic Press, San Diego, New York, 408 pp.

Haugen DA (ed) (1973) Workshop on Micrometeorology. Am. Meteorol. Soc., Boston, 392 pp.

Henderson-Sellers A and Robinson PJ (1986) Contemporary Climatology. John Wiley & Sons, Inc., New York, 439 pp.

Högström U (1988) Non-dimensional wind and temperature profiles in the atmospheric surface layer: A re-evaluation. Boundary-Layer Meteorol. 42:55–78.

Högström U (1990) Analysis of turbulence structure in the surface layer with a modified similarity formulation for near neutral conditions. J Atmos Sci. 47:1949–1972.

Houghton DD (1985) Handbook of applied meteorology. Wiley, New York, XV, 1461 pp.

Houghton JT (2015) Global Warming, The complete Briefing. Cambridge University Press, Cambridge, 396 pp.

Hupfer P and Kuttler W (eds) (2005) Witterung und Klima, begründet von Ernst Heyer. B.G. Teubner, Stuttgart, Leipzig, 554 pp.

Izumi Y (1971) Kansas 1968 field program data report. Air Force Cambridge Research Laboratory, Bedford, MA, 79 pp.

Jiang B, Zhang Y, Liang S, Wohlfahrt G, Arain A, Cescatti A, Georgiadis T, Jia K, Kiely G, Lund M, Montagnani L, Magliulo V, Ortiz PS, Oechel W, Vaccari FP, Yao Y and Zhang X (2015) Empirical estimation of daytime net radiation from shortwave radiation and ancillary information. Agrical Forest Meteorol. 211–212:23–36.

Kaimal JC and Businger JA (1963) A continuous wave sonic anemometer-thermometer. J Climate Appl Meteorol 2:156–164.

Kaimal JC and Wyngaard JC (1990) The Kansas and Minnesota experiments. Boundary-Layer Meteorol. 50:31–47.

Kiehl J and Trenberth KE (1997) Earth annual global mean energy budget. Bull Amer Meteorol Soc. 78:197–208.

Kleinschmidt E (ed) (1935) Handbuch der meteorologischen Instrumente und ihrer Auswertung. Springer, Berlin, 733 pp.

Kolmogorov AN (1941a) Lokalnaja struktura turbulentnosti v neschtschimaemoi schidkosti pri otschen bolschich tschislach Reynoldsa (The local structure of turbulence in incompressible viscous fluid for very large Reynolds numbers). Dokl AN SSSR. 30:299–303.

Kolmogorov AN (1941b) Rassejanie energii pri lokolno-isotropoi turbulentnosti (Dissipation of energy in locally isotropic turbulence). Dokl AN SSSR. 32:22–24.

Kopp G and Lean JL (2011) A new, lower value of total solar irradiance: Evidence and climate significance. Geophys Res Letters. 38:L01706.

Korzun VI (ed) (1978) World Water Balance and Water Resources of the Earth. UNESCO, Paris, 663 pp.

Kraus H (2004) Die Atmosphäre der Erde. Springer, Berlin, Heidelberg, 422 pp.

Kraus H (2008) Grundlagen der Grenzschichtmeteorologie. Springer, Berlin, Heidelberg, 211 pp.

Lehmann A and Kalb M (1993) 100 Jahre meteorologische Beobachtungen an der Säkularstation Potsdam 1893–1992. Deutscher Wetterdienst, Offenbach, 32 pp.

Lettau H (1939) Atmosphärische Turbulenz. Akad. Verlagsges., Leipzig, 283 pp.

Lettau H (1949) Isotropic and non-isitropic turbulence in the atmospheric surface layer. Geophys Res Pap. 1:86 pp.

Lettau HH and Davidson B (eds) (1957) Exploring the Atmosphere's First Mile. Pergamon Press, London, New York, 376 pp.

Liebethal C, Huwe B and Foken T (2005) Sensitivity analysis for two ground heat flux calculation approaches. Agrical Forest Meteorol. 132:253–262.

Liebethal C and Foken T (2007) Evaluation of six parameterization approaches for the ground heat flux. Theor Appl Climat. 88:43–56.

Liou KN (1992) Radiation and Cloud Processes in the Atmosphere. Oxford University Press, Oxford, 487 pp.

Lothon M, Lohou F, Pino D, Couvreux F, Pardyjak ER, Reuder J, Vilà-Guerau de Arellano J, Durand P, Hartogensis O, Legain D, Augustin P, Gioli B, Lenschow DH, Faloona I, Yagüe C, Alexander DC, Angevine WM, Bargain E, Barrié J, Bazile E, Bezombes Y, Blay-Carreras E, van de Boer A, Boichard JL, Bourdon A, Butet A, Campistron B, de Coster O, Cuxart J, Dabas A, Darbieu C, Deboudt K, Delbarre H, Derrien S, Flament P, Fourmentin M, Garai A, Gibert F, Graf A, Groebner J, Guichard F, Jiménez MA, Jonassen M, van den Kroonenberg A, Magliulo V, Martin S, Martinez D, Mastrorillo L, Moene AF, Molinos F, Moulin E, Pietersen HP, Piguet B, Pique E, Román-Cascón C, Rufin-Soler C, Saïd F, Sastre-Marugán M, Seity Y, Steeneveld GJ, Toscano P, Traullé O, Tzanos D, Wacker S, Wildmann N and Zaldei A (2014) The BLLAST field experiment: Boundary-Layer Late Afternoon and Sunset Turbulence. Atmos Chem Phys. 14:10931–10960.

Lumley JL and Yaglom AM (2001) A century of turbulence. Flow, Turbulence and Combustion. 66:241–286.

Mitsuta Y (1966) Sonic anemometer-thermometer for general use. J Meteor Soc Japan. Ser. II, 44:12–24.

Miyake M, Stewart RW, Burling RW, Tsvang LR, Kaprov BM and Kuznecov OA (1971) Comparison of acoustic instruments in an atmospheric flow over water. Boundary-Layer Meteorol. 2:228–245.

Monin AS and Obukhov AM (1954) Osnovnye zakonomernosti turbulentnogo peremesivanija v prizemnom sloe atmosfery (Basic laws of turbulent mixing in the atmosphere near the ground). Trudy geofiz inst AN SSSR. 24 (151):163–187.

Monin AS and Yaglom AM (1973) Statistical Fluid Mechanics: Mechanics of Turbulence, Volume 1. MIT Press, Cambridge, London, 769 pp.

Monin AS and Yaglom AM (1975) Statistical Fluid Mechanics: Mechanics of Turbulence, Volume 2. MIT Press, Cambridge, London, 874 pp.

Montgomery RB (1948) Vertical eddy flux of heat in the atmosphere. Journal Meteorology. 5:265–274.

Obukhov AM (1946) Turbulentnost' v temperaturnoj - neodnorodnoj atmosfere (Turbulence in an atmosphere with a non-uniform temperature). Trudy Inst Theor Geofiz AN SSSR 1:95–115.

Obukhov AM (1951) Charakteristiki mikrostruktury vetra v prizemnom sloje atmosfery (Characteristics of the micro-structure of the wind in the surface layer of the atmosphere). Izv AN SSSR, ser Geofiz. 3:49–68.

Obukhov AM (1960) O strukture temperaturnogo polja i polja skorostej v uslovijach konvekcii (Structure of the temperature and velocity fields under conditions of free convection). Izv AN SSSR, ser Geofiz. 9:1392–1396.

Obukhov AM (1971) Turbulence in an atmosphere with a non-uniform temperature. Boundary-Layer Meteorol. 2:7–29.

Oertel H (ed) (2004) Prandtl's essentials of fluid mechanics. Springer, New York, VII, 723 pp.

Oke TR (1987) Boundary Layer Climates. Methuen, New York, 435 pp.

Oncley SP, Foken T, Vogt R, Kohsiek W, DeBruin HAR, Bernhofer C, Christen A, van Gorsel E, Grantz D, Feigenwinter C, Lehner I, Liebethal C, Liu H, Mauder M, Pitacco A, Ribeiro L and Weidinger T (2007) The energy balance experiment EBEX-2000, Part I: Overview and energy balance. Boundary-Layer Meteorol. 123:1–28.

Orlanski I (1975) A rational subdivision of scales for atmospheric processes. Bull. Am. Meteorol. Soc. 56:527–530.

Persson POG, Fairall CW, Andreas EL, Guest PS and Perovich DK (2002) Measurements near the atmospheric surface flux group tower at sheba: Near-surface conditions and surface energy budget. J Geophys Res. 107:8045.

Poulos GS, Blumen W, Fritts DC, Lundquist JK, Sun J, Burns SP, Nappo C, Banta R, Newsom R, Cuxart J, Terradellas E, Balsley B and Jensen M (2002) CASES-99: A comprehensive investigation of the stable nocturnal boundary layer. Bull Amer Meteorol Soc. 83:55–581.

Prandtl L (1925) Bericht über Untersuchungen zur ausgebildeten Turbulenz. Z angew Math Mech. 5:136–139.

Priestley CHB and Swinbank WC (1947) Vertical transport of heat by turbulence in the atmosphere. Proceedings Royal Society London. A189:543–561.

Reynolds O (1894) On the dynamical theory of turbulent incompressible viscous fluids and the determination of the criterion. Phil Trans R Soc London. A 186:123–161.

Richardson LF (1920) The supply of energy from and to atmospheric eddies. Proceedings Royal Society. A 97:354–373.

Roedel W and Wagner T (2011) Physik unserer Umwelt: Die Atmosphäre. Springer, Berlin, Heidelberg pp.

Schlichting H and Gersten K (2003) Boundary-Layer Theory. McGraw Hill, New York, XXIII, 799 pp.

Schmidt W (1925) Der Massenaustausch in freier Luft und verwandte Erscheinungen. Henri Grand Verlag, Hamburg, 118 pp.

Schoonmaker PK (1998) Paleoecological perspectives on ecological scales. In: Peterson DL and Parker VT (eds.), Ecological Scale. Columbia University Press, New York, 79–103.

Schotland RM (1955) The measurement of wind velocity by sonic waves. J Meteorol. 12:386–390.

Seibert P, Beyrich F, Gryning S-E, Joffre S, Rasmussen A and Tercier P (2000) Review and intercomparison of operational methods for the determination of the mixing height. Atmos Environm. 34:1001–1027.

Sellers PJ, Hall FG, Asrar G, Strebel DE and Murphy RE (1988) The first ISLSCP field experiment (FIFE). Bull Amer Meteorol Soc. 69:22–27.

Shen S and Leclerc MY (1995) How large must surface inhomogeneous be before they influence the convective boundary layer structure? A case study. Quart J Roy Meteorol Soc. 121: 1209–1228.

Stull RB (1988) An Introduction to Boundary Layer Meteorology. Kluwer Acad. Publ., Dordrecht, Boston, London, 666 pp.

Suomi VE (1957) Sonic anemometer - University of Wisconsin. In: Lettau HH and Davidson B (eds.), Exploring the atmosphere's first mile, vol 1. Pergamon Press, London, New York, 256–266.

Sutton OG (1953) Micrometeorology. McGraw Hill, New York, 333 pp.

Swinbank WC (1951) The measurement of vertical transfer of heat and water vapor by eddies in the lower atmosphere. J Meteorol. 8:135–145.

Taylor GI (1915) Eddy motion in the atmosphere. Phil Trans R Soc London. A 215:1–26.

Taylor GI (1938) The spectrum of turbulence. Proceedings Royal Society London. A 164: 476–490.

Trenberth KE, Fasullo JT and Kiehl J (2009) Earth's Global Energy Budget. Bull Amer Meteorol Soc. 90:311–323.

Tsvang LR, Kaprov BM, Zubkovskij SL, Dyer AJ, Hicks BB, Miyake M, Stewart RW and McDonald JW (1973) Comparison of turbulence measurements by different instuments; Tsimlyansk field experiment 1970. Boundary-Layer Meteorol. 3:499–521.

Tsvang LR, Zubkovskij SL, Kader BA, Kallistratova MA, Foken T, Gerstmann W, Przandka Z, Pretel J, Zelený J and Keder J (1985) International turbulence comparison experiment (ITCE-81). Boundary-Layer Meteorol. 31:325–348.

Tsvang LR, Fedorov MM, Kader BA, Zubkovskii SL, Foken T, Richter SH and Zelený J (1991) Turbulent exchange over a surface with chessboard-type inhomogeneities. Boundary-Layer Meteorol. 55:141–160.

Vogel H-J and Roth K (2003) Moving through scales of flow and transport in soil. J Hydrol. 272:95–106.

von Kármán T and Howarth L (1938) On the statistical theory of isotropic turbulence. Proceedings Royal Society London. A 164:192–215.

Wendisch M and Yang P (2012) Theory of Atmospheric Radiative Transfer. Wiley & Sons, Inc., Weinheim pp.

Wendling U, Fuchs P and Müller-Westermeier G (1997) Modellierung des Zusammenhangs von Globalstrahlung, Sonnenscheindauer und Bewölkungsgrad als Beitrag der Klimaüberwachung. Dt Wetterdienst, Forsch. Entwicklung, Arbeitsergebnisse. 45:29 pp.

Wichura B, Buchmann N, Foken T, Mangold A, Heinz G and Rebmann C (2001) Pools und Flüsse des stabilen Kohlenstoffisotops ^{13}C zwischen Boden, Vegetation und Atmosphäre in verschiedenen Pflanzengemeinschaften des Fichtelgebirges. Bayreuther Forum Ökologie. 84:123–153.

Wieringa J (1980) A revaluation of the Kansas mast influence on measurements of stress and cup anemometer overspeeding. Boundary-Layer Meteorol. 18:411–430.

Wild M, Folini D, Schär C, Loeb N, Dutton E and König-Langlo G (2013) The global energy balance from a surface perspective. Climate Dynamics. 40:3107–3134.

Wild M, Folini D, Hakuba M, Schär C, Seneviratne S, Kato S, Rutan D, Ammann C, Wood E and König-Langlo G (2015) The energy balance over land and oceans: an assessment based on direct observations and CMIP5 climate models. Climate Dynamics. 44:3393–3429.

Wulfmeyer V, Behrendt A, Kottmeier C, Corsmeier U, Barthlott C, Craig G, Hagen M, Althausen D, Aoshima F, Arpagaus M, Bauer HS, Bennett L, Blyth A, Brandau C, Champollion C, Crewell S, Dick G, Di Girolamo P, Dorninger M, Dufournet Y, Eigenmann R, Engelmann R, Flamant C, Foken T, Gorgas T, Grzeschik M, Handwerker J, Hauck C, Höller H, Junkermann W, Kalthoff N, Kiemle C, Klink S, König M, Krauß L, Long CN, Madonna F, Mobbs S, Neininger B, Pal S, Peters G, Pigeon G, Richard E, Rotach M, Russchenberg H, Schwitalla T, Smith V, Steinacker R, Trentmann J, Turner DD, van Baelen J, Vogt S,

Volkert H, T. W, Wernli H, Wieser A and Wirth M (2011) The convective and orographically induced precipitation study (COPS): The scientific strategy, the field phase, and research highlights. Quart J Roy Meteorol Soc. 137:3–30.

Wyngaard JC, Coté OR and Izumi Y (1971) Local free convection, similarity and the budgets of shear stree and heat flux. J Atmos Sci. 28:1171–1182.

Wyngaard JC, Businger JA, Kaimal JC and Larsen SE (1982) Comments on 'A revaluation of the Kansas mast influence on measurements of stress and cup anemometer overspeeding'. Boundary-Layer Meteorol. 22:245–250.

Chapter 2
Basic Equations of Atmospheric Turbulence

Before starting the derivation of the equations for the turbulent fluxes of momentum, heat and trace gases (Sect. 2.3), we present a short introduction into the basic equations. These include the equations of mean and turbulent motions, describing the transport and for energy and matter (Sect. 2.1), and the conservation equation for the turbulence kinetic energy (Sect. 2.2). To illustrate the importance of micrometeorological equations and parameterizations for modelling on all scales, different closure techniques of the turbulent differential equations are described (Sect. 2.1.3). The more practical user of this book can proceed directly to Sect. 2.3.

2.1 Equation of Motion

2.1.1 Navier-Stokes Equation of Mean Motion

The Navier-Stokes equations describe the balance of all the forces in the earth's atmosphere without consideration of the centrifugal force (Stull 1988; Arya 1999; Etling 2008; Wyngaard 2010; Hantel 2013):

$$\frac{\partial u}{\partial t} = -u\frac{\partial u}{\partial x} - v\frac{\partial u}{\partial y} - w\frac{\partial u}{\partial z} - \frac{1}{\rho}\frac{\partial p}{\partial x} + f\,v + v\,\nabla^2 u$$
$$\frac{\partial v}{\partial t} = -u\frac{\partial v}{\partial x} - v\frac{\partial v}{\partial y} - w\frac{\partial v}{\partial z} - \frac{1}{\rho}\frac{\partial p}{\partial y} - f\,u + v\,\nabla^2 v \qquad (2.1)$$
$$\frac{\partial w}{\partial t} = -u\frac{\partial w}{\partial x} - v\frac{\partial w}{\partial y} - w\frac{\partial w}{\partial z} + g + v\,\Delta w$$

where u is the horizontal wind in the x-direction (east); v is the horizontal wind in the y-direction (north), and w is the vertical wind; p is the atmospheric pressure; f is the Coriolis parameter; g is the gravity acceleration; ρ is the air density; v is the

Table 2.1 Definitions of Einstein's summation notation

Running index of the velocity components	i = 1, 2, 3	j = 1, 2, 3	k = 1, 2, 3
	$u_1 = u$	$u_2 = v$	$u_3 = w$
Length components	$x_1 = x$	$x_2 = y$	$x_3 = z$
Variables	No free index: scalar	One free index: vector	Two free indexes: tensor
Kronecker delta-operator δ_{ij}	= +1, for i = j	= 0, for i ≠ j	
Levi-Civita symbol (alternating unit tensor) ε_{ijk}	= +1, for ijk = 123, 231 or 312	= −1, for ijk = 321, 213 or 132	= 0, for ijk = all other combinations

kinematic viscosity, and ∇^2 is the Laplace operator. From left-to-right, the terms of the equation are the tendency, the advection, the pressure gradient force, the Coriolis force, and the (molecular) stress. In a turbulent atmosphere, a turbulent stress term, the Reynolds stress, must be applied. All the terms in the horizontal motion equations are of the order of $10^{-4} - 10^{-3}$ m s^{-2}. Under certain condition, some terms are very small and can be neglected. For example, for steady-state flow, the tendency can be neglected; above horizontally homogeneous surfaces, the advection can be neglected; in the centre of high and low pressure areas or for small scale processes the pressure gradient force can be neglected; at the equator or for small scale processes the Coriolis force can be neglected, and above the atmospheric boundary layer the stress terms can be neglected.

The three equations of the wind components can be combined applying Einstein's summation notation and partial derivatives:

$$\frac{\partial u_i}{\partial t} = -u_j \frac{\partial u_i}{\partial x_j} - \delta_{i3} g + f \varepsilon_{ij3} u_j - \frac{1}{\rho} \frac{\partial p}{x_i} + \frac{1}{\rho} \left(\frac{\partial \tau_{ij}}{\partial x_j} \right) \tag{2.2}$$

The shear stress tensor with dynamic viscosity μ is given in the form (Stull 1988):

$$\tau_{ij} = \mu \left(\frac{\partial u_i}{\partial x_j} + \frac{\partial u_j}{\partial x_i} \right) - \frac{2}{3} \mu \frac{\partial u_k}{\partial x_k} \delta_{ij} \tag{2.3}$$

The generalizations and applications of the Einstein summation operators are summarized in Table 2.1.

2.1.2 Turbulent Equation of Motion

The modification of the Navier-Stokes equations to include turbulent motions requires the decomposition of all the variables into a mean part, $\bar{x}$, and a random

Fig. 2.1 Schematic presentation of Reynolds's decomposition of the value x
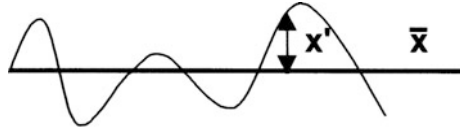
fluctuating part, x'. This is called the Reynolds's decomposition (Fig. 2.1), and is represented by:

$$x = \bar{x} + x'. \tag{2.4}$$

The application of Reynolds's decomposition requires some averaging rules for the turbulent value x' and y' (a represents a constant), which are termed Reynolds's postulates:

$$
\begin{array}{ll}
\text{I} & \overline{x'} = 0 \\
\text{II} & \overline{xy} = \bar{x}\,\bar{y} + \overline{x'y'} \\
\text{III} & \overline{\bar{x}\,y} = \bar{x}\,\bar{y} \\
\text{IV} & \overline{a\,x} = a\bar{x} \\
\text{V} & \overline{x+y} = \bar{x} + \bar{y}
\end{array}
\tag{2.5}
$$

It is assumed that the postulates are universal, but for special spectral regions or for intermitted turbulence this is not valid (Bernhardt 1980). The second postulate is the basis for the determination of turbulent fluxes according to the direct eddy-covariance method (see Sect. 4.2).

The turbulent equations of motion follow after application of Reynolds's decomposition and postulates into Eq. (2.2). It is also assumed (Businger 1982; Stull 1988), that:

$$
\begin{array}{l}
|p'/\bar{p}| \ll |\rho'/\bar{\rho}| \\
|p'/\bar{p}| \ll |T'/\bar{T}| \\
|\rho'/\bar{\rho}| \ll 1 \\
|T'/\bar{T}| \ll 1
\end{array}
\tag{2.6}
$$

These assumptions are not trivial and need further inspections for individual cases. A very important simplification results from the Boussinesq-approximation (Boussinesq 1877), which neglects density fluctuations except for the buoyancy (gravitation) term. This is because the acceleration of gravity is relatively large in comparison with the other accelerations in the equation. Therefore, shallow convective conditions (Stull 1988) are permitted. This form of averaging is not without consequences for the determination of turbulent fluxes (see Sect. 4.2.3). Applying all these simplifications it follows that:

$$\frac{\partial \overline{u_i}}{\partial t} + \frac{\partial}{\partial x_j}\left(\overline{u_j}\,\overline{u_i} + \overline{u_j' u_i'}\right) = -\frac{1}{\rho}\frac{\partial \overline{p}}{\partial x_i} + v\frac{\partial^2 \overline{u_i}}{\partial x_i^2} + g\delta_{i3} + \varepsilon_{ijk} f\overline{u_k} \qquad (2.7)$$

Completely analogous equations for the heat transfer and the transfer of trace gases such as water vapour can be derived

$$\frac{\partial \overline{T}}{\partial t} + \frac{\partial}{\partial x_i}\left(\overline{u_i}\,\overline{T} + \overline{u_i' T'}\right) = a_T \frac{\partial^2 \overline{T}}{\partial x_i^2} + R, \qquad (2.8)$$

$$\frac{\partial \overline{c}}{\partial t} + \frac{\partial}{\partial x_i}\left(\overline{u_i}\,\overline{c} + \overline{u_i' c'}\right) = D\frac{\partial^2 \overline{c}}{\partial x_i^2} + S, \qquad (2.9)$$

where R and S are source and sink terms respectively, and a_T and D are the molecular heat conduction and diffusion coefficients, respectively.

An important simplification is possible in the atmospheric boundary layer where only the equations for j = 3, i.e. $u_3 = w$, are important, and steady state conditions ($\partial/\partial t = 0$) and horizontal homogeneity ($\partial/\partial x_1 = 0$, $\partial/\partial x_2 = 0$) are assumed. This assumption is far reaching because all the following applications are valid only under these conditions. For instance, for all micrometeorological measurements steady state conditions are implied (see Sect. 4.2.4), and a mostly homogeneous surface is necessary. Under these assumptions and including the components u_g und v_g of the geostrophic wind velocity and the angular velocity of the earth's rotation, Ω, the three equations of motion become:

$$\frac{\partial \overline{u'w'}}{\partial z} = f\left(\overline{v} - \overline{v_g}\right) + v\frac{\partial^2 \overline{u}}{\partial z^2}, \quad \overline{v_g} = \frac{1}{\rho f}\frac{\partial \overline{p}}{\partial x} \qquad (2.10)$$

$$\frac{\partial \overline{v'w'}}{\partial z} = -f\left(\overline{u} - \overline{u_g}\right) + v\frac{\partial^2 \overline{v}}{\partial z^2}, \quad \overline{u_g} = -\frac{1}{\rho f}\frac{\partial \overline{p}}{\partial y} \qquad (2.11)$$

$$\frac{\partial \overline{w'^2}}{\partial z} = \frac{1}{\rho}\frac{\partial \overline{p}}{\partial z} - g - 2[\Omega_u \overline{v} - \Omega_v \overline{u}], \quad f = 2\,\Omega\,\sin\varphi \qquad (2.12)$$

Equations (2.10) and (2.11) are the basis of the so-called ageostrophic method for the determination of the components of the shear stress tensor using differences between the wind velocity in the atmospheric boundary layer and the geostrophic wind (Lettau 1957; Bernhardt 1970). The practical application of the ageostrophic method is limited because of baroclinicity, nonsteady-state conditions, and inhomogeneities (Schmitz-Peiffer et al. 1987). For example, they can be applied only for the determination of the shear stress at the ground surface using a large number of aerological observations (Bernhardt 1975).

In addition, the continuity equation in the incompressible form is assumed:

$$\frac{\partial \overline{u_i}}{\partial x_i} = 0, \quad \frac{\partial \overline{w}}{\partial z} = 0, \quad \overline{w} = 0 \tag{2.13}$$

The gas law with the specific gas constant for dry air R_L and the virtual temperature T_v (temperature of the dry air, which has the same density as the moist air)

$$T_v = T(1 + 0.61 \cdot q), \tag{2.14}$$

with the specific humidity q, completes the system of equations:

$$p = \rho R_L T_v \tag{2.15}$$

In an analogous way, the equations for heat and trace gas transfer are:

$$\frac{\partial \overline{w'T'}}{\partial z} = a_T \frac{\partial^2 \overline{T}}{\partial z^2}, \quad for \quad R = 0 \tag{2.16}$$

$$\frac{\partial \overline{w'c'}}{\partial z} = D \frac{\partial^2 \overline{c}}{\partial z^2}, \quad for \quad S = 0 \tag{2.17}$$

The influence of the individual terms in the different layers of the atmospheric boundary layer can be estimated using similarity numbers. These numbers are dimensionless values describing the relations between characteristic scales of the forces. Two physical systems are similar if the similarity numbers of both systems are on the same order. This is imported if atmospheric processes are investigated in a wind tunnel or water channel.

The ratio of the inertia to the pressure gradient force is called the Euler number

$$Eu = \frac{\rho V^2}{\Delta P}, \tag{2.18}$$

where V is the characteristic velocity, and ΔP is the characteristic pressure gradient.

The ratio of the inertia force to the Coriolis force is the Rossby number

$$Ro = \frac{V}{f L_h}, \tag{2.19}$$

where L_h is the characteristic large-area horizontal length scale.

The ratio of the inertia force to the molecular stress is the Reynolds number

$$Re = \frac{L_z V}{\nu}, \tag{2.20}$$

where L_z is the characteristic small-scale vertical length scale.

The ratio of the buoyancy production or destruction (stratification of the atmosphere) to the shear production of turbulence kinetic energy is the Richardson flux number (see Sect. 2.3.3). A bulk Richardson number can be defined as

$$Ri = -\frac{g}{\overline{T}} \frac{\Delta_z T \ \Delta z}{(\Delta_z u)^2},$$ (2.21)

where $\Delta_z T$ is the characteristic temperature gradient, and $\Delta_z u$ is the characteristic vertical wind gradient (see Sect. 2.3.2).

For heights above 10 m the temperature must be replaced by the potential temperature θ. Due to the decrease of atmospheric pressure with height it follows from Poisson's equation (Kraus 2004; Salby 2012):

$$\theta = T \left(\frac{1000}{p}\right)^{R_L/c_p}$$ (2.22)

Replacing potential by air temperature is only valid for heights below 10 m resulting in errors of less than 0.1 K.

The relevant processes in the atmospheric boundary layer can be identified using dimensional analysis and the similarity numbers. Using the logarithms of the similarity numbers the relevant processes can be identified for logarithms smaller than zero (Bernhardt 1972) as listed in Table 2.2. From the structure of the atmospheric boundary layer presented in Fig. 1.4, this is a logical organization.

It can be shown that the pressure gradient force is important only in the upper boundary layer. Molecular viscosity is only relevant in the viscous and molecular sub-layer. The effect of the Coriolis force can be neglected in the flux gradient relationships (see Sect. 2.3) in the surface layer, but not in general (see Sect. 2.4). On the other hand, the turbulent stress is relevant in the whole boundary layer.

In the dynamical and viscous sub-layers, the stratification does not play a role. Under these circumstances, it is possible that the vertical gradients are nearly zero:

Table 2.2 Order of the similarity numbers in the layers of the atmospheric boundary layer (**bold**: Processes characterized by the similarity numbers are relevant)

Layer	Height	lg Ro	lg Eu	lg Re	lg $|Ri|$
Upper layer	~ 1000 m	**<0**	**<0**	>0 $Re > 10^8$	**> −2**
Surface layer	$\sim 10 \ldots 50$ m	~ 0	<0	>0 $Re \sim 10^7 \ldots 10^8$	**> −2**
Dynamical sub-layer	~ 1 m	>0	~ 0	>0 $Re < 10^7$	~ -2
Viscous sub-layer	~ 0.01 m	>0	>0	**~0**	< −2
Molecular or laminar boundary layer	~ 0.001 m	>0	>0	**<0**	< −2

$$\frac{\partial \overline{u'w'}}{\partial z} \approx 0, \quad \frac{\partial \overline{v'w'}}{\partial z} \approx 0, \quad \frac{\partial \overline{T'w'}}{\partial z} \approx 0, \quad \frac{\partial \overline{c'w'}}{\partial z} \approx 0 \tag{2.23}$$

These equations mean that the covariances are constant with height in the surface layer. An error in this assumption of approximately 10% is typical.

The covariance of the vertical wind velocity, w, and a horizontal wind component or a scalar x can be determined by:

$$\begin{aligned}
\overline{w'x'} &= \frac{1}{N-1} \sum_{k=0}^{N-1} \left[(w_k - \overline{w_k})(x_k - \overline{x_k}) \right] \\
&= \frac{1}{N-1} \left[\sum_{k=0}^{N-1} w_k \cdot x_k - \frac{1}{N} \left(\sum_{k=0}^{N-1} w_k \sum_{k=0}^{N-1} x_k \right) \right]
\end{aligned} \tag{2.24}$$

According to the second Reynolds's postulate (Eq. 2.5, II), in the case of a negligible vertical wind the total flux is equal to the covariance. This equation is implemented in the eddy-covariance method, a method to directly measure turbulent fluxes (see Sect. 4.2). The dimensions of the turbulent fluxes of momentum (expressed as square of the friction velocity), sensible and latent heat, and matter are in kinematic units m^2 s^{-2}, K m s^{-1}, and kg kg^{-1} m s^{-1}, respectively. For water vapour flow, the units are hPa m s^{-1}:

$$u_*^2 = -\overline{u'w'}, \quad \frac{Q_H}{\rho \cdot c_p} = \overline{T'w'}, \quad \frac{Q_E}{\rho \cdot \lambda} = \overline{q'w'}, \quad \frac{Q_c}{\rho} = \overline{c'w'} \tag{2.25}$$

The equation for the friction velocity is valid only if u is the direction of the mean wind velocity. This simplification is typically used in micrometeorology and is equivalent to a coordinate rotation around the z-axis (see Sect. 4.2.3). The covariance of u' and w' is negative except below the crown in a forest (Amiro 1990). For a Cartesian coordinate system that is not aligned with the flow streamlines the friction velocity is given by:

$$u_* = \left[\left(\overline{u'w'} \right)^2 + \left(\overline{v'w'} \right)^2 \right]^{1/4} \tag{2.26}$$

The friction velocity is a generalized velocity, i.e., it is the shear stress divided by the density

$$u_* = \sqrt{\frac{\tau}{\rho}}. \tag{2.27}$$

2.1.3 Closure Techniques

The transition from the equation of motion from mean to turbulent flow gives a system of differential equations with more unknown parameters than equations. To solve the system of equations, assumptions have to be made to calculate the unknown parameters. These assumptions, for example for the covariance terms, are called closure techniques.

The order of the closure refers to the highest order of the parameters that must be calculated with the prognostic equations. Therefore, the moments of the next higher order must be determined (Table 2.3). Simple closure techniques are bulk approaches (see Sect. 4.1.1). Closer techniques of higher order require extensive calculations (Table 2.4). The most important approaches are presented here.

2.1.3.1 Local or first-order closure

First-order closure is analogous to molecular diffusion approaches, i.e. an assumed proportionality between the vertical flux and the vertical gradient of the relevant state parameter ξ. In the turbulent case, the proportionality factor is the eddy diffusion coefficient, K, and the approach is called K-theory. The gradient will be determined at the same place where the flux is to be calculated; therefore it is a local closure:

$$\overline{u_i'\xi'} = -K\frac{\partial \overline{\xi}}{\partial z} \tag{2.28}$$

The product of air density and turbulent diffusion coefficient (Eq. 1.22) is called "Austausch"-coefficient or exchange coefficient. The turbulent diffusion coefficients

Table 2.3 Characterization of closure techniques (Stull 1988)

Order of closure	Prognostic equation for	To be approximate in the equation	Number of equations	Number of unknown parameters
1st order	$\overline{u_i}$	$\overline{u_i u_j}$	3	6
2nd order	$\overline{u_i u_j}$	$\overline{u_i u_j u_k}$	6	10
3rd order	$\overline{u_i u_j u_k}$	$\overline{u_i u_j u_k u_l}$	10	15

Table 2.4 Realization of closure techniques

Order of closure	Realization	
0. order	No prognostic equation (bulk and similarity approaches)	
½ order	Forecast with simple bulk approaches	
1. order	K-approach (local)	Transilient closure (non-local)
1½ order	TKE equation with variance terms	
2. order	Prognostic equation for fluxes	
3. order	Prognostic equation for triple correlations	

Fig. 2.2 Schematic view of the movement of an air parcel z' to explain the mixing length approach
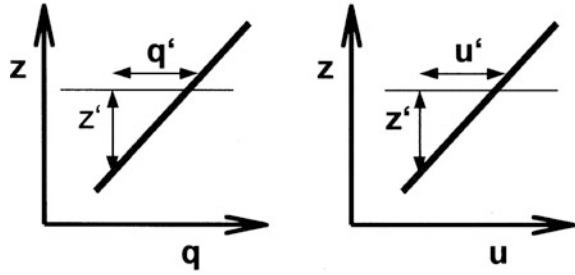
are formed for momentum, sensible heat, water vapour (latent heat), etc. For the single fluxes in kinematic units, the following relations are used:

$$\overline{u'w'} = K_m \frac{\partial \overline{u}}{\partial z} \tag{2.29}$$

$$\overline{w'T'} = -K_H \frac{\partial \overline{T}}{\partial z} \tag{2.30}$$

$$\overline{w'q'} = -K_E \frac{\partial \overline{q}}{\partial z} \tag{2.31}$$

For the determination of the turbulent diffusion coefficients, the mixing length parameterization is used, which is based on the work of Prandtl (1925). This approach describes the turbulent diffusion coefficient in terms of geometric and flux parameters. This is illustrated in the following example for the moisture flux. If an air parcel moves to a slightly different height, it will have a humidity and velocity slightly different than its new environment. This change of the environmental velocity and humidity can be described with gradients (Fig. 2.2):

$$u' = -\left(\frac{\partial \overline{u}}{\partial z}\right)z' \quad q' = -\left(\frac{\partial \overline{q}}{\partial z}\right)z' \tag{2.32}$$

The vertical velocity, which is necessary for the movement of the parcel, is assumed proportional to the horizontal velocity (c: constant factor):

$$w' = \pm c\, u' = c\left|\frac{\partial \overline{u}}{\partial z}\right| z' \tag{2.33}$$

The water vapour flux and the turbulent diffusion coefficient for evaporation are then given by

$$\overline{w'q'} = -c\overline{(z')^2}\left|\frac{\partial \overline{u}}{\partial z}\right| \cdot \left(\frac{\partial \overline{q}}{\partial z}\right) = -l^2\left|\frac{\partial \overline{u}}{\partial z}\right| \cdot \left(\frac{\partial \overline{q}}{\partial z}\right), \tag{2.34}$$

$$K_E = l^2 \left| \frac{\partial \overline{u}}{\partial z} \right|, \tag{2.35}$$

where l is called the mixing length. The mixing length is usually assumed to be

$$l = \kappa\, z, \tag{2.36}$$

where κ is the von-Kármán constant and z is the height above the ground surface. The value of κ is currently taken to be 0.4 (see Sect. 2.3.3).

The turbulent diffusion coefficient of momentum is:

$$K_m = \kappa^2\, z^2 \left[\left(\frac{\partial \overline{u}}{\partial z} \right)^2 + \left(\frac{\partial \overline{v}}{\partial z} \right)^2 \right]^{1/2} \tag{2.37}$$

With Eqs. (2.24) and (2.28), the widely used exchange approach (*K*-approach) for neutral stratification in the surface layer is:

$$K_m = \kappa\, z\, u_* \tag{2.38}$$

Applications of local closure for the stratified surface layer are discussed in Sect. 2.3.3. Outside of the surface layer, closure parameterizations for greater heights in the atmospheric boundary layer are used (see Sect. 2.6.2). The *K*-theory approach can be always applied when the exchange process takes place between direct neighbouring atmospheric layers or turbulence elements. *K*-theory cannot be applied in convective boundary layers (i.e. the daytime mixed layer). Also, *K*-theory should not be used within high vegetation (see Sect. 3.5) or for very stable stratification (see Sect. 3.7).

2.1.3.2 Non-local first-order closure

Local scaling approaches are no longer sufficient once larger eddies contribute to the exchange process, resulting in an overall flux that is greater than the flux due to the smaller eddies alone. This is e.g. the case for turbulent transport processes in tall vegetation and convective boundary layers. Possible solutions are given by either the transilient theory or the spectral diffusion theory.

The transilient theory (Stull 1984) approximates the turbulent exchange process between adjoining atmospheric layers or boxes, and also admits the exchange between non-adjoining boxes. The change of a scalar ξ with time in a box i is given by a fixed matrix of exchange coefficients, c_{ij} between the boxes i and j and the size of the scalar in the box j:

$$\overline{\xi}_i(t + \Delta t) = \sum_{j=1}^{N} c_{ij}(t, \Delta t)\overline{\xi}_j(t) \tag{2.39}$$

Fig. 2.3 Schematic view of the mixing of eddies from the central layer (**a**) and by superposition of similar mixing of the three layers in the centre (**b**) (Adapted from Stull 1988, with kind permission of © Kluwer Academic Publisher B. V. Dordrecht 1988, All rights reserved)
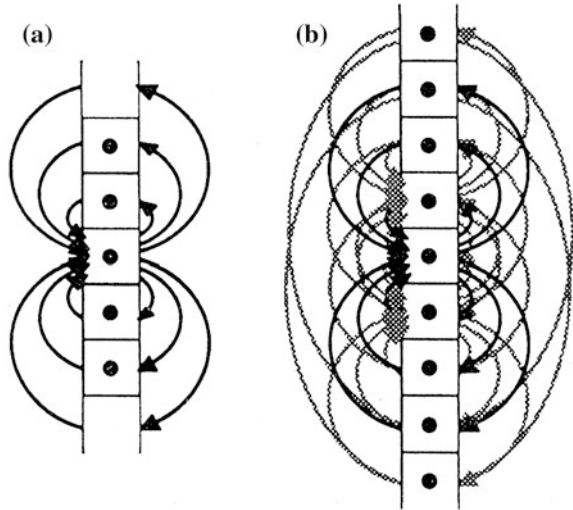
The matrix of mixing coefficients is called a transilient matrix. The flux in the k-layer is given by:

$$\overline{w'\xi'}(k) = \left(\frac{\Delta z}{\Delta t}\right) \sum_{i=1}^{k} \sum_{j=1}^{N} c_{ij}(\overline{\xi_i} - \overline{\xi_j}) \tag{2.40}$$

Figure 2.3 illustrates the possibilities for mixing between boxes. In principle all possibilities of mixing can be realized by the definition of the transilient matrix, which must be parameterized using external parameters such as the wind field or the radiation (Stull 1988). The difficulties of getting these parameters are the reasons why this form of the closure is rarely used.

2.1.3.3 Higher order closure

Closures higher than first order are now quite typical. But most of the parameterizations are poorly validated against observations. Commonly used, is a closure of 1.5th order. This is a closure using variances, which can be partially determined with the equation of the turbulence kinetic energy (TKE, see Sect. 2.2). 2nd order closure approaches use triple correlations (see Table 2.4).

2.2 Equation of the Turbulence Kinetic Energy

The equation of the turbulence kinetic energy, (TKE) in kinematic form is obtained by multiplication of the Navier-Stokes equation for turbulent flow Eq. (2.7) with u_i'. With the kinetic energy defined as (Stull 1988; Etling 2008; Wyngaard 2010)

Table 2.5 Meaning of the terms of the TKE equation

Term	Process
I	Local TKE storage or tendency
II	TKE advection
III	Buoyancy production or consumption
IV	Product from momentum flux (<0) and wind shear (>0) mechanical (or shear) production or loss term of turbulent energy
V	Turbulent TKE transport
VI	Pressure correlation term
VII	Energy dissipation

$$\overline{e} = 0.5\left(\overline{u'^2} + \overline{v'^2} + \overline{w'^2}\right) = 0.5\,\overline{u_i'^2} \tag{2.41}$$

it follows:

$$\underbrace{\frac{\partial \overline{e}}{\partial t}}_{\text{I}} = \underbrace{-\overline{u}_j \frac{\partial \overline{e}}{\partial x_j}}_{\text{II}} + \underbrace{\delta_{i3}\frac{g}{\theta_v}\left(\overline{u_i'\theta_v'}\right)}_{\text{III}} - \underbrace{\overline{u_i'u_j'}\frac{\partial \overline{u_i}}{\partial x_j}}_{\text{IV}} - \underbrace{\frac{\partial \left(\overline{u_j'e'}\right)}{\partial x_j}}_{\text{V}} - \underbrace{\frac{1}{\rho}\frac{\partial \left(\overline{u_i'p'}\right)}{\partial x_i}}_{\text{VI}} - \underbrace{\varepsilon}_{\text{VII}} \tag{2.42}$$

Descriptions of the terms in Eq. (2.42), which are in the order of 10^{-4} m^2 s^{-3}, are given in Table 2.5. The changes of the magnitudes of the terms in Eq. (2.42) with height in the boundary layer are shown in Fig. 2.4, whereby the terms are normalized by $w_*^3 z_i^{-1}$ (order $6 \cdot 10^{-3}$ m^2 s^{-3}). In a boundary layer that is strongly influenced by convective processes, the terms are usually normalized by the characteristic convective or Deardorff velocity (Deardorff 1970):

$$w_* = \left[\frac{g \cdot z_i}{\theta_v}\left(\overline{w'\theta_v'}\right)\right]^{1/3} \tag{2.43}$$

By application of the Obukhov-length L (see Sect. 2.3.3) it follows

$$w_* \approx 0,7 u_*\left(-\frac{z_i}{L}\right)^{1/3}, \tag{2.44}$$

while the conditions of free convection are given for $-z_i/L < -5\ldots10$ (Wyngaard 2010).
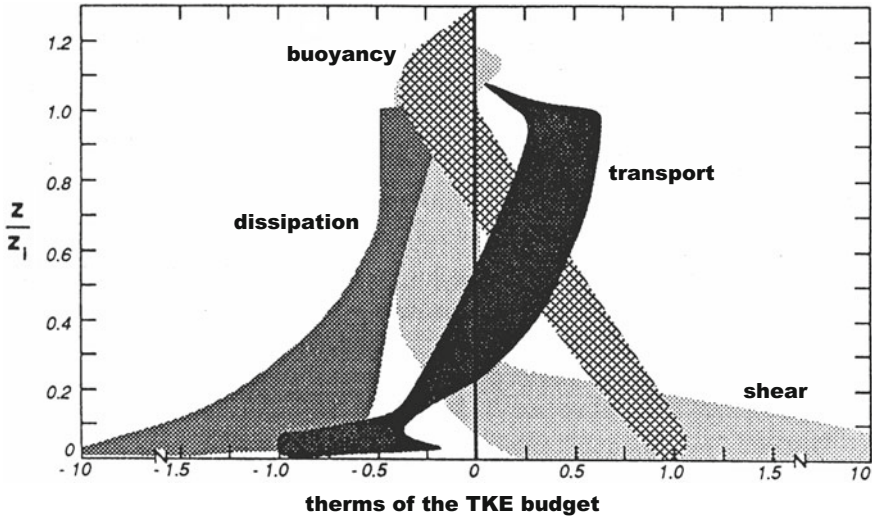
Fig. 2.4 Order of the terms of the TKE equation in the atmospheric boundary layer at daytime (Stull 1988) normalized with $w_*^3 z_i^{-1}$ (about 6×10^{-3} m^2 s^{-3}) (Adapted from Stull 1988, with kind permission of © Kluwer Academic Publisher B. V. Dordrecht 1988, All rights reserved)

Convection is the vertical transport or mixing of properties of the air (horizontal transport: advection). Forced convection results from mechanical forces (wind field) and inhomogeneities of the ground surface. It occurs for $1 > z/L > -1$ and appropriate scaling parameters are u_* and T_*. In contrast, free convection is caused by density differences and occurs for $z/L < -1$, and the scaling parameter is w_*. The fluxes in the case of free convection are typically not proportional to the local gradient (in the literature this is often referred to as counter gradient fluxes, Deardorff 1966).

Comparing the magnitudes of the terms of the TKE equation near the surface, terms I, II, V, and VI can be neglected relative to terms III, IV, and VII. The resulting equation is:

$$0 = \delta_{i3} \frac{g}{\theta_v} \left(\overline{u_i' \theta_v'} \right) - \overline{u_i' u_j'} \frac{\partial \overline{u_i}}{\partial x_j} - \varepsilon \tag{2.45}$$

This equation can be used in the surface layer to determine the energy dissipation ε, i.e., the decay of turbulent eddies into heat:

$$\varepsilon = \frac{g}{\theta_v} \left(\overline{w' \theta_v'} \right) - \overline{w' u'} \frac{\partial \overline{u}}{\partial z} \tag{2.46}$$

2.3 Flux-Gradient Similarity

2.3.1 Profile Equations for Neutral Stratification

In Sect. 2.1.3.1, it was shown that the flux could be determined by the vertical gradient of the state variable and a diffusion coefficient. These relations are called flux-gradient similarities. Thus, the turbulent diffusion coefficient for momentum can be parameterized in a simple way using Eq. (2.38). For the shear stress, it follows:

$$\tau = \rho \, K_m \frac{\partial u}{\partial z} \tag{2.47}$$

As discussed above, the friction velocity Eq. (2.26), is often used instead of the shear stress.

The turbulent fluxes of momentum, Eq. (2.29), sensible heat, Eq. (2.30), and latent heat, Eq. (2.31), can be calculated using the turbulent diffusion coefficient for momentum in the case of neutral stratification, Eq. (2.38), as the profile equations:

$$u_* = \sqrt{-\overline{u'w'}} = \kappa \cdot z \cdot \frac{\partial u}{\partial z} = \kappa \cdot \frac{\partial u}{\partial \ln z} \tag{2.48}$$

$$\overline{w'T'} = -\kappa \cdot u_* \cdot \frac{1}{Pr_t} \frac{\partial T}{\partial \ln z} \tag{2.49}$$

$$\overline{w'q'} = -\kappa \cdot u_* \cdot \frac{1}{Sc_t} \frac{\partial q}{\partial \ln z} \tag{2.50}$$

In Eq. (2.48) the friction velocity was defined in a simplified way in comparison to Eq. (2.26) by using the mean horizontal wind u. This first-order approximation is possible in the case of small wind fluctuations as shown by (Foken 1990).

Because the diffusion coefficients for momentum, sensible and latent heat are not identical, the turbulent Prandtl number Pr_t and the turbulent Schmidt number Sc_t are introduced. The turbulent Prandtl number is

$$Pr_t = \frac{K_m}{K_H}, \tag{2.51}$$

which is $Pr_t \sim 0.8$ for air (see Table 2.6). This definition is analogous to the Prandtl number of molecular exchange conditions

$$Pr = \frac{\nu}{\nu_T}, \tag{2.52}$$

with the thermal diffusion coefficient ν_T.

Table 2.6 Turbulent Prandtl number according to different authors

Author	Pr_t
Businger et al. (1971)	0.74
• Correction according to Wieringa (1980)	1.00
• Correction according to Högström (1988)	0.95
Kader and Yaglom (1972)	0.72–0.87
Foken (1990)	0.80
Högström (1996)	0.92 ± 0.03

Similarly, for the latent heat flux the Schmidt number

$$Sc = \frac{v}{D},\tag{2.53}$$

of the molecular diffusion coefficient for water vapour, D, and the turbulent Schmidt number are applied:

$$Sc_t = \frac{K_m}{K_E}\tag{2.54}$$

For the latent heat flux (water vapour flux) and the matter flux the turbulent diffusion coefficients for heat are applied, even when this is not fully justified. The turbulent Prandtl- and Schmidt numbers can be determined only by the comparisons of profile measurements (see Sect. 4.1) and flux measurements with the eddy-covariance method (see Sect. 4.2) for neutral conditions. Because of the inaccuracies in these methods the coefficients contain remarkable errors and for the turbulent Schmidt number the same values as for the turbulent Prandtl number are applied. Table 2.6 gives an overview of the currently available data.

Transferring the given equations in kinematic units into energetic units requires multiplication by the air density, which can be determined according to the ideal gas law and either the specific heat for constant pressure c_p (for sensible heat flux) or the latent heat of evaporation λ (for latent heat flux). These values are temperature and pressure dependent (see Appendix A.3):

$$\rho = \frac{p[\text{hPa}] \cdot 100}{R_L \cdot T_v} \quad \left[\text{kg m}^{-3}\right]\tag{2.55}$$

$$c_p = 1004.834 \quad \left[\text{J K}^{-1} \text{ kg}^{-1}\right]\tag{2.56}$$

$$\lambda = 2500827 - 2360(T - 273.15 \text{ K}) \quad \left[\text{J kg}^{-1}\right]\tag{2.57}$$

If the kinematic latent heat flux was based on water vapour pressure data, an additional correction factor of $0.62198/p$ (p in hPa) must be applied that accounts for the conversion into specific humidity in kg kg^{-1}. To achieve an accuracy better than 1% of the fluxes, the temperature must be determined with an accuracy of 1 K

and the pressure should be determined as a mean value with the barometric equation (Supplement 2.1) for the height above sea level. The following transformation relations are given:

$$Q_H[\text{W m}^{-2}] = c_p\,\rho\overline{w'T'}[\text{K m s}^{-1}]$$
$$= 1004.832\frac{p[\text{hPa}]\cdot 100}{287.0586\cdot T}\overline{w'T'}[\text{K m s}^{-1}] \tag{2.58}$$

$$Q_E[\text{W m}^{-2}] = \rho\,\lambda\,\overline{w'q'}[\text{kg kg}^{-1}\ \text{m s}^{-1}]$$
$$= \frac{p[\text{hPa}]\cdot 100}{287.0586\,T}\frac{0.62198}{p[\text{hPa}]}\left[2500827 - 2360\,(T - 273.15\ \text{K})\right] \tag{2.59}$$
$$\cdot\,\overline{w'e'}[\text{hPa m s}^{-1}]$$

Supplement 2.1 Barometric equation

The pressure at some height Z can be calculated from the pressure at sea level $p(Z = 0)$ and the mean virtual temperature, T_v between sea level and Z,

$$p(Z) = p(Z = 0)\ e^{\frac{g_0}{R_L\,T_v}Z}, \tag{S2.1}$$

where T_v is given by Eq. (2.14). Z is the geopotential height (Stull 2000), i.e. the geopotential Φ normalized with the constant gravity acceleration $g_0 = 9.81$ m s^{-2} (Hantel 2013),

$$Z = \frac{\Phi}{g_0}, \tag{S2.2}$$

In the lower troposphere, the geopotential height differs only slightly from the geometric height. Also, depending on the required accuracy the virtual temperature can be replaced by the actual temperature.

For hydrological applications the latent heat flux is often converted into the evaporated amount of water with the evaporation equivalent (0.0347 mm d^{-1} are equal to 1 Wm^{-2} as the daily average).

The profile equations Eqs. (2.48)–(2.50) give the opportunity to determine the fluxes in a simple way using either semi-log paper or similar computer outputs as shown in Fig. 2.5. Such graphs are helpful for a quick check of the measurement results or the functioning of the sensors. An overview of applicable humidity units is given in Supplement 2.2. Relative humidity observations should never be used for computing latent heat fluxes. When converting relative humidity into other humidity variables, air temperature observations are needed, which can lead to cross-correlations between latent and sensible heat fluxes. For heights above 10 m potential temperature (Eq. 2.22) instead of air temperature must be used.
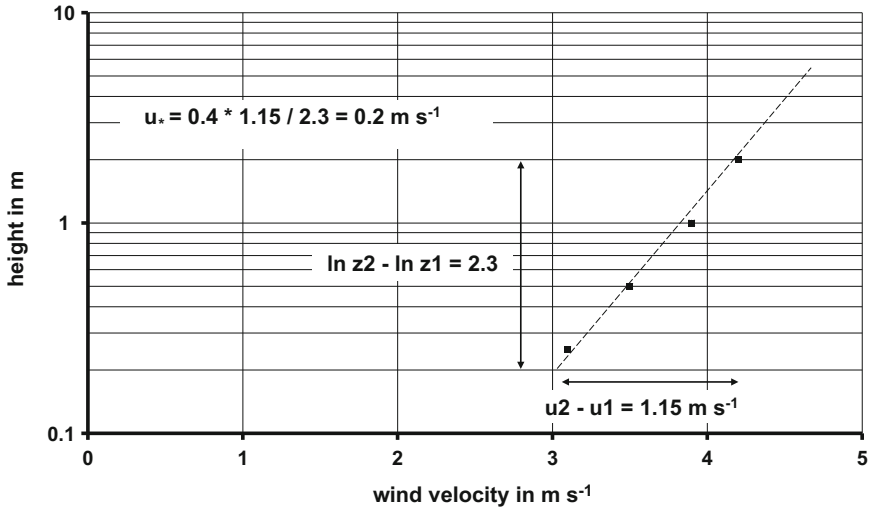
Fig. 2.5 Determination of the friction velocity from the wind profile with a semi-log plot

Supplement 2.2 Humidity units

Humidity unit	Equation
Water vapour pressure: partial pressure of the water vapour in hPa	e
Relative humidity: ratio of the water vapour pressure and the water vapor pressure at saturation in %	$R = (e/E)\,100\%$
Dew point τ: temperature, at which the water vapour pressure for saturation can be reached in °C	$E(\tau)$
Water vapour pressure for saturation in with Tetens' equation over water (Stull 2000)	$E = 6.11\,e^{\frac{17.6294\cdot(T-273.16\,K)}{T-35.86\,K}}$
Water vapour pressure for saturation with Magnus's equation (-45–60 °C over water) according to Sonntag (1990) in hPa	$E = 6.112\,e^{\frac{17.62\,t}{243.12+t}}$
Water vapour pressure for saturation with Magnus's equation (-65–0.01 °C over ice) according to Sonntag (1990) in hPa	$E = 6.112\,e^{\frac{22.46\,t}{272.62+t}}$
Absolute humidity: mass water vapour per volume moist air in kg m^{-3}	$a = \frac{0.21667\,e}{T}$
Specific humidity: mass water vapour per mass moist air in kg kg^{-1}, can be replaced with sufficient accuracy by the mixing ratio or visa versa	$q = 0.622\,\frac{e}{p-0.378\,e}$
Mixing ratio: mass water vapour per mass dry air in kg kg^{-1}	$m = 0.622\,\frac{e}{p-e}$

2.3.2 Integration of the Profile Equation—Roughness and Zero-Plane Displacement

The integration of the profile equation for the momentum flux Eq. (2.48) from height z_0 up to height z is

$$u(z) - u(z_0) = u(z) = \frac{u_*}{\kappa} \ln \frac{z}{z_0}, \tag{2.60}$$

where z_0 is the height of the extrapolated logarithmic wind profile where $u(z_0) = 0$ as illustrated in Fig. 2.6. Thus, z_0 is simply an integration constant. Because this parameter depends on the characteristics of the surface it is called roughness length, roughness parameter, or roughness height . It varies from 10^{-3} to 10^{-6} m for water and ice, 10^{-2} m for grassland, and up to 0.2 m for small trees. More values are given in Table 2.7.

For neutral conditions, the roughness length z_0 can be determined by extrapolating the wind profile according to Fig. 2.6 to the point $u(z_0) = 0$. This method is limited to roughness elements of small vertical extension (at a maximum forests or settlements with low houses). For more details see Sect. 3.1.1.

For water surfaces, the roughness length z_0 is generally parameterized as a function of the friction velocity. The parameterization by Charnock (1955)

$$z_0 = \frac{u_*^2}{81.1 \, g} \tag{2.61}$$

Fig. 2.6 Determination of the roughness length z_0 by extrapolation of the log-linear wind profile to the point $u(z_0) = 0$
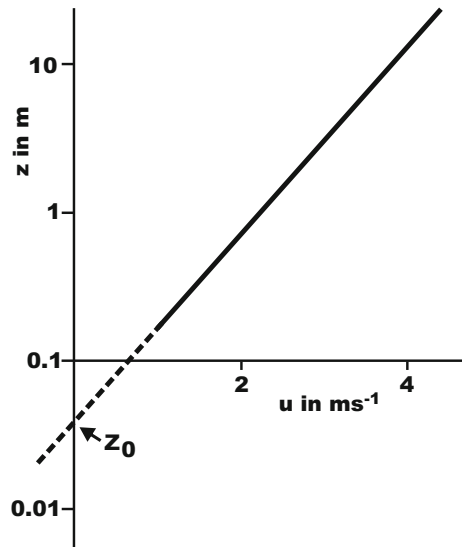
Table 2.7 Roughness length in m from different sources (Reithmaier et al. 2006, updated)

Surface	ESDU (1972)	Troen and Lundtang Petersen (1989)	Wieringa (1992)	Fiedler according to Hasager and Jensen (1999)	Davenport et al. (2000)
Ice	10^{-5}				
Water	$10^{-4} - 10^{-3}$				
Snow	0.002				
Bare soil		0.03	0.004	0.03	0.005
Grassland	0.005–0.02	0.03	0.06	0.08	0.03
Winter crops (winter)		0.1	0.09	0.12	0.1
Winter crops	0.05	0.1	0.18	0.09	0.25
Summer crops	0.05	0.1	0.18	0.09	0.25
Clearings		0.1	0.35	0.004	0.2
Shrubs	0.2	0.4	0.45	0.3	0.5
Conifer forest	1–2	0.4	1.6	0.9	1.0
Deciduous forest	1–2	0.4	1.7	1.2	2.0
Settlement	0.5–2	0.4	0.7	0.5	2.0

is often used in models. However, Eq. (2.61) underestimates z_0, for low wind velocities, because under these circumstances existing capillary waves are very rough. It is highly recommended to use the relation by Zilitinkevich (1969), which is a combination of Eq. (2.61) and the relation by Roll (1948) in the form

$$z_0 = c_1 \frac{v}{u_*} + \frac{u_*^2}{c_2 \, g},$$
(2.62)

where the coefficients, c_1 and c_2 are given in Table 2.8 and plotted in Fig. 2.7. For high friction velocities, the data given by Zilitinkevich et al. (2002) show slightly higher roughness-length values in the coastal zone than for the open sea. Because of the remarkable scatter of experimental data for the determination of the roughness length (Kitajgorodskij and Volkov 1965), all combinations of both parameterizations as well the Roll-type for $u_* < 0.1$ m s^{-1} and the Charnock-type for $u_* > 0.1$ m s^{-1} are applicable.

The integration of the equations for the sensible and the latent heat flux is formally identical to those of the momentum flux (Eq. 2.60). The integration constants are the so-called roughness length for temperature and roughness length for humidity. At these heights, the temperature and the humidity are assumed to

Table 2.8 Coefficients for Eq. (2.62)

Author	c_1	c_2
Roll (1948)	0.48	∞
Charnock (1955)	0.0	81.1
Zilitinkevich (1969)	0.1	20.8
Brocks and Krügermeier (1970)	0.0	28.5
Foken (1990)	0.48	81.1
Beljaars (1995)	0.11	55.6
Zilitinkevich et al. (2002)	0.1	56 open ocean 32 coastal zone
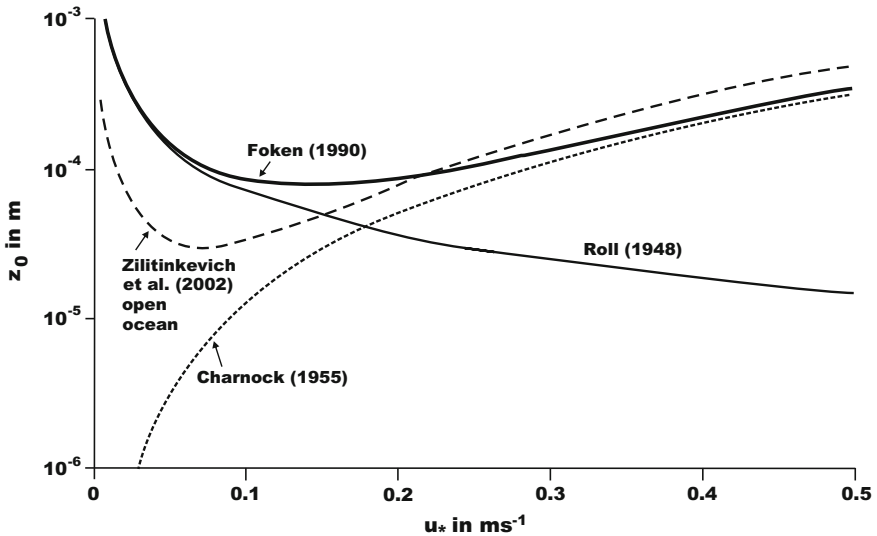
Fig. 2.7 Dependence of the roughness length over water on the friction velocity according to different authors

have approximately the same values as at the ground surface. That this cannot be true was already shown in Fig. 1.5, because near the surface large temperature gradients occur. Therefore, the roughness lengths for scalars cannot be precisely determined. Typically, their values are assumed to be equal to 10% of the roughness length z_0 for momentum.

For atmospheric models these roughness lengths are parameterized (see Sect. 5.3) and used in the following equations

$$T(z) - T(z_{0T}) = \frac{\mathrm{Pr}_t\, T_*}{\kappa}\, \ln \frac{z}{z_{0T}}, \tag{2.63}$$

$$q(z) - q(z_{0q}) = \frac{Sc_t\, q_*}{\kappa} \ln \frac{z}{z_{0q}}, \tag{2.64}$$

where

$$T_* = -\frac{\overline{w'T'}}{u_*} \tag{2.65}$$

is the temperature scale or friction temperature and

$$q_* = -\frac{\overline{w'q'}}{u_*} \tag{2.66}$$

is the humidity scale.

For dense vegetation (grass, grain), the canopy can be considered as a porous medium. The zero-level for the wind field according to Eq. (2.60) is no longer at the ground surface but at a distance d above the surface within the plant canopy. At this level, often called displacement height or zero-plane displacement height d, all equations given thus far are valid analogues to the case of bare soil (Paeschke 1937). The length scale, which is based on this level, is called the aerodynamic scale with $z'(d) = 0$. In contrast, the geometric scale, which is measured from the ground surface, is $z = z' + d$ (Fig. 2.8). Because Eq. (2.60) is valid only for the aerodynamic scale, the expression for low vegetation using the geometric scale as reference gives:
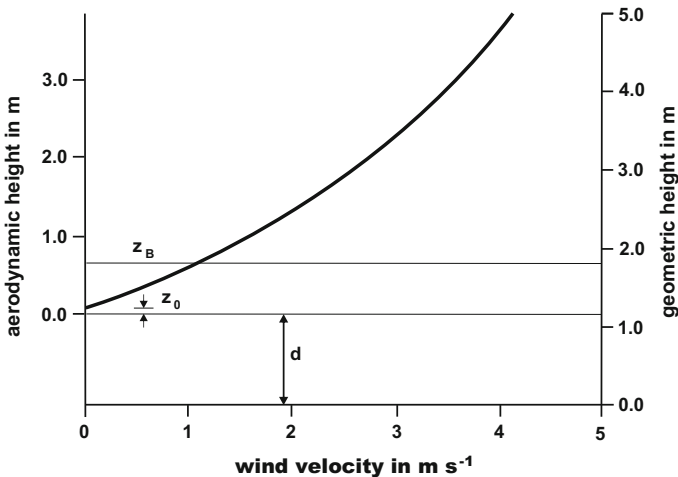

Fig. 2.8 Aerodynamic and geometric scale for dense vegetation ($d = 1.2$ m)

$$u(z) = \frac{u_*}{\kappa} \ln \frac{z - d}{z_0} \qquad (2.67)$$

Consequently, all profile equations and equations for integral turbulence characteristics, which are used in this and the following chapters, must be modified for low vegetation by replacing "z" with "$z - d$". The roughness length z_0 in Eq. (2.67) is related to the new aerodynamic zero-level and Table 2.7 can be applied. Sometimes in the literature the denominator is given as $z_0 - d$. In this case z_0 is measured from the ground. High vegetation (forest) and tall buildings require special considerations (see Sect. 3.1.2).

The log-linear extrapolated plot of the wind profile above a dense plant canopy with the geometric height as the ordinate cuts the ordinate at $u(z_0 + d) = 0$. Thus, it is not possible to determine the roughness and displacement heights in a simple way. Instead, a system of equations must be solved. However, it is possible to use a value of z_0 from Table 2.7 and then calculate d. A simple approximation is also given by

$$z_0 = 0.1 \, z_B, \qquad (2.68)$$

where z_B is the canopy height. Another method is to assume that the displacement height is about 2/3 of the canopy height. Therefore, with a known value of $z_0 + d$ the roughness length can be determined by:

$$z_0 = [z_0 + d] - \frac{2}{3} z_B \qquad (2.69)$$

The determination of the zero-plane displacement for heterogeneous surfaces, high vegetation and buildings is discussed in Sect. 3.1.2.

2.3.3 Monin-Obukhov's Similarity Theory

The equations given in Sect. 2.3.1 are strictly speaking only valid in the dynamic sub-layer in which the influence of thermal stratification can be neglected. Monin and Obukhov (1954) used dimensional analysis according to Buckingham's Π-theorem (Supplement 2.3), to extend these equations to the non-neutral (diabatic) case (Foken 2006a). In this analysis, the dependent parameters in the surface layer are the height z in m, the friction velocity u_* in m s^{-1}, the kinematic heat flux

$$\overline{w'T'} = \frac{Q_H}{\rho \, c_p} \qquad (2.70)$$

in K m s^{-1}, and the buoyancy parameter g/T in m s^{-2} K^{-1}. The independent dimensions are the length in meters, the time in seconds, and the temperature in K

degrees. The dimensionless parameter that characterizes the processes in the surface layer is (also called Obukhov number or Obukhov stability parameter)

$$\varsigma = z/L, \tag{2.71}$$

where

$$L = -\ \frac{u_*^3}{\kappa \frac{g}{T} \frac{Q_H}{\rho \cdot c_p}}. \tag{2.72}$$

Supplement 2.3   Buckingham's Π-theorem

Buckingham's Π-theorem (Buckingham 1914; Kantha and Clayson 2000) states that for n + 1 dependent parameters and k independent dimensions, there exist exactly n + 1 − k dimensionless parameters which characterize the process. This can be demonstrated for the free throw of an object (Kitajgorodskij 1976), where z, u_0, g and x are the n + 1 dependent parameters corresponding to the dropping height, velocity of the throw, gravity acceleration, and distance of the impact point. The independent dimensions are the length in m and the time in s. The benefit of the dimension analysis is shown stepwise:

- The determination of $x = f(z, u_0, g)$ from many single experiments is very expensive.
- The assumption $g = $ const gives an array of curves for different dropping heights.
- Using Buckingham's Π-theorem one can determine both dimensionless values $x^+ = x/z$ and $z^+ = g\ z\ u_0^2$, which gives a direct functional relation between x^+ and z^+.
- If you increase the number of dimensions by separation of the length scale for the horizontal and vertical direction, the process can be described with only one dimensionless parameter $x^* = c\ u_0\ (z\ g^{-1})^{1/2}$. With some experiments it is even possible to determine for the constant c the standard deviation.

The difficulty in the application of Buckingham's Π-theorem is the selection of the parameters, the dimensions, and the determination of the suitable dimensionless parameters. Because of the many influencing parameters in meteorology, this theorem is very important.

The characteristic length scale L is called the Obukhov length (Obukhov 1946). Initially, the notation Monin-Obukhov-length was used, but this is, in the historical sense, not exact (Businger and Yaglom 1971). The Obukhov length gives a relation

between dynamic, thermal, and buoyancy processes, and is proportional to the height of the dynamic sub-layer (Obukhov 1946), but is not identical with it (Monin and Yaglom 1973, 1975).

Currently (Stull 1988), the Obukhov length is derived from the TKE-equation Eq. (2.42). A physical interpretation of L was made by Bernhardt (1995), i.e., the absolute value of the Obukhov length is equal to the height of an air column in which the production ($L < 0$) or the loss ($L > 0$) of TKE by buoyancy forces is equal to the dynamic production of TKE per volume unit at any height z multiplied by z.

It is more accurate to define the Obukhov length using the potential temperature. Furthermore, for buoyancy considerations the content of water vapour is important, which changes the air density. Therefore, virtual potential temperature θ_v should be applied. The Obukhov length is then defined as:

$$L = -\frac{u_*^3}{\kappa \frac{g}{\theta_v} \overline{w'\theta_v'}} \tag{2.73}$$

This is precise, but is not often used because the universal functions, discussed below, were determined in the lower surface layer and often in dry regions. Observations made in other regions showed within the accuracy of the measurements no significant differences.

The application of Monin-Obukhov similarity theory on the profile equations Eqs. (2.46)–(2.48) is done using the so-called universal functions $\varphi_m(\varsigma)$, $\varphi_H(\varsigma)$ and $\varphi_E(\varsigma)$ for the momentum, sensible and latent heat exchange respectively. Therefore, a new functional dependence on the dimensionless parameter ζ, is given along with Eqs. (2.51) and (2.54):

$$u_* = \sqrt{-\overline{u'w'}} = \frac{\kappa z}{\varphi_m(\varsigma)} \frac{\partial u}{\partial z} = \frac{\kappa}{\varphi_m(\varsigma)} \frac{\partial u}{\partial \ln z} \tag{2.74}$$

$$\overline{w'T'} = -\frac{\kappa / \Pr_t u_*}{\varphi_H(\varsigma)} \frac{\partial T}{\partial \ln z} \tag{2.75}$$

$$\overline{w'q'} = -\frac{\kappa / Sc_t u_*}{\varphi_E(\varsigma)} \frac{\partial q}{\partial \ln z} \tag{2.76}$$

The universal functions account for the effects of stronger mixing in the unstable case, which leads to a decrease of the gradient and an increase of the flux. In the stable case the opposite conditions apply. The universal functions can be approximated by a Taylor series (Monin and Obukhov 1954) with the argument ς:

$$\varphi(\varsigma) = 1 + \beta_1 \varsigma + \beta_2 \varsigma^2 + \cdots \tag{2.77}$$
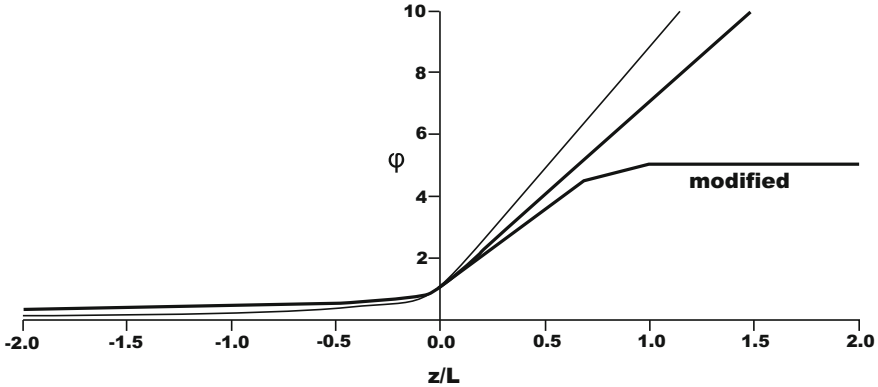
Fig. 2.9 Typical graph of the universal functions for momentum flux (*bold line*) and sensible and latent heat flux (*fine line*); 'modified' indicates the function is characterized under the conditions of *z*-less-scaling

Based on **O**bukhov's (1946) investigations, the so-called O'KEYPS-function (**K**aimal, **E**lliot, **Y**amamoto, **P**anofsky, **S**ellers) followed from the studies made in the 1950s and 60s (Panofsky 1963; Businger and Yaglom 1971; Businger 1988):

$$[\varphi_m(\varsigma)]^4 - \gamma_1 \cdot \varsigma \cdot [\varphi_m(\varsigma)]^3 = 1 \tag{2.78}$$

According to Businger et al. (1971) it follows that $\gamma_1 \approx 9$ ($-2 < \zeta < 0$) and that the form $\varphi_m(\zeta) \cong (-\gamma_1\zeta)^{-1/3}$ fulfills the O'KEYPS-equation which applies to the conditions of free convection. The currently used form of the universal functions (Fig. 2.9) is numerically only slightly different (Kramm and Herbert 2009):

$$\varphi_m(\varsigma) = (1 + \gamma_2 \cdot \varsigma)^{-1/4}, \tag{2.79}$$

which is called the Businger-Dyer-Pandolfo-relationship (Pandolfo 1966; Businger 1988).

The relationships between the universal functions for momentum and sensible heat are given by:

$$\begin{aligned} \varphi_H &\approx \varphi_m^2 \quad \text{for } \varsigma < 0 \\ \varphi_H &\approx \varphi_m \quad \text{for } \varsigma \geq 0 \end{aligned} \tag{2.80}$$

Consequently, the influence of stratification in the surface layer on the universal functions can be described with the stability parameter ς. The universal functions are generally defined in the range of $-1 < \varsigma < 1$. In the stable case ($\varsigma > 1$) a height-independent scaling occurs, the so-called *z-less* scaling (Wyngaard 1973). In this case, the eddy sizes do not depend on the height above the ground surface but on the local Obukhov-length (Table 2.9, Fig. 2.9).

Table 2.9 Determination of the stratification in the surface layer dependent on the dimensionless parameter ς and the universal function $\varphi(\varsigma)$

Stratification	Remark	ς	$\varphi(\varsigma)$
Unstable	Free convection, independent from u_*	$-1 > \varsigma$	No definition
	Dependent from u_*, T_*	$-1 < \varsigma < 0$	$\varphi(\varsigma) < 1$
Neutral	Dependent from u_*	$\varsigma \sim 0$	$\varphi(\varsigma) = 1$
Stable	Dependent from u_*, T_*	$0 < \varsigma < 0.5 \dots 2$	$1 < \varphi(\varsigma) < 3 \dots 5$
	Independent from z	$0.5 \dots 1 < \varsigma$	$\varphi(\varsigma) \sim const \sim 4 \dots 7$

Table 2.10 Universal function according to Businger et al. (1971), recalculated by Högström (1988)

Stratification	$\varphi_m(\varsigma)$	$\varphi_H(\varsigma) \sim \varphi_E(\varsigma)$, $Pr_t = Sc_t = 1$
Unstable	$(1 - 19.3\,\varsigma)^{-1/4}$	$0.95\,(1 - 11.6\,\varsigma)^{-1/2}$
Stable	$1 + 6.0\,\varsigma$	$0.95 + 7.8\,\varsigma$

Presently the universal functions derived from the Kansas-experiment of 1968 by Businger et al. (1971) and later modified by Högström (1988) are widely used. Högström (1988) considered important criticisms of the Kansas-experiment, for example of the wind measurements (Wieringa 1980), and has re-calculated the von-Kármán constant from $\kappa = 0.35$ to the presently used value of $\kappa = 0.40$ (Table 2.10).

The universal functions given in Table 2.10 are recommended for use. In the last 40 years, many universal functions where determined. The most important of these are given in Appendix A.4. A difficulty in applying the universal functions is the normalization. The basics were discussed by Yaglom (1977). For applying the universal functions, one must consider if the turbulent Prandtl number is part of the universal function, is used in the profile equation, or even included in the Obukhov length (Skeib 1980). Furthermore, all universal functions must be recalculated for the updated value of the von-Kármán constant of 0.4 (Högström 1988). It must be noted that the universal functions by Zilitinkevich and Tschalikov (1968) and Dyer (1974) are widely used in the Russian and English literature respectively. Also interesting, is the universal function by Skeib (1980) which is based on the separation of the atmospheric boundary layer into a dynamical sub-layer (without influence of stratification) and a surface layer. In analogy with hydrodynamics, critical values for the separation of both layers are used. A disadvantage is the non-continuous function, but the integration gives a physically rational function.

There are only a few papers with results using the universal function for the water vapor exchange. Therefore, the universal function for the sensible heat flux is

Table 2.11 The von-Kármán constant according to different authors (Foken 1990, 2006), where the value by Högström (1996) is recommended

Author	κ
Monin and Obukhov (1954)	0.43
Businger et al. (1971)	0.35
Pruitt et al. (1973)	0.42
Högström (1974)	0.35
Yaglom (1977)	0.40
Kondo and Sato (1982)	0.39
Högström (1985, 1996)	0.40 ± 0.01
Andreas et al. (2004)	0.387 ± 0.004

used widely for the latent heat flux and the fluxes of trace gases with accordingly identical numbers for the turbulent Prandtl and Schmidt number.

Applying the universal function in the stable case is difficult. It is already well known that the universal function in the above form underestimates the turbulent exchange process. The assumption of a nearly constant universal function, which also supports the z-less scaling is obvious. The lack of measurements has not allowed a general applied formulation (Andreas 2002). Handorf et al. (1999) based on measurements in Antarctica that for $\zeta > 0.6$ the universal function becomes constant $\varphi_m \sim 4$. Cheng and Bruntseart (2005) found for $\zeta > 0,6$ a value of $\varphi_m \sim 7$ for the CASES-99-experiment.

The uncertainty of the universal functions is similar to those of the turbulent Prandtl number (Table 2.6), and is also dependent on the accuracy of the measurement methods. Furthermore, the determination of Pr_t and κ for neutral conditions is relevant for the universal function at $\zeta = 0$. The von-Kármán constant is presently accepted as $\kappa = 0.40 \pm 0.01$ (Högström 1996). But a slight dependency on the Rossby and Reynolds numbers was discovered (Oncley et al. 1996), which is probably a self-correlation effect (Andreas et al. 2004). An overview of values of the von-Kármán constant appearing in the literature is shown in Table 2.11. Regarding the universal function, the following accuracies are given by Högström (1996), where normally the virtual temperature is not applied:

$$
\begin{aligned}
|z/L| &\le 0.5: \quad |\delta\varphi_H| \le 10\,\% \\
|z/L| &\le 0.5: \quad |\delta\varphi_m| \le 20\,\% \\
z/L &> 0.5: \quad \varphi_m, \ \varphi_H = \text{const }?
\end{aligned}
\tag{2.81}
$$

The discussion of the accuracy of the parameters and functions is still ongoing. For example, a dependence on the mixed layer height cannot be excluded (Johansson et al. 2001). This means that processes in the surface layer may be influenced non-locally by the whole boundary layer.

In addition to the Obukhov number ς, the Richardson number Eq. (2.20) is used to determine atmospheric stability. The definitions of the gradient, bulk, and flux Richardson numbers are:

Gradient Richardson number:

$$Ri = -\frac{g}{\overline{T}} \cdot \frac{\partial T / \partial z}{(\partial u / \partial z)^2} \tag{2.82}$$

Bulk Richardson number:

$$Ri_B = -\frac{g}{\overline{T}} \frac{\Delta T \, \Delta z}{(\Delta u)^2} \tag{2.83}$$

Flux Richardson number:

$$Rf = \frac{g}{\overline{T}} \frac{\overline{w'T'}}{\overline{w'u'}(\partial u / \partial z)} \tag{2.84}$$

Analogous to the Obukhov length, the temperature can be replaced by the virtual potential temperature.

The critical Richardson numbers are $Ri_c = 0.2$ and $Rf_c = 1.0$, for which in the case of stable stratification the turbulent flow changes suddenly to a quasi laminar, non-turbulent, flow or turbulence becomes intermittent. The conversion of ς into Ri is stratification-dependent according to the relations (Businger et al. 1971; Arya 2001):

$$\begin{array}{ll} \varsigma = Ri & \text{for} \quad Ri < 0 \\ \varsigma = \frac{Ri}{1 - 5\,Ri} & \text{for} \quad 0 \le Ri \le 0.2 = Ri_c \end{array} \tag{2.85}$$

An overview about the ranges of different stability parameters is shown Table 2.12.

The integration of the profile Eqs. (2.74)–(2.76) using the universal functions in the form of Eq. (2.79) for the unstable case is not trivial and was first presented by Paulson (1970). For the wind profile, the integration from z_0 to z using the definition of the roughness length $u(z_0) = 0$ is

$$u(z) - u(z_0) = u(z) = \frac{u_*}{\kappa}\left[\ln\frac{z}{z_0} - \int \varphi_m(\varsigma)\,d\varsigma\right], \tag{2.86}$$

$$u(z) = \frac{u_*}{\kappa}\left[\ln\frac{z}{z_0} - \psi_m(\varsigma)\right], \tag{2.87}$$

Table 2.12 Overview about different stability parameters

Stratification	Temperature	Ri	L	$\varsigma = z/L$
Unstable	$T(0) > T(z)$	< 0	< 0	< 0
Neutral	$T(0) \sim T(z)$	~ 0	$\pm\infty$	~ 0
Stable	$T(0) < T(z)$	$0 < Ri < 0.2 = Ri_c$	> 0	$0 < \varsigma < \sim 1$

where the integral of the universal function, $\psi_m(\varsigma)$, is:

$$\psi_m(\varsigma) = \int\limits_{z_0/L}^{z/L} [1 - \varphi_m(\varsigma)]\frac{d\varsigma}{\varsigma} \tag{2.88}$$

Accordingly, it follows for the integrated version for the sensible heat flux, which can also be applied for other scalars:

$$T(z) - T(z_{0T}) = \frac{\mathrm{Pr}_t\, T_*}{\kappa}\left[\ln\frac{z}{z_{0T}} - \int \varphi_h(\varsigma)d\varsigma\right] \tag{2.89}$$

$$T(z) - T(z_{0T}) = \frac{\mathrm{Pr}_t\, T_*}{\kappa}\left[\ln\frac{z}{z_{0T}} - \psi_h(\varsigma)\right] \tag{2.90}$$

$$\psi_h(\varsigma) = \int\limits_{z_{0T}/L}^{z/L} [1 - \varphi_h(\varsigma)]\frac{d\varsigma}{\varsigma} \tag{2.91}$$

The integration of the universal function for the momentum and sensible heat flux for unstable conditions according to Businger et al. (1971) in the form of Högström (1988) is

$$\psi_m(\varsigma) = \ln\left[\left(\frac{1+x^2}{2}\right)\left(\frac{1+x}{2}\right)^2\right] - 2\tan^{-1}x + \frac{\pi}{2} \quad \text{for } \frac{z}{L} < 0, \tag{2.92}$$

$$\psi_h(\varsigma) = 2\ln\left(\frac{1+y}{2}\right) \quad \text{for } \frac{z}{L} < 0, \tag{2.93}$$

with

$$x = (1 - 19.3\varsigma)^{1/4} \quad y = 0.95(1 - 11.6\varsigma)^{1/2}. \tag{2.94}$$

It is obvious that the cyclic term in Eq. (2.92) is not physically realistic. But this term is relatively small and has no remarkable influence on the result. In the stable case there are very simple solutions for the integrals of the universal functions:

$$\psi_m(\varsigma) = -6\frac{z}{L} \quad \text{for } \frac{z}{L} \geq 0 \tag{2.95}$$

$$\psi_h(\varsigma) = -7.8\frac{z}{L} \quad \text{for } \frac{z}{L} \geq 0 \tag{2.96}$$

The universal function according to the Businger-Dyer-Pandolfo relation Eq. (2.79) shows a good asymptotic behaviour for neutral stratification. A further version for the integration was proposed by Berkowicz and Prahm (1984).

2.3.4 Bowen-Ratio Similarity

The Bowen ratio (Bowen 1926) is defined as the ratio of the sensible to the latent heat flux:

$$Bo = \frac{Q_H}{Q_E} \qquad (2.97)$$

Using Eqs. (2.75) and (2.76), and taking the conversion between kinematic and energetic units into consideration according to Eqs. (2.58) and (2.59) a very simple relation develops. With the assumption $\varphi_H(\varsigma) \sim \varphi_E(\varsigma)$, for neutral stratification or restriction to the dynamic sub-layer, $Pr_t \sim Sc_t$, and replacing the partial derivatives by finite-differences gives

$$Bo = \frac{c_p}{\lambda} \frac{\Delta T}{\Delta q} = \frac{c_p}{\lambda} \frac{p}{0.622} \frac{\Delta T}{\Delta e} = \gamma \frac{\Delta T}{\Delta e}, \qquad (2.98)$$

where the psychrometric constant is $\gamma = 0.667$ hPa K^{-1} for $p = 1013.25$ hPa and $T = 20$ °C.

A special case of the flux-gradient similarity Eq. (2.98), is the so-called Bowen-ratio similarity. The ratio of the gradients of temperature and humidity between two heights behaves like the Bowen ratio. This simplification is the basis of the Bowen-ratio method (see Sect. 4.1.1). It must be noted that the simplifications used are also limitations of the method.

The generalization of this similarity is

$$\frac{F_x}{F_y} \approx \frac{\Delta x}{\Delta y}, \qquad (2.99)$$

i.e., the ratio of two fluxes is proportional to the ratio of the differences of the relevant state parameters between two heights.

This equation opens the possibility of determining the flux of an inert gas if the energy flux is known, if the differences of the trace gas concentrations can be determined with a high accuracy, and if the above made simplifications can be accepted. This method was proposed as a modified Bowen-ratio method by Businger (1986), compare with Sect. 4.1.1.

2.4 Flux-Variance Similarity

Analogous to the derivation of the *TKE* equation, Eq. (2.42), the balance equations for the momentum and sensible heat flux can be derived (Wyngaard et al. 1971a; Foken et al. 1991):

$$\frac{\partial \overline{w'u'}}{\partial t} = -\overline{w'^2}\frac{\partial \overline{u}}{\partial z} - \frac{g}{\overline{T}}\left(\overline{u'T'}\right) - \frac{\partial}{\partial z}\overline{u'w'^2} - \frac{1}{\rho}\frac{\partial\left(\overline{w'p'}\right)}{\partial z} - \varepsilon \qquad (2.100)$$

$$\text{II} \hspace{6.5cm} \text{VII}$$

$$\frac{\partial \overline{w'T'}}{\partial t} = -\overline{w'^2}\frac{\partial \overline{T}}{\partial z} - \frac{g}{\overline{T}}\left(\overline{T'^2}\right) - \frac{\partial}{\partial z}\overline{T'w'^2} - \frac{1}{\rho}\frac{\partial\left(\overline{T'p'}\right)}{\partial z} - N_T \qquad (2.101)$$

$$\text{III} \hspace{6.5cm} \text{VII}$$

These equations include the standard deviations of the vertical wind component and the temperature:

$$\sigma_w = \sqrt{\overline{w'^2}} \quad und \quad \sigma_T = \sqrt{\overline{T'^2}} \qquad (2.102)$$

For steady state conditions and after estimation of the magnitude of the terms II and VII in Eq. (2.100) and terms III and VII in Eq. (2.101) it follows for the surface layer (Wyngaard et al. 1971a; Foken et al. 1991):

$$\sigma_w/u_* \cong \text{const.} \quad und \quad \sigma_T/T_* \cong \text{const.} \qquad (2.103)$$

These normalized standard deviations are also called integral turbulence characteristics (Tillman 1972), because they integrally characterize the state of turbulence over all frequencies. For the integral turbulence characteristics of the three wind components, the following values are given (Lumley and Panofsky 1964; Panofsky and Dutton 1984):

$$\sigma_w/u_* \cong 1.25$$
$$\sigma_u/u_* \cong 2.45 \qquad (2.104)$$
$$\sigma_v/u_* \cong 1.9$$

The constancy is only valid for neutral stratification. From similarity relations for diabatic conditions it follows (Foken et al. 1991):

$$\sigma_w/u_* = a[\varphi_m(z/L)]^{-0.5} \qquad (2.105)$$

$$\sigma_T/T_* = b\left[\frac{z}{L}\varphi_h(z/L)\right]^{-0.5}. \qquad (2.106)$$

Many dependencies are reported in the literature for the integral turbulence characteristics under diabatic conditions (see Appendix A.4). Therefore, for the integral turbulence characteristics a general form is used for the wind components

$$\sigma_{u,v,w}/u_* = c_1(z/L)^{c_2}, \tag{2.107}$$

and for temperature and other scalars

$$\sigma_T/T_* = c_1(z/L)^{c_2}, \tag{2.108}$$

where $c_2 = -1/3$ is often applied (Wyngaard 1973). At least for the vertical wind, there are no significant differences between the available parameterizations. The most common parameterization by Panofsky et al. (1977) can be applied in the neutral and unstable case too:

$$\sigma_w/u_* = 1.3\left(1 - 2\,\frac{z}{L}\right)^{1/3} \tag{2.109}$$

Based on these findings, the experimentally verified relationships are given in Table 2.13.

The integral turbulence characteristics for temperature and other scalars in the case of neutral stratification are not exact because $T_* \to 0$. In the case of unstable stratification for wind components and scalars, dependencies on stratification were found. Thus, some authors (Panofsky et al. 1977; Peltier et al. 1996; Johansson et al. 2001) reported a dependency on the mixed layer height in the case of strong unstable stratification. But the difference is relevant only for free convection (Thomas and Foken 2002). For stable stratification, only a few verified measurements are available. Therefore, the use of the given parameterizations for the unstable case with the argument $|(z - d)/L|$ is recommended as a first approximation. For temperature, a slightly modified approach is given in Table 2.13 (Thomas and Foken 2002).

Based on Rossby similarity (Garratt 1992, see Sect. 2.6.2) some authors (Yaglom 1979; Tennekes 1982; Högström 1990; Smedman 1991) assumed, at least in the neutral case, a visible dependency on the Coriolis parameter. The verification

Table 2.13 Integral turbulence characteristics for diabatic stratification (Foken et al. 1991, 1997; Thomas and Foken 2002)

Parameter	z/L	c_1	c_2
σ_w/u_*	$0 > z/L > -0.032$	1.3	0
	$-0.032 > z/L$	2.0	1/8
σ_u/u_*	$0 > z/L > -0.032$	2.7	0
	$-0.032 > z/L$	4.15	1/8
σ_T/T_*	$0.02 < z/L < 1$	1.4	$-1/4$
	$0.02 > z/L > -0.062$	0.5	$-1/2$
	$-0.062 > z/L > -1$	1.0	$-1/4$
	$-1 > z/L$	1.0	$-1/3$

Parameter	$-0.2 < z/L < 0.4$
σ_w/u_*	$0.21 \ln\left(\frac{z_+ f}{u_*}\right) + 3.1 \quad z_+ = 1\ m$
σ_u/u_*	$0.44 \ln\left(\frac{z_+ f}{u_*}\right) + 6.3 \quad z_+ = 1\ m$

Table 2.14 Parameterization of the integral turbulence characteristics for neutral and slightly unstable and stable stratification (Thomas and Foken 2002)

was developed by Högström et al. (2002). A parameterization according to this finding for the neutral and slightly unstable and stable range is given in Table 2.14. For scalars, such a parameterization cannot be found due to the high dependency on the stratification in this range.

2.5   Turbulence Spectrum

Knowledge of the turbulence spectrum (see Sect. 1.4.3) is critically important for choosing sensors and defining optimal sensing strategies for given atmospheric conditions. Many sensing and also modelling techniques are possible only within certain portions of the turbulence spectrum, or are based on assumptions about the distribution of spectral energy density. Turbulence spectra vary depending on the state parameters, fluxes, and micrometeorological conditions. In the frequency range of interest to micrometeorology, i.e. periods shorter than about 30 min, three ranges can be identified. The range of production of the turbulent energy by the mean flow is characterized by the integral turbulent length scale Λ, which is in the order of 10–500 m (Kaimal and Finnigan 1994). The typical frequency range is $f \sim 10^{-4}$ Hz (note that here f is not the Coriolis parameter). This range is followed by the inertial sub-range in which turbulence is assumed to be isotropic, i.e. the turbulent movements have no preferential direction. In this range, a well defined energy decrease with increasing frequency occurs according to Kolmogorov's laws (Kolmogorov 1941a, b). The decrease of energy is proportional to $f^{-5/3}$. After multiplying the energy by the frequency the Kolmogorov laws predict an $f^{-2/3}$ decrease for state parameters and an $f^{-4/3}$ decrease for the fluxes. In the third range, with frequencies of $10-30$ Hz the kinetic energy of the small eddies is transformed into thermal energy (energy dissipation). The typical dissipation length scale is the Kolmogorov's microscale

$$\eta = \left(\frac{\nu^3}{\varepsilon}\right)^{1/4}, \tag{2.110}$$

which is about 10^{-3} m.

   The three parts of the turbulence spectrum in the micrometeorological range are plotted against wave number in Fig. 2.10. Maximum energy occurs at the integral turbulence length $\sim 1/k$. Note that $\Lambda = \pi/k$, is the Eulerian integral turbulence

Fig. 2.10 Schematic plot of the turbulence spectra and the ranges of energy production (A), the inertial sub-range (B) and the dissipation range (C) dependent on the wave number k (Adapted from Kaimal and Finnigan 1994, with kind permission of © Oxford University Press, Oxford 1994, All rights reserved)
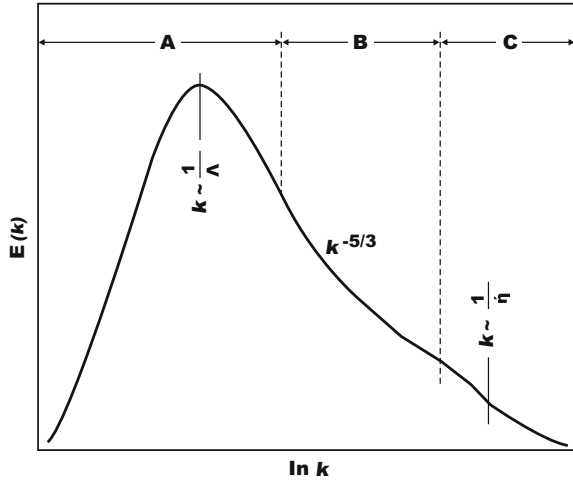
length scale. This length scale can be given for all wind components and scalars. According to Taylor's frozen turbulence hypothesis (Taylor 1938), wave number and frequency are related as:

$$k = 2\pi f / \overline{u} \tag{2.111}$$

Using Eq. (2.111), the integral turbulence length scale can be transferred into an integral turbulence time scale T_u which is defined by the autocorrelation function ρ_u for the horizontal velocity perturbation (Monin and Yaglom 1973; 1975; Schlichting and Gersten 2003; Wyngaard 2010),

$$\Lambda_u = \overline{u} \cdot T_u = \overline{u} \int\limits_0^\infty \rho_u(\xi)\, d\xi = \overline{u} \int\limits_0^\infty \frac{\overline{u'(t)\, u'(t+\xi)}}{\sigma_u^2}\, d\xi. \tag{2.112}$$

Because the autocorrelation function is usually an exponential function, the integral time scale, τ, is given $\rho(\tau) = 1/e \sim 0.37$. This is schematically illustrated in Fig. 2.11.

The energy spectrum under the assumption of local isotropy along with the Kolmogorov constant $\beta_u \sim 0.5-0.6$ (Kolmogorov 1941b) can be given in the inertial sub-range by the so-called −5/3-law, here presented for the horizontal wind component:

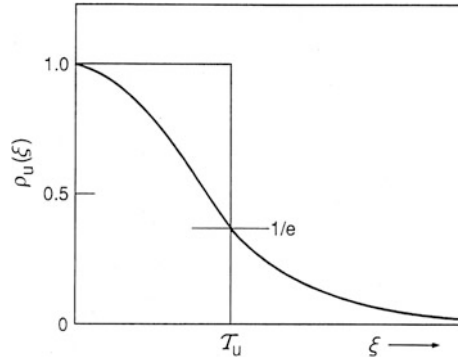$$E_u(k) = \beta_u\, \varepsilon^{2/3}\, k^{-5/3} \tag{2.113}$$

Fig. 2.11 Autocorrelation function and its relation to the integral time scale. The value 1/e is a good approximation for which the area of the shown rectangle is equal to the area below the exponential plot (Adapted from Kaimal and Finnigan 1994, with kind permission of © Oxford University Press, Oxford 1994, All rights reserved)

In an analogous way, the energy spectrum of the temperature in the inertial sub-range is

$$E_T(k) = \beta_T \, N_T \, \varepsilon^{-1/3} \, k^{-5/3}, \tag{2.114}$$

with the Kolmogorov constant $\beta_T \sim 0.75\text{–}0.85$ (Corrsin 1951), and N_T is the dissipation rate of the variance of the temperature Eq. (2.94). For humidity, the inertial sub-range spectrum is

$$E_q(k) = \beta_q \, N_q \, \varepsilon^{-1/3} \, k^{-5/3} \tag{2.115}$$

with the Kolmogorov constant $\beta_q \sim 0.8\text{–}1.0$. The mathematical background for spectral diagrams is briefly given in Supplement 2.4.

Supplement 2.4 Fourier series and frequency spectrum

A function f, e.g., a time series of a meteorological parameter with turbulent fluctuations (Fig. 1.13), can be represented by a system of orthogonal functions:

$$f(x) = \frac{a_0}{2} + \sum_{k=1}^{\infty} (a_k \cos kx + b_k \sin kx) \tag{S2.3}$$

$$a_k = \frac{1}{\pi} \int_0^{2\pi} f(x) \cos kx \, dx \quad b_k = \frac{1}{\pi} \int_0^{2\pi} f(x) \sin kx \, dx \tag{S2.4}$$

In an analogous way, its representation by an exponential function is possible:

$$f(x) = \sum_{k=-\infty}^{\infty} \left(c_k \, e^{ikx} \right) \quad c_k = \frac{1}{2\pi} \int_{-\pi}^{\pi} f(x) \, e^{-ikx} dx \qquad (S2.5)$$

The Fourier transformation is an integral transformation, which converts a function of time into a function of frequency:

$$F(\omega) = \frac{1}{\sqrt{2\pi}} \int_{-\infty}^{\infty} f(t) \, e^{i\omega t} dt \qquad (S2.6)$$

The square root of the time integral over the frequency spectrum (energy spectrum, power spectrum) corresponds to the standard derivation. The frequency spectrum of two time series is called the cross spectrum. Its real part is the co-spectrum, and the time integral of the co-spectrum corresponds to the covariance.

Multiplying the TKE equation, Eq. (2.42), by the factor $\kappa z/u_*^3$ and assuming steady state conditions ($\partial \overline{e}/\partial t = 0$), gives the dimensionless TKE equation for the surface layer (Wyngaard and Coté 1971; Kaimal and Finnigan 1994):

$$\varphi_m - \frac{z}{L} - \varphi_t - \varphi_\varepsilon + I = 0 \qquad (2.116)$$

The imbalance term I is based on the pressure term. I disappears in the unstable case and is of order z/L in the stable case. The transport term, φ_t, is of order $-z/L$ in the unstable case, and disappears in the stable case. The dimensionless energy dissipation term is

$$\varphi_\varepsilon = \frac{\kappa z \varepsilon}{u_*^3}, \qquad (2.117)$$

which can be described by a universal function (Kaimal and Finnigan 1994):

$$\varphi_\varepsilon^{2/3} = \left\{ \begin{array}{ll} 1 + 0.5|z/L|^{2/3} & for \quad z/L \leq 0 \\ (1 + 5z/L)^{2/3} & for \quad z/L \geq 0 \end{array} \right\}$$

$$\varphi_\varepsilon^{2/3} = \left\{ \begin{array}{ll} 1 + 0.5|z/L|^{2/3} & for \quad z/L \leq 0 \\ (1 + 5z/L)^{2/3} & for \quad z/L \geq 0 \end{array} \right\} \qquad (2.118)$$

Additional universal functions for the energy dissipation are given in Appendix A.4. A practical application of these equations is the determination of the friction velocity using a scintillometer (see Sect. 6.2.5). Also, the energy spectrum of the horizontal wind can be derived in the inertial sub-range (Kaimal and Finnigan 1994):

$$
\frac{f \cdot S_u(f)}{u_*^2} = \frac{0.55}{(2\pi)^{2/3}} \left(\frac{\varepsilon^{2/3} z^{2/3}}{u_*^2} \right) \left(\frac{fz}{\overline{u}} \right)^{-2/3}
$$
$$
= \frac{0.55}{(2\pi\kappa)^{2/3}} \varphi_\varepsilon^{2/3} \left(\frac{fz}{\overline{u}} \right)^{-2/3}
\tag{2.119}
$$

The turbulence spectra of various parameters differ significantly in peak frequency (maximum of the energy density) and their dependence on the stratification. The peak frequency of the vertical wind corresponds to the highest frequencies (0.1–1 Hz), and those of the horizontal wind are one order of magnitude lower (Fig. 2.12). The vertical wind shows this typical form of spectrum for stable (peak frequency shifted to higher frequencies) and unstable stratification. For the other wind components and scalars, the peak frequencies are shifted to lower frequencies,
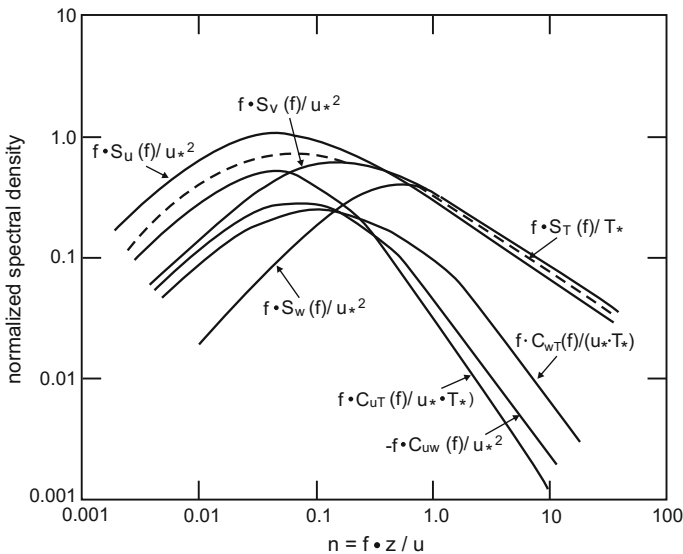

Fig. 2.12 Models of the energy density spectrum of state variables and fluxes (Adapted from Kaimal et al. 1972, with kind permission of © John Wiley & Sons Inc., New York 1972, All rights reserved)

and because of large scatter in the data, they are often not clearly seen. In this range, mixed layer height often becomes an important, additional scaling parameter.

Energy density spectra are often used for the correction of measurement data (see Sect. 4.1.2). Because of the difficulty in calculating spectra, models of spectra are often applied. Such models were parameterized by Kaimal et al. (1972) on the basis of the data of the Kansas experiment. With the usual normalization of the frequency according to Eq. (1.19)

$$n = f \frac{z}{\bar{u}}, \tag{2.120}$$

the wind components for neutral and slightly unstable stratification (Kaimal and Finnigan 1994) are:

$$\frac{f\, S_u(f)}{u_*^2} = \frac{102\, n}{(1 + 33\, n)^{5/3}} \tag{2.121}$$

$$\frac{f\, S_v(f)}{u_*^2} = \frac{17\, n}{(1 + 9.5\, n)^{5/3}} \tag{2.122}$$

$$\frac{f\, S_w(f)}{u_*^2} = \frac{2.1\, n}{1 + 5.3\, n^{5/3}} \tag{2.123}$$

Højstrup (1981) proposed a stability-dependent parameterization for the vertical wind for unstable stratification:

$$\frac{f\, S_w(f)}{u_*^2} = \frac{2\, n}{1 + 5.3\, n^{5/3}} + \frac{32\, n(z/-L)^{2/3}}{(1 + 17n)^{5/3}} \tag{2.124}$$

For the temperature spectrum, which can also be used for other scalars, Kaimal et al. (1972) published the following parameterization:

$$\frac{f\, S_T(f)}{T_*^2} = \left\{ \begin{array}{ll} \frac{53.4\, n}{(1 + 24\, n)^{5/4}} & \text{for} \quad n < 0.5 \\ \frac{24.4\, n}{(1 + 12.5\, n)^{5/3}} & \text{for} \quad n \geq 0.5 \end{array} \right\} \tag{2.125}$$

For the co-spectra, (Kaimal and Finnigan 1994) proposed for the unstable case $(-2 < z/L < 0)$

$$-\frac{f\, C_{uw}(f)}{u_*^2} = \frac{12\, n}{(1 + 9.6\, n)^{7/3}}, \tag{2.126}$$

$$- \frac{f\ C_{wT}(f)}{u_*\ T_*} = \left\{ \begin{array}{ll} \frac{11\ n}{(1+13.3\ n)^{7/4}} & \text{for} \quad n \leq 1.0 \\ \frac{4\ n}{(1+3.8\ n)^{7/3}} & \text{for} \quad n > 1.0 \end{array} \right\}, \tag{2.127}$$

and for the stable case $(0 < z/L < 2)$:

$$- \frac{f\ C_{uw}(f)}{u_*^2} = 0.05\ n^{-4/3}\left(1 + 7.9\frac{z}{L}\right) \tag{2.128}$$

$$- \frac{f\ C_{wT}(f)}{u_*\ T_*} = 0.14\ n^{-4/3}\left(1 + 6.4\frac{z}{L}\right) \tag{2.129}$$

A log–log plot of $f\ S_X(f)$ versus f (see e.g. Figure 2.12) can be used to illustrate the power law relationships in the form $f\ S_X(f) \approx f^{-2/3}$ and $S_X(f) \approx f^{-5/3}$ (X is an arbitrary parameter). In a linear-linear plot of $S_X(f)$ versus f, the area below the graph in the range Δf is equal to the standard deviation $\sigma_A(\Delta f)$. The resolution at low frequencies is often bad. In a log-linear plot the area below the graph of $f \cdot S_X(f)$ versus f, is equal to the energy density. The multiplication of the values of the ordinate by f and logarithmic abscissa, gives a better representation of the low frequencies.

Figure 2.12 illustrates that the frequency of the energy maximum of the spectra is one order larger for the vertical than for the horizontal wind velocity. Accordingly, vertically moving turbulence elements are smaller and have a higher frequency than horizontally moving turbulence elements.

An alternative statistical parameter to the autocorrelation function, Eq. (2.112), is the structure function. It is a relation between the value of a variable at time t, $X(t)$, and its value at a later time, $X(t + L)$, note L is not the Obukhov length. If the time between the measurements is ΔT, then $L = j\ \Delta T$ and

$$D_{XX}(L) = \frac{1}{N}\sum_{k=0}^{N-j}\left(X_k - X_{k+j}\right)^2. \tag{2.130}$$

If simultaneous measurements are made at several locations, the structure function can be computed using $L = j\Delta r$ where Δr is the spatial separation between measurement sites.

The energy density in the inertial sub-range according to Eq. (2.112) can also be determined using the structure function (Tatarski 1961), which is with the spatial distance r

$$D_u(r) = c_u\ \varepsilon^{2/3}\ r^{2/3}, \tag{2.131}$$

with the structure constant $c_u \sim 4.02\ \beta_u$, $\beta_u \sim 0.5$ (Sreenivasan 1995), and the structure function parameter

$$C_u^2 = c_u \, \varepsilon^{2/3}. \tag{2.132}$$

The structure function for the temperature is given by

$$D_T(r) = c_T \, N_T \, \varepsilon^{-1/3} \, r^{2/3}, \tag{2.133}$$

with the structure constant $c_T \sim 4.02 \, \beta_T$, with β_T Obukhov-Corrsin constant (Obukhov 1949; Corrsin 1951), and the structure function parameter

$$C_T^2 = c_T \, N_T \, \varepsilon^{-1/3}. \tag{2.134}$$

The Obukhov-Corrsin constant is about 0.4 (Sreenivasan 1996). The ratio β_T/β_u is equal to the turbulent Prandtl number.

The structure function for moisture is given by

$$D_q(r) = c_q \, N_q \, \varepsilon^{-1/3} \, r^{2/3}, \tag{2.135}$$

with the structure constant $c_q \sim 4.02 \, \beta_q$ and the structure function parameter

$$C_q^2 = c_q \, N_q \, \varepsilon^{-1/3}. \tag{2.136}$$

The structure function parameters are very relevant for meteorological measuring techniques (Kohsiek 1982; Beyrich et al. 2005), because they are directly connected to the refraction structure function parameter C_n^2 (Hill et al. 1980),

$$C_n^2 = \left(79.2 \cdot 10^{-6} \frac{p}{T^2} \right)^2 C_T^2 \tag{2.137}$$

which is proportional to the backscatter echo of ground-based remote sensing techniques:

$$C_n^2 = A^2 C_T^2 + 2ABC_{Tq} + B^2 C_q^2 \tag{2.138}$$

The coefficients A and B are dependent on temperature, humidity, pressure and the electromagnetic wave length (Hill et al. 1980; Andreas 1989; Beyrich et al. 2005). While a dependence on temperature and humidity exists for microwaves, the humidity dependence on visible and near infrared light is negligible.

The stability dependence of the structure function parameter is given by a dimensionless function of the energy dissipation, which has the character of a universal function (Wyngaard et al. 1971b). For the surface layer, they are given in the form (Kaimal and Finnigan 1994):

$$\frac{C_u^2 \, z^{2/3}}{u_*^2} = \begin{cases} 4\left(1+0.5\frac{-z}{L}\right)^{2/3} & \text{for} \quad z/L \leq 0 \\ 4\left(1+5\frac{z}{L}\right)^{2/3} & \text{for} \quad z/L > 0 \end{cases} \tag{2.139}$$

$$\frac{C_T^2 \, z^{2/3}}{T_*^2} = \begin{cases} 5\left(1+6.4\frac{-z}{L}\right)^{-2/3} & \text{for} \quad z/L \leq 0 \\ 5\left(1+3\frac{z}{L}\right) & \text{for} \quad z/L > 0 \end{cases} \tag{2.140}$$

Other universal functions are listed in Appendix A.4. These will be used later for the determination of the sensible heat flux with scintillometers (see Sect. 6.2.5). Within the range of uncertainties of the measurements, all functions for C_T^2 can be applied.

The temperature structure function parameter C_T^2 can be determined according to Wyngaard et al. (1971b) by the vertical temperature profile

$$C_T^2 = z^{-4/3} \left(\partial\theta/\partial z\right)^2 f_T(Ri) \tag{2.141}$$

with the empirical stability function $f_T(Ri)$.

2.6   Atmospheric Boundary Layer

Even though micrometeorological measurements and modelling primarily focus on the surface layer it could be shown that the characteristics of the atmospheric boundary layer are important for many processes. As an example, the mixed-layer depth limits the vertical mixing of emissions. Therefore, in the following a short overview of the determination of the mixed layer height and of boundary-layer profile relationships is presented. More in-depth descriptions are given in the literature (Stull 1988; Garratt 1992; Jacobson 2005; Kraus 2008).

2.6.1   Mixed Layer Height

For practical issues the boundary-layer height, which includes the capping inversion and entrainment layer, is less important than the mixed-layer height. In the mixed layer (see Sect. 1.3), emissions from the surface and any material passing through the entrainment layer are mixed by convection and mechanical turbulence at time scales of about 1 h (Seibert et al. 2000). However, there is no standard method available to determine the mixed-layer height. Several observational methods and modelling approaches have been adopted.

Traditional methods use data from radiosondes, but can also be applied to observations from tethered balloons and aircrafts. For convective conditions, the

Fig. 2.13 Determination of the mixed layer height with the parcel method using the thermodynamic diagram
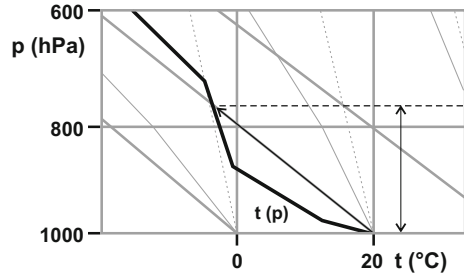
simplest method is the parcel method (Holzworth 1964, 1967). It is assumed that an air parcel lifts up adiabatically in the unstable boundary layer up to a level, where the surrounding potential temperature is warmer than those of the parcel (Fig. 2.13). One shortcoming of this method is finding the right surface temperature due to strong vertical temperature gradients near the surface. For instance, Troen and Mahrt (1986) proposed to apply an additional correction term to the surface temperature. According to Seibert et al. (2000) the same effect is achieved by using the virtual potential temperature of the surface level. A method proposed by Busch et al. (1976) and applied by Troen and Mahrt (1986) was operationally implemented by Beyrich and Leps (2012). It based on the calculation of the bulk-Richardson number

$$Ri_B(z) = -z\frac{g}{\theta_0} \cdot \frac{(\theta(z) - \theta_0)}{u(z)^2 + v(z)^2}. \tag{2.142}$$

The mixed-layer height is the level where Ri_B reaches a critical value of about 0.2.

Sounding techniques like sodars and lidars, which can detect temperature inhomogeneities, or strong gradients of moisture or aerosol concentrations, are also suitable to determine the mixed-layer height. However, due to measurement-range limitations, sodars can typically only detect the mixed layer evolution in the morning (Beyrich 1997). Lidars, on the other hand, cannot be applied in the case of low clouds because the backscatter from the cloud base is very strong and areas above the clouds cannot be seen. Recently, it was shown that mixed-layer height can also be reliably estimated with ceilometers, which are widespread to detect cloud base height, if the general shortcomings of lidar techniques are accepted (Münkel et al. 2007). Finally, mixed layer heights determined with remote techniques are in a good agreement with numerical simulations (Helmis et al. 2012).

2.6.2 Resistance Law

Analogue to the surface layer, similarity laws can also be derived for the boundary layer if the geostrophic wind speed u_g is factored in. Besides the roughness length, the Obukhov length and the Coriolis parameter the geostrophic drag coefficient u_*/u_g and the Rossby number,

$$Ro = \frac{u_g}{fz_0},$$

(2.143)

are the scaling parameters (here and in Eq. 2.146 u_g is the mean geostrophic wind velocity and not the component of the geostrophic wind in x-direction like in Eq. 2.11 and the following text). Thus type of scaling is called Rossby number similarity (Garratt 1992; Kraus 2008; Salby 2012; Hantel 2013). On this basis, Kazanski und Monin (1960, 1961) developed a stability parameter for the whole boundary layer

$$\mu = \frac{z_i}{L},$$

(2.144)

with the boundary layer height determined by

$$z_i = \frac{\kappa u_*}{f}$$

(2.145)

Furthermore, Kazanski und Monin (1960, 1961) formulated the so-called resistance law, which can be applied for the calculation of wind profiles:

$$\ln Ro = A - \ln \frac{u_*}{u_g} + \left[\frac{\kappa^2}{\left(u_*/u_g\right)^2} - B^2 \right]$$

(2.146)

For both horizontal wind components u_g und v_g (perpendicular to u_g) of the geostrophic wind follows:

$$\frac{u_g}{u_*} = \frac{1}{\kappa} \left(\ln \frac{u_*}{fz_0} - A \right)$$

(2.147)

$$\frac{v_g}{u_*} = \frac{B}{\kappa}$$

(2.148)

The coefficients A and B are functions of the stability parameter μ.

The resistance low was subject of intensive theoretical and experimental investigations in the 1960s and 1970s (Csanady 1967; Blackadar and Tennekes 1968; Clarke 1970; Wippermann and Yordanov 1972; Clarke and Hess 1974; Zilitinkevich 1970, 1975). Due to high uncertainties in the determination of A and

B and progress in numerical modeling techniques the resistance law is nowadays rarely discussed in textbook**s** (Blackadar 1997; Kraus 2008). More recently is has however again received attention in wind energy studies that require relatively simple methods to determine the wind profile and wind resource in the whole boundary layer (Gryning et al. 2007; Peña et al. 2010).

2.6.3 Integral Turbulence Characteristics

Integral turbulence characteristics can also be applied above the surface layer. For free convection ($z/L < -1$), scaling with the Deardorff velocity Eq. (2.42) and the mixed layer height, z_i, is necessary (Garratt 1992). Such parameterizations must show the decrease of the integral characteristics with increasing height as well as the increase in the entrainment layer. The following parameterizations were given by Sorbjan (1989, 2008):

$$\sigma_w/w_* = 1.08(z/z_i)^{1/3}(1 - z/z_i)^{1/3} \tag{2.149}$$

$$\sigma_\theta/T_* = 2(z/z_i)^{-2/3}(1 - z/z_i)^{4/3} + 0.94(z/z_i)^{4/3}(1 - z/z_i)^{-2/3} \tag{2.150}$$

References

Amiro BD (1990) Comparison of turbulence statistics within three boreal forest canopies. Boundary-Layer Meteorol. 51:99–121.

Andreas EL (1989) Two-wavelength method of measuring path-averaged turbulent surface heat fluxes. J Atm Oceanic Techn. 6:280–292.

Andreas EL (2002) Parametrizing scalar transfer over snow and ice: A review. J Hydrometeorol. 3:417–432.

Andreas EL, Claffey KJ, Fairall CW, Grachev AA, Guest PS, Jordan RE and Persson POG (2004) Measurements of the von Kármán constant in the atmospheric surface layer - further discussions. 16th Conference on Boundary Layers and Turbulence, Portland ME2004. Am. Meteorol. Soc., pp. 1–7, paper 7.2.

Arya SP (1999) Air Pollution Meteorology and Dispersion. Oxford University Press, New York, Oxford, 310 pp.

Arya SP (2001) Introduction to Micrometeorology. Academic Press, San Diego, 415 pp.

Beljaars ACM (1995) The parametrization of surface fluxes in large scale models under free convection. Quart J Roy Meteorol Soc. 121:255–270.

Berkowicz R and Prahm LP (1984) Spectral representation of the vertical structure of turbulence in the convective boundary layer. Quart J Roy Meteorol Soc. 110:35–52.

Bernhardt K-H (1995) Zur Interpretation der Monin-Obuchovschen Länge. Meteorol Z. 4:81–82.

Bernhardt K (1970) Der ageostrophische Massenfluß in der Bodenreibungsschicht bei beschle-unigungsfreier Strömung. Z Meteorol. 21:259–279.

Bernhardt K (1972) Vorlesung 'Dynamik der Atmosphäre'. Humboldt-Universität zu Berlin

Bernhardt K (1975) Some characteristics of the dynamic air-surface interaction in Central Europe. Z Meteorol. 25:63–68.

Bernhardt K (1980) Zur Frage der Gültigkeit der Reynoldsschen Postulate. Z Meteorol. 30:361–368.

Beyrich F (1997) Mixing height estimation from sodar data — A critical discussion. Atmos Environm. 31:3941–3953.

Beyrich F, Kouznetsov RD, Leps J-P, Lüdi A, Meijninger WML and Weisensee U (2005) Structure parameters for temperature and humidity from simultaneous eddy-covariance and scintillometer measurements. Meteorol Z. 14:641–649.

Beyrich F and Leps J-P (2012) An operational mixing height data set from routine radiosoundings at Lindenberg: Methodology. Meteorol Z. 21:337–348.

Blackadar AK and Tennekes H (1968) Asymptotic similarity in neutral barotropic planetary boundary layers. J Atmos Sci. 25:1015–1020.

Blackadar AK (1997) Turbulence and Diffusion in the Atmosphere. Springer, Berlin, Heidelberg, 185 pp.

Boussinesq J (1877) Essai sur la théorie des eaux courantes. Mem Savants Etrange. 23:46 pp.

Bowen IS (1926) The ratio of heat losses by conduction and by evaporation from any water surface. Phys Rev. 27:779–787.

Brocks K and Krügermeyer L (1970) Die hydrodynamische Rauhigkeit der Meeresoberfläche. Ber Inst Radiometeorol Marit Meteorol. 14:55 pp.

Buckingham E (1914) On physically similar systems; illustrations of the use of dimensional equations. Phys Rev. 4:345–376.

Busch NE, Chang SW and Anthes RA (1976) A Multi-Level Model of the Planetary Boundary Layer Suitable for Use with Mesoscale Dynamic Models. J Appl Meteorol. 15:909–919.

Businger JA and Yaglom AM (1971) Introduction to Obukhov's paper "Turbulence in an atmosphere with a non-uniform temperature". Boundary-Layer Meteorol. 2:3–6.

Businger JA, Wyngaard JC, Izumi Y and Bradley EF (1971) Flux-profile relationships in the atmospheric surface layer. J Atmos Sci. 28:181–189.

Businger JA (1982) Equations and concepts. In: Nieuwstadt FTM and Van Dop H (eds.), Atmospheric turbulence and air pollution modelling: A course held in The Hague, 21–25 September 1981. D. Reidel Publ. Co., Dordrecht, 1–36.

Businger JA (1986) Evaluation of the accuracy with which dry deposition can be measured with current micrometeorological techniques. J Appl Meteorol. 25:1100–1124.

Businger JA (1988) A note on the Businger-Dyer profiles. Boundary-Layer Meteorol. 42:145–151.

Charnock H (1955) Wind stress on water surface. Quart J Roy Meteorol Soc. 81:639–642.

Cheng Y and Bruntseart W (2005) Flux-profile relationships for wind speed and temperature in the stable atmospheric boundary layer. Boundary-Layer Meteorol. 114:519–538.

Clarke RH (1970) Observational studies in the atmospheric boundary layer. Quart J Roy Meteorol Soc. 96:91–114.

Clarke RH and Hess GD (1974) Geostrophic departure and the functions A and B of Rossby-number similarity theory. Boundary-Layer Meteorol. 7:267–287.

Corrsin S (1951) On the spectrum of isotropic temperature fluctuations in an isotropic turbulence. J Appl Phys. 22:469–473.

Csanady GT (1967) On the "resistance law" of a turbulent Ekman-Layer. J Atmos Sci. 24:467–471.

Davenport AG, Grimmond CSB, Oke TR and Wieringa J (2000) Estimating the roughness of cities and shelterred country. 12th Conference on Applied Climatology, Ashville, NC2000. American Meteorological Society, pp. 96–99.

Deardorff JW (1966) The counter-gradient heat flux in the lower atmosphere and in the laboratory. J Atmos Sci. 23:503–506.

Deardorff JW (1970) Convective Velocity and Temperature Scales for the Unstable Planetary Boundary Layer and for Rayleigh Convection. J Atmos Sci. 27:1211–1213.

Dyer AJ (1974) A review of flux-profile-relationships. Boundary-Layer Meteorol. 7:363–372.

ESDU (1972) Characteristics of wind speed in the lowest layers of the atmosphere near the ground: strong winds. Engl. Sci. Data Unit Ltd. Regent St., London, 35 pp.

Etling D (2008) Theoretische Meteorologie. Springer, Berlin, Heidelberg, 376 pp.

Foken T (1990) Turbulenter Energieaustausch zwischen Atmosphäre und Unterlage - Methoden, meßtechnische Realisierung sowie ihre Grenzen und Anwendungsmöglichkeiten. Ber Dt Wetterdienstes. 180:287 pp.

Foken T, Skeib G and Richter SH (1991) Dependence of the integral turbulence characteristics on the stability of stratification and their use for Doppler-Sodar measurements. Z Meteorol. 41:311–315.

Foken T, Jegede OO, Weisensee U, Richter SH, Handorf D, Görsdorf U, Vogel G, Schubert U, Kirzel H-J and Thiermann V (1997) Results of the LINEX-96/2 Experiment. Dt Wetterdienst, Forsch. Entwicklung, Arbeitsergebnisse. 48:75 pp.

Foken T (2006) 50 years of the Monin-Obukhov similarity theory. Boundary-Layer Meteorol. 119:431–447.

Garratt JR (1992) The Atmospheric Boundary Layer. Cambridge University Press, Cambridge, 316 pp.

Gryning S-E, Batchvarova E, Brümmer B, Jørgensen H and Larsen S (2007) On the extension of the wind profile over homogeneous terrain beyond the surface boundary layer. Boundary-Layer Meteorol. 124:251–268.

Handorf D, Foken T and Kottmeier C (1999) The stable atmospheric boundary layer over an Antarctic ice sheet. Boundary-Layer Meteorol. 91:165–186.

Hantel M (2013) Einführung Theoretische Meteorologie. Springer Spektrum, Berlin, Heidelberg, 430 pp.

Hasager CB and Jensen NO (1999) Surface-flux aggregation in heterogeneous terrain. Quart J Roy Meteorol Soc. 125:2075–2102.

Helmis CG, Sgouros G, Tombrou M, Schäfer K, Münkel C, Bossioli E and Dandou A (2012) A comparative study and evaluation of mixing-height estimation based on sodar-RASS, ceilometer data and numerical model simulations. Boundary-Layer Meteorol. 145:507–526.

Hill RJ, Clifford SF and Lawrence RS (1980) Refractive index and absorption fluctuations in the infrared caused by temperature, humidity and pressure fluctuations. J Opt Soc Am. 70:1192–1205.

Högström U (1974) A field study of the turbulent fluxes of heat water vapour and momentum at a 'typical' agricultural site. Quart J Roy Meteorol Soc. 100:624–639.

Högström U (1985) Von Kármán constant in atmospheric boundary flow: Reevaluated. J Atmos Sci. 42:263–270.

Högström U (1988) Non-dimensional wind and temperature profiles in the atmospheric surface layer: A re-evaluation. Boundary-Layer Meteorol. 42:55–78.

Högström U (1990) Analysis of turbulence structure in the surface layer with a modified similarity formulation for near neutral conditions. J Atmos Sci. 47:1949–1972.

Högström U (1996) Review of some basic characteristics of the atmospheric surface layer. Boundary-Layer Meteorol. 78:215–246.

Högström U, Hunt JCR and Smedman A-S (2002) Theory and measurements for turbulence spectra and variances in the atmospheric neutral surface layer. Boundary-Layer Meteorol. 103:101–124.

Højstrup J (1981) A simple model for the adjustment of velocity spectra in unstable conditions downstream of an abrupt change in roughness and heat flux. Boundary-Layer Meteorol. 21:341–356.

Holzworth GC (1964) Estimates of mean maximum mixing depth in the contiguous United States. Monthly Weather Review. 92:235–242.

Holzworth GC (1967) Mixing depths, wind speeds and air pollution potential for selected locations in the United States. J Appl Meteorol. 6:1039–1044.

Jacobson MZ (2005) Fundamentals of Atmospheric Modelling. Cambridge University Press, Cambridge, 813 pp.

Johansson C, Smedman A, Högström U, Brasseur JG and Khanna S (2001) Critical test of Monin-Obukhov similarity during convective conditions. J Atmos Sci. 58:1549–1566.

Kader BA and Yaglom AM (1972) Heat and mass transfer laws for fully turbulent wall flows. Int J Heat Mass Transfer. 15:2329–2350.

Kaimal JC, Wyngaard JC, Izumi Y and Coté OR (1972) Spectral characteristics of surface layer turbulence. Quart J Roy Meteorol Soc. 98:563–589.

Kaimal JC and Finnigan JJ (1994) Atmospheric Boundary Layer Flows: Their Structure and Measurement. Oxford University Press, New York, NY, 289 pp.

Kantha LH and Clayson CA (2000) Small scale processes in geophysical fluid flows. Academic Press, San Diego, 883 pp.

Kazanski AB and Monin AS (1960) A turbulent regime above the surface atmospheric layer (in Russian). Izv AN SSSR, ser Geofiz. 1:165–168.

Kazanski AB and Monin AS (1961) On the dynamical interaction between the atmosphere and the Earth's surface (in Russian). Izv AN SSSR, ser Geofiz. 5:786–788.

Kitajgorodskij SA and Volkov JA (1965) O rascete turbulentnych potokov tepla i vlagi v privodnom sloe atmosfery (The calculation of the turbulent fluxes of temperature and humidity in the atmosphere near the water surface) Izv AN SSSR, Fiz Atm Okeana. 1:1317–1336.

Kitajgorodskij SA (1976) Die Anwendung der Ähnlichkeitstheorie für die Bearbeitung der Turbulenz in der bodennahen Schicht der Atmosphäre. Z Meteorol. 26:185–204.

Kohsiek W (1982) Measuring C_T^2, C_Q^2, and C_{TQ} in the unstable surface layer, and relations to the vertical fluxes of heat and moisture. Boundary-Layer Meteorol. 24:89–107.

Kolmogorov AN (1941a) Rassejanie energii pri lokolno-isotropoi turbulentnosti (Dissipation of energy in locally isotropic turbulence). Dokl AN SSSR. 32:22–24.

Kolmogorov AN (1941b) Lokalnaja struktura turbulentnosti v neschtschimaemoi schidkosti pri otschen bolschich tschislach Reynoldsa (The local structure of turbulence in incompressible viscous fluid for very large Reynolds numbers). Dokl AN SSSR. 30:299–303.

Kondo J and Sato T (1982) The determination of the von Kármán constant. J Meteor Soc Japan. 60:461–471.

Kramm G and Herbert F (2009) Similarity hypotheses for the atmospheric surface layer expressed by non-dimensional characteristic invariants – A review Open Atmos Sci J. 3:48–79.

Kraus H (2004) Die Atmosphäre der Erde. Springer, Berlin, Heidelberg, 422 pp.

Kraus H (2008) Grundlagen der Grenzschichtmeteorologie. Springer, Berlin, Heidelberg, 211 pp.

Lettau HH (1957) Windprofil, innere Reibung und Energieumsatz in den untersten 500 m über dem Meer. Beitr Phys Atm. 30:78–96.

Lumley JL and Panofsky HA (1964) The structure of atmospheric turbulence. Interscience Publishers, New Yotk, 239 pp.

Monin AS and Obukhov AM (1954) Osnovnye zakonomernosti turbulentnogo peremesivanija v prizemnom sloe atmosfery (Basic laws of turbulent mixing in the atmosphere near the ground). Trudy Geofiz inst AN SSSR. 24 (151):163–187.

Monin AS and Yaglom AM (1973) Statistical Fluid Mechanics: Mechanics of Turbulence, Volume 1. MIT Press, Cambridge, London, 769 pp.

Monin AS and Yaglom AM (1975) Statistical Fluid Mechanics: Mechanics of Turbulence, Volume 2. MIT Press, Cambridge, London, 874 pp.

Münkel C, Eresmaa N, Räsänen J and Karppinen A (2007) Retrieval of mixing height and dust concentration with lidar ceilometer. Boundary-Layer Meteorol. 124:117–128.

Obukhov AM (1946) Turbulentnost' v temperaturnoj - neodnorodnoj atmosfere (Turbulence in an atmosphere with a non-uniform temperature). Trudy Inst Theor Geofiz AN SSSR 1:95–115.

Obukhov AM (1949) Struktura temperaturnogo polja v turbulentnom potoke (Structure of the temperature field in the turbulent stream). Izv AN SSSR, ser geogr geofiz. 13:58–69.

Oncley SP, Friehe CA, Larue JC, Businger JA, Itsweire EC and Chang SS (1996) Surface-layer fluxes, profiles, and turbulence measurements over uniform terrain under near-neutral conditions. J Atmos Sci. 53:1029–1054.

Paeschke W (1937) Experimentelle Untersuchungen zum Rauhigkeitsproblem in der bodennahen Luftschicht. Z Geophys. 13:14–21.

Pandolfo JP (1966) Wind and temperature profiles for constant-flux boundary layers in lapse conditions with a variable eddy conductivity to eddy viscosity ratio. J Atmos Sci. 23:495–502.

Panofsky HA (1963) Determination of stress from wind and temperature measurements. Quart J Roy Meteorol Soc. 89:85–94.

Panofsky HA, Tennekes H, Lenschow DH and Wyngaard JC (1977) The characteristics of turbulent velocity components in the surface layer under convective conditions. Boundary-Layer Meteorol. 11:355–361.

Panofsky HA and Dutton JA (1984) Atmospheric Turbulence - Models and Methods for Engineering Applications. John Wiley and Sons, New York, 397 pp.

Paulson CA (1970) The mathematical representation of wind speed and temperature profiles in the unstable atmospheric surface layer. J Climate Appl Meteorol. 9:857–861.

Peltier LJ, Wyngaard JC, Khanna S and Brasseur JG (1996) Spectra in the unstable surface layer. J Atmos Sci. 53:49–61.

Peña A, Gryning S-E and Hasager C (2010) Comparing mixing-length models of the diabatic wind profile over homogeneous terrain. Theor Appl Climat. 100:325–335.

Prandtl L (1925) Bericht über Untersuchungen zur ausgebildeten Turbulenz. Z Angew Math Mech. 5:136–139.

Pruitt WO, Morgan DL and Lourence FJ (1973) Momentum and mass transfer in the surface boundary layer. Quart J Roy Meteorol Soc. 99:370–386.

Reithmaier LM, Göckede M, Markkanen T, Knohl A, Churkina G, Rebmann C, Buchmann N and Foken T (2006) Use of remotely sensed land use classification for a better evaluation of micrometeorological flux measurement sites. Theor Appl Climat. 84:219–233.

Roll HU (1948) Wassernahes Windprofil und Wellen auf dem Wattenmeer. Ann Meteorol. 1:139–151.

Salby ML (2012) Physics of the Atmosphere and Climate. Cambridge University Press, Cambridge, 666 pp.

Schlichting H and Gersten K (2003) Boundary-Layer Theory. McGraw Hill, New York, XXIII, 799 pp.

Schmitz-Peiffer A, Heinemann D and Hasse L (1987) The ageostrophic methode - an update. Boundary-Layer Meteorol. 39:269–281.

Seibert P, Beyrich F, Gryning S-E, Joffre S, Rasmussen A and Tercier P (2000) Review and intercomparison of operational methods for the determination of the mixing height. Atmos Environm. 34:1001–1027.

Skeib G (1980) Zur Definition universeller Funktionen für die Gradienten von Windgeschwindigkeit und Temperatur in der bodennahen Luftschicht. Z Meteorol. 30:23–32.

Smedman A-S (1991) Some turbulence characteristics in stable atmospheric boundary layer flow. J Atmos Sci. 48:856–868.

Sonntag D (1990) Important new values of the physical constants of 1986, vapour pressure formulations based on the ITC-90, and psychrometer formulae. Z Meteorol. 40:340–344.

Sorbjan Z (1989) Structure of the Atmospheric Boundary Layer. Prentice Hall, New York, 317 pp.

Sorbjan Z (2008) Gradient-based similarity in the atmospheric boundary layer. Acta Geophys. 56:220–233.

Sreenivasan KR (1995) On the universality of the Kolmogorov constant. Phys Fluids. 7:2778–2784.

Sreenivasan KR (1996) The passive scalar spectrum and the Obukhov–Corrsin constant. Phys Fluids. 8:189–196.

Stull RB (1984) Transilient turbulence theorie, Part 1: The concept of eddy mixing across finite distances. J Atmos Sci. 41:3351–3367.

Stull RB (1988) An Introduction to Boundary Layer Meteorology. Kluwer Acad. Publ., Dordrecht, Boston, London, 666 pp.

Stull RB (2000) Meteorology for Scientists and Engineers. Brooks/Cole, Pacific Grove, 502 pp.

Tatarski VI (1961) Wave Propagation in a Turbulent Medium. McGraw-Hill, New York, 285 pp.

Taylor GI (1938) The spectrum of turbulence. Proceedings Royal Society London. A 164:476–490.

Tennekes H (1982) Similarity relations, scaling laws and spectral dynamics. In: Nieuwstadt FTM and Van Dop H (eds.), Atmospheric turbulence and air pollution modelling. D. Reidel Publ. Comp., Dordrecht, Boston, London, 37–68.

Thomas C and Foken T (2002) Re-evaluation of integral turbulence characteristics and their parameterisations. 15th Conference on Turbulence and Boundary Layers, Wageningen, NL, 15–19 July 2002. Am. Meteorol. Soc., pp. 129-132.

Tillman JE (1972) The indirect determination of stability, heat and momentum fluxes in the atmospheric boundary layer from simple scalar variables during dry unstable conditions. J Climate Appl Meteorol. 11:783–792.

Troen I and Lundtang Peterson E (1989) European Wind Atlas. Risø National Laboratory, Roskilde, 656 pp.

Troen IB and Mahrt L (1986) A simple model of the atmospheric boundary layer; sensitivity to surface evaporation. Boundary-Layer Meteorol. 37:129–148.

Wieringa J (1980) A revaluation of the Kansas mast influence on measurements of stress and cup anemometer over speeding. Boundary-Layer Meteorol. 18:411–430.

Wieringa J (1992) Updating the Davenport roughness classification. J Wind Eng Industry Aerodyn. 41:357–368.

Wippermann F and Yordanov D (1972) A note on the Rossby similarity for flows of barotropic planetary boundary layers. Beitr Phys Atm. 45:66–71.

Wyngaard JC, Coté OR and Izumi Y (1971a) Local free convection, similarity and the budgets of shear stree and heat flux. J Atmos Sci. 28:1171–1182.

Wyngaard JC and Coté OR (1971) The budgets of turbulent kinetic energy and temperature variance in the atmospheric surface layer. J Atmos Sci. 28:190–201.

Wyngaard JC, Izumi Y and Collins SA (1971b) Behavior of the refractive-index-structure parameter near the ground. J Opt Soc Am. 61:1646–1650.

Wyngaard JC (1973) On surface layer turbulence. In: Haugen DH (ed.), Workshop on Micrometeorology. Am. Meteorol. Soc., Boston, 101–149.

Wyngaard JC (2010) Turbulence in the Atmosphere. Cambridge University Press, Cambridge, 393 pp.

Yaglom AM (1977) Comments on wind and temperature flux-profile relationships. Boundary-Layer Meteorol. 11:89–102.

Yaglom AM (1979) Similarity laws for constant-pressure and pressure-gradient turbulent wall flow. Ann Rev Fluid Mech. 11:505–540.

Zilitinkevich SS and Tschalikov DV (1968) Opredelenie universalnych profilej skorosti vetra i temperatury v prizemnom sloe atmosfery (Determination of universal profiles of wind velocity and temperature in the surface layer of the atmosphere). Izv AN SSSR, Fiz Atm Okeana. 4:294–302.

Zilitinkevich SS (1969) On the computation of the basic parameters of the interaction between the atmosphere and the ocean. Tellus. 21:17–24.

Zilitinkevich SS (1970) Dinamika pogranichnogo sloia atmosfery (Dynamics of the atmospheric boundary layer). Gidrometeorologicheskoe Izdatelstvo, Leningrad pp.

Zilitinkevich SS (1975) Resistance laws and prediction equations for the depth of the planetary boundary layer. J Atmos Sci. 32:741–752.

Zilitinkevich SS, Perov VL and King JC (2002) Near-surface turbulent fluxes in stable stratification: Calculation techniques for use in general circulation models. Quart J Roy Meteorol Soc. 128:1571–1587.

Chapter 3
Specifics of the Near-Surface Turbulence

The equations given in Chap. 2 describe atmospheric turbulence near the surface for ideal conditions such as horizontally homogeneous surfaces free of obstacles, steady-state conditions, and others. Such conditions are rarely found in the nature, since the Earth's surface is never completely flat and surface properties vary. Furthermore, all processes are not steady-state because of changing cloudiness and the diurnal cycle of irradiation. In this chapter, the properties of a vegetated and heterogeneous surface and its influences on the exchange process are described. Because these effects are substantial, they must be taken into account in all measurements and modelling efforts of atmospheric turbulence.

3.1 Properties of the Underlying Surface

Underlying surfaces are distinguished according to their thermal properties, roughness, canopy height and other obstacles, and unevenness. For low vegetation, the surface can be approximated as a porous sponge-like layer, which can be described by simple mathematical equations. The results do not differ significantly from the results described in previous chapters. Much more complicated to handle are obstacles and tall vegetation. Therefore, a special paragraph on this subject is included in this chapter.

3.1.1 Roughness—Additional Remarks

As illustrated in Fig. 3.1, there are two different ways to determine roughness: the determination of the geometric surface structure, and the calculation of the
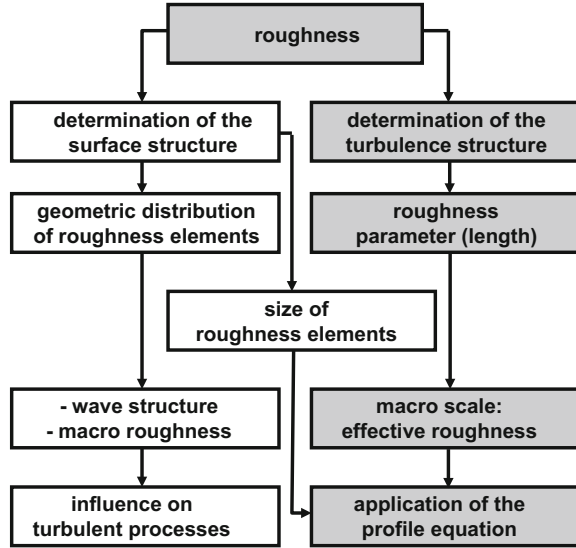
roughness from the turbulence near the surface. There have been many investigations of both methods, but the second way has the highest practical relevance.

The possibility of the determination of the surface roughness as an integration constant of the profile equation Eq. (2.47) for neutral conditions Eq. (2.60) was shown in Sect. 2.3.2 with the roughness length z_0 (Table 2.7). Principally the method can also be applied on the profile equation for more complex landscapes, towns and others, which are higher than the surface layer. These heights are called effective roughness (Fiedler and Panofsky 1972). Such heights are 0.42 m for flat terrain, 0.99 m for low hills, and 1.42 m for high hills. Effective roughness lengths are used in connection with the *blending-height*-concept (see Sect. 3.2.4) and area averaging (see Sect. 5.8).

If the roughness length values in Table 2.7 are not accurate enough, then estimates of the roughness length can be made using wind measurements at different levels (see Sect. 4.1.2). From a log–linear plot analogous to Fig. 2.5, the roughness length can be determined for neutral stratification. In the case of low roughness (ice or water) this method can be very inaccurate, because small errors in the measurements of the wind velocity can cause large changes in the estimated roughness length. This is the reason for the large scatter in the reported roughness lengths over water.

Panofsky (1984), proposed an interesting way of determining the roughness length using the integral turbulence characteristics or turbulence intensities. From the combination of Eqs. (2.60) and (2.104) for neutral stratification, one gets:

$$\frac{\sigma_w}{\overline{u}} = \frac{1.25\,\kappa}{\ln(z/z_0)} \tag{3.1}$$

A more exact method is to use the morphological determination of the roughness from the surface structures. For solid surfaces, this method was used for a long time in hydrodynamics where the roughness elements are exactly measured. In hydrodynamic investigations, the so-called equivalent sand roughness k_s according to Nikuradse (1933) is applied, which can be determined in a way analogous to the profile method Eq. (2.60) with the integration constant B of about 2.5:

$$u(z) = \frac{u_*}{\kappa} \ln \frac{z}{k_s} + B \tag{3.2}$$

This method is the connection between the exact determination of the surface structures and the application of the profile equation. Errors in the determination of the surface structure and the influence of stratification are transferred into the integration constant B. This method has been used mostly in wind tunnel experiments (Raupach 1992); however, in urban meteorology it is a good method to estimate and classify roughness (Lettau 1969; Grimmond and Oke 1999; Grimmond and Oke 2000).

In some applications, roughness parameters based on the statistical distribution of the roughness elements have been used. One example is the replacement of the roughness length in the roughness-Reynolds-number

$$\mathrm{Re}_s = \frac{z_0 \cdot u_*}{\nu} \tag{3.3}$$

with the standard deviation of the height of water waves (Kitajgorodskij and Volkov 1965), which was used successfully by Russian scientists. A further example is the so-called macro roughness which is based on the standard deviation of the topography or geometric structures within a certain horizontal scale (Zelený and Pretel 1986), a first step towards the footprint calculation. For both cases, a direct connection with the profile equation is not possible, but e.g. integral turbulence characteristics have significant correlations with these parameters.

For real land surfaces, estimating roughness parameters is complicated because landscapes are often complex, and do not have uniform roughness which is comparable with the data given in Table 2.7. A further complication is that single roughness elements such as trees can have a significant influence on the roughness of the area. Furthermore, it is impossible to calculate a simple area-average roughness from the roughness of individual regions because Eq. (2.48) is non-linear. For example, an area comprised of 50% bush land and 50% open water is on average a bush land with a lower surface roughness length. The wind field calculated with this new roughness length will not be representative of the smooth water surface. In spite of these findings, the arithmetic averaging is still widely applied in modelling. This is

because the heterogeneity of the landscape exists on spatial scales that are smaller than the grid size of most of the models (see Sect. 5.8).

The determination of surface roughness for wind power applications is of high practical significance. Therefore, for the European Wind Atlas an averaging scheme

Table 3.1 Averaging scheme for the mean roughness length z_0^R in the European Wind Atlas (Troen and Lundtang Peterson 1989). In the table, the different portions of the roughness classes 0–3 to the whole study area are given

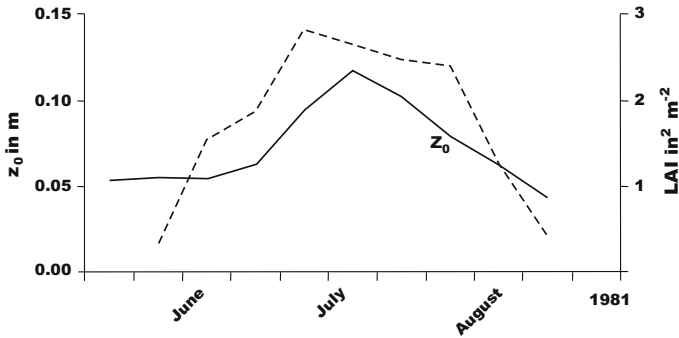| Type	0	1	2	3	z_0^R
z_0 in m	0.0002	0.03	0.1	0.4	in m
	3	1			0.001
	3		1		0.002
	3			1	0.003
	2	2			0.004
	2	1	1		0.006
	2	1		1	0.010
	2				0.009
	2		1	1	0.015
	2			2	0.025
	1	3			0.011
	1	2	1		0.017
	1	2		1	0.027
	1	1	2		0.024
	1	1	1	1	0.038
	1	1		2	0.059
	1		3		0.033
	1		2	1	0.052
	1		1	2	0.079
	1			3	0.117
		3	1		0.042
		3		1	0.064
		2	2		0.056
		2	1	1	0.086
		2		2	0.127
		1	3		0.077
		1	2	1	0.113
		1	1	2	0.163
		1		3	0.232
			3	1	0.146
			2	2	0.209
			1	3	0.292

Fig. 3.2 Change of the roughness length and the leaf-area index (*LAI*) during the growth of a corn field according to Hurtalová et al. (1983), added by data given by Hurtalova et al. (1988). Adapted with kind permission of © WILEY-VCH Verlag Weinheim 1983, All rights reserved

was developed (Troen and Lundtang Peterson 1989) which takes into account the non-linear character of averaging and integrating low roughness surfaces into the area roughness. For simplicity, the authors classify only four types (0–3) of surface roughness (class 0: water; class 1: open landscape with flat meadows; class 2: croplands with bushes; class 3: forest and suburban). The whole area is divided into quarters; then depending on the combination of the surfaces of each quarter a mean surface roughness is determined as in Table 3.1. This is a special form of parameter averaging, which is described in more detail in Sect. 5.8.1. The calculation must be done for the windward side of the wind turbine. More sophisticated approaches use flux averaging so that the roughness distributions can be determined, e.g., by remote sensing (Hasager and Jensen 1999). The application of footprint models makes this application more objective (Foken 2013).

Specifics of the determination of the roughness length over water were already shown in Sect. 2.3.2. For the case of roughness calculations over vegetated land, the annual change of foliage and the growth of plants must also be taken into account. An example of these changes is given in Fig. 3.2.

3.1.2 Zero-Plane Displacement—Additional Remarks

In addition to the arguments given in Sect. 2.3.2, the determination of the zero-plane displacement for high vegetation or vegetation with changing density and for urban areas is described thereafter.

Table 3.2 Dependence of the ratio of zero-plane displacement and canopy height on the canopy density for a winter wheat field (Koitzsch et al. 1988)

Canopy density stems with ears m^{-2}	Canopy height in m	Ratio d/z_B
390	0.80	0.60
660	0.97	0.73
570	0.40	0.76

The relation between zero-plane displacement and canopy height is independent of the plant species, but changes during the growth of the plants (Table 3.2). There are also approaches available which include the plant cover (Raupach 1994).

There is a wind-velocity dependence caused by the changing of the canopy structure with wind speed (Marunitsch 1971). For low wind velocities over the forest, the ratio d/z_B increases up to values of about 0.8, while for high wind velocities values of about 0.5 are found. In the opposite way, the ratio z_0/z_B changes from about 0.01 to 0.2. It is recommended to use zero-plane displacements which are variable in time (Maurer et al. 2015).

Of great difficulty, is the determination of the canopy height. This is because the top of the canopy often has a non-uniform height, and the highest parts of the canopy have a disproportionably large influence on the roughness (Foken 1990). It is therefore recommended to determine the canopy height as well as the roughness length using the largest canopy heights or roughness lengths covering 10% of the area.

For a more exact determination of the zero-plane displacement, it is necessary to measure the friction velocity using the eddy-covariance method (see Sect. 4.1) and the wind profile above the canopy. With an iterative model, the zero-plane displacement is varied until the friction velocity of the profile method is equal to the friction velocity from the eddy-covariance. For high vegetation the influence of the roughness sublayer must be taken into account (see Sect. 3.5.3).

The determination of the zero-plane displacement height for an urban surface is more complicated. Widely used are morphometric methods (Grimmond and Oke 1999) where the roughness length and the zero-plane displacement are calculated as simple fractions of the average height $\overline{z_H}$ of the buildings:

$$d = f_d \, \overline{z_H}, \quad z_0 = f_o \, \overline{z_H}, \tag{3.4}$$

with $f_d = 0.67$ and $f_0 = 0.1$ or alternatively $f_d = 0.8$ for densely built-up cities (Roth et al. 2006).

Another method was proposed by MacDonald et al. (1998) which uses also the density of the buildings as well as the mean building height

$$d = \overline{z_H}\left[1 + \alpha^{-\lambda_P}(\lambda_P - 1)\right], \tag{3.5}$$

with the empirical coefficient $\alpha = 4.43$ and λ_P the plan areal fraction calculated as the fraction of the total area that is built up.

Another approach was introduced by Raupach (1994), which uses the frontal areal index λ_F

$$d = \overline{z_H}\left(1 - \frac{1 - e^{-\sqrt{c_{d1}\lambda_F}}}{\sqrt{c_{d1}\lambda_F}}\right) \tag{3.6}$$

with the empirical coefficient $c_{d1} = 7.5$.

The experimental determination of the zero-plane displacement height in an urban area is principally possible from profile and flux measurements as described above. More simple is the use of two scintillometers (see Sect. 6.2.5) placed at two different heights. Applying the constant flux layer assumption for the sensible heat flux and the friction velocity the displacement height can be determined (Kanda et al. 2002).

3.1.3 Profiles in Plant Canopies

Meteorological measurements within low plant canopies are very rare because they cannot be made with the usual measurement techniques without disturbing the canopy. Temperature measurements are very costly because of the difficulties in measuring temperature without a radiation error (see Sect. 6.2.3). An introduction to the principle structures of temperature, wind speed, relative humidity, water vapour pressure, and the saturation deficit are given in Fig. 3.3.

Fig. 3.3 Profiles of different meteorological elements in a dense grass canopy on a sunny day in June, 3–4 p.m., in Scotland (Adapted from Waterhouse 1955, with kind permission of © Royal Meteorological Society Reading 1955, All rights reserved)
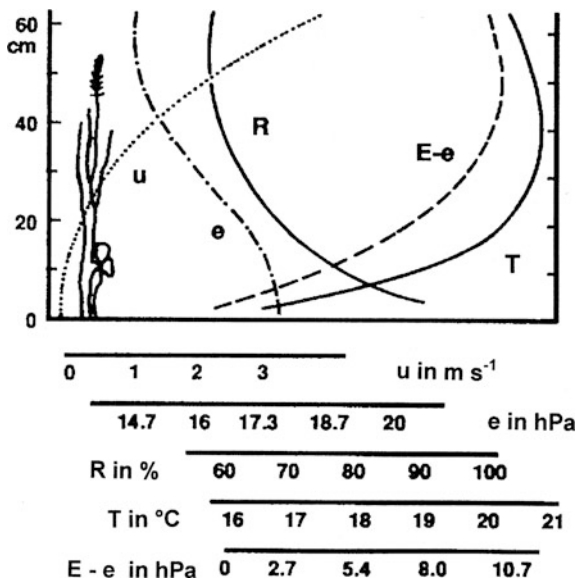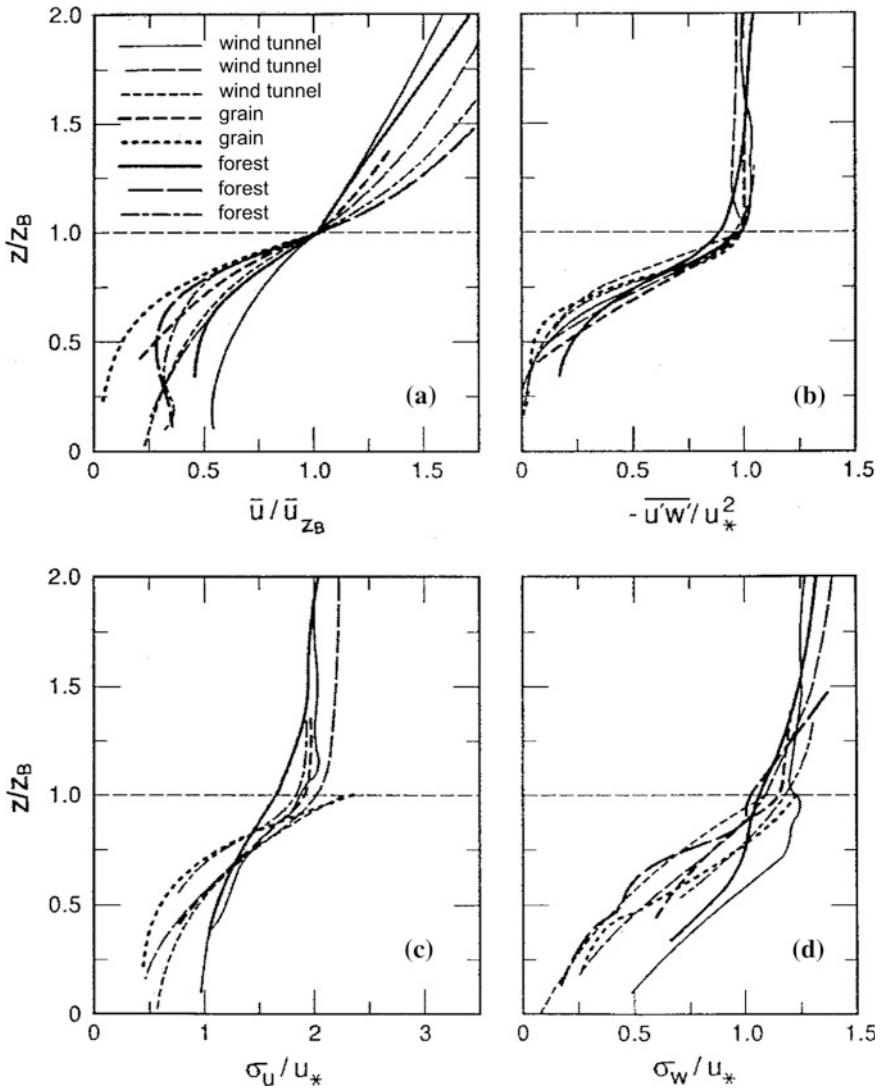
Fig. 3.4 Profiles of the mean wind velocity, the friction velocity and the standard deviations of the horizontal and vertical wind velocity normalized with their values at the canopy height according to different authors (Adapted from Kaimal and Finnigan 1994, with kind permission of © Oxford University Press New York 1994, All rights reserved)

By normalizing the profiles of turbulence parameters with their mean values at the canopy height, the profiles become very similar regardless of the character of the surface, i.e. obstacles in a wind tunnel, low vegetation, or forest (Fig. 3.4). For the determination of the wind profile, exponential expressions are used with coefficients dependent on the plant species and the leaf-area index:

Table 3.3 Values of the profile parameter of the wind profile within the plant canopy in Eq. (3.8)

Plant canopy	Profile parameter α	References
Wheat	2.45	Cionco (1978)
	1.6	Brunet et al. (1994)
Corn	1.97	Cionco (1978)
	2.4	Shaw et al. (1974)
	4.1	Wilson et al. (1982)
Rice	1.62	Cionco (1978)
Sun flowers	1.32	Cionco (1978)
Larch tree plantation	1.00	Cionco (1978)
Fruit plantation	0.44	Cionco (1978)
Forest. 20 m high	1.7	Denmead and Bradley (1987)

$$\overline{u(z)} = \overline{u(z_B)}\, e^{\alpha(z/z_B - 1)}, \tag{3.7}$$

with the canopy height z_B. Table 3.3 contains the values of profile coefficient, α, for different plant canopies (Cionco 1978). An explicit expression for α was given by Goudriaan (1977) and cited by Campbell and Norman (2013),

$$\alpha \cong \left(\frac{0.2\ LAI\ z_B}{l_m} \right), \tag{3.8}$$

where *LAI* is the leaf-area index, l_m is the mean separation of leaves. For plant physiological investigations, the distribution of light is important in the calculation of photosynthesis. Relevant contributions to this topic were made by Ross (1981), Jones (2013). For physiological details see Hari et al. (2013).

3.2   Internal Boundary Layers

3.2.1   Definition

The statements so far are based on the assumption of a homogeneous surface. More typical for our landscapes are heterogeneous surfaces with a change in the surface characteristics within about 100 m. In Fig. 3.5, it is shown that a complicated flow system is developing above such an inhomogeneous surface. The reason is that over each surface a wind profile is generated dependent on the surface roughness or a temperature profile dependent on the surface temperature. Due to the horizontal wind field the different profiles are shifted downwind forming a layer of discontinuity, which is called an internal boundary layer. Therefore, neighbouring areas can also affect the exchange of energy and matter above a different downwind area. The internal boundary layers are caused by different surface roughness and different
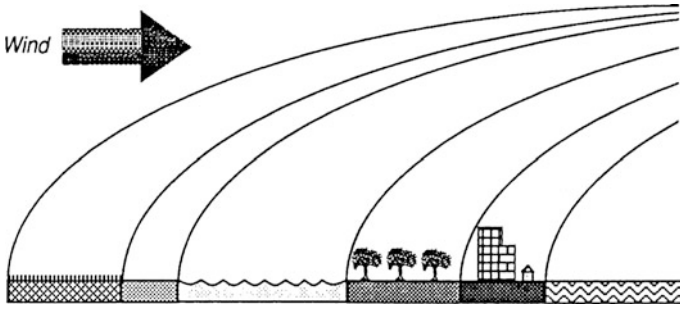
Fig. 3.5 Generation of internal boundary layers above an inhomogeneous surface (Adapted from Stull 1988, with kind permission of © Kluwer Academic Publisher B.V. Dordrecht 1988, All rights reserved)

source areas of surface temperature, moisture etc. Internal boundary layers can be found for neutral, stable, and unstable stratifications. In the case of free convection, the exchange process is more vertically dominated.

> Internal boundary layers are significantly developed disturbance layers in the near-surface layer, which are generated by horizontal advection over discontinuities of the surface properties (roughness, thermal properties, etc.).

The internal boundary layer is sometimes composed of several layers each with a different thickness. The layer below the discontinuity layer is called new equilibrium layer (NEL). Their properties come from the new surface. Above the discontinuity layer (internal boundary layer, IBL) the layer is influenced by the surface upwind of the site (Fig. 3.6). Relevant to the development of mechanical internal boundary layers are the roughness lengths upwind and downwind of the site of a sudden change of the surface roughness and the friction velocities related to the wind field on both sides of the change. The height of the internal boundary layer depends on the fetch (distance to the roughness change). For large fetches the

Fig. 3.6 Schematic structure of the internal boundary layer at a sudden change of the surface roughness according to Rao et al. (1974)
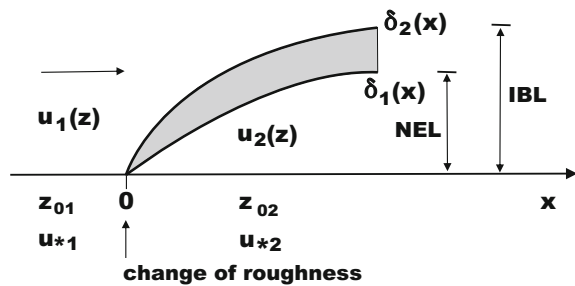
differences between both sides of an internal boundary layer decreases. Overviews are given by Stull (1988), Garratt (1990, 1992), Savelyev and Taylor (2001, 2005).

Figure 3.6 illustrates that the internal boundary layer includes a large transition layer above the new equilibrium layer. To determine the height δ of the internal boundary layer several methods are available.

In the simplest case, the height of an internal boundary layer can be determined by extrapolation of the wind profiles from both sides of the internal boundary layer (Elliott 1958; Raabe 1983):

$$u_1(\delta) = u_2(\delta) \tag{3.9}$$

This method has the disadvantage that the point of intersection may be outside the internal boundary layer.

More successful is the assumption that if the undisturbed wind profiles can be measured below and above the internal boundary layer, than the point of intersection is taken to be the height of the internal boundary layer:

$$\delta = \frac{\delta_1 + \delta_2}{2} \tag{3.10}$$

This method is nearly identical with the determination of the height of the internal boundary layer as the height of the inflection point of the wind profile (Logan and Fichtl 1975).

The height of the internal boundary layer can also be determined by the change of the friction velocity (Peterson 1969; Taylor 1969; Shir 1972; Savelyev and Taylor 2001):

$$z = \delta \quad \text{for} \quad \frac{u_*(x, z) - u_{*1}}{u_{*2} - u_{*1}} < c \sim 0.1 \tag{3.11}$$

Equation (3.11) is often used by modellers. It should be mentioned that the internal boundary layer defined this way is higher than those derived from wind profiles (Shir 1972).

For practical reasons, it is useful to use the lower level of the layer of disturbances as the height of the internal boundary layer, $\delta = \delta_1$, because the new equilibrium layer can be assumed as undisturbed above the new surface (Rao et al. 1974), and is therefore relevant for making measurements.

Mechanical internal boundary layers occur for flow from rough to smooth or from smooth to rough surfaces. Because of the different wind gradients above smooth and rough surfaces, there are characteristic forms of internal boundary layers as shown in Fig. 3.7. This figure further illustrates the currently most widely applied methods (Savelyev and Taylor 2005) to determine the height of the internal boundary layer according to the layered structure shown in Fig. 3.6 (Rao et al. (1974) or from the inflection point of the wind profile (Logan and Fichtl 1975).
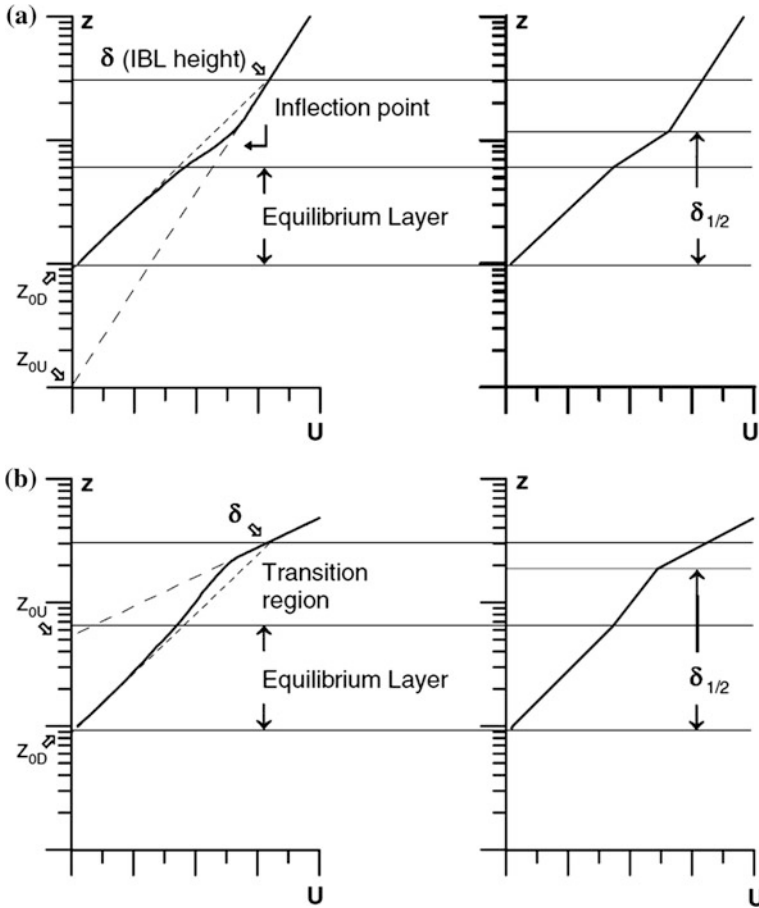
Fig. 3.7 The wind profile at an internal boundary layer for neutral stratification for **a** for roughness change from smooth to rough, **b** from rough to smooth, for the layered structure of the internal boundary layer (*left*) and definition of the height of the internal boundary layer using the wind-profile inflection point (*right*) according to Savelev and Taylor (2005), published with kind permission of © Springer Berlin Heidelberg 2005, All rights reserved

The classical model for the height of an internal boundary layer based on Eq. (2.60) was given by Elliott (1958):

$$\delta_{\text{Elliott}} = z_{02} \left(\frac{z_{01}}{z_{02}} \right)^{1/(1-R)} \quad \text{with} \quad R = u_{*2}/u_{*1} \tag{3.12}$$

Current parameterizations give a value that is multiplied by the base of the natural logarithm. i.e.

$$\delta \approx \mathrm{e}\, \delta_{\mathrm{Elliott}} \tag{3.13}$$

These parameterizations are also based on Eq. (2.60) and lead to Radikevitsch (1971), Logan and Fichtl (1975):

$$\frac{u_{*2}}{u_{*1}} = 1 \;-\; \frac{\ln \frac{z_{01}}{z_{02}}}{\ln \frac{\delta}{z_{01}}} \tag{3.14}$$

The height of an internal boundary layer as a function of fetch was found in hydrodynamical investigations, and is given by a 4/5-exponential law (Shir 1972; Garratt 1990; Savelyev and Taylor 2001):

$$\delta = f_1\!\left(z_{01}/z_{02}\right) x^{4/5 + f_2\left(z_{01}/z_{02}\right)} \tag{3.15}$$

3.2.2 Experimental Findings

There are many experimental results available about internal boundary layers, but more fundamental experiments which could update our present models and parameterizations in a more physical way are missing (Garratt 1990; Raabe 1991). Consequently classical experiments, such as Bradley (1968), are still used for model comparisons (Fig. 3.8). The first experimental investigations in nature were

Fig. 3.8 Ratio of the friction velocities on both sides of a sudden roughness change (Adapted from Bradley 1968, with kind permission of © Royal Meteorological Society Reading 1968, All rights reserved)
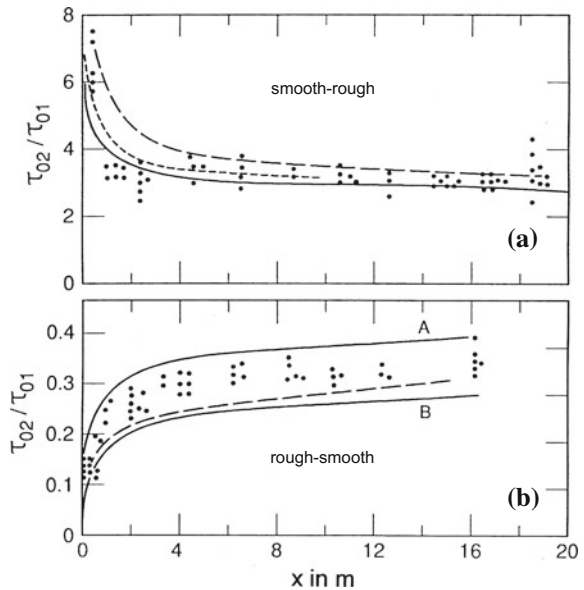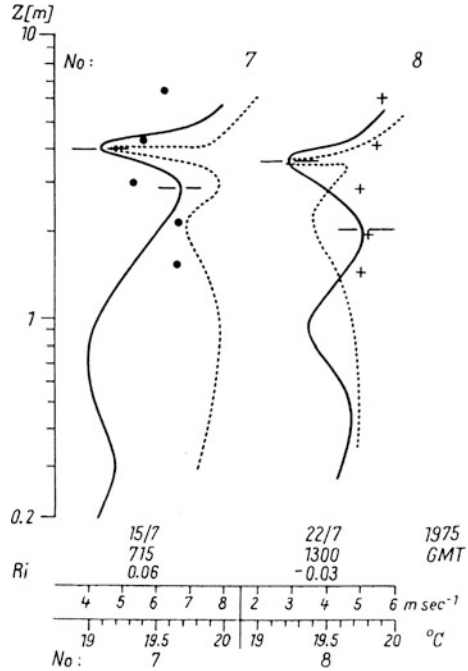
made by Taylor (1969), Peterson (1969) in a coastal zone. An example (Fig. 3.9) of
the difficulties in the experimental evaluation is given by measurements made with
an ascending and descending probe by Hupfer et al. (1976). Their high-resolution
temperature and wind profile measurements showed a narrow internal boundary
layer, which cannot be found in the mean wind profile.

A number of experiments were done to determine the heights of either the
internal boundary layer or the new equilibrium layer using an equation comparable
to Eq. (3.15). At this time, the influences on the IBL height of the stratification,
which increases the exponent from 0.8 to 1.4 according Rao et al. (1974), and the
possible differences in the transitions from smooth to rough or from rough to
smooth are not yet determined. Garratt (1990) assumed a greater increase of the IBL
height in the case of the transition from smooth to rough than from rough to
smooth. A comprehensive overview of all known relationships is given by Savelyev
and Taylor (2005). Because of the large scatter of the results from all experiments,
most authors assume a simplified relation

$$\delta = a \, x^b \tag{3.16}$$

instead of Eq. (3.15). Experimental data for this equation are given in Table 3.4.
These data are related to the new equilibrium layer according to Rao et al. (1974).

Table 3.4 Experimental results for the coefficients in Eq. (3.16) to estimate the height of the internal boundary layer (new equilibrium layer)

Author	a	b	Conditions
Bradley (1968), Shir (1972)	0.11	0.8	z_{01}/z_{02} = 125 and 0.08
			Artificial roughness
Antonia and Luxton (1971, 1972)	0.28	0.79	$x \leq 10$ m, rough–smooth, wind tunnel
	0.04	0.43	$x \leq 10$ m, smooth–rough, wind tunnel
Raabe (1983)	0.30 ± 0.05	0.50 ± 0.05	Beach, on- and off-shore winds, 5 m < x < 1000 m

The depth of the new equilibrium layer is also reliably predicted by a relation proposed by Raabe (1983):

$$\delta = 0.3 \sqrt{x} \tag{3.17}$$

Jegede and Foken (1999) found good agreement with internal boundary layers determined from wind profile data for smooth-to-rough and rough-to-smooth roughness changes for different wind directions which are related to different fetches (Fig. 3.10). Evaluated was the intersection of both wind profiles above and below the internal boundary layer. The height of the middle of the internal boundary layer is well represented by Eq. (3.16) with $a = 0.43$ and $b = 0.5$. The prominent disagreement for a wind direction of about 270° is caused by an additional internal boundary layer due to a group of bushes about 500 m away, which makes the actual internal boundary layer not verifiable. The remarkable scatter for wind directions < 230° is caused by changing wind directions which are partly connected with short fetches.

Fig. 3.10 Measured heights of the internal boundary layer from the boundary layer measurement site Falkenberg of the German Meteorological Service (Jegede and Foken 1999), roughness changes from smooth ($z_o = 0.008$ m) to rough ($z_0 = 0.032$ m). Published with kind permission of © Springer Vienna 1999, All rights reserved
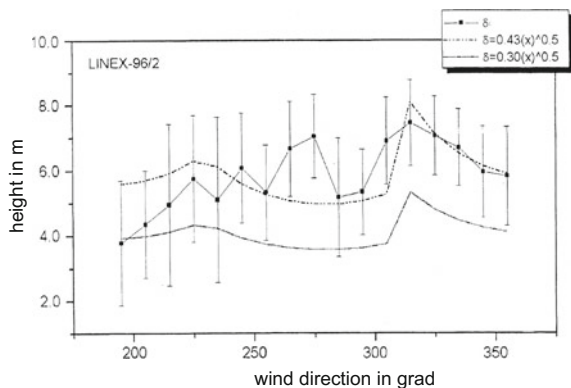
3.2.3 Thermal Internal Boundary Layer

In analogy to the mechanical internal boundary layer caused by a step change in surface roughness, a thermal internal boundary layer develops after a step change in the surface temperature. Such changes in temperature may be triggered by differences in land use characteristics, soil moisture content, or turbulent exchange conditions. Few experimental results are available because the investigations are often made in costal zones where the thermal internal boundary layer is combined with the mechanical internal boundary layer.

The height of the thermal internal boundary layer is given by Raynor et al. (1975):

$$\delta_T = c\left(\frac{u_*}{u}\right)\left[\frac{x(\theta_1 - \theta_2)}{|\partial T/\partial z|}\right]^{1/2} \tag{3.18}$$

The temperature gradient is measured on either the upwind side of the surface temperature change or above the internal boundary layer; all other parameters are measured at a reference level. The coefficient c depends on the reference level and is in the order of one (Arya 2001). Such parameterizations are probably as robust as Eq. (3.16) for the mechanical internal boundary layer.

A special case is the thermal internal boundary layer in the afternoon mainly due to the so-called oasis effect (see Sect. 1.4.3, Stull 1988). Above a strongly evaporating surface, the temperature near the ground surface decreases in the afternoon and a surface-based inversion develops. The height of the inflection point between the stable stratification near the surface and the unstable stratification in the upper
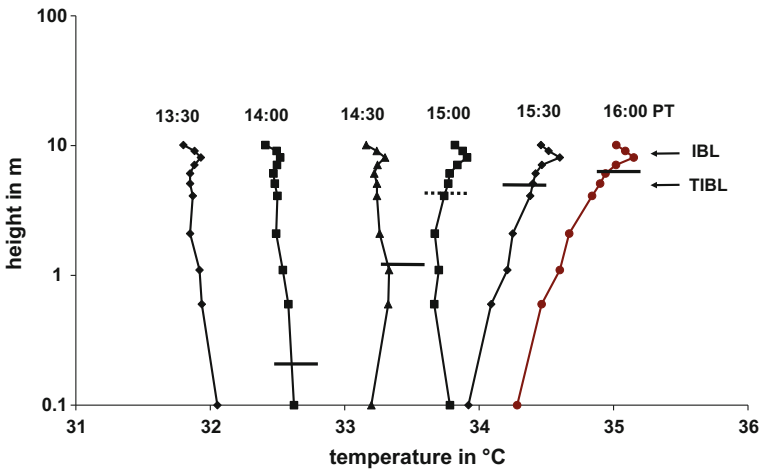

Fig. 3.11 Generation of the afternoon thermal internal boundary layer (TIBL) during the experiment EBEX-2000 above an irrigated cotton field on Aug. 17, 2000 (PT: Pacific time)

layer grows with time (Fig. 3.11). Within the inversion layer, the sensible heat flux is downwards, and above the inversion it is upwards. In the evening, the height of the internal boundary layer increases to about 50–100 m above the ground, but later at night it coincides with the depth of the nocturnal stable boundary layer (Zelený and Foken 1991). In the early morning, a similar effect can be found but with a much shorter duration. Since the late afternoon or early evening thermal internal boundary layer persists over many hours, it is of relevance for the measurement and modelling of gradients near the surface. As a consequence, measurements of temperature gradients near the surface may e.g. not be representative of atmospheric stability higher up in the atmospheric boundary layer (see Sect. 4.1.3).

Another special case of a thermal internal boundary layer, is a near-surface inversion layer (height about 1 m), which cannot be described by any of the phenomena already discussed. This layer was observed first by Andreev et al. (1969) above the Black Sea. Further results are available from the Caspian Sea (Foken and Kuznecov 1978), from Antarctica (Sodemann and Foken 2005), and the Arctic (Lüers and Bareiss 2010). In all cases, the surface was relatively smooth and the stratification was either neutral or stable. Explanations for the layer include a release of heat by chemical reactions, or eddy dissipation (Chundshua and Andreev 1980) or condensation processes (Foken and Kuznecov 1978); also possible are decoupling effects due to a large wind shearing near the surface or potentially counter-gradient fluxes may play a role (see Sect. 3.5.2).

3.2.4   Blending-Height Concept

An important question for modellers is the possible height of an internal boundary layer. According to the structure of internal boundary layers, it can be assumed that layers are separate only up to a certain height (Fig. 3.6). At a greater horizontal distance from the change in surface roughness, they merge. This so-called blending height is assumed to be about 30–100 m above the ground surface. Above this height, an area-averaged flux is assumed. This means that the properties near the surface are smoothed (Taylor 1987). This idea was proposed by Mason (1988) and updated by (Claussen 1991; Claussen and Walmsley 1994; Claussen 1995; Philip 1997). The concept considers especially larger-scale changes of surface roughness with characteristic horizontal distances of $L_c > 1$ km. The blending height can be estimated by

$$L_b = 2\left(\frac{u_*}{u}\right)^2 L_c \approx 2\left(\frac{\sigma_w}{u}\right)^2 L_c \qquad (3.19)$$

(compare with Eqs. 2.60 and 3.1) or $L_b = L_c/200$. Relevant approaches according to different authors are given in Table 3.5. The blending height concept has practical applications for area averaging in numerical models (see Sect. 5.7) because it can be assumed that for the model level at approximately the height of the blending height, the fluxes above a heterogeneous surface are area averaged.

Table 3.5 Parameterization approaches for the blending height L_b (L_c: characteristic horizontal scale)

References	Equation
Mason (1988)	$\frac{L_b}{L_c}\left(ln\frac{L_b}{z_0}\right)^2 \approx 2\kappa^2$
Claussen (1991)[a]	$\frac{L_b}{L_c}\left(ln\frac{L_b}{z_0}\right) \approx 1.57\kappa$
Mahrt (1996)	$L_b = 2\left(\frac{\sigma_w}{u}\right)^2 L_c$

[a]*Here* L_b is the diffusion height

From the experimental point of view, this concept is not much accepted. In an atmospheric boundary layer with free convection (Eigenmann et al. 2009), the various surfaces can be detected by aircraft measurements through the depth of the boundary layer if the single areas are large enough for convection to develop above them. This is the case for horizontal scales greater than 200 m (Shen and Leclerc 1994), which is also basic knowledge for glider pilots. Free convection does not start at the surface, but in the surface layer above a growing internal boundary layer when $\delta/L < -1$ (Andreas and Cash 1999).

Because the structure of the atmospheric boundary layer over heterogeneous surfaces is very complicated, the blending height is meaningful for models with grid sizes greater than 2–10 km. In smaller scale models, the blending height concept seems not to be the best tool.

3.2.5 Practical Relevance of Internal Boundary Layers

Internal boundary layers are disturbances, which cannot be adequately treated in experiments and models. However, for measuring and modelling the properties of the near-surface layer the identification of internal boundary layers is essential.

Experimentally internal boundary layers can be identified as the region in which wind and temperature profile measurements or measurements of turbulence characteristics disagree with typical values for homogenous boundary layers. The actual measurements must be made in the new equilibrium layer or above the internal boundary layer. Problematical are methods that are based on gradient measurements. Extreme errors may occur if an internal boundary layer falls within the profile. Measurements should be done in the new equilibrium layer because due to the logarithmic profile functions the gradients above an internal boundary layer are often very small. When thermal internal boundary layers are present during the daily cycle, the measured gradients are not proportional to a flux.

For modelling, internal boundary layers should be taken into account if the grid size is less than 1 km. Such models are presently very rare because models with high spatial resolution were developed from large-scale low-resolution models. By applying these model physics, the modelling of internal boundary layers is impossible (Herzog et al. 2002).
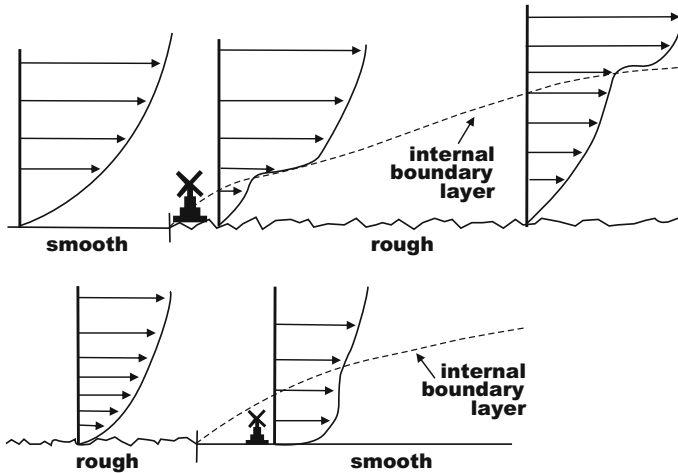
Fig. 3.12 Position of a wind power station in relation to an internal boundary layer (Adapted from WMO 1981, with kind permission of © World Meteorological Organization, Geneva 1981, All rights reserved)

Investigations of internal boundary layers are very important in the use of wind power (WMO 1981). To realize an optimal energy output, wind power stations should be installed on the side of a roughness change that has the smoothest surface for most of the wind directions as illustrated in Fig. 3.12.

3.3   Obstacles

Obstacles have a remarkable influence on meteorological measurements, though the disturbance is not only at the downwind side but also on the windward side of the obstacle. In general, measurements should thus be placed far away from large obstacles. However, this is impossible in forest, mountain regions, and urban environments. Often, modelling approaches are compared with wind tunnel simulations (Schatzmann et al. 1986). However, wind tunnel measurements are typically limited to neutral stratification, and the atmospheric turbulence structures can only be partially replicated.

For classical meteorological measurements and especially for micrometeorological measurements, the influences of obstacles should be excluded to the greatest possible extent. Therefore, the available rough approximations presented in this section are relevant only for mean meteorological parameters. For measurements of energy fluxes, the distances should be increased by a factor 2–5, and the footprint conditions must be applied (see Sect. 3.4).
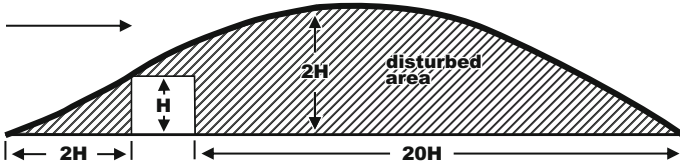
Fig. 3.13 Disturbance area of an obstacle (Adapted from WMO 1981, with kind permission of ©
World Meteorological Organization, Geneva 1981, All rights reserved)

The following engineering approximation technique is used for wind measure-
ments and of wind power assessments. This simple approach (WMO 1981) is
illustrated in Fig. 3.13.

In Germany (VDI 2000), for meteorological standard measurements of the wind
velocity at 10 m height, the necessary distance from an obstacle, A, is a function of
the height, H, and the width, B, of the obstacle. In the exceptional case of a short
distance to the obstacle, D, the measurement height should be increased by an
amount h' where

$$h' = \frac{H}{A}(A - D), \tag{3.20}$$

see also Table 3.6.

The European Wind Atlas (Troen and Lundtang Peterson 1989) applies a
method to determine the lee side of an obstacle on the basis of a paper by Perera
(1981). Accordingly, a corrected wind velocity can be calculated from the measured
velocity and the porosity P of the obstacle (buildings: 0.0; trees: 0.5):

$$u_{\text{corr}} = u[1 - R_2 R_1 (1 - P)] \tag{3.21}$$

The factor R_1 is given in Fig. 3.14. and R_2 can be determined from

$$R_2 = \begin{cases} \left(1 + 0.2\frac{x}{L}\right)^{-1} & \text{for} \quad \frac{L}{x} \geq 0.3 \\ 2\frac{L}{x} & \text{for} \quad \frac{L}{x} < 0.3 \end{cases}, \tag{3.22}$$

where x is the distance between the obstacle and the measurement site, and L is the
length of the obstacle).

Table 3.6 Minimal distance
of meteorological
measurements, especially
wind measurements, to an
obstacle (VDI 2000)

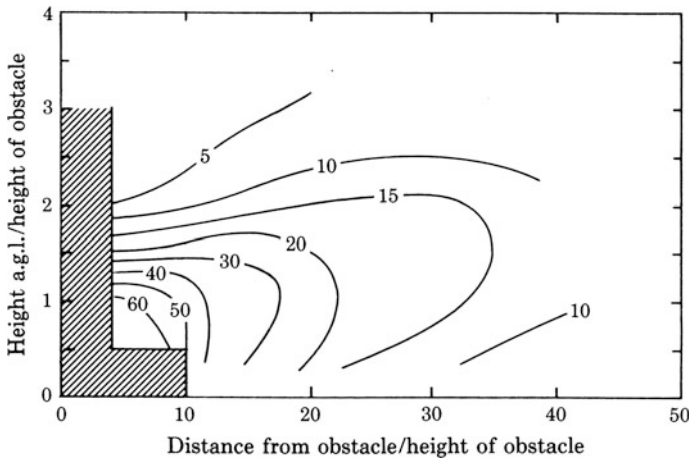| Height $\gg$ wide	Height $\approx$ wide	Height $\ll$ wide
$A \geq 0.5\,H + 10\,B$ for $B \ll H \leq 10\,B$	$A = 5\,(H + B)$	$A \geq 0.5\,B + 10\,H$ for $H \ll B \leq 10\,H$
$A \geq 15\,B$ for $H > 10\,B$		$A \geq 15\,H$ for $B > 10\,H$

Fig. 3.14 Determination of the factor R_1 (Adapted from Troen and Lundtang Peterson 1989, with kind permission of © Danish Technical University Roskilde 1989, All rights reserved)

Results from the three methods are not comparable because the length of the obstacle in each case is used in a different way. However, for similar obstacles the results are not greatly different.

It should be noted that an instrument tower can also influence the measurements. Generally, measurements should not be made in the lee of a tower, and on the windward side the distance of wind and flux sensors from the mast should be large. For the installation of sensors, helpful rules of thumb for distances are 5-times the diameter of the mast for lattice masts, and 10-times the diameter of the mast for concrete masts.

Obstacles in connection with the generation of internal boundary layers have practical applications. For example, bushes used as windbreak lines reduce soil erosion on the lee side remarkable well, and distances less than 100 m from these break lines are optimal. Windbreaks are also used to shelter rain gauges, and snow fences are used to collect snow in the lee side.

3.4 Footprint

3.4.1 Definition

Measurements made at a particular site and at a particular height do not represent the properties or the fluxes below that sensor. Instead, the measurements represent the conditions of the underlying surface upwind of the sensor (Gash 1986). This effective area of influence is called the *footprint*. While the phenomenon of the footprint has been well known for a long time the term footprint is not much older
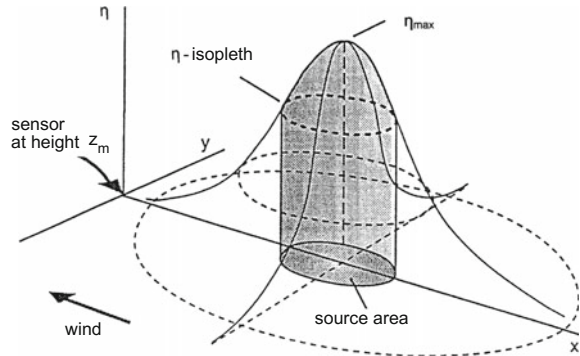
than 20 years. Thus, different forms of presentation and notation can be found in the
literature. For example Schmid and Oke (1988) call this a source-weight function,
and Leclerc and Thurtell (1989) call it a footprint function. In subsequent papers,
the footprint description was widely used (Leclerc and Thurtell 1990; Schmid and
Oke 1990; Schuepp et al. 1990), but the final mathematical form according to our
present knowledge was given by Horst and Weil (1992, 1994). The footprint
function f describes the source area Q_η of a measured signal η (scalar, flux) in
relation to its spatial extent and its distribution of intensity, as illustrated in
Fig. 3.15, and is given by:

$$\eta(x_m, y_m, z_m) = \int\limits_{-\infty}^{\infty} \int\limits_{-\infty}^{\infty} Q_\eta(x', y', z' = z_0) \cdot$$
$$\cdot f(x_m - x', y_m - y', z_m - z_0) dx' dy' \qquad (3.23)$$

> The footprint of a special point (measurement device) is the influence of the
> properties of the upwind source area weighted with the footprint function.

It is interesting, that the horizontal and vertical scales of internal boundary layers
and footprint concepts are also identical with the blending height concept (Horst
1999). A textbook about the footprint issue was recently published by Leclerc and
Foken (2014).

3.4.2 Footprint Models

Footprint models can be classified based on dimension and theoretical background
of the model. Dimensions are given for the source and the footprint (Table 3.7).
The first and relatively simple models (1D) used a line source and determined the
footprint along a horizontal axis. They integrated the footprint along the cross-wind

Table 3.7 Definition of dimensions of source area and footprint (Leclerc and Foken 2014)

Dimension	1-dimensional (1D)	2-dimensional (2D)	3-dimensional (3D)
Source area	Line source $Q\eta(x)$	Two dimensional source in x and y, while z is constant, $Q\eta(x, y)$	Three dimensional source, $Q\eta(x, y, z)$
Footprint	Distribution of the concentration or flux density along a horizontal line, $\eta(x)$	Distribution of the concentration or flux density along a horizontal plane, $\eta(x, y)$	Distribution of the concentration or flux density in a non-horizontal plane like in a hilly region, $\eta(x, y, z)$

component. Recently, more sophisticated models, applicable for heterogeneous surfaces and variable heights, were developed.

The first footprint models (Schmid and Oke 1990; Schuepp et al. 1990) were diffusion models based on the assumptions of homogeneous surfaces, uniform fluxes with height, and constant advection. Important input parameters were the measurement height, the roughness length, the stratification, the standard deviation of the lateral wind component, and the wind velocity. The core of analytical footprint models are dispersion models such as the often-used model developed by Gryning et al. (1983). In parallel, Lagrangian footprint models were developed (Leclerc and Thurtell 1990), in which particles from a source area were emitted and detected at the measurement level (forward trajectory). For heterogeneous surfaces, models with backward trajectories are appropriate, where the particles are emitted from the measurement sensor and detected at the surface (Kljun et al. 2002). Also other model types can be applied for the footprint detection. Sogachev and Lloyd (2004) were successful with a numerical model with 1.5–order closure. Large-Eddy-Simulation models (LES) are ideal due to their high spatial resolution. These models either generate the meteorological fields for the Lagrangian simulation (Leclerc et al. 1997) or the Lagrangian simulation is directly embedded into the LES model (Steinfeld et al. 2008). An overview about the development of footprint models and the recent state is given by Schmid (2002), Vesala et al. (2008), Rannik et al. (2012), Leclerc and Foken (2014). The available footprint models are listed in Table 3.8.

While footprint models are widely used, their experimental validation is still an outstanding issue (Finn et al. 1996). This validation is all the more necessary because the models are often applied under conditions that are not in agreement with the model assumptions. Currently, two methods of validation are available. The first method is the classical validation of dispersion models with tracer gases (Finn et al. 1996, 2001), and the second method tries to find the influences of obstacles in the footprint area by examination of the integral turbulence characteristics (Foken and Leclerc 2004). In the second method, the differences in the integral turbulence characteristics of the footprint area due to changes of stability are investigated. This approach was validated using natural tracers (Foken and Leclerc 2004). These natural tracers are surfaces with different properties which can

Table 3.8 Overview about some of the most important footprint models with their dimension, adapted from Leclerc and Foken (2014)

Author	Remarks
Schuepp et al. (1990)	Analytical footprint model; use of source areas, but neutral stratification and averaged wind velocity (1D)
Leclerc and Thurtell (1990)	Lagrangian footprint model (1D)
Horst and Weil (1992)	Analytical footprint model (1D)
Schmid (1994)	Separation of footprints for scalars and fluxes (1D)
Schmid (1997)	2D version of Horst and Weil (1992)
Kaharabata et al. (1997)	Analytical footprint model (2D)
Leclerc et al. (1997)	LES model for footprints (1D)
Baldocchi (1997)	Lagrangian footprint model within forests (1D)
Rannik et al. (2000, 2003)	Lagrangian model for forests (2D)
Hsieh et al. (2000)	Analytical footprint model (1D)
Kormann and Meixner (2001)	Analytical model with exponential wind profile (1D)
Kljun et al. (2002)	Back trajectories Lagrangian model for varying stratifications and heterogeneous surfaces (3D), 1D analytical version by Kljun et al. (2004), 2D analytical version by Kljun et al. (2015)
Sogachev and Lloyd (2004)	Boundary-layer model with 1.5 order closure (2 and 3D)
Cai and Leclerc (2007)	Concentration footprints from backward and forward in-time particle simulations driven with LES data (3D)
Prabha et al. (2008)	Footprint inside a canopy using LES (3D)
Steinfeld et al. (2008)	Footprint model with LES embedded particles (3D)
Hsieh and Katul (2009)	Second order closure model for heterogeneous surfaces (2D)

be verified with measurements according their footprint (Göckede et al. 2005). At this time, we are at the beginning of footprint model validation, and to a large extent only comparisons between different footprint models are available. To make these comparisons more objective, Markkanen et al. (2009) developed a method to validate footprint models in terms of the position of the maximum of the footprint and the relevant source area.

3.4.3 Application of Footprint Models

The first applications of footprint models were in the planning of field experiments (Horst and Weil 1994, 1995), i.e. how complex is the target surface in the footprint

area of the measurement site. Changes in the underlying surface create internal boundary layers, which can change the local turbulence structure by adding mechanical or thermal-induced turbulence. An example of such a footprint calculation is shown in Fig. 3.16, where it is clearly seen that only the lowest measurement height can measure the influence of the surface on which the mast is standing. The upper measurement heights record increasing parts of the neighbouring surfaces. The measurements of gradients can no longer be used for the determination of fluxes; it would more likely reflect horizontal differences.

Another important application is the so-called footprint climatology (Amiro 1998), which is shown in Fig. 3.17 for a selected measurement site. Depending on the stratification and the standard deviation of the lateral wind component, a data set over a long time period is necessary in order to calculate the climatology of the footprint areas. It can then be estimated, which land use types contributed to the measured fluxes over a longer time period.

For measurement sites with changing roughness in the surrounding region, surface maps are used. The averaging of the roughness lengths can be made according to Table 3.1, and the results used with some iterations optimal to the footprint model (Göckede et al. 2004). With an averaging model for fluxes (Hasager and Jensen 1999) the approach can be further augmented for heterogeneous surfaces (Göckede et al. 2006). With this approach for estimating the roughness lengths of heterogeneous surfaces the footprint climatology can be significantly improved.
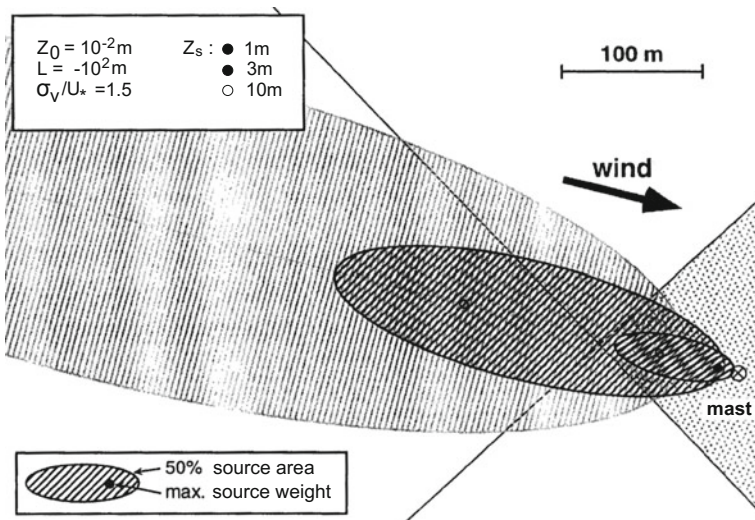

Fig. 3.16 Schematic picture of footprint areas according the model by Schmid (1997). It is seen that for different measurement heights different footprints and influences of underlying surfaces occur. Published with kind permission of © Elsevier Science AG Oxford 1997, All rights reserved
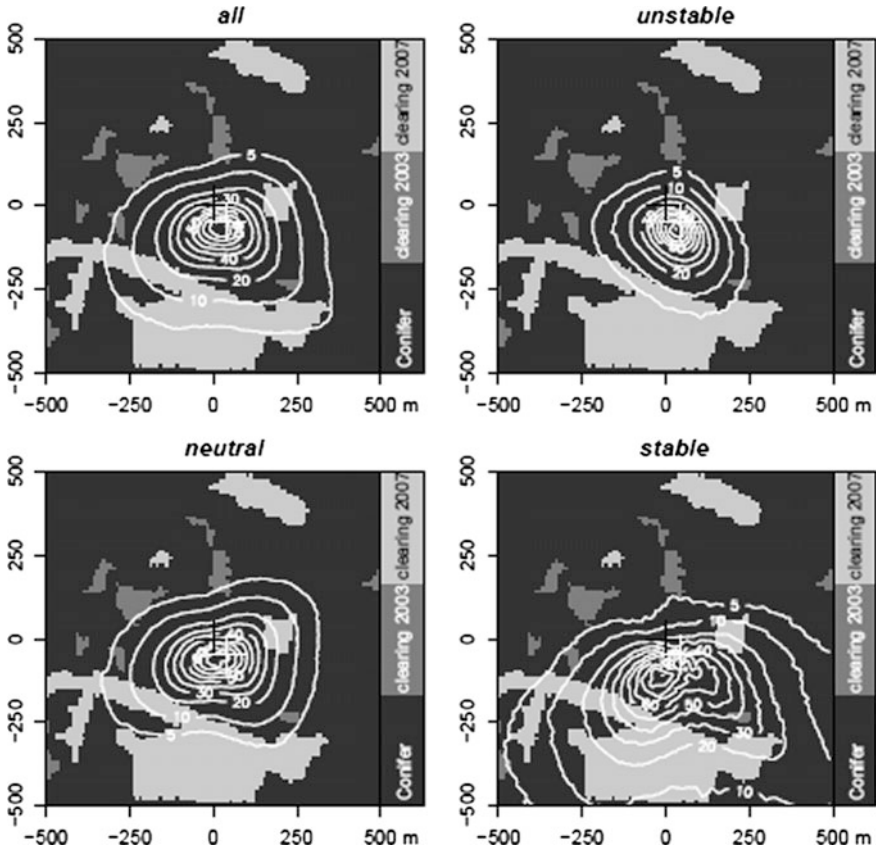
Fig. 3.17 Footprint climatology of the FLUXNET station Waldstein-Weidenbrunnen (DE-Bay), Turbulence Tower, based on the data set 2007, Sept. 09 to Oct. 07. (Adapted from Siebicke 2008, published with kind permission of © Author 2008, All rights reserved)

Another application is the evaluation of the quality of carbon dioxide flux measurement sites with respect to the target surface in the footprint area and the spatial distribution of the estimated data quality within the footprint (see Sect. 4.2.5 and Rebmann et al. 2005; Göckede et al. 2008). From Fig. 3.18, it can be seen that in the NW- and S-sectors the data quality is not sufficient for the calculation of the latent heat flux. The reason for this is that clouds and precipitation often occur in the NW-sector at the station Waldstein-Weidenbrunnen.

The footprint of a single measurement can be used to connect measurements with a certain surface type. Using the footprint calculation, measured fluxes can be separated proportional to the different surfaces. For instance, it is possible to make chamber measurements exactly in the footprint of the flux measurements (Reth et al. 2005). If models are used in parallel for different surfaces, fluxes can be determined for each surface type and continuously monitored by flux measurements for each footprint area (Biermann et al. 2014).

Fig. 3.18 Spatial distribution of the data quality according to Table 4.3 for the latent heat flux at the measurement station Waldstein-Weidenbrunnen for stable stratification. The relevant footprint climatology is underlined with contour lines, according to Göckede et al. (2006). The measurement tower is located at point (0, 0). Published with kind permission of © Springer, Berlin, Heidelberg 2006, All rights reserved
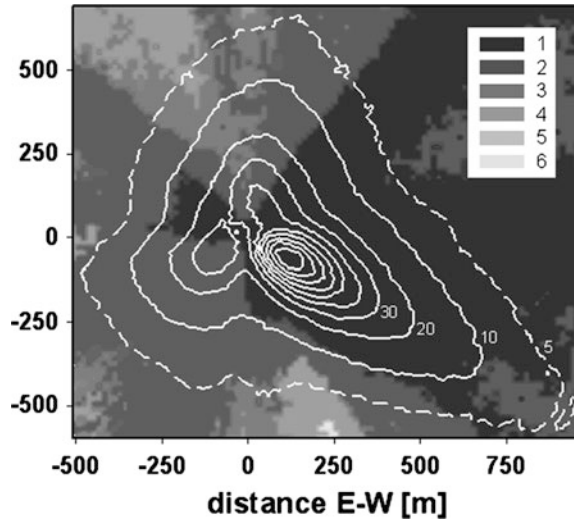
Figure 3.19 shows the measured and modelled integral turbulence characteristics of the vertical wind velocity for stable and unstable stratification at the Waldstein-Weidenbrunnen station. Significant differences can be seen between the model and experiment in the wind sector 180°–230°. However, for neutral stratification this is not the case. The reason is that the Waldstein massif is about 1 km from the measurement site, and its effects on the measurements are seen only for stable stratification. Thus, the disturbances of the vertical wind can explain the low data quality of the latent heat flux in the S-sector. Similar influences on the integral turbulence characteristics were found by DeBruin et al. (1991). They distinguish between heterogeneities in the surface roughness and in the thermal or other surface properties, with the former affecting the integral characteristics of wind observations and the latter the characteristics of scalars. The influence of heterogeneous surfaces on the wind field motivated Foken (2013) to apply footprint models to find the optimal positions for wind power stations with minimal influences of the surface.

3.5 High Vegetation

The description of meteorological processes over high vegetation is opposite to that for dense vegetation (e.g. grain), which was described in Sect. 3.1.2 as a porous layer with a vertical displacement of the height (zero-plane displacement) in the profile equation. In a forest, the canopy and the understory are regions where complex micrometeorological processes occur. Therefore the crown is a layer that often decouples the understory from the atmosphere above the forest canopy. The energy and matter exchange between the atmosphere and the upper crown is often completely different than those between the lower crown and the trunk space and the soil. The
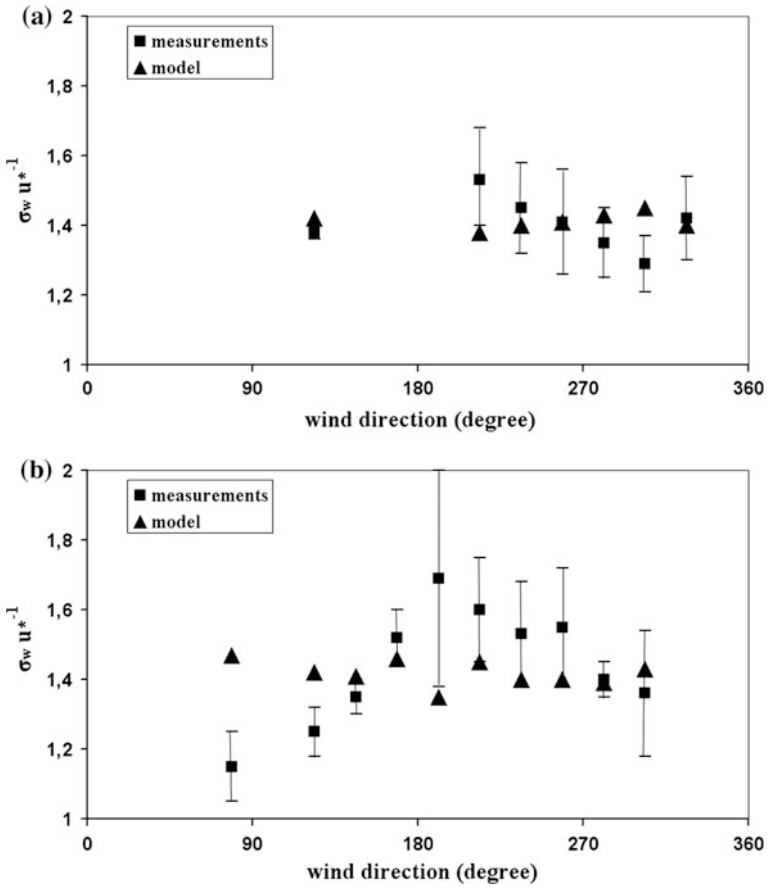
Fig. 3.19 Integral turbulence characteristics of the vertical wind velocity at the station Waldstein-Weidenbrunnen as a function of wind direction for **a** unstable and **b** stable stratification; measurements are plotted as ● and model calculations according to Table 2.11 as ▲ (Adapted from Foken and Leclerc 2004, with kind permission of © Elsevier AG Oxford 2004, All rights reserved)

stratification in both layers can be different, and the gradients in each layer can be of opposite sign. This has significant influence on measurement and modelling of exchange processes, which are very complex. Currently, these processes and their consequences are not fully understood (Finnigan 2000; Monson and Baldocchi 2014).

3.5.1 Behaviour of Meteorological Parameters in a Forest

The typical daily cycle of the temperature in a forest (Baumgartner 1956; Lee 1978) is illustrated in Fig. 3.20. The maximum air temperature occurs in the upper crown

Fig. 3.20 Daily cycle of the air temperature in and above a forest according to Baumgartner ([1956](#), published with kind permission of © German Meteorological Service Offenbach 1956, All rights reserved)
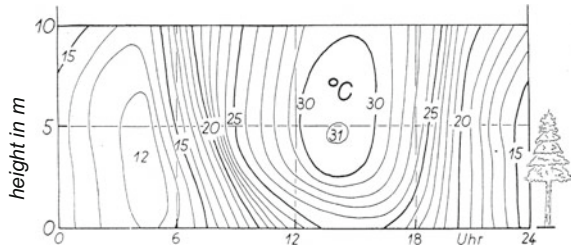
usually about 1–2 h after local noon. Below the crown, the daytime temperatures are lower. During the night, the minimum temperature occurs in the upper crown due to radiation cooling. Because the cool air in the crown drops to the ground surface, the minimum of the temperature near the ground occurs a short time later. Especially in the evening, it is warmer in the forest than in the surroundings. Fields near the forest edges may be damaged by frost in the morning due to the outflow of cold air, especially on slopes. The temperature structure in a forest has an absolutely different stratification than commonly observed above low vegetation. During day time above low vegetation and above the crown, unstable stratification is typical, and during the night stable stratification is typical. Due to the relatively cool forest ground during daytime and warm forest ground during the nighttime, inside the forest the opposite stratifications are realized.

A typical phenomenon of the exchange processes in and above a forest is a decoupling due to the crown. For example, during a calm night the upper canopy is relatively warm, but cool air is stored in the understory. A very small increase of the wind speed (gust, sweep) can cause a sudden inflow of warm air into the understory as seen in the historical measurements by Siegel (1936) in Fig. 3.21 at 01:40. Also, the opposite effect (burst, ejection) often occurs during the day, when warm or moist air is suddenly ejected from the understory. Therefore, the exchange of energy and matter within and above a forest is not a continuous process but is limited to a sequence of single events.

The wind velocity in and above a forest is greatly reduced due to friction. But in a clear trunk space with nearly no understory growth a secondary maximum of the wind appears (Shaw 1977; Yi 2008). This can change the momentum flux below the crown (Fig. 3.22). The wind profile near the top of the canopy has an inflection point, and at forest edges internal boundary layers can develop. Near the edge, as shown by measurements and modelling studies, increased turbulent fluxes occur (Klaassen et al. 2002).

3.5.2 Counter Gradient Fluxes—Coherent Structures

It is typical in the convective boundary layer that the flux—generated by convection —is not correlated to the mean, local gradient. The flux remains positive as the
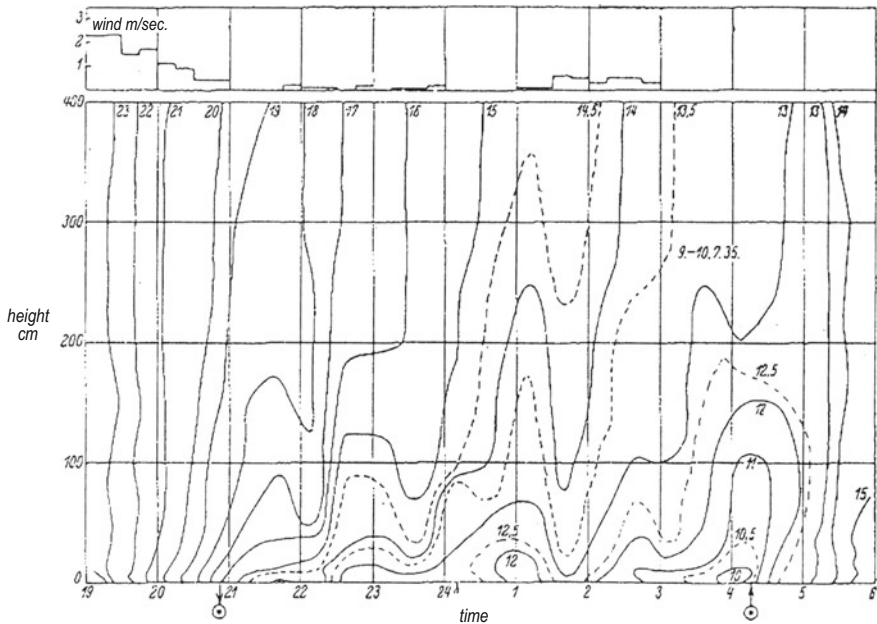
Fig. 3.21 Nigh time plot of the temperature in a forest with a sudden inflow of warm air connected with a short increase of the wind velocity at 01:40 according to Siegel (1936), published again by Geiger (2013, published with kind permission of © Springer Berlin, Heidelberg 2013, All rights reserved)

gradients approach zero or even slightly positive. This phenomenon is called counter gradient flux. It can be explained by the triple correlations (Deardorff 1966). Such a behaviour exists also in a forest. Air parcels from the trunk space penetrate through the crown into the atmosphere or a gust can penetrate into the forest. This was found to be the case not only for the fluxes of sensible and latent heat but also for the fluxes of matter, e.g. carbon dioxide (Denmead and Bradley 1985, 1987) and schematically shown in Fig. 3.23.

Counter-gradient fluxes are not limited to forest sites. They also occur in connection with decoupling effects in the near-water air layer (Foken and Kuznecov 1978) or above ice shields (Sodemann and Foken 2005; Lüers and Bareiss 2010). It is interesting from the point of view of the history of science, that experimental findings were already known before the book chapter by Denmead and Bradley (1985) which opened the possibility to publish these investigations in reviewed journals.

While the profiles are determined by the mean structures, the turbulence fluxes contain short-time transports by gusts and bursts, which cause little change to the profiles. Relatively large turbulence eddies called coherent structures, which are not comparable with the turbulent elements of the gradient transport, make remarkable flux contributions (Holmes et al. 1996; Venditti et al. 2013):
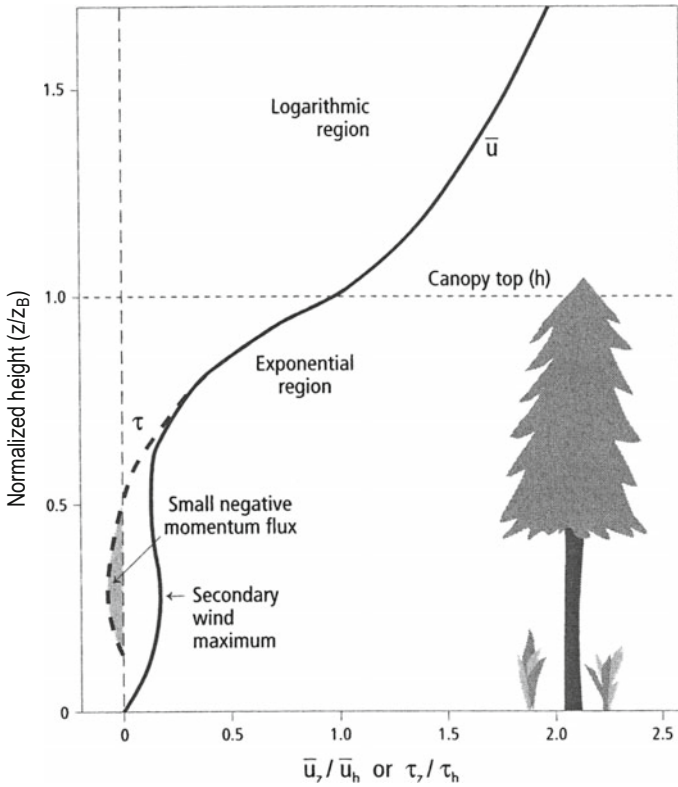
Fig. 3.22 Typical wind profile in a forest, adapted from Bailey et al. (1997) using the data by Amiro (1990, published with kind permission of © Kluwer Academic Publisher B.V. Dordrecht 1990, All rights reserved)
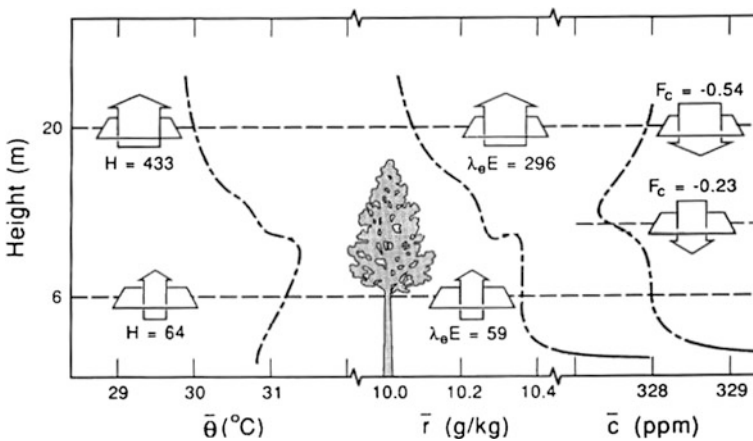
Fig. 3.23 Profile of the temperature θ, the mixing ratio r, and the trace gas concentration c, as well as the sensible heat flux H, the latent heat flux λE, and the trace gas flux F_c in a forest with counter-gradients (Adapted from Denmead and Bradley 1985, with kind permission of © D. Reidel Publ. Comp. Dordrecht 1985, All rights reserved)

> Coherent structures, in contrast to stochastically distributed turbulence
> eddies, are well organized, relatively stable long-living eddy structures,
> which occur mostly with regularity in either time or space.

Therefore, fluxes cannot be determined from gradient of state parameters
according to Sect. 2.3, rather higher order closure approaches must be applied for
modelling (compare Table 2.3). With these findings, the application of either the
Monin-Obukhov similarity theory or the *K*-approach for the exchange process at a
forest site gives only meaningful results in the case of a good coupling of the
atmosphere with the forest (Staudt et al. 2011). Alternatives are modelling with the
transilient theory if the transilient matrix is well parameterized (Inclán et al. 1996,
see Sect. 2.1.3), LES modelling (see Sect. 5.7, Dupont and Brunet 2009; Finnigan
et al. 2009; Schlegel et al. 2012), or higher-order closure approaches (Meyers and
Paw U 1986, 1987; Pyles et al. 2000).

In contrast to low vegetation, above a forest ramp-like structures in the time
series as seen in Fig. 3.24 typically occur. These generally are short-lived but strong
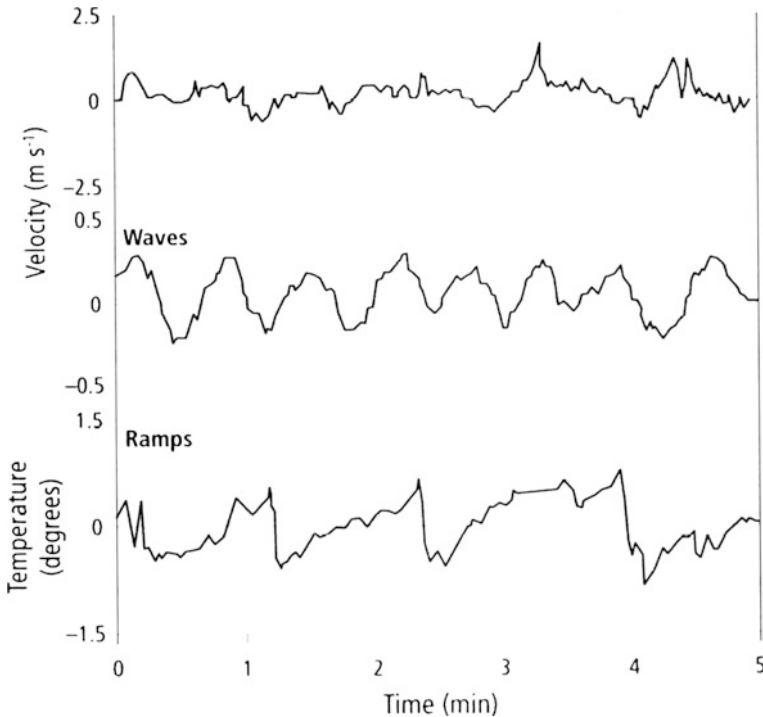

Fig. 3.24 Fluctuations, waves and ramp structures above a forest, adapted from Amiro and
Johnson (1991, *upper* and *middle graph*, with kind permission of © Authors 1991, All rights
reserved) and from Gao et al (1989, *lower graph*, with kind permission of © Kluwer Academic
Publisher B.V. Dordrecht 1990, All rights reserved)

turbulent events, which make remarkable contributions to the transport process (Bergström and Högström 1989; Gao et al. 1989). These ramps have some regularity, and persist for time periods typically ranging from tens of seconds to a few minutes; they are different from the normal fluctuations and gravity waves, which can be observed above the canopy in the night.

The structures shown in Fig. 3.21 are probably the first observations of coherent structures. More systematic investigations require the applications of statistical approaches, for example the wavelet analysis (Supplement 3.1), to clearly isolate time and frequency scales. This is not possible with spectral analysis, which gives only the frequency distribution. The first papers on this technique were presented by Collineau and Brunet (1993a, b).

Supplement 3.1 Wavelet Analysis

The wavelet transformation $T_p(a, b)$ of a function $f(t)$ is the convolution of a time series $f(t)$ with a family of Wavelet functions $\Psi_{a,b}(t)$ (see Torrence and Compo 1998)

$$T_p(a, b) = \int_{-\infty}^{\infty} f(t)\, \overline{\Psi_{p,a,b}(t)}\, dt = \frac{1}{a^p} \int_{-\infty}^{\infty} f(t)\, \overline{\Psi\left(\frac{t-b}{a}\right)}\, dt, \qquad \text{(S3.1)}$$

where $T_p(a, b)$ is the wavelet transform; $\Psi_{p,1,0}(t)$ is the mother wavelet; b is the translation parameter, a is the dilatation parameter (time scale), $1/a$ is a frequency scale, and $p = 0.5$. If $a > 1$, then a widening of the mother wavelet occurs, and if $a < 1$ then a contracting of the mother wavelet occurs. Wavelet functions differ in their response to time and frequency, and so they must be selected according to the application. A wavelet that responds equally well in both scales is the Mexican-hat:

$$\Psi(t) = \frac{2}{\sqrt{3\sqrt{\pi}}} \left(1 - t^2\right) e^{-t^2/2} \qquad \text{(S3.2)}$$

Wavelet plots show the time on the x-axis and the period or frequency on the y-axis. In the wavelet plot in Fig. 3.26 light areas correspond to high energy densities and the dark areas to low energy densities. Thus, an explicit localization of frequencies and energy densities in time is possible. This is not possible in spectral analysis.

The turbulent fluctuations of the vertical wind are shown in the upper part of Fig. 3.25. Below this but on the same time axis is the wavelet energy plot. On the ordinate, the logarithm of the reciprocal time scale (frequency in Hz) is plotted. Long periods of minimum and maximum energy are seen, which are correlated with the ramp structures. These structures show a maximum in the variances at 300 s
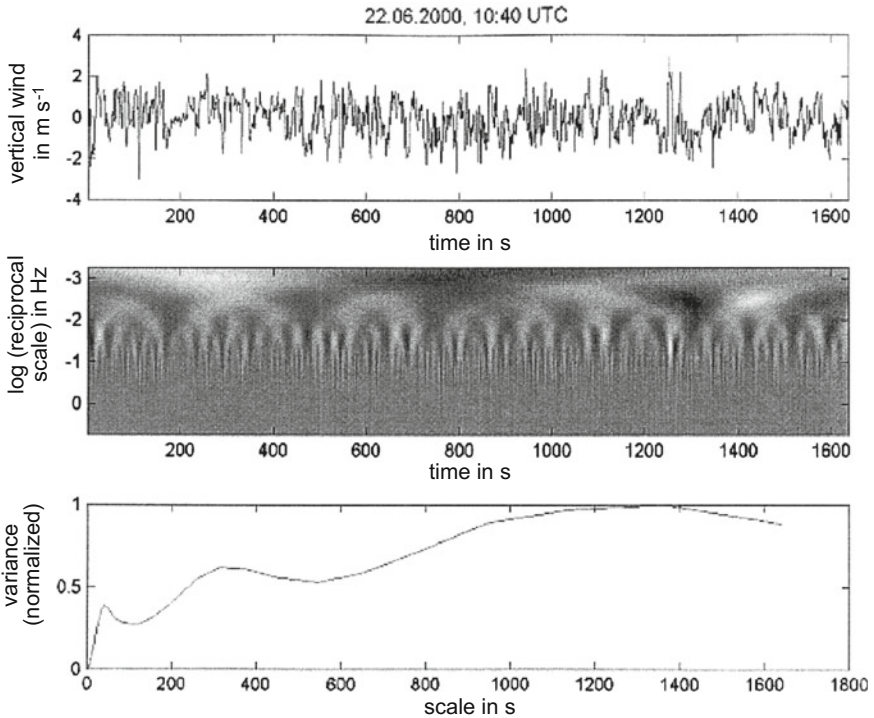
Fig. 3.25 Structure of the vertical wind velocity above a forest, *above* time series, *middle* wavelet analysis, *below* scale of typical variances (Wichura et al. 2001, adapted with kind permission of © Authors 2001, All rights reserved)

(lower part of the Figure). We also see in Fig. 3.26, a maximum variance in the micro-turbulence range at about 50 s, and another maximum for the very long waves. Ruppert et al. (2006) have shown that not all meteorological variables have the same coherent structure, in contrast to stochastically organized eddies (Pearson jr. et al. 1998). The main reasons are different sources. This phenomenon is called scalar similarity.

Scalar similarity is also shown in Fig. 3.26. While the ramp structures in the vertical wind are not well developed, the ramp structures in the temperature, water vapour, ozone, and carbon dioxide fluctuations are; however, the characteristics of the ramps are not similar. For example, due to the different sources of carbon dioxide and water vapour, their ramps are mirror images.

Above forests, coherent structures contribute about 20% to the total flux with smaller partitions at daytime and larger in the case of stable stratification at night (see Sect. 3.5.4). At the canopy height sweeps dominate in comparison to ejections. In the trunk space and above the forest the relationship is vice versa (Fig. 3.27, Thomas and Foken 2007b).
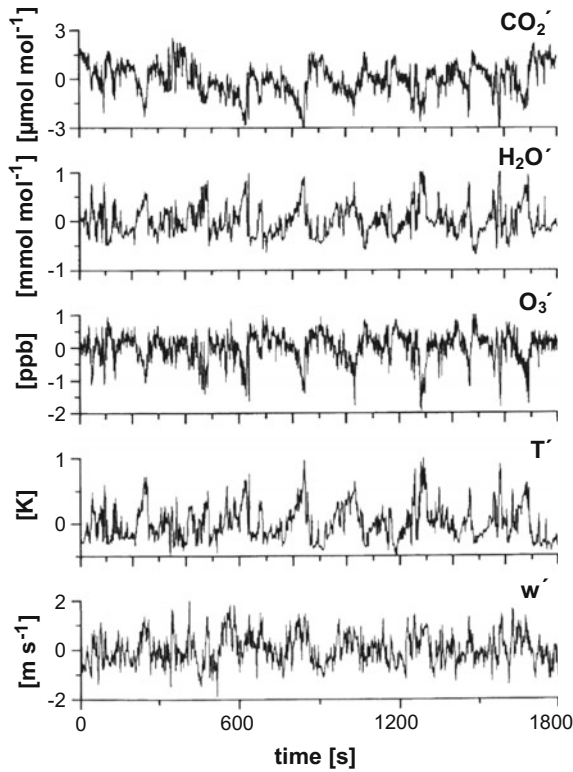
Fig. 3.26 Turbulent structures above a tropical rain forest (Rummel et al. 2002, adapted with kind permission of © Authors 2002, All rights reserved)
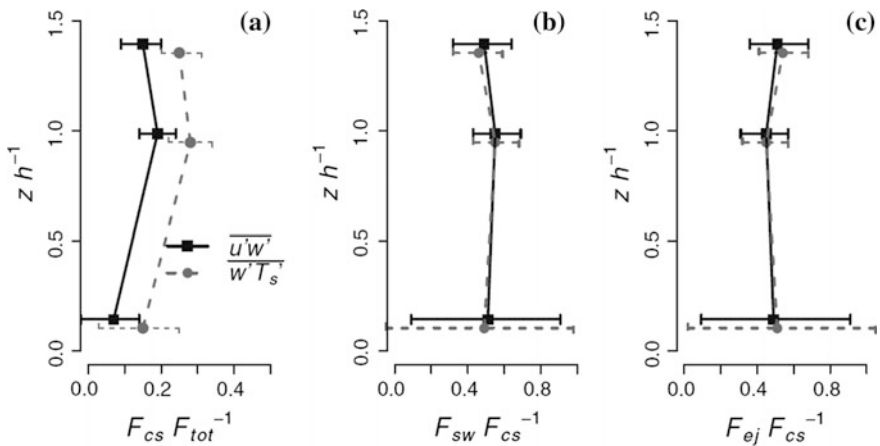
Fig. 3.27 Vertical profile of the relative momentum (*squares*) and buoyancy (*circles*) flux partition of coherent structures of the total flux (**a**), sweeps (**b**), and ejections (**c**) in a spruce forest, h: canopy height (Eder et al. 2013, published with kind permission of © Springer, Berlin, Heidelberg 2013, All rights reserved)

Coherent structures are found over all surfaces. Their characteristics above highly heterogeneous surfaces are much greater than those over low uniform surfaces. Obstacles such as forest edges can generate additional structures, which generate periods that are dependent on the distance from the edge (Zhang et al. 2007; Eder et al. 2013).

3.5.3 Roughness Sublayer—Mixing Layer

Above a forest canopy, the profiles of state parameters are modified due to the high roughness compared with the ideal profile equations given in Sect. 2.3. The gradients of the wind velocity and of scalars are reduced above the canopy, while the fluxes are increasing. This layer together with the canopy is called the roughness sublayer, which has a thickness of about three times of the canopy height. This means that above a forest within a distance of two times of the canopy height undisturbed conditions can be found (Thom et al. 1975; Garratt 1978). Under neutral or unstable stratification for moderately high canopies, part of the surface layer, for which the constant flux layer approach can be applied, persists above the roughness sublayer.

The same phenomena of high wind shear can also be described by a mixing layer approach for the exchange processes (Raupach et al. 1996). The mixing layer is characterized by a sequence of coherent eddies, which have the wavelength of the initial Kelvin-Helmholtz instability and primarily cause the mixing layer. The development of the mixing layer is very similar to wind tunnel experiments as illustrated in Fig. 3.28. Turbulent exchange is possible if the characteristic turbulence scales of the vertical wind velocity and a scalar are similar to the scales of the mixing layer. If this is not the case, then decoupling may occur. An attempt to combine both concepts was made by Harman and Finnigan (2007, 2008).
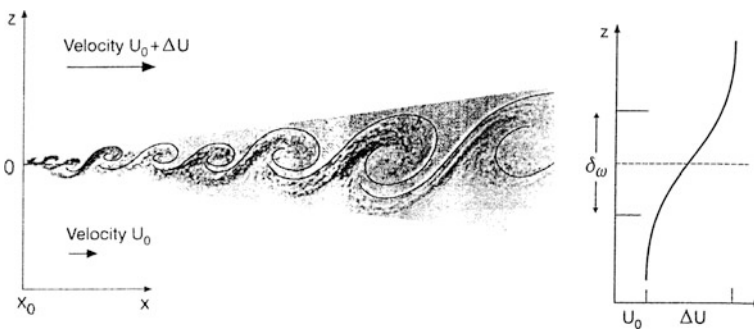

Fig. 3.28 Developing of the mixing layer of the height δ_w (Adapted from Raupach et al. 1996, with kind permission of © Kluwer Academic Publisher B.V. Dordrecht 1994, All rights reserved)

The verification of the roughness sublayer was made first in the wind tunnel (Raupach et al. 1980). Experiments in nature were done, for example, by Shuttleworth (1989). While above low vegetation the ratio z/z_0 for typical measurement heights has values of 100–1000, above a forest roughness sublayer this ratio is typically 5–10 (Garratt 1980). Accordingly, the profile equations (Eqs. 2.74 to 2.76) must be changed by including functions which compensate for the effects of the increased turbulent diffusion coefficient in the roughness sublayer (Garratt 1992; Graefe 2004)

$$u_* = \sqrt{-\overline{u'w'}} = \frac{\kappa}{\varphi_*(z/z_*)\varphi_m(\varsigma)} \frac{\partial u}{\partial \ln z}, \tag{3.24}$$

$$\overline{w'T'} = -\frac{\kappa/\operatorname{Pr}_t}{\varphi_*(z/z_*)\varphi_H(\varsigma)} \frac{u_*}{} \frac{\partial T}{\partial \ln z}, \tag{3.25}$$

$$\overline{w'q'} = -\frac{\kappa/Sc_t}{\varphi_*(z/z_*)\varphi_E(\varsigma)} \frac{u_*}{} \frac{\partial q}{\partial \ln z}, \tag{3.26}$$

where z_* is the height of the roughness sublayer. Below the roughness sublayer the profile equations (Eqs. 2.74 to 2.76) are no longer valid. The expression $1/\varphi_*(z/L)$ is called enhancement factor (Raupach and Legg 1984; Simpson et al. 1998). The correction functions do not change with stratification and can be determined as empirical exponentials according to Garratt (1992) and Graefe (2004):

$$\varphi_*(z/z_*) = \exp[-0.7(1 - z/z_*)] \quad \text{for} \quad z < z_* \tag{3.27}$$

Cellier and Brunet (1992) found the following function ($\eta = 0.6$),

$$\varphi_{*_u}\left(\frac{z}{z_*}\right) = \left(\frac{z}{z_*}\right)^{\eta} \quad \text{for} \quad z < z_*, \tag{3.28}$$

Which was verified by Mölder et al. (1999), Foken et al. (2012, supplement). For temperature and humidity Mölder et al. (1999) found a linear relationship, i.e. $\eta = 1$:

$$\varphi_{*_{T,q}}\left(\frac{z}{z_*}\right) = \frac{z}{z_*} \quad \text{for} \quad z < z_*, \tag{3.29}$$

The measurement of the sensible and latent heat fluxes requires according to Eqs. (3.25) and (3.26) the consideration of Eq. (3.24) and therefore of the universal functions for the roughness sublayer. In practice, the friction velocity is often directly measured and only the universal function for scalars of the roughness sublayer is applied.

The corrected functions must be used above the forest in all cases; otherwise the profile method (see Sect. 4.1) gives false values. The application of Bowen-ratio

similarity (see Sect. 2.3.4) is in principal possible as long as the corrected functions for both fluxes are identical. However, for the application of Bowen-ratio similarity the relatively small gradients above the forest are the more limiting factors.

Another possibility for the correction of the roughness sublayer was proposed by DeBruin and Moore (1985), which was however rarely applied. They assumed that the mass flow inside the forest compensates the missing mass flow above the forest. The mathematical application needs either a detailed assumption about the wind profile in the forest or better measurements. From the mass flow in the forest, the mass flow above the forest and the resulting wind profile can be determined.

The mixing layer is characterized by the characteristic scales of the Kelvin-Helmholtz instability, where the characteristic length scale of the mixing layer is the shearing scale. Assuming that the inflection point of the wind profile is at the top of the canopy and that the wind velocity within the canopy is significantly lower it follows (Raupach et al. 1996):

$$L_s = \frac{\delta_w}{2} = \frac{u(z_B)}{(\partial u/\partial z)_{z=z_B}} \tag{3.30}$$

The development of the mixing layer above a plant canopy was comprehensively described by Finnigan (2000). The second length scale is the characteristic distance between coherent eddies, which is the wavelength of the initial Kelvin-Helmholtz instability which is the underlying cause of the developing mixing layer. This length scale, Λ_x, can be determined, for example, by a wavelet analysis. According to Raupach et al. (1996) a linear relation exists between both scales

$$\Lambda_x = m L_s, \tag{3.31}$$

with values for m ranging from 7 to 10 for neutral stratification, whereby this value is strongly site dependent (Thomas and Foken 2007a).

A relationship between the shear scale and the height of the roughness sublayer was proposed by Verhoef et al. (1997),

$$z_* = z_B + cL_s, \tag{3.32}$$

with $c = 2$ for the momentum exchange and $c = 3$ for the heat exchange (Mölder et al. 1999).

3.5.4 Coupling Between the Atmosphere and Plant Canopies

The determination of energy exchange above a forest is extremely complicated. Not only the crown space but also the wind shearing above the canopy can decouple the forest from the atmosphere. Therefore, the exchange processes between the forest

and the atmospheric boundary layer is occasionally intermitted. Tall plant canopies are coupled with the atmosphere by turbulent eddies most often during the daytime. Then, the energy and matter exchange takes place between the ground, the trunk space, and the atmosphere above the canopy. Reasons for the occasional decoupling between the canopy and the atmosphere are the high roughness at the upper part of the canopy, which damps the wind field, and the stable stratification in the canopy. The latter is responsible for the enhancement of emitted gases from the ground in the trunk space and large concentrations above the canopy. This can be seen for nitrogen monoxide and carbon dioxide produced by microbiological and respiration processes in the ground. As a rule these concentrations will be removed by turbulent mixing and, in the case of nitrogen monoxide, by reactions with ozone (Foken et al. 2012). However, during calm conditions high concentrations may occur above low vegetation.

Coherent structures are very effective for the characterization of the turbulent exchange process if they can be measured at least at three different heights in the canopy (Thomas and Foken 2007b; Thomas et al. 2013). The dependence of the penetration depth of coherent structures into the canopy can be classified by five states of coupling (Table 3.9). In the case of gravity waves, (Wa) or no penetration of turbulence into the canopy (Dc) no coupling exists. In the case of penetration of turbulence into the crown (Ds), at least the crown is coupled with the atmosphere. A complete coupling (C) is given only for short time periods. More often is seen an occasional or partial coupling of the trunk space and the crown with the atmosphere (Cs). Often it is sufficient to combine the classes Wa and Dc as well as Cs and C to characterize the exchange regime. The typical daily cycle of the phase of coupling together with the contribution of the coherent structures to the flux is shown in Fig. 3.29.

Table 3.9 Characterization of the states of coupling between the atmosphere and tall plant canopies (Thomas and Foken 2007b). The signature with letter is according to the coupling stages in Fig. 3.29 (Figures from Göckede et al. 2007, published with kind permission of © Authors 2007, CC Attribution 4.0 Licence, All rights reserved)

Wa	Dc	Ds	Cs	C
Gravity waves above the canopy	Turbulent eddies only above the canopy	Turbulent mixing up to the crown	Occasionally complete mixing of the canopy	Complete mixing of the canopy
No coupling	No coupling	Occasionally weak coupling	Occasionally coupling	Good coupling
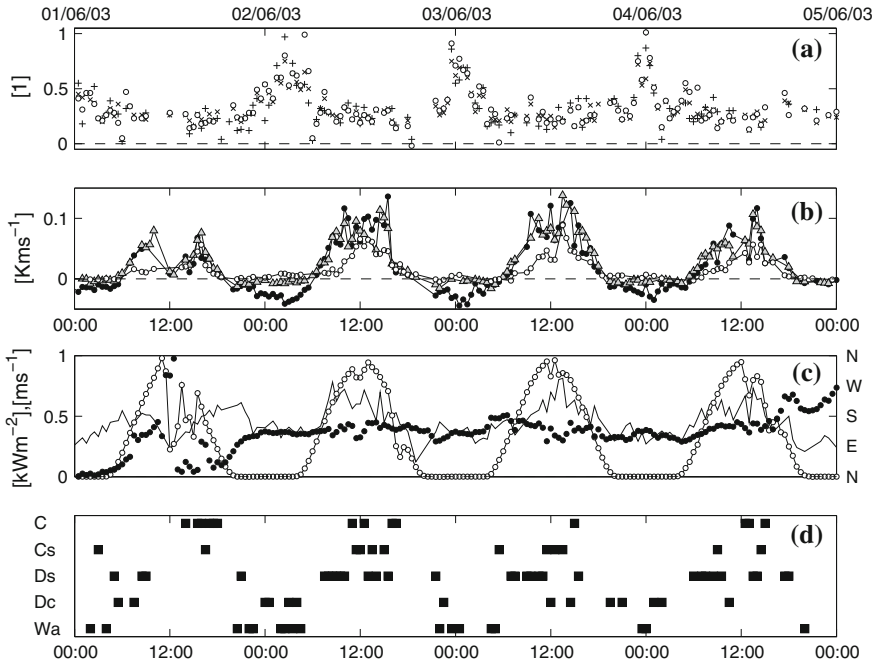
Fig. 3.29 Measurements of the characteristics of the turbulent exchange in the period from June 1 to June 4, 2003 during the experiment WALDATEM-2003 (Waldstein/Weidenbrunnen) in a 19 m high spruce forest in the Fichtelgebirge mountains: **a** Relative contribution of coherent structures to the carbon dioxide exchange (○), buoyancy flux (□) and latent heat flux (+) at 1,74 z_B (z_B: canopy height); **b** Kinematic buoyancy flux of the coherent structure at 1.74 z_B (●), 0.93 z_B (▲) and 0.72 z_B (○); **c** Friction velocity (——), global radiation (○) and wind direction (●) at 1.74 z_B; **d** States of coupling between the atmosphere and the forest (abbreviations see Table 3.9) according to Thomas and Foken (2007b, published with kind permission of © Springer, Berlin, Heidelberg 2007, All rights reserved)

3.6 Advection

Divergences and convergences of the wind field occur above inhomogeneous surfaces, which generates gradients of fluxes, wind velocities and scalars. In a volume element (Fig. 3.30), differences are visible in the horizontal inflow and outflow, characterized by the horizontal wind velocity or the horizontal fluxes. This phenomenon is called horizontal advection. To compensate for the horizontal divergence or convergence, a flow through the upper boundary of the volume element—called vertical advection—is necessary. Therefore, the energy and matter fluxes between the surface and the upper boundary are no longer height-independent. The advection terms are of relevance in micrometeorology, since their influence on the matter exchange must be accounted for in when the eddy covariance method is applied (see Sect. 4.2). Initially a correction for the vertical
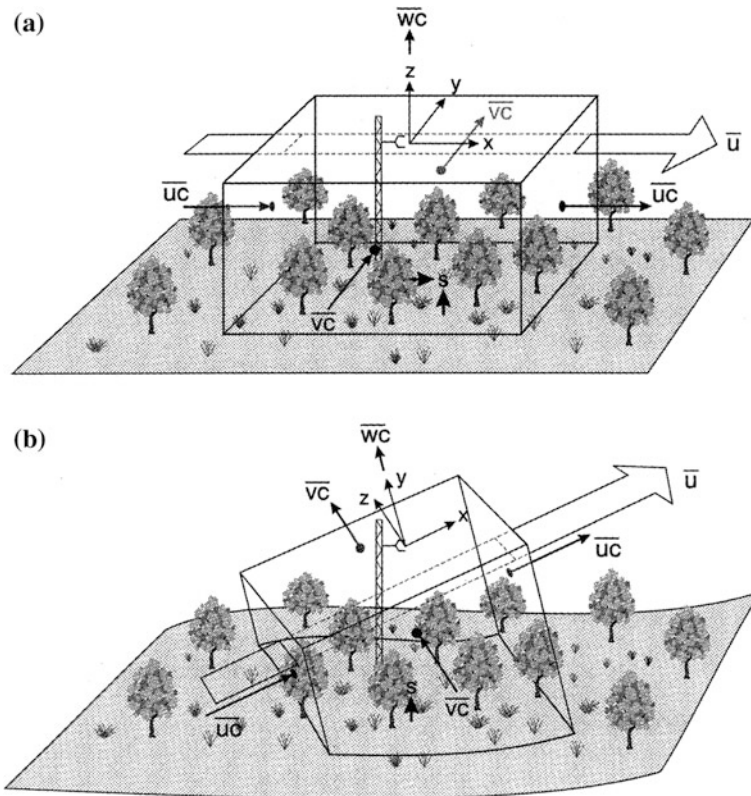
Fig. 3.30 Schematic view of the advection through a volume element for homogeneous terrain (**a**) and for complex topography (**b**). The *x-y* coordinate plane is defined by an ensemble of mean wind vectors and the lid of the control volume is not parallel to the average surface. Adapted from Finnigan et al. (2003, with kind permission of © Kluwer Academic Publisher B.V. Dordrecht 2003, All rights reserved)

advection was proposed (Lee 1998), however the horizontal advection was of the same order (Finnigan 1999; Baldocchi et al. 2000). The balance equation of the net flux $F\chi$ of a volume element is

$$F_\chi = \underbrace{\overline{\rho_d w' \chi'}\big|_h}_{\text{I}} + \underbrace{\int\limits_0^{z_m} \overline{\rho_d \frac{\partial \overline{\chi}}{\partial t}} dz}_{\text{II}} + \underbrace{\int\limits_0^{z_m} \left[\overline{\rho_d u \frac{\partial \overline{\chi}_x}{\partial x}} + \overline{\rho_d v \frac{\partial \overline{\chi}_y}{\partial y}} \right]}_{\text{III}} + \underbrace{\int\limits_0^{z_m} \left[\overline{\rho_d w \frac{\partial \overline{\chi}}{\partial z}} \right]}_{\text{IV}} \quad (3.33)$$

Therefore, the net flux is the sum of the flux above the volume element (I. term), the storage and sink term—determined from the change of the partial density with time—(2. Term, Finnigan 2006), and finally from the horizontal (III. term) and vertical advection (IV. Term). Paw U et al. (2000) showed that the vertical
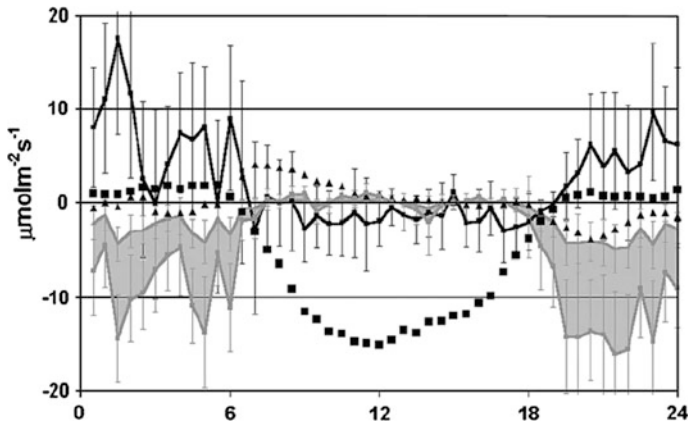
Fig. 3.31 Mean daily cycle of the carbon dioxide exchange: Eddy covariance measurements: *black squares*; storage term: *black triangles* with error bars; vertical advection: *black line* with error bars; horizontal advection: *shadowed area* with error bars, the *upper* and *lower values* are for a height of 3 m or 10 m (Adapted from Aubinet et al. 2003b, with kind permission of © Kluwer Academic Publisher B.V. Dordrecht 2003, All rights reserved)

advection term includes the effect of an additional vertical velocity due to the WPL-correction (Webb et al. 1980) as well as the vertical advection discussed by Lee (1998). The presentation of the advection terms for horizontal fluxes was omitted, because these are probably very small and it is nearly impossible to measure these. The advection terms in Eq. (3.33) are only significant and larger than the vertical flux at night and they probably compensate each other (Fig. 3.31, Aubinet et al. 2003b).

Through extensive measurement campaigns in the last years above heterogeneous surfaces it was found that advection cannot be fully neglected by the application of the eddy-covariance technique (see Sect. 4.2). But, the results were inconsistent (Aubinet 2008). These studies were done under the assumption of prevailing katabatic flow in a terrain with a slide slope. However, concentration differences in tall vegetation can also be generated by coherent structures (Siebicke 2011). This hypothesis appears realistic because in the trunk space of tall vegetation the horizontal coupling (see Sect. 3.5.4) of turbulent structures is not very effective (Serafimovich et al. 2011) and the scale for wind and temperatures are not identical (Thomas 2011).

The influence of micro-fronts should not be confused with advection (Bergström and Högström 1989; Mahrt 1991; Gamage and Hagelberg 1993). They do not move with the wind field but with the phase velocity, which is only identical with the wind velocity at about 4 m s^{-1}, but is otherwise larger (Zubkovskij and Sushko 1987).

3.7   Conditions Under Stable Stratification

During the last few years, the stable or nocturnal atmospheric boundary layer has become an important research topic. In contrast to the convective boundary layer, the stable boundary layer is remarkably shallow. Often it reaches a depth of only 10–100 m. It is referred to as a long-living stable (nocturnal) atmospheric boundary layer if, as in polar regions, it continues over a long time. The stable free atmosphere and the stable boundary layer are often connected by internal gravity waves (Zilitinkevich and Calanca 2000). Due to the negative buoyancy of the stable stratification, the turbulence is strongly damped, and longwave radiation processes have an especially strong influence. These processes have an important role in the development of ground inversions under calm and widely non-turbulent conditions. Under these situations, the phenomenon of a low level jet often occurs at heights of 10–300 m, which can also significantly affect and intensify the fluxes near the surface (Karipot et al. 2008; Mahrt et al. 2013; Duarte et al. 2015). As a general rule, intermittent turbulence and gravity waves are present, and steady-state conditions do not exist. The stability of the layer is most often greater than that at the critical Richardson number.

In Fig. 3.32 it is shown that under stable conditions scalar time series have a turbulent and wavy part. Because of gravity waves, perturbations of the vertical wind velocity are highly connected with changes of scalar quantities, and thus the correlation coefficients may be significantly greater than those for turbulent flow alone (see Sect. 4.1.3). Under this circumstances, flux measurements according to the eddy-covariance method would give an unrealistic overestimation of the turbulent fluxes if the time series were not filtered to remove the wave signal (Foken and Wichura 1996).

Under stable conditions, intermittent flow often occurs. According to a classification of the stable atmospheric boundary layer by Holtslag and Nieuwstadt (1986), this occurs in a range beyond the z-less scaling, i.e. for local Obukhov length $z/\Lambda > 10$ (Fig. 3.33). The exact definition of intermittency is somewhat

Fig. 3.32 Examples of turbulence time series (*above* temperature, experiment FINTUTREX Antarctica) with selection of the wave (*middle*) and the turbulent signal (*below*) after filtering (Handorf and Foken 1997)
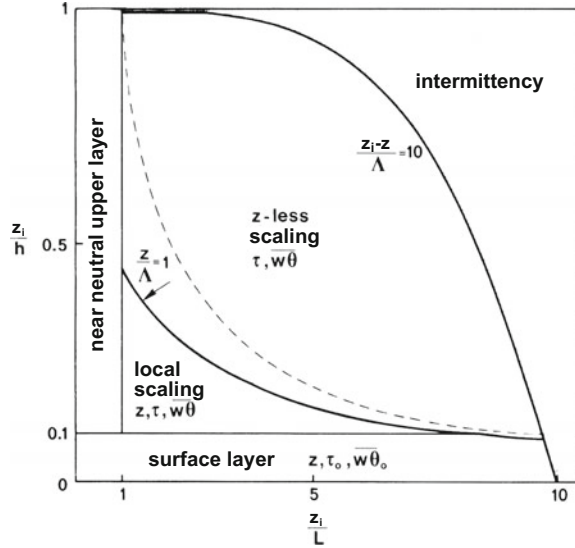
vague because the events must be characterized by relatively long periods with
quasi laminar condition and interruptions by turbulent processes and their inten-
sities. Therefore intermittency cannot be defined only in the micrometeorological
scale. Intermittency factors are the ratio between the local (spatial and temporal)
turbulent fluctuations and those over a longer time period or spatial area. Relatively
convenient is the definition of a local intermittency factor using the wavelet coef-
ficients (Supplement 3.1) according to Farge (1992).

$$I(a,b) = \frac{\left|T_p(a,b_0)\right|^2}{\left(\left|T_p(a,b_0)\right|^2\right)_b}, \tag{3.34}$$

where the contribution to the energy spectrum at the moment b_0 in the scale a can
be considered as the time average in this scale. For $I(a, b) = 1$, no intermittency
occurs. Because the intermittency factor must be determined for all values of a, it is
obvious that intermittent events develop differently at different scales.

A typical phenomenon at stable stratification is the occurrence of gravity waves.
The frequencies of gravity waves at each height are lower than the corresponding
Brunt-Väisälä frequency (Stull 1988):

$$N_{BV}^2 = \frac{g}{\theta_v} \frac{\partial \overline{\theta_v}}{\partial z} \tag{3.35}$$

Using the Brunt-Väisälä frequency, the influence of the stable atmospheric
boundary layer on the near surface exchange processes can be determined
(Zilitinkevich et al. 2002) and this can be used in modelling (see Sect. 5.5).

3.8   Energy Balance Closure

According to experimental results the energy balance equation (Eq. 1.1) is not fulfilled due to limitations of the measurement methods:

$$-Q_s^* - Q_G = Q_H + Q_E + Res \qquad (3.36)$$

The residual *Res* balances the turbulent fluxes, which are lower than the available energy given by the sum of net radiation and ground heat flux. Figure 3.34 shows that even over a homogeneous surface, a large residual of the energy balance closure exists. Thus, during the day the ground surface gets more energy by radiation than can be carried away by turbulent fluxes. Consequently, the ground heat flux and energy storage must be large. In the night, the opposite conditions exist but often within the error bars of the fluxes (Foken 1998; Wilson et al. 2002; Culf et al. 2004; Foken 2008; Foken et al. 2011; Leuning et al. 2012). Panin and Bernhofer (2008) discussed results from different experiments and found a closure-gap especially for heterogeneous surfaces, while for homogeneous surfaces a full closure is given (Heusinkveld et al. 2004; Haverd et al. 2007; Mauder et al. 2007b).

After a workshop held in 2004 in Grenoble (Foken and Oncley 1995) the closure gap of the energy balance was systematically investigated. First studies identified the relatively large measurement errors of the individual components of the energy balance equation as reasons but also the use of different measurement methods (Fig. 3.35) can lead to errors. The individual terms of the energy balance equation are not measured directly at the surface, but either in the air above it or in the soil. Furthermore, the information of the measured fluxes comes from different source
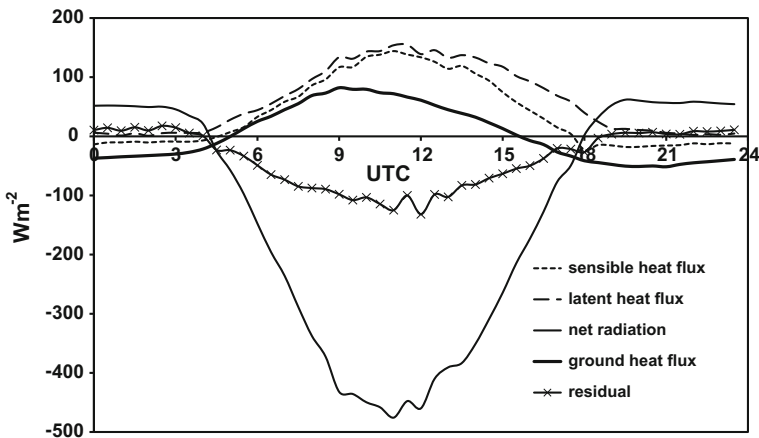
Fig. 3.34 Mean daily cycle of the components of the energy balance above a corn field during LITFASS-2003 (Liebethal 2006)

Fig. 3.35 Schematic view of the measurement area of the different terms of the energy balance equation
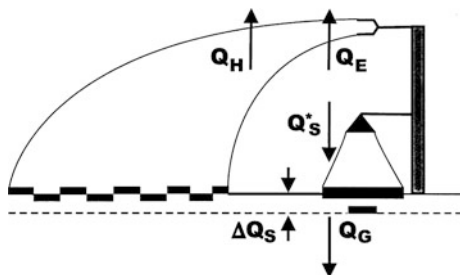
areas. This is very critical for the turbulent fluxes where the measurement, e.g., at 2 m height is connected with a much larger area according to the footprint (see Sect. 3.4), which is up to 200 m upwind from the measurement point (ratio about 1:100).

Of special relevance for the energy balance closure, is energy storage in the upper soil layer (above the soil heat flux measurement). If this heat storage and those of the biomass of high plants (Haverd et al. 2007; Lindroth et al. 2010) is not carefully determined, hysteresis will affect the daily cycle of the energy balance closure (Leuning et al. 2012). Due to the high variability of the irradiation the storage terms may be highly unsteady (Kukharets et al. 2000). At night, when the turbulent fluxes can be neglected, optimal measurements and an exact determination of the ground heat flux at the surface gives a very good closure of the energy balance (Heusinkveld et al. 2004; Mauder et al. 2007b). Thus, the reasons for the energy balance closure problem are no longer assumed to be caused by the soil heat flux. In most cases, storage in low vegetation and in the air column below the turbulence measurements, as well as the energy loss by photosynthesis, are negligible relative to the high energy storage in the soil and in tall vegetation (Oncley et al. 2007).

A focus of the investigations was the measurement errors of the radiative and turbulent fluxes, which more recently were again identified as reasons for the closure gap of the energy balance (e.g Nakai et al. 2006). The experiment EBEX-2000 (Oncley et al. 2007), which was designed for this purpose, yielded some progress regarding the sensor configuration and correction methods. For the determination of the net radiation, a relatively high effort is necessary (see Sect. 6.2.1), because inexpensive net radiometers underestimate the net radiation, and can cause an apparent more accurate closure of the energy balance (Kohsiek et al. 2007). The turbulent fluxes must be carefully corrected (see Sect. 4.2.3), and their quality must be comprehensively controlled (see Sect. 4.2.5). Highly relevant, are the measurements of the moisture fluctuations and the calibration (also during experiments) of the sensors. A careful calculation of the turbulent fluxes can reduce the energy balance closure gap significantly (Mauder and Foken 2006; Mauder et al. 2007a) but cannot close it.

Energy balance closures cannot be used as a quality criteria for turbulent fluxes (Aubinet et al. 2000). This is because the influencing factors are so greatly different,

wrong conclusions are possible. In comparison with similar experiments, energy balance can give only a rough criterion about the accuracy of the fluxes (Aubinet et al. 2003a).

Panin et al. (1998) have shown that heterogeneous surfaces in the vicinity of the measurements can cause low frequency turbulent structures, which cannot be measured with the turbulence systems. A significantly longer averaging time, say over several hours, gives nearly a closure (Finnigan et al. 2003), while averaging times up to 2 h show no significant effects (Foken et al. 2006). Also, the assumption by Kanda et al. (2004) that organized turbulent structures in the lower boundary layer make a contribution to the energy balance closure support these findings. In this context, two experiments are of special interest; one in areas with large-scale homogeneous surfaces in the dessert (Heusinkveld et al. 2004), and the other in the African bush land (Mauder et al. 2007b). In both cases, a closed energy balance was found. Considering the results of these experiments, Foken et al. (2010) have attempted to close the energy balance by investigating secondary circulations and low frequency structures using for the LITFASS-2003 experiment (Beyrich and Mengelkamp 2006). This was followed by determination of circulations using large-eddy simulation and the determination of spatially-averaged fluxes using scintillometer measurements (Meijninger et al. 2006). These low-frequency structures can be considered as meso-scale fluxes (Nakamura and Mahrt 2006), which in contrast to the microscale fluxes measured with the eddy-covariance method show sources and sinks that can be attributed to different land cover types (Charuchittipan et al. 2014).

Although for the absolute clarity about these phenomena, further investigations are necessary, it can be stated that the energy balance closure problem is a scale problem. This is illustrated schematically in Fig. 3.36. Spatial heterogeneities result in stronger vertical exchange (Schmid and Bünzli 1995; Friedrich et al. 2000; Klaassen et al. 2002), which transports energy in meso-scale structures above the surface layer that are not adequately captured by micro-scale measurements in the surface layer. Consequently, very small advective fluxes that cannot easily be measured must prevail in the surface layer. However, according to calculations by Leuning et al. (2012) these advective fluxes cannot completely explain the closure gap of the energy balance.

Fig. 3.36 Schematic of the generation of secondary circulations and the hypothesis of turbulent fluxes at different scales based on small eddies (*s*) and large eddies (*l*) according to Foken (2008, adapted with kind permission of © Ecological Society of America 2008, All rights reserved)
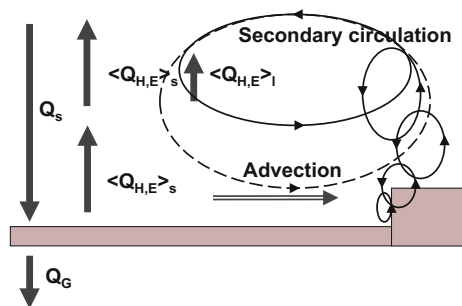
These findings have far ranging consequences. For the determination of turbulent fluxes in heterogeneous areas, methods based on the energy balance equation should not be used. As an example, the Bowen-ratio method (see Sect. 4.2.2) should not be used if it is not accepted that the closure gap is distributed according to the Bowen ratio to the sensible and latent heat flux. Other methods measure the right flux on the small scale, but these methods cannot be transferred to larger areas and do not close the energy balance. In a first approximation, a correction can be made with the Bowen-ratio (Twine et al. 2000) by the distribution of the residual to both turbulent fluxes according this ratio:

$$Q_H^{EBC-Bo} = Q_H + \frac{Bo}{1+Bo} Res \qquad (3.37)$$

$$Q_E^{EBC-Bo} = Q_E + \frac{1}{1+Bo} Res \qquad (3.38)$$

This method is based on the assumption that measurement errors uniformly affect the sensible and latent heat flux. Because scalar similarity is not always fulfilled (Ruppert et al. 2006), this method can cause large errors. Assuming that possible secondary circulations are generated by buoyancy effects, a correction based on the buoyancy flux would be meaningful, e.g. the residual of the energy balance closure is distributed to the sensible and latent heat flux according to the ratio of the temperature and the moisture contribution to the buoyancy effect (Charuchittipan et al. 2014):

$$Q_H^{EBC-HB} = Q_H + f_{HB} Res, \qquad (3.39)$$

$$Q_E^{EBC-HB} = Q_E + (1 - f_{HB}) Res \qquad (3.40)$$

With the factor (see Sect. 4.1.1)

$$f_{HB} = \frac{Q_H}{Q_B} = \left(1 + 0.61 \overline{T} \frac{c_p}{\lambda Bo} \right)^{-1}. \qquad (3.41)$$

This correction method supports the hypothesis that the sensible heat flux has a larger contribution to the energy balance closure than the latent heat flux (Foken et al. 2011; Ingwersen et al. 2011). First applications appear to confirm this hypothesis (Babel et al. 2014). The comparison of the effects of both methods is illustrated in Fig. 3.37.

The energy balance equation is the basis for most atmospheric models, in which the energy balance is closed by definition. Therefore, the energy balance closure problem is still an ongoing issue of research to validate models with experimental data. In these comparisons, one of the energy fluxes is often calculated as a residual, which can lead to large errors. Another approach is to calculate all fluxes assuming one reference surface temperature (Kracher et al. 2009). The latter approach is
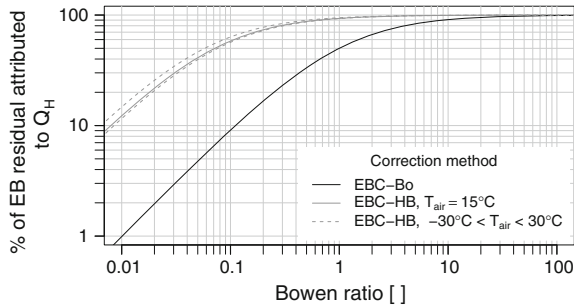
Fig. 3.37 Fraction of the residual attributed to the sensible heat flux at different Bowen ratios from two different approaches. The Bowen ratio approach (EBC-Bo, *black line*) assumes the scalar similarity between the sensible and latent heat fluxes by preserving the Bowen ratio (Twine et al. 2000). The buoyancy flux ratio approach (EBC-HB, *grey lines*) partitions the residual according to the ratio between the sensible heat flux and the buoyancy flux, and is shown at different temperatures from −30 to 30 °C. Although both approaches are identical at very large Bowen ratios, in most cases EBC-HB would attribute a larger fraction of the residual to the sensible heat flux than would EBC-Bo (Adapted from Charuchittipan et al. 2014, with kind permission of © Springer, Berlin, Heidelberg 2014, All rights reserved)

nearly equal to the correction of the energy balance closure with the Bowen ratio (Eqs. 3.37 and 3.38). The high uncertainties for the turbulent fluxes even in the climatological mean are a further indication of the closure problem (Table 1.1).

References

Amiro BD (1990) Comparison of turbulence statistics within three boreal forest canopies. Boundary-Layer Meteorol. 51:99–121.

Amiro BD and Johnson FL (1991) Some turbulence features within a boreal forest canopy during winter. 20th Conference on Agricultural and Forest Meteorology, Salt Lake City, 10–13 Sept. 1991 1991. Am. Meteorol. Soc., pp. 135–138.

Amiro BD (1998) Footprint climatologies for evapotranspiration in a boreal catchment. Agrical Forest Meteorol. 90:195–201.

Andreas EL and Cash BA (1999) Convective heat transfer over wintertime leads and polynyas. J Geophys Res. 104:15.721–725.734.

Andreev EG, Lavorko VS, Pivovarov AA and Chundshua GG (1969) O vertikalnom profile temperatury vblizi granicy rasdela more - atmosphera (About the vertical temperature profile close to to ocean - atmosphere interface). Okeanalogija. 9:348–352.

Antonia RA and Luxton RE (1971) The response of turbulent boundary layer to a step change in surface roughness, Part 1. J Fluid Mech. 48:721–761.

Antonia RA and Luxton RE (1972) The response of turbulent boundary layer to a step change in surface roughness, Part 2. J Fluid Mech. 53:737–757.

Arya SP (2001) Introduction to Micrometeorology. Academic Press, San Diego, 415 pp.

Aubinet M, Grelle A, Ibrom A, Rannik Ü, Moncrieff J, Foken T, Kowalski AS, Martin PH, Berbigier P, Bernhofer C, Clement R, Elbers J, Granier A, Grünwald T, Morgenstern K, Pilegaard K, Rebmann C, Snijders W, Valentini R and Vesala T (2000) Estimates of the annual net carbon and water exchange of forests: The EUROFLUX methodology. Adv Ecol Res. 30:113–175.

Aubinet M, Clement R, Elbers J, Foken T, Grelle A, Ibrom A, Moncrieff H, Pilegaard K, Rannik U and Rebmann C (2003a) Methodology for data acquisition, storage and treatment. In: Valentini R (ed.), Fluxes of Carbon, Water and Energy of European Forests. Ecological Studies, Vol. 163. Springer, Berlin, Heidelberg, 9–35.

Aubinet M, Heinesch B and Yernaux M (2003b) Horizontal and vertical CO_2 advection in a sloping forest. Boundary-Layer Meteorol. 108:397–417.

Aubinet M (2008) Eddy covariance CO_2 flux measurements in nocturnal conditions: An analysis of the problem. Ecol Appl. 18:1368–1378.

Babel W, Biermann T, Coners H, Falge E, Seeber E, Ingrisch J, Schleuß PM, Gerken T, Leonbacher J, Leipold T, Willinghöfer S, Schützenmeister K, Shibistova O, Becker L, Hafner S, Spielvogel S, Li X, Xu X, Sun Y, Zhang L, Yang Y, Ma Y, Wesche K, Graf HF, Leuschner C, Guggenberger G, Kuzyakov Y, Miehe G and Foken T (2014) Pasture degradation modifies the water and carbon cycles of the Tibetan highlands. Biogeosci. 11:6633–6656.

Bailey WG, Oke TR and Rouse WR (eds) (1997) The Surface Climate of Canada. Mc Gill-Queen's University Press, Montreal, Kingston, 369 pp.

Baldocchi D (1997) Flux footprints within and over forest canopies. Boundary-Layer Meteorol. 85:273–292.

Baldocchi DD, Finnigan J, Wilson K, Paw U KT and Falge E (2000) On measuring net ecosystem carbon exchange over tall vegetation on complex terrain. Boundary-Layer Meteorol. 96:257–291.

Baumgartner A (1956) Untersuchungen über den Wärme- und Wasserhaushalt eines jungen Waldes. Ber Dt Wetterdienstes. 28:53 pp.

Bergström H and Högström U (1989) Turbulent exchange above a pine forest. II. Organized structures. Boundary-Layer Meteorol. 49:231–263.

Beyrich F and Mengelkamp H-T (2006) Evaporation over a heterogeneous land surface: EVA_GRIPS and the LITFASS-2003 experiment - an overview. Boundary-Layer Meteorol. 121:5–32.

Biermann T, Babel W, Ma W, Chen X, Thiem E, Ma Y and Foken T (2014) Turbulent flux observations and modelling over a shallow lake and a wet grassland in the Nam Co basin, Tibetan Plateau. Theor Appl Climat. 116:301–316.

Bradley EF (1968) A micrometeorological study of velocity profiles and surface drag in the region modified by change in surface roughness. Quart J Roy Meteorol Soc. 94:361–379.

Brunet Y, Finnigan JJ and Raupach MR (1994) A wind tunnel study of air flow in waving wheat: single-point velocity statistics. Boundary-Layer Meteorol. 70:95–132.

Cai X and Leclerc MY (2007) Forward-in-time and backward-in-time dispersion in the convective boundary layer: The concentration footprint. Boundary-Layer Meteorol. 123:201–218.

Campbell GS and Norman JM (2013) Introduction to Environmental Biophysics. Springer, New York, 312 pp.

Cellier P and Brunet Y (1992) Flux-gradient relationships above tall plant canopies. Agrical Forest Meteorol. 58:93–117.

Charuchittipan D, Babel W, Mauder M, Leps J-P and Foken T (2014) Extension of the averaging time of the eddy-covariance measurement and its effect on the energy balance closure Boundary-Layer Meteorol. 152:303–327.

Chundshua GG and Andreev EG (1980) O mechanizme formirovanija inversii temperatury v privodnoim sloe atmosfery nad morem (About a mechanism of the development of a temperature inversion in the near surface layer above the ocean). Dokl AN SSSR. 255:829–832.

Cionco RM (1978) Analysis of canopy index values for various canopy densities. Boundary-Layer Meteorol. 15:81–93.

Claussen M (1991) Estimation of areally-averaged surface fluxes. Boundary-Layer Meteorol. 54:387–410.

Claussen M and Walmsley JL (1994) Modification of blending procedure in a proposed new PBL resistance law. Boundary-Layer Meteorol. 68:201–205.

Claussen M (1995) Flux aggregation at large scales: on the limits of validity of the concept of blending height. J Hydrol. 166:371–382.

Collineau S and Brunet Y (1993a) Detection of turbulent coherent motions in a forest canopy. Part I: Wavelet analysis. Boundary-Layer Meteorol. 65:357–379.

Collineau S and Brunet Y (1993b) Detection of turbulent coherent motions in a forest canopy. Part II: Time-scales and conditional averages. Boundary-Layer Meteorol. 66:49–73.

Culf AD, Foken T and Gash JHC (2004) The energy balance closure problem. In: Kabat P et al. (eds.), Vegetation, Water, Humans and the Climate. A new Perspective on an Interactive System. Springer, Berlin, Heidelberg, 159–166.

Deardorff JW (1966) The counter-gradient heat flux in the lower atmosphere and in the laboratory. J Atmos Sci. 23:503–506.

DeBruin HAR and Moore JC (1985) Zero-plane displacement and roughness length for tall vegetation, derived from a simple mass conservation hypothesis. Boundary-Layer Meteorol. 38:39–49.

DeBruin HAR, Bink NJ and Kroon LJ (1991) Fluxes in the surface layer under advective conditions. In: Schmugge TJ and André JC (eds.), Workshop on Land Surface Evaporation, Measurement and Parametrization. Springer, New York, 157–169.

Denmead DT and Bradley EF (1985) Flux-gradient relationships in a forest canopy. In: Hutchison BA and Hicks BB (eds.), The Forest-Atmosphere Interaction. D. Reidel Publ. Comp., Dordrecht, Boston, London, 421–442.

Denmead DT and Bradley EF (1987) On scalar transport in plant canopies. Irrig Sci. 8:131–149.

Duarte H, Leclerc M, Zhang G, Durden D, Kurzeja R, Parker M and Werth D (2015) Impact of Nocturnal Low-Level Jets on Near-Surface Turbulence Kinetic Energy. Boundary-Layer Meteorol. 156:349–370.

Dupont S and Brunet Y (2009) Coherent structures in canopy edge flow: a large-eddy simulation study. J Fluid Mech. 630:93–128.

Eder F, Serafimovich A and Foken T (2013) Coherent structures at a forest edge: Properties, coupling and impact of secondary circulations. Boundary-Layer Meteorol. 148:285–308.

Eigenmann R, Metzger S and Foken T (2009) Generation of free convection due to changes in the local circulation system. Atmos Chem Phys. 9:8587–8600.

Elliott WP (1958) The growth of the atmospheric internal boundary layer. Trans Am Geophys Union. 39:1048–1054.

Farge M (1992) Wavelet transforms and their application to turbulence. Annu. Rev. Fluid Mech. 24:395–347.

Fiedler F and Panofsky HA (1972) The geostrophic drag coefficient and the 'effective' roughness length. Quart J Roy Meteorol Soc. 98:213–220.

Finn D, Lamb B, Leclerc MY and Horst TW (1996) Experimental evaluation of analytical and Lagrangian surface-layer flux footprint models. Boundary-Layer Meteorol. 80:283–308.

Finn D, Lamb B, Leclerc MY, Lovejoy S, Pecknold S and Schertzer D (2001) Multifractal analysis of line-source plume concentration fluctuations in surface-layer flows. J Appl Meteorol. 40:229–245.

Finnigan J (1999) A comment on the paper by Lee (1998): "On micrometeorological observations of surface-air exchange over tall vegetation". Agrical Forest Meteorol. 97:55–64.

Finnigan J (2000) Turbulence in plant canopies. Ann Rev Fluid Mech. 32:519–571.

Finnigan J (2006) The storage term in eddy flux calculations. Agrical Forest Meteorol. 136:108–113.

Finnigan JJ, Clement R, Malhi Y, Leuning R and Cleugh HA (2003) A re-evaluation of long-term flux measurement techniques, Part I: Averaging and coordinate rotation. Boundary-Layer Meteorol. 107:1–48.

Finnigan JJ, Shaw RH and Patton EG (2009) Turbulence structure above a vegetation canopy. J Fluid Mech. 637:687–424.

Foken T and Kuznecov OA (1978) Die wichtigsten Ergebnisse der gemeinsamen Expedition "KASPEX-76" des Institutes für Ozeanologie Moskau und der Karl-Marx-Universität Leipzig. Beitr. Meeresforsch. 41:41–47.

Foken T (1990) Turbulenter Energieaustausch zwischen Atmosphäre und Unterlage - Methoden, meßtechnische Realisierung sowie ihre Grenzen und Anwendungsmöglichkeiten. Ber Dt Wetterdienstes. 180:287 pp.

Foken T and Oncley SP (1995) Results of the workshop 'Instrumental and methodical problems of land surface flux measurements'. Bull Amer Meteorol Soc. 76:1191–1193.

Foken T and Wichura B (1996) Tools for quality assessment of surface-based flux measurements. Agrical Forest Meteorol. 78:83–105.

Foken T (1998) Die scheinbar ungeschlossene Energiebilanz am Erdboden - eine Herausforderung an die Experimentelle Meteorologie. Sitzungsberichte der Leibniz-Sozietät. 24:131–150.

Foken T and Leclerc MY (2004) Methods and limitations in validation of footprint models. Agrical Forest Meteorol. 127:223–234.

Foken T, Wimmer F, Mauder M, Thomas C and Liebethal C (2006) Some aspects of the energy balance closure problem. Atmos Chem Phys. 6:4395–4402.

Foken T (2008) The energy balance closure problem – An overview. Ecolog Appl. 18:1351–1367.

Foken T, Mauder M, Liebethal C, Wimmer F, Beyrich F, Leps J-P, Raasch S, DeBruin HAR, Meijninger WML and Bange J (2010) Energy balance closure for the LITFASS-2003 experiment. Theor Appl Climat. 101:149–160.

Foken T, Aubinet M, Finnigan J, Leclerc MY, Mauder M and Paw U KT (2011) Results of a panel discussion about the energy balance closure correction for trace gases. Bull Amer Meteorol Soc:ES13-ES18.

Foken T, Meixner FX, Falge E, Zetzsch C, Serafimovich A, Bargsten A, Behrendt T, Biermann T, Breuninger C, Dix S, Gerken T, Hunner M, Lehmann-Pape L, Hens K, Jocher G, Kesselmeier J, Lüers J, Mayer JC, Moravek A, Plake D, Riederer M, Rütz F, Scheibe M, Siebicke L, Sörgel M, Staudt K, Trebs I, Tsokankunku A, Welling M, Wolff V and Zhu Z (2012) Coupling processes and exchange of energy and reactive and non-reactive trace gases at a forest site – results of the EGER experiment. Atmos Chem Phys. 12:1923–1950.

Foken T (2013) Application of footprint models for wind turbine locations. Meteorol Z. 22:111–115.

Friedrich K, Mölders N and Tetzlaff G (2000) On the influence of surface heterogeneity on the Bowen-ratio: A theoretical case study. Theor Appl Climat. 65:181–196.

Gamage N and Hagelberg C (1993) Detection and analysis of microfronts and associated coherent events using localized transforms. J Atmos Sci. 50:750–756.

Gao W, Shaw RH and Paw U KT (1989) Observation of organized structure in turbulent flow within and above a forest canopy. Boundary-Layer Meteorol. 47:349–377.

Garratt JR (1978) Flux profile relations above tall vegetation. Quart J Roy Meteorol Soc. 104:199–211.

Garratt JR (1980) Surface influence upon vertical profiles in the atmospheric near surface layer. Quart J Roy Meteorol Soc. 106:803–819.

Garratt JR (1990) The internal boundary layer - A review. Boundary-Layer Meteorol. 50:171–203.

Garratt JR (1992) The Atmospheric Boundary Layer. Cambridge University Press, Cambridge, 316 pp.

Gash JHC (1986) A note on estimating the effect of a limited fetch on micrometeorological evaporation measurements. Boundary-Layer Meteorol. 35:409–414.

Geiger R (2013) Das Klima der bodennahen Luftschicht. Springer Vieweg, Wiesbaden, 646 pp.

Göckede M, Rebmann C and Foken T (2004) A combination of quality assessment tools for eddy covariance measurements with footprint modelling for the characterisation of complex sites. Agrical Forest Meteorol. 127:175–188.

Göckede M, Markkanen T, Mauder M, Arnold K, Leps J-P and Foken T (2005) Validation footprint models using natural tracer. Agrical Forest Meteorol. 135:314–325.

Göckede M, Markkanen T, Hasager CB and Foken T (2006) Update of a footprint-based approach for the characterisation of complex measuring sites. Boundary-Layer Meteorol. 118:635–655.

Göckede M, Thomas C, Markkanen T, Mauder M, Ruppert J and Foken T (2007) Sensitivity of Lagrangian stochastic footprints to turbulence statistics. Tellus. 59B:577–586.

Göckede M, Foken T, Aubinet M, Aurela M, Banza J, Bernhofer C, Bonnefond J-M, Brunet Y, Carrara A, Clement R, Dellwik E, Elbers JA, Eugster W, Fuhrer J, Granier A, Grünwald T, Heinesch B, Janssens IA, Knohl A, Koeble R, Laurila T, Longdoz B, Manca G, Marek M, Markkanen T, Mateus J, Matteucci G, Mauder M, Migliavacca M, Minerbi S, Moncrieff JB, Montagnani L, Moors E, Ourcival J-M, Papale D, Pereira J, Pilegaard K, Pita G, Rambal S, Rebmann C, Rodrigues A, Rotenberg E, Sanz MJ, Sedlak P, Seufert G, Siebicke L, Soussana JF, Valentini R, Vesala T, Verbeeck H and Yakir D (2008) Quality control of CarboEurope flux data – Part 1: Coupling footprint analyses with flux data quality assessment to evaluate sites in forest ecosystems. Biogeosci. 5:433–450.

Goudriaan J (1977) Crop micrometeorology: A simulation study. Center for Agricultural Publishing and Documentation, Wageningen, 249 pp.

Graefe J (2004) Roughness layer corrections with emphasis on SVAT model applications. Agrical Forest Meteorol. 124:237–251.

Grimmond CSB and Oke TR (1999) Aerodynamic properties of urban areas derived from analysis of surface form. J Appl Meteorol. 38:1262–1292.

Grimmond CSB and Oke TR (2000) Corrigendum. J Appl Meteorol. 39:2494.

Gryning S-E, van Ulden AP and Larsen S (1983) Dispersions from a ground level source investigated by a K model. Quart J Roy Meteorol Soc. 109:355–364.

Handorf D and Foken T (1997) Analysis of turbulent structure over an Antarctic ice shelf by means of wavelet transformation. 12th Symposium on Boundary Layer and Turbulence, Vancouver BC, Canada, 28 July - 1 August 1997 1997. Am. Meteorol. Soc., pp. 245–246.

Hari P, Heliövaara K and Kulmala L (eds) (2013) Physical and Physiological Forest Ecology. Springer, Dordrecht, Heidelberg, New York, London, 534 pp.

Harman IN and Finnigan JJ (2007) A simple unified theory for flow in the canopy and roughness sublayer. Boundary-Layer Meteorol. 123:339–363.

Harman IN and Finnigan JJ (2008) Scalar concentration profiles in the canopy and roughness sublayer. Boundary-Layer Meteorol. 129:323–351.

Hasager CB and Jensen NO (1999) Surface-flux aggregation in heterogeneous terrain. Quart J Roy Meteorol Soc. 125:2075–2102.

Haverd V, Cuntz M, Leuning R and Keith H (2007) Air and biomass heat storage fluxes in a forest canopy: Calculation within a soil vegetation atmosphere transfer model. Agrical Forest Meteorol. 147:125–139.

Herzog H-J, Vogel G and Schubert U (2002) LLM - a nonhydrostatic model applied to high-resolving simulation of turbulent fluxes over heterogeneous terrain. Theor Appl Climat. 73:67–86.

Heusinkveld BG, Jacobs AFG, Holtslag AAM and Berkowicz SM (2004) Surface energy balance closure in an arid region: role of soil heat flux. Agrical Forest Meteorol. 122:21–37.

Holmes P, Lumley JL and Berkooz G (1996) Turbulence, coherent structures, dynamical systems and symmetry. Cambridge University Press, Cambridge, 420 pp.

Holtslag AAM and Nieuwstadt FTM (1986) Scaling the atmospheric boundary layer. Boundary-Layer Meteorol. 36:201–209.

Horst TW and Weil JC (1992) Footprint estimation for scalar flux measurements in the atmospheric surface layer. Boundary-Layer Meteorol. 59:279–296.

Horst TW and Weil JC (1994) How far is far enough?: The fetch requirements for micrometeorological measurement of surface fluxes. J Atm Oceanic Techn. 11:1018 - 1025.

Horst TW and Weil JC (1995) Corrigenda: How far is far enough?: The fetch requirements for micrometeorological measurement of surface fluxes. J Atm Oceanic Techn. 12:447.

Horst TW (1999) The footprint for estimation of atmosphere-surface exchange fluxes by profile techniques. Boundary-Layer Meteorol. 90:171–188.

Hsieh C-I, Katul G and Chi T-W (2000) An approximate analytical model for footprint estimation of scalar fluxes in thermally stratified atmospheric flows. Adv Water Res. 23:765–772.

Hsieh C-I and Katul G (2009) The Lagrangian stochastic model for estimating footprint and water vapor fluxes over inhomogeneous surfaces. Int J Biometeorol. 53:87–100.

Hupfer P, Foken T and Bachstein U (1976) Fine structure of the internal boundary layer in the near shore zone of the sea. Boundary-Layer Meteorol. 10:503–505.

Hurtalova T, Vidovitsch J, Matejka F and Mudry P (1988) Dinamitscheskaja sherochovatost i biometritscheskie charakteristiki kukuruzy v ontogeneze (Dynamical roughness and biometric characteristics of corn during the ontogenesis). Contr Geophys Inst Slovak Akad Sci. 8:46–53.

Hurtalová T, Matejka F and Vidovic J (1983) Untersuchung der Oberflächenrauhigkeit und ihrer Variation auf Grund von Strukturveränderungen des Maisbestandes während der Ontogenese. Z Meteorol. 33:368–372.

Inclán MG, Forkel R, Dlugi R and Stull RB (1996) Application of transilient turbulent theory to study interactions between the atmospheric boundary layer and forest canopies. Boundary-Layer Meteorol. 79:315–344.

Ingwersen J, Steffens K, Högy P, Warrach-Sagi K, Zhunusbayeva D, Poltoradnev M, Gäbler R, Wizemann H-D, Fangmeier A, Wulfmeyer V and Streck T (2011) Comparison of Noah simulations with eddy covariance and soil water measurements at a winter wheat stand. Agrical Forest Meteorol. 151:345–355.

Jegede OO and Foken T (1999) A study of the internal boundary layer due to a roughness change in neutral conditions observed during the LINEX field campaigns. Theor Appl Climat. 62:31–41.

Jones HG (2013) Plants and Microclimate. Cambridge Univ. Press, Cambridge, 423 pp.

Kaharabata SK, Schuepp PH, Ogunjemiyo S, Shen S, Leclerc MY, Desjardins RL and MacPherson JI (1997) Footprint considerations in BOREAS. J Geophys Res. 102 (D24):29113–29124.

Kaimal JC and Finnigan JJ (1994) Atmospheric Boundary Layer Flows: Their Structure and Measurement. Oxford University Press, New York, NY, 289 pp.

Kanda M, Moriwaki R, Roth M and Oke T (2002) Area-averaged sensible heat flux and a new method to determine zero-plane displacement length over an urban surface using scintillometry. Boundary-Layer Meteorol. 105:177–193.

Kanda M, Inagaki A, Letzel MO, Raasch S and Watanabe T (2004) LES study of the energy imbalance problem with eddy covariance fluxes. Boundary-Layer Meteorol. 110:381–404.

Karipot A, Leclerc MY, Zhang G, Lewin KF, Nagy J, Hendrey GR and Starr D (2008) Influence of nocturnal low-level jet on turbulence structure and CO_2 flux measurements over a forest canopy J Geophys Res. 113:D10102.

Kitajgorodskij SA and Volkov JA (1965) O rascete turbulentnych potokov tepla i vlagi v privodnom sloe atmosfery (The calculation of the turbulent fluxes of temperature and humidity in the atmosphere near the water surface) Izv AN SSSR, Fiz Atm Okeana. 1:1317–1336.

Klaassen W, van Breugel PB, Moors EJ and Nieveen JP (2002) Increased heat fluxes near a forest edge. Theor Appl Climat. 72:231–243.

Kljun N, Rotach MW and Schmid HP (2002) A three-dimensional backward Lagrangian footprint model for a wide range of boundary layer stratification. Boundary-Layer Meteorol. 103:205–226.

Kljun N, Calanca P, Rotach M and Schmid HP (2004) A simple parameterization for flux footprint predictions. Boundary-Layer Meteorol. 112:503–523.

Kljun N, Calanca P, Rotach MW and Schmid HP (2015) A simple two-dimensional parameterisation for Flux Footprint Prediction (FFP). Geosci Model Dev. 8:3695–3713.

Kohsiek W, Liebethal C, Foken T, Vogt R, Oncley SP, Bernhofer C and DeBruin HAR (2007) The Energy Balance Experiment EBEX-2000. Part III: Behaviour and quality of radiation measurements. Boundary-Layer Meteorol. 123:55–75.

Koitzsch R, Dzingel M, Foken T and Mücket G (1988) Probleme der experimentellen Erfassung des Energieaustausches über Winterweizen. Z Meteorol. 38:150–155.

Kormann R and Meixner FX (2001) An analytical footprint model for non-neutral stratification. Boundary-Layer Meteorol. 99:207–224.

Kracher D, Mengelkamp H-T and Foken T (2009) The residual of the energy balance closure and its influence on the results of three SVAT models. Meteorol Z. 18:647–661.

Kukharets VP, Nalbandyan HG and Foken T (2000) Thermal interactions between the underlying surface and a nonstationary radiation flux. Izv Atmos Ocenanic Phys. 36:318–325.

Leclerc MY and Thurtell GW (1989) Footprint Predictions of Scalar Fluxes and Concentration Profiles using a Markovian Analysis 19th Conference of Agricultural and Forest Meteorology, Charleston, SC, March 7–10, 1989 1989. American Meteorological Society.

Leclerc MY and Thurtell GW (1990) Footprint prediction of scalar fluxes using a Markovian analysis. Boundary-Layer Meteorol. 52:247–258.

Leclerc MY, Shen S and Lamb B (1997) Observations and large-eddy simulation modeling of footprints in the lower convective boundary layer. J Geophys Res. 102(D8):9323–9334.

Leclerc MY and Foken T (2014) Footprints in Micrometeorology and Ecology. Springer, Heidelberg, New York, Dordrecht, London, XIX, 239 pp.

Lee R (1978) Forest Microclimatology. Columbia University Press, New York, 276 pp.

Lee X (1998) On micrometeorological observations of surface-air exchange over tall vegetation. Agrical Forest Meteorol. 91:39–49.

Lettau H (1969) Note on aerodynamic roughness-parameter estimation on the basis of roughness-element description. J Appl Meteorol. 8:828–832.

Leuning R, van Gorsel E, Massman WJ and Isaac PR (2012) Reflections on the surface energy imbalance problem. Agrical Forest Meteorol. 156:65–74.

Liebethal C (2006) On the determination of the ground heat flux in micrometeorology and its influence on the energy balance closure. PhD thesis, University of Bayreuth, Bayreuth, 143 pp.

Lindroth A, Mölder M and Lagergren F (2010) Heat storage in forest biomass improves energy balance closure. Biogeosci. 7:301–313.

Logan E and Fichtl GH (1975) Rough to smooth transition of the equilibrium neutral constant stress layer. Boundary-Layer Meteorol. 8:525–528.

Lüers J and Bareiss J (2010) The effect of misleading surface temperature estimations on the sensible heat fluxes at a high Arctic site – the Arctic Turbulence Experiment 2006 on Svalbard (ARCTEX-2006). Atmos Chem Phys. 10:157–168.

MacDonald RW, Griffiths RF and Hall DJ (1998) An improved method for the estimation of surface roughness of obstacle arrays. Atmos Environm. 32:1857–1864.

Mahrt L (1991) Eddy asymmetry in the sheared heated boundary layer. J Atmos Sci. 48:472–492.

Mahrt L (1996) The bulk aerodynamic formulation over heterogeneous surfaces. Boundary-Layer Meteorol. 78:87–119.

Mahrt L, Thomas C, Richardson S, Seaman N, Stauffer D and Zeeman M (2013) Non-stationary generation of weak turbulence for very stable and weak-wind conditions. Boundary-Layer Meteorol. 147:179–199.

Markkanen T, Steinfeld G, Kljun N, Raasch S and Foken T (2009) Comparison of conventional Lagrangian stochastic footprint models against LES driven footprint estimates. Atmos Chem Phys. 9:5575–5586.

Marunitsch SV (1971) Charakteristiki turbulentnosti v yslovijach lesa po gradientnym i strukturnym nabljudenijam (Turbulence characteristics of gradients in a forest from structure observations). Trudy Gos Gidrometeorol Inst. 198:154–165.

Mason PJ (1988) The formation of areally-averaged roughness length. Quart J Roy Meteorol Soc. 114:399–420.

Mauder M and Foken T (2006) Impact of post-field data processing on eddy covariance flux estimates and energy balance closure. Meteorol Z. 15:597–609.

Mauder M, Oncley SP, Vogt R, Weidinger T, Ribeiro L, Bernhofer C, Foken T, Kohsiek W, DeBruin HAR and Liu H (2007a) The Energy Balance Experiment EBEX-2000. Part II: Intercomparison of eddy covariance sensors and post-field data processing methods. Boundary-Layer Meteorol. 123:29–54.

Mauder M, Jegede OO, Okogbue EC, Wimmer F and Foken T (2007b) Surface energy flux measurements at a tropical site in West-Africa during the transition from dry to wet season. Theor Appl Climat. 89:171–183.

Maurer KD, Bohrer G, Kenny WT and Ivanov VY (2015) Large-eddy simulations of surface roughness parameter sensitivity to canopy-structure characteristics. Biogeosci. 12:2533–2548.

Meijninger WML, Lüdi A, Beyrich F, Kohsiek W and DeBruin HAR (2006) Scintillometer-based turbulent surface fluxes of sensible and latent heat over heterogeneous a land surface — A contribution to LITFASS-2003. Boundary-Layer Meteorol. 121:89–110.

Meyers TP and Paw U KT (1986) Testing a higher-order closure model for modelling airflow within and above plant canopies. Boundary-Layer Meteorol. 37:297–311.

Meyers TP and Paw U KT (1987) Modelling the plant canopy microenvironment with higher-order closure principles. Agrical Forest Meteorol. 41:143–163.

Mölder M, Grelle A, Lindroth A and Halldin S (1999) Flux-profile relationship over a boreal forest - roughness sublayer correction. Agrical Forest Meteorol. 98–99:645–648.

Monson R and Baldocchi D (2014) Terrestrial Biosphere-Atmosphere Fluxes. Cambridge University Press, New York, XXI, 487 pp.

Nakai T, van der Molen MK, Gash JHC and Kodama Y (2006) Correction of sonic anemometer angle of attack errors. Agrical Forest Meteorol. 136:19–30.

Nakamura R and Mahrt L (2006) Vertically integrated sensible-heat budgets for stable nocturnal boundary layers. Quart J Roy Meteorol Soc. 132:383–403.

Nikuradse J (1933) Strömungsgesetze an rauhen Rohren. VDI Forschungshefte. 361.

Oncley SP, Foken T, Vogt R, Kohsiek W, DeBruin HAR, Bernhofer C, Christen A, van Gorsel E, Grantz D, Feigenwinter C, Lehner I, Liebethal C, Liu H, Mauder M, Pitacco A, Ribeiro L and Weidinger T (2007) The energy balance experiment EBEX-2000, Part I: Overview and energy balance. Boundary-Layer Meteorol. 123:1–28.

Panin G and Bernhofer C (2008) Parametrization of turbulent fluxes over inhomogeneous landscapes. Izvestiya Atmospheric and Oceanic Physics. 44:701–716.

Panin GN, Tetzlaff G and Raabe A (1998) Inhomogeneity of the land surface and problems in the parameterization of surface fluxes in natural conditions. Theor Appl Climat. 60:163–178.

Panofsky HA (1984) Vertical variation of roughness length at the Boulder Atmospheric Observatory. Boundary-Layer Meteorol. 28:305–308.

Paw U KT, Baldocchi D, Meyers TP and Wilson KB (2000) Correction of eddy covariance measurements incorporating both advective effects and density fluxes. Boundary-Layer Meteorol. 97:487–511.

Pearson jr. RJ, Oncley SP and Delany AC (1998) A scalar similarity study based on surface layer ozone measurements over cotton during the California Ozone Deposition Experiment. J Geophys Res. 103 (D15):18919–18926.

Perera MD (1981) Shelder behind two dimensional solit and porous fences. J Wind Engin Industrial Aerodyn. 8:93–104.

Peterson EW (1969) Modification of mean flow and turbulent energy by a change in surface roughness under conditions of neutral stability. Quart J Roy Meteorol Soc. 95:561–575.

Philip JR (1997) Blending and internal boundary-layer heights, and shear stress. Boundary-Layer Meteorol. 84:85–89.

Prabha T, Leclerc MY and Baldocchi D (2008) Comparison of in-canopy flux footprints between Large-Eddy Simulation and the Lagrangian simulation. J Appl Meteorol Climatol. 47:2115–2128.

Pyles RD, Weare BC and Paw U KT (2000) The UCD Advanced Canopy-Atmosphere-Soil Algorithm: comparisons with observations from different climate and vegetation regimes. Quart J Roy Meteorol Soc. 126:2951–2980.

Raabe A (1983) On the relation between the drag coefficient and fetch above the sea in the case of off-shore wind in the near shore zone. Z Meteorol. 33:363–367.

Raabe A (1991) Die Höhe der internen Grenzschicht. Z Meteorol. 41:251–261.

Radikevitsch VM (1971) Transformazija dinamitscheskich charakteristik vozduschnogo potoka pod vlijaniem izmenenija scherochovatosti postilajustschej poverchnosti (Transformation of

the dynamical characteristics of the wind field under the influence of a changing surface roughness) Izv AN SSSR, Fiz Atm Okeana. 7:1241–1250.

Rannik Ü, Aubinet M, Kurbanmuradov O, Sabelfeld KK, Markkanen T and Vesala T (2000) Footprint analysis for measurements over heterogeneous forest. Boundary-Layer Meteorol. 97:137–166.

Rannik Ü, Markkanen T, Raittila T, Hari P and Vesala T (2003) Turbulence statistics inside and above forest: Influence on footprint prediction. Boundary-Layer Meteorol. 109:163–189.

Rannik Ü, Sogachev A, Foken T, Göckede M, Kljun N, Leclerc MY and Vesala T (2012) Footprint analysis. In: Aubinet Met al (eds.), Eddy Covariance: A Practical Guide to Measurement and Data Analysis. Springer, Berlin, Heidelberg, 211–261.

Rao KS, Wyngaard JC and Coté OR (1974) The structure of the two-dimensional internal boundary layer over a sudden change of surface roughness. J Atmos Sci. 31:738–746.

Raupach MR, Thom AS and Edwards I (1980) A wind-tunnel study of turbulent flow close to regularly arrayed rough surface. Boundary-Layer Meteorol. 18:373–379.

Raupach MR and Legg BJ (1984) The uses and limitations of flux-gradient relationships in micrometeorology. Agricult Water Managem. 8:119–131.

Raupach MR (1992) Drag and drag partition on rough surfaces. Boundary-Layer Meteorol. 60:375–395.

Raupach MR (1994) Simplified expressions for vegetation roughness length and zero-plane displacement as functions of canopy height and area index. Boundary-Layer Meteorol. 71:211–216.

Raupach MR, Finnigan JJ and Brunet Y (1996) Coherent eddies and turbulence in vegetation canopies: the mixing-layer analogy. Boundary-Layer Meteorol. 78:351–382.

Raynor GS, Michael P, Brown RM and SethuRaman S (1975) Studies of atmospheric diffusion from a nearshore oceanic site. J Climate Appl Meteorol. 14:1080–1094.

Rebmann C, Göckede M, Foken T, Aubinet M, Aurela M, Berbigier P, Bernhofer C, Buchmann N, Carrara A, Cescatti A, Ceulemans R, Clement R, Elbers J, Granier A, Grünwald T, Guyon D, Havránková K, Heinesch B, Knohl A, Laurila T, Longdoz B, Marcolla B, Markkanen T, Miglietta F, Moncrieff H, Montagnani L, Moors E, Nardino M, Ourcvial J-M, Rambal S, Rannik U, Rotenberg E, Sedlak P, Unterhuber G, Vesala T and Yakir D (2005) Quality analysis applied on eddy covariance measurements at complex forest sites using footprint modelling. Theor Appl Climat. 80:121–141.

Reth S, Göckede M and Falge E (2005) CO_2 efflux from agricultural soils in Eastern Germany - comparison of a closed chamber system with eddy covariance measurements. Theor Appl Climat. 80:105–120.

Ross J (1981) The radiation regime and architecture of plant stands. Dr. W. Junk Publishers, The Hague, 391 pp.

Roth M, Salmond J and Satyanarayana A (2006) Methodological considerations regarding the measurement of turbulent fluxes in the urban roughness sublayer: The role of scintillometry. Boundary-Layer Meteorol. 121:351–375.

Rummel U, Ammann C and Meixner FX (2002) Characterizing turbulent trace gas exchange above a dense tropical rain forest using wavelet and surface renewal analysis. 15th Symposium on Boundary Layer and Turbulence, Wageningen, NL, 15–19 July 2002 2002. Am. Meteorol. Soc., pp. 602–605.

Ruppert J, Thomas C and Foken T (2006) Scalar similarity for relaxed eddy accumulation methods. Boundary-Layer Meteorol. 120:39–63.

Savelyev SA and Taylor PA (2001) Notes on an internal boundary-layer height formula. Boundary-Layer Meteorol. 101:293–301.

Savelyev SA and Taylor PA (2005) Internal boundary layers: I. Height formulae for neutral and diabatic flow. Boundary-Layer Meteorol. 115:1–25.

Schatzmann M, König G and Lohmeyer A (1986) Physikalische Modellierung mikrometeorologischer Vorgänge im Windkanal. Meteorol Rundschau. 39:44–59.

Schlegel F, Stiller J, Bienert A, Maas H-G, Queck R and Bernhofer C (2012) Large-Eddy Simulation of Inhomogeneous Canopy Flows Using High Resolution Terrestrial Laser Scanning Data. Boundary-Layer Meteorol. 142:223–243.

Schmid HP and Oke TR (1988) Estimating the source area of a turbulent flux measurement over a patchy surface. 8th Symposium on Turbulence and Diffusion, San Diego, CA., April 26–29, 1988 1988. Am. Meteorol. Soc., pp. 123–126.

Schmid HP and Oke TR (1990) A model to estimate the source area contributing to turbulent exchange in the surface layer over patchy terrain. Quart J Roy Meteorol Soc. 116:965–988.

Schmid HP (1994) Source areas for scalars and scalar fluxes. Boundary-Layer Meteorol. 67:293–318.

Schmid HP and Bünzli D (1995) The influence of the surface texture on the effective roughness length. Quart J Roy Meteorol Soc. 121:1–21.

Schmid HP (1997) Experimental design for flux measurements: matching scales of observations and fluxes. Agrical Forest Meteorol. 87:179–200.

Schmid HP (2002) Footprint modeling for vegetation atmosphere exchange studies: A review and perspective. Agrical Forest Meteorol. 113:159–184.

Schuepp PH, Leclerc MY, MacPherson JI and Desjardins RL (1990) Footprint prediction of scalar fluxes from analytical solutions of the diffusion equation. Boundary-Layer Meteorol. 50:355–373.

Serafimovich A, Thomas C and Foken T (2011) Vertical and horizontal transport of energy and matter by coherent motions in a tall spruce canopy. Boundary-Layer Meteorol. 140:429–451.

Shaw RH, Silversides RH and Thurtell GW (1974) Some observations of turbulence and turbulent transport within and above plant canopies. Boundary-Layer Meteorol. 5:429–449.

Shaw RH (1977) Secondary wind speed maxima inside plant canopies. J Appl Meteorol. 16:514–521.

Shen S and Leclerc MY (1994) Large-eddy simulation of small scale surface effects on the convective boundary layer structure. Atmosphere-Ocean. 32:717–731.

Shir CC (1972) A numerical computation of the air flow over a sudden change of surface roughness. J Atmos Sci. 29:304–310.

Shuttleworth WJ (1989) Micrometeorology of temperate and tropical forest. Phil Trans R Soc London. B 324:299–334.

Siebicke L (2008) Footprint synthesis for the FLUXNET site Waldstein/Weidenbrunnen (DE-Bay) during the EGER experiment. Arbeitsergebn, Univ Bayreuth, Abt Mikrometeorol, ISSN 1614–8916. 38:45 pp.

Siebicke L (2011) Advection at a forest site – an updated approach. PhD Thesis, University of Bayreuth, Bayreuth, 113 pp.

Siegel S (1936) Messungen des nächtlichen thermischen Gefüges in der bodennahen Luftschicht. Gerl Beitr Geophys. 47:369–399.

Simpson IJ, Thurtell GW, Neumann HH, Hartog GD and Edwards GC (1998) The validity of similarity theory in the roughness sublayer above forests. Boundary-Layer Meteorol. 87:69–99.

Sodemann H and Foken T (2005) Special characteristics of the temperature structure near the surface. Theor Appl Climat. 80:81–89.

Sogachev A and Lloyd J (2004) Using a one-and-a-half order closure model of atmospheric boundary layer for surface flux footprint estimation. Boundary-Layer Meteorol. 112:467–502.

Staudt K, Serafimovich A, Siebicke L, Pyles RD and Falge E (2011) Vertical structure of evapotranspiration at a forest site (a case study). Agrical Forest Meteorol. 151:709–729.

Steinfeld G, Raasch S and Markkanen T (2008) Footprints in homogeneously and heterogeneously driven boundary layers derived from a Lagrangian stochastic particle model embedded into large-eddy simulation. Boundary-Layer Meteorol. 129:225–248.

Stull RB (1988) An Introduction to Boundary Layer Meteorology. Kluwer Acad. Publ., Dordrecht, Boston, London, 666 pp.

Taylor PA (1969) On wind and shear stress profiles above a change in surface roughness. Quart J Roy Meteorol Soc. 95:77–91.

Taylor PA (1987) Comments and further analysis on the effective roughness length for use in numerical three-dimensional models: A research note. Boundary-Layer Meteorol. 39:403–418.

Thom AS, Stewart JB, Oliver HR and Gash JHC (1975) Comparison of aerodynamic and energy budget estimates of fluxes over a pine forest. Quart J Roy Meteorol Soc. 101:93–105.

Thomas C and Foken T (2007a) Organised motion in a tall spruce canopy: Temporal scales, structure spacing and terrain effects. Boundary-Layer Meteorol. 122:123–147.

Thomas C and Foken T (2007b) Flux contribution of coherent structures and its implications for the exchange of energy and matter in a tall spruce canopy. Boundary-Layer Meteorol. 123:317–337.

Thomas CK (2011) Variability of sub-canopy flow, temperature, and horizontal advection in moderately complex terrain. Boundary-Layer Meteorol. 139:61–81.

Thomas CK, Martin JG, Law BE and Davis K (2013) Toward biologically meaningful net carbon exchange estimates for tall, dense canopies: Multi-level eddy covariance observations and canopy coupling regimes in a mature Douglas-fir forest in Oregon. Agrical Forest Meteorol. 173:14–27.

Torrence C and Compo GP (1998) A practical guide to wavelet analysis. Bull Amer Meteorol Soc. 79:61–78.

Troen I and Lundtang Peterson E (1989) European Wind Atlas. Risø National Laboratory, Roskilde, 656 pp.

Twine TE, Kustas WP, Norman JM, Cook DR, Houser PR, Meyers TP, Prueger JH, Starks PJ and Wesely ML (2000) Correcting eddy-covariance flux underestimates over a grassland. Agrical Forest Meteorol. 103:279–300.

VDI (2000) Umweltmeteorologie, Meteorologische Messungen für Fragen der Luftreinhaltung - Wind, VDI 3786 Blatt2. Beuth Verlag, Berlin, VDI 3786, Blatt 2, 33 pp.

Venditti JG, Best JL, Church M and Hardy RJ (2013) Coherent Flow Structures at Earth's Surface. John Wiley & Sons, Ltd., Chichester, 387 pp.

Verhoef A, McNaughton KG and Jacobs AFG (1997) A parameterization of momentum roughness length and displacement height for a wide range of canopy densities. Hydrol Earth Syst Sci. 1:81–91.

Vesala T, Kljun N, Rannik U, Rinne J, Sogachev A, Markkanen T, Sabelfeld K, Foken T and Leclerc MY (2008) Flux and concentration footprint modelling: State of the art. Environm Pollution. 152:653–666.

Waterhouse FL (1955) Micrometeorological profiles in grass cover in relation to biological problems. Quart J Roy Meteorol Soc. 81:63–71.

Webb EK, Pearman GI and Leuning R (1980) Correction of the flux measurements for density effects due to heat and water vapour transfer. Quart J Roy Meteorol Soc. 106:85–100.

Wichura B, Buchmann N, Foken T, Mangold A, Heinz G and Rebmann C (2001) Pools und Flüsse des stabilen Kohlenstoffisotops ^{13}C zwischen Boden, Vegetation und Atmosphäre in verschiedenen Pflanzengemeinschaften des Fichtelgebirges. Bayreuther Forum Ökologie. 84:123–153.

Wilson JD, Ward DP, Thurtell GW and Kidd GE (1982) Statistics of atmospheric turbulence within and above a corn canopy. Boundary-Layer Meteorol. 24:495–519.

Wilson KB, Goldstein AH, Falge E, Aubinet M, Baldocchi D, Berbigier P, Bernhofer C, Ceulemans R, Dolman H, Field C, Grelle A, Law B, Meyers T, Moncrieff J, Monson R, Oechel W, Tenhunen J, Valentini R and Verma S (2002) Energy balance closure at FLUXNET sites. Agrical Forest Meteorol. 113:223–234.

WMO (1981) Meteorological aspects of the utilization of wind as an energy source. WMO, Techn Note. 175:180 pp.

Yi C (2008) Momentum transfer within canopies. J Appl Meteorol Climatol. 47:262–275.

Zelený J and Pretel J (1986) Zur Problematik der Bestimmung der aerodynamischen Rauhigkeit der Erdoberfläche. Z Meteorol. 36:325.

Zelený J and Foken T (1991) Ausgewählte Ergebnisse des Grenzschichtexperimentes in Bohunice 1989. Z Meteorol. 41:439–445.

Zhang G, Thomas C, Leclerc MY, Karipot A, Gholz HL and Foken T (2007) On the effect of clearcuts on turbulence structure above a forest canopy. Theor Appl Climat. 88:133–137.

Zilitinkevich SS and Calanca P (2000) An extended similarity theory for the stably stratified atmospheric surface layer. Quart J Roy Meteorol Soc. 126:1913–1923.

Zilitinkevich SS, Perov VL and King JC (2002) Near-surface turbulent fluxes in stable stratification: Calculation techniques for use in general circulation models. Quart J Roy Meteorol Soc. 128:1571–1587.

Zubkovskij SL and Sushko AA (1987) Eksperimentalnoe issledovanie prostranstvennoj struktury temperaturnogo polja v prizemnom sloe atmosfery (Experimental investigations spatial structure of the temperature field in the near surface layer of the atmosphere). Meteorol Issledovanija. 28:36–41.

Chapter 4
Experimental Methods for Estimating the Fluxes of Energy and Matter

In meteorology and climatology, typically only specific atmospheric variables are measured in operational networks and energy and matter fluxes cannot easily be determined. In the last 20 years, the growing interest and research on climate change has increased the demand for reliable measurements of evaporation, carbon dioxide uptake by forests, and fluxes of other greenhouse gases. So far, these measurements were primarily for research purposes but their integration into operational networks is increasing. The measurements are very complex and need comprehensive micrometeorological knowledge. Most of the measurement methods are based on simplifications and special conditions, and therefore their implementation is not trivial. In the following chapter, overview tables provide guidance to the reader about areas of applications and related costs of the various methods.

4.1 Profile Method

Under the general term profile method, all approaches are combined which are based on the flux-gradient similarity (see Sect. 2.3). Because of the progress of the eddy-covariance measurement technique (see Sect. 4.2), the profile method with measurements at several heights has become increasingly irrelevant in the last 10–15 years. The disturbing influence of internal boundary layers makes this technique only applicable in homogeneous terrain with a large uniform fetch. Nevertheless, simple approaches with measurements at only two levels are common; analogue to many parameterization schemes used in atmospheric models.

4.1.1 Profile Method with Two Measurement Heights

4.1.1.1 Bulk Approaches

The most simple profile method to determine the energy exchange is the bulk approach, which is also used in models as a zero order closure approach. Bulk approach means that a uniform (linear) gradient is assumed for the given layer and only values at the upper and lower boundaries are used (Mahrt 1996). If the lower boundary of this layer is identical to the surface, than the method is strictly speaking only applicable over water bodies, because only there the gradient between surface values and measurement data at a certain measurement height (mostly 10 m) can be explicitly determined. For instance, the surface temperature and moisture for land surfaces cannot be determined exactly because of roughness elements (plant cover and others). Nevertheless, the method is partly applied by the calculation of surface information measured with satellites, even when considerable losses in the accuracy must be accepted. It is also possible to fix the lowest level at a certain distance above the surface. As a general rule, this should be double the canopy height.

The application of the actual bulk method above water bodies is not without problems, because normally it is not the water surface temperature that is measured but rather the temperature some decimetres below the water surface. Because of the cold film at the surface caused by evaporative cooling, this temperature is about 0.5 K lower than the temperature at the measurement level. The absolute accuracy of the determination of the surface temperature with remote sensing methods is of the same order. Instead of the turbulent diffusion coefficients, bulk coefficients are used. Then the friction velocity can be determined with the drag coefficient C_D and the wind velocity

$$u_* = \sqrt{C_D(z)}\, u(z),\tag{4.1}$$

where it is assumed that the wind velocity at the ground surface is zero.

The sensible heat flux is parameterized with the Stanton number C_H and the latent heat flux with the Dalton number C_E:

$$\frac{Q_H}{\rho\, c_p} = C_H(z)\, u(z)[T(z) - T(0)],\tag{4.2}$$

$$\frac{Q_E}{\rho\, \lambda_p} = C_E(z)\, u(z)[e(z) - e(0)]\tag{4.3}$$

The bulk coefficients are stability and wind velocity dependent. Over the ocean with mostly neutral stratification, the first sensitivity is not a problem. Over the land, the application for non-neutral stratification should be limited to the dynamical sublayer because the bulk coefficients have a remarkable dependency on stratification with differences up to 50% (Brocks and Krügermeyer 1970; Panin

Table 4.1 Coefficients for the determination of the drag coefficient above water bodies according to Eq. (4.4) for $u_{10} < 20$ m s^{-1}

Author	a	b	c in m s^{-1}	u_{10} in m s^{-1}
Foken (1990)	1.2	0	0	<7
	1.2	0.065	7	≥7
Garratt (1992)	1.0	0	0	<3.5
	0.75	0.067	0	≥3.5

1983; Foken 1990). In the literature, a number of relations for the drag coefficient are given (Smith et al. 1996; Geernaert 1999). Currently, the parameterization dependent on the wind velocity at the 10 m reference level is the most useful version. Mean coefficients from a large number of experiments are given in Table 4.1 for the following equation:

$$C_{D10} = [a + b[u_{10} - c]] \cdot 10^{-3} \tag{4.4}$$

For greater wind velocities, the bulk coefficients increase dramatically, and are no longer clearly determined because energy fluxes are much higher under storm conditions than under normal conditions. The values over lakes are slightly higher and over land, where nearly no data are available, they are at least one order of magnitude higher than over the ocean.

The Stanton and Dalton numbers over water are about 20% lower than the drag coefficient. For the same wind velocity classes as given in Table 4.1, the coefficients for Eq. (4.4) have the values $a = 1.0$, $b = 0.054$, $c = 7$ m s^{-1} according to Foken (1990). With increasing roughness the differences compared to the drag coefficient increase (Garratt 1992).

By comparison of Eq. (4.1) with the profile equation for neutral stratification, the relation between the drag coefficient and the roughness height follows as:

$$C_D = \frac{\kappa^2}{\left[\ln\left(\frac{z}{z_0}\right)\right]^2} \tag{4.5}$$

For the determination of the Stanton number, the roughness length for temperature must be considered (for the Dalton number use the roughness length for specific humidity):

$$C_H = \frac{(\kappa/Pr_t)^2}{ln\left(\frac{z}{z_0}\right) ln\left(\frac{z}{z_{0T}}\right)} \tag{4.6}$$

In a similar way, the stability dependence of the bulk coefficients can be determined. Note that slight errors in the determination of the roughness length have a remarkable influence on the bulk coefficients. Therefore, these bulk coefficients are not really an alternative to experimental parameterizations.

Table 4.2 Evaluation of the bulk method

Criterion	Evaluation
Area of application	Application over water, modelling, if no other possibilities
Financial expense	1–3 k€ per system
Personal expense	Low technical maintenance
Education	Introduction
Error	According to the micrometeorological conditions 10–50%
Sampling	1–10 s
Time resolution of fluxes	10–30 min, higher accuracy for daily averages
Application for chemical compounds	For selected inert gases possible
Restrictions in the application	Turbulent conditions necessary

Bulk approaches for the determination of the momentum and energy exchange over water bodies are widely used because the input data are routinely available or can be easily determined, i.e. these data are contained in models. Thus, the roughness parameter is often determined with the Charnock approach, Eq. (2.61).

An overall evaluation, including information about areas of application, cost, and accuracy etc., of the bulk approach is given in Table 4.2. In the following, similar tables are presented for all methods, which allows the reader to easily compare the pros and cons of each approach.

4.1.1.2   Bowen-Ratio Method

The Bowen-ratio method is one of the most common methods used to determine the fluxes of sensible and latent heat. The method is based on Bowen-ratio similarity (see Sect. 2.3.3) and the energy balance equation

$$Bo = \gamma \frac{\Delta T}{\Delta e}, \qquad (4.7)$$

$$-Q_s^* = Q_H + Q_E + Q_G, \qquad (4.8)$$

where the psychrometric constant $\gamma = 0.667$ hPa K^{-1} for $p = 1013.25$ hPa and $t = 20\ ^{\circ}$C. From both equations, the sensible and latent heat fluxes can be determined:

$$Q_H = (-Q_s^* - Q_G)\frac{Bo}{1 + Bo} \qquad (4.9)$$

$$Q_E = \frac{-Q_s^* - Q_G}{1 + Bo} \qquad (4.10)$$

Fig. 4.1 Bowen-ratio measurement system (Published with kind permission of © Campbell Scientific, Inc. Logan UT, USA, All rights reserved)
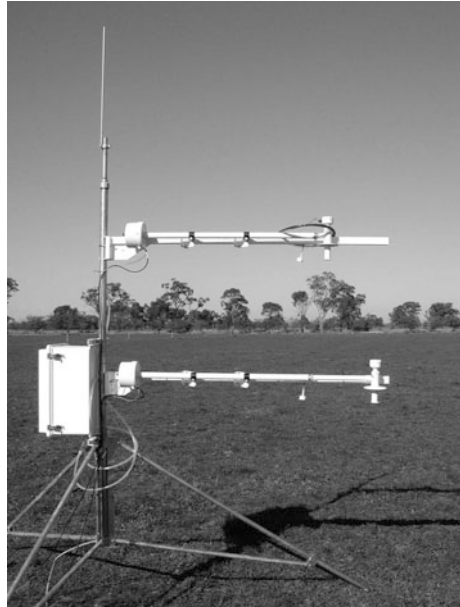
In addition to net radiation also the ground heat flux, and the temperature and humidity at two levels (see Fig. 4.1) must be determined according to Eq. (4.7).

In addition to the simplifications discussed in Sect. 2.3.4, it is apparent that the equations do not include the wind velocity and do not prescribe a certain difference between the measurement heights. To ensure that a sufficient turbulent regime exists, Foken et al. (1997a) recommend that only measurements with a wind velocity at the upper height greater than 1 m s^{-1} and a difference of the wind velocities between both heights greater than 0.3 m s^{-1} should be used. This requires additional instrumentation with anemometers. Even though the height difference of the measurements (Δz) is not included into the equations, an increase of Δz also increases the difference of the temperature and the humidity. Consequently the influence of the measurement errors decreases. It is therefore recommended to choose a ratio of the measurement heights greater than 4–8 (Foken et al. 1997a). In practice, these requirements are rarely taken into account because measurements over high vegetation have ratios of the aerodynamical heights of about 1.5 (Bernhofer 1992; Barr et al. 1994.). Equations (4.9) and (4.10) are singular for $Bo = -1$. Consequently, unrealistic energy fluxes are predicted for the morning and evening hours. Therefore, the range $-1.25 < Bo < -0.75$ should be excluded from further analysis. To determine the correct sign of the fluxes in the case $Bo < 0$ the following decision criteria are necessary (Ohmura 1982):

$$\begin{aligned} \text{If} \quad (-Q_s^* - Q_G) > 0 \quad \text{then} \quad (\lambda\Delta q + c_p\Delta T) > 0. \\ \text{If} \quad (-Q_s^* - Q_G) < 0 \quad \text{then} \quad (\lambda\Delta q + c_p\Delta T) < 0. \end{aligned} \tag{4.11}$$

If these criteria are not fulfilled, the fluxes must be deleted.

The crucial disadvantage of the Bowen-ratio method is that because of the apparent unclosed energy balance (see Sect. 3.8) the residual is either added to the net radiation or distributed according to the Bowen ratio to the sensible and latent heat flux. In general, the fluxes determined with the Bowen-ratio method are larger than those determined with the eddy-covariance method. By definition, the Bowen ratio method fulfils the energy balance equation, but the quantitative accuracy of the fluxes may be limited.

Error analyses for the Bowen-ratio method are widely available (Fuchs and Tanner 1970; Sinclair et al. 1975; Foken et al. 1997a, and references therein). Many of these investigations are based on either single measurements or false assumptions. Often, only the electrical error of the sensor is used (about 0.01–0.001 K), but not the error in the adaptation of the sensor to the surrounding medium and atmosphere with radiation, ventilation and other influences. Only with much effort in measurement techniques is it possible that sensors under the same meteorological conditions and mounted close together show differences as low as 0.05–0.1 K or hPa. Therefore, the errors in temperature and humidity measurements in the atmosphere are significantly higher than the pure electrical error (Dugas et al. 1991).

The error plots given in Fig. 4.5 are taken from Foken et al. (1997a), and are based on an accepted measurement error of ±0.05 K or hPa. From Fig. 4.2 we see that a 20 and 40% error in the Bowen ratio corresponds to about a 10 and 20% error
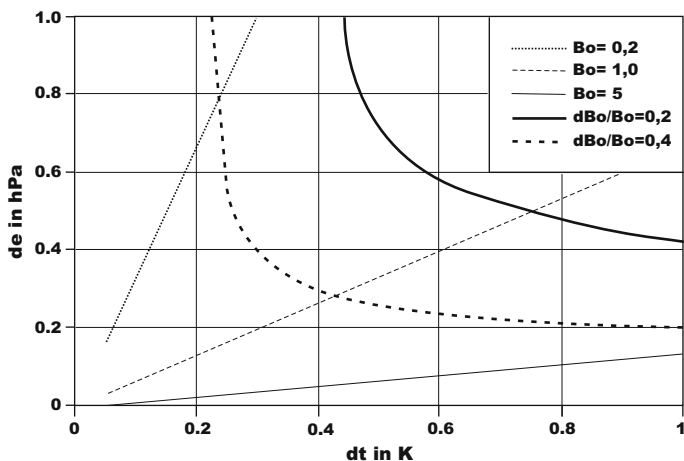
Fig. 4.2 Error of the Bowen ratio (20 und 40%) dependent on the measured temperature and water vapour differences (Adapted from Foken et al. 1997a, with kind permission of © Austrian Meteorological Society, Vienna 1997, All rights reserved)

Table 4.3 Evaluation of the Bowen-ratio method

Criterion	Evaluation
Area of application	Applied research, partly continuously running programs
Financial expense	10–15 k€ per system
Personal expense	Continuous scientific and technical support
Education	Knowledge in micrometeorology and measurement technique
Error	According to the micrometeorological conditions 10–30% (assumption of a closed energy balance)
Sampling	1–10 s
Time resolution of fluxes	10–30 min
Application for chemical compounds	For selected inert gases possible
Restrictions in the application	Sufficient footprint area, turbulent conditions necessary

in the sensible and latent heat flux respectively. Consideration of the three values of Bowen ratios in Fig. 4.5 shows that optimal conditions exist for $Bo = 0.677$ and the Bowen ratio should not significantly differ from this value. To realize errors of <20% (<40%) for the Bowen ratio, the temperature and humidity differences must be >0.6 (>0.4) K or hPa. This underlines the requirement for large differences in the measurement heights. Limitations result from internal boundary layers and possible roughness sublayers, which should be avoided within the measurement range. Note that in this error analysis, possible errors due to energy imbalance were not taken into account.

An overall evaluation of the method is given in Table 4.3. The evaluations of the errors of the method are based on the assumption of accurate net radiometer measurements (see Sect. 6.2.1), which require sensors costing at least 4 k€. Furthermore, the heat storage in the soil should be calculated very accurately to reduce the influence of the residual of the energy balance closure.

4.1.1.3 Modified Bowen-Ratio Method

According to Businger (1986), the modified Bowen-ratio method (see Eq. 2.89) is based on the application of Bowen-ratio similarity (see Sect. 2.3.4) and does not use the energy balance equation, i.e. it avoids the related energy balance closure issues (see Sect. 3.8). The method benefits both from the Bowen-ratio similarity (Eq. 2.99) and also from direct measurements of the buoyancy flux with a sonic anemometer according to the eddy-covariance method (see Sect. 4.2), which can be re-calculated into the sensible heat flux (Schotanus et al. 1983; Liu et al. 2001). Such a measurement system is shown in Fig. 4.3 (Liu and Foken 2001). Usual limitations of the Bowen-ratio method are not valid when the modified Bowen-ratio is used. However, the recommended ratio of the measurement heights of $z_2/z_1 = 4$–8 is still required to reduce the measurement errors. Also, the observed data are not

Fig. 4.3 Measurement
system for the modified
Bowen-ratio method
(METEK GmbH Elmshorn
and Th. Friedrichs & Co.
Schenefeld near Hamburg;
Photograph Foken)

useful when the friction velocity $u_* < 0.07$ m s^{-1} and the Bowen ratio $Bo \sim 0$. Because of the decreasing cost of sonic anemometers, they are now in the price range of good net radiation sensors, the overall measurement costs do not increase. Furthermore, the expensive measurements of the soil heat flux and the heat storage in the soil are no longer necessary. The Bowen ratio can be calculated with Eq. (4.7), and the latent heat flux can be calculated with:

$$Q_E = \frac{Q_H}{Bo}. \tag{4.12}$$

The modified Bowen-ratio method was originally developed for the determination of trace gas fluxes (Businger 1986; Müller et al. 1993). According to Eq. (2.99) a turbulent flux, e.g. the sensible heat flux, can be directly determined, and from the relevant difference (here temperature difference, ΔT) and the concentration difference, Δc, between two measurement levels, the trace gas flux (dry deposition) can be calculated using:

$$Q_c = Q_H \frac{\Delta_c}{\Delta T} \tag{4.13}$$

Table 4.4 Evaluation of the modified Bowen-ratio method

Criterion	Evaluation
Area of application	Applied research, partly continuously running programs
Financial expense	10–15 k€ per system
Personal expense	Continuous scientific and technical support
Education	Knowledge in micrometeorology and measurement technique
Error	According to the micrometeorological conditions 10–30%
Sampling	1–10 s, 10–20 Hz for turbulent flux
Time resolution of fluxes	10–30 min
Application for chemical compounds	For selected inert gases possible
Restrictions in the application	Sufficient footprint area, turbulent conditions necessary, similarity of the turbulence characteristics necessary

In an analogues way to the Bowen-ratio method, criteria for and limitations of the method, which are dependent on the deposited or emitted matter, must be developed. The wind or friction velocity criteria can be used; also, the turbulent scales of both scalars must be similar (see Sects. 2.5 and 4.4). An overall evaluation of the methods is given in Table 4.4.

4.1.1.4 Further Parameterization Methods

The determination of turbulent fluxes with observations at only two heights is an interesting measurement approach because the fluxes can be estimated in a simple way. While the bulk method requires a uniform (linear) gradient between both measurement heights and the Bowen-ratio method requires similar gradients of both parameters, there is also the possible solution of the profile equations with stability influences (Eqs. 2.74–2.76) for two heights. Corresponding proposals (Itier 1980; Lege 1981) were used by Richter and Skeib (1984) for a method to determine the turbulent fluxes in an iterative way. They introduced a critical height, z_c, which is approximately equal to the height of the dynamical sublayer. Below this height, the equations for neutral stratification can be applied. The use of the universal functions by Skeib (1980), which allows for this method a simple layer-wise integration, gives the following equations for the flux calculation (Richter and Skeib 1991):

$$u(z_2) - u(z_1) = \frac{u_*}{\kappa} \left\{ \begin{array}{ll} \ln\left(\frac{z_2}{z_1}\right) & z_1 < z_2 < z_c \\ \ln\left(\frac{z_c}{z_1}\right) + \frac{1}{n_u}\left[1 - \left(\frac{z_2}{z_c}\right)^{-n_u}\right] & z_1 \leq z_c \leq z_2 \\ \frac{1}{n_u}\left[\left(\frac{z_1}{z_c}\right)^{-n_u} - \left(\frac{z_2}{z_c}\right)^{-n_u}\right] & z_c < z_1 < z_2 \end{array} \right\} \quad (4.14)$$

In an analogues way, follow the equation for the sensible and latent heat flux:

Table 4.5 Coefficients for Eqs. (4.14) and (4.15)

Stability range	$\varsigma < 0$	$\varsigma > 0$
ς_c	−0.0625	0.125
n_u	0.25	−1
n_T	0.5	−2

Table 4.6 Weighting factor R for Eq. (4.16) according to Richter and Skeib (1984)

z_2/z_1	2	4	8	16
$-0.0625 \leq \varsigma \leq 0.125$	0.693	0.462	0.297	0.185
$-1 < \varsigma < -0.0625$	0.691	0.456	0.290	0.178
$0.125 < \varsigma < 1$	0.667	0.400	0.222	0.118

$$T(z_2) - T(z_1) = \Pr_t \frac{\overline{w'T'}}{\kappa\, u_*} \left\{ \begin{array}{ll} \ln\left(\frac{z_2}{z_1}\right) & z_1 < z_2 < z_c \\ \ln\left(\frac{z_c}{z_1}\right) + \frac{1}{n_T}\left[1 - \left(\frac{z_2}{z_c}\right)^{-n_T}\right] & z_1 \leq z_c \leq z_2 \\ \frac{1}{n_T}\left[\left(\frac{z_1}{z_c}\right)^{-n_T} - \left(\frac{z_2}{z_c}\right)^{-n_T}\right] & z_c < z_1 < z_2 \end{array} \right\} \quad (4.15)$$

The coefficients in Eqs. (4.14) and (4.15) are given in Table 4.5. The critical height, which is a function of the bulk-Richardson number (Eq. 2.83) and a weighting factor R (the stability-dependent curvature of the profile according to Table 4.6), is given by:

$$z_c = \frac{\varsigma_c}{\varsigma_1} z_1 = \frac{\varsigma_c}{R\, Ri_B} \quad (4.16)$$

The application of the method requires an iterative solution of the equation. Starting with an initial estimate of ς_c, the friction velocity and then the sensible heat flux are calculated. Using these values, an updated value for ς_c is calculated, and the process is repeated. After about 3–6 iteration steps, the method converges. As a measurement technique the Bowen-ratio system without net radiometer but with anemometers at both measurement heights can be used. The wind velocity criterion of the Bowen-ratio method, which is a test on developed turbulence, must also be applied here. Also, measurements must be excluded when the wind and temperatures differences between the two levels are of the order of the measurement error. The method can be extend in principle by using humidity and/or concentration measurements to measure the latent heat and/or deposition flux. An overall evaluation is given in Table 4.7.

4.1.1.5 Quality Assurance

For all profile measurements with two measurement levels, it should be demonstrated that the measurement accuracy is at least 10-fold greater than the expected difference between the two measurement heights such that the flux can at least be determined with an accuracy of 20% (positive and negative measurement errors are

Table 4.7 Evaluation of the parameterization approach according to Richter and Skeib (1991)

Criterion	Evaluation
Area of application	Applied research, partly continuously running programs
Financial expense	10–15 k€ per system
Personal expense	Continuous scientific and technical support
Education	Knowledge in micrometeorology and measurement technique
Error	According to the micrometeorological conditions 10–30%
Sampling	1–10 s
Time resolution of fluxes	10–30 min
Application for chemical compounds	For selected inert gases possible
Restrictions in the application	Sufficient footprint area, turbulent conditions necessary

assumed). It is further assumed that wind and temperature measurements can be made with a sufficient accuracy. According to a method proposed by Foken (1998), the profile equations Eqs. (2.74)–(2.76) can be divided into a turbulence-related part and in the difference of the state parameter between both heights:

$$Q_c = Q_N[u_*, \varphi(z/L), \ln(z - d)]\Delta_c \tag{4.17}$$

The normalized flux Q_N is plotted in Fig. 4.4. The minimal measurable flux with 20% accuracy is the 10-fold resolution of the measurement system c_{min}:

$$Q_{c,\min} = Q_N 10\, c_{\min} \tag{4.18}$$
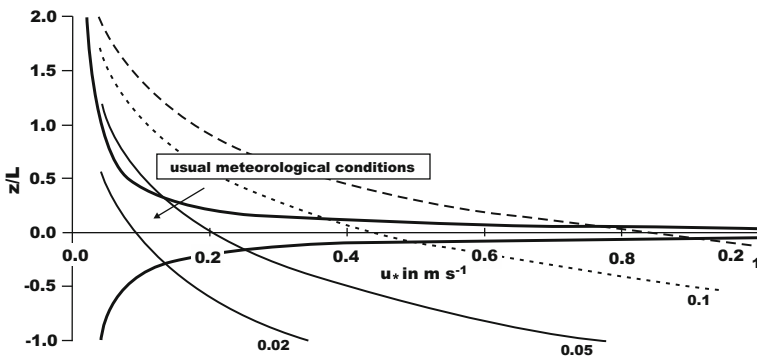
Fig. 4.4 Course of the normalized flux Q_N in dependency of the stratification and the friction velocity for m = z_2/z_1 = 8 (Adapted from Foken 1998, with kind permission of © German Meteorological Service, Offenbach 1998, All rights permitted)

Table 4.8 Minimal determinable flux (20% error) for energy and different matter fluxes above low ($m = z_2/z_1 = 8$) and tall ($m = 1.25$) vegetation for neutral stratification and $u_* = 0.2$ m s^{-1} (units µg m^{-3} for concentrations and µg s^{-1} m^{-2} for fluxes), the italic fluxes are larger than the typical fluxes (Foken 1998, completed)

Energy or matter flux	c_{min}	$\Delta_{c.min}$	Flux $m = 8$	Flux $m = 1.25$
Sensible heat	0.05 K	0.5 K	0.025 m K s^{-1} 30 W m^{-2}	0.05 m K s^{-1} 60 W m^{-2}
Latent heat	0.05 hPa	0.5 hPa	0.025 hPa m s^{-1} 45 W m^{-2}	0.05 hPa m s^{-1} 90 W m^{-2}
Nitrate particles	0.01	0.1	0.005	0.01
Ammonium particles	0.02	0.2	0.01	*0.02*
CO_2	100	1000	50	100
NO	0.06	0.6	*0.03*	*0.06*
NO_2	0.1	1.0	0.05	0.1
O_3	1.0	10.0	0.5	*1.0*
NH_3	0.014	0.14	0.007	0.014
HNO_3	0.2	2.0	*0.1*	0.2
HNO_2	0.25	2.5	*0.125*	0.25

Typical values of minimum measurable fluxes over low and high vegetation are given in Table 4.8.

4.1.2 Profile Measurements with Several Measurement Heights

In Sect. 4.1.1, special cases of the profile method with only two measurement heights were discussed. The classical profile method (Fig. 4.5) is based on wind, temperature and moisture measurements made at 3–6 levels, where 4–6 levels are optimum (Foken and Skeib 1980). These measurements were more widely used about 20 years ago because the eddy-covariance method was too costly. Today, profile measurements are applied most often in basic research to determine parameters of the profile equation or disturbances by internal and stable boundary layers.

The basis for the profile method in the neutral case are Eqs. (2.48)–(2.50) or in the integral form as in Eq. (2.60). The simplest case is the linear approximation, which is more or less also the basis of the bulk and Bowen-ratio method:

$$\left(\frac{\partial X}{dz}\right)_{z_a} \cong \frac{\Delta X}{\Delta z} = \frac{X_2 - X_1}{z_2 - z_1}$$
$$z_a = (z_1 - z_2)^{1/2}$$

(4.19)

Fig. 4.5 Measurement mast for profile measurements (*Photograph* Foken)
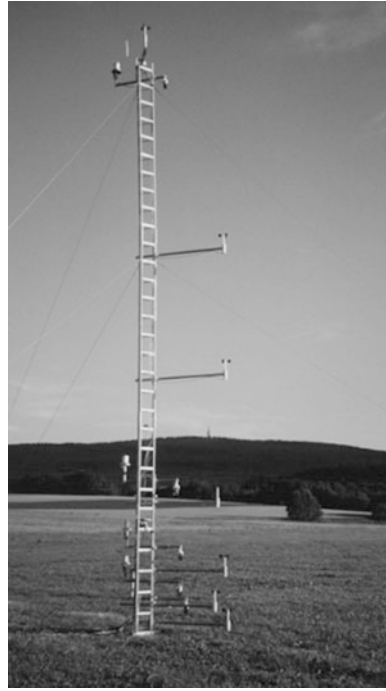
The logarithmic approximation is a much better representation of the physical facts with a geometric average of the heights:

$$\left(\frac{\partial X}{\partial \ln z}\right)_{z_m} \cong \frac{\Delta X}{\Delta \ln z} = \frac{X_2 - X_1}{\ln(z_2/z_1)}$$

$$z_m = (z_1 \, z_2)^{1/2}$$

(4.20)

The basis for the profile method in the diabatic case are Eqs. (2.74)–(2.76). For a simple graphical analysis, the integral form (Eq. 2.86) is used with $\ln z - \psi(z/L)$ on the ordinate and u or T on the abscissa according to the following equations (Arya 2001):

$$\ln z - \psi_m(z/L) = \frac{\kappa}{u_*} u + \ln z_0$$

(4.21)

$$\ln z - \psi_H\left(\frac{z}{L}\right) = \frac{\kappa/Pr_t}{T_*} T - \ln\frac{\kappa/Pr_t}{T_*} T_0 + \ln z_{0T}$$

(4.22)

Before both equations can be calculated, either the Richardson number (Eq. 2.82 or 2.83) or the Obukhov length (Eq. 2.72) must be determined. The method can be solved iteratively.

There are approximations that are not directly based on the profile equation. The simplest is the series expansion:

$$u(z) = a_0 + a_1 \ln z + a_2 z \tag{4.23}$$

A more commonly used expansion is one developed by Kader and Perepelkin (1984), which is superior to Eq. (4.23):

$$u(z) = a_0 + \frac{a_1 \ln z + a_3 + a_4 z^{2/3}}{5 + z} \tag{4.24}$$

For the interpolation of profiles, several approaches are used, for example, spline methods. To insure that these methods do not overcorrect measurement errors and falsify the result, special cubic interpolation methods between neighbouring grid points should be used (see e.g. Akima 1970).

Because of the availability of powerful personal computers, lavish interpolation methods are used such as the Nieuwstadt-Marquardt approach. In this approach, a quadratic cost function is calculated as a measure of the tolerance between the measured data and the model based on the profile equations (Nieuwstadt 1978). The nonlinear system of equations to minimize the cost function can be solved using the method described by Marquardt (1983).

As with the Bowen ratio method, the profile method requires high accuracies in the measurements. High ratios of the upper to the lower measurement height, and negligible influences from the surface are also necessary. The wind criteria for the Bowen ratio method to exclude non-turbulent cases can be also used. A complete error analysis was made by Foken and Skeib (1980). An overall evaluation is given in Table 4.9.

Table 4.9 Overall evaluation of the profile method with 4–6 measurement heights

Criterion	Evaluation
Area of application	Basic and applied research, partly continuously running programs
Financial expense	10–15 k€ per system
Personal expense	Continuous scientific and technical support
Education	Good knowledge in micrometeorology and measurement technique
Error	According to the micrometeorological conditions 5–20%
Sampling	1–10 s
Time resolution of fluxes	10–30 min
Application for chemical compounds	For selected inert gases possible
Restrictions in the application	Sufficient footprint area, turbulent conditions necessary

4.1.3 Power-Law

For many applied methods, the power-law is widely used for the determination of the wind distribution near the ground surface. Such power-law expressions approximately agree only with respect to shape with the physical equations given in Sect. 2.3. They are not only applied in the surface layer but also in the lower part of the atmospheric boundary layer (Doran and Verholek 1978; Sedefian 1980; Joffre 1984; Wieringa 1989; Hsu et al. 1994):

$$\frac{u_1}{u_2} = \left(\frac{z_1}{z_2}\right)^p \tag{4.25}$$

For wind power applications, an exponent of $p = \frac{1}{7}$ is often applied (Peterson and Hennessey 1978). Detailed approaches use a stability and roughness dependency on the exponent. After differentiation of Eq. (4.25), it follows according to Huang (1979):

$$p = \frac{z}{u}\frac{\partial u}{\partial z} \tag{4.26}$$

This version allows complicated approaches including the roughness of the surface and the stratification expressed with universal functions. Irvin (1978) proposed the approach

$$p = \frac{u_*}{u\,\kappa}\varphi_m(\varsigma). \tag{4.27}$$

Similar is the approach by Sedefian (1980):

$$p = \frac{\varphi_m\left(\frac{\bar{z}}{L}\right)}{\left[\ln\left(\frac{\bar{z}}{z_0}\right) - \psi_m\left(\frac{\bar{z}}{L}\right)\right]} \tag{4.28}$$

Huang (1979) used this form of the exponent with the universal function given by Webb (1970) and Dyer (1974) and a special integration for large roughness elements. For unstable stratification, it follows that

$$p = \frac{\left(1 - 19.3\frac{z}{L}\right)^{-1/4}}{\ln\frac{(\eta-1)(\eta_0+1)}{(\eta+1)(\eta_0-1)} + 2\tan^{-1}\eta - 2\tan^{-1}\eta_0}$$
$$\eta = \left(1 - 19.3\frac{z}{L}\right)^{1/4} \quad \eta_0 = \left(1 - 19.3\frac{z_0}{L}\right)^{1/4} \tag{4.29}$$

and for stable stratification:

$$p = \frac{1 + 6\frac{z}{L}}{\ln\frac{z}{z_0} + 6\frac{z}{L}} \qquad (4.30)$$

The numbers in both equations differ from those in the original reference according to the investigations by Högström (1988). This approach is for instance used in the footprint model by Kormann and Meixner (2001).

The application of this method is not without problems. In the morning daylight hours, these approaches are in a good agreement with measurements, but in the early afternoon—with the start of the thermal internal boundary layer (see Sect. 3.2.3)— the values of the stratification measured in the surface layer cannot be applied to the whole profile. An overall evaluation of the method is given in Table 4.10.

An interesting approach was given with the definition of the radix layer (Santoso and Stull 1998), which is approximately one fifth of the atmospheric boundary layer (surface layer and lower part of the upper layer). In the uniform layer above the radix layer, no increase of the wind velocity occurs and a constant wind velocity u_{RS} predominates:

$$\frac{u(z)}{u_{RS}} = \left\{ \begin{array}{ll} \left(\frac{z}{z_{RS}}\right)^A \exp\left[A\left(1 - \frac{z}{z_{RS}}\right)\right] & z \leq z_{Rs} \\ 1 & z > z_{Rs} \end{array} \right\} \qquad (4.61)$$

Until now, the radix-layer method has been rarely used and it is limited to convective conditions. Furthermore there are difficulties to determine the height z_{RS} of the radix layer.

Table 4.10 Evaluation of exponential approaches for the determination of the wind profile in the lowest 100 m

Criterion	Evaluation
Area of application	Engineer-technical applications, continuously running programs
Financial expense	1–3 k€ per system
Personal expense	Continuous technical support
Education	Experiences in measurement technique
Error	According to the micrometeorological conditions 5–20% (unstable stratification), otherwise significant larger errors
Sampling	1–5 s
Time resolution of the gradients	10–30 min
Restrictions in the application	Only for unstable stratification sufficient accuracy, significant influences by internal boundary layers, band thermal internal boundary layers at the afternoon for near surface measurements, turbulent conditions necessary

4.2   Eddy-Covariance Method

4.2.1   General Basics

Flux measurements using the eddy-covariance method (often also called eddy-correlation method, but this can bring some confusions, see Sect. 4.3) are a direct measurement method without any applications of empirical constants (Haugen 1973; Businger 1986; Kaimal and Finnigan 1994; Foken et al. 1995, 2012b Lee et al. 2004; Aubinet et al. 2012a). However, the derivation of the mathematical algorithm is based on a number of simplifications so that the method can be applied only if these assumptions are exactly fulfilled (see Sect. 2.1.2). The quality of the measurements primarily depends more on the on-site conditions and the application of necessary corrections than on the presently available highly sophisticated measurement systems. Therefore experimental experience and knowledge of the special character of atmospheric turbulence have a high relevance. The most limiting conditions are the assumptions of horizontally homogeneous surfaces and steady-state conditions. The exact determination of the footprint area (see Sect. 3.4), which should be over a uniform underlying surface for all stability conditions, and the exclusion of internal boundary layers and obstacle influences (see Sects. 3.2 and 3.3) are critical for the selection of the measurement site. This is especially relevant for forest sites, where additional specifics of tall vegetation must be taken into account (see Sect. 3.5).

The basic equations are comparatively simple (see Eqs. 2.23 and 2.24):

$$u_*^2 = \overline{-u'w'}, \frac{Q_H}{\rho\, c_p} = \overline{T'w'}, \frac{Q_E}{\rho\, \lambda} = \overline{q'w'}, \frac{Q_c}{\rho} = \overline{c'w'} \tag{4.32}$$

The covariance of the vertical wind velocity, w, and either one of the horizontal wind components or of a scalar x can be determined in the following way:

$$\begin{aligned}
\overline{w'x'} &= \frac{1}{N-1} \sum_{k=0}^{N-1} \left[(w_k - \overline{w_k})(x_k - \overline{x_k}) \right] \\
&= \frac{1}{N-1} \left[\sum_{k=0}^{N-1} w_k x_k - \frac{1}{N} \left(\sum_{k=0}^{N-1} w_k \sum_{k=0}^{N-1} x_k \right) \right]
\end{aligned} \tag{4.33}$$

Since the method is not applied directly at the surface but at a certain height above the surface and partially also above heterogeneous terrain, further assumption must be made. Figure 3.30 schematically illustrates for flat and sloped terrain that in addition to the vertical flux at the upper boundary of a volume element horizontal and vertical fluxes through the volume exist, which in the simplest case balance each other. For flat terrain the net flux of a scalar is:

$$F_\chi = \underbrace{\overline{\rho_d}\,\overline{w'\chi'}\Big|_h}_{I} + \underbrace{\int\limits_0^{z_m} \overline{\rho_d}\frac{\overline{\partial\chi}}{\partial t}\,dz}_{II} \tag{4.34}$$

The term II is the source or sink term between the surface and the measurement height, which can be ignored for the momentum and sensible heat or buoyancy flux. In most cases, it is also negligible for the latent heat flux. However, for other gases, like carbon dioxide, its contribution can be significant. In particular, in the morning hours, when the storage near the ground disappears, the source term is important. Term I is the *flux at the upper boundary of the volume element measured with the eddy-covariance method*.

In heterogeneous terrain, the net flux is the flux at the upper boundary of the volume element (term I), the source and sink term II (calculated from the change in time of the partial density of the investigated matter), and also a horizontal (term III) and vertical (term IV) advection term (see Eq. 3.33) must be taken into account:

$$F_\chi = \underbrace{\overline{\rho_d w'\chi'}\Big|_h}_{I} + \underbrace{\int\limits_0^{z_m} \overline{\rho_d}\frac{\overline{\partial\chi}}{\partial t}\,dz}_{II} + \underbrace{\int\limits_0^{z_m} \left[\overline{\rho_d u}\frac{\overline{\partial\chi_x}}{\partial x} + \overline{\rho_d v}\frac{\overline{\partial\chi_y}}{\partial y}\right]}_{III} + \underbrace{\int\limits_0^{z_m} \left[\overline{\rho_d w}\frac{\overline{\partial\chi}}{\partial z}\right]}_{IV}$$

$$\tag{4.35}$$

The advection term of the fluxes was neglected, because it is obviously very small and it cannot be measured with a sufficient accuracy. In this form the method is called *Generalized Eddy-Covariance Method*.

Lee (1998) showed that term IV should also include the change of the vertical velocity, $\int_0^{z_m} \left[\overline{\rho_d w}\frac{\overline{\partial\chi}}{\partial x} + \overline{\rho_d \chi}\frac{\overline{\partial w}}{\partial z}\right]$. In the discussion of this paper, Paw U et al. (2000) concluded that the change of the vertical velocity is already part of the WPL-correction (Webb et al. 1980), which further includes the vertical advection term discussed by Lee (1998). However, it is required that the coordinate system follows the stream lines after a coordinate transformation (see Sect. 4.2.3).

Especially in complex terrain, the advection problem is still subject of ongoing research efforts and expensive experiments (Aubinet et al. 2003a, 2005, see Sect. 3.6). Due to the large errors in the determination of the advection terms it is recommended that no corrections are applied at sites without obvious indication of advection being an important factor (Aubinet et al. 2010). Instead it is recommended to exclude data sets collected at night under low-turbulence conditions. In such cases, the fluxes should be parameterized (see Sect. 4.2.6, Aubinet et al. 2012b).

4.2.2   Basics in Measurement Technique

According to Eq. (4.32), the turbulent fluctuations of the components of the wind vector and of scalar parameters must be measured at a high sampling frequency (see Sect. 6.1.2) so that the turbulence spectra (see Sect. 2.5) can be extended to 10–20 Hz. The measurement devices used for such purposes are sonic anemometers for the wind components and sensors that can measure scalars with the required high resolution in time. The latter are often optical measurement methods (see Sect. 6.2.3). The measurement or sampling time depends on the atmospheric stratification, the wind velocity, and the measurement height. For heights of 2–5 m, 10–20 min would be required for daytime unstable stratification (summer) and about 30–60 and sometimes as high as 120 min for nighttime stable stratification. The measurement errors are not significant if a sampling time of 30 min is used over the entire day. For short sampling times, the low frequency contributions to the fluxes are missed, and for long sampling times the steady state condition may not be fulfilled. Accordingly, the flux can be determined only after the measurements have been made. It is also possible to use filtering options. Low pass filters or trend eliminations can create errors in the fluxes, (Rannik and Vesala 1999; Finnigan et al. 2003), thus block averaging with an averaging time of 30 min is now recommended. Due to the spectral character of turbulence, fluxes are measured only partially if only short averaging intervals are available (5–10 min). The simple summation over longer time periods is incorrect. Special correction algorithms are necessary, and these need further statistical parameters of the short time periods. For the covariance of a long time series of M data points, based on N short-time series each with U data points, where $N = M/U$, it follows (Foken et al. 1997b, method was proposed by G. Peters):

$$\overline{w'x'} = \frac{1}{M-1}\left[(U-1)\sum_{j=1}^{N}(\overline{w'x'})_j + U\sum_{j=1}^{N}\overline{w_j}\,\overline{x_j} - \frac{U^2}{M}\sum_{j=1}^{N}\overline{w_j}\sum_{j=1}^{N}\overline{x_j} \right] \quad (4.36)$$

The height of the measurements depends on the path length and the separation between a sonic anemometer and an additional device (e.g. hygrometer). Devices with a path length less than 12 cm should not be used below 2 m, and devices with a path length more than 20 cm should not be used below 4 m. The minimum distance between a sonic anemometer and an additional device, depends on the flow distortions caused by the devices and should be determined in a wind tunnel. Typically, for fine-wire temperature sensors, the minimum distance is 5 cm, and for hygrometers it is 20–30 cm. These additional instruments should be mounted downwind of the sonic anemometers and 5–10 cm below the wind measurement path (Kristensen et al. 1997). Therefore, to reduce the corrections of the whole system (see Sect. 4.2.3) the measurement height must be estimated not only dependent on the path length of the sonic anemometer but also dependent on the separation of the measurement devices. Also, the measurement height should be twice the canopy height in order to exclude effects of the roughness sublayer. Flow distortions due to the measurement system can hardly be avoided (Dyer 1981),

Fig. 4.6 Eddy-covariance
measurement complex of the
University of Bayreuth with a
sonic anemometer CSAT3,
IR-hygrometer LiCor 7500,
and hygrometer KH20 in the
back ground (*Photograph*
Foken)

however corrections with coordinate rotations are possible (Sect. 4.2.3). Nevertheless, care must be taken that instrument mounts, tower elements, or other sensors are installed at a sufficient distance to the turbulence measurements (distance 5–10fold of the dimension, Wieringa 1980; Wyngaard 1981; Wyngaard et al. 1982; Barthlott and Fiedler 2003).

In basic research, sonic anemometers (Fig. 4.6, see Sect. 6.2.2) with a selected inflow sector to exclude flow distortion are used. For most applications, wind direction-independent omni-directional sonic anemometers are sufficient, but these have flow distortions due to mountings and sensor heads. For flux measurements, it is important that interfering parts of devices are kept at a minimum, in particular below the measurement path for the vertical component of the wind, because the vertical oscillations of relatively small turbulence elements are much faster than the horizontal movements of larger turbulence elements. This difference can be noted in the frequency shift of the spectral maximum for vertical and horizontal wind fluctuations by more than one order (see Sect. 2.5).

Most of the sonic anemometers also measure the fluctuations of the sound velocity and therefore indicate the so-called sonic temperature (nearly identical with the virtual temperature). The flux calculated with this temperature is the buoyancy flux, about 10–20% greater than the sensible heat flux:

$$\frac{Q_{HB}}{\rho c_p} = \overline{w'T_v'} \tag{4.37}$$

The sensible heat flux can be determined by applying additional corrections, which need additional moisture measurements (see Sect. 4.2.3.5). More expensive are direct temperature measurements made with thin thermocouples or free spanned resistance wires (diameter <15 µm to reduce the radiation error, see Sect. 6.2.3.2).

Hygrometers are used for the determination of the latent heat flux (evaporation). Such devices are nowadays mostly optical devices. These have either an open path or are a closed path. The open path hygrometer is mounted near the sonic anemometer, and the closed path is mounted some meters away and the air is aspirated below the sonic anemometer. The first works in the UV and IR range, and the second works only in the IR range. UV devices should be used for low humidity conditions (water vapour pressure 0–20 hPa) and IR devices for high moistures (10–40 hPa). Closed path devices need extensive data corrections. One correction accounts for the time delay of the measurement signal in relation to the wind measurements, and another correction accounts for the filtering of the fluctuations by the tube (Leuning and Judd 1996; Aubinet et al. 2000; Ibrom et al. 2007a, b). These devices have the benefit of directly measuring the mixing ratio, while open-path devices measure the absolute concentration and need a density correction (WPL-correction, see Sect. 4.2.3.6). The effort for maintenance and calibration for all devices is considerable. The lifetime of UV devices is very limited (<1000 h). Very fast optical devices for other gaseous components (e.g. ozone, nitrogen oxide, sulphur dioxide) are also available and the deposition flux can be measured in a similar way. Nowadays increasingly tuneable lasers are applied (Bowling et al. 2003; Pattey et al. 2006), which are commercially available for carbon dioxide, carbon isotopes 12 and 13, methane, nitrous oxide, and other gases.

Recently, extensive software packages for the analysis of eddy-covariance measurements have become available, mostly free of charge, from universities, institutions and commercial companies (Appendix A.7). They differ in their application for users without extensive knowledge of the methods and researches, who need a high variability in the data analysis. Comparison studies, which are available for most of the programs, have shown that software packages can be reliably applied (Mauder et al. 2008; Fratini and Mauder 2014). Nevertheless, they differ slightly in the applications of correction and quality control methods. Therefore, the user needs some basic knowledge about these methods. Based on recent knowledge, versions of the software developed by McMillen (1988), which includes an internal rotation of the coordinates with a moving average, should no longer be applied. Furthermore, only well documented software packages should be used.

4.2.3 Applicable Correction Methods

The eddy-covariance method is based on a number of assumptions (see Sect. 2.1.2), and if these assumptions are not met, corrections must be applied to the collected data. However, it is often not clear which corrections are necessary. The data are thus screened with extensive tests (see Sect. 4.2.5), primarily after all corrections

are applied to the data. Important are the tests for steady-state conditions and developed turbulence.

4.2.3.1 Control of the Raw Data

The application of correction methods is closely connected with the data quality control (see Sects. 4.2.5 and 6.3). It starts with the exclusion of missing values and outliers, which can be found by electrical and meteorological plausibility tests.

Further tests should detect unfavourable meteorological conditions or technical problems of the instruments, whereby separating these two factors is often difficult (Vickers and Mahrt 1997). Spikes, i.e. values that are significantly above the normal measurement value but still within the possible range, are often electronically caused. The usual test is the determination of the standard deviation. All values greater than 3.5σ (Højstrup 1993) are considered as spikes. If single spikes are large, it is recommended to repeat the test 2–3 times, because otherwise erroneous data cannot be identified. Measurement series with more than 1% of spikes should not be used. More robust is the application of the absolute deviation from the median (MAD, Hoaglin et al. 2000), $MAD = median_i\left(\left|x_i - median_j\left(x_j\right)\right|\right)$, where all values are identified as spikes, which are larger or lower than a multiple of the MAD-value

$$median(x) - \frac{q\,MAD}{0.6745} \leq x_i \leq \frac{q\,MAD}{0.6745} + median(x), \qquad (4.38)$$

where 0.6745 is the corresponding value of the normal distribution by Gauß. It is recommended to use $q = 7$ for this application (Mauder et al. 2013).

If the same data logger records several measurement signals, it may occur that the data measured at the same point of time are not stored at the same point of time. This can be partially corrected in the software of the data logger, but such time delays can change with time. A typical example is a measurement system where a gas is aspirated with a tube at the sonic anemometer. Then, depending on the flow velocity within the tube, concentration measurements can be recorded significantly later than the wind component. A cross-correlation analysis is recommended and the concentration time series are shifted relative to the vertical wind measurements by the time difference of maximum cross-correlation. This must be done before any further calculations are made.

After the time shift is applied, initial covariances can be calculated. It is helpful to store these, because the first two steps use most of the calculation time. The next step is the rotation of the coordinates. In research studies, the *planar-fit* method (Wilczak et al. 2001) is currently most often used. This rotation method is applied to the data over the entire measurement campaign. Therefore, only preliminary results are available up to the end of the experiment.

The following corrections are given in the order of their application. Because some quantities, such as the stability parameter, must be calculated from the

corrected data, but are also used in the correction algorithms, their values should be updated iteratively. The iterations often converge after a few cycles, leading to an improvement of the fluxes by 1% (Mauder et al. 2006).

4.2.3.2 Coordinate Rotation (Tilt Correction)

A basic condition for applying the eddy-covariance method is the assumption of a negligible mean vertical wind component (see Eq. 2.5). Otherwise advective fluxes must be corrected (see Sect. 3.6). This correction is called tilt correction and includes the rotation of a horizontal axis into the mean wind direction. It is based on works by Tanner and Thurtell (1969) and Hyson et al. (1977). The first correction is the rotation of the coordinate system around the z-axis into the mean wind. Using the measured wind components (subscript m), the new components are given by (Kaimal and Finnigan 1994)

$$
\begin{aligned}
u_1 &= u_m \cos \theta + v_m \sin \theta, \\
v_1 &= -u_m \sin \theta + v_m \cos \theta, \\
w_1 &= w_m,
\end{aligned}
\tag{4.39}
$$

where

$$
\theta = \tan^{-1}\left(\frac{\overline{v_m}}{\overline{u_m}}\right).
\tag{4.40}
$$

For an exact orientation of the anemometer into the mean wind and for small fluctuations of the wind direction ($<30°$), this rotation is not necessary (Foken 1990). The friction velocity can be calculated from the horizontal wind component orientated into the mean wind direction; otherwise Eq. (2.26) must be applied. With today's high computer power, this special case has little significance.

The second rotation is around the new y-axis until the mean vertical wind disappears (Kaimal and Finnigan 1994)

$$
\begin{aligned}
u_2 &= u_1 \cos \phi + w_1 \sin \phi \\
v_2 &= v_1, \\
w_2 &= -u_1 \sin \phi + w_1 \cos \phi,
\end{aligned}
\tag{4.41}
$$

where

$$
\phi = \tan^{-1}\left(\frac{\overline{w_1}}{\overline{u_1}}\right).
\tag{4.42}
$$

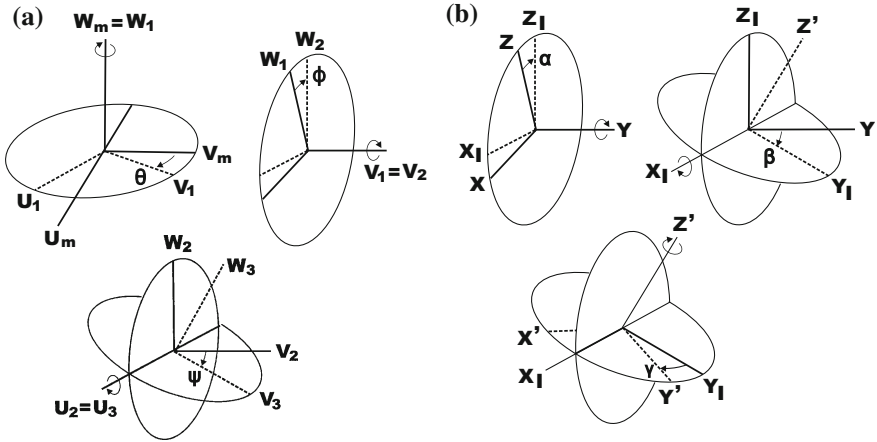Both rotations are graphically shown in Fig. 4.7a, above.

Fig. 4.7 Definition of the coordinate rotations: **a** double rotation (both upper figures) including a possible third rotation (*below*), the measurement parameters are described with m and the numbers indicate the rotations; **b** planar-fit method according to Wilczak et al. (2001), consisting in two rotations after a linear multiple regression (both upper figures) followed by a rotation into the mean wind field (*below*), with the index I describing subrotations and the apostrophe the coordinates after rotation (Adapted from Wilczak et al. 2001, with kind permission of © Kluwer Academic Publisher B. V. Dordrecht 2001, All rights reserved)

With these rotations, the coordinate system of the sonic anemometer is aligned with the streamlines. Over flat terrain, these rotations correct errors in the vertical orientation of a sonic anemometer. In sloped terrain, the streamlines are not implicitly normal to the gravity force, and at least for short averaging periods rotations may be questionable. This is especially true for short convective events or for flow distortion problems of the sensor, which may significantly affect the vertical wind components, but are not associated with the coordinate rotations. For convection or periods of low wind velocities, rotation angels up to 20–40° are typical.

Therefore, the two-rotation approach requires certain quality control procedures. However, it is the standard method in many routine monitoring networks due to its easy application (Rebmann et al. 2012). If the data are screened for low wind velocities (see Sect. 4.2.6) questionable large rotation angles are also excluded.

The third rotation (Fig. 4.7a, below) around the new *x*-axis was proposed by McMillen (1988) to eliminate the covariance from the vertical and the horizontal, normal to the mean wind direction, wind component (Kaimal and Finnigan 1994)

$$
\begin{aligned}
u_3 &= u_2, \\
v_3 &= v_2 \cos \psi + w_2 \sin \psi, \\
w_3 &= -v_2 \sin \psi + w_2 \cos \psi,
\end{aligned}
\tag{4.43}
$$

where

$$\psi = \tan^{-1}\left(\frac{\overline{v_2 w_2}}{\overline{v_2^2} - \overline{w_2^2}}\right). \tag{4.44}$$

This rotation does not significantly influence the fluxes, and introduces some problems. Therefore, it is recommended to use only the first two rotations (Aubinet et al. 2000).

A rotation into the mean stream lines was proposed by Paw U et al. (2000) and Wilczak et al. (2001). With this so called planar-fit method, the differences between the anemometer alignment and the mean stream field for a given measurement site is estimated over a long time period (days to weeks). The mounting and orientation of the anemometer should not change over this period. It is therefore recommended to combine the sonic anemometer with an inclinometer and to observe the inclinometer data regularly. If necessary, the anemometer must be regularly realigned with its initial orientation.

A matrix form is suitable to describe the planar-fit method (Wilczak et al. 2001)

$$\vec{u}_p = P(\vec{u}_m - \vec{c}), \tag{4.45}$$

where $\vec{u}_m$ is the vector of the measured wind velocities, $\vec{u}_p$ is the vector of the planar-fit rotated wind velocities, $\vec{c}$ is an offset vector, and P is a transformation matrix. The equations of rotations are then:

$$\begin{aligned}
\overline{u_p} &= p_{11}(\overline{u_m} - c_1) + p_{12}(\overline{v_m} - c_2) + p_{13}(\overline{u_m} - c_3) \\
\overline{v_p} &= p_{21}(\overline{u_m} - c_1) + p_{22}(\overline{v_m} - c_2) + p_{23}(\overline{w_m} - c_3) \\
\overline{w_p} &= p_{31}(\overline{u_m} - c_1) + p_{32}(\overline{v_m} - c_2) + p_{33}(\overline{w_m} - c_3)
\end{aligned} \tag{4.46}$$

The offset vector is necessary because, for example, the flow distortion of the sonic anemometer generates a slightly positive vertical wind velocity (Dyer 1981), and therefore a value of c_3 which differs from zero. The offset of the horizontal wind components can be assumed negligible. Nevertheless, before using a sonic anemometer the offset values during calm conditions (or observed in a box) should be controlled and if necessary corrected (see Sect. 6.2.2).

The planar-fit coordinate system fitted to the mean-flow streamlines is characterized by $\overline{w_p} = 0$. The tilt angels can be calculated according Eq. (4.46) with multiple linear regressions

$$\overline{w_m} = c_3 - \frac{p_{31}}{p_{33}}\overline{u_m} - \frac{p_{32}}{p_{33}}\overline{v_m}, \tag{4.47}$$

where $p_{31} = \sin\alpha$, $p_{32} = -\cos\alpha \sin\beta$ and $p_{33} = \cos\alpha \cos\beta$. Knowing these angles, the coordinate system can be rotated according to Fig. 4.7b, above, in the proposed order. This means that the rotation is first around angle α and then around β. The rotation

angles for this method are only a few degrees. If the rotation angels differ for different wind directions and velocities, then this method must be applied for single wind sectors and velocity classes. Of special importance is the length of the period for which the coordinate rotation should be applied. Dependent on the canopy structure (deciduous forest) and other factors this length must be individually determined (Su et al. 2008; Siebicke et al. 2012). Therefore, with the planar-fit method fluxes cannot be measured in real time.

After the rotation into the mean streamline level, each single measurement must be rotated into the mean wind direction according to (Fig. 4.7b, below):

$$\gamma = \arctan\left(\frac{\overline{v_p}}{\overline{u_p}}\right) \tag{4.48}$$

This is an absolute analogue to other rotation methods, but is applied as last step. In general, for the single measurements a block averaging over 30 min is used.

4.2.3.3 Spectral Correction in the High Frequency Range

An important correction to the actual available turbulence spectra is the adjustment of the spectral resolution of the measurement system. Hence, the time resolution (time constant) of the sensor, the measurement path length, and the separation between different measurement paths must be corrected. Currently, the correction method according to Moore (1986) is usually applied (Foken et al. 2012c), but it should be noted that the published software program has errors. Thus, the stability-dependent spectral function must be taken from the original source (Kaimal et al. 1972), see Sect. 2.5. Furthermore, the published aliasing correction should not be applied. The spectral functions are based on a few measurements from the Kansas experiment, and therefore its universal validity is limited.

The spectral correction is made using transfer functions (see Sect. 6.1.3). For each combination of the path length for the vertical wind velocity of a sonic anemometer (w) and the sensor for the determination of the relevant flux parameter (x), there are separate filters for the time constant (τ), the measurement path length (d), and the senor separation (s), which must be determined. The product of these single functions is the total transfer function:

$$T_{w,x}(f) = \sqrt{T_{\tau,w}(f)}\,\sqrt{T_{\tau,x}(f)}\,\sqrt{T_{d,w}(f)}\,\sqrt{T_{d,x}(f)}\,T_{s,w,x}(f) \tag{4.49}$$

If the sensors are aligned parallel to the mean wind, the spectral correction is partially done using the above-mentioned cross-correlation correction.

The method can also be applied using different transfer functions according to Horst (1997) and Moncrieff et al. (1997). A comparison of both methods was presented by Fratini and Mauder (2014). For a chosen measurement system, it is also possible to use a simple analytical correction for a site that takes into account

the observed spectra (Massman 2000). From Eugster and Senn (1995), a method was proposed which is based on an electronic damping circuit.

4.2.3.4 Spectral Correction in the Low Frequency Range

Often a sampling time of 30 min is not long enough to measure the low frequency part of the fluxes. In principle, the averaging interval can be extended by an elimination of a trend, and in most cases it is sufficient to subtract only the linear trend. This of course involves the danger that the low frequency events, which are not associated with turbulent fluxes, contribute to the calculated flux (Finnigan et al. 2003).

It is therefore advised to test if the flux has its maximum value within the usual averaging time. This is done using the so called *ogive* test (Desjardins et al. 1989; Oncley et al. 1990; Foken et al. 1995). It is calculated using the cumulative integral of the co-spectrum of the turbulent flux beginning with the highest frequencies:

$$Og_{w,x}(f_0) = \int\limits_{\infty}^{f_0} Co_{w,x}(f) df \tag{4.50}$$

If the value of the integral approaches a constant value (flux) for low frequencies, and if an enhancement of the averaging interval gives no significant changes, then no additional correction is necessary (Fig. 4.8).
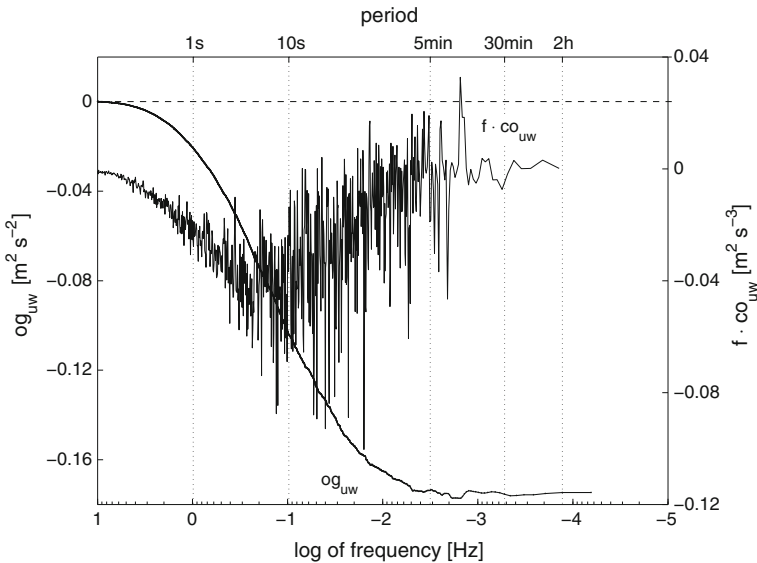

Fig. 4.8 Converging ogive (Og_{uw}) and co-spectrum ($f\,CO_{uw}$) of the momentum flux during the LITFASS-2003 experiment (June 09, 2003, 12:30–16:30 UTC, Foken et al. 2006, published with kind permission of © Authors 2006, CC Attribution 3.0 License, All rights reserved)

For the LITFASS-2003 experiment, the ogive converged within an averaging time of 30 min in about 80% of all cases (Foken et al. 2006; Charuchittipan et al. 2014). In the remaining cases, which occurred mainly during the transition periods of the day when fluxes are typically low, the ogives did not converge or reached a maximum value before the integration time of 30 min, and then decreased. By applying the ogive correction for low frequency fluxes of the investigated data set, the fluxes would increase less than 5%. The ogive correction is currently not routinely applied.

4.2.3.5 Correction of the Buoyancy Flux

The temperature measured with sonic anemometers is the so-called sonic temperature (Kaimal and Gaynor 1991):

$$T_s = T(1 + 0.32\, e/p) \tag{4.51}$$

It differs only slightly from the virtual temperature (see Eq. 2.14):

$$T_v = T(1 + 0.38\, e/p) \tag{4.52}$$

Therefore, the heat flux measured with the sonic temperature is approximately equal to the buoyancy flux. To transfer the measured buoyancy flux into the sensible heat flux, the Reynolds decomposition of Eq. (4.51) must be used in Eq. (4.33). It must be noted that the sound signal is modified depending on the construction of the sonic anemometer and the cross wind velocity. Schotanus et al. (1983) developed a correction method which is widely used. Analogue to the WPL correction, which is described in the following section, it should be named SND-correction after the three developers *S*chotanus, *N*ieuwstadt, and *D*eBruin. It is valid only for vertical measurement paths. For currently available sonic anemometers, Liu et al. (2001) adapted the method including the so called crosswind correction:

$$\rho c_p \overline{(w'T')} = \rho\, c_p\, \frac{\overline{w'T_s'} + \frac{2\overline{T}}{c^2}\left(\overline{u}\,\overline{u'w'}\,A + \overline{v}\,\overline{v'w'}B\right)}{1 + \frac{0.51\,\overline{T}c_p}{\lambda\,Bo}} \tag{4.53}$$

Because most of the producers include the crosswind correction in the sensor software, the second term in the enumerator of Eq. (4.53) can be neglected. The coefficients *A* and *B* for different types of sonic anemometers are given in Table 4.11.

Table 4.11 Coefficients for Eq. (4.53) according to Liu et al. (2001), φ: angle between the measurement axis and the *horizontal line* for different presently used sonic anemometer types. Except for the USA-1 without turbulence module, these corrections are already included in the sensor software

Factor	CSAT3	USA-1	Solent	Solent-R2
A	7/8	3/4	$1–1/2 \cdot \cos^2\varphi$	½
B	7/8	3/4	$1–1/2 \cdot \cos^2\varphi$	1

4.2.3.6 WPL-Correction

Webb et al. (1980), discussed the necessity for a density correction (*WPL*-correction according to *W*ebb, *P*earman, and *L*euning, formerly also called Webb-correction), which is caused by ignoring density fluctuations, a finite humidity flux at the surface, and the measurement of gas concentration per volume unit instead of per mass unit. A review of the continuing discussions over the last 20 years is given by Fuehrer and Friehe (2002). A different approach uses density-weighted averaging according to Hesselberg (1926), Kramm et al. (1995), and Kramm and Meixner (2000). However, the application of this approach would lead to inconsistencies in this book; therefore in the following, the version by Webb et al. (1980) is used. Webb et al. (1980) begin their derivation assuming dry air while Bernhardt and Piazena (1988) assume moist air. The differences between both methods are negligible. Nevertheless, recently several critical notes related to the *WPL* correction were published (see Sect. 4.2.4). Therefore Leuning (2007) summarized the method again (see also Foken et al. 2012c).

The total flux measured per unit mass, must be represented by the specific content of the matter q_c, according to the relation

$$F_c = \overline{\rho w q_c} = \overline{\rho w} \, \overline{q_c} + \overline{(\rho w)' q_c'}. \tag{4.54}$$

Using the partial density

$$\rho_c = \rho \, q_c \tag{4.55}$$

the relation per unit volume is

$$F_c = \overline{\rho w q_c} = \overline{w} \, \overline{q_c} + \overline{w' \rho_c'}, \tag{4.56}$$

which is applied in measurements. The mean vertical wind velocity is included in a correction term, which is given in the following form (Webb et al. 1980; Foken et al. 2012c):

$$F_c = \overline{w' \rho_c'} + 1.61 \frac{\overline{\rho_c}}{\overline{\rho_w}} \overline{w' \rho_w'} + (1 + 1.61\overline{q}) \frac{\overline{\rho_c}}{\overline{T}} \overline{w' T'}, \tag{4.57}$$

with $M_L/M_w = 1.61$. Thus, it this follows that the measurement of trace gas fluxes always requires simultaneous measurements of the water vapour concentration and the latent heat flux. For the measurement of the latent heat flux a simpler equation can be applied:

$$\frac{Q_E}{\lambda\,\rho} = (1 + 1.61\,\overline{q})\left(\overline{w'\rho w'} + \frac{\overline{\rho_c}}{\overline{T}}\,\overline{w'T'}\right), \tag{4.58}$$

The WPL-correction is large if the turbulent fluctuations are small relative to the mean concentration. For example, this is the case for carbon dioxide where corrections up to 50% are typical. For water vapour flux, the corrections are only a few percent because the effects of the Bowen ratio and the sensible heat flux balance each other (Liebethal and Foken 2003, 2004).

The conversion from volume into mass-related values using the WPL-correction is not necessary if the water vapour concentrations or the concentrations of other gases are transferred into mol per mol dry air before the eddy-covariance is calculated. Some manufacturers offer this sensor-internal conversion. The WPL-correction can be omitted for closed path sensors and if heated tubes that eliminate temperature fluctuations are used. However, this must be controlled and possibly corrected (Leuning and Judd 1996; Ibrom et al. 2007a; Foken et al. 2012c), otherwise too low fluxes are measured.

4.2.4 Corrections in Question

4.2.4.1 Flow Distortion Correction

Already Dyer (1981) pointed out that sonic anemometers generate a small updraft, which can be corrected with a coordinate rotation (see Sect. 4.2.3.2). The applications of the flow distortion correction need some care because these are determined in the wind tunnel, but these corrections have much lower values in the atmosphere (Högström and Smedman 2004). In the literature the transducer correction and the angle of attack correction are discussed.

4.2.4.2 Transducer Correction

Disturbances of the wind field are the most important sources of errors for sonic anemometers. The reasons are the installations of the sensors and the size of the transducers. For new sensors, a large ratio of the path length, d, to the transducer diameter, a, of up to $d/a = 50$ is required, because under these circumstances the influences of flow distortion are small. Furthermore, the angle, θ, between the wind vector and the path should be large. The results are based on wind tunnel

investigations of Kaimal (1978) and Kaimal et al. (1990) for a sonic anemometer with orthogonal measurement paths. For a ratio $d/a = 15$, the deviations are (Kaimal and Finnigan 1994):

$$(u_d)_{means} \begin{cases} u_d(0.82 + 0.18 \cdot \theta/75), & 0° \leq \theta \leq 75° \\ u_d, & 75° \leq \theta \leq 90° \end{cases} \qquad (4.59)$$

Due to these results the vertical wind velocity should not be measured with a vertical path but with a path that is not affected by the wind direction (omni-directional, Fig. 6.14, Zhang et al. 1986).

Recently some papers explained a reduction of the vertical wind velocity by a transducer effect (Frank et al. 2013; Horst et al. 2015) and proposed to apply corrections similar to Eq. (4.59). These measurements were not done in a wind tunnel and a benchmark is missing. Therefore, applying these corrections is not recommended.

4.2.4.3 Angle of Attack Correction

The angle of attack correction assumes that turbulence elements move through the sonic anemometer on waveform patterns and thus reach the anemometer at a specific angle. As a consequence, the vertical and horizontal wind component should be highly correlated, which is however not the case (see Sect. 4.2.5). Nakai et al. (2006) developed a correction approach in the wind tunnel. The measurements were repeated in a turbulent field with inclined sonic anemometers (Nakai and Shimoyama 2012), but the measurement setup was questionable. The correction should only be applied with care. Only corrections for non-inclined streamlines that correct the effects of anemometer mounts should be used.

4.2.4.4 Modification of the WPL-Correction

Using an alternative approach based on moist air, Liu (2005) found significant differences in the corrections of carbon dioxide fluxes. However, Kowalski (2006), Massman and Tuovinen (2006), and Leuning (2007) have shown that this alternative correction is based on wrong assumptions.

Liu also proposed a correction of the energy balance closure (see Sect. 3.8, Liu et al. 2006), which is however based on the correction with the Bowen-ratio method (Twine et al. 2000). Assuming more realistic corrections for energy balance closure, this method would be definitely applicable.

4.2.4.5   Correction of the Specific Heat

Due to the presentation by Stull (1988) of the correction of humidity-dependent fluctuations of the specific heat proposed by Brook (1978), which is some percentage of the flux, this correction is often used. However, shortly after the publication of this correction several authors (Leuning and Legg 1982; Nicholls and Smith 1982; Webb 1982) showed the this correction is based on incorrect conditions, and should never be used.

4.2.4.6   Advection Correction

Matter exchange and especially vertical fluxes in complex terrain motivated the advection corrections proposed by Lee (1998). This correction increases the low fluxes at night by application of the following equation for the vertical advection

$$F_{VA} = \overline{w}\left[\overline{\chi_c(Z_m)} - \overline{\chi_c}\right] \qquad (4.60)$$

where $\overline{\chi_c}$ is the mixing ratio measured from the ground up to the measurement height. The discussion has shown (Finnigan 1999; Paw U et al. 2000) that the vertical advection cannot be separated from other advection terms as shown in Sect. 3.6. The correction is no longer recommended (Foken et al. 2012c).

4.2.4.7   Burba Correction

Erroneous measurements with open-path gas analysers for low temperatures triggered investigations of the effects of free convection on the measured flux between the heated radiation source and the receiver (LiCor 7500, Grelle and Burba 2007) and to formulate a correction (Burba et al. 2008). At times, these corrections were found to be too large (Järvi et al. 2009; Oechel et al. 2014). Additionally, miss-interpretations may have affected the derivation. Thus, applying the correction is not recommended. Instead, open-path gas analysers should be tilted such that any possible convection does not reach the receiver. Furthermore, the temperature of the radiation source was reduced by the producer.

4.2.5   Quality Assurance

Turbulence measurements with the eddy-covariance method cannot be controlled in a simple way with plausibility tests (see Sect. 6.3.1). The quality assurance of turbulence measurements is a combination of the complete application of all corrections and the exclusion of meteorological influences such as internal boundary

layers, gravity waves, and intermitted turbulence. The main aim of the control of the data quality is to validate if, under given meteorological conditions, the simplifications of Eq. (4.32) are warranted (see Sect. 2.1.2). Quality tests (Kaimal and Finnigan 1994; Foken and Wichura 1996; Foken et al. 2004) are used to validate the theoretical assumptions of the method such as steady-state conditions, homogeneous surfaces, and developed turbulence.

For the eddy-covariance method, steady states are required. Meteorological measurements fulfil these conditions for short time periods up to one hour only roughly. There are several tests, which can be used directly or indirectly. For example, stationarity can be determined by examining the fluxes for different averaging times (Gurjanov et al. 1984; Foken and Wichura 1996). In this way, the flux is determined once over M short intervals each of only about 5 min duration, and then the average over the short time intervals is calculated (Remark: $\left[\overline{x'y'}\right]_{5min}$ means that this is a 30 min average calculated from 5 min averages):

$$
\begin{aligned}
\left(\overline{x'y'}\right)_i &= \frac{1}{N-1}\left[\sum_j x_j\, y_j - \frac{1}{N}\left(\sum_j x_j \sum_j y_j\right)\right] \\
\left[\overline{x'y'}\right]_{5\,\text{min}} &= \frac{1}{M}\sum_j \left(\overline{x'y'}\right)_i
\end{aligned}
\tag{4.61}
$$

Next, the flux is calculated over the whole averaging interval (e.g. 30 min):

$$
\left[\overline{x'y'}\right]_{30\,\text{min}} = \frac{1}{M\cdot N-1}\left\{\sum_i\left(\sum_j x_j\cdot y_j\right)_i - \frac{1}{M\cdot N}\left[\sum_i\left(\sum_j x_j\right)_i \cdot \sum_i\left(\sum_j y_j\right)_i\right]\right\}
\tag{4.62}
$$

Steady-state conditions can be assumed, if both results do not differ by more than 30%. A gradation of the differences can be used as a classification of the data quality:

$$
Stat = \left|\frac{\left[\overline{x'y'}\right]_{5\,\text{min}} - \left[\overline{x'y'}\right]_{30\,\text{min}}}{\left[\overline{x'y'}\right]_{30\,\text{min}}}\right| \cdot 100\%
\tag{4.63}
$$

From Vickers and Mahrt (1997), two tests were proposed, which give similar results. They calculate the skewness and excess of the time series. For values of skewness >|2| and values of excess <1 and >8, the authors suggested a bad data quality, and for skewness >|1| and excess <2 and >5 medium data quality is assumed. For wind components, the data at the beginning and end of a time series are compared. The difference of these values normalized by the mean wind velocity must fulfill the relation

$$\left| \frac{u_1 - u_N}{\bar{u}} \right| < 0.5, \qquad (4.64)$$

if the time series can be accepted as steady-state. This method does not always correctly identify unsteady conditions in the middle of the measurement interval.

The steady-state test often identifies large sudden jumps in the signal, a constant signal for a certain time, or changes of the signal level. The reason for these events is often an electronic one. Mahrt (1991) proposed a test using the Haar-wavelet for which the time of events can be well located. The test can also identify periods of intermittent turbulence.

The development of the turbulence can be investigated with the flux-variance similarity described in Sect. 2.4 (Foken and Wichura 1996). In this case, the measured integral turbulence characteristics (ITC) are compared with the modelled characteristics according to Tables 2.13 and 2.14. A good data quality is assumed for differences less than about 30%.

$$ITC = \left| \frac{\left(\frac{\sigma_X}{X_*}\right)_{Modell} - \left(\frac{\sigma_X}{X_*}\right)_{Messung}}{\left(\frac{\sigma_X}{X_*}\right)_{Modell}} \right| \cdot 100\% \qquad (4.65)$$

In a similar way, the comparison of the correlation coefficient between values used in the flux calculations with the mean values can be used for quality assurance testing (see Table 4.16 in Sect. 4.3, Kaimal and Finnigan 1994).

Additionally, the wind components should be included in a system of quality control tests. The mean vertical wind must be low such that over flat terrain and for horizontal wind velocities <5 m s^{-1} it is <0.15–0.20 m s^{-1}. For sonic anemometers with a limited range of acceptable wind directions, measurements within an inflow sector that is affected by instrument mounts should be excluded. The excluded region should be based on the typical standard deviation of the wind direction at a particular site and given micrometeorological conditions, but is typically ±30–40°. For sonic anemometers with unlimited inflow angles (omni-directional) the flow through instrument mounts and sensor heads can reduce the overall data quality.

An evaluation system for turbulent fluxes consists of two steps: The single tests should be evaluated according to the threshold values and corresponding data quality classes (Table 4.12) and the overall quality of a measurement is expressed as an appropriate combination of the single tests (Table 4.13). The highest priority should be given to the steady-state test. Note that for the test on integral turbulence characteristics for neutral stratification, the errors in the determination of the characteristics for scalars can be very high. This test should not be overly inter-preted, and the test on the characteristics of the wind parameters should dominate. In any case, the classification results of the single tests should be stored to have them available later in cases of doubt. The classification according to Table 4.12 was done such that classes 1–3 have a high accuracy and the data can be used for basic research. Classes 1–6 can be used for long-term measurements of fluxes

Table 4.12 Classification of the data quality of the steady-state test according to Eq. (4.63); the comparison of the integral turbulence characteristics with model assumptions according to Eq. (4.65) and Tables 2.13 and 2.14, and the wind criteria, for example for the sonic anemometer CSAT3 (Foken et al. 2004, 2012c)

Steady state, differences		Integral turbulence characteristics, differences		Horizontal inflow sector for CSAT3	
Class	Range (%)	Class	Range (%)	Class	Range (°)
1	0–15	1	0–15	1	±0–30
2	16–30	2	16–30	2	±31–60
3	31–50	3	31–50	3	±60–100
4	51–75	4	51–75	4	±101–150
5	76–100	5	76–100	5	±101–150
6	101–250	6	101–250	6	±151–170
7	251–500	7	251–500	7	±151–170
8	501–1000	8	501–1000	8	±151–170
9	>1000	9	>1000	9	>±171

Table 4.13 Proposal for the combination of single quality tests (Table 4.12) to an overall data quality of flux measurements (Foken et al. 2004, 2012c)

Overall quality	Steady state	Integral turbulence characteristics	Horizontal inflow sector
1	1	1–2	1–5
2	2	1–2	1–5
3	1–2	3–4	1–5
4	3–4	1–2	1–5
5	1–4	3–5	1–5
6	5	≤ 5	1–5
7	≤ 6	≤ 6	≤ 8
8	≤ 8	≤ 8	≤ 8
	≤ 8	6–8	≤ 8
9	One ranging 9		

without limitations. Measurements of the classes 7–8 should only be used for ballpark estimates and should, if necessary, be deleted while data in class 9 are always removed. In several papers, certain classes were also combined (Rebmann et al. 2005; Mauder et al. 2013).

With the discussed approach, any erroneous measurements should be successfully detected and removed. If this is not the case, or if the tests can only be partially applied, it is possible to screen the data using final tests (Papale et al. 2006).

Analogue to Eq. (4.38), this final screening also uses the absolute deviation from the median *MAD* but the parameter *q* can be reduced (4 or 5.5).

4.2.5.1 Gap Filling

The application of the eddy-covariance method in long-term measurement programs such as the international FLUXNET programme (Baldocchi et al. 2001) requires objective methods on how to handle missing data. This is because with such measurement programs annual sums such as the Net Ecosystem Exchange (NEE) are determined. In substance, two types of missing data must be corrected. One type is missing data from single systems due to meteorological influences such as heavy rain or failure of the whole system. The second type is data that must be replaced. If, for example, during the night no turbulent exchange conditions exist, then the measurement method no longer works satisfactorily. For the measurements of carbon dioxide fluxes, the methods of gap filling are well developed (Falge et al. 2001; Hui et al. 2004; Gu et al. 2005; Reichstein et al. 2005; Moffat et al. 2007; Lasslop et al. 2010). Nevertheless these methods, which use an approach for the carbon assimilation at daytime and a different approach for respiration, are still under discussion. Recently, gap filling with models (e.g. Papale and Valentini 2003) are applied.

The determination of the carbon uptake (NEE) at daytime takes place with the so called Michaelis-Menton function (Michaelis and Menton 1913; Falge et al. 2001), which must be evaluated for different temperature classes and the global radiation:

$$Q_{c,Tag} = \frac{a\,K\downarrow Q_{c,sat}}{a\,K\downarrow + Q_{c,sat}} + Q_{R,Tag} \qquad (4.67)$$

where $Q_{c,sat}$ is the carbon flux for light saturation ($K\downarrow = \infty$), Q_R is the respiration at daytime, and a and $Q_{c,sat}$ must be determined with multiple regression using data from an available dataset for the specific measurement site.

The respiration of an ecosystem can be determined with the Lloyd-Taylor-function (Lloyd and Taylor 1994; Falge et al. 2001)

$$Q_R = Q_{R,10}e^{E_0\left[\frac{1}{283.15K-T_0} - \frac{1}{T-T_0}\right]}, \qquad (4.68)$$

where $Q_{R,10}$ is the respiration at 10 °C, $T_0 = 227.13$ K (Lloyd and Taylor 1994), and E_0 describes the temperature dependence of the respiration. The parameters of this equation are determined from nighttime ($K\downarrow < 10$ W m^{-2}) eddy-covariance measurements with the assumption that for such low radiation fluxes only the respiration can be measured. The coefficients are determined also for temperature classes (Fig. 4.9).

While the Michaelis-Menton function is in general used for gap filling for the daytime, the Lloyd-Taylor function must be used at night because of low

Fig. 4.9 Calculation of the respiration from NEE measurements at night as a function of air temperature at 2 m height according to Eq. (4.67), *grey line*. Circles are the medians of 2°-classes, points are individual values (Adapted from Ruppert et al. 2006b, with kind permission of © Elsevier Science AG Oxford 2006, All rights reserved)
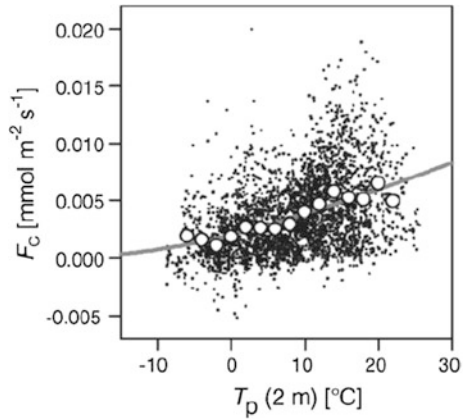
turbulence. The decision regarding the application follows from the so called u_*-criterion (Goulden et al. 1996). Therefore, the respiration is normalized to exclude the temperature sensitivity using a model calculation according to Eq. (4.67), and plotted as a function of the friction velocity u_*. Above a certain friction velocity, the normalized respiration is constant. Measurements with a lower friction velocity are gap filled. Typical threshold values are in the range $u_* = 0.3–0.4$ m s^{-1}. However, such a threshold value cannot be determined for all stations (Gu et al. 2005).

It must be noted that for both methods the equations for the carbon flux during the day and the respiration during the night are climatological parameterizations. These can have significant differences from the individual values. The determination of the respiration relationships is particularly difficult because of the large scatter of the data (Fig. 4.9). It is recommended to use medians for the temperature classes. Due to the application of the u_*-criterion only few data are available with low turbulent conditions. Therefore, an over-parameterization of the respiration may be possible. Very critical is the situation in winter, when many data are missing. In this case, data for many years should be used for the calculation of the parameterization. Also the assimilation is difficult to parametrize in winter time, because the parametrization is based on few sunny weather periods. It is very useful to set the assimilation to zero for periods without biological activity if the investigations aim at the determination of annual sums (Lindauer et al. 2014).

A more objective approach seems to be the application of the quality criterion for turbulent fluxes as introduced in Sect. 4.1.3 (Ruppert et al. 2006b). According to this, very high data quality is used to determine the Michaelis-Menton and Lloyd-Taylor functions. Then both functions are used to fill gaps of data with low data quality. The benefit of this method is that nighttime data with high data quality and low friction velocity can be used to parameterize the Lloyd-Taylor function. On the other hand, daytime values with low data quality must be gap filled. However, this approach requires the availability of raw data.

For the gap filling of evapotranspiration data the modelling with the Penman-Monteith-approach or, if using a correction factor, also with the Priestley-Taylor-approach can be applied (see Sect. 5.1.2).

4.2.6 Overall Evaluation

Due to the very complicated algorithms of the eddy-covariance method, errors cannot easily be estimated according to the error propagation law (Huges and Hase 2010). Nevertheless Mauder et al. (2006) have tried using sensor and software comparisons during the experiments EBEX-2000 and LITFASS-2003 to determine the accuracy of the measurement method. A significant dependence was found on the type of sonic anemometer (compare Table 6.8) and on the data quality. The results are summarized in Table 4.14.

Hollinger and Richardson (2005) have tried to evaluate the uncertainty of the eddy-covariance method using data from two instrumented towers with the same footprint. For climatological analyses, a comparison of different years is possible (Richardson et al. 2006). Quite promising are statistical methods. Hereby, it must be noticed that the time series used for the eddy-covariance are auto-correlated and the usual statistical criterions for random numbers cannot be applied (Bartels 1935). Approaches by Lenschow et al. (1994) and Finkelstein and Sims (2001) obviously account for this limitation. Thus, according to Mauder et al. (2013) the noise of the errors εx and εy is

$$\sigma^{noice}_{covariance} = \sqrt{\frac{1}{N}} \sqrt{\overline{\varepsilon x^2 y'^2} + \overline{\varepsilon y^2 x'^2}} \qquad (4.68)$$

and the statistical error following the error propagation law (Huges and Hase 2010), e.g. for the friction velocity, is

$$\sigma_{\tau} = \frac{\rho}{u_*} \sqrt{\overline{u'w'}^2 \sigma^2_{u'w'} + \overline{v'w'}^2 \sigma^2_{v'w'}}. \qquad (4.69)$$

Table 4.14 Evaluation of the accuracy of the eddy-covariance method on the basis of the results of the experiments EBEX-2000 and LITFASS-2003 (Mauder et al. 2006) dependent on the data quality (Sect. 4.2.5) and from the type of the sonic anemometer (Table 6.8, Foken and Oncley 1995)

Sonic anemometer	Data quality class	Sensible heat flux	Latent heat flux
Type A, e.g. CSAT3	1–3	5% or 10 W m^{-2}	10% or 20 W m^{-2}
	4–6	10% or 20 W m^{-2}	15% or 30 W m^{-2}
Type B, e.g. USA-1	1–3	10% or 20 W m^{-2}	15% or 30 W m^{-2}
	4–6	15% or 30 W m^{-2}	20% or 40 W m^{-2}

Table 4.15 Evaluation of the eddy-covariance method

Criterion	Evaluation
Area of application	Basic research and expensive continuous measurement programs
Financial expense	10–50 k€ per system
Personal expense	Continuous scientific and technical support
Education	Good micrometeorological and measurement technique knowledge
Error	Depending on the micrometeorological conditions 5–10%
Sampling	10–20 Hz
Time resolution of fluxes	10–60 min
Application for chemical compounds	Selected inert gases (gas analysers with high time resolution)
Restrictions in the application	Sufficient footprint area, turbulent conditions necessary, depending on the senor, possible precipitation

The method leads to results comparable with Table 4.14. Systematic errors essentially are the unclosed energy balance (see Sect. 3.8) and a limited footprint (see Sect. 3.4).

It is seen that the eddy-covariance method (Table 4.15) is the only direct measurement method and the most accurate with the largest time resolution. However, it needs also the most comprehensive knowledge and great experimental effort.

4.3 Flux-Variance Relations

The flux-variance relation (variance method) according to Sect. 2.4 allows the calculation of fluxes using the measured variance of a meteorological parameter and the integral turbulence characteristics. Many investigations of this method have been made. However, the variance method has never reached a practical relevance even though the method has an accuracy comparable to the eddy-covariance method (Tsvang et al. 1985). Thus, the application of the variance method according to Eqs. (2.105) and (2.106) as well as Tables 2.13 and 2.14 is possible.

The equations can also be derived from the definition of the correlation coefficient or the covariance. Therefore, the method is often called eddy-correlation method, which should not be confused with the eddy-covariance method:

$$r_{wX} = \frac{\overline{w'X'}}{\sigma_w \, \sigma_X} = \frac{F_X}{\sigma_w \, \sigma_X} \tag{4.70}$$

$$r_{wY} = \frac{\overline{w'Y'}}{\sigma_w \, \sigma_Y} = \frac{F_Y}{\sigma_w \, \sigma_Y} \tag{4.71}$$

Table 4.16 Typical values of the correlation coefficient between the vertical and horizontal wind components and between vertical wind component and temperature

Author	r_{uw}	r_{wT}
Kaimal and Finnigan (1994)	−0.35	0.5 (unstable)
		−0.4 (stable)
Arya (2001)	−0.15	0.6 (unstable)

By assuming the same values for the correlation coefficients (Table 4.16), well-known standard deviations, and one well-known flux, a second flux can be determined. The sign of the flux must be determined by additional measurements, e.g. by measurements of the temperature gradient:

$$|F_X| = |F_Y|\frac{\sigma_X}{\sigma_Y} \tag{4.72}$$

The standard deviations can be determined using a lower frequency spectral range, than the necessary spectral range of the eddy-covariance method for the reference flux. This method can, for example, be applied, if only one of the two gas fluxes can be measured with high time resolution using the eddy-covariance method.

Furthermore the flux can also be determined according to Eq. (4.65), if the correlation coefficient is well known:

$$F_X = r_{wX}\sigma_w\,\sigma_X \tag{4.73}$$

The correlation coefficient can be roughly parameterized according to the stratification (Table 4.16)

$$r_{wX} = \tilde{\varphi}(\varsigma). \tag{4.74}$$

But the parameterization lacks a sufficient data basis.

An evaluation of the practically rarely used flux-variance method is given in Table 4.17. Due to the methodical and technical progress of the eddy-covariance method, this method has only historical relevance.

4.4 Accumulation Methods

4.4.1 Eddy-Accumulations-Method (EA)

The basic idea of the eddy-accumulation method (conditional sampling) originates in the work of Desjardins beginning in 1972 (Desjardins 1977). He assumed that the covariance of the turbulent flux could be averaged separately for positive and negative vertical wind velocities:

Table 4.17 Evaluation of the flux-variance method

Criterion	Evaluation
Area of application	Basic research
Financial expense	2–10 k€ per system
Personal expense	Continuous scientific and technical support
Education	Good micrometeorological and measurement technique knowledge
Error	Depending on the micrometeorological conditions 10–30%
Sampling	10–20 Hz (probably lower)
Time resolution of fluxes	10–30 min
Application for chemical compounds	Selected inert gases (gas analysers with high time resolution)
Restrictions in the application	Sufficient footprint area, turbulent conditions necessary, if necessary similarity of the scalars

$$\overline{w'c'} = \overline{w^+c} + \overline{w^-c} = (\overline{w^+} + \overline{w^-})\bar{c} + \overline{w^+c'} + \overline{w^-c'}$$
$$(\overline{w^+} + \overline{w^-}) = \bar{w} = 0 \tag{4.75}$$

Realization of this direct measurement technique should be done by concentration measurements in two separate reservoirs for positive and negative vertical wind velocities weighted with the actual vertical wind velocity (Fig. 4.10). However, the therefore necessary valve control technology did not yet exist.

However, the conditional sampling method has still a practical relevance in data analysis. For data with a high temporal resolution of the vertical wind velocity and a scalar, the time series can be conditionally sampled according to Eq. (4.75). If it is possible to fulfil the condition $\bar{w} = 0$, fluxes can be calculated without the assumption of steady state conditions.

Fig. 4.10 Schematic view of the eddy-accumulation method (Adapted from Foken et al. 1995, with kind permission of © Gebr. Borntraeger Verlagsgesellschaft Stuttgart 1995, www.schweizerbart.de, All rights reserved)
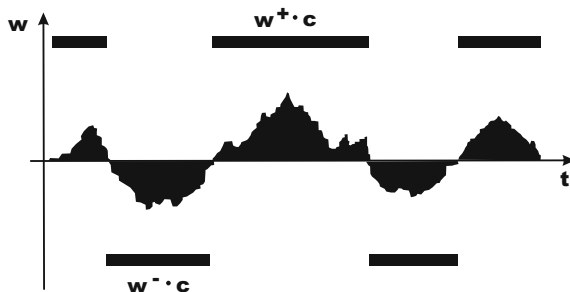
4.4.2 Relaxed Eddy-Accumulation Method (REA)

The work of Businger and Oncley (1990) was a technical breakthrough for the accumulation method. They combined the eddy-accumulation method (EA) according to Eq. (4.75) with the flux-variance similarity according to Eq. (2.97). Their method becomes an indirect method:

$$\overline{w'c'} = b\sigma_w(\overline{c^+} - \overline{c^-}) \tag{4.76}$$

where the coefficient $b = 0.627$ for an ideal Gaussian frequency distribution (Wyngaard and Moeng 1992), otherwise low variations occur which are also probably different for different gases (Businger and Oncley 1990; Oncley et al. 1993; Pattey et al. 1993):

$$b = \frac{r_{wc}\sigma_c}{(\overline{c^+} - \overline{c^-})} = 0.6 \pm 0.06 \tag{4.77}$$

The coefficient b is to a large extent independent of the stratification. This is probably due to the opposite stability dependency of the integral turbulence characteristics for the vertical wind and matter (Foken et al. 1995). The relaxed eddy-accumulation (REA) method is schematically shown in Fig. 4.11. The weighting of the concentrations is no longer necessary, but the high switching frequency of the valves for zero passages of the vertical wind is still necessary.

A further improvement was realized with the modified relaxed eddy-accumulation method (MREA) according to Businger and Oncley (1990), which is of practical use and generally called REA. In this method, the air in the case of positive and negative maximal values of the vertical wind velocity are collected into two separate reservoirs; for fluctuations around zero the air is rejected or collected in a control volume (Fig. 4.12).

Equations (4.76) and (4.77) get the following modifications

$$\overline{w'c'} = b\sigma_w\left(\overline{c^+(w > w_0)} - \overline{c^-(w < -w_0)}\right) \tag{4.78}$$

Fig. 4.11 Schematic view of the relaxed eddy-accumulation method (Adapted from Foken et al. 1995, with kind permission of © Gebr. Borntraeger Verlagsgesellschaft Stuttgart 1995, www.schweizerbart.de, All rights reserved)
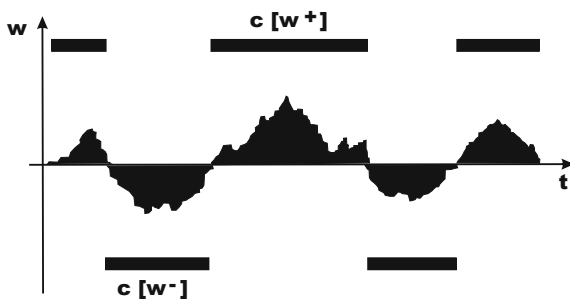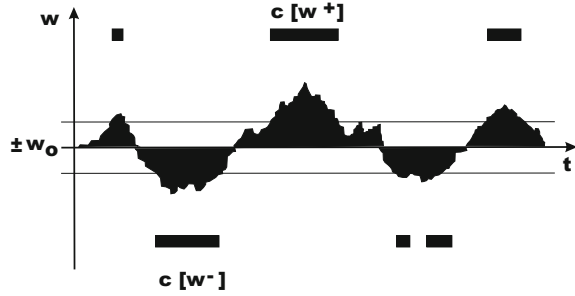
with

$$\frac{b(w_0/\sigma_w)}{b(0)} = e^{-\frac{3}{4}w_0/\sigma_w} \pm 0.012. \tag{4.79}$$

The threshold value w_0 depends on the experimental conditions and the sampled gas. Thus, the parameter b must be updated using a parallel simulation with a proxy parameter, e.g. the temperature or the water vapour:

$$b = \frac{\overline{w'c'_{proxy}}}{\sigma_w \left(\overline{c^+_{proxy}}(w > w_0) - \overline{c^-_{proxy}}(w < -w_0) \right)} \tag{4.80}$$

Simulation experiments have shown (Ruppert et al. 2006a) that the optimal value for b is approximately 0.6. The accuracy of the method is up to one order lower if a constant b-value is used as compared to the determination with a proxy value. It must be taken into consideration that scalars act similar only for small eddies (Pearson et al. 1998). This is not the case for the application of larger eddies (Ruppert et al. 2006a). This so-called scalar similarity can also change during the daily cycle (see also Sect. 3.5.5). Therefore the choice of the proxy scalar must be made very carefully. The method fails for low fluxes, which are not only caused by the daily cycle but also the ecosystem. For instance, this is the case about two weeks after the mowing of a meadow (Riederer et al. 2014).

For the implementation of the method, the measurement system must be adapted to the streamlines by a coordinate transformation, and the planar-fit method (Wilczak et al. 2001) is recommended (see Sect. 4.2.3.2). Furthermore attention must be paid so that the integral turbulence characteristics of the vertical wind velocity, which must follow the known dependencies, are not specifically modified by the measurement site. An overall evaluation is given in Table 4.18.

Often, the accuracy of gas analyzers is not high enough to accurately detect concentration differences between both reservoirs. This can be overcome by the hyperbolic relaxed eddy-accumulation method (HREA), which is based on an idea by Shaw (1985). Bowling et al. (1999) and Wichura et al. (2000) expanded this method for operational applications for carbon dioxide isotope fluxes. In this

Table 4.18 Evaluation of the relaxed eddy accumulation method (REA)

Criterion	Evaluation
Area of application	Basic research and extravagant continuous measurement programs
Financial expense	10–50 k€ per system
Personal expense	Continuous scientific and technical support
Education	Good micrometeorological and measurement technique and probably also chemical knowledge
Error	Depending on the micrometeorological conditions 5–20%
Sampling	10–20 Hz
Time resolution of fluxes	30–60 min
Application for chemical compounds	Selected inert gases (gas analysers with high time resolution)
Restrictions in the application	Sufficient footprint area, turbulent conditions necessary, similarity of turbulent scales of the scalars, no local influences on integral turbulence characteristics

Fig. 4.13 Schematic view of the hyperbolic relaxed eddy-accumulation method (Adapted from Ruppert et al. 2002, with kind permission of © Authors 2002, All rights reserved)
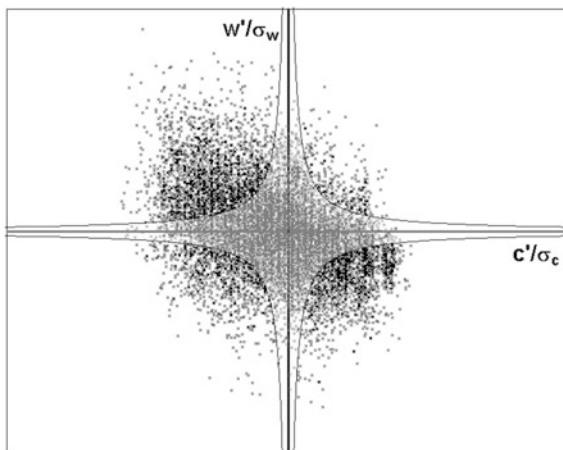
method, only air is collected outside a hyperbolic curve, which must be defined for each particular study (Fig. 4.13)

$$\left| \frac{w'}{\sigma_w} \frac{c'}{\sigma_c} \right| > D \quad \text{for w} > 0, \tag{4.81}$$

$$\left| \frac{w'}{\sigma_w} \frac{c'}{\sigma_c} \right| > D \quad \text{for w} < 0. \tag{4.82}$$

The hyperbolic relaxed eddy-accumulation method requires considerable efforts to accurately determine the dead band. The value calculated by Bowling et al. (1999) $D = 1.1$ is probably too large so that only extreme events are collected

Table 4.19 Evaluation of the hyperbolic relaxed eddy accumulation method (HREA)

Criterion	Evaluation
Area of application	Basic research
Financial expense	10–50 k€ per system
Personal expense	Intensive scientific and technical support
Education	Good micrometeorological and measurement technique and probably also chemical knowledge
Error	Depending on the micrometeorological conditions 5–20%
Sampling	10–20 Hz
Time resolution of fluxes	30–60 min
Application for chemical compounds	Selected inert gases (gas analysers with high time resolution)
Restrictions in the application	Sufficient footprint area, turbulent conditions necessary, similarity of turbulent scales of the scalars, no local influences on integral turbulence characteristics

which are not adequately distributed among the quadrants. A simulation study by Ruppert et al. (2006a) showed that an optimal value is $D \sim 0.8$. An adequate choice of the proxy scalar and the control of the scalar similarity of the measured quantity and proxy parameters are very important. Deviations have a much larger effect than in the case of the simple REA method.

The benefit of the hyperbolic relaxed eddy-accumulation method, the significant increase of the concentration differences in both reservoirs, may be compensated by the high standards needed for turbulent similarity relations being applicable. An overall evaluation is given in Table 4.19.

Besides improved analyzers for trace gases, which allows the application of the eddy-covariance method (see Sect. 4.2) or at least of the disjunct eddy-covariance method (see Sect. 4.4.3), there are still single REA applications such as for nitrous acid (HONO, Ren et al. 2011), peroxyacetyl nitrate (PAN, Moravek et al. 2014) or ^{13}C isotopes (Riederer et al. 2014). Because these systems need longer suction tubes, the triggering of the valves based on the vertical wind velocity must be highly accurate and timed correctly (Moravek et al. 2013).

4.4.3 Disjunct Eddy-Covariance Method (DEC)

Up to now, only methods have been discussed which can be used for inert gases or gases that do not react during their stay in the reservoirs. Gas analyzers with sampling rates of about 10–20 Hz are necessary for the measurement of turbulent fluxes with the eddy-covariance method. Such instruments are available for only a few gases such as ozone. The basic idea of the disjunct eddy-covariance method borrows from the eddy-covariance method for aircraft measurements and is therefore a direct measurement method. Due to the velocity of the aircraft and the

Table 4.20 Evaluation of the disjunct eddy-covariance method (DEC)

| Criterion	Evaluation
Area of application	Basic research
Financial expense	10–100 k€ per system
Personal expense	Intensive continuous scientific and technical support
Education	Good micrometeorological, measurement technique and chemical knowledge
Error	Depending on the micrometeorological conditions 5–20%
Sampling	1–30 s, sampling duration <0.1 s
Time resolution of fluxes	30–60 min
Application for chemical compounds	Selected inert gases (gas analysers with time resolution <30 s)
Restrictions in the application	Sufficient footprint area, turbulent conditions necessary

nearly identical sampling frequencies as for surface measurements, the sampling frequency cannot be optimized according to the sampling theorem (see Sect. 6.1.2) to resolve the turbulent eddies. According to investigations by Lenschow et al. (1994), it is possible to estimate fluxes for a fully-developed turbulent regime even when the sampling frequency is low in comparison to the eddy size. This means a larger separation in time (disjunct) of the single samples.

This is the benefit of the disjunct eddy-covariance method where samples are taken only in certain time intervals. Although the direct sampling is taken over a time interval <0.1 s, it may take the gas analyzer several seconds to record the data due to its high inertia, assuming no remarkable reactions occur during this time. Based on simulations, the time difference between two samplings should be in the range of 1–30 s to get the errors comparable to the eddy-covariance method. The method was successfully applied several times (Rinne et al. 2000; Ammann et al. 2006; Held et al. 2007; Schmidt and Klemm 2008; Turnipseed et al. 2009), amongst others with mass spectrometers for reactive gases and aerosols. An overview of the method was given by Rinne and Ammann (2012) and an evaluation of the method is given in Table 4.20.

4.4.4 Surface Renewal Method

The surface renewal method (Paw U et al. 1995) is based on the concept of eddy accumulation (conditional sampling). Instead of turbulence measurements, ramp structures in concentration time series over the vegetation are detected of (see Sect. 3.5.2). Due to the constant *renewal* of these structures, the flux can be defined based on storage depletion. The concept was derived for the sensible heat flux but it can also be applied for matter fluxes. The sensible heat flux is defined as the
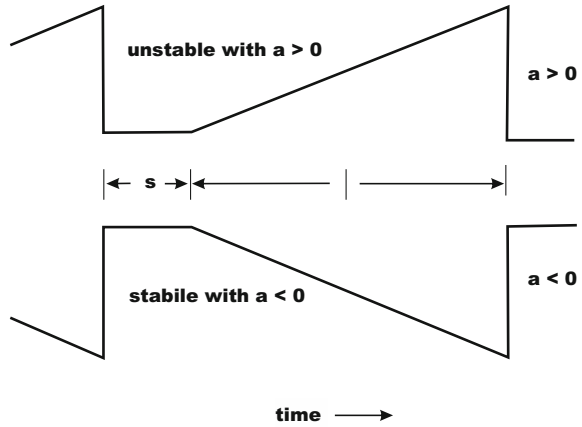
temperature change in time in a volume V above an area A, where V/A can be used
as canopy height z_B:

$$Q_H = \rho\, c_p \frac{dT}{dt}\left(\frac{V}{A}\right) \tag{4.83}$$

Ramp structures such as those shown in Fig. 4.14 for stable and unstable
stratification form the basis (Paw U et al. 1995; Snyder et al. 1996). Accordingly,
the temperature change in time dT/dt in Eq. (4.83) can be substituted by a/l and is
multiplied with the relative duration of the heating or cooling $l/(l + s)$:

$$Q_H = \rho\, c_p \frac{a}{l + s} z_B \tag{4.84}$$

The method needs careful analysis of the turbulence structure and promises
possibilities for the application of fluxes above high vegetation, especially for
predominant stabile stratification with significant ramp structures. There are only a
few experimental studies available (Katul et al. 1996; Snyder et al. 1996; Castellví
and Snyder 2010; Castellví et al. 2012). An evaluation is given in Table 4.21.

4.5 Fluxes of Chemical Substances

The deposition of chemical substances occurs in three different ways (Foken et al.
1995; Finlayson-Pitts and Pitts 2000):

- wet deposition of solute gases and substances in rain water,
- moist deposition of solute gases and substances in fog water,
- dry deposition by turbulent transport of gases and particles (aerosols).

Table 4.21 Evaluation of the surface renewal method

Criterion	Evaluation
Area of application	Basic research and extensive continuous measurement programs for special cases
Financial expense	5–10 k€ per system
Personal expense	Intensive continuous scientific and technical support
Education	Good micrometeorological and measurement technique and probably also chemical knowledge
Error	Depending on the micrometeorological conditions 10–30%
Sampling	10–20 Hz
Time resolution of fluxes	30–60 min
Application for chemical compounds	Selected inert gases (gas analysers with high time resolution)
Restrictions in the application	Sufficient footprint area, turbulent conditions necessary, only over vegetation with ramp structures

Only the dry deposition can be measured with the previously described methods of energy and matter exchange. The wet deposition is a precipitation measurement made with so-called wet-only collectors, which open only during precipitation to avoid the collection of dry deposition and sedimentation. The problems with this measurement are similar to those for precipitation measurement (see Sect. 6.2.4). The moist deposition is important only in areas with frequent fog conditions such as hilly regions (Wrzesinsky and Klemm 2000).

In ecological studies, bulk deposition is measured with open collectors located in the trunk space of a forest. These measurements are the sums of the wet deposition, the sedimentation, the wash up of deposited substances from leafs, and partly dry deposition. The crown-eaves method attempts to compare the bulk deposition with the wet deposition outside the forest, and to estimate the dry deposition as a difference term (Guderian 2000). This method cannot measure the dry deposition quantitatively, because substances are also directly absorbed by the plant surfaces or deposited in the under story or the soil. Also, the sampling time cannot be equated with the time of deposition.

The distribution of the total deposition of the three deposition paths depends significantly on the properties of the surface. High vegetation with a large surface roughness more efficiently absorbs matter by dry deposition from the air (comb out) than by wet or moist deposition. Depending on the substances, dry deposition makes a contribution to the total deposition of about 3/4 above high vegetation and 2/3 above low vegetation (Foken et al. 1995). The substance-dependent differences are shown in Table 4.22.

The dry deposition can be determined, in principle, with all the methods described thus far. One of the difficulties is the limited number of gases for which high-frequency gas analyzers are available for the eddy-covariance method. For profile measurements, the absolute accuracy of the gas analyzers is often too poor to provide for the necessary resolution or the sampling times are larger than the typical

Table 4.22 Ratio of the dry deposition (TD) to the wet deposition (WD) resp. dry particle deposition (TPD) over rural areas (Foken et al. 1995)

Matter	High roughness (forest)		Low roughness (meadow)	
SO_2/SO_4^-	3–4:1	TD/WD	1–1.5:1	TD/WD
	1:1	TD/TPD	3–10:1	TD/TPD
$NO_2 + HNO_3$	1.8–4:1	TD/WD	1–2:1	TD/WD
NO_3^-	1.2–2:1	TD/TPD	2–10:1	TD/TPD
NH_3/NH_4^+	0.2–5:1	TD/WD	?	TD/WD
	0.2–5:1	TD/TPD	1:1	TD/TPD
metal	$\sim$1:1	TD/WD	1:20	TD/WD

meteorological averaging times. Often, modified Bowen-ratio methods, flux-variance similarities, or accumulation methods are utilized. All these methods are not suitable for continuous, operational measurement programs. For recording of the dry deposition estimates, the so-called deposition velocity is used. For climate research worldwide, carbon dioxide exchange is measured with the eddy-covariance method within the FLUXNET programme (Baldocchi et al. 2001). Therefore, extensive technical guides are available (Moncrieff et al. 1997; Aubinet et al. 2000, 2003b, 2012a). Recently efforts have been made to standardize measurement and analysis methods within larger national (NEON, SanClements et al. 2014) and international (ICOS) programs. However, limitations exist due to the variability of atmospheric turbulence and the adaption of instruments and models.

All mentioned methods are unsuitable for routine measurements. A simple and routinely applicable, but physically unrealistic, method is based on the deposition velocity defined by Chamberlain (1961):

$$v_D(z) = -\frac{Q_c}{c(z)} \quad (4.85)$$

This definition is inconsistent with the gradient approach (Roth 1975). But the deposition velocity can be assumed to be a reciprocal transport resistance (see Sect. 5.3), in which the concentration can be replaced by the concentration difference between the measurement height and a second reference height (in the ground), where the concentration is constant or very low. In this way, the physical incorrectness can be overcome. This assumption has the disadvantage that short time changes of the dry deposition (daily cycle or shorter) cannot be exactly reproduced. The method is therefore only applicable for long-term measurements.

Deposition velocities are on the order of 10^{-3} m s^{-1} and are highly variable depending on the surface and the meteorological conditions (Table 4.23). For countrywide investigations, the deposition velocity listed by the relevant agencies is dependent on the time of the year in which the averaged dry deposition was measured.

The proportionality given in Eq. (4.85) between the flux and the concentration is generally fulfilled only for unstable and neutral stratification. Figure 4.15 shows

Table 4.23 Examples for the deposition velocity (Helbig et al. 1999)

Gas	Surface	v_D in 10^{-2} m s^{-1}	Conditions
SO$_2$	Grass	0.5	Neutral stratification
	Needle forest	0.3–0.6	Averaged value
O$_3$	Grass	0.55	Neutral, 5 m s^{-1}
	Spruce forest	0.4	Averaged value
NO	Grass	0.05	Neutral, 5 m s^{-1}
	Spruce forest	0.1–0.4	Averaged value
NO$_2$	Grass	0.6	Neutral, 5 m s^{-1}
	Spruce forest	1.2	In spring

Fig. 4.15 Dependency of the sulphur dioxide deposition on the concentration under the assumption of a constant deposition velocity; filled symbols are values at noon time with unstable stratification, and open symbols values with stable stratification (Adapted from Hicks and Matt 1988, with kind permission of © Kluwer Academic Publisher B. V. Dordrecht 1988, All rights reserved)
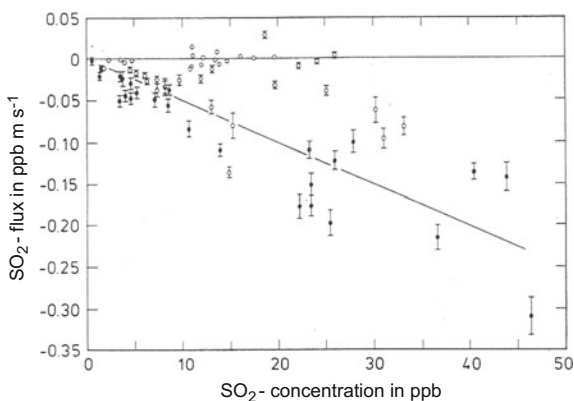
that this proportionality can be realized only with a large scatter. For stable strat-ification, changes of the concentration are nearly independent of the flux.

Due to the non-physical definition of the deposition velocity, there are also problems with its experimental determination. The exact definition would be the transport or transfer velocity (Roth 1975; Arya 1999):

$$v_D(z) = -\frac{Q_c}{c(z) - c(0)} \tag{4.86}$$

Only for the case $c(0) = 0$, i.e. for matter which disappears nearly completely by reactions at the surface, the deposition velocity would be identical with the transfer velocity. Otherwise one obtains unrealistic values (Businger 1986). The determination of the transfer velocity can be made with all the methods described in this chapter; however, the profile method (see Sect. 4.1) is the simplest method.

Most common is the determination of the deposition velocity with the resistance approach (Seinfeld and Pandis 1998), which is described in detail in Sect. 5.3. Thus, the calculation using simple models is possible (Hicks et al. 1987). An evaluation of the method with the deposition velocity is given in Table 4.24.

Table 4.24 Evaluation of the determination of the dry deposition with the deposition velocity

Criterion	Evaluation
Area of application	Operational measurement programs
Financial expense	2–15 k€ per system
Personal expense	Technical support
Education	Knowledge in measurement technique
Error	According to the micrometeorological conditions 20–50%, partly >50%
Sampling	1–10 s, determination of averages over 10–30 min
Time resolution of fluxes	Decadal and monthly averages
Application for chemical compounds	Selected inert gases
Restrictions in the application	Only for rough estimates usable

The previous remarks are only valid for inert gases like carbon dioxide or sulphur dioxide. For reactive gases, the methods can be used only if one gas is significantly in surplus or the measurement time is significantly shorter than the reaction time (e.g. application of the disjunct eddy-covariance method) and reactions do not play an important role, for example ozone deposition during daytime in a rural area. It is also possible to combine complexes of matter, for instance the NO_x-triade consisting of nitrogen monoxide, nitrogen dioxide, and ozone, or the ammonium-tirade consisting of ammoniac, ammonium ions and ammonium nitrate. With the application of the profile method, it must be taken into account that due to reactions the gradient does not always represent the direction of the flux (Kramm et al. 1996). For the application of the eddy-covariance and eddy-accumulation methods, it must be considered that the reaction times of typical chemical reactions are in the order of 10^1–10^4 s and therefore just in the range of the turbulence fluctuations (Fig. 4.16). Very critical are the conditions of stable stratification. Therefore, these methods are basically unusable except if turbulent eddies are tracked with multipoint measurements under the assumption of isotropic turbulence (Foken et al. 1995).

A measure for the ratio of the transport time to the reaction time is the Damköhler number (Molemaker and Vilà-Guerau de Arellano 1998)

$$Da_t = \frac{t_d}{t_c} k \langle c^* \rangle, \tag{4.87}$$

where k is the kinematic reaction constant and $\langle c^* \rangle$ is a dimensionless volume-averaged concentration of one of the reaction partners in equilibrium. Other definitions scale with the emission flux (Schumann 1989). Because the reactions often occur within the smallest eddies, the Kolmogorov-Damköhler number is applied
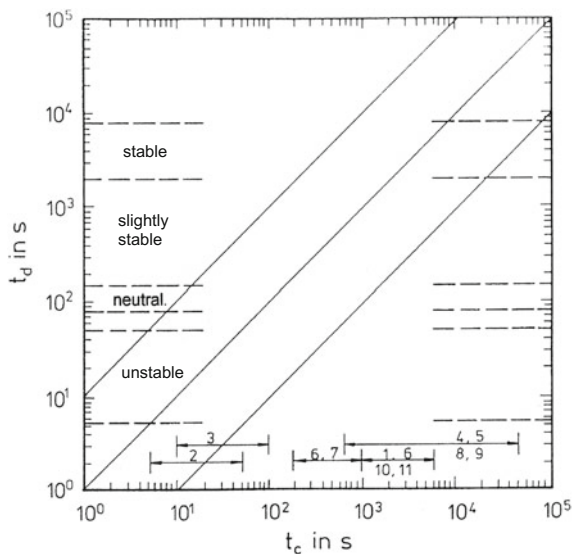
Fig. 4.16 Relation between the characteristic transport time t_d and characteristic reaction time t_c for different chemical reactions for a layer of 10 m thickness and different thermal stratifications according to Dlugi (1993), 1: $HO_2 + HO_2 \rightarrow H_2O_2 + O_2$, 2: $HNO_3 + NH_3 \leftrightarrow NH_4NO_3$, 3: $O_3 + NO \rightarrow NO_2 + O_2$, 4: $O_3 + isoprene \rightarrow$ reaction products (R), 5: $O_3 + monoisoprene \rightarrow$ R, 6: $NO_3 + monoisoprene \rightarrow$ R, 7: $NO_3 + isoprene \rightarrow$ R, 8: $OH + isoprene \rightarrow$ R, 9: $OH + monoisoprene \rightarrow$ R, 10: $O_3 + olefins \rightarrow$ R, 11: $O_3 + NO_2 \rightarrow NO_3 + O_2$ (Published with kind permission of © SPB Academic Publisher, The Hague 1993, All rights reserved)

$$Da_k = \sqrt{\frac{v}{\varepsilon}} k \langle c^* \rangle \tag{4.88}$$

with the kinematic viscosity, v, and the energy dissipation ε. An estimate of the dependence of chemical reactions on the Damköhler number was given by Bilger (1980):

$$
\begin{array}{ll}
Da_t \ll 1 & \text{slow chemistry} \\
Da_k < 1 < Da_t & \text{moderate chemistry} \\
Da_k \gg 1 & \text{fast chemistry}
\end{array}
\tag{4.89}
$$

The determination of the exact transfer and reaction times is important. For the transfer times the method by Vilà-Guerau de Arellano and Duynkerke (1992) is widely applied:

$$t_d = \frac{\kappa \cdot (z + z_0)}{\frac{\sigma_w^2}{u_*^2} \cdot u_*} \tag{4.90}$$

Often the value for σ_w^2/u_*^2 is parametrized using a value of 1.6 according Eq. (2.102). Consequently, Eq. (4.90) is then only valid for neutral stratification (Wyngaard 1982). An estimate for single layers in the surface layer by considering of the stratification based on Eq. (2.75) was given by Mayer et al. (2011):

$$t_d = \frac{\Delta z^2 \cdot \varphi_H(\varsigma) \cdot Sc_t}{\kappa \cdot z_m \cdot u_*}. \tag{4.91}$$

The reaction time, e.g. for the reaction of ozone and nitrogen monoxide with the reaction rate k by Atkinson et al. (2004)

$$O_3 + NO \xrightarrow{k} NO_2 + O_2, k = 1.40 \cdot 10^{-12} exp\left(\frac{-1310}{T}\right), \tag{4.92}$$
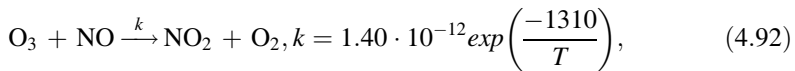
according to Lenschow (1982) is given by

$$t_c = \frac{2}{\sqrt{j_{NO_2} + k^2(N_{O_3} + N_{NO})^2 + 2kj_{NO_2}(N_{O_3} + N_{NO} + 2N_{NO_2})}} \tag{4.93}$$

with the photolysis rate for NO_2 (j_{NO_2}) and the molecule density N in mol cm^{-3}.

Vilà-Guerau de Arellano (2003) explicitly recommended that chemical reactions and turbulent transport are always being considered together and that the determination of the Damköhler number is of vital importance. Foken et al. (2012a), among others, confirmed this for the matter exchange in high vegetation, where the diurnal cycle of the Damköhler number was found being highly variable.

References

Akima H (1970) A new method of interpolation and smooth curve fitting based on local procedures. J Assc Comp Mach. 17:589–602.

Ammann C, Brunner A, Spirig C and Neftel A (2006) Technical note: Water vapour concentration and flux measurements with PTR-MS. Atmos Chem Phys. 6:4643–4651.

Arya SP (1999) Air Pollution Meteorology and Dispersion. Oxford University Press, New York, Oxford, 310 pp.

Arya SP (2001) Introduction to Micrometeorology. Academic Press, San Diego, 415 pp.

Atkinson R, Baulch DL, Cox RA, Crowley JN, Hampson RF, Hynes RG, Jenkin ME, Rossi MJ and Troe J (2004) Evaluated kinetic and photochemical data for atmospheric chemistry: Volume I - gas phase reactions of O$_x$, HO$_x$, NO$_x$ and SO$_x$ species. Atmos Chem Phys. 4:1461–1738.

Aubinet M, Grelle A, Ibrom A, Rannik Ü, Moncrieff J, Foken T, Kowalski AS, Martin PH, Berbigier P, Bernhofer C, Clement R, Elbers J, Granier A, Grünwald T, Morgenstern K, Pilegaard K, Rebmann C, Snijders W, Valentini R and Vesala T (2000) Estimates of the annual net carbon and water exchange of forests: The EUROFLUX methodology. Adv Ecol Res. 30:113–175.

Aubinet M, Heinesch B and Yernaux M (2003a) Horizontal and vertical CO_2 advection in a sloping forest. Boundary-Layer Meteorol. 108:397–417.

Aubinet M, Clement R, Elbers J, Foken T, Grelle A, Ibrom A, Moncrieff H, Pilegaard K, Rannik U and Rebmann C (2003b) Methodology for data acquisition, storage and treatment. In: Valentini R (ed.), Fluxes of Carbon, Water and Energy of European Forests. Ecological Studies, Vol. 163. Springer, Berlin, Heidelberg, 9–35.

Aubinet M, Berbigier P, Bernhofer C, Cescatti A, Feigenwinter C, Granier A, Grünwald T, Havrankova K, Heinesch B, Longdoz B, Marcolla B, Montagnani L and Sedlak P (2005) Comparing CO_2 storage and advection conditions at night at different CarboEuroflux sites. Boundary-Layer Meteorol. 116:63–94.

Aubinet M, Feigenwinter C, Heinesch B, Bernhofer C, Canepa E, Lindroth A, Montagnani L, Rebmann C, Sedlak P and van Gorsel E (2010) Direct advection measurements do not help to solve the night-time CO_2 closure problem: Evidence from three different forests. Agrical Forest Meteorol. 150:655–664.

Aubinet M, Vesala T and Papale D (eds) (2012a) Eddy Covariance: A Practical Guide to Measurement and Data Analysis. Springer, Dordrecht, Heidelberg, London, New York, 438 pp.

Aubinet M, Feigenwinter C, Heinesch B, Laffineur Q, Papale D, Reichstein M, Rinne J and Van Gorsel E (2012b) Nighttime flux correction. In: Aubinet Met al (eds.), Eddy Covariance: A Practical Guide to Measurement and Data Analysis. Springer, Berlin, Heidelberg, 133–157.

Baldocchi D, Falge E, Gu L, Olson R, Hollinger D, Running S, Anthoni P, Bernhofer C, Davis K, Evans R, Fuentes J, Goldstein A, Katul G, Law B, Lee XH, Malhi Y, Meyers T, Munger W, Oechel W, PawU KT, Pilegaard K, Schmid HP, Valentini R, Verma S and Vesala T (2001) FLUXNET: A new tool to study the temporal and spatial variability of ecosystem-scale carbon dioxide, water vapor, and energy flux densities. Bull Amer Meteorol Soc. 82:2415–2434.

Barr AG, King KM, Gillespie TJ, Hartog GD and Neumann HH (1994) A comparison of Bowen ratio and eddy correlation sensible and latent heat flux measurements above deciduous forest. Boundary-Layer Meteorol. 71:21–41.

Bartels J (1935) Zur Morphologie geophysikalischer Zeitfunktionen. Sitzungsberichte Preuß Akad Wiss. 30:504–522.

Barthlott C and Fiedler F (2003) Turbulence structure in the wake region of a meteorological tower. Boundary-Layer Meteorol. 108:175–190.

Bernhardt K and Piazena H (1988) Zum Einfluß turbulenzbedingter Dichteschwankungen auf die Bestimmung turbulenter Austauschströme in der Bodenschicht. Z Meteorol. 38:234–245.

Bernhofer C (1992) Estimating forest evapotranspiration at a non-ideal site. Agrical Forest Meteorol. 60:17–32.

Bilger RW (1980) Turbulent flows with nonpremixed reactants. In: Libby PA and Willimas FA (eds.), Turbulent Reacting Flows. Springer, Berlin, Heidelberg, 65–113.

Bowling DR, Delany AC, Turnispseed AA, Baldocchi DD and Monson RK (1999) Modification of the relaxed eddy accumulation technique to maximize measured scalar mixing ratio differences in updrafts and downdrafts. J Geophys Res. 104:9121–9133.

Bowling DR, Pataki DE and Ehleringer JR (2003) Critical evaluation of micrometeorological methods for measuring ecosystem-atmosphere isotopic exchange of CO_2. Agrical Forest Meteorol. 116:159–179.

Brocks K and Krügermeyer L (1970) Die hydrodynamische Rauhigkeit der Meeresoberfläche. Ber Inst Radiometeorol Marit Meteorol. 14:55 pp.

Brook RR (1978) The influence of water vapor fluctuations on turbulent fluxes. Boundary-Layer Meteorol. 15:481–487.

Burba G, McDermitt DK, Grelle A, Anderson DJ and Xu L (2008) Addressing the influence of instrument surface heat exchange on the measurements of CO2 flux from open-path gas analyzers. Global Change Biology. 14:1854–1876.

Businger JA (1986) Evaluation of the accuracy with which dry deposition can be measured with current micrometeorological techniques. J Appl Meteorol. 25:1100–1124.

Businer JA and Oncley SP (1990) Flux measurement with conditional sampling. J Atm Oceanic Techn. 7:349–352.

Castellví F and Snyder RL (2010) A comparison between latent heat fluxes over grass using a weighing lysimeter and surface renewal analysis. J Hydrol. 381:213–220.

Castellví F, Consoli S and Papa R (2012) Sensible heat flux estimates using two different methods based on surface renewal analysis. A study case over an orange orchard in Sicily. Agrical Forest Meteorol. 152:58–64.

Chamberlain AC (1961) Aspects of travel and deposition of aerosol and vapour clouds. A.E.R.E., Harwell, Berkshire, 38 pp.

Charuchittipan D, Babel W, Mauder M, Leps J-P and Foken T (2014) Extension of the averaging time of the eddy-covariance measurement and its effect on the energy balance closure Boundary-Layer Meteorol. 152:303–327.

Desjardins RL (1977) Description and evaluation of a sensible heat flux detector. Boundary-Layer Meteorol. 11:147–154.

Desjardins RL, MacPherson JI, Schuepp PH and Karanja F (1989) An evaluation of aircraft flux measurements of CO_2, water vapor and sensible heat. Boundary-Layer Meteorol. 47:55–69.

Dlugi R (1993) Interaction of NO_x and VOC's within vegetation. In: Borrell PW (ed.), Proceedings EUROTRAC-Symposium 92. SPB Acad. Publ., The Hague, 682–688.

Doran JC and Verholek MG (1978) A note on vertical extrapolation formulas for Weibull velocity distribution parameters. J Climate Appl Meteorol. 17:410–412.

Dugas WA, Fritschen LJ, Gay LW, Held AA, Matthias AD, Reicosky DC, Steduto P and Steiner JL (1991) Bowen ratio, eddy correlation, and portable chamber measurements of sensible and latent heat flux over irrigated spring wheat. Agrical Forest Meteorol. 56:12–20.

Dyer AJ (1974) A review of flux-profile-relationships. Boundary-Layer Meteorol. 7:363–372.

Dyer AJ (1981) Flow distortion by supporting structures. Boundary-Layer Meteorol. 20:363–372.

Eugster W and Senn W (1995) A cospectral correction for measurement of turbulent NO_2 flux. Boundary-Layer Meteorol. 74:321–340.

Falge E, Baldocchi D, Olson R, Anthoni P, Aubinet M, Bernhofer C, Burba G, Ceulemans R, Clement R, Dolman H, Granier A, Gross P, Grunwald T, Hollinger D, Jensen NO, Katul G, Keronen P, Kowalski A, Lai CT, Law BE, Meyers T, Moncrieff H, Moors E, Munger JW, Pilegaard K, Rannik U, Rebmann C, Suyker A, Tenhunen J, Tu K, Verma S, Vesala T, Wilson K and Wofsy S (2001) Gap filling strategies for long term energy flux data sets. Agrical Forest Meteorol. 107:71–77.

Finkelstein PL and Sims PF (2001) Sampling error in eddy correlation flux measurements. J Geophys Res. D106:3503–3509.

Finlayson-Pitts BJ and Pitts JN (2000) Chemistry of the Upper and Lower Atmosphere. Academic Press, San Diego, 963 pp.

Finnigan J (1999) A comment on the paper by Lee (1998): "On micrometeorological observations of surface-air exchange over tall vegetation". Agrical Forest Meteorol. 97:55–64.

Finnigan JJ, Clement R, Malhi Y, Leuning R and Cleugh HA (2003) A re-evaluation of long-term flux measurement techniques, Part I: Averaging and coordinate rotation. Boundary-Layer Meteorol. 107:1–48.

Foken T (1990) Turbulenter Energieaustausch zwischen Atmosphäre und Unterlage - Methoden, meßtechnische Realisierung sowie ihre Grenzen und Anwendungsmöglichkeiten. Ber Dt Wetterdienstes. 180:287 pp.

Foken T (1998) Genauigkeit meteorologischer Messungen zur Bestimmung des Energie- und Stoffaustausches über hohen Pflanzenbeständen. Ann Meteorol. 37:513–514.

Foken T and Skeib G (1980) Genauigkeit und Auswertung von Profilmessungen zur Energieaustauschbestimmung. Z Meteorol. 30:346–360.

Foken T and Oncley SP (1995) Results of the workshop 'Instrumental and methodical problems of land surface flux measurements'. Bull Amer Meteorol Soc. 76:1191–1193.

Foken T and Wichura B (1996) Tools for quality assessment of surface-based flux measurements. Agrical Forest Meteorol. 78:83–105.

Foken T, Dlugi R and Kramm G (1995) On the determination of dry deposition and emission of gaseous compounds at the biosphere-atmosphere interface. Meteorol Z. 4:91–118.

Foken T, Richter SH and Müller H (1997a) Zur Genauigkeit der Bowen-Ratio-Methode. Wetter und Leben. 49:57–77.

Foken T, Jegede OO, Weisensee U, Richter SH, Handorf D, Görsdorf U, Vogel G, Schubert U, Kirzel H-J and Thiermann V (1997b) Results of the LINEX-96/2 Experiment. Dt Wetterdienst, Forsch. Entwicklung, Arbeitsergebnisse. 48:75 pp.

Foken T, Göckede M, Mauder M, Mahrt L, Amiro BD and Munger JW (2004) Post-field data quality control. In: Lee X et al (eds.), Handbook of Micrometeorology: A Guide for Surface Flux Measurement and Analysis. Kluwer, Dordrecht, 181–208.

Foken T, Wimmer F, Mauder M, Thomas C and Liebethal C (2006) Some aspects of the energy balance closure problem. Atmos Chem Phys. 6:4395–4402.

Foken T, Meixner FX, Falge E, Zetzsch C, Serafimovich A, Bargsten A, Behrendt T, Biermann T, Breuninger C, Dix S, Gerken T, Hunner M, Lehmann-Pape L, Hens K, Jocher G, Kesselmeier J, Lüers J, Mayer JC, Moravek A, Plake D, Riederer M, Rütz F, Scheibe M, Siebicke L, Sörgel M, Staudt K, Trebs I, Tsokankunku A, Welling M, Wolff V and Zhu Z (2012a) Coupling processes and exchange of energy and reactive and non-reactive trace gases at a forest site—results of the EGER experiment. Atmos Chem Phys. 12:1923–1950.

Foken T, Aubinet M and Leuning R (2012b) The eddy-covarianced method. In: Aubinet M et al (eds.), Eddy Covariance: A Practical Guide to Measurement and Data Analysis. Springer, Dordrecht, Heidelberg, London, New York, 1–19.

Foken T, Leuning R, Oncley SP, Mauder M and Aubinet M (2012c) Corrections and data quality In: Aubinet M et al (eds.), Eddy Covariance: A Practical Guide to Measurement and Data Analysis. Springer, Dordrecht, Heidelberg, London, New York, 85–131.

Frank JM, Massman WJ and Ewers BE (2013) Underestimates of sensible heat flux due to vertical velocity measurement errors in non-orthogonal sonic anemometers. Agrical Forest Meteorol. 171–172:72–81.

Fratini G and Mauder M (2014) Towards a consistent eddy-covariance processing: an intercomparison of EddyPro and TK3. Atmos Meas Techn. 7:2273–2281.

Fuchs M and Tanner CB (1970) Error analysis of Bowen ratios measured by differential psychrometry. Agric Meteorol. 7:329–334.

Fuehrer PL and Friehe CA (2002) Flux correction revised. Boundary-Layer Meteorol. 102:415–457.

Garratt JR (1992) The Atmospheric Boundary Layer. Cambridge University Press, Cambridge, 316 pp.

Geernaert GL (ed) (1999) Air-Sea Exchange: Physics, Chemistry and Dynamics. Kluwer Acad. Publ., Dordrecht, 578 pp.

Goulden ML, Munger JW, Fan F-M, Daube BC and Wofsy SC (1996) Measurements of carbon sequestration by long-term eddy covariance: method and critical evaluation of accuracy. Global Change Biol. 2:159–168.

Grelle A and Burba G (2007) Fine-wire thermometer to correct CO_2 fluxes by open-path analyzers for artificial density fluctuations. Agrical Forest Meteorol. 147:48–57.

Gu L, Falge EM, Boden T, Baldocchi DD, Black T, Saleska SR, Sumi T, Verma SB, Vesala T, Wofsy SC and Xu L (2005) Objective threshold determination for nighttime eddy flux filtering. Agrical Forest Meteorol. 128:179–197.

Guderian R (ed) (2000) Handbuch der Umweltveränderungen und Ökotoxikologie, Atmosphäre. Springer, Berlin, Heidelberg, 424, 516 pp.

Gurjanov AE, Zubkovskij SL and Fedorov MM (1984) Mnogokanalnaja avtomatizirovannaja sistema obrabotki signalov na baze EVM (Automatic multi-channel system for signal analysis with electronic data processing). Geod Geophys Veröff, R II. 26:17–20.

Haugen DA (ed) (1973) Workshop on Micrometeorology. Am. Meteorol. Soc., Boston, 392 pp.

Helbig A, Baumüller J and Kerschgens MJ (eds) (1999) Stadtklima und Luftreinhaltung. Springer, Berlin, Heidelberg, 467 pp.

Held A, Niessner R, Bosveld F, Wrzesinsky T and Klemm O (2007) Evaluation and application of an electrical low pressure impactor in disjunct eddy covariance aerosol flux measurements. Aerosol Science and Technology. 41:510–519.

Hesselberg T (1926) Die Gesetze der ausgeglichenen atmosphärischen Bewegungen. Beitr Phys Atm. 12:141–160.

Hicks BB and Matt DR (1988) Combining biology, chemistry and meteorology in modelling and measuring dry deposition. J Atm Chem. 6:117–131.

Hicks BB, Baldocchi DD, Meyers TP, Hosker jr. RP and Matt DR (1987) A preliminary multiple resistance routine for deriving dry deposition velocities from measured quantities. Water, Air and Soil Pollution. 36:311–330.

Hoaglin DC, Mosteller F and Tukey JW (2000) Understanding robust and exploratory data analysis. John Wiley & Sons, New York, 447 pp.

Högström U (1988) Non-dimensional wind and temperature profiles in the atmospheric surface layer: A re-evaluation. Boundary-Layer Meteorol. 42:55–78.

Högström U and Smedman A (2004) Accuracy of sonic anemometers: Laminar wind-tunnel calibrations compared to atmospheric in situ calibrations against a reference instrument. Boundary-Layer Meteorol. 111:33–54.

Højstrup J (1993) A statistical data screening procedure. Meas Sci Techn. 4:153–157.

Hollinger DY and Richardson AD (2005) Uncertainty in eddy covariance measurements and its application to physiological models. Tree Phys. 25:873–885.

Horst TW (1997) A simple formula for attenuation of eddy fluxes measured with first-order-response scalar sensors. Boundary-Layer Meteorol. 82:219–233.

Horst TW, Semmer SR and Maclean G (2015) Correction of a non-orthogonal, three-component sonic aanemometer for flow Distortion by transducer shadowing. Boundary-Layer Meteorol. 155:371–395.

Hsu SA, Meindl EA and Gilhousen DB (1994) Determination of power-law wind-profile exponent under near- neutral stability conditions at sea. J Appl Meteorol. 33:757–765.

Huang CH (1979) A theory of dispersion in turbulent shear flow. Atmos Environm. 13:453–463.

Huges IG and Hase TPA (2010) Measurements and their Uncertainties. Oxford University Press, Oxford, 136 pp.

Hui DF, Wan SQ, Su B, Katul G, Monson R and Luo YQ (2004) Gap-filling missing data in eddy covariance measurements using multiple imputation (MI) for annual estimations. Agrical Forest Meteorol. 121:93–111.

Hyson P, Garratt JR and Francey RJ (1977) Algebraic und elektronic corrections of measured uw covariance in the lower atmosphere. Boundary-Layer Meteorol. 16:43–47.

Ibrom A, Dellwik E, Larsen SE and Pilegaard K (2007a) On the use of the Webb–Pearman–Leuning theory for closed-path eddy correlation measurements. Tellus. B 59:937–946.

Ibrom A, Dellwik E, Flyvbjerg H, Jensen NO and Pilegaard K (2007b) Strong low-pass filtering effects on water vapour flux measurements with closed-path eddy correlation systems. Agrical Forest Meteorol. 147:140–156.

Irvin JS (1978) A theoretical variation of the wind profile power-law exponent as a function of surface roughness and stability. Atmos Environm. 13:191–194.

Itier B (1980) Une méthode simplifièe pour la mesure du flux de chaleur sensible. J Rech Atm. 14:17–34.

Järvi L, Mammarella I, Eugster W, Ibrom A, Siivola E, Dellwik E, Keronen P, Burba G and Vesala T (2009) Comparison of net CO_2 fluxes measured with open- and closed-path infrared gas analyzers in urban complex environment. Boreal Environm Res. 14:499–514.

Joffre SM (1984) Power laws and the empirical representation of velocity and directional sheer. J Climate Appl Meteorol. 23:1196–1203.

Kader BA and Perepelkin VG (1984) Profil skorosti vetra i temperatury v prizemnom sloje atmosfery v uslovijach nejtralnoj i neustojtschivoj stratifikacii (The wind and temperature profile in the near surface layer for neutral and unstable stratification). Izv AN SSSR, Fiz Atm Okeana. 20:151–161.

Kaimal JC (1978) Sonic Anemometer Measurement of Atmospheric Turbulence. In: Hansen B (ed.), Proceedings of the Dynamic Flow Conference 1978 on Dynamic Measurements in Unsteady Flows. Springer Netherlands, 551–565.

Kaimal JC and Gaynor JE (1991) Another look to sonic thermometry. Boundary-Layer Meteorol. 56:401–410.

Kaimal JC and Finnigan JJ (1994) Atmospheric Boundary Layer Flows: Their Structure and Measurement. Oxford University Press, New York, NY, 289 pp.

Kaimal JC, Wyngaard JC, Izumi Y and Coté OR (1972) Spectral characteristics of surface layer turbulence. Quart J Roy Meteorol Soc. 98:563–589.

Kaimal JC, Gaynor JE, Zimmerman HA and Zimmerman GA (1990) Minimizing flow distortion errrors in a sonic anemometer. Boundary-Layer Meteorol. 53:103–115.

Katul G, Hsieh C-I, Oren R, Ellsworth D and Phillips N (1996) Latent and sensible heat flux predictions from a uniform pine forest using surface renewal and flux variance methods. Boundary-Layer Meteorol. 80:249–282.

Kormann R and Meixner FX (2001) An analytical footprint model for non-neutral stratification. Boundary-Layer Meteorol. 99:207–224.

Kowalski A (2006) Comment on "An Alternative Approach for CO_2 Flux Correction Caused by Heat and Water Vapour Transfer" by Liu. Boundary-Layer Meteorol. 120:353–355.

Kramm G and Meixner FX (2000) On the dispersion of trace species in the atmospheric boundary layer: a re-formulation of the governing equations for the turbulent flow of the compressible atmosphere. Tellus. 51A:500–522.

Kramm G, Dlugi R and Lenschow DH (1995) A re-evaluation of the Webb correction using density weighted averages. J Hydrol. 166:293–311.

Kramm G, Beier M, Foken T, Müller H, Schröder P and Seiler W (1996) A SVAT-skime for NO, NO_2, and O_3—Model description and test results. Meteorol Atmos Phys. 61:89–106.

Kristensen L, Mann J, Oncley SP and Wyngaard JC (1997) How close is close enough when measuring scalar fluxes with displaced sensors. J Atm Oceanic Techn. 14:814–821.

Lasslop G, Reichstein M, Papale D, Richardson AD, Arneth A, Barr A, Stoy P and Wohlfahrt G (2010) Separation of net ecosystem exchange into assimilation and respiration using a light response curve approach: critical issues and global evaluation. Global Change Biology. 16:187–208.

Lee X (1998) On micrometeorological observations of surface-air exchange over tall vegetation. Agrical Forest Meteorol. 91:39–49.

Lee X, Massman WJ and Law B (eds) (2004) Handbook of Micrometeorology: A Guide for Surface Flux Measurement and Analysis. Kluwer, Dordrecht, 250 pp.

Lege D (1981) Eine Betrachtung zur Bestimmung des Stroms fühlbarer Wärme und der Schubspannungsgeschwindigkeit aus Temperatur- und Windgeschwindigkeitsdifferenzen. Meteorol Rundschau. 34:1–4.

Lenschow DH (1982) Reactive trace species in the boundary layer from a micrometeorological perspective. J Meteor Soc Japan. 60:472–480.

Lenschow DH, Mann J and Kristensen L (1994) How long is long enough when measuring fluxes and other turbulence statistics? J Atm Oceanic Techn. 11:661–673.

Leuning R (2007) The correct form of the Webb, Pearman and Leuning equation for eddy fluxes of trace gases in steady and non-steady state, horizontally homogeneous flows Boundary-Layer Meteorol. 123:263–267.

Leuning R and Legg BJ (1982) Comments on 'The influence of water vapor fluctuations on turbulent fluxes' by Brook. Boundary-Layer Meteorol. 23:255–258.

Leuning R and Judd MJ (1996) The relative merits of open- and closed path analysers for measurements of eddy fluxes. Global Change Biology. 2:241–254.

Liebethal C and Foken T (2003) On the significance of the Webb correction to fluxes. Boundary-Layer Meteorol. 109:99–106.

Liebethal C and Foken T (2004) On the significance of the Webb correction to fluxes, Corrigendum. Boundary-Layer Meteorol. 113:301.

Lindauer M, Schmid HP, Grote R, Mauder M, Steinbrecher R and Wolpert B (2014) Net ecosystem exchange over a non-cleared wind-throw-disturbed upland spruce forest— Measurements and simulations. Agrical Forest Meteorol. 197:219–234.

Liu H (2005) An alternative approach for CO_2 flux correction caused by heat and water vapour transfer. Boundary-Layer Meteorol. 115:151–168.

Liu H and Foken T (2001) A modified Bowen ratio method to determine sensible and latent heat fluxes. Meteorol Z. 10:71–80.

Liu H, Peters G and Foken T (2001) New equations for sonic temperature variance and buoyancy heat flux with an omnidirectional sonic anemometer. Boundary-Layer Meteorol. 100:459–468.

Liu H, Randerson JT, Lindfors J, Massman WJ and Foken T (2006) Consequences of incomplete surface energy balance closure for CO_2 fluxes from open-path CO_2/H_2O infrared gas analyzers. Boundary-Layer Meteorol. 120:65–85.

Lloyd J and Taylor JA (1994) On the temperature dependence of soil respiration. Functional Ecol. 8:315–323.

Mahrt L (1991) Eddy asymmetry in the sheared heated boundary layer. J Atmos Sci. 48:472–492.

Mahrt L (1996) The bulk aerodynamic formulation over heterogeneous surfaces. Boundary-Layer Meteorol. 78:87–119.

Marquardt D (1983) An algorithm for least-sqares estimation of nonlinear parameters. J Soc Indust Appl Math. 11:431–441.

Massman WJ (2000) A simple method for estimating frequency response corrections for eddy covariance systems. Agrical Forest Meteorol. 104:185–198.

Massman WJ and Tuovinen J-P (2006) An analysis and implications of alternative methods of deriving the density (WPL) terms for eddy covariance flux measurements. Boundary-Layer Meteorol. 121:221–227.

Mauder M, Liebethal C, Göckede M, Leps J-P, Beyrich F and Foken T (2006) Processing and quality control of flux data during LITFASS-2003. Boundary-Layer Meteorol. 121:67–88.

Mauder M, Foken T, Clement R, Elbers J, Eugster W, Grünwald T, Heusinkveld B and Kolle O (2008) Quality control of CarboEurope flux data - Part 2: Inter-comparison of eddy-covariance software. Biogeoscience. 5:451–462.

Mauder M, Cuntz M, Drüe C, Graf A, Rebmann C, Schmid HP, Schmidt M and Steinbrecher R (2013) A strategy for quality and uncertainty assessment of long-term eddy-covariance measurements. Agrical Forest Meteorol. 169:122–135.

Mayer JC, Bargsten A, Rummel U, Meixner FX and Foken T (2011) Distributed Modified Bowen Ratio method for surface layer fluxes of reactive and non-reactive trace gases. Agrical Forest Meteorol. 151:655–668.

McMillen RT (1988) An eddy correlation technique with extended applicability to non-simple terrain. Boundary-Layer Meteorol. 43:231–245.

Michaelis L and Menton ML (1913) Die Kinetik der Invertinwirkung. Biochem Z. 49:333.

Moffat AM, Papale D, Reichstein M, Barr AG, Beckstein C, Braswell BH, Churkina G, Desai A, Falge E, Gove JH, Heimann M, Hollinger DY, Hui D, Jarvis AJ, Kattge J, Noormets A, Richardson AD and Stauch VJ (2007) Comprehensive comparison of gap filling techniques for eddy covariance net carbon fluxes. Agrical Forest Meteorol. 47:209–232.

Molemaker MJ and Vilà-Guerau de Arellano J (1998) Control of chemical reactions by convective turbulence in the boundary layer. J Atmos Sci. 55:568–579.

Moncrieff JB, Massheder JM, DeBruin H, Elbers J, Friborg T, Heusinkveld B, Kabat P, Scott S, Søgaard H and Verhoef A (1997) A system to measure surface fluxes of momentum, sensible heat, water vapor and carbon dioxide. J Hydrol. 188–189:589–611.

Moore CJ (1986) Frequency response corrections for eddy correlation systems. Boundary-Layer Meteorol. 37:17–35.

Moravek A, Trebs I and Foken T (2013) Effect of imprecise lag time and high-frequency attenuation on surface-atmosphere exchange fluxes determined with the relaxed eddy accumulation method. J Geophys Res: Atmosph. 118:10, 210–210, 224.

Moravek A, Foken T and Trebs I (2014) Application of a GC-ECD for measurements of biosphere–atmosphere exchange fluxes of peroxyacetyl nitrate using the relaxed eddy accumulation and gradient method. Athmospheric Measurement Techniques. 7:2097–2119.

Müller H, Kramm G, Meixner FX, Fowler D, Dollard GJ and Possanzini M (1993) Determination of HNO_3 dry deposition by modified Bowen ratio and aerodynamic profile techniques. Tellus. 45B:346–367.

Nakai T and Shimoyama K (2012) Ultrasonic anemometer angle of attack errors under turbulent conditions. Agrical Forest Meteorol. 162–163:14–26.

Nakai T, van der Molen MK, Gash JHC and Kodama Y (2006) Correction of sonic anemometer angle of attack errors. Agrical Forest Meteorol. 136:19–30.

Nicholls S and Smith FB (1982) On the definition of the flux of sensible heat. Boundary-Layer Meteorol. 24:121–127.

Nieuwstadt FTM (1978) The computation of the friction velocity u_* and the temperature scale T_* from temperature and wind velocity profiles by least-square method. Boundary-Layer Meteorol. 14:235–246.

Oechel WC, Laskowski CA, Burba G, Gioli B and Kalhori AAM (2014) Annual patterns and budget of CO_2 flux in an Arctic tussock tundra ecosystem. Journal of Geophysical Research: Biogeosciences. 119:2013JG002431.

Ohmura A (1982) Objective criteria for rejecting data for Bowen ratio flux calculations. J Climate Appl Meteorol. 21:595–598.

Oncley SP, Businger JA, Itsweire EC, Friehe CA, LaRue JC and Chang SS (1990) Surface layer profiles and turbulence measurements over uniform land under near-neutral conditions. 9th Symposium on Boundary Layer and Turbulence, Roskilde, Denmark, April 30 - May 3, 1990. Am. Meteorol. Soc., pp. 237–240.

Oncley SP, Delany AC, Horst TW and Tans PP (1993) Verification of flux measurement using relaxed eddy accumulation. Atmos Environm. 27A:2417–2426.

Panin GN (1983) Metodika rastscheta lokalnogo teplo- i vlagoobmena v sisteme vodoem - atmosfera (Method for calculation of local heat and humidity exchange of the system water - atmosphere). Vodnye resursy. 4:3–12.

Papale D and Valentini R (2003) A new assessment of European forests carbon exchanges by eddy fluxes and artificial neural network spatialization. Global Change Biology. 9:525–535.

Papale D, Reichstein M, Aubinet M, Canfora E, Bernhofer C, Kutsch W, Longdoz B, Rambal S, Valentini R, Vesala T and Yakir D (2006) Towards a standardized processing of Net Ecosystem Exchange measured with eddy covariance technique: algorithms and uncertainty estimation. Biogeoscience. 3:571–583.

Pattey E, Desjardins RL and Rochette P (1993) Accuracy of the relaxed eddy accumulation technique. Boundary-Layer Meteorol. 66:341–355.

Pattey E, Strachan IB, Desjardins RL, Edwards GC, Dow D and MacPherson IJ (2006) Application of a tunable diode laser to the measurement of CH_4 and N_2O fluxes from field to landscape scale using several micrometeorological techniques. Agrical Forest Meteorol. 136:222–236.

Paw U KT, Qiu J, Su H-B, Watanabe T and Brunet Y (1995) Surface renewal analysis: a new method to obtain scalar fluxes. Agrical Forest Meteorol. 74:119–137.

Paw U KT, Baldocchi D, Meyers TP and Wilson KB (2000) Correction of eddy covariance measurements incorporating both advective effects and density fluxes. Boundary-Layer Meteorol. 97:487–511.

Pearson jr. RJ, Oncley SP and Delany AC (1998) A scalar similarity study based on surface layer ozone measurements over cotton during the California Ozone Deposition Experiment. J Geophys Res. 103 (D15):18919–18926.

Peterson EW and Hennessey jr. JP (1978) On the use of power laws for estimates of wind power potential. J Climate Appl Meteorol. 17:390–394.

Rannik U and Vesala T (1999) Autoregressive filtering versus linear detrending in estimation of fluxes by the eddy covariance method. Boundary-Layer Meteorol. 91:259–280.

Rebmann C, Göckede M, Foken T, Aubinet M, Aurela M, Berbigier P, Bernhofer C, Buchmann N, Carrara A, Cescatti A, Ceulemans R, Clement R, Elbers J, Granier A, Grünwald T, Guyon D, Havránková K, Heinesch B, Knohl A, Laurila T, Longdoz B, Marcolla B, Markkanen T, Miglietta F, Moncrieff H, Montagnani L, Moors E, Nardino M, Ourcvial J-M, Rambal S, Rannik U, Rotenberg E, Sedlak P, Unterhuber G, Vesala T and Yakir D (2005) Quality analysis applied on eddy covariance measurements at complex forest sites using footprint modelling. Theor Appl Climat. 80:121–141.

Rebmann C, Kolle O, Heinesch B, Queck R, Ibrom A and Aubinet M (2012) Data acquisition and flux calculations. In: Aubinet Met al (eds.), Eddy Covariance: A Practical Guide to Measurement and Data Analysis. Springer, Dordrecht, Heidelberg, London, New York, 59–83.

Reichstein M, Falge E, Baldocchi D, Papale D, Aubinet M, Berbigier P, Bernhofer C, Buchmann N, Gilmanov T, Granier A, Grünwald T, Havránková K, Ilvesniemi H, Janous D, Knohl A, Laurila T, Lohila A, Loustau D, Matteucci G, Meyers T, Miglietta F, Ourcival J-M, Pumpanen J, Rambal S, Rotenberg E, Sanz M, Tenhunen J, Seufert G, Vaccari F, Vesala T, Yakir D and Valentini R (2005) On the separation of net ecosystem exchange into assimilation and ecosystem respiration: review and improved algorithm. Global Change Biology. 11:1424–1439.

Ren X, Sanders JE, Rajendran A, Weber RJ, Goldstein AH, Pusede SE, Browne EC, Min KE and Cohen RC (2011) A relaxed eddy accumulation system for measuring vertical fluxes of nitrous acid. Atmos. Meas. Tech. 4:2093–2103.

Richardson AD, Hollinger DY, Burba GG, Davis KJ, Flanagan LB, Katul GG, Munger JW, Ricciuto DM, Stoy PC, Suyker AE, Verma SB and Wofsy SC (2006) A multi-site analysis of random error in tower-based measurements of carbon and energy fluxes. Agrical Forest Meteorol. 136:1–18.

Richter SH and Skeib G (1984) Anwendung eines Verfahrens zur Parametrisierung des turbulenten Energieaustausches in der atmosphärischen Bodenschicht. Geod Geophys Veröff, R II. 26:80–85.

Richter SH and Skeib G (1991) Ein Verfahren zur Parametrisierung von Austauschprozessen in der bodennahen Luftschicht. Abh Meteorol Dienstes DDR. 146:15–22.

Riederer M, Hübner J, Ruppert J, Brand WA and Foken T (2014) Prerequisites for application of hyperbolic relaxed eddy accumulation on managed grasslands and alternative net ecosystem exchange flux partitioning. Atmos Meas Techn. 7:4237–4250.

Rinne HJI, Delany AC, Greenberg JP and Guenther AB (2000) A true eddy accumulation system for trace gas fluxes using disjunct eddy sampling method. J Geophys Res. 105(D20):24791–24798.

Rinne J and Ammann C (2012) Disjunct eddy covariance method. In: Aubinet Met al (eds.), Eddy Covariance: A Practical Guide to Measurement and Data. Springer, Dordrecht, Heidelberg, London, New York, 291–307.

Roth R (1975) Der vertikale Transport von Luftbeimengungen in der Prandtl-Schicht und die Depositionsgeschwindigkeit. Meteorol Rundschau. 28:65–71.

Ruppert J, Wichura B, Delany AC and Foken T (2002) Eddy sampling methods, A comparison using simulation results. 15th Symposium on Boundary Layer and Turbulence, Wageningen, 15–19 July 2002. Am. Meteorol. Soc., pp. 27–30.

Ruppert J, Thomas C and Foken T (2006a) Scalar similarity for relaxed eddy accumulation methods. Boundary-Layer Meteorol. 120:39–63.

Ruppert J, Mauder M, Thomas C and Lüers J (2006b) Innovative gap-filling strategy for annual sums of CO_2 net ecosystem exchange. Agrical Forest Meteorol. 138:5–18.

SanClements M, Metzger S, Luo H, Pingintha-Durden N, Zulueta RC and Loescher HW (2014) The National Ecological Observatory Network (NEON): Providing free long-term ecological data on a continental scale. iLEAPS newsletter, Special issue on Environmental Research Infrastructures:23–26.

Santoso E and Stull RB (1998) Wind and temperature profiles in the Radix layer: The botton fifth of the convective boundary layer. J Appl Meteorol. 37:545–558.

Schmidt A and Klemm O (2008) Direct determination of highly size-resolved turbulent particle fluxes with the disjunct eddy covariance method and a 12 – stage electrical low pressure impactor. Atmos Chem Phys. 8:7405–7417.

Schotanus P, Nieuwstadt FTM and DeBruin HAR (1983) Temperature measurement with a sonic anemometer and its application to heat and moisture fluctuations. Boundary-Layer Meteorol. 26:81–93.

Schumann U (1989) Large-eddy simulation of turbulent diffusion with chemical reactions in the convective boundary layer. Atmos Environm. 23:1713–1727.

Sedefian L (1980) On the vertical extrapolation of mean wind power density. J Climate Appl Meteorol. 19:488–493.

Seinfeld JH and Pandis SN (1998) Atmospheric chemistry and physics. Wiley, New York, 1326 pp.

Shaw RH (1985) On diffusive and dispersive fluxes in forest canopies. In: Hutchinson BA and Hicks BB (eds.), The Forest-Atmosphere interaction. Reidel Publishing Company, 407–419.

Siebicke L, Hunner M and Foken T (2012) Aspects of CO_2-advection measurements. Theor Appl Climat. 109:109–131.

Sinclair TR, Allen jr. LH and Lemon ER (1975) An analysis of errors in the calculation of energy flux densities above vegetation by Bowen-ratio profile method. Boundary-Layer Meteorol. 8:129–139.

Skeib G (1980) Zur Definition universeller Funktionen für die Gradienten von Windgeschwindigkeit und Temperatur in der bodennahen Luftschicht. Z Meteorol. 30:23–32.

Smith SD, Fairall CW, Geernaert GL and Hasse L (1996) Air-sea fluxes: 25 years of progress. Boundary-Layer Meteorol. 78:247–290.

Snyder RL, Spano D and Paw U KT (1996) Surface renewal analysis for sensible and latent heat flux density. Boundary-Layer Meteorol. 77:249–266.

Stull RB (1988) An Introduction to Boundary Layer Meteorology. Kluwer Acad. Publ., Dordrecht, Boston, London, 666 pp.

Su HB, Schmid HP, Grimmond CSB, Vogel CS and Curtis PS (2008) An assessment of observed vertical flux divergence in long-term eddy-covariance measurements over two Midwestern forest ecosystems. Agrical Forest Meteorol. 148:186–205.

Tanner CB and Thurtell GW (1969) Anemoclinometer measurements of Reynolds stress and heat transport in the atmospheric surface layer. ECOM, United States Army Electronics Command, Research and Developement, ECOM-66-G22-F, Fort Huachuca, AZ, 82 pp.

Tsvang LR, Zubkovskij SL, Kader BA, Kallistratova MA, Foken T, Gerstmann W, Przandka Z, Pretel J, Zelený J and Keder J (1985) International turbulence comparison experiment (ITCE-81). Boundary-Layer Meteorol. 31:325–348.

Turnipseed AA, Pressley SN, Karl T, Lamb B, Nemitz E, Allwine E, Cooper WA, Shertz S and Guenther AB (2009) The use of disjunct eddy sampling methods for the determination of ecosystem level fluxes of trace gases. Athmospheric Chemistry and Physics. 9:981–994.

Twine TE, Kustas WP, Norman JM, Cook DR, Houser PR, Meyers TP, Prueger JH, Starks PJ and Wesely ML (2000) Correcting eddy-covariance flux underestimates over a grassland. Agrical Forest Meteorol. 103:279–300.

Vickers D and Mahrt L (1997) Quality control and flux sampling problems for tower and aircraft data. J Atm Oceanic Techn. 14:512–526.

Vilà-Guerau de Arellano J (2003) Bridging the gap between atmospheric physics and chemistry in studies of small-scale turbulence. Bull Amer Meteorol Soc. 84:51–56.

Vilà-Guerau de Arellano J and Duynkerke P (1992) Influence of chemistry on the flux-gradient relationships for the $NO-O_3-NO_2$ system. Boundary-Layer Meteorol. 61:375–387.

Webb EK (1970) Profile relationships: the log-linear range, and extension to strong stability. Quart J Roy Meteorol Soc. 96:67–90.

Webb EK (1982) On the correction of flux measurements for effects of heat and water vapour transfer. Boundary-Layer Meteorol. 23:251–254.

Webb EK, Pearman GI and Leuning R (1980) Correction of the flux measurements for density effects due to heat and water vapour transfer. Quart J Roy Meteorol Soc. 106:85–100.

Wichura B, Buchmann N and Foken T (2000) Fluxes of the stable carbon isotope ^{13}C above a spruce forest measured by hyperbolic relaxed eddy accumulation method. 14th Symposium on Boundary Layer and Turbulence, Aspen, CO., 7–11 Aug. 2000. Am. Meteorol. Soc., Boston, pp. 559–562.

Wieringa J (1980) A revaluation of the Kansas mast influence on measurements of stress and cup anemometer overspeeding. Boundary-Layer Meteorol. 18:411–430.

Wieringa J (1989) Shapes of annual frequency distribution of wind speed observed on high meteorological masts. Boundary-Layer Meteorol. 47:85–110.

Wilczak JM, Oncley SP and Stage SA (2001) Sonic anemometer tilt correction algorithms. Boundary-Layer Meteorol. 99:127–150.

Wrzesinsky T and Klemm O (2000) Summertime fog chemistry at a mountainous site in Central Europe. Atmos Environm. 34:1487–1496.

Wyngaard JC (1981) The effects of probe-indused flow distortion on atmospheric turbulence measurements. J Appl Meteorol. 20:784–794.

Wyngaard JC (1982) Boundary-Layer Modelling. In: Nieuwstadt FTM and Van Dop H (eds.), Atmospheric Turbulence and Air Pollution Modelling. Reidel, Dordrecht, 69–106.

Wyngaard JC and Moeng C-H (1992) Parameterizing turbulent diffusion through the joint probability density. Boundary-Layer Meteorol. 60:1–13.

Wyngaard JC, Businger JA, Kaimal JC and Larsen SE (1982) Comments on 'A revaluation of the Kansas mast influence on measurements of stress and cup anemometer overspeeding'. Boundary-Layer Meteorol. 22:245–250.

Zhang SF, Wyngaard JC, Businger JA and Oncley SP (1986) Response characteristics of the U.W. sonic anemometer. J Atm Oceanic Techn. 2:548–558.

Chapter 5
Modeling of the Energy and Matter Exchange

Within micrometeorology the term *modeling* is not uniquely defined. It refers to various methods covering a range of complexity extending from simple regressions up to complicated numerical models. In applied meteorology (agro meteorology and hydro meteorology) simple analytical models are very common. Modeling of evaporation is particularly important but sophisticated numerical methods are not yet widely used in this research area. The following chapter describes different types of models and their limitations beginning with simple analytical methods up to numerical models of near-surface energy and matter transport. The application of models in heterogeneous terrain receives special attention and related flux averaging approaches are addressed in a separate subchapter.

5.1 Energy Balance Methods

Energy exchange measurements and modeling form the bases for many applied investigations. Methods that are based on the surface energy balance equation (e.g. Bowen-ratio method, Sect. 4.2.2) are widespread regardless of the related open issues in terms of measurement techniques (see Sect. 3.8). Many applied models are based on similar theoretical backgrounds. Often, the general limitations of the various methods are unknown to the user. Most applications can be used only for hourly values at noon with unstable stratification or for daily and weekly averages (see below). Various models distinguish between potential evaporation from free water bodies or water saturated surfaces. The actual evapotranspiration, which is the sum of the evaporation of the soil and transpiration from plants, is typically lower.

In most of the models, parameters are used which were empirically determined by experiments. Strictly speaking, these parameters are only valid for the climatological conditions prevailing during the original experiments. The parameter values can vary from place to place, and more importantly they are valid only for special mean climatological conditions. Thus, the parameters are functions of the place, the time

of the year, and the weather or climate of the period when the experiment was done. These conditions may currently or in the future no longer be valid (Houghton 2015). Therefore, hourly and daily values have only a low representativeness. Depending on the sensitivity of the parameterization, decade or monthly averages have an acceptable accuracy. Accordingly, it is necessary to associate the time scale of the model with the intended use and the geographically valid region.

5.1.1 Determination of the Potential Evaporation

5.1.1.1 Dalton Approach

The simplest way to determine the potential evaporation over open water is the Dalton approach, which is comparable to the bulk approach discussed in Sect. 4.2.1 . It is not part of the energy balance methods. Instead of the Dalton number alone, simple correction functions are used which account for the wind-speed dependency,

$$
\begin{aligned}
Q_E &= f(u)\,[E(T_0) - e(z)],\\
f(u) &= a + b\,u^c,
\end{aligned}
\tag{5.1}
$$

where $a = 0.16$; $b = 0.2$; $c = 0.5$ for lakes in Northern Germany (Richter 1977). Possible areas of application for this method are given in Table 5.1.

5.1.1.2 Turc Approach

Many approaches are based on radiation measurements, e.g. the evaporation calculation, where only the air temperature (t in °C) and the global radiation (in W m^{-2}) are used as input parameters (Turc 1961):

$$
Q_{E\text{-}TURK} = k\,(K \downarrow + 209)\frac{0.0933t}{t + 15}
\tag{5.2}
$$

Table 5.1 Possible areas of application of the Dalton approach

Criterion	Evaluation
Defining quantity	Potential evaporation of free water bodies
Area of application	According to the validity of the area specific constants (DVWK 1996)
Resolution of ten input parameters	10–60 min averages
Representativeness of the results	(daily-), decade and monthly averages
Error	20–40%

Table 5.2 Possible areas of application of the Turc approach

Criterion	Evaluation
Defining quantity	Potential evaporation of free water bodies, possible for well saturated meadows
Area of application	Mediterranean Sea, Germany (lowlands) with correction factor k = 1.1
Resolution of ten input parameters	10–60 min averages
Representativeness of the results	Decade and monthly averages
Error	20–40%

The method was developed for the Mediterranean Sea and for the application in Germany Eq. (5.2) needs a correction factor of about $k = 1.1$ (DVWK 1996). Possible areas of application for this method are given in Table 5.2.

5.1.1.3   Priestley–Taylor Approach

The Bowen ratio is the starting point for the derivation of several methods for the determination of sensible and latent heat fluxes. The Priestley–Taylor approach starts with Eqs. (2.98) and (4.7) respectively, which can be written with the potential temperature and the dry adiabatic temperature gradient as:

$$Bo = \gamma \frac{\partial \overline{\theta}/\partial z}{\partial \overline{q}/\partial z} = \frac{\gamma \left[(\partial \overline{T}/\partial z) + \Gamma_d\right]}{\partial \overline{q}/\partial z} \tag{5.3}$$

With the temperature dependence of saturation water vapor pressure according to the Clausius–Clapeyron's equation

$$\frac{d\,q_s}{dT} = s_c(\overline{T}) \tag{5.4}$$

it follows that

$$Bo = \frac{\gamma \left[(\partial \overline{T}/\partial z) + \Gamma_d\right]}{s_c \left(\partial \overline{T}/\partial z\right)} = \frac{\gamma}{s_c} + \frac{\gamma \, \Gamma_d}{s_c \left(\partial \overline{T}/\partial z\right)}, \tag{5.5}$$

where γ is the psychrometric constant in K^{-1}.

For the further derivation, the second term on the right-hand-side of (5.5) will be ignored; however, this is valid only if the gradient in the surface layer is significantly greater than the dry adiabatic gradient of $\Gamma_d = 0.0098$ K m^{-1}. This is not the case for neutral stability, because under such conditions the fluxes are generally small. After introducing the Priestley–Taylor coefficient of $\alpha_{PT} \sim 1.25$ for water

Table 5.3 Values for the temperature dependent parameters γ und s_c based on the specific moisture (Stull 1988)

Temperature in K	γ in K^{-1}	s_c in K^{-1}
270	0.00040	0.00022
280	0.00040	0.00042
290	0.00040	0.00078
300	0.00041	0.00132

Table 5.4 Possible areas of application of the Priestley–Taylor approach

Criterion	Evaluation
Defining quantity	Potential evaporation of free water bodies
Area of application	Universally
Resolution of ten input parameters	10–60 min averages
Representativeness of the results	(daily-), decade and monthly averages
Error	10–20%

saturated surfaces and applying the energy balance equations (1.1) and (4.8) respectively, follows the Priestley–Taylor approach (Priestley and Taylor 1972):

$$Q_H = \frac{\left[(1 - \alpha_{PT}) \, s_c + \gamma\right] \left(-Q_s^* - Q_G\right)}{s_c + \gamma} \tag{5.6}$$

$$Q_E = \alpha_{PT} \, s_c \, \frac{-Q_s^* - Q_G}{s_c + \gamma} \tag{5.7}$$

Typical values of the ratios $c_p/\lambda = \gamma$ and $de_s/dT = s_c$ are given in Table 5.3 and can be calculated approximately with the following relation:

$$\frac{s_c}{\gamma} = -0.40 + 1.042 \, e^{0.0443 \cdot t} \tag{5.8}$$

The method can be used for vegetated surfaces if the Priestley–Taylor coefficient is varied to account for the dependence on stomata resistance (DeBruin 1983). Possible areas of application for this method are given in Table 5.4.

5.1.1.4 Penman Approach

A commonly used method for the determination of the potential evaporation is that proposed by Penman (1948). This method was developed for Southern England and underestimates the evaporation for arid regions. The derivation is based on the Dalton approach and the Bowen ratio, whereas the equation of the Priestley–Taylor type is an intermediate stage (DVWK 1996). The evaporation in mm d^{-1} is

Table 5.5 Wind factors in the ventilation term of Eq. (5.10)

Surface and reference	f_1 in mm d^{-1} h Pa^{-1}	f_2 in mm d^{-1} h Pa^{-1} m^{-1} s
Original approach for water bodies (Hillel 1980)	0.131	0.141
Small water bodies (DVWK 1996)	0.136	0.105
Water bodies (Dommermuth and Trampf 1990)	0.0	0.182
Grass surfaces (Doorenbos and Pruitt 1977; Schrödter 1985)	0.27	0.233

$$Q_E\left[\text{mm d}^{-1}\right] = \frac{s_c\left(-Q_s^* - Q_G\right)\left[\text{mm d}^{-1}\right] + \gamma\, E_a\left[\text{mm d}^{-1}\right]}{s_c + \gamma}, \qquad (5.9)$$

where the available energy must be used in mm d^{-1}. The conversion factor from mm d^{-1} to W m^{-2} is 0.0347. The second term in the numerator of Eq. (5.9) is called the ventilation term E_a (also in mm d^{-1}) and contains the influence of turbulence according to the Dalton approach. It is significantly smaller than the first term and is often ignored in the simplified Penman approach (Arya 2001). The Priestley–Taylor approach follows when $\alpha_{PT} = 1.0$.

The ventilation term is a function of the wind velocity and the saturation deficit:

$$E_a = (E - e)\,(f_1 + f_2\, u)\,\left[\text{mm d}^{-1}\right] \qquad (5.10)$$

While one can use daily averages in Eq. (5.10), the use of 10–60 min averages is considerably more meaningful; however, in this case the units must be converted. Typical values for both wind factors f_1 and f_2 are given in Table 5.5. These values are valid for water surfaces, but they can also be used for well-saturated grass surfaces, which to a large degree is the actual evaporation. To include the effects of larger roughness, the ventilation term according to the approach by van Bavel (1986) can be applied in h Pa ms^{-1}:

$$E_a = \frac{314\ \text{K}}{T}\,\frac{u}{[\ln(z/z_0)]^2}\,(E - e)\,\left[\text{h Pa m s}^{-1}\right] \qquad (5.11)$$

Possible areas of application for this method are given in Table 5.6.

Table 5.6 Possible areas of application of the Penman approach

Criterion	Evaluation
Defining quantity	Potential evaporation of free water bodies
Area of application	Universally
Resolution of ten input parameters	10–60 min averages
Representativeness of the results	(daily-), decade and monthly averages
Error	10–20%

Table 5.7 Methods for the determination of the potential evaporation of water bodies. The underlying grey scale corresponds to the accuracies given in the last line

minute				
hour day decade month	Dalton approach	Turc approach	Priestley- Taylor approach	Penman approach
very good	good	satisfactory	rough estimate	inadequately
5–10 %	10–20 %	20–40 %	40–100 %	> 100 %

5.1.1.5 Overall Evaluation of Approaches for the Determination of the Potential Evaporation

All approaches presented thus far are valid only for computing longer-term averages. Less sophisticated approaches have only low accuracy for short averaging intervals (Table 5.7).

The inherent non-linearity of the approaches requires calculations using 30–60 min averages, but the results are not reliable for these short time periods.

5.1.2 Determination of the Actual Evaporation

Empirical methods for the determination of evaporation are widely used, but are only applicable in the specific areas for which they were developed. Therefore, these types of approaches were not included in the following chapter. However, methods developed by Haude (1955) and Sponagel (1980) or the modified Turc approach according to Wendling et al. (1991), which are commonly used in Germany, are described in detail in the German versions of this book (Foken 2016).

5.1.2.1 Penman–Monteith Approach

The transition from the Penman to the Penman–Monteith approach (Penman 1948; Monteith 1965; DeBruin and Holtslag 1982) included the consideration of non-saturated surfaces and cooling due to evaporation, which reduces the energy of

the sensible heat flux. Including both aspects leads to the Penman–Monteith method for the determination of the actual evaporation (evapotranspiration)

$$Q_H = \frac{\gamma \left(-Q_s^* - Q_G\right) - \rho c_p F_w}{R_G s_c + \gamma}, \tag{5.12}$$

$$Q_E = \frac{R_G s_c \left(-Q_s^* - Q_G\right) + \rho c_p F_w}{R_G s_c + \gamma}, \tag{5.13}$$

with the so-called ventilation term

$$F_w = C_E \bar{u} \left(R_G - R_s\right) q_{sat}, \tag{5.14}$$

where R_G is the relative humidity of the surface; R_s is the relative humidity close to the surface, and q_{sat} is the specific humidity for saturation. Eq. (5.14) can also be formulated according the resistance concept (see Sect. 5.3) without the molecular-turbulent resistance:

$$F_w = \frac{q_{sat} - q_a}{r_a + r_c} \tag{5.15}$$

In the simplest case, the canopy resistance, r_c, will be replaced by the stomatal resistance r_s. The stomatal resistance can be calculated from the stomatal resistance of a single leaf r_{si} and the leaf-area index (LAI, leaf surface of the upper side per area element of the underlying surface)

$$r_s = \frac{r_{si}}{LAI_{aktiv}}, \tag{5.16}$$

where LAI_{aktiv} is the leaf area index of the active sunlight leafs. Generally, this is only the upper part of the canopy, and therefore $LAI_{aktiv} = 0.5$ LAI (Allen et al. 1998). In the simplest case, the turbulent resistance is given (Stull 1988) as:

$$r_a = \frac{1}{C_E \bar{u}}. \tag{5.17}$$

But usually r_a is calculated from Eqs. (2.60) and (2.64):

$$r_a = \frac{\ln\left(\frac{z-d}{z_0}\right) \ln\left(\frac{z-d}{z_{oq}}\right)}{\kappa^2 u(z)} \tag{5.18}$$

In the non-neutral case, universal functions can be used in Eq. (5.18). Typical values of the parameters are given in Table 5.8. Possible areas of application for this method are given in Table 5.9.

Table 5.8 Typical values of the *LAI* (Kaimal and Finnigan 1994) and the stomata resistance of single leafs (Garratt 1992)

Surface	Height in m	*LAI* in m^2 m^{-2}	r_{si} in s m^{-1}
Seat (begun to grow)	0.05	0.5	
Cereal	2	3.0	50–320
Forest	12–20	1–4	120–2700

Table 5.9 Possible areas of application of the Penman–Monteith approach

Criterion	Evaluation
Defining quantity	Actual evaporation
Area of application	Universally
Resolution of ten input parameters	10–60 min averages
Representativeness of the results	Hourly and daily averages
Error	10–40%

The Food and Agriculture Organization of the United Nations (FAO) has put much effort into the development of a uniform method to determine the evaporation, and recommended a more convenient equation with a limited input data set (Allen et al. 1998; Moene and van Dam 2014):

$$Q_E = \frac{s_c \left(-Q_s^* - Q_G\right) + \rho \, c_p \frac{0.622}{p} \frac{E-e}{r_a}}{s_c + \gamma \left(1 + \frac{r_s}{r_a}\right)}, \tag{5.19}$$

where r_s and r_a are given by Eqs. (5.16) and (5.18), respectively. The factor $0.622/p$ was included contrary to the original reference, and is necessary for consistency; the constants s_c and γ are used in the dimension K^{-1} and not as in the original reference, i.e. h Pa K^{-1}. Further improvements are still proposed like e.g. including the surface temperature such that parametrizations for the resistances are no longer needed (Mallick et al. 2015).

To compare worldwide evaporation rates and to use input parameters, which are available everywhere, the FAO has formulated a (grass) reference evaporation (Allen et al. 1998). This is based in principle on Eq. (5.19), but includes the estimated input parameters given in Table 5.10. A further standardization was made by ASCI (American Society of Civil Engineers) by the unification of the calculation steps and application to grass and alfalfa (Allen et al. 2005).

The Penman–Monteith approach is widely used in diverse applications, for example, in the atmospheric boundary conditions of many hydrological and ecological models. During the daytime, the accuracy of computed hourly data is satisfactory, and the determination of daily sums of the evaporation and sensible heat fluxes is generally acceptable.

Table 5.10 Fixing of the input parameters for the FAO-(grass)-reference evaporation (Allen et al. 1998)

Parameter	Value	Remark
r_a	$d = 2/3\ z_B$; $z_0 = 0.123\ z_B$; $z_{0q} = 0.1\ z_0$ with $z_B = 0.12$ m and $z = 2$ m follows $r_a = 208/u$ (2 m)	It is $\kappa = 0.41$ applied
r_s	$LAI_{aktiv} = 0.5\ LAI$; $LAI = 24\ z_B$ with $r_{si} = 100$ s m^{-1} and $z_B = 0.12$ m follows $r_s = 70$ s m^{-1}	
$-Q_s^* - Q_G$	Various simplifications possible with an albedo of 0.23	Allen et al. (1998)

The available energy is the main forcing, but because the atmospheric turbulence and the control by the plants influence the ventilation term, the method is inaccurate if the turbulent conditions differ from an average stage. Therefore, this approach is often not used in meteorological models that have several layers in the surface layer (see Sect. 5.3).

Other approaches not discussed here require long averaging intervals and thus have low accuracy for short averaging periods. Water balance methods use the water balance equation Eq. (1.23) while runoff and precipitation are measured parameters.

5.1.3 Determination from Routine Weather Observations

The equations presented up to here are generally not adequate to determine the energy exchange from routinely available observations. Holtslag and van Ulden (1983) developed a method to determine the sensible heat flux under application of the Priestley–Taylor approach. They included an advection factor $\beta = 20$ W m^{-2} according to DeBruin and Holtslag (1982), and varied α_{PT} with the soil moisture between 0.95 and 0.65; however, for summer conditions with good water supply $\alpha_{PT} = 1.0$ can be assumed. Eq. (5.6) then has the following form with temperature-dependent constants according to Table 5.3:

$$Q_H = \frac{[(1 - \alpha_{PT})\, s_c + \gamma]\left(-Q_s^* - Q_G\right)}{s_c + \gamma} + \beta \qquad (5.20)$$

To estimate the available energy an empirical equation is used

$$\left(-Q_s^* - Q_G\right) = 0.9\frac{(1 - \alpha)K\downarrow + c_1 T^6 - \sigma T^4 + c_2 N}{1 + c_3}, \qquad (5.21)$$

where T is the air temperature; N is the cloud cover; $K\downarrow$ is the downward radiation; α is the surface albedo, and the constants $c_1 = 5.3 \cdot 10^{-13}$ W m^{-2} K^{-6}, $c_2 = 60$ W m^{-2} and $c_3 = 0.12$. The disadvantage of this method is that the cloud cover

Table 5.11 Possible areas of application of the Holtslag-van-Ulden approach

Criterion	Evaluation
Defining quantity	Sensible heat flux and actual evaporation
Important input parameters	Cloud cover (original method) Global radiation (modified method)
Area of application	Universally
Resolution of ten input parameters	10–60 min averages
Representativeness of the results	Hourly and daily averages
Error	10–30%

from routine weather observations is often not available. The application is limited to daylight hours with either neutral or unstable stratification and neither rain nor fog.

Göckede and Foken (2001) have tried to only use, instead of the cloud cover, the widely-measured global radiation as input parameter. They applied a parameterization for the radiation fluxes based on cloud observations proposed by Burridge and Gadd (1977), see Stull (1988), to determine a general formulation for the transmission in the atmosphere, see Eqs. (1.5) and (1.7). The available energy is then given by

$$\left(-Q_s^* - Q_G\right) = 0.9 \text{ K} \downarrow \left(1 - \alpha - \frac{0.08 \text{ K m s}^{-1}}{K \downarrow_G}\right), \qquad (5.22)$$

where $K\downarrow$ is the measured global radiation, and $K\downarrow_G$ is the global radiation near the surface which can be calculated from the extraterrestrial radiation and the angle of incidence:

$$K \downarrow_G = K \downarrow_{extr} (0.6 + 0.2 \sin \Psi) \qquad (5.23)$$

With Eq. (5.25) it is only necessary to calculate the angle of incidence for hourly data using astronomical relations (Appendix A.4). The method can be applied to both Eq. (5.20) and the Penman–Monteith approach Eq. (5.12). As shown in Table 5.11, the areas of application of this method are similar to the ones of the method by Holtslag and van Ulden (1983). Both methods as well as the method by Burridge and Gadd (1977) give comparable results.

5.2   Hydrodynamical Multilayer Models

The development of multilayer models began soon after the start of hydrodynamic investigations (see Sect. 1.3). In these models, the energy exchange in the molecular boundary layer, the viscous buffer layer, and the turbulent layer of the surface layer (Fig. 1.4) was separately parameterized according to the particular exchange conditions. The exchange of sensible heat can be shown to be dependent on the
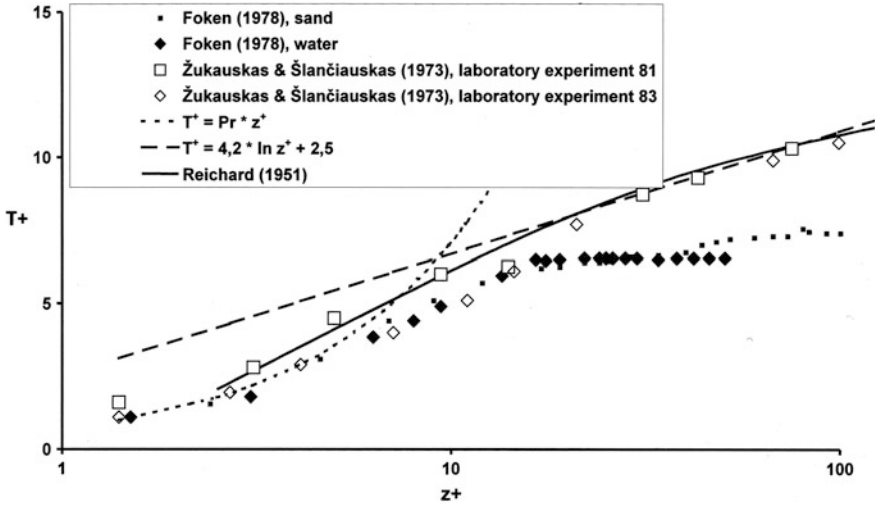
Fig. 5.1 Dimensionless temperature profile (T^+: dimensionless temperature, z^+: dimensionless height) according to laboratory measurements (Shukauskas and Schlantschiauskas 1973), and outdoor measurements (Foken 1978) and balanced profiles for the molecular layer (*dotted line*) and the turbulent layer (*broken line*) as well as profiles according to Reichardt (1951), from Foken (2002, with kind permission of © Borntraeger, Stuttagrt 2002, www.schweizerbart.de, All rights reserved)

temperature profile in dimensionless coordinates (Fig. 5.1) with the dimensionless height $z^+ = zu_*/v$ and the dimensionless temperature $T^+ = T/T_*$ (T_*: dynamical temperature) analogous to the wind profile with dimensionless velocity $u^+ = u/u_*$ (Landau and Lifschitz 1987; Csanady 2001; Schlichting and Gersten 2006). For the molecular boundary layer, $T^+ \sim z^+$, and for the laminar boundary layer $u^+ \sim z^+$. Above the viscous buffer layer, the flow is turbulent. Therefore, the typical logarithmic profile equations $T^+ \sim \ln z^+$ and $u^+ \sim \ln z^+$ are valid. The greatest problem for the parameterization is the formulation for the buffer layer, where empirical approaches must be applied. According to Fig. 5.1, profiles in the nature and in hydrodynamic studies (Foken 2002) are similar, which can be applied,

The hydrodynamic multilayer models based on bulk approaches, where instead of the bulk coefficients the so-called profile coefficient Γ is included, can be determined by integration over all layers

$$Q_H = -\Gamma[T(z) - T_0], \tag{5.24}$$

$$\Gamma = \left(\int_0^z \frac{dz}{K_T + v_{Tt} + v_T} \right)^{-1}, \tag{5.25}$$

where K_T is the turbulent diffusion coefficient for heat, v_{Tt} is the molecular-turbulent diffusion coefficient in the buffer layer, and v_T is the molecular diffusion coefficient.

The first integrations were done by Sverdrup (1937/38) and Montgomery (1940) using a single viscous sublayer consisting of the buffer layer and the molecular boundary layer. For this combined layer, a dimensionless height $\delta_{vT}^+ \approx 27.5$ was assumed (this value is slightly larger than the values assumed today), and for the turbulent layer a logarithmic wind profile with roughness length z_0 was applied. For smooth surfaces an integration constant instead of the roughness length was used (von Kármán 1934).

An integral approach for all layers including the turbulent layer was presented by Reichard (1951), who parameterized the ratio of the diffusion coefficient and the kinematic viscosity

$$\frac{K_m}{v} = \kappa \left(z^+ - z_T^+ \, \tanh \frac{z^+}{z_T^+} \right). \tag{5.26}$$

This approach is in good agreement with experimental data as shown in Fig. 5.1, and can be used for the parameterization of exchange processes between the atmosphere and the surface (Kramm et al. 1996a) .

In the 1960s and 1970s, several papers were published with an integration of the profile coefficient over all three layers (Kitajgorodskij and Volkov 1965; Mangarella et al. 1972, 1973; Bjutner 1974). These models were based on new hydrodynamic data sets and took into account the wavy structure of the water surface (Foken et al. 1978) in the determination of the thickness of the molecular boundary layer

$$\delta_T = 7.5 \frac{v}{u_*} [2 + \sin (\zeta - \pi/2)], \tag{5.27}$$

where $\varsigma = 0$ is valid for the windward and $\varsigma = \pi$ for the leeward site.

From measurements of the dimensionless temperature profile near the sea surface, it was possible to determine the dimensionless temperature difference in the buffer layer as $\delta_T^+ \approx 4$ (Foken et al. 1978; Foken 1984); also compare with Fig. 5.1. Following this approach, by applying of Eq. (5.27) with $\varsigma = 0$ or $\delta_T \approx 6$ respectively for smooth surfaces and low friction velocities ($u_* < 0.23 \, \mathrm{m \, s^{-1}}$) the profile coefficient is given by:

$$\Gamma = \frac{\kappa \, u_*}{\kappa \, \mathrm{Pr} \, \frac{\delta_T u_*}{v} + \kappa \, \delta_T^+ + \ln \frac{u_* z}{30 \, v}} \tag{5.28}$$

This model shows good results in comparison with experimental data (Foken 1984, 1986; Biermann et al. 2014), and can be used for the calculation of the surface temperature for known sensible heat flux (Lüers and Bareiss 2010). However, these approaches have not been widely used, which is primarily due to the fact that current models use fundamentally different approaches to describe the energy exchanges in the surface layer (Geernaert 1999), as it is further discussed in Sect. 5.5.

5.3   Resistance Approach

Recent models for the determination of the turbulent exchange are layer models. These models generally use the resistance approach for the energy and matter exchange between the atmosphere and the ground surface. They can be classified in three types:

One-layer-models consider only soil, plants and atmosphere at a close range. The plants are not separated into different layers. Instead, it is assumed that plants act like a big leaf covering the soil (*big leaf model*). Many of the so-called Soil-Vegetation-Atmosphere-Transfer (SVAT) models can be considered big-leaf models, but some SVAT models are multilayer models. These models are mainly based on surface layer physics (partly several layers) and are schematically illustrated in Fig. 5.2 (Hicks et al. 1987; Sellers and Dorman 1987; Schädler et al. 1990; Groß 1993; Kramm et al. 1996b; Gusev and Nasonova 2010). A special case is the hybrid model according to Baldocchi et al. (1987). One important requirement is the closure of the energy balance at the earth's surface. This can be reached with an iterative determination of the surface temperature (Mengelkamp et al. 1999), with is used in the parameterizations for both the energy fluxes and the longwave radiation.

Multilayer models simulate the atmosphere in several layers. The simplest models have no coupling with the atmospheric boundary layer, and only the surface layer is solved in detail. These models are available using simple (1st and 1.5th
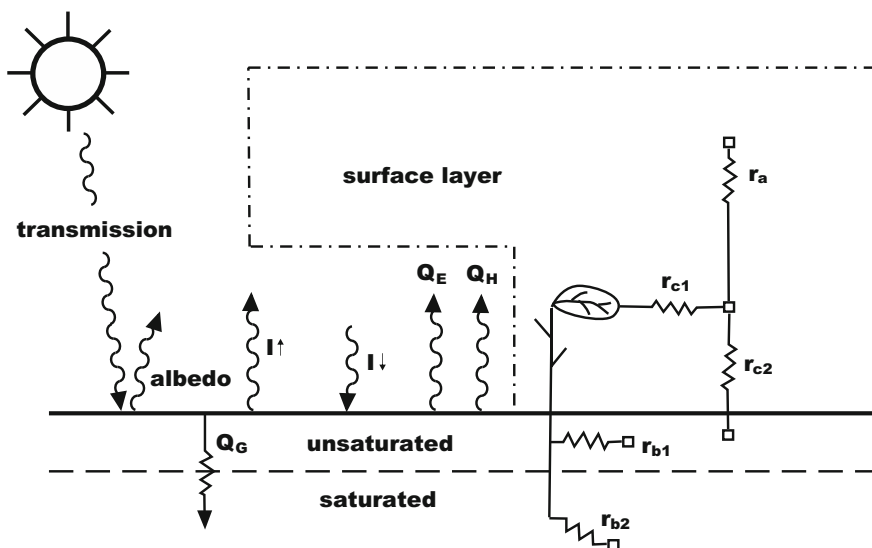

Fig. 5.2 Schematic representation of the modeling of the atmospheric surface layer including plants and soil (Blackadar 1997, adapted with kind permission of © Springer Berlin, Heidelberg 1997, All rights reserved)

order) and higher order closure techniques (Meyers and Paw U 1986, 1987;
Baldocchi 1988; Pyles et al. 2000).

Multilayer models with boundary layer coupling best represent the current state
of model development. In these models, the lower layers deal with balance equa-
tions, and the upper layers use assumptions based on mixing length approaches
(Fig. 5.3, see Sect. 2.1.3). These models are also available with simple (1st and
1.5th order) and higher order closure techniques. The most widely used models use
a 1st order closure with a local mixing length approach (Mix et al. 1994) or a
non-local transilient approach (Inclán et al. 1996). The complicated transport
conditions in high vegetation (see Sect. 3.5) may be best realized with a higher
order closure technique (Pyles et al. 2000), which also accounts for the effects of
coherent structures. An intercomparison showed that first order closure models do
not adequately describe the fluxes at night (Staudt et al. 2011).

The resistance concept is based on the assumption that in the turbulent layer the
turbulence resistance counteracts the turbulent flux, in the viscous and molecular
layer a molecular-turbulence resistance counteracts the flux, and in the plant and
soil all resistances can be combined into a total resistance (canopy resistance). The
canopy resistance can be divided into different transfer pathways, where the main
transport paths are stomata–mesophyll, cuticula, or direct transfer to the soil, which
are schematically illustrated in Fig. 5.4. The simplest picture is the comparison with
Ohm's law:
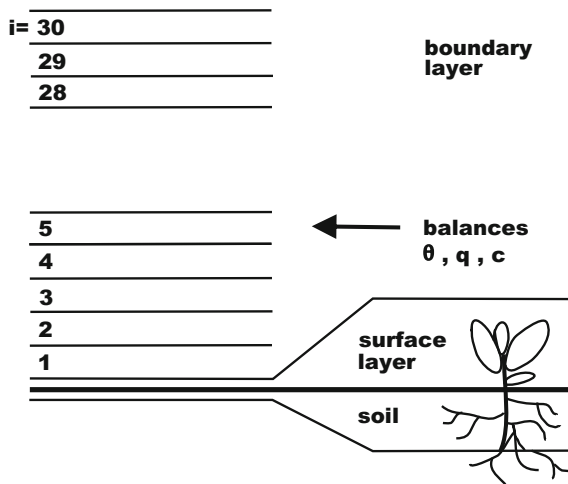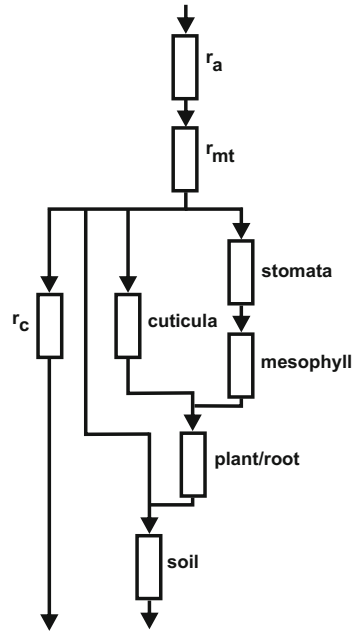
$$I = \frac{U}{R} \tag{5.29}$$

Fig. 5.3 Schematic representation of a boundary layer model (Blackadar 1997, adapted with kind
permission of © Springer Berlin, Heidelberg 1997, All rights reserved)

Fig. 5.4 Schematic representation of the resistance concept

Here, the flux is analogous with the current, I, and the vertical difference of wind speed or temperature with the voltage, U. The resistance, R, can be described as a network of individual resistances (Fig. 5.4) in the following simple form:

$$r_g = r_a + r_{mt} + r_c \tag{5.30}$$

The consideration of the resistance concept in the profile equations (Eqs. 2.48–2.50) is illustrated in the example of the sensible heat flux:

$$Q_H = -K(z)\frac{\partial T}{\partial z} = \frac{\int_{T(0)}^{T(z)} dT}{\int_0^z \frac{dz}{K(z)}} = \frac{T(z) - T(0)}{\int_0^z \frac{dz}{K(z)}} \tag{5.31}$$

For the bulk approaches (Eqs. 4.1–4.3) follows

$$Q_H = -C_H\, u(z)\, [T(z) - T(0)] = -\Gamma_H\, [T(z) - T(0)], \tag{5.32}$$

where the total resistance is:

$$r_{g(0,z)} = \int_0^z \frac{dz}{K(z)}, \tag{5.33}$$

$$r_{g(0,z)} = \frac{1}{\Gamma_{H(0,z)}} \tag{5.34}$$

The individual parts of the total resistance must be parameterized. For the turbulent resistance Eq. (2.86) under consideration of Eq. (2.67) is applied (Foken et al. 1995)

$$r_a = \int\limits_{\delta}^{z_R} \frac{dz}{K(z)} = \frac{1}{\kappa u_*} \left[\ln \frac{z_R - d}{\delta - d} - \psi_H \left(\varsigma_{z_R}, \varsigma_{\delta} \right) \right], \tag{5.35}$$

where z_R is the reference level of the model, i.e. the upper layer of the model in the surface layer. The lower boundary, δ, is identical with the upper level of the molecular-turbulent layer. The resistance in the molecular-turbulent range is

$$r_{mt} = \int\limits_{z_0}^{\delta} \frac{dz}{(D + K_H)} = (u_* B)^{-1}, \tag{5.36}$$

with the so-called sublayer-Stanton number B (Kramm et al. 1996a, 2002)

$$B^{-1} = Sc \int\limits_{0}^{\eta} \frac{d\eta}{1 + ScK_m/v}, \tag{5.37}$$

$$\eta = u_* (z - z_0)/v, \tag{5.38}$$

and the Schmidt number in the case of the exchange of gases including water vapor

$$Sc = v/D. \tag{5.39}$$

For the exchange of sensible heat, the Schmidt number in Eq. (5.37) is replaced by the Prandtl number.

While parameterization with multilayer models (see Sect. 5.2) could be an obvious choice, presently most models use roughness length parameterizations (Jacobson 2005)

$$r_{mt} = \ln \left(\frac{z_0}{z_{0q}} \right) \frac{(Sc/Pr)^{2/3}}{\kappa u_*}, \tag{5.40}$$

with $Pr = 0.71$ and $Sc = 0.60$ valid in the temperature range of 0–40 °C. For the sensible heat flux follows for the sublayer -Stanton number according to Eqs. (5.36) and (5.40), (Owen and Thomson 1963):

$$\kappa\, B^{-1} = \ln \frac{z_0}{z_{0T}} \qquad (5.41)$$

This equation is defined only for $z_0 > z_{0T}$, otherwise negative molecular-turbulent resistances would be calculated which are non-physical (Kramm et al. 1996a; Kramm et al. 2002). Nevertheless, in the literature negative values can be found (Brutsaert 1982; Garratt 1992), which can compensate for too large resistances in the turbulent layer and in the canopy, but in reality these negative values are due to inaccurate concepts of roughness lengths for scalars. For $\kappa\, B^{-1}$ values of 2–4 are typical. The application of the Reichardt (1951) approach would lead to a value of 4 (Kramm and Foken 1998).

The canopy resistance is often approximated as a stomatal resistance (Jarvis 1976):

$$r_c \approx r_{st} = \frac{r_{st,\min}\left(1 + \frac{b_{st}}{PAR}\right)}{g_\delta(\delta_e)\, g_\Psi(\Psi)\, g_T(T_f)\, g_C(c_{CO_2})\, g_D} \qquad (5.42)$$

Thus, the parameterization depends primarily on the minimal stomatal resistance (Table 5.8) and the photosynthetically active radiation (PAR) with empirical constant b_{st}. The correction functions in the denominator of Eq. (5.44) have values from 0 to 1, and include the saturation deficit between the atmosphere and leafs (δ_e), the water stress (Ψ), the leaf temperature (T_f), and the local carbon dioxide concentration (c_{CO2}). Furthermore, g_D is a correction factor for the molecular diffusivity of different gases. Current model approaches are often based on the works of Farquhar et al. (1980) and Ball et al. (1987) with modifications by Leuning (1995). The parameterizations are very complicated, and are essentially independent models (Falge et al. 1997; Blümel 1998; Müller 1999; Jacobson 2005). A detailed description of these models is beyond the scope of this textbook and the reader is referred to the literature (Moene and van Dam 2014; Monson and Baldocchi 2014).

5.4 Modelling of Water Surfaces

It is generally easier to model the energy and matter exchange over water surfaces than over land surfaces (Smith et al. 1996; Geernaert 1999; Csanady 2001). However, methods for high wind velocities (>20 m s^{-1}) are very inaccurate. The usual approaches are comparable with bulk approaches (see Sect. 4.1.1). Thus, Eqs. (4.1)–(4.3) can be directly used for the open ocean where water and air temperatures became more similar, and a nearly-neutral stratification occurs. Otherwise it is recommended to use the profile equations with universal functions. Furthermore, the influence of surface waves should be included with the roughness-Reynolds number (Rutgersson and Sullivan 2005), see Eq. 3.3. A well-verified approach was

given by Panin ([1985](#)), in which Eqs. ([4.2](#)) and ([4.3](#)) are multiplied by the following factors respectively:

$$
\cdot \left\{
\begin{array}{ll}
(1 - z/L) \left[1 + 10^{-2} (z_0\, u_* / v)^{3/4} \right] & z/L < 0 \\
\left[1/(1 + 3.5\, z/L) \right] \left[1 + 10^{-2} (z_0\, u_* / v)^{3/4} \right] & z/L > 0
\end{array}
\right\}
\tag{5.43}
$$

The Stanton and Dalton numbers are those for neutral stratification.

Along the same line, the approaches used in hydrodynamics can also be applied over water bodies. For example Eq. ([5.28](#)) can be inserted in Eq. ([4.2](#)) instead of the product $u\, C_H$ and in Eq. ([4.3](#)) instead of the product $u\, C_E$.

These approaches fail for shallow water bodies. For shallow lakes the fluxes can be calculated from the temperature regime (Jacobs et al. [1998](#)). However, the approaches given above can be applied assuming that over flat water the exchange is increased by steep waves and better mixing of the water body. According to Panin et al. ([1996a](#)) a correction function dependent on the water depth and the wave height should be included to determine fluxes in shallow water areas (depth lower than 20 m)

$$
\begin{aligned}
Q_H{}^{SW} &\approx Q_H (1 + 2h/H), \\
Q_E{}^{SW} &\approx Q_E (1 + 2h/H),
\end{aligned}
\tag{5.44}
$$

where H is the water depth and h the wave height, which can be calculated using

$$
h \approx \frac{0.07\, u_{10}{}^2 \left(gH/u_{10}{}^2 \right)^{3/5}}{g},
\tag{5.45}
$$

where u_{10} is the wind velocity measured at 10 m (Davidan et al. [1985](#)). This approach is also well verified for German lakes (Panin et al. [2006](#)).

5.5 Boundary Layer Modelling

The determination of profiles of meteorological parameters for the entire boundary layer and of the mixed-layer height are the main objectives of atmospheric boundary layer models. Such models recently attracted increased interest due to wind power applications. Prognostic calculations of the mixed-layer height, which are feasible for the convective boundary layer, play also important roles when planning field experiments and can provide valuable guidance to observational meteorologists. There is a lot of literature related to this subject, and Seibert et al. ([2000](#)) and Hess ([2004](#)) give good overview papers.

5.5.1 Prognostic Models for the Mixed Layer Height

Prognostic equations for the mixed layer height go back to Tennekes (1973), who determined this height based on a sudden increase of the virtual potential temperature $\Delta\theta_v$. Furthermore, he postulated a small downward sensible heat flux and a change of the virtual potential temperature in the boundary layer (index BL). Above the mixed layer stable stratification with a lapse rate of γ is assumed:

$$\frac{d\Delta\theta_v}{dt} = \gamma\frac{dz_i}{dt} - \left(\frac{d\theta_v}{dt}\right)_{BL} \tag{5.46}$$

Defining an entrainment velocity w_e, the buoyancy flux at the mixed layer height is given by:

$$\left(\overline{w'\theta'_v}\right)_i = -w_e\Delta\theta_v. \tag{5.47}$$

To solve these equations a linear dependence between the buoyancy flux at mixed layer height and at the surface is assumed:

$$-\left(\overline{w'\theta'_v}\right)_i = A\left(\overline{w'\theta'_v}\right)_s, \tag{5.48}$$

whereby the entrainment parameter A assumes values between 0 and 1 (Seibert et al. 2000). Using these assumptions, a simple relationship follows:

$$\frac{dz_i}{dt} = A\frac{\left(\overline{w'\theta'_v}\right)_s}{\gamma z_i} \tag{5.49}$$

Instead of A often also $(1 + A)$ is used. This relationship is called bulk or slab model, and it reliably predicts the development of the boundary layer until noon. Required input parameters are the buoyancy flux at the ground and the lapse rate γ in the free atmosphere which can be estimated the morning radio sounding. If the buoyancy flux and lapse rate are constant in time, the integration of Eq. (5.49) yields (Stull 1988):

$$z_i^2 - z_{i_0}^2 = \frac{2A}{\gamma}\left(\overline{w'\theta'_v}\right)_s(t - t_0) \tag{5.50}$$

More complicated parameterizations are also available (Batchvarova and Gryning 1991; Rigby et al. 2015).

5.5.2 Parametrization of the Wind Profile in the Boundary Layer

The closure approaches discussed in Sect. 2.1.3 form the basis for the determination of the wind profile in the entire boundary layer. Therefore, the change of the wind velocity with height is given by first order closure according to Eq. (2.29) and the turbulent diffusion coefficient according to Eq. (2.38):

$$\frac{\partial u}{\partial z} = \frac{u_*}{\kappa \cdot l}. \tag{5.51}$$

Contrary to Eq. (2.36), the mixing length l is defined as $l = z$ not as $l = \kappa z$ (i.e. the von-Kármán constant is ignored here). This approach, which is valid in the surface layer, can be extended for the boundary layer by assuming that the friction velocity increases exponentially with height

$$u_*(z) = u_{*0}(1 - z/z_i)^\alpha, \tag{5.52}$$

whereby values for the exponent α discussed by various authors are given in Table 5.12. The mixing length can also be extended for the entire boundary layer (Arya 2001):

$$\frac{\partial u}{\partial z} = \frac{u_{*0}(1 - z/z_i)^\alpha}{\kappa}\left(\frac{1}{l_{SL}} + \frac{1}{l_{MBL}} + \frac{1}{l_{UBL}}\right) \tag{5.53}$$

Thereby $l_{SL} = z$ is the mixing length in the surface layer and l_{MBL} and l_{UBL} are the mixing lengths in the middle and upper boundary. With the assumption $\alpha = 1$ and a mixing length for the upper boundary layer it follows

$$\frac{\partial u}{\partial z} = \frac{u_{*0}}{\kappa}(1 - z/z_i)\left(\frac{1}{z} + \frac{1}{l_{MBL}} + \frac{1}{(z_i - z)}\right). \tag{5.54}$$

Table 5.12 Exponent of the vertical profile of the friction velocity in the atmospheric boundary layer according to Eq. (5.52)

Author	α
Panofsky (1973)	1.0 (neutral, from geostrophic drag coefficients)
Yokoyama et al. (1979)	0.5–1.5
Stull (1988)	0.5–1.0 (stabil) 0.5 (neutral) 0.5 (unstable, with additional term in Eq. 5.52)
Zilitinkevich u. Esau (2005)	0.75 (from LES-modelling)
Gryning et al. (2007)	1.0 (simplified assumption)

The determination of the mixing length l_{MBL} in the middle boundary layer remains a challenging problem. Gryning et al. (2007) used a resistance law (Gl. 2.145) which yields

$$\frac{1}{l_{MBL}} = \frac{2}{z_i} \left\{ \left[\left(ln\frac{u_{*0}}{fz_0} - B \right)^2 + A^2 \right]^{1/2} - ln\frac{z_i}{z_0} \right\} \tag{5.55}$$

with $A = 4.9$ and $B = 1.9$ (Zilitinkevich and Esau 2005). These equations are valid for the neutral boundary layer but they can be extended to the diabatic boundary layer by application of the universal functions of the surface layer and by assuming a dependence of A and B on the stability parameter μ (Eq. 2.143). The wind profile follows by integration of Eq. (5.54) and consideration of Eq. (5.57) (Gryning et al. 2007; Peña et al. 2010). These authors could show that the models give satisfactory results for homogeneous surfaces.

5.6 Modeling in Large-Scale Models

The modeling of the momentum, energy, and matter exchange in global circulation models is very simple in comparison to resistance models (Brutsaert 1982; Beljaars and Viterbo 1998; Zilitinkevich et al. 2002; Jacobson 2005). The limited computer time does not allow the application of complicated and iterative methods. The determination of the momentum and energy exchange uses bulk approaches (see Sect. 4.1.1), which are calculated for the layer between the surface (index s) and the first model layer (index 1). The surface fluxes are then given by:

$$u_*^2 = C_m \left| \overrightarrow{u_1} \right|^2 \tag{5.56}$$

$$\left(\overline{w'\theta'} \right)_0 = C_h \left| \overrightarrow{u_1} \right| (\theta_s - \theta_1) \tag{5.57}$$

$$\left(\overline{w'q'} \right)_0 = C_q \left| \overrightarrow{u_1} \right| (q_s - q_1) \tag{5.58}$$

In these equations, constant fluxes between the surface and the first model level (i.e. 30 m) are assumed. In the case of stable stratification, this assumption is questionable. The transfer coefficients $C_{m,h,q}$ can be calculated according to an approach by Louis (1979) or using a modified form proposed by Louis et al. (1982) with the coefficient for neutral stratification $C_{mn,hn,qn}$ and correction factors that are functions of atmospheric stability and the roughness of the underlying surface:

$$C_m = C_{mn} \, F_m \left(Ri_B, z_1/z_0 \right) \tag{5.59}$$

$$C_h = C_{hn} \, F_h\big(Ri_B, z_1/z_0, z_1/z_{0T}\big) \tag{5.60}$$

$$C_q = C_{qn} \, F_q\big(Ri_B, z_1/z_0, z_1/z_{0q}\big) \tag{5.61}$$

In the neutral case, the transfer coefficients depend only on the roughness length (Eq. 4.5):

$$C_{mn} = \left(\frac{\kappa}{\ln \frac{z_1 + z_0}{z_0}} \right)^2 \tag{5.62}$$

C_{hn} and C_{qn} can be determined according to Eq. (4.2) with z_{0T} and Eq. (4.3) with z_{0q}.

The bulk-Richardson number, Ri_B is given by:

$$Ri_B = \frac{g}{\theta_v} \, \frac{\theta_{v1} - \theta_{vs}}{|\vec{u_1}|^2} \tag{5.63}$$

Based on a limited number of experimental data (Louis 1979; Louis et al. 1982) the original expressions for the correction functions were derived as

$$F_m = \left(\frac{1 + 2\,b\,Ri_B}{\sqrt{1 + d\,Ri_B}} \right)^{-1}, \tag{5.64}$$

$$F_h = \left(\frac{1 + 3\,b\,Ri_B}{\sqrt{1 + d\,Ri_B}} \right)^{-1}, \tag{5.65}$$

where the empirical parameters are $b = 5$ and $d = 5$. Although these methods have been questioned (Beljaars and Holtslag 1991), they remain in use. Some corrections regarding the stability functions (Högström 1988) are sometimes used. However, the potential of modern micrometeorology is to a large extend not exhausted. An important criticism on the use of the Louis-(1979)-scheme is the application of roughness lengths for scalars. Their physical meaning is controversial, and they are nearly identical with the aerodynamic roughness length. Above the ocean, the roughness is determined according to either the Charnock equation or preferrably by a combination approach (see Sect. 2.3.2 and Table 2.8). The roughness lengths for scalars are parameterized according to the Roll (1948) approach for smooth surfaces (Beljaars 1995):

$$z_{0T} = 0.40 \frac{v}{u_*}, \quad z_{0q} = 0.62 \frac{v}{u_*} \tag{5.66}$$

For a better consideration of convective cases (Beljaars 1995) the wind vector can be enhanced by a gustiness component

$$\left| \overrightarrow{u_1} \right| = \left(u_1^2 + v_1^2 + \beta\, w_*^{\,2} \right)^{1/2} \tag{5.67}$$

with $\beta = 1$. The Deardorff velocity scale w_* (Eq. 2.43) can be simplified with the use of a mixed layer height of $z_i = 1$ km. This approach is in good agreement with experimental data, and represents the moisture exchange well.

The parameterization of stable stratification is especially difficult, as atmospheric stability may not be constant within the first model layer, the universal functions are not well defined, and the dynamics of the stable surface layer depends on external, larger scale parameters (Zilitinkevich and Mironov 1996; Handorf et al. 1999). In the simplest case, modified correction functions Eqs. (5.64) and (5.65) can be assumed (Louis et al. 1982)

$$F_m = \frac{1}{1 + 2\,b\,Ri_B\,(1 + d\,Ri_B)^{-1/2}}, \tag{5.68}$$

$$F_h = \frac{1}{1 + 3\,b\,Ri_B\,(1 + d\,Ri_B)^{1/2}} \tag{5.69}$$

with $b = 5$ and $d = 5$.

A parameterization applying external parameters was presented by Zilitinkevich and Calanca (2000)

$$F_m = \left(\frac{1 - \alpha_u\,Fi_0}{1 + \frac{C_u}{\ln z/z_0} \frac{z}{L}} \right)^2, \tag{5.70}$$

$$F_h = \left(\frac{1 - \alpha_\theta\,Fi\,\frac{Fi_0^2}{Ri_B}}{1 + \frac{C_\theta}{\ln z/z_0} \frac{z}{L}} \right), \tag{5.71}$$

where Fi is the inverse Froude-number and Fi_0 the inverse external Froude-number

$$Fi_0 = \frac{N\,z}{u} \tag{5.72}$$

where N is the Brunt-Väisälä frequency (Eq. 3.35), $C_u = \alpha_u \kappa / C_{uN}$, and $C_\theta = \alpha_\theta Pr_{\mathrm t}^{-1} \kappa / C_{\theta N}$. The first experimental assessments of the coefficients are given in Table 5.13.

Table 5.13 Constants of the parameterization according to Zilitinkevich and Calanca (2000) in Eqs. (5.70) and (5.71)

Author	Experiment	C_{uN}	$C_{\theta N}$
Zilitinkevich and Calanca (2000)	Greenland experiment (Ohmura et al. 1992)	0.2…0.5	
Zilitinkevich et al. (2002)	Greenland experiment (Ohmura et al. 1992)	0.3	0.3
Zilitinkevich et al. (2002)	Cabauw tower, The Netherlands	0.04…0.9	
Sodemann and Foken (2004)	FINTUREX, Antarctica (Foken 1996), *Golden days*	0.51 ± 0.03	0.040 ± 0.001
Sodemann and Foken (2004)	FINTUREX, Antarctica (Foken 1996)	2.26 ± 0.08	0.022 ± 0.002

5.7   Large-Eddy Simulation

The model approaches discussed up to here have been primarily based on mean relations and averaged input parameters. They do not allow a spectral-dependent view, where the effects of single eddies can be shown. The reasons for this are the significant difficulties in spectral modeling and the large range of scales in atmospheric boundary layers. The spatial scale extends from the mixed layer height of about 10^3 m down to the Kolmogorov micro scale

$$\eta = \left(v^3/\varepsilon\right)^{1/4} \tag{5.73}$$

of about 10^{-3} m. The energy dissipation, ε, is identical with the energy input from the energy conserving scale $l \sim z_i$ and the relevant characteristic velocity:

$$\varepsilon = u^3/l \tag{5.74}$$

For the convective boundary layer, the energy dissipation is approximately 10^{-3} m^2 s^{-3}. The turbulent eddies in the atmospheric boundary layer cover a range from kilometers to millimeters. Thus, a numerical solution of the Navier-Stokes equation would need 10^{18} grid points. Because the large eddies, which are easily resolvable in a numerical model, are responsible for the transports of momentum, heat and moisture, it is necessary to estimate the effects of the small dissipative eddies which are not easily resolvable. The simulation technique for large eddies (Large-Eddy-Simulation: LES) consists in the modeling of the important contributions of the turbulent flow and to parameterize integral effects of small eddies (Moeng 1998). For technical applications with low Reynolds numbers, almost all eddy sizes can be resolved. The latter method is called Direct Numerical Simulation (DNS).

The basic equations for LES are the Navier-Stokes equations, where single terms must be transferred into volume averages

$$\tilde{u}_i = \iiint (u_i \, G) \, dx \, dy \, dz \, , \qquad (5.75)$$

where G is a filter function which filters out small eddies and regards only large eddies. The total contribution of the small eddies is taken into account in an additional term of the volume averaged Navier-Stokes equations and parameterized with a special model. The widely used approach is the parameterization according to Smagorinsky-Lilly (Smagorinsky 1963; Lilly 1967), where the diffusion coefficient is described in terms of the wind and temperature gradients. For small eddies in the inertial subrange, the $-5/3$ law is assumed so that the relevant constants can be determined (Moeng and Wyngaard 1989). If small-scale phenomena have an important influence, the application of LES modeling requires a lot of care, for example, near the surface or when including chemical reactions.

The LES technique is currently no longer just a research tool, which allows investigating simple situations with high resolution in space and time, but at the cost of large computation times. Results from LES studies led to significant advancements in the understanding of the atmospheric boundary layer. Beginning with the first simulations by (Deardorff 1972), LES has been mainly applied to the convective boundary layer (Schmidt and Schumann 1989; Schumann 1989). In most cases, the ground surface is assumed homogeneous or only simply structured. Recently, the stably stratified boundary layer has become a topic of investigations. In the last 20 years, LES is a rapidly developing research field with many publications (Garratt 1992; Moeng 1998; Kantha and Clayson 2000; Raasch and Schröter 2001, Moeng et al. 2004, and others). Increasingly, heterogeneous surfaces like forests (Kanani-Sühring and Raasch 2015; Schlegel et al. 2015), valleys (Brötz et al. 2014), urban areas (Letzel et al. 2008) are modelled, and technical applications related to the use of wind power (Vollmer et al. 2015) are becoming common.

5.8 Area Averaging

All methods to determine the turbulent momentum and energy fluxes are related to the surface above which the fluxes are measured. But in most cases, the problem is to determine for example the evapotranspiration within a catchment, or over a large agricultural area or even over entire landscapes. Area-averaged fluxes are necessary in numerical weather and climate forecast models as input or validation parameters. It is impossible to calculate them by a simple averaging of the input parameters because complicated non-linear relations could cause large errors. Nevertheless this method has recently been used for weather and climate models, which use simple parameterizations of the interaction of the atmosphere with the surface.

Using the resistance concept in the form of Eq. (5.30), the total resistance of the area is a *parallel connection* of the total resistances of areas with different land use:

$$\frac{1}{r_g} = \frac{1}{r_{g1}} + \frac{1}{r_{g2}} + \frac{1}{r_{g3}} + \cdots \qquad (5.76)$$

Applying the method of parameter aggregation, it follows from Eq. (5.76) for an averaging of individual resistances as in Eq. (5.32):

$$\frac{1}{r_g} = \frac{1}{\frac{1}{N}\sum_i r_{a_i}} + \frac{1}{\frac{1}{N}\sum_i r_{mt_i}} + \frac{1}{\frac{1}{N}\sum_i r_{c_i}} \qquad (5.77)$$

It is immediately clear that Eq. (5.77) is physically incorrect. Nevertheless this approach is practicable because, for example, the mean resistance of the turbulent layer can be determined by averaging the roughness lengths of individual areas as it is done in most of weather prediction and climate models. However, one must be aware that because of non-linear relations significant estimation errors of the turbulent fluxes can occur (Stull and Santoso 2000).

In contrast, for the flux aggregation the total resistance must be calculated for each individual area, which also implies different boundary conditions for the different areas:

$$\frac{1}{r_g} = \sum_i \frac{1}{r_{a_i} + r_{mt_i} + r_{c_i}} \qquad (5.78)$$

The more simple methods of flux averaging differ in the ways Eq. (5.78) is used for the individual areas.

An overview about different area averaging methods is given in Table 5.14. In this table statistical-dynamical methods, which give only a rough resolution of the land use types, are not mentioned.

The area averaging is also important for the experimental determination of turbulent fluxes, because different land use types are often in the footprint of the sensors, which generates a mixed signal. This problem can be solved if additional measurements are taken for parts of the area, which allows a footprint dependent correction (Göckede et al. 2005; Leclerc and Foken 2014). In a similar way, the correction can be determined if at least for one part of the area the fluxes are modelled (Biermann et al. 2014).

5.8.1 Simple Area Averaging Methods

A very simple, but still-used method is the calculation of fluxes for dominant areas. For each grid element of a numerical model, the dominate land use must be

Table 5.14 Methods of area averaging

Averaging method	Procedure	Example/reference
Parameter aggregation	Averaging for example of the roughness length	$\overline{z_0} = \frac{1}{N}\sum_i^N z_{0i}$
	Averaging of *effective* parameters	i.e. Troen and Lundtang Peterson (1989), see Sect. 3.1.1
Flux aggregation	Averaging for example of the roughness length with Fourier analysis	Hasager and Jensen (1999), Hasager et al. (2003)
	Mixing method for resistances	Mölders et al. (1996), Mölders (2012)
	Flux determination for dominant areas	Avissar and Pielke (1989)
	Mosaic approach	Mölders et al. (1996), Mölders (2012)
	• *tile* approach	
	• subgrid approach	

determined over which the fluxes are calculated. It is assumed that over all grid elements the different land uses are statistically balanced. Therefore, each grid element has only one land use type. The averaging within a grid element is a quasi parameter-averaging process because the individual estimations of the parameters of the grid elements are largely intuitive and therefore parameter averaged.

The *blending-height* concept (see Sect. 3.2.4) can also be used for area averaging. It is assumed that at a certain height above the ground (for example 50 m) the fluxes above the heterogeneities of the surface do not differ and can be presented as an averaged flux. The fluxes for this height can be parameterized using effective parameters. A typical case is the application of effective roughness length, where the friction velocities are averaged instead of the roughness lengths (Taylor 1987; Blyth 1995; Schmid and Bünzli 1995a, 1995b; Mahrt 1996; Hasager and Jensen 1999; Hasager et al. 2003). From Eq. (2.60), it follows that by averaging the friction velocities of the individual areas an effective roughness length is given by:

$$z_{0eff} = \frac{\overline{u_* \ln z_0}}{\overline{u_*}} \tag{5.79}$$

A more empirical averaging of roughness lengths as presented by Troen and Lundtang Petersen (1989) for the European Wind Atlas (Table 3.1) can be classified as an early stage of the above given method. A good effective averaging is of increasing importance for many practical reasons, for example micrometeorological processes in the urban boundary layer (Grimmond et al. 1998).
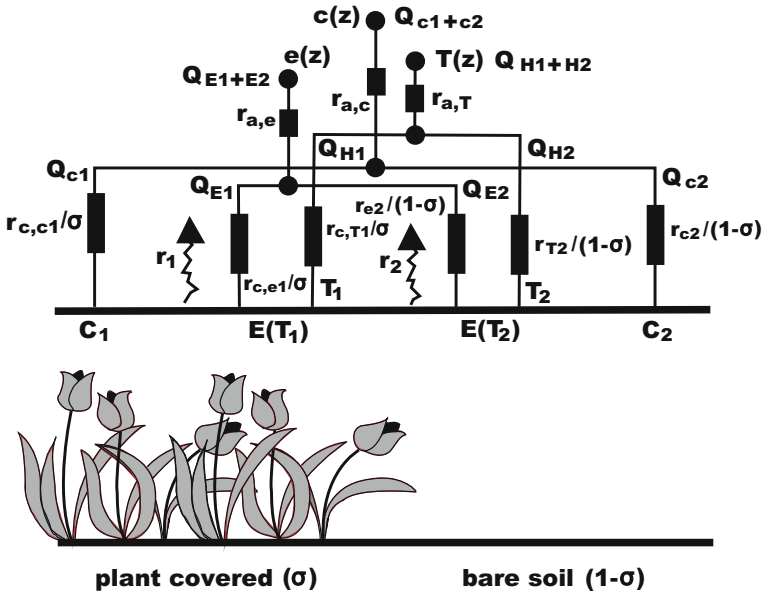
Fig. 5.5 Schematic representation of the mixing method (modified according to Mölders 2012, with kind permission of © Springer Berlin, Heidelberg 2012, All rights reserved)

The procedure of roughness averaging with an effective roughness length is widely applied in the determination of turbulent resistances. In a mixing method, only those resistances are averaged which are obviously different for the different individual areas. Generally, uniform values are assumed for the turbulent and the molecular-turbulent resistances, and only the canopy resistance is averaged according—comparable with the mosaic approach (see Sect. 5.8.2)—to the land use (Fig. 5.5). This method uses the fact that in most cases meteorological information is not available for different land uses within a grid element. However, for the determination of the turbulent and molecular-turbulent resistances a parameter averaging is used because these are often not parameterized for a specific underlying surface.

5.8.2 Complex Area-Averaging Methods

The mosaic approach belongs to the complex methods (Avissar and Pielke 1989; Mölders et al. 1996). This description is currently often used as a generic term for different applications. In the simplest case, (*tile*-approach) for each grid cell, contributions of similar land use types are combined and the parameterization of all resistances and the fluxes for each type will be separately calculated. The mean flux

Fig. 5.6 Schematic representation of the mosaic approach (Mölders et al. 1996). The initial distribution of the surface structures will be combined according their contributions for further calculations. Adapted with kind permission of © Author(s) 1996, CC Attribution 4.0 Licence, All rights reserved
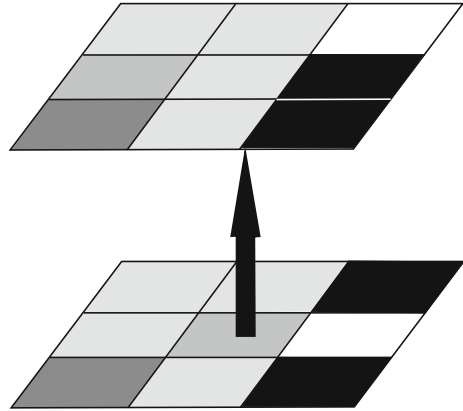
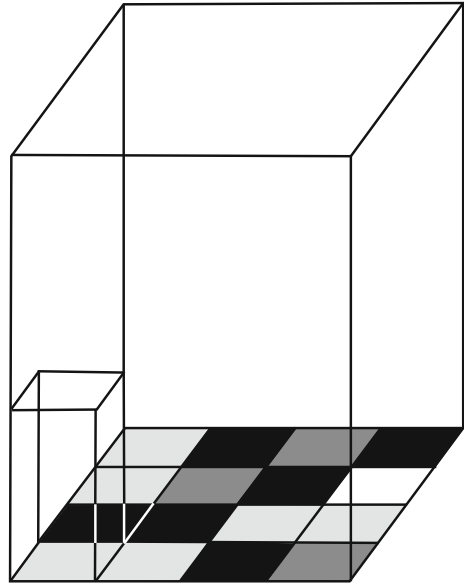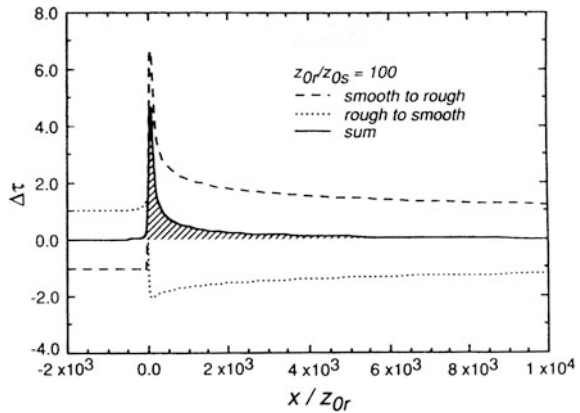is the weighted average according to the contribution of the single land uses (Fig. 5.6):

$$Q_x = \sum_{i=1}^{N} a_i Q_{xi} \tag{5.80}$$

whereby Q_x is the averaged flux and Q_{xi} are the fluxes of partial areas with an area fraction of a_i. This method is widely used for high-resolution models in space (100 m grid size), but it does not allow horizontal fluxes (advection) between the areas.

This disadvantage is overcome with the subgrid method (Fig. 5.7)

$$Q_x = \frac{1}{N} \sum_{i=1}^{N} Q_{xi} \tag{5.81}$$

where for each land use a small multi-layer model is used, which takes advection into account. For a certain height according to the blending-height concept, an average of the fluxes for a grid element is assumed. Such models correspond well with the reality, but they require very large computer capacity. Therefore, the subgrid method has been applied only for single process studies.

Model calculations with subgrid models and experiments (Panin et al. 1996b; Klaassen et al. 2002) show that fluxes above one surface are not independent of the neighbourhood surfaces. Accordingly, these model studies for highly heterogeneous surfaces show an increase of the flux for the total area (Friedrich et al. 2000). According to numerical studies by Schmid and Bünzli (1995a) this increase of the fluxes occurs on the lee side of boundaries between the single surfaces (Fig. 5.8).

5.8.3 Model Coupling

Averaging concepts are often used in the coupling of models. For model coupling,
different approaches have been tested and are promising (Mölders 2001). The
simplest versions are the direct data transfer and the one-way coupling, where the
plant, soil, or hydrological model (SVAT and others) get their forcing from a
meteorological model. In a two-way coupling, the SVAT model for example, gives
its calculated fluxes back to the meteorological model. If sufficient computer time is
available, then complete couplings are possible.

Instead of a coupling with effective parameters, a coupling with fluxes is preferred (Best et al. 2004), because effective parameters cannot adequately describe the high non-linearity of the fluxes. Instead of a coupling with area-averaged fluxes (Herzog et al. 2002), modules between the models should be included (Mölders 2001), which allow suitable coupling of the heterogeneous surface in different models, e.g. an averaging according to the mosaic or subgrid approach (Mölders et al. 1996; Albertson and Parlange 1999). It very important that the coupled models use consistent parameterizations (Mölders and Kramm 2014). This issue is relevant for the development of Earth system models, which are discussed in climate research.

For model coupling, an unsolved problem is the usage sufficient grid structures. Meteorological models are based on rectangular grids, while land use models are based on polygons. A promising development is the use of adaptive grids (Behrens et al. 2005) that fit themselves to the respective surface conditions of each model, and have a high resolution in regions where the modeling is very critical or where the largest heterogeneities occur.

References

Albertson JD and Parlange MB (1999) Natural integration of scalar fluxes from complex terrain. Adv Water Res. 23:239–252.

Allen RG, Pereira LS, Raes D and Smith M (1998) Crop evaporation. FAO Irrigation Drainage Pap. 56:XXVI + 300 pp.

Allen RG, Walter IA, Elliott R, Howell T, Itenfisu D and Jensen M (2005) The ASCE standardized reference evapotranspiration equation. Environmental and Water Resources Institute of the American Society of Civil Engineers, X + 59 pp.

Arya SP (2001) Introduction to Micrometeorology. Academic Press, San Diego, 415 pp.

Avissar R and Pielke RA (1989) A parametrization of heterogeneous land surface for atmospheric numerical models and its impact on regional meteorology. Monthly Weather Review. 117:2113–2136.

Baldocchi D (1988) A multi-layer model for estimating sulfor dioxid deposition to a deciduous oke forest canopy. Atmos Environm. 22:869–884.

Baldocchi D, Hicks BB and Camara P (1987) A canopy stomatal resistance model for gaseous deposition to vegetated surfaces. Atmos Environm. 21:91–101.

Ball JT, Woodrow IE and Berry JA (1987) A model predicting stomatal conductance and its contribution to the control of photosynthesis under different environmental conditions. In: Biggens J (ed.), Progress in Photosynthesis Research. Vol. IV. Martinus Nijhoff Publisher, Dordrecht, IV.5.221–IV.5.224.

Batchvarova E and Gryning S-E (1991) Applied model for the growth of the daytime mixed layer. Boundary-Layer Meteorol. 56:261–274.

Behrens J, Rakowsky N, Hiller W, Handorf D, Läuter M, Päpke J and Dethloff K (2005) amatos: parallel adaptive mesh generator for atmospheric and oceanic simulation. Ocean Modelling. 10:171–183.

Beljaars ACM (1995) The parametrization of surface fluxes in large scale models under free convection. Quart J Roy Meteorol Soc. 121:255–270.

Beljaars ACM and Holtslag AAM (1991) Flux parametrization over land surfaces for atmospheric models. J Appl Meteorol. 30:327–341.

Beljaars ACM and Viterbo P (1998) Role of the boundary layer in a numerical weather prediction model. In: Holtslag AAM and Duynkerke PG (eds.), Clear and Cloudy Boundary Layers, vol VNE 48. Royal Netherlands Academy of Arts and Sciences, Amsterdam, 287–304.

Best MJ, Beljaars A, Polcher J and Viterbo P (2004) A proposed structure for coupling tiled surfaces with the planetary boundary layer. J Hydrometeorol. 5:1271–1278.

Biermann T, Babel W, Ma W, Chen X, Thiem E, Ma Y and Foken T (2014) Turbulent flux observations and modelling over a shallow lake and a wet grassland in the Nam Co basin, Tibetan Plateau. Theor Appl Climat. 116:301–316.

Bjutner EK (1974) Teoreticeskij rascet soprotivlenija morskoj poverchnosti (Theoretical calculation of the resistance at the surface of the ocean). In: Dubov AS (ed.), Processy perenosa vblizi poverchnosti razdela okean - atmosfera (Exchange processes near the ocean - atmosphere interface). Gidrometeoizdat, Leningrad, 66–114.

Blackadar AK (1997) Turbulence and Diffusion in the Atmosphere. Springer, Berlin, Heidelberg, 185 pp.

Blümel K (1998) Estimation of sensible heat flux from surface temperature wave and one-time-of-day air temperature observations. Boundary-Layer Meteorol. 86:193–232.

Blyth EM (1995) Comments on 'The influence of surface texture on the effective roughness length' by H. P. Schmid and D. Bünzli (1995, **121**, 1–21). Quart J Roy Meteorol Soc. 121:1169–1171.

Brötz B, Eigenmann R, Dörnbrack A, Foken T and Wirth V (2014) Early-morning flow transition in a valley in low-mountain terrain. Boundary-Layer Meteorol. 152:45–63.

Brutsaert WH (1982) Evaporation into the atmosphere: Theory, history and application. D. Reidel, Dordrecht, 299 pp.

Burridge DM and Gadd AJ (1977) The Meteorological Office operational 10-level numerical weather prediction model (December 1975). Meteorological Office Technical Notes. 34:39 pp.

Csanady GT (2001) Air-sea interaction, Laws and mechanisms. Cambridge University Press, Cambridge, New York, 239 pp.

Davidan IN, Lopatuhin LI and Rogkov VA (1985) Volny v okeane (Waves in the ocean). Gidrometeoizdat, Leningrad, 256 pp.

Deardorff JW (1972) Numerical investigation of neutral und unstable planetary boundary layer. J Atmos Sci. 29:91–115.

DeBruin HAR (1983) A model for the Priestley–Taylor parameter α. J Climate Appl Meteorol. 22:572–578.

DeBruin HAR and Holtslag AAM (1982) A simple parametrization of the surface fluxes of sensible and latent heat during daytime compared with the Penman–Monteith concept. J Climate Appl Meteorol. 21:1610–1621.

Dommermuth H and Trampf W (1990) Die Verdunstung in der Bundesrepublik Deutschland, Zeitraum 1951-1980, Teil 1. Deutscher Wetterdienst, Offenbach, 10 pp.

Doorenbos J and Pruitt WO (1977) Guidelines for predicting crop water requirements. FAO Irrigation Drainage Pap. 24, 2nd ed.:145 pp.

DVWK (1996) Ermittlung der Verdunstung von Land- und Wasserflächen. DVWK-Merkblätter zur Wasserwirtschaft. 238:134 pp.

Falge EM, Ryel RJ, Alsheimer M and Tenhunen JD (1997) Effects on stand structure and physiology on forest gas exchange: A simulation study for Norway spruce. Trees. 11:436–448.

Farquhar GD, von Caemmerer S and Berry JA (1980) A biochemical of photosynthetic CO_2 assimilation in leaves of C_3 species. Planta. 149:78–90.

Foken T (1978) The molecular temperature boundary layer of the atmosphere over various surfaces. Archiv Meteorol Geophys Bioklim, Ser. A. 27:59–67.

Foken T (1984) The parametrisation of the energy exchange across the air-sea interface. Dynamics Atm Oceans. 8:297–305.

Foken T (1986) An operational model of the energy exchange across the air-sea interface. Z Meteorol. 36:354–359.

Foken T (1996) Turbulenzexperiment zur Untersuchung stabiler Schichtungen. Ber Polarforschung. 188:74–78.

Foken T (2002) Some aspects of the viscous sublayer. Meteorol Z. 11:267–272.

Foken T (2016) Angewandte Meteorologie. Springer-Spektrum, Berlin, Heidelberg, 394 pp.

Foken T, Kitajgorodskij SA and Kuznecov OA (1978) On the dynamics of the molecular temperature boundary layer above the sea. Boundary-Layer Meteorol. 15:289–300.

Foken T, Dlugi R and Kramm G (1995) On the determination of dry deposition and emission of gaseous compounds at the biosphere-atmosphere interface. Meteorol Z. 4:91–118.

Friedrich K, Mölders N and Tetzlaff G (2000) On the influence of surface heterogeneity on the Bowen-ratio: A theoretical case study. Theor Appl Climat. 65:181–196.

Garratt JR (1992) The Atmospheric Boundary Layer. Cambridge University Press, Cambridge, 316 pp.

Geernaert GL (ed) (1999) Air-Sea Exchange: Physics, Chemistry and Dynamics. Kluwer Acad. Publ., Dordrecht, 578 pp.

Göckede M and Foken T (2001) Ein weiterentwickeltes Holtslag-van Ulden-Schema zur Stabilitätsparametrisierung in der Bodenschicht. Österreichische Beiträge zu Meteorologie und Geophysik. 27:(Extended Abstract and pdf-file on CD) 210.

Göckede M, Markkanen T, Mauder M, Arnold K, Leps JP and Foken T (2005) Validation of footprint models using natural tracer measurements from a field experiment. Agrical Forest Meteorol. 135:314–325.

Grimmond CSB, King TS, Roth M and Oke TR (1998) Aerodynamic roughness of urban areas derived from wind observations. Boundary-Layer Meteorol. 89:1–24.

Groß G (1993) Numerical Simulation of Canopy Flows. Springer, Berlin, Heidelberg pp.

Gryning S-E, Batchvarova E, Brümmer B, Jørgensen H and Larsen S (2007) On the extension of the wind profile over homogeneous terrain beyond the surface boundary layer. Boundary-Layer Meteorol. 124:251–268.

Gusev EM and Nasonova ON (2010) Modelirovanie teplo- i vlagoobmena poverchnosti sushi s atmosferoj (Modelling of the heat and moisture exchange of land surfaces with the atmosphere). Nauka, Moskva, 327 pp.

Handorf D, Foken T and Kottmeier C (1999) The stable atmospheric boundary layer over an Antarctic ice sheet. Boundary-Layer Meteorol. 91:165–186.

Hasager CB and Jensen NO (1999) Surface-flux aggregation in heterogeneous terrain. Quart J Roy Meteorol Soc. 125:2075–2102.

Hasager CB, Nielsen NW, Jensen NO, Boegh E, Christensen JH, Dellwik E and Soegaard H (2003) Effective roughness calculated from satellite-derived land cover maps and hedge-information used in a weather forecasting model. Boundary-Layer Meteorol. 109:227–254.

Haude W (1955) Bestimmung der Verdunstung auf möglichst einfache Weise. Mitt Dt Wetterdienst. 11:24 pp.

Herzog H-J, Vogel G and Schubert U (2002) LLM - a nonhydrostatic model applied to high-resolving simulation of turbulent fluxes over heterogeneous terrain. Theor Appl Climat. 73:67–86.

Hess GD (2004) The neutral, barotropic planetary layer capped by a low-level inversion. Boundary-Layer Meteorol. 110:319–355.

Hicks BB, Baldocchi DD, Meyers TP, Hosker jr. RP and Matt DR (1987) A preliminary multiple resistance routine for deriving dry deposition velocities from measured quantities. Water, Air and Soil Pollution. 36:311–330.

Hillel D (1980) Applications of Soil Physics. Academic Press, New York, 385 pp.

Högström U (1988) Non-dimensional wind and temperature profiles in the atmospheric surface layer: A re-evaluation. Boundary-Layer Meteorol. 42:55–78.

Holtslag AAM and van Ulden AP (1983) A simple scheme for daytime estimates of the surface fluxes from routine weather data. J Climate Appl Meteorol. 22:517–529.

Houghton JT (2015) Global Warming, The complete Briefing. Cambridge University Press, Cambridge, 396 pp.

Inclán MG, Forkel R, Dlugi R and Stull RB (1996) Application of transilient turbulent theory to study interactions between the atmospheric boundary layer and forest canopies. Boundary-Layer Meteorol. 79:315–344.

Jacobs AFG, Heusinkveld BG and Nieveen JP (1998) Temperature behavior of a natural shallow water body during a summer periode. Theor Appl Climat. 59:121–127.

Jacobson MZ (2005) Fundamentals of Atmospheric Modelling. Cambridge University Press, Cambridge, 813 pp.

Jarvis PG (1976) The interpretation of the variations in leaf water potential and stomatal conductance found in canopies in the field. Phil Trans Roy. Soc London B: Biolog Sci. 273:593–610.

Kaimal JC and Finnigan JJ (1994) Atmospheric Boundary Layer Flows: Their Structure and Measurement. Oxford University Press, New York, NY, 289 pp.

Kanani-Sühring F and Raasch S (2015) Spatial variability of scalar concentrations and fluxes downstream of a clearing-to-forest transition: A Large-Eddy Simulation study. Boundary-Layer Meteorol. 155:1–27.

Kantha LH and Clayson CA (2000) Small scale processes in geophysical fluid flows. Academic Press, San Diego, 883 pp.

Kitajgorodskij SA and Volkov JA (1965) O rascete turbulentnych potokov tepla i vlagi v privodnom sloe atmosfery (The calculation of the turbulent fluxes of temperature and humidity in the atmosphere near the water surface) Izv AN SSSR, Fiz Atm Okeana. 1:1317–1336.

Klaassen W, van Breugel PB, Moors EJ and Nieveen JP (2002) Increased heat fluxes near a forest edge. Theor Appl Climat. 72:231–243.

Kramm G and Foken T (1998) Ucertainty analysis on the evaporation at the sea surface. Second Study Conference on BALTEX, Juliusruh, 25–29 May 1998. BALTEX Secretariat, pp. 113–114.

Kramm G, Foken T, Molders N, Muller H and Paw U KT (1996a) The sublayer-Stanton numbers of heat and matter for different types of natural surfaces. Contr Atmosph Phys. 69:417–430.

Kramm G, Beier M, Foken T, Müller H, Schröder P and Seiler W (1996b) A SVAT-skime for NO, NO_2, and O_3 - Model description and test results. Meteorol Atmos Phys. 61:89–106.

Kramm G, Dlugi R and Mölders N (2002) Sublayer-Stanton numbers of heat and matter for aerodynamically smooth surfaces: basic considerations and evaluations. Meteorol Atmos Phys. 79:173–194.

Landau LD and Lifschitz EM (1987) Fluid Mechanics. Butterworth-Heinemann, Oxford, 539 pp.

Leclerc MY and Foken T (2014) Footprints in Micrometeorology and Ecology. Springer, Heidelberg, New York, Dordrecht, London, XIX, 239 pp.

Letzel MO, Krane M and Raasch S (2008) High resolution urban large-eddy simulation studies from street canyon to neighbourhood scale. Atmos Environm. 42:8770–8784.

Leuning R (1995) A critical appraisal of a combined stomatal-photosynthesis model for C_3 plants. Plant, Cell & Environment. 18:339–355.

Lilly DK (1967) The representation of small-scale turbulence in numerical simulation experiments. In: Goldstein HH (ed). IBM Scientific Computing Symposium on Environmental Science, Yorktown Heights, N.Y., November 14-16, 1966 1967, pp. IBM Form No. 320-1951, 1195–1210.

Louis JF (1979) A parametric model of vertical fluxes in the atmosphere. Boundary-Layer Meteorol. 17:187–202.

Louis JF, Tiedtke M and Geleyn JF (1982) A short history of the PBL parametrization at ECMWF. Workshop on Boundary Layer parametrization, Reading1982. ECMWF, pp. 59–79.

Lüers J and Bareiss J (2010) The effect of misleading surface temperature estimations on the sensible heat fluxes at a high Arctic site – the Arctic Turbulence Experiment 2006 on Svalbard (ARCTEX-2006). Atmos Chem Phys. 10:157–168.

Mahrt L (1996) The bulk aerodynamic formulation over heterogeneous surfaces. Boundary-Layer Meteorol. 78:87–119.

Mallick K, Boegh E, Trebs I, Alfieri JG, Kustas WP, Prueger JH, Niyogi D, Das N, Drewry DT, Hoffmann L and Jarvis AJ (2015) Reintroducing radiometric surface temperature into the Penman–Monteith formulation. Water Resources Res. 51:6214–6243.

Mangarella PA, Chambers AJ, Street RL and Hsu EY (1972) Laboratory and field interfacial energy and mass flux and prediction equations. J Geophys Res. 77:5870–5875.

Mangarella PA, Chambers AJ, Street RL and Hsu EY (1973) Laboratory studies of evaporation and energy transfer through a wavy air-water interface. J. Phys. Oceanogr. 3:93–101.

Mengelkamp H-T, Warrach K and Raschke E (1999) SEWAB a parameterization of the surface energy and water balance for atmospheric and hydrologic models. Adv Water Res. 23:165–175.

Meyers TP and Paw U KT (1986) Testing a higher-order closure model for modelling airflow within and above plant canopies. Boundary-Layer Meteorol. 37:297–311.

Meyers TP and Paw U KT (1987) Modelling the plant canopy microenvironment with higher-order closure principles. Agrical Forest Meteorol. 41:143–163.

Mix W, Goldberg V and Bernhardt K-H (1994) Numerical experiments with different approaches for boundary layer modelling under large-area forest canopy conditions. Meteorol Z. 3:187–192.

Moene AF and van Dam JC (2014) Transport in the Atmosphere-Vegetation-Soil Continuum. Cambridge University Press, Cambridge, 436 pp.

Moeng C-H (1998) Large eddy simulation of atmospheric boundary layers. In: Holtslag AAM and Duynkerke PG (eds.), Clear and cloudy boundary layers, vol VNE 48. Royal Netherlands Academy of Arts and Science, Amsterdam, 67–83.

Moeng C-H and Wyngaard JC (1989) Evaluation of turbulent transport and dissipation closure in second-order modelling. J Atmos Sci. 46:2311–2330.

Moeng C-H, Sullivan PP and Stevens B (2004) Large-eddy simulation of cloud-topped mixed layers. In: Fedorovich Eet al (eds.), Atmospheric Turbulence and mesoscale Meteorology. Cambridge University Press, Cambridge, 95–114.

Mölders N (2001) Concepts for coupling hydrological and meteorological models. Wiss. Mitt. aus dem Inst. für Meteorol. der Univ. Leipzig und dem Institut für Troposphärenforschung e. V. Leipzig. 22:1–15.

Mölders N (2012) Land-Use and Land-Cover Changes, Impact on climate and air quality. Springer, Dordrecht, Heidelberg, London, New York, 189 pp.

Mölders N and Kramm G (2014) Lectures in Meteorology. Springer, Cham Heidelberg New York Dordrecht London XIX, 591 pp.

Mölders N, Raabe A and Tetzlaff G (1996) A comparison of two strategies on land surface heterogeneity used in a mesoscale ß meteorological model. Tellus. 48A:733–749.

Monson R and Baldocchi D (2014) Terrestrial Biosphere-Atmosphere Fluxes. Cambridge University Press, New York, XXI, 487 pp.

Monteith JL (1965) Evaporation and environment. Symp Soc Exp Biol. 19:205–234.

Montgomery RB (1940) Observations of vertical humidity distribution above the ocean surface and their relation to evaporation. Pap Phys Oceanogr Meteorol. 7:1–30.

Müller C (1999) Modelling Soil-Biosphere Interaction. CABI Publishing, Wallingford, 354 pp.

Ohmura A, Steffen K, Blatter H, Greuell W, Rotach M, Stober M, Konzelmann T, Forrer J, Abe-Ouchi A, Steiger D and Neiderbäumer G (1992) Greenland Expedition, Progress Report No. 2, April 1991 to Oktober 1992. Swiss Federal Institute of Technology, Zürich, 94 pp.

Owen PR and Thomson WR (1963) Heat transfer across rough surfaces. J Fluid Mech. 15:321–334.

Panin GN (1985) Teplo- i massomen meszdu vodoemom i atmospheroj v estestvennych uslovijach (Heat- and mass exchange between the water and the atmosphere in the nature). Nauka, Moscow, 206 pp.

Panin GN, Nasonov AE and Souchintsev MG (1996a) Measurements and estimation of energy and mass exchange over a shallow see. In: Donelan M (ed.), The air-sea interface, Miami, 489–494.

Panin GN, Tetzlaff G, Raabe A, Schönfeld H-J and Nasonov AE (1996b) Inhomogeneity of the land surface and the parametrization of surface fluxes - a discussion. Wiss Mitt Inst Meteorol Univ Leipzig und Inst Troposphärenforschung Leipzig. 4:204–215.

Panin GN, Nasonov AE, Foken T and Lohse H (2006) On the parameterization of evaporation and sensible heat exchange for shallow lakes. Theor Appl Climat. 85:123–129.

Panofsky HA (1973) Tower micrometeorology. In: Haugen DA (ed.), Workshop on Micrometeorology. American Meteorological Society, Boston, 151–176.

Peña A, Gryning S-E and Hasager C (2010) Comparing mixing-length models of the diabatic wind profile over homogeneous terrain. Theor Appl Climat. 100:325–335.

Penman HL (1948) Natural evaporation from open water, bare soil and grass. Proceedings Royal Society London. A193:120–195.

Priestley CHB and Taylor JR (1972) On the assessment of surface heat flux and evaporation using large-scale parameters. Monthly Weather Review. 100:81–92.

Pyles RD, Weare BC and Paw U KT (2000) The UCD Advanced Canopy-Atmosphere-Soil Algorithm: comparisons with observations from different climate and vegetation regimes. Quart J Roy Meteorol Soc. 126:2951–2980.

Raasch S and Schröter M (2001) PALM - A large-eddy simulation model performing on massively parallel computers. Meteorol Z. 10:363–372.

Reichardt H (1951) Vollständige Darstellung der turbulenten Geschwindigkeitsverteilung in glatten Röhren. Z angew Math Mech. 31:208–219.

Richter D (1977) Zur einheitlichen Berechnung der Wassertemperatur und der Verdunstung von freien Wasserflächen auf statistischer Grundlage. Abh Meteorol Dienstes DDR. 119:35 pp.

Rigby JR, Yin J, Albertson J and Porporato A (2015) Approximate Analytical Solution to Diurnal Atmospheric Boundary-Layer Growth Under Well-Watered Conditions. Boundary-Layer Meteorol. 156:73–89.

Roll HU (1948) Wassernahes Windprofil und Wellen auf dem Wattenmeer. Ann Meteorol. 1:139–151.

Rutgersson A and Sullivan PP (2005) Investigating the effects of water waves on the turbulence structure in the atmosphere using direct numerical simulations. Dynamics Atm Oceans. 38:147–171.

Schädler G, Kalthoff N and Fiedler F (1990) Validation of a model for heat, mass and momentum exchange over vegetated surfaces using LOTREX-10E/HIBE88 data. Contr Atmosph Phys. 63:85–100.

Schlegel F, Stiller J, Bienert A, Maas H-G, Queck R and Bernhofer C (2015) Large-Eddy Simulation study of the effects on flow of a heterogeneous forest at sub-tree resolution. Boundary-Layer Meteorol. 154:27–56.

Schlichting H and Gersten K (2006) Grenzschicht-Theorie. Springer, Berlin, Heidelberg, 799 pp.

Schmid HP and Bünzli D (1995a) The influence of the surface texture on the effective roughness length. Quart J Roy Meteorol Soc. 121:1–21.

Schmid HP and Bünzli D (1995b) Reply to comments by E. M. Blyth on 'The influence of surface texture on the effective roughness length'. Quart J Roy Meteorol Soc. 121:1173–1176.

Schmidt H and Schumann U (1989) Coherent structures of the convective boundary layer derived from large eddy simulations. J Fluid Mech. 200:511–562.

Schrödter H (1985) Verdunstung, Anwendungsorientierte Meßverfahren und Bestimmungsmethoden. Springer, Berlin, Heidelberg, 186 pp.

Schumann U (1989) Large-eddy simulation of turbulent diffusion with chemical reactions in the convective boundary layer. Atmos Environm. 23:1713–1727.

Seibert P, Beyrich F, Gryning S-E, Joffre S, Rasmussen A and Tercier P (2000) Review and intercomparison of operational methods for the determination of the mixing height. Atmos Environm. 34:1001–1027.

Sellers PJ and Dorman JL (1987) Testing the simple biospere model (SiB) for use in general circulation models. J Climate Appl Meteorol. 26:622–651.

Shukauskas A and Schlantschiauskas A (1973) Teplootdatscha v turbulentnom potoke shidkosti (Heat exchange in the turbulent fluid). Izd. Mintis, Vil'njus, 327 pp.

Smagorinsky J (1963) General circulation experiments with the primitive equations: I. The basic experiment. Monthly Weather Review. 91:99–164.

Smith SD, Fairall CW, Geernaert GL and Hasse L (1996) Air-sea fluxes: 25 years of progress. Boundary-Layer Meteorol. 78:247–290.

Sodemann H and Foken T (2004) Empirical evaluation of an extended similarity theory for the stably stratified atmospheric surface layer. Quart J Roy Meteorol Soc. 130:2665–2671.

Sponagel H (1980) Zur Bestimmung der realen Evapotranspiration landwirtschaftlicher Kulturpflanzen. Geologisches Jahrbuch. F9:87 pp.

Staudt K, Serafimovich A, Siebicke L, Pyles RD and Falge E (2011) Vertical structure of evapotranspiration at a forest site (a case study). Agrical Forest Meteorol. 151:709–729.

Stull RB (1988) An Introduction to Boundary Layer Meteorology. Kluwer Acad. Publ., Dordrecht, Boston, London, 666 pp.

Stull R and Santoso E (2000) Convective transport theory and counter-difference fluxes. 14th Symposium on Boundary Layer and Turbulence, Aspen, CO., 7.-11. Aug. 2000. Am. Meteorol. Soc., Boston, pp. 112–113.

Sverdrup HU (1937/38) On the evaporation from the ocean. J. Marine Res. 1:3–14.

Taylor PA (1987) Comments and further analysis on the effective roughness length for use in numerical three-dimensional models: A research note. Boundary-Layer Meteorol. 39:403–418.

Tennekes H (1973) A Model for the Dynamics of the Inversion Above a Convective Boundary Layer. J Atmos Sci. 30:558–567.

Troen I and Lundtang Peterson E (1989) European Wind Atlas. Risø National Laboratory, Roskilde, 656 pp.

Turc L (1961) Évaluation des besoins en eau d'irrigation évapotranspiration potentielle. Ann Agron. 12:13–49.

van Bavel CHM (1986) Potential evapotranspiration: The combination concept and its experimental verification. Water Resources Res. 2:455–467.

Vollmer L, van Dooren M, Trabucchi D, Schneemann J, Steinfeld G, Witha B, Trujillo J and Kühn M (2015) First comparison of LES of an offshore wind turbine wake with dual-Doppler lidar measurements in a German offshore wind farm. J Phys: Conf Ser. 625:012001.

von Kármán T (1934) Turbulence and skin friction. J. Aeronautic Sci. 1:1–20.

Wendling U, Schellin H-G and Thomä M (1991) Bereitstellung von täglichen Informationen zum Wasserhaushalt des Bodens für die Zwecke der agrarmeteorologischen Beratung. Z Meteorol. 41:468–475.

Yokoyama O, Gamo M and Yamamoto S (1979) The vertical profiles of the turbulent quantities in the atmospheric boundary layer. J Meteor Soc Japan. 57:264–272.

Zilitinkevich SS and Calanca P (2000) An extended similarity theory for the stably stratified atmospheric surface layer. Quart J Roy Meteorol Soc. 126:1913–1923.

Zilitinkevich SS and Esau IN (2005) Resistance and heat transfer laws for stable and neutral planetary layers: Old theory advanced and re-evaluated. Quart J Roy Meteorol Soc. 131:1863–1892.

Zilitinkevich SS and Mironov DV (1996) A multi-limit formulation for the equilibrium depth of a stable stratified atmospheric surface layer. Boundary-Layer Meteorol. 81:325–351.

Zilitinkevich SS, Perov VL and King JC (2002) Near-surface turbulent fluxes in stable stratification: Calculation techniques for use in general circulation models. Quart J Roy Meteorol Soc. 128:1571–1587.

Chapter 6
Measurement Technique

Because meteorological measurements are primarily taken in the near-surface layer, they are carried out in the micrometeorological scale. While some textbooks about meteorological measurements—starting with the classical book by Kleinschmidt (1935)—are available (DeFelice 1998; Brock and Richardson 2001; Emeis 2010; Hebra 2010; Harrison 2015), it can be challenging to find detailed information about micrometeorological measurement and data processing techniques. For this reason, a special chapter is dedicated to micrometeorological measurements. Unlike other books with extensive descriptions of meteorological instrumentation, only general principles of the micrometeorological measurement techniques are described. Of special importance are techniques for the optimal adaptation of the sensors to the surrounding environment—the turbulent atmosphere. The quality assurance of observations is another focal point.

6.1 Data Collection

Digital data collection systems have recently replaced analogue systems. Due to their inertia, analogue systems often required only simple filter functions; however, for digital recording systems these functions are not simple. This is a topic for the users but not the producers, who developed their loggers mostly for universal applications. For the development of micrometeorological measurement systems, the following basic considerations must be made.

6.1.1 Principles of Digital Data Collection

Modern data collection systems use data loggers that collect quasi-parallel signals and create a serial digital signal for transmission to a computer or a storage unit.

Thus, each signal is sampled regularly in time, which is the sampling frequency. This sampling frequency must be adapted very precisely to the frequency of the measured signal. For sensors with a high time resolution (e.g. sonic anemometers), the sensor itself is no longer a low pass filter (LP). An additional low-pass filtering (see Sect. 6.1.2) must be provided so that at the input of the logger no frequencies occur that are greater than half of the sampling frequency. Often, the low pass filtering is done with the software of the sensor. Thus, the signal of the sensor is sampled with a frequency, which is much greater than necessary. The signal is then averaged over several samplings (over sampling). This low pass filtering has the benefit that often-present noise of 60 (50) Hz from the power supply has no influence on the input signal of the logger, which could otherwise affect spectral analyses (aliasing).

With a multiplexer (MUX), the signals of the individual sensors are successively sampled. Then, the sampling process starts again from the beginning. For turbulence measurements, covariances are often calculated between different logger channels, and the logger must be programmed in such a way that signals for covariance calculations are sampled at neighbouring channels. Grounding unused logger channels prevents noise from influencing the system. The logger submits the measured signals one after the other over a sample and hold circuit (SH) to an analogue-to-digital converter (A/D), whose configuration influences the accuracy of the system. While often in the past only 11 or 12 bits were resolved, recent converters have mostly 16-bit resolution of the signal. For the configuration of the logging system, attention must be paid so that there is enough time available for converting the signals, which must be tuned with the sampling frequency. The high sampling frequencies required for turbulence measurements are close to the limits of the loggers. A basic circuit of a data sampling system is shown in Fig. 6.1.
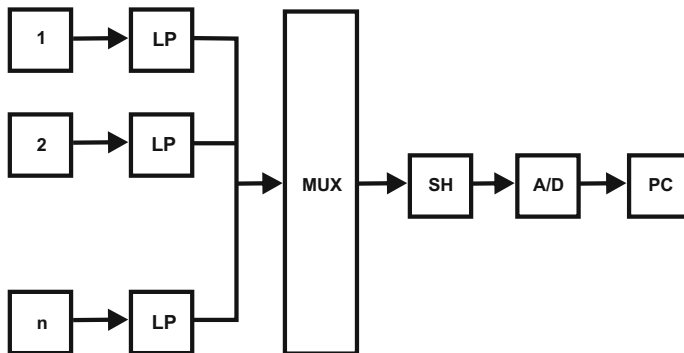

Fig. 6.1 Basic circuit of a data sampling system with 1 to n signals, low passes (LP), multiplexer (MUX), sample and hold circuit (SH), analogue-digital converter (A/D), all integrated in a modern logger and a data collection computer (PC) or storage medium

The analogue-to-digital converter is responsible for the discretization of the signal amplitude. The specification must be dependent on the noise level, S, between the signal level and the mean noise level, where the logarithmic measure $S_{dB} = 10 \lg S$ is used. Using

$$S_{dB} = 1.76 + 6.02n, \qquad (6.1)$$

with the bit resolution, n, of the A/D converter, the minimal distance to the noise level in decibel (dB, see Supplement 6.1) or the separation from the noise level (Profos and Pfeifer 1997) can be determined.

Supplement 6.1 Specification of amplification and damping in decibel

The amplification or damping of a measurement system is given by a logarithmic proportion (Bentley 2005):

$$X_{dB} = 20 \lg \frac{X_2}{X_1} \qquad (S6.1)$$

This ratio is applied for amplifiers with the output voltage X_2 and the input voltage X_1 respectively for the damping of filters. The measurement unit is the logarithmic proportion expressed in decibel (dB). For power (e.g. product of voltage and current) one uses:

$$P_{dB} = 10 \lg \frac{P_2}{P_1} \qquad (S6.2)$$

This measure is also used to express the noise level. If the signal differs from the noise level by factor 10^6, then the distance to the noise level is 60 dB.

6.1.2   Signal Sampling

Micrometeorological data often must be sampled with a high time resolution, e.g. for eddy covariance measurements, the sampling frequency is about 20 Hz. Even for standard meteorological data the sampling rate is 1 Hz. The sampling rate determines the discretization in time. Accordingly, the measured signal must be on the A/D converter a long enough time so that the signal level can be adjusted and digitized. The time difference between two samples depends on the conversion time and the number of measurement channels. The sampling of a periodic function g (t) must be done in such a way that the measured data can be reconstructed for the given sampling time Δt. The necessary number of samples is given by the sampling theorem (Schrüfer et al. 2014):

According to the sampling theorem a function $g(t)$ with sampling values $g(x_i)$ in a time period Δt can be exactly reconstructed, if their Fourier spectra $S(k)$ for $k > \pi/\Delta t$ disappears. The sampling period Δt must be chosen so that $\Delta t < 1/(2 f_g)$ where f_g is the highest resolvable frequency.

This means that periodic oscillations must be sampled more than two times per period or the sampling frequency must be double of the measurement frequency (Bentley 2005; Schrüfer et al. 2014). The frequency

$$f_N = \frac{1}{2\Delta t} > f_g \tag{6.2}$$

is called Nyquist frequency. Therefore, the highest appearing frequency, f_g, must be limited by low pass filtering, and is equal to the frequency where a damping of 3 dB occurs. If higher frequencies nevertheless occur, e.g. by noise of the power frequency, the so-called aliasing effect will appear (Bentley 2005):

The aliasing effect is a false reconstruction of a continuous function $g(t)$ made from discreetly-sampled values $g(x_i)$ with a time resolution of Δt, resulting in higher frequencies appearing as lower ones.

In Fig. 6.2, it is shown that for accurate sampling the function (f1) can be correctly reconstructed while functions with higher frequencies (f2) cannot be reconstructed. In spectra of signals with aliasing the energy of lower frequencies increases ($< f_g$). The increase is equal to the energy of the not-included frequencies above f_g. Therefore, no energy loss happens, but the frequencies are not correctly reconstructed. For frequencies that are not related to the measurement process (electrical power frequency), false measurements occur. If the power frequency cannot filtered, then the sampling frequency should be chosen in such a way that the power frequencies compensate each other, e.g. for 60 Hz power frequency a sampling frequency of 30 Hz and for 50 Hz one of 25 Hz (Kaimal and Finnigan 1994).

Meteorological measurement systems are already low pass filters (see Sect. 4.2.3.3). Due to the finite extension of the sensors, the only turbulence elements that can be measured are larger than or equal to the measurement path d. Furthermore, due to the turbulence spectrum the filter frequency depends on the wind velocity and the measurement height. As a simple approximation for the upper frequency limit with 10% damping and a height of 5–10 m, one can use according to Mitsuta (1966):
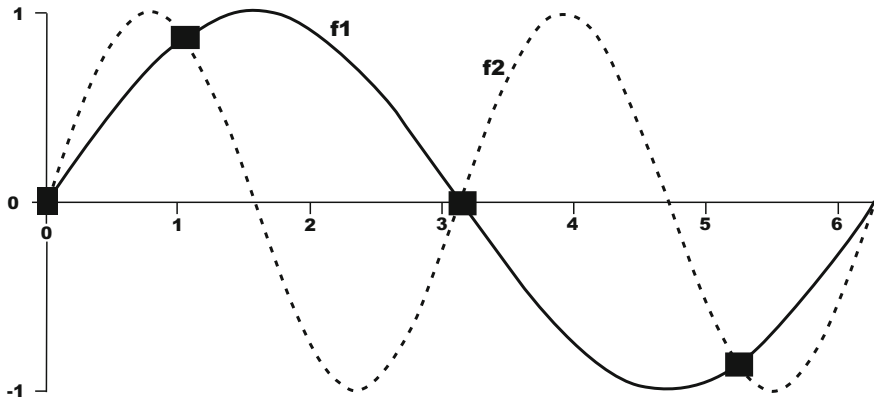
$$f_{g10\%} = \frac{u}{d} \tag{6.3}$$

Fig. 6.2 Sampling of periodic signals: f1 is correctly represented in contrast to f2

Another simple approximation with the wind velocity and the measurement height (Kaimal and Finnigan 1994) is:

$$f_g > 8\frac{\overline{u}}{z} \tag{6.4}$$

The length of a measured time series depends on the lowest frequency of the turbulence spectrum to be constructed. Attention must be paid so that for an acceptable accuracy of the standard deviations and covariances a minimum of samples is necessary. According to Haugen (1978), this is at least 1000, and is illustrated for different quantities in Fig. 6.3. In the case of statistical independence, the error is approximately $N^{-1/2}$ (N: umber of samples). Because the independence of time series is generally uncertain a higher error must be assumed (Bartels 1935; Taubenheim 1969).

For spectral analysis, the length of the necessary time series is determined by the accuracy of the low frequency part of the spectrum. Assuming an error of 10%, the length, T, must be chosen so that either it is the 10 times the longest period to reconstruct or the lower frequency limit given by $f_{gl} = 10/T$ (Taubenheim 1969). This measurement length is generally significantly longer than those for the error calculation for standard deviations and covariances.

6.1.3 Transfer Function

In addition to inadequate sampling of the measurement signal an inadequate resolution in time and space of the sensor itself can also cause measurement errors. A transfer function of a measurement system describes the time delay between the output signal and the input signal (phase shift) and the damping of the amplitude.
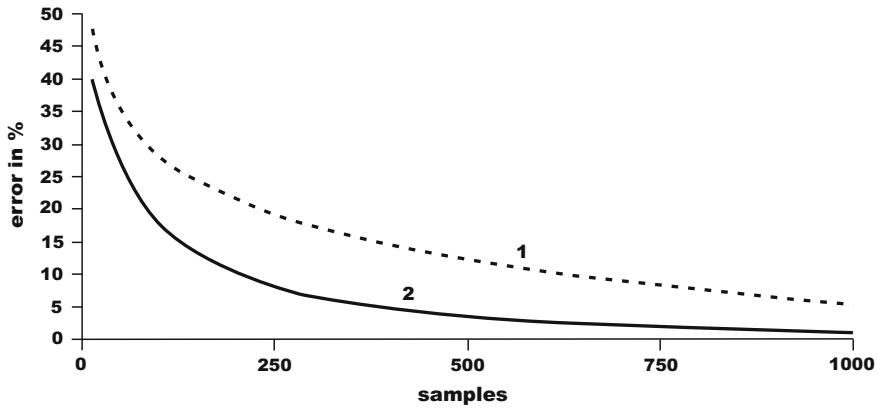
Fig. 6.3 Error in the measurements of (*1*) the friction velocity or the sensible heat flux; (*2*) error in the standard deviation of the vertical wind component as functions of the number of samples. Processed on the basis of the results of Haugen (1978)

A transfer function can be defined in the space of the complex Laplace operator $s = \delta + i\omega$, with δ as a damping parameter (see Supplement 6.2):

$$T(s) = \frac{L\{X_s(T)\}}{L\{X_i(T)\}} \tag{6.5}$$

The determination of the Laplace transform of the sensor output signal, X_s, from the Laplace transform of the input signal, X_i, is given by:

$$X_s(s) = X_i(s)T(s) \tag{6.6}$$

This description is very simple for many practical applications. For example, the product of the single functions can determine the transfer function of a measurement system. For a turbulence measurement system, the transfer function can be determined as the product of the transfer functions of the response in time, of the averaging by the sensor in space, and by the averaging in space of sensors that are used for eddy-covariance measurements at a certain distance (Eq. 4.49).

The error of a standard deviation or of a flux is given by the ratio of the spectrum multiplied with the transfer function to the undamped spectrum:

$$\frac{\Delta F}{F} = 1 - \frac{\int\limits_0^\infty T_{x(y)}(f)S_{x(y)}(f)df}{\int\limits_0^\infty S_{x(y)}(f)df} \tag{6.7}$$
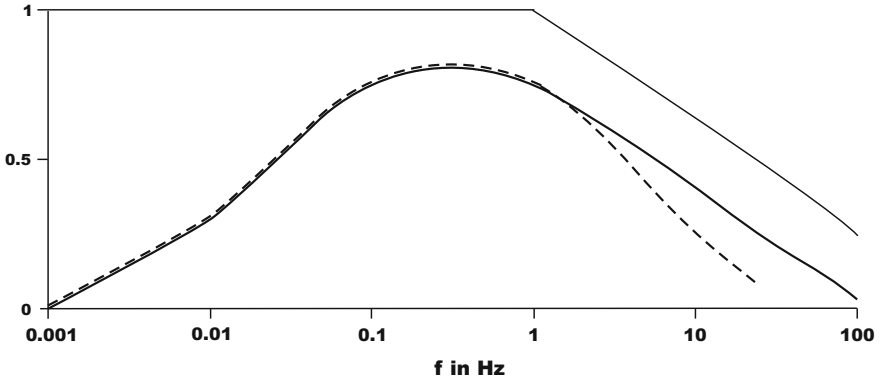
Fig. 6.4 Schematic graph of the transfer function T (*thin line*) and the turbulence spectra S (*thick line*) with the resulting spectra $T\,S$ (*dotted line*)

Figure 6.4 shows schematically that the turbulence spectrum is reduced if the transfer function is less than one. Because in most of the cases the damping starts in the inertial subrange, the correction of turbulence measurements for well-known turbulence spectra is relatively simple. The spectrum in the inertial subrange is extrapolated or corrected relative to the modelled spectra, e.g. Moore (1986).

Supplement 6.2 Laplace transformation

In contrast to the Fourier transformation (see Supplement 2.3), which is a function of circular frequency, the Laplace transform transformation of an aperiodic signal, which disappears for $t < 0$, is a function of a complex operator $s = \delta + i\omega$ (Bentley 2005). The Laplace transformed L is defined as:

$$X(s) = L\{X(t)\} = \int_{0}^{\infty} X(t)\, e^{-st} dt \qquad (S6.3)$$

For the backward transformation is:

$$X(t) = L^{-1}\{X(s)\} = \frac{1}{2\pi i} \int_{s=\delta-i\omega}^{\delta+i\omega} X(s)\, e^{st} ds \qquad (S6.4)$$

A benefit of the Laplace transformation is that extensive tables and software for the determination of the transformation are available (Doetsch 1985; Graf 2004).

6.1.4 Inertia of a Measurement System

A special case of a transfer function is the sharp change of the signal from $X = X_0$ for $t \leq t_0$ to $X = X_\infty$ for $t > t_0$. A first-order measurement system, e.g. temperature measurements, can be described by the differential equation (Profos and Pfeifer 1997; Brock and Richardson 2001):

$$X_s(t) = X_i(t) + \tau \frac{dX_i}{dt} \tag{6.8}$$

The dependency of the input X_i and output X_s signals can be presented with the time constant τ. To have an indicator number, which is dependent only on the sensor and not on the size of the quantity for different meteorological systems, different indicator numbers are used. For second order measurement systems (wind vane) see DeFelice (1998) or Brock and Richardson (2001).

6.1.4.1 Time Constant

For a first order measurement systems and assuming $X_0 = 0$ the differential equation Eq. (6.8) has an exponential solution

$$X(t) = X_\infty \left(1 - e^{-\frac{t}{\tau}} \right), \tag{6.9}$$

where X_∞ is the final value after complete adjustment to the surrounding conditions and τ is the time constant which is a measure of the inertia of the measurement system:

> The time constant of a measurement system is the time required for the measurement system to reach 63% of its final or equilibrium value. The value of 63% is equal to $(1 - 1/e)$.

To determine the real final value due to a sharp change of the input signal, it is necessary to measure significantly longer than the time constant. This value depends on the required accuracy, and should be at least five times the time constant. The response of the measurement signal after a sharp change is schematically shown in Fig. 6.5.

6.1.4.2 Distance Constant

Anemometers have a wind-speed dependent time constant, i.e. time constants are not representative specifications for anemometers. Instead, a distance constant, can
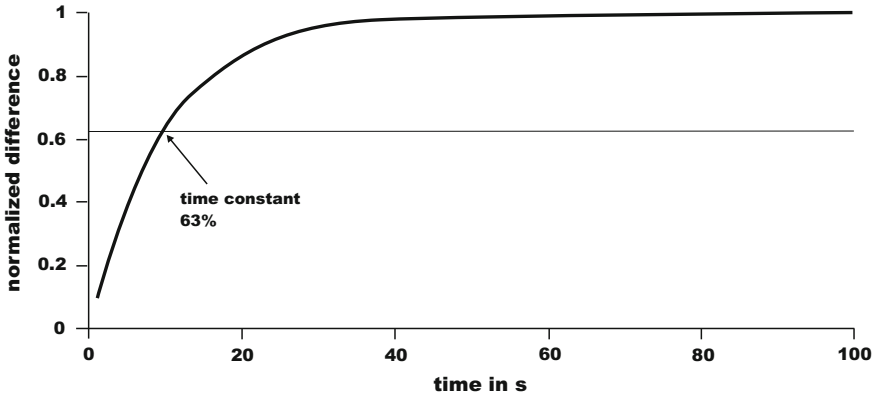
Fig. 6.5 Schematic graph for the documentation of the time constant for a change of the measured signal by a normalized signal difference

be defined, which allows comparing the time performance of different anemometers independent of wind speed:

> The distance constant is the length of the wind path necessary for the anemometer to reach 63% of the final velocity.

The relation between the time constant and the distance constant L can be calculated with the final velocity V_∞:

$$L = V_\infty \cdot \tau \tag{6.10}$$

6.1.4.3   Dynamic Error

The time constant describes the dynamic error of a measurement system. The typical case in meteorology of dynamic errors is, when a nearly linear change of the meteorological element occurs over a given time span. Instead of a change in time, a change in space is also possible which is typical for moving measurement systems such as radiosondes and tethersondes. For this case, Eq. (6.8) can be written in the form (Brock and Richardson 2001):
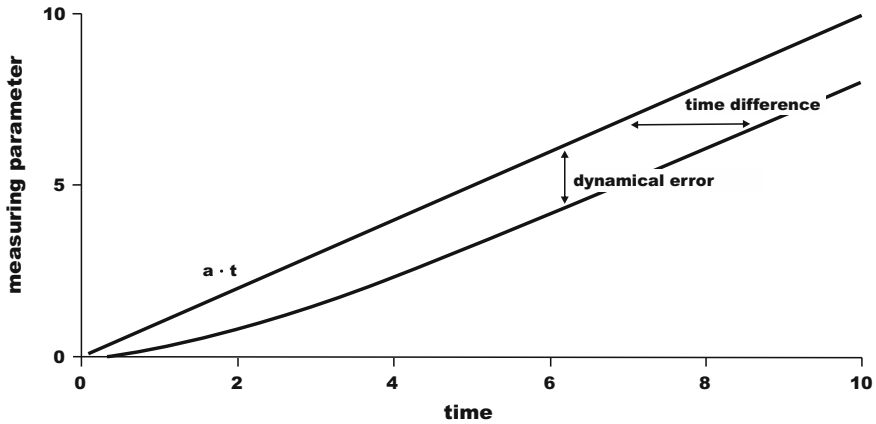
$$a \cdot t = X_i(t) + \tau \frac{dX_i}{dt} \tag{6.11}$$

Fig. 6.6 Schematically graph of the dynamical error and of the time difference by a linear change of the input signal

The solution of this equation is:

$$X(t) = a\,t - a\,\tau\left(1 - \mathrm{e}^{-\frac{t}{\tau}}\right) \tag{6.12}$$

The second term on the right-hand-side in Eq. (6.12) is responsible for the lag in the measured signal relative to the input signal and is called dynamical error:

$$\Delta X_d(t) = a\,\tau\left(1 - \mathrm{e}^{-\frac{t}{\tau}}\right) \tag{6.13}$$

In the case of an input signal linearly varying with time, the output signal is shifted in relation to the input signal by the time difference $\Delta t = \tau$. The dynamic error is schematically shown in Fig. 6.6. Often dynamic errors are a reason for hysteresis.

For known input signal functions, the dynamic error can be easily corrected either mathematically or by correction networks. This may be relevant for the exact determination of the temperature gradient of an inversion layer of small vertical thickness. For measurements near the earth's surface this was also demonstrated for vertically (Mayer et al. 2009) and horizontally (Hübner et al. 2014) moving measurement systems.

6.2 Measurement of Meteorological Elements

Measurements in the atmosphere are different to other media, because of the influence of the wind field. Thus, atmospheric measurements are not point measurements. Rather turbulent eddies are measured, which move within a certain time

interval through the measurement volume. These eddies originate on the windward site of the sensor and can be attributed to a certain source area. These source areas are quite large for scalars and for fluxes their dimension is still of the order of 100 times the measurement height. Their exact determination is possible with footprint models (see Sect. 3.4). Consequently, some requirements for meteorological measurements are necessary.

Standard measurements in meteorological networks are made according to the international guide of the World Meteorological Organization (WMO 2008). Often, such regulations are extensive in order to guaranty a high and constant data quality for climate and environmental monitoring stations (see Appendix A.6). In contrast, at weather stations, which supply only data for weather forecasts or for the current weather state (nowcasting), less accurate sensors can be used. Research and special practical applications require specialized measurement stations (VDI 2006), which are listed in Table 6.1. The typical parameters collected at such sites are given in Appendix A.6.

Micrometeorological measurements are related to the meteorological scales according to Orlanski (1975) (see Fig. 1.2). These relations are relevant as well for

Table 6.1 Classification of meteorological measurement stations (VDI 2006), except stations of meteorological services which are classified by WMO (2008)

Number	Indication	Feature
1	Agrometeorological station	Agrometeorological basic parameters e.g. for the determination of evaporation
2	Microclimatological or micrometeorological station	Miscellaneous application with different instrumentations, e.g. biometeorological measurements
3	Micrometeorological station with turbulence measurements	Including eddy-covariance measurements for research purposes
4	Air pollution stations	Determination of parameters for air pollution calculations; with additional meteorological measurements
5	Disposal site stations	Mainly for the determination of the water balance
6	Noise station	Determination of parameters (mainly wind) for the meteorological influence (ISO 1996)
7	Roadside station	Measurement of meteorological elements which may affect the traffic
8	Hydrological station	Mainly precipitation measurements
9	Forest climate station	Measurement of meteorological elements in clearing and below trees
10	Nowcasting station	Measurement of the actual weather state, e.g. with present weather sensors
11	"Hobby station"	Measurement of meteorological elements with simple sensors but according the relevant installation instructions

Table 6.2 Assignment of direct and remote sensing systems to meteorological scales (the grey shading shows the degree of scale assignment)

Sensor system	macro	meso			micro		
	β	α	β	γ	α	β	γ
Radio sonde	▓	▓					
Boundary layer sonde			▓	▓			
Tower > 100 m			�(light)	▓			
Mast < 50 m				▓(light)	▓	▓	
Turbulence sensors					▓	▓	▓
Satellite (vertical resolved)	▓						
Wind profiler		▓	▓	▓(light)			
Sodar			▓	▓			
RASS			▓	▓			
Lidar			▓	▓			

Table 6.3 Assignment of scales of models to the necessary resolution of input parameters (the grey shading shows the degree of scale assignment)

Resolving structures	macro	meso			micro		
	β	α	β	γ	α	β	γ
Horizontal fields	▓	▓	▓(light)	▓(light)			
Vertical distributions			▓(light)	▓	▓	▓(dark)	▓(dark)
Boundary layer parameters		▓(light)	▓(light)	▓	▓(dark)	▓(dark)	▓(dark)
Specified surface layer parameters				▓(light)	▓	▓(dark)	▓(dark)

both in situ and remote sensing measurement techniques (Table 6.2). In the case of in situ techniques the sensor mast determines the scale.

Knowing the scale of the measurement systems is very important if the data are used as input parameters of models. The smaller the scales of the models, the greater the importance of vertical structures, boundary layer structures, and soil layer conditions (Table 6.3).

6.2.1 Radiation Measurements

Most radiation sensors are based on the principle of a radiation-caused heating and therefore an increase of the surface temperature of a receptor. For absolute devices (used for calibration) the temperature is directly measured on a black receiver

surface, which is irradiated without any filters directly by the sun. Due to the selective measurement of the direct sun radiation, the longwave radiation can be neglected, and therefore absolute devices measure only the shortwave radiation. Relative devices measure the temperature difference between two different irradiated areas one black and one white. Nowadays, silicon sensors are also available. Furthermore radiation sensors are classified depending on if they measure radiation from the half space or directed (from the sun) and if they measure short or long wave radiation. For measurements of the short wave diffuse radiation the sun is shadowed. Net radiometers measure the upper and lower half space. The possible spectral range can be selected by the material, which is used for the dome (receiver protection). Domes made of quartz glass are only permeable for short wave radiation (0.3–3.0 μm). For measurements of short and longwave radiation (0.3–100 μm) domes with Lupolen (special polyethylene) are used, and for longwave radiation (5.0–100 μm) domes made from silicon are used. The spectral gap region (3.0–5.0 μm) is accounted for in the calibration of the longwave radiation sensors but it has no significant influence on the measurements due to the low amount of energy in this range. Using a special set of filters or spectrally sensitive photoelectric cells, the photosynthetic active radiation (PAR) can be measured. PAR has dimensions of $\mu\text{mol m}^{-2}\text{s}^{-1}$, and the numerical value is approximately twice the numerical value of the global radiation in Wm^{-2}. Radiation instruments working in the small or large atmospheric window of the longwave range and a relatively small dihedral angle are used for measuring surface temperature. An overview is given in Table 6.4.

Table 6.4 Classification of radiation sensors

Measurement device	Sensor type		Wave length		Opening angle	
	absolute	relative	short wave	long wave	half space	directed
Absolute radiometer	x		x			x
Pyrheliometer		x	x			x
Pyranometer		x	x		x	
Albedometer		x	x		x[a]	
Pyrgeometer		x		x	x	
Net pyrgeometer		x		x	x[a]	
Radiometer		x	x	x	x	
Net radiometer		x	x	x	x[a]	
PAR radiation sensor		x	x (partly)		x	
IR radiation thermometer		x		x		x

[a]upper and lower half space

Table 6.5 Quality requirements for pyranometers (ISO 1990; WMO 2008), percents are related to the full measurement range

Property	Secondary standard	First class	Second class
Time constant (99%)	<15 s	<30 s	<60 s
Offset (200 W m^{-2})	±10 W m^{-2}	±15 W m^{-2}	±40 W m^{-2}
Resolution	±1 W m^{-2}	±5 W m^{-2}	±10 W m^{-2}
Long term stability	±1%	±2%	±5%
Non-linearity	±0.5%	±2%	±5%
Cosine response 10° solar elevation, clear	±3%	±7%	±15%
Spectral sensitivity	±2%	±5%	±10%
Temperature response	±1%	±2%	±5%

In the last 15–20 years, remarkable progress was achieved regarding the accuracy of radiation sensors. This success is based on the classification of radiation sensors by the World Meteorological Organization (Kasten 1985; WMO 2008) with clear guidelines for the error limits (Table 6.5) and also on the creation of the Basic Surface Radiation Network (BSRN) of the World Climate Research Program with a well-formulated quality control scheme (Gilgen et al. 1994; Ohmura et al. 1998). Therefore, the world radiation centre in Davos (Schwitzerland) maintains a collection of sensors called the World Radiation Reference. The other world centers regularly compare their Primary Standard devices (ISO 1990) with this reference. Regional and national radiation centres should compare their Secondary Standard devices with the world centres at least every 5 years. Currently, the widely used pyranometers PSP (Eppley Lab. Inc., USA), CM11, and especially CM21 (producer: Kipp & Zonen, The Netherlands) conform to the Secondary Standard.

For radiation sensors, a cosine correction is of special importance because the radiation power does not exactly follow the cosine of the solar angle of incidence. The reasons for the corrections are the unequal thickness of the domes and the changing thickness of the atmosphere with changes of the angle of incidence. Therefore, the exact horizontal levelling of the sensor and the clearness of the domes should be controlled.

In any case, the radiation instruments should be permanent (1–3 years) compared with national sensors for comparison (etalon). Because Secondary Standard devises are widely used, the comparisons with the sensors of different users are possible.

In contrast to shortwave radiation sensors, longwave radiation sensors are insufficiently calibrated. Serious differences were pointed out by Halldin and Lindroth (1992). While shortwave radiation sensors can be calibrated relatively easily against sun or with a lamp of defined radiation, calibration of longwave radiation sensors requires that radiation of the sensors themselves must be taken into account. The measured signal is simply the difference between the incoming longwave radiation and the longwave radiation of the housing in the form

$$I \downarrow = \frac{U_{rec}}{C} + k\sigma_{SB}T_G^4, \tag{6.14}$$

where U_{rec} is the voltage measured at the receiver, C and k are calibration coefficients, and T_G is the housing temperature which must be measured.

Progress in sensor development was made by Philipona et al. (1995), who installed thermistors in the silicone domes of the longwave radiation sensor to measure the temperature of the dome to correct the effects of dome temperature and local heating by shortwave radiation. The correction requires the temperatures of the housing and the dome (T_D):

$$I \downarrow = \frac{U_{rec}}{C}\left(1 + k_1\sigma_{SB}T_G^3\right) + k_2\sigma_{SB}T_G^4 - k_3\sigma_{SB}\left(T_D^4 - T_G^4\right) \tag{6.15}$$

To take into account the influence of the shortwave radiation, the so-called *f*-correction (Philipona et al. 1995) is added in Eq. (6.15), where the temperature differences between the North and South, North and Southeast, and North and Southwest sides of the dome must be considered. The *f*-correction is nowadays not very often applied because the accuracy of the temperature measurements is not good enough and cross-sensitivities occur. Good pyrgeometers can reach an accuracy of ± 2 Wm^{-2} if they are carefully calibrated according to Eq. (6.15) (Philipona et al. 2001), which is comparable with the characteristics of pyranometers.

In micrometeorology, net radiation measurements are highly relevant, and thus a high accuracy is required. Instead of the formerly used radiometers, which measured the short and longwave radiation together, sensors that measure all four radiation components are now quite common (Fig. 6.7). Of special importance is the ventilation of the sensor such that the body temperature, which is measured with a temperature sensor (Eq. 6.14), is uniform. As an additional effect, the ventilation averts dew formation on the calottes, which tampers the radiation fluxes in the morning hours.

Fig. 6.7 Net radiometer CNR4 with two as albedometer installed pyranometern (*right*) and pyrgeometern (*middle*) and a common ventilation (published with kind permission of © Kipp & Zonen, All rights reserved)

Net radiometer measurements must also meet some requirements regarding the underlying surface: It should be homogeneous to avoid errors it should reflect or emit the entire radiation from the lower half space. According to Latimer (1972), for an installation height of 2 m 90% of the radiation comes from a circle with a 12 m diameter, 95% from a circle of 18 m diameter, and 99% from a circle of 40 m diameter. This relationship is linear and the proportionality factor between the measurement height and the diameter of the circle is 6, 9, and 20.

6.2.2   Wind Measurements

Classical wind measurement devices are based on a mechanical principle, where the wind path is transformed into a rotation movement. Over the last 10 years, the application of ultra sonic anemometers that transmit and receive sound signals have become more common and have started to replace traditional rotation anemometers. Also remote sensing methods with e.g. radar became more widespread. The sensors can be further classified based on whether they can be used for standard measurements or for turbulence measurements using the eddy-covariance method. An overview is given in Table 6.6.

For mechanical anemometers (Fig. 6.8), the knowledge of the transfer function between the velocity in a wind tunnel and the velocity measured with the anemometer is of high importance, which must be determined in the wind tunnel (ISO 2007):

> The transfer function is the linear dependence between the wind velocity and the rotation velocity of the anemometer within a defined working range.

This calibration relation is linear over a wide range of velocities, but for low velocities (<2–4 ms^{-1}) is exponential. This is shown in Fig. 6.9 where c is the threshold velocity, which should not be confused with the intersection of the linearly extrapolated transfer function to the point with zero revolutions, a:

Table 6.6 Classification of wind sensors (anemometer)

Type of sensor	Measurement principle				Application	
	Mech.	Sound	Therm.	Other	Mean	Turb.
Cup anemometer	x				x	
Propeller anemometer	x				x	(x)
Hot wire anemometer			x			x
Sonic anemometer		x			x	x
Laser anemometer				x	(x)	x

Fig. 6.8 Cup anemometer (published with kind permission of © Th. Friedrichs & Co., Schenefeld near Hamburg,)

> The threshold velocity of a rotating anemometer is the lowest wind speed that transfers the rotating anemometer into a continuous movement.

Beyond the threshold velocity (about 0.1–0.3 m s^{-1}), the so-called distance constant is important. It is a measure of inertia, and gives the necessary wind path required for an anemometer to register 63% of a wind velocity difference (see Sect. 6.1.4.2). The distance constant is an important parameter for mechanical anemometers; for sensitive propeller anemometers it is about 1 m; for small cup anemometers it is about 2–3 m, and for larger anemometers it is about 5 m. Note that sonic and hot wire anemometers in the usual application range are free of inertia. The distance constant should be used for the assessment of the measurement quality instead of the threshold velocity, because the starting velocity is generally within a range below 0.5–1.0 ms^{-1}, where the turbulent wind field is not fully developed.

In a turbulent flow, additional problems for mechanical anemometers exist (Kristensen 1998). With increasing distance constant, the wind velocity will be overestimated due to the mechanical inertia (over speeding):

> Overspeeding is the turbulence-caused over estimation of the measured wind velocity relative to the true wind velocity.
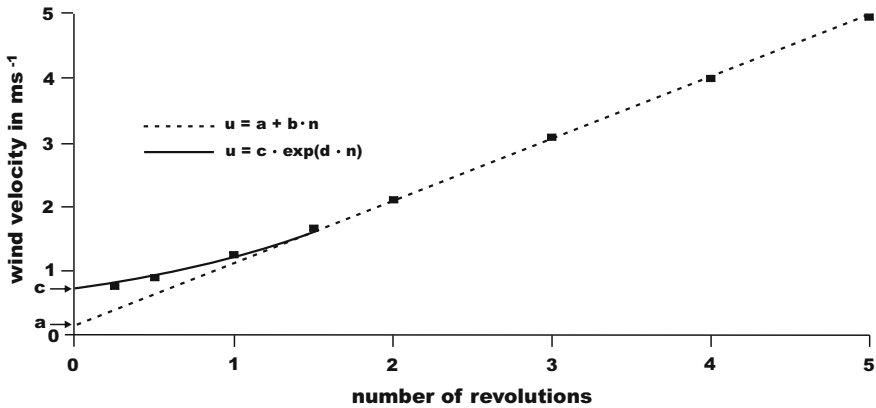
Fig. 6.9 Transfer function of a cup anemometer (VDI 2000) with n: number of revolutions of the anemometer, u: wind velocity and a, b, c and d: constants. Adapted with kind permission of © VDI e.V. and Beuth-Verlag, Berlin 2000, All rights reserved

Wind gusts will bring a mechanical anemometer into high rotation; however, after the gust the anemometer will require some time to adjust to the lower wind speeds. There is no compensation of these additional rotations in the case of low wind speeds. Overspeeding can be as large as 10% of the wind velocity, and is particularly large for low wind velocities and high distance constants. The value is proportional to $(\sigma_u/u)^2$. For micrometeorological measurements it is especially important that the overspeeding is small because otherwise wind gradients near the ground will be inaccurate.

The cosine response of an anemometer is of importance:

> The cosine response is the ratio of the measured wind velocity for a special angle of incidence to the wind velocity of the horizontal wind field multiplied by the cosine of the angle.

$$F(\alpha) = \frac{u(\alpha)}{u(0) \cdot \cos \alpha} \tag{6.16}$$

An ideal cosine response is given by $F(\alpha) = 1$. For propeller anemometers, deviations up to 15% occur for incidence angles of about 45° (Figs. 6.10 and 6.11). These deviations can be relatively simply corrected with the relation:

$$u_{korr}(\alpha) = u_{mess}(\alpha) \cdot [\cos \alpha - a \cdot \sin(2\alpha)] \tag{6.17}$$

where $a = 0.085$ (Drinkov 1972) or $a = 0.140 - 0.009\, u$ (Foken et al. 1983). For crosswinds, a dead zone of approximately $\pm 2°$ exists where the propeller does not
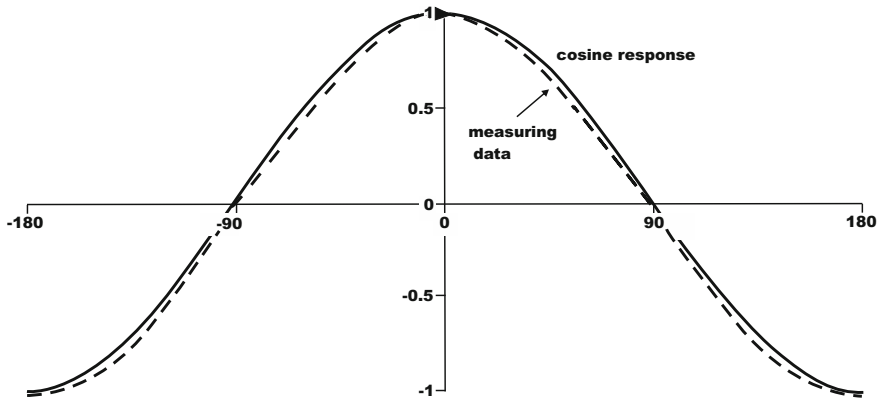
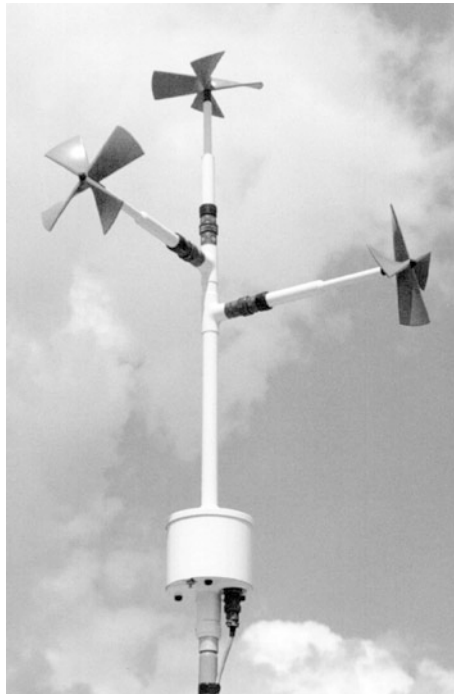**Fig. 6.10** Cosine response of a propeller anemometer

Fig. 6.11 UVW three-component propeller anemometer by Gill, model 27005T (published with kind permission of © R. M. YOUNG Company/GWU-Umwelttechnik GmbH, All rights reserved)

rotate. For measurements of the vertical wind, the dead zone is overcome with two inclined sensors. A shank extension is recommended for flow from the front (Bowen and Teunissen 1986) so that the dynamical conditions of a propeller for flow from the front and behind are nearly identical.

For cup anemometers, a cosine response cannot be assumed. If the inclination of the flow is not very great, then nearly the same wind velocity is always measured. This means that for an inclined flow the cup anemometers overestimate the wind velocity (Brock and Richardson 2001).

The first sonic anemometers used the phase shift method (Bovscheverov and Voronov 1960; Kaimal and Businger 1963). In this method, the ultrasonic signal of the transmitter is received at several points, and the phase difference between the transmitted and received signals is a function of wind velocity. The disadvantage of this method is that for different wind velocities (5–10 ms^{-1} steps) identical values will be observed, but the sound wave is shifted several times of 2π.

Modern sonic anemometers use the travel time principle and a direct time determination (Hanafusa et al. 1982). In this method, a sonic signal (about 100 kHz) is transmitted from both sides of a measurement path and received on the opposite sides. Due to the wind velocity, one signal is faster than the other. The exact travel times of the sonic signals are used for the determination of the wind velocity:

$$t_{1,2} = \frac{\sqrt{c^2 - u_n^2} \pm u_d}{c^2 - u^2}\, d \qquad (6.18)$$

where d is the path length, u_d is the wind component along the path, u_n is the normal component of the wind, and c is the sound speed. This relation is based on the assumption that the flow in the sonic anemometer is generally slightly shifted by an angle γ from the measurement path (Fig. 6.12), and for the travel times follows (Kaimal and Finnigan 1994; Brock and Richardson 2001):

$$t_{1,2} = \frac{d}{c\,\cos\gamma \pm u_d} \qquad (6.19)$$

The difference of the reciprocal travel times gives the wind velocity and the sum of the reciprocal travel times gives the sound velocity:
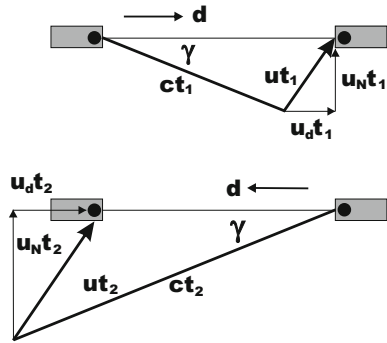
$$\frac{1}{t_1} - \frac{1}{t_2} = \frac{2}{d}\,u_d \qquad (6.20)$$

$$\frac{1}{t_1} + \frac{1}{t_2} = \frac{2}{d}\,c\,\sqrt{1 - \frac{u_n^2}{c^2}} \approx \frac{2}{d}\,c \qquad (6.21)$$

The first sonic anemometers with the travel time principle (Mitsuta 1966) could only measure the time difference. Measuring the wind velocity depended on the sound velocity and therefore on the temperature and the moisture:

$$c^2 = 403T(1 + 0.32\,e/p) \qquad (6.22)$$

Fig. 6.12 Vector graph of the sound paths of a sonic anemometer

From this equation the so-called sonic temperature can be calculated (Kaimal and Gaynor 1991), which is similar to the virtual temperature:

$$T_s = T(1 + 0.32e/p) = \frac{d^2}{1612}\left(\frac{1}{t_1} + \frac{1}{t_2}\right)^2 \tag{6.23}$$

A recalculation into the true temperature is possible by applying the geometric parameters of the sonic anemometer (see Sect. 4.2.3.5).

Initially, the measurement paths of the sonic anemometers were predominantly Cartesian orientated (Mitsuta 1966; Hanafusa et al. 1982). Modern sonic anemometers have increased angles of the measurement paths, e.g. 120° (Fig. 6.13)

Fig. 6.13 Sonic anemometer CSAT3 (Campbell Sci. Inc.) with inclined measurement paths and large inflow sector; additionally an IR gas analyzer LI7500 (Li-Cor) is mounted (*Photograph* Foken)
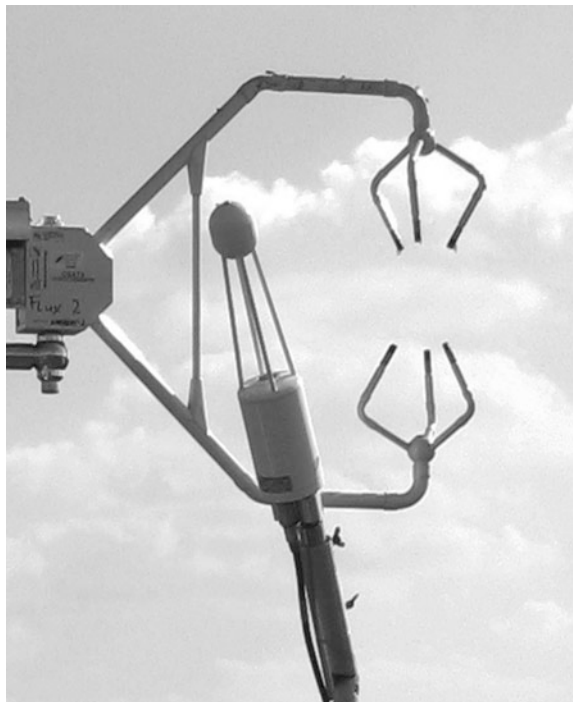
Fig. 6.14 Sonic anemometer
USA-1 with inclined paths
and omni-directional
construction (published with
kind permission of © METEK
GmbH, Elmshorn, All rights
reserved)

so as to get lower flow distortion. Also, sensors were developed, which can be used
for all flow directions (omni-directional, Fig. 6.14). A problem yet to be investi-
gated, is the significant self-correlation of the Cartesian wind components from the
inclined wind components, which influences the statistical independence for the
calculation of the covariances.

The calibration of sonic anemometers is very stable. However, before the
application a zero-point test should be done in a closed chamber (ISO 2002). Due to
the construction of the anemometer a reduction of the wind field is possible. In a
turbulent flow, the errors due to flow distortion are often smaller than those for the
laminar flow in the wind tunnel. Therefore, the application of the wind tunnel
correction may lead to an overcorrection. For flux measurements, it is important that
there are no sensor mountings below the measurement path for the vertical wind
component, otherwise flow corrections up to 10% are possible. For more details see
Sect. 4.2.3.2.

The number of different sonic anemometer types has increased in the last few
years. Thus, a type of classification is necessary, which is given in Table 6.7. The
accuracy is not only dependent on the type of the sonic anemometer but also on the
turbulent flow field. This influence can be taken into account by data quality
investigations (see Sects. 4.2.5, 4.2.7, and Table 4.14).

Table 6.7 Classification of sonic anemometers (based on a classification by Foken and Oncley 1995; Mauder et al. 2006)

Anemometer class		Sensor type
A	Basic research	Kaijo-Denki typ A
		Campbell CSAT3, Gill HS
B	General use for flux measurements	Kaijo-Denki typ B
		Gill Wind Master, R2, R3
		METEK USA-1, Young 81000
C	General use for wind measurements	Sensors of class B
		2D-anemometer of different producers

6.2.3 Temperature and Humidity Measurements

6.2.3.1 General Statements

The classical mercury thermometers (recently liquid-in-glass thermometers with alcohol), bimetal thermometers, and hair hygrometers have mostly been replaced by electrical measurement principles. The measurement of electrical resistance is used most frequently for temperature measurements. Thermocouples and thermistors are reserved mostly for special measurements with small sensors. Due to the temperature sensitivity of the sound velocity, sonic anemometers are often used for temperature measurements (remark: the sonic temperature is not absolutely equal to the temperature, see Sect. 4.2.3.5). For humidity measurements, ceramic material or polymers are used to measure the relative humidity, and optical techniques are used to measure the absolute humidity. The dew point temperature is measured by detecting condensation on a chilled mirror. An overview is given in Table 6.8

Table 6.8 Classification of temperature (T) and humidity sensors (H)

Type of sensor	Measurement principle				Application	
	Therm.	Electr.	Optical	Other	Mean	Turb.
Psychrometer (T,H)	x	x			x	
Liquate-in-glass thermometer (T)	x				x	
Bimetal thermometer	x				x	
Resistance thermometer (T)		x			x	(x)
Thermistor (T)		x			x	
Thermocouple (T)		x			x	(x)
Sonic thermometer (T)				x	x	x
Hair hygrometer (H)				x	x	
Capacity hygrometer (H)		x			x	
Dew point hygrometer (H)		x		x	x	
Infrared hygrometer ((H)			x		(x)	x
Ultraviolet hygrometer (H)			x			x

Table 6.9 Time constant of temperature and humidity measurement systems

Type of sensor	Time constant in s
Sonic thermometer	<0.01
Optical humidity measurement system	<0.01
Thin resistance wires (<20 μm)	<0.01
Thermocouples (<20 μm)	<0.01
Thermistors	0.1–1
Resistance thermometers	10–30
Liquate-in-glass thermometers	80–150

where it is also indicated if the sensor can be used for the observation of mean or turbulent quantities.

An important parameter for temperature and moisture sensors is the time constant (see Sect. 6.1.4.1). Typical time constants are given in Table 6.9. It is seen that the wet sensors (e.g. at a psychrometer) are less inert than dry sensors.

6.2.3.2 Temperature Measurement

Accurate measurements of the true air temperature are one of the most challenging problems in meteorology. Even today, it is worth reading the paper by Albrecht (1927). While improved technical possibilities are available, the measurement problems are often significantly underestimated. Because temperature sensors warm if they are exposed to radiation, they work better as a radiation sensor than a temperature sensor. Therefore, at least the incidence of direct solar radiation on the sensor must be eliminated. Furthermore, the thermometer must be ventilated to prevent heating and to promote turbulent exchange of heat. Both of these requirements are realized (ideally) with Assmann's aspirated psychrometer (Assmann 1887, 1888; Sonntag 1966–1968, 1994). The device consists of two thermometers ventilated at a rate >2.5 ms^{-1} and equipped with a double radiation shield. There are several duplicated sensors available, whereby not all have the quality of the original sensor. Even electrical versions of the sensor are most accurate if Assmann's dimensions of the double radiation shield are met and if the ventilation velocity is larger than 2.5 ms^{-1} (Fig. 6.15, Frankenberger 1951).

Given the difficulties in measuring temperature, measurement accuracy outside of closed rooms is typically about 0.1 K, and only for very well maintained devices the accuracy can reach 0.05 K. Therefore, the errors due to radiation and turbulence conditions are much greater than the possibilities of the recent electrical measurement techniques (<0.001 K).

The radiation influence on the temperature measurement is called radiation error and can be estimated as an additional heating by the absorption of radiation by the sensor. This heating depends on the Prandtl number,

Fig. 6.15 Electrical aspiration psychrometer according to Frankenberger (1951) (published with kind permission of © Th. Friedrichs & Co., Schenefeld near Hamburg,

$$Pr = v/a_T \tag{6.24}$$

which is the ratio of the kinematic viscosity to the molecular thermal conductivity and has the value 0.71 for air; the Reynolds number (Eq. 2.20), which is the ratio of inertial forces to frictional forces (see Sect. 2.1.2); and the Nusselt number,

$$Nu = f(Re, Pr) \tag{6.25}$$

which is a function of the heat conductance and the flow characteristics. The radiation error is therefore a function of the radiation balance at the sensor surface Q_s, the sensor surface area F, and the heat transfer properties, α,

$$Sf = \frac{Q_s}{\alpha F} \tag{6.26}$$

where

$$\alpha = \frac{Nu\,\lambda}{d}, \tag{6.27}$$

$$Q_s = a\,K \downarrow F_R, \tag{6.28}$$

and a is the absorption capacity of the surface, λ is the molecular heat transfer number, d is the sensor length, and F_R is the area affected directly by the radiation.
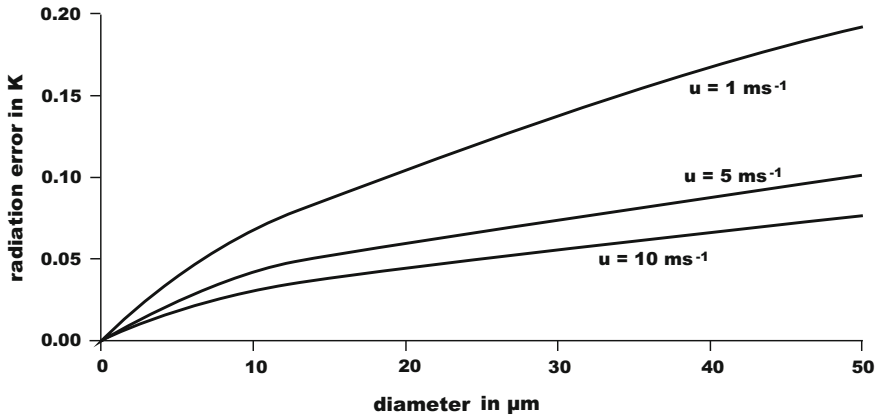
Fig. 6.16 Radiation error of thin platinum wires for $K\downarrow = 800$ W m^{-2} and $a = 0.5$ (adapted from Foken 1979, with kind permission of © Wiley-VCH, Weinheim 1979, All rights reserved)

For forced convection $(0.01 < Re < 10,000)$ it follows (van der Hegge Zijnen 1956) that:

$$
\begin{aligned}
Nu &= 0.42 \, Pr^{0.2} + 0.57 \, Pr^{0.33} Re^{0.5} \\
Nu_{air} &= 0.39 + 0.51 \, Re^{0.5}
\end{aligned}
\tag{6.29}
$$

For the absorption capacity of platinum $(a = 0.5)$, the radiation errors are given in Fig. 6.16. Thus, radiation errors below 0.1 K are realized only for wire diameters <20 µm.

The radiation error can be excluded only for very thin and spread-out resistance wires and for thermocouples of the same dimension. The use of thin resistance wires for turbulence measurements is based on Kretschmer (1954). Extensive investigations of the use of resistance wires were made, for example, by Tsvang (1960), Foken (1979), and Jacobs and McNaughton (1994). For thin platinum wires, it must be taken into consideration that the specific resistance in $\Omega \cdot$ m for diameters <50 µm, but especially for diameters <10 µm, increases because the diameter is in the order of the free path length of the electrons. Such sensors are nowadays commercially no longer available.

For the measurement of the mean temperature, a suitable radiation shield, e.g. double protection tube or weather hut with double Venetian blind, is necessary to reduce the radiation error. Huts have the disadvantage that they heat up, and the so-called hut error of up to 1 K can occur (WMO 2008). For micrometeorological measurements, small cylindrical huts designed by Gill (Fig. 6.17) are often used. These huts were described regarding their dynamic and radiation properties by Richardson et al. (1999). The hut error can be removed by sufficient ventilation. Therefore, the Reynolds number should be above the critical Reynolds number to achieve a turbulent flow:

Fig. 6.17 Temperature hut according to Gill (model 41003) for micrometeorological investigations (published with kind permission of © R. M. YOUNG Company/GWU-Umwelttechnik GmbH, All rights reserved)

$$\text{Re} = \frac{L\,V}{\nu} \geq \text{Re}_{krit} = \begin{pmatrix} 2300 & \text{tube} \\ 2800 & \text{plate} \end{pmatrix} \tag{6.30}$$

Below the critical Reynolds number, a laminar flow occurs near the sensor, and increases the response time of the measurement. The laminar flow boundary layer is thinner than the molecular temperature boundary layer (von Driest 1959):

$$\frac{\delta}{\delta_T} = \sqrt{Pr} = 0.85 \ \text{(air)} \tag{6.31}$$

Except for thermocouples, platinum wires have prevailed over all other temperature measurement sensors because of the stable temperature-resistance dependency. The resistance can be determined with the following equation

$$R(T) = R(0°C) \cdot \left(1 + \alpha T + \beta T^2\right), \tag{6.32}$$

Table 6.10 Maximal differences for 100 Ω platinum resistance thermometers (DIN-EN 2009)

Temperature °C	Maximal difference					
	Class A		Class B		Class AA[a]	
	K	Ω	K	Ω	K	Ω
−100	±0.35	±0.14	±0.8	±0.32	±0.27	±0.11
0	±0.15	±0.06	±0.3	±0.12	±0.10	±0.04
100	±0.35	±0.13	±0.8	±0.30	±0.27	±0.11

[a]formerly class 1/3 class B

where α is a temperature-dependent coefficient which ranges from 0.00385 to 0.00392 K^{-1} depending on the purity of the platinum. By adding iridium, the brittleness of the wire can be reduced so that lower temperature coefficients are typical. Under these circumstances β is about $-5.85 \cdot 10^{-7}$ K^{-2}. In the meteorological measurement range of –50 to 50 °C nearly linear temperature dependence is obtained. Typically, platinum thermometers are produced with a resistance of R (0 ° C) = 100 Ω (1000 Ω is also available). The quality of resistance thermometers in Germany and other countries is standardized (DIN-EN 2009). The sensors are separated into classes A, B, and AA (Table 6.10), where selected resistance thermometers with differences of only 1/3 or 1/10 of the DIN-class are also available. Regularly, thermometers are used with class AA, formerly 1/3 DIN class B, which is better than class A.

The electrical measurement of the resistance is made with bridge circuits. The classical Wheatstone bridge with two and three wire circuits is seldom used because of non-linearity and a poor compensation for wire resistances. Recently, e.g. Thompson bridges or constant- current sources with four-wire circuits are used.

The progress of resistance measurements using integrated electronic circuits, has widely replaced the thermistor (Rink 1961) as a measurement sensor, because even though it has a tenfold higher temperature sensitivity, it has nonlinear characteristics. Before its use, thermistor must undergo heat and quench ageing, and during operation frequent recalibrations are often necessary. The temperature dependence is given by

$$R(T) = R(0°C) \cdot e^{\left(\frac{\alpha}{T} + \frac{\beta}{T^3}\right)} \tag{6.33}$$

with typical values of $\alpha \sim 4500$ K and $\beta \sim -1.5 \cdot 10^7$ K^3 (Brock and Richardson 2001). The most important areas of application are radiosondes and the measurements of body and dome temperatures in radiation sensors.

6.2.3.3   Humidity Measurement

Assmann's aspirated psychrometers are most reliable devices for measuring humidity, and can also be used for comparison measurements (see Sect. 6.2.3.2).

This instrument has a second thermo-meter with a wet bulb for measuring the wet bulb temperature. Both thermometers must be ventilated with velocities >2.5 ms^{-1}. It uses the effect of evaporative cooling. The water vapour pressure can be determined from the temperature difference between the dry (t) and wet (t') bulb temperatures using Sprung's psychrometric equation (psychrometer constant $\gamma = 0.666$ hPa K^{-1} for $p_0 = 1013.25$ hPa, $t = 20$ °C):

$$e = E(t') - \gamma \cdot \frac{p}{p_0} \cdot (t - t') \tag{6.34}$$

Meanwhile the improved relationship by Sonntag et al. (1989) is recommended by the World Meteorological Organization (WMO 2008) and widely applied. Above water follows

$$e = E(p, t') - 6.53 \cdot 10^{-4} \cdot p \left(1 + 9.44 \cdot 10^{-4} \cdot t'\right) \cdot (t - t'), \tag{6.35}$$

and above ice

$$e = E(p, t') - 5.75 \cdot 10^{-4} \cdot p \cdot (t - t'). \tag{6.36}$$

For wet temperatures above 30 °C a further modification is recommended (Sonntag et al. 1989):

$$e = E(p, t') - 6.53 \cdot 10^{-4} \cdot (p - E(p, t')) \cdot \left(1 + 9.44 \cdot 10^{-4} \cdot t'\right) \cdot (t - t') \tag{6.37}$$

For high accuracies, there are dew- and frost-point hygrometers. These expensive sensors can be used for comparison experiments (Sonntag 1994). In meteorological networks, capacitive sensors are widely used. These have replaced the hair hygrometer, which is still used for temperatures below 0 °C when the psychrometer has insufficient accuracy.

For many micrometeorological measurements of turbulent fluxes, the absolute humidity is necessary. For relative humidity sensors such as capacitive and hair hygrometers, the absolute humidity must be calculated with the temperature. This introduces temperature sensitivity, and makes temperature-independent humidity measurements impossible.

For the measurement of turbulent humidity fluctuations optical measurement methods are primarily used, which are based on the Lambert-Beer's law

$$I = I_0 \cdot e^{-k \cdot d \cdot \frac{c}{c_0}}, \tag{6.38}$$

where k is the absorption coefficient, d is the path length, and I_0 the radiation intensity at absorber concentration c_0. The measurement is made per unit volume. The measurement principle is schematically illustrated in Fig. 6.18.

The application of these techniques for turbulence measurements in the IR range are based on Elagina (1962) and in the UV range on Buck (1973), Kretschmer and

Fig. 6.18 Schematically construction of an absorption hygrometer
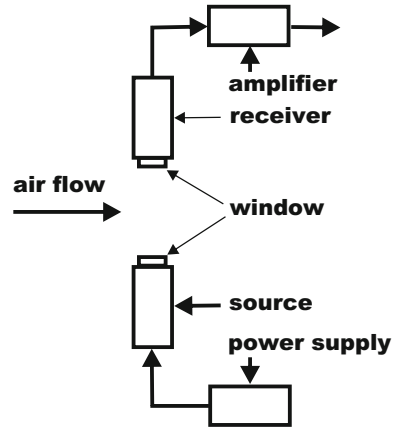
Karpovitsch (1973), and Martini et al. (1973). Many commercial developments followed, which were summarized by Foken et al. (1995). Today, only commercial sensors are used.

Instruments with either UV or IR radiation are used (Table 6.11). For measurements of low absolute humidity instruments in the UV-range are preferred, and for water vapour pressures larger than 10 hPa the IR-range is preferred. Due to the low absorptivity of the IR-range relatively long (>0.12 m) measurement paths are necessary. For a suitable wavelength, IR devices can also be used to measure carbon dioxide concentration. The lifetime of UV devices is limited due to changes of the lamp after about 1000 h. For these sensors, the surfaces of the optical windows are treated with hygroscopic material such as magnesium fluoride, which must be taken into account when the humidity is high. Therefore, IR hygrometers have become the preferred instruments for many users and vendors. Besides the IR open path systems (see Fig. 6.13), closed-path sensors, in which the air is withdrawn near the sonic anemometer and measured some meters away in an IR measurement cell are also applied (Leuning and Judd 1996; Moncrieff et al. 1997). These systems have the benefit that density fluctuations do not occur if heated tubes are used, and the WPL correction (see Sect. 4.2.3.6) can be dropped. However,

Table 6.11 Selected spectral lines for the water vapour absorption

Range	Wave length	Radiation source	Measurement length	Absorber
UV	0.12156 μm	Atomic hydrogen (Lyman-α)	3–10 mm	H_2O
	0.12358 μm 0.11647 μm	Krypton	5–15 mm	H_2O, (O_2, O_3)
IR	Different wave length	Stable electric light bulb	0.125–1 m	H_2O, CO_2

these are very complicated dynamical systems with low-pass characteristics. The time delay between the wind and concentration measurements is especially important and must be taken into account in flux calculations.

The calibration characteristics can change during the application time, and the devices working in the UV range are affected more than those in the IR range. Two calibration methods are commonly used: One method uses the calibration within a gas flow with a constant concentration of water vapour or other trace gases, and the other method uses a climate chamber. Also, the in situ calibration is possible by changing the path length for nearly constant background humidity (Foken et al. 1998; Foken and Falke 2012). This method works because according to Eq. (6.38) the trace gas concentration as well as the path length is in the exponent.

The application of very sensitive tuneable diode lasers (Edwards et al. 1994; Werle et al. 2008) increased during the last few years (e.g. Pattey et al. 2006; Sturm et al. 2012) because different gases such as methane, nitrogen oxides, and carbon isotopes can be measured and the instruments are now commercially available.

6.2.4 Precipitation Measurements

Precipitation measurements are one of the standard meteorological measurement techniques. In Germany, the rain gauge according to Hellmann should have a $200 \, cm^2$ collection area, but in other countries it is $500 \, cm^2$. The daily emptying of a collection bucket is often replaced by automatic rain gauges. Various measurement principles are available. The tipping-bucket gauge collects a certain amount of water in a bucket, and when the full bucket tips it is emptied, and electrical signal is sent. The droplet counter counts the number of droplets of a uniform size. Recently, weight scale rain gauges are used; this type has the benefit that the danger of freezing is low. It should be noticed that the rain gauge according to Hellmann has a very adverse ratio of the wettable surface and the collection area ($200 \, cm^2$) with a value of 7.55.

Precipitation measurements play an important role in the calculations of the water balance. It should be noted that precipitation data listed in climatological tables are typically not corrected. The moisten error and the wind error (Sevruk 1981; Richter 1995) must be corrected. For solid precipitation, the wind error can be very large (Fig. 6.19). The correction equation for both errors is:

$$N_{korr} = N_{mess} + b \, N_{mess}^{\varepsilon} \tag{6.39}$$

The coefficients are given in Table 6.12. Correction values are for different seasons and regions in Germany (Richter 1995).

For wind exposure on slopes with 40% inclination, up to 10% more precipitation can be expected due to the increasing horizontal contribution. A calculation of this effect was presented by Junghans (1967)
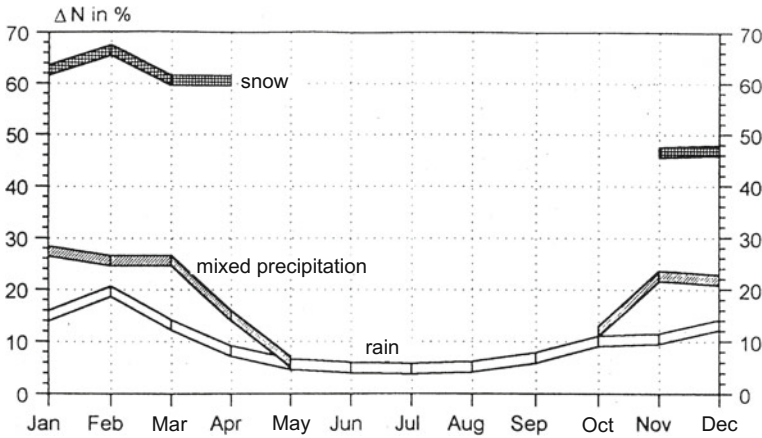
Fig. 6.19 Measurement error of precipitation measurements (adapted from Richter 1995, published with kind permission of © Deutscher Wetterdienst, Offenbach 1995, All rights reserved)

Table 6.12 Coefficients of the precipitation correction according Eq. (6.43) according to Richter (1995)

Type of precipitation	ε	Horizontal shading (b-value)			
		2°	5°	9.5°	16°
Rain (summer)	0.38	0.345	0.310	0.280	0.245
Rain (winter)	0.46	0.340	0.280	0.240	0.190
Mixed precipitation	0.55	0.535	0.390	0.305	0.185
Snow	0.82	0.720	0.510	0.330	0.210

$$\frac{N_H}{N} = 1 + 0.113 \, tg \, g \, \sin A_j, \tag{6.40}$$

where N_H is the precipitation on the slope, N is the measured precipitation on a horizontal surface, g is the inclination of the slope, and A_j is the azimuth angle of the jth wind direction.

For accurate and comparable precipitation measurements, rain gauges should be protected by a wind screen and should be placed at a distance equal to at least four times the height of any nearby obstacles, (WMO 2008). Nevertheless, the absolute accuracy is hardly better than 5% and for single, low-intensity precipitation events it is even larger. Open questions concerning the accuracy of accumulated sums (month, year) remain even after field intercomparisons were conducted (Vuerich et al. 2009). However, the scatter of the single data indicates that systematic errors are rather small and the measurement error for most instruments are approximately 5–10%.

6.2.5 *Remote Sensing Methods*

Increasingly, remote sensing techniques are being used in micrometeorology and applied meteorology. The techniques use sound waves (Sodar), light (Lidar) or radio waves (RADAR), and by applying the Doppler effect the wind velocity can be measured remotely. The use of lasers and microwaves makes moisture measurements possible. These instruments do not provide reliable observations below 20–50 m above the ground, but for micrometeorologists they cover an important region of the atmospheric boundary layer. Additionally, in the lower atmospheric boundary layer scintillometers can be used to measure the structure functions of the refractive index over horizontal path lengths from which fluxes can be determined indirectly. The electromagnetic spectrum, which is used by the remote sensing methods, is summarized in Table 6.13.

6.2.5.1 Sodar-RASS

The development of profiling techniques using sound are based on Russian theoretical work on wave propagation in the atmosphere (e.g. Tatarski 1961), while the first Sodar devices (**So**nic **D**etecting **A**nd **R**anging) by Kallistratova (1959) and McAllister et al. (1969) were constructed and used. The measurement principle is based on the fact that a sound pulse emitted into the atmosphere will be backscattered by temperature inhomogeneities. The degree of backscatter is directly proportional to the temperature structure function parameter. The classical range for application of these "monostatic" Sodars was the detection of inversion layers for air pollution purposes. By calibration of theses devices, the determination of the sensible heat flux using Eq. (2.140) is possible.

Subsequently, the Doppler effect was explored as a way to measure the three-dimensional wind field. These investigations lead to bistatic devices, which have low vertical operation range, and monostatic devices with one vertical and two sloping antennae. The accuracy of these Sodars is in the range of mechanical sensors (Table 6.14). However, these measurements are volume averages, and the horizontal wind components are measured in different sampling volumes, which may be far apart at high altitudes. For the standard deviation of the vertical wind it was found that the high values are underestimated and the low values are overestimated; this can be corrected.

Table 6.13 Ranges of the electromagnetic spectrum, which are used for remote sensing techniques in the atmospheric boundary layer

Frequency/wave length	Description	Sounding technique
1–5 kHz	Sound	Sodar
100 MHz–3 GHz	Ultra short waves (VHF), decimetre waves (UHF)	RASS, windprofiler
3–30 GHz	Centimetre waves	Microwave scintillometer
0.3–3 μm	Visible, infrared	Lidar
0.8–5 μm	Infrared	Scintillometer

Table 6.14 Measurement range and accuracy of Doppler-Sodar and RASS systems (Neff and Coulter 1986)

Parameter	Max. height in m	Resolution in m	Accuracy
Horizontal wind velocity	1000	15–50	± 0.5 m s^{-1}
Vertical wind velocity	1000	15–50	± 0.2 m s^{-1}
Structure function parameter	1500	2–10	$\pm 30\%$
Temperature (RASS)	600	15–50	± 0.5 K
Boundary layer height	600	2–10	$\pm 10\%$
Sensible heat flux	500	15–50	± 50 W m^{-2}

Modern Sodars use a "phased-array" arrangement, where a large number of loudspeakers are triggered in such a way that the sound pulse can be emitted in any direction. Thus, ground echoes and obstacles can be excluded. Also, the emission of single frequency pulses can be replaced by a continuous multi-frequency emission. The sampling frequency must be chosen in such a way that the cross sensitivity to the humidity is minimal.

The combination of a Sodar and a RADAR (Fig. 6.20) makes the measurement of the temperature field possible (RASS: **R**adio **A**coustic **S**ounding **S**ystem). In the RASS system, a Sodar emits vertically an acoustic wave, which is observed by the radar. Using the propagation speed of the sound wave, the sound temperature can be determined with Eqs. (6.22). Periodic inhomogeneities (turbulence elements) can only be detected if their size is approximately half of the wavelength of the sounding signal (Bragg condition).

While Sodar and Sodar-RASS systems offer reliable data at heights as low as 10–30 m, wind profilers have their first values at larger heights. The boundary-layer wind profiler works in the UHF range and is still interesting for micrometeorological applications; however, the tropospheric wind profiler works in the VHF rang and gives little data below 500 m.

6.2.5.2 Lidar

Due to the availability of improved laser techniques Lidar devices (**Li**ght **d**etection **a**nd **r**anging) have become quite popular (Weitkamp 2005). Depending on the type

Fig. 6.20 Sodar-RASS system consistent on a "phased-array" Sodar (*middle*) and two radar antenna (published with kind permission of © METEK GmbH, Elmshorn, All rights reserved)

of Lidar, in addition to aerosol measurements, which can be used to determine the mixed layer height, also wind profiles can be measured with Doppler-type instruments. The resolution of Doppler Lidars is similar to those given in Table 6.14 for Doppler-sodar devices. The benefit in comparison to Sodar technique is the noise-free sounding, but the measurements fail in the case of cloud cover.

Of special interest for boundary layer investigations are ceilometers. These are relatively simple back-scatter Lidars with an infrared laser with a wavelength of 0.9 μm, which were primarily used to detect the height of the clouds. Additionally, boundary-layer height can be detected from the vertical gradient of the back-scatter intensity as the height, where the gradient shows the largest negative deviation (Hayden et al. 1997). This method, which was originally developed for Lidar devices, can be transferred to ceilometers (Münkel et al. 2007; Helmis et al. 2012). Therefore, operational weather services are able to continuously produce boundary layer heights more easily than from radio soundings (see Sect. 2.6.1)

6.2.5.3   Scintillometer

The so-called scintillometer (Hill et al. 1980; Hill 1997) measures the refraction structure function parameter, C_n^2, and offers a method for the determination of the sensible heat flux and the friction velocity (Wyngaard and Clifford 1978). The bases for this are Eqs. (2.137) and (2.140) as well as other parameterizations for the dependency of the sensible heat flux on the temperature structure function parameter, C_T^2. The friction velocity can be calculated from the inner scale of the temperature fluctuations (Hill and Clifford 1978). Temperature or humidity inhomogeneities (IR or microwave scintillometer) cause a scintillation of the measurement beam, which can be evaluated.

Essentially, scintillometers are separated into two classes (DeBruin 2002) the large aperture scintillometer (LAS) and the small aperture scintillometer (SAS). The latter instrument is commercially available as a displaced-beam small aperture laser scintillometer (DBSAS). The LAS works in the IR range, has a measurement path length of several kilometers, and can determine only the sensible heat flux. In contrast, the DBSAS works with two laser beams over a distance of about 100 m (Andreas 1989). These systems can determine also the path-length-averaged turbulence scale, which is associated with the energy dissipation according to Eqs. (2.110) and by using the TKE equation Eq. (2.42), the direct determination of the friction velocity is possible when a stability dependence is taken into account (Thiermann and Grassl 1992). Note that scintillometers are not able to determine the sign of the sensible heat flux. Additional measurements (temperature gradient) are necessary, if the sign cannot simply be determined by the daily cycle because possibly unclear situations can occur in the afternoon. Scintillometers have a sensitivity that is in the middle of the measurement path rather than near the transmitter and receiver. This must be taken into account for footprint analyses of the measurement sector (Meijninger et al. 2002). Both scintillometer types have been successfully used in long-term measurement programs (Beyrich et al. 2002;

DeBruin et al. 2002). Relatively new is the microwave scintillometer, which measures the humidity structure function parameter $C_q^{\,2}$, see Eq. (2.136), and has the possibility of determining the latent heat flux (Meijninger et al. 2002, 2006).

6.2.6 Other Measurement Techniques

From the micrometeorological point of view, parameters other than those discussed are of special interest. In this section, a short overview of important measurements is given. But in some cases, the study of additional literature is necessary (DeFelice 1998; Brock and Richardson 2001; Moene and van Dam 2014).

6.2.6.1 Measurements in the Soil

Soil temperature, soil moisture, and the soil heat flux are especially relevant micrometeorological parameters (see Sect. 1.4.2). The soil temperature is a standard measurement using water-protected thermometers at 5, 10, 20, 50, and 100 cm depth. Micrometeorological investigations often need an increase of the measurement density close to the surface, e.g. in 2 cm depth. The heterogeneity of the soil and the plant cover make the positioning of the sensors difficult.

The soil moisture as a control parameter for evaporation is of special importance. The most accurate version for measurement is still the gravimetric method, where the soil probe is made with a soil core sampler and the soil is weighted after drying at a temperature of 105 °C. The measured change in weight is equivalent to the gravimetric water content (θ_g). Using a cylinder of known volume the volumetric water content (θ_v) can be determined. For a conversion of both parameters, the knowledge of the bulk density of the soil (dry density ρ_b) is necessary (ρ_w water density):

$$\theta_v = \theta_g \frac{\rho_b}{\rho_w} \tag{6.41}$$

A special electrical method for dry soil is the use of gypsum blocks, which include electrodes for measuring the electric conductivity. However, these devices must be calibrated individually in the laboratory. Note that the gypsum blocks have a strong hysteresis between moistening and drying.

For not very dry soils, tensiometers are widely used for the determination of the soil moisture tension by capillary forces. This technique uses a fine porous ceramic cup filled with water and placed in good contact with the moist soil. A balance of water pressure develops between the inner and outer sides of the cup. Using a glass tube extended into the cup, the pressure can be measured directly or the tube is closed with a septum and the pressure is measured with puncture devices. The matrix potential, ψ, in the depth, L (distance between the middle of the cup and the top of the tensiometer) can be calculated by

$$\psi = \psi_0 + (L - L_{bubble}) \tag{6.42}$$

where L is reduced by the height of the air bubble, L_{bubble}, in the glass tube. The pressure measured in the bubble (negative) is expressed as a length (ψ_0). There is a soil-type specific and characteristic connection (water tension curve) between the matrix potential and the volumetric water content that is used for the calculation. The use of tensiometers is diminishing because of the effort needed for the measurements and the indirect calculation.

Widely used today, is the capacitive TDR-method (time domain reflection). The instrument consists of two or more electrodes separated 2–5 cm and placed into the soil. The dielectric constant is measured by the travel time of an electric wave in the medium. The reflection properties are influenced in a characteristic way by the soil moisture. Because the electrical field develops over a large soil volume, an absolutely exact determination of the measurement height is not possible. With this method only the volumetric soil moisture is measured.

Soil heat flux can be measured using soil heat flux plates. These consist of two metallic plates separated by a layer of resin, with a heat conductance matching the one of the soil. The temperature difference measurement between both plats is made with thermocouples, where according to Eq. (1.12) the output signal is proportional to the soil heat flux. The plates require calibration.

There are numerous sources of errors for the soil heat flux plates. Especially important are the differences of the heat conductivities between the plates and the soil and at the edges of the plates, which are insufficiently included in the temperature measurement (van Loon et al. 1998). The first published and widely used correction method is the Philip correction (Philip 1961). The correction factor f between the measured soil heat flux, Q_G', and the soil heat flux through the surrounding soil, Q_G, is given by

$$f = \frac{Q_G'}{Q_G} = \frac{\varepsilon}{1 + (\varepsilon - 1)H'} \tag{6.43}$$

where ε is the ratio of the heat conductivities $\lambda_{plate}/\lambda_{soil}$. The factor H is dependent on the geometry of the heat flux plate and is given for square plates as:

$$H = 1 - \frac{1.70T}{L} \tag{6.44}$$

and for round plates as:

$$H = 1 - \frac{1.92T}{D} \tag{6.45}$$

where T is the thickness of the plate, L is the length of the square plate, and D is the diameter of the round plate. The Philip correction is recommended by Fuchs (1986), but it is doubted by other authors (van Loon et al. 1998). Also different types of plates have significant differences (Sauer et al. 2002). By applying self- calibrating

heat flux plates (Hukseflux HFP01SC), which determine a correction value by using a short and well-defined heating, the Philip correction can be omitted (Liebethal and Foken 2006). In contrast, these sensors (Hukseflux HFP01SC and TF01) are however less suitable to determine the heat conductance and the volumetric heat capacity by in situ measurements.

Generally, for micrometeorological measurements only the soil heat flux at the surface is necessary. Therefore, according to Eq. (1.14) the storage term above the heat flux plate must be determined by additional temperature measurements. It is also possible to eliminate the heat flux plates, if in a certain depth according to Eq. (1.12) the heat flux can be determined from the temperature gradient. It is recommended to determine the temperature gradient or to locate the heat flux plates at a depth of 10–20 cm to reduce errors. Both methods (using soil heat flux plates or temperature gradients for determining the storage) have approximately the same accuracy in an undisturbed soil profile (Liebethal et al. 2005).

The volumetric heat capacity, necessary for the determination of the storage term, can be determined with the method of de Vries (1963)

$$C_G = C_{G,m} x_m + C_{G,o} x_o + C_{G,w} \theta, \tag{6.46}$$

with the heat capacity of the mineral and organic compounds ($C_{G,m} = 1.9 \cdot 10^6$ J m^{-3} K^{-1}, $C_{G,o} = 2.479 \cdot 10^6$ J m^{-3} K^{-1}) and for water ($C_{G,w} = 4.12 \cdot 10^6$ J m^{-3} K^{-1}). The contribution of mineral components (assumed mineral 2650 kgm^{-3}), x_m, and can be determined by volume measurements of the soil. For depths up to 20 cm, x_o can often be neglected. The volumetric moisture of the soil is θ and given in m^3 m^{-3} as is x_m.

For the calculation of soil heat flux from the temperature gradient, the coefficient of heat conductance, a_G, is necessary:

$$a_G = C_G v_T \tag{6.47}$$

where v_T is the thermal diffusion coefficient and C_G is given by Eq. (6.46).

The thermal diffusion coefficient can also be determined using the method by Horton et al. (1983), in which the temperatures sensors are installed at three depths (10, 15 and 20 cm) and the temperature difference between two time steps ($\Delta t = 1$ min) is determined:

$$\frac{T_{15cm}^{n+1} - T_{15cm}^n}{v_T \Delta t} = \frac{T_{20cm}^n - 2T_{15cm}^n + T_{10cm}^n}{(\Delta z)^2} \tag{6.48}$$

A relatively simple yet reliable approach (Liebethal and Foken 2007) for the determination of the soil heat flux was presented by Braud et al. (1993). It is based on a heat flux measurement at $z = 10$ cm depth and temperature measurements at 1 and 10 cm depth as well as an estimate of the soil moisture for the determination of the volumetric heat capacity:

$$Q_G(0,t) = Q_G(-z,t)$$
$$+ C_G z \frac{T_1(t) - T_1(t-\Delta t) + 0.5[\Delta T(t-\Delta t) - \Delta T(t)]}{\Delta t} \qquad (6.49)$$

The time interval for such investigations is 10 min.

6.2.6.2 Soil Chamber Measurements

Ecologists use soil chambers to investigate the matter exchange between the atmosphere and the soil. With this method fluxes can be determined for very small plots. A good overview about this technique is given by Rochette and Hutchinson (2005). From the micrometeorological point of view these measurements are often criticized because of two reasons (Denmead 2008). First, chambers separate the near surface volume from the atmosphere such that typical atmospheric turbulent conditions are not present within the chamber and the longwave net radiation inside the chamber is nearly zero. Secondly, chamber measurements are often made manually and the daily cycle cannot be fully reproduced and the sampling theorem is not fulfilled. To overcome these problems, the chamber is often ventilated, but the typical wind profile of a boundary layer cannot be realized. Cooling pads are used to prevent overheating due to shortwave radiation. Sporadic chamber measurements are based on the assumption of a constant emission flux from the soil into the atmosphere. Thereby it is ignored that the pressure field, the stratification of the atmosphere and the turbulence can modify the emission rate, at least the emission at the top of the surface. But it is impossible to abstain from chamber measurements, because measurements in the atmosphere have a too large footprint for probing single plots. Furthermore, non-transparent chambers can measure the respiration at daytime too. To reduce errors under atmospheric conditions, the following measurement design is possible: Parallel measurements with eddy-covariance techniques on a nearby larger plot with a chamber in the maximum of the footprint for comparison.

One of the oldest chamber types and nearly 100 years in use is the non-flow-through steady-state chamber. These chambers are fully closed with an absorber inside. As an example, the respired carbon dioxide can be measured with an alkali absorber. After some hours or days, the absorber must be chemically analyzed. This type of chamber is however nowadays rarely used except for isotope labeling techniques. Non-steady-state chambers are now the most common. Thereby, in the case of emission from the soil, the concentration inside the chamber increases in a time interval of some minutes, while the concentration is continuously measured. From the slope of the concentration increase the emission can be calculated. To realize a linear slope the chamber must be ventilated or equipped with a pressure vent at the top of the chamber (Xu et al. 2006). Another system, the flow-through non-steady-state chamber, works with a constant air flow through the ventilated chamber, where the concentration is measured at the in- and out-flow. The benefit is a high time resolution of the measurements, but the gas analyzers

need a high accuracy and sampling frequency. Accordingly, these chambers are only available for some gases.

Due to the large number of chamber types and the relatively low number of commercially available chambers, chamber comparison studies were often conducted (Pumpanen et al. 2004; Pihlatie et al. 2013) and good agreement was generally observed. Also the comparison automatic chamber and eddy-covariance measurements compare well over longer time periods (Rochette et al. 1997; Wang et al. 2013; Riederer et al. 2014). However, single measurements often differ significantly due to various factors. The dependence on the degree of turbulence (friction velocity) shows good agreement for chambers when turbulence is low and underestimation for higher levels of turbulence (Lai et al. 2012). Obviously, in the range of a good agreement the ventilation of the chamber is similar to the conditions outside the chamber. The adjusted longwave net radiation inside the chamber is often very much underestimated, while outside large values are possible with cooling at the surface resulting in stable stratification. Under these conditions, during the night or during the oasis effect in the late afternoon, chambers overestimate the fluxes significantly. But in the case of coherent structures, which realize a well-mixed situation over a short period, even at night, smaller fluxes are measured in the chamber (Riederer et al. 2014). These complex findings corroborate the above given recommendation, to permanently measure at the same site with both eddy-covariance and chamber methods, such that corrections for single cases are possible.

6.2.6.3 Measurements at Plants

Even though measurements at plants are not the task of meteorologists, many plant parameters are used for modelling the energy and matter exchange (see Chap. 5). Since good textbooks are now available (Monteith and Unsworth 2008; Hari et al. 2013; Moene and van Dam 2014; Monson and Baldocchi 2014), only the most important parameters are described.

Probably the most important parameter is the leaf-area-index (*LAI*), which gives the contribution of the leaf surface per area element (see Table 5.11). It can be determined by spectral radiation measurements in the photosynthetic active range (*PAR*). Thus, the radiation below leafs will be compared with the radiation without any influence of the biomass.

The leaf area index can be relatively easily determined with remote sensing methods. The satellite images must be corrected for atmospheric influences before application to ensure the comparability of different pictures. For evaluation of single pictures, such corrections are not needed (Song et al. 2001). For the determination of the *LAI* value the Normalized Difference Vegetation Index (*NDVI*) is applied, which is the difference of the spectral channels of the red light (0.63–0.69 μm) and the near infrared (0.76–0.90 μm):

$$NDVI = \frac{NIR - red}{NIR + red} \tag{6.50}$$

Often the vertical distribution of the leaf area density (*LAD*) is also necessary and sometimes even the available leaf mass is of interest, but for this determination a harvesting of leaves is necessary. Instead of the leaf area index the plant area index (*PAI*), which includes besides the leaves also the branches and the steam, can also be used. It must be taken into account that the dependence of the *LAI* and *NDVI* becomes saturated for *LAI* > 8–10 and in this range the *LAI* cannot be accurately determined from *NDVI* data.

While the *NDVI* has a strong sensitivity on chlorophyll, the Enhanced Vegetation Index (*EVI*) better represents the plant structure together with *LAI* (Huete et al. 2002). It can be determined by including the blue light (0.459–0.479 μm):

$$EVI = G \cdot \frac{NIR - red}{NIR + C1 \cdot red - C2 \cdot blue + L} \tag{6.51}$$

The amplification factor is *G* = 2.5, the other factors are *C1* = 6, *C2* = 7.5, and *L* = 1. If no spectral measurements of the blue band are available, the factors are *C1* = 2.4 and *C2* = 0.

6.2.6.4   *Direct Evaporation Measurement*

The determination of the evaporation is a very important task. Prior to micrometeorological studies various devices were developed, especially in agrometeorology such as the evaporimeter according to Piche with absorbent paper as evaporation area or the evaporation instrument according to Czeratzki with porous clay plates, all of which are no longer used (Hupfer and Kuttler 2006).

For evaporation measurements in agrometeorology lysimeters are applied, which are a good direct measurement technique if applied correctly. The benefit is that contrary to micrometeorological measurements, only small areas are necessary.

Especially in hydrological networks, evaporation pans are still used, mainly the Class-A-Pan (DeFelice 1998). It is a round pan with 1.14 m^2 water surface (diameter 120.65 cm, height 25.4 cm) and 15.2–17.8 cm water depth. The evaporation is measured by the water loss in the pan, and complicated corrections (Linacre 1994; Sentelhas and Folegatti 2003) based on wind velocity, atmospheric moisture, and water temperature must be made. A greatly simplified but reliable method for daily sums of the evaporation (Smajstrla et al. 2000) uses the height difference of the water level in the evaporation pan corrected with the precipitation

$$Q_E = Kp \left(h_{day \, before} - h_{measuring \, day} \right) \tag{6.52}$$

Table 6.15 Coefficient Kp for the determination of the evaporation with the Class-A-Pan according to Eq. (6.55) for meadows or grain (in brackets for bare soil) in the vicinity of the device (Doorenbos and Pruitt 1977; Smajstrla et al. 2000)

Mean wind velocity at the measurement date	Extension of the area in the surrounding in m	Minimum of the relative humidity at the measurement date	
		>40%	<40%
low ≤ 2 ms^{-1}	1	0.65 (0.80)	0.75 (0.85)
	10	0.75 (0.70)	0.85 (0.80)
	100	0.80 (0.65)	0.85 (0.75)
	1000	0.85 (0.60)	0.85 (0.70)
moderate 2.1–4.4 ms^{-1}	1	0.60 (0.75)	0.65 (0.80)
	10	0.70 (0.65)	0.75 (0.70)
	100	0.75 (0.60)	0.80 (0.65)
	1000	0.80 (0.55)	0.80 (0.60)
strong ≥ 4.5 ms^{-1}	1	0.50 (0.65)	0.60 (0.70)
	10	0.60 (0.55)	0.65 (0.65)
	100	0.65 (0.50)	0.70 (0.60)
	1000	0.70 (0.45)	0.75 (0.55)

(in mm d^{-1}). Correction factors, which are functions of wind velocity, minimum relative humidity, and the conditions in the surrounding environment of the pan are given in Table 6.15.

6.3 Quality Assurance

Measurements are now widely automated, and based on modern measurement and electronic data storage techniques. But it is a fallacy to believe this saves man-power, because uncontrolled measurement data are not very reliable or may be worthless. The expense of measurements has moved from manpower for obser-vation to manpower for quality assurance (QA), which requires measures that were formally covered by visual observations. Quality assurance includes several

important steps, which are partly interconnected (Shearman 1992; Smith et al. 1996; DeFelice 1998; VDI 2013).

6.3.1 Measurement Planning

During the planning of a measurement system, numerous questions must be taken into account. This starts with the data user giving clear instructions about the measurement resolutions in time and space, the requested representativeness, the accuracy, and the availability of the data, etc. This sounds easy, but it is often a big problem because users often have little knowledge of measurement methodology and technology, and unrealistic requirements can occur. An interdisciplinary and iterative planning is necessary before a specification of the parameters can be made. This includes the technical parameters of the sensors, the units of the whole data sampling, transmitting and storing of the data, and data transfer to the user.

After this, follows the choice of suitable sensors, measurement sites, and data systems. Often large differences in price exist for apparently similar sensors. Therefore, detailed knowledge of the sensor characteristics and their influence on the whole project is necessary. Often in brochures, important information is missing and cannot be found elsewhere, because many low cost instruments are insufficiently investigated. Sensor lifetime, maintenance expenditure, and application under expected or extreme weather conditions are the deciding factors for high-end instruments. Sometimes special sensors must be developed. The micrometeorological requirements for the measurement sites are often so great that compromises are necessary, such as the exclusion of wind sectors or nighttime conditions with stable stratification. This must be done in agreement with the user requirements. For expensive measurement programs, it is required to test the measurement sites with a pre-experiment.

The largest part of the costs in running an experiment is the necessity for calibration and maintenance. Therefore, the periods for calibration (every 6–12 month for most of the systems) and maintenance (from a few days to several weeks depending on the specific maintenance work) must be determined, as well as the type of maintenance without data loss. This needs partly also investigation into calibration systems. Consideration of work safety is an important issue. In this complex, necessary corrections must be included, not only based on the calibration but also on the weather conditions.

A very important point is the definition of quality control (QC). This includes a possible daily control (visual or partly automatic) so that data failure or other defects can be immediately found. Only controlled and marked data must be stored in the database or go to the end user. Appropriate possibilities are extensively discussed in Sect. 6.3.2.

Because the data quality depends not only on the state of the sensor but also on the meteorological constraints, a complex quality management is necessary. Accordingly, the data should be flagged regarding the data control, if the data have

the necessary quality for usage, or if it can only be used for orientation. Such a system for the eddy-covariance method is shown in Sect. 4.2.5.

Feedback from the data user on further qualification of the system should not be underestimated. It is definitely a duty of the user and the initiator of the measurement program to insure that the data fulfil the desired objectives regarding the type of measurements and their quality. This can require some improvements or even reductions of the expenditure.

Quality assurance is a work package, which should not be underestimated with respect to the scope of the experiment. An increased attention for the running of the system helps in all cases.

6.3.2 Quality Control

Quality control has extremely important considerations. These include the control of the observations applying different criteria, and the indication of the data quality depending on the sensor and the meteorological conditions. Finally, the measured value gets a quality stamp.

The quality control can be made in different steps. The first step is the exclusion of missing data and obviously false data especially based on an electronic plausibility. The second step is assurance that the measured values are in the range of the measurement devices and in the possible meteorological range, which can change with the season. The resolution of the measured signal and its dependence on the digitalization must be controlled for the further calculations.

The meteorological tests follow, where typically comparisons are made with other observations. Complicated meteorological measurements need test models, e.g. boundary layer models, which test the combinations of all measured parameters. As a result of the test, a decision is necessary about the use of a manual or an automatic data correction, and the further use of the data. The storage in the database follows with a sufficient flagging, and information about the controls made, and probably also a quality stamp. All necessary steps are shown in Fig. 6.21.

After the initial tests, which can be automated, special tests on single parameters must be done (Fiebrich and Crawford 2001). The simplest cases are plausibility tests, e.g. for wind velocity and wind direction as shown in Table 6.16.

Tests for radiation components, more heavily use checks based on other meteorological parameters (Gilgen et al. 1994), where at least the components of the longwave radiation cannot easily be visually evaluated. For the upwelling longwave radiation, the test is to see if the radiation is within a certain difference of the radiation according to Stefan-Boltzmann law with the body temperature of the sensor:

$$\sigma(T_G - 5K)^4 \leq I \uparrow \leq \sigma(T_G + 5K)^4 \tag{6.53}$$

For strong longwave upwelling radiation during the night or strong heating of a dry soil, the threshold value of 5 K must be increased. For the atmospheric

Fig. 6.21 Flow diagram of the quality control steps for measured data (adapted from VDI 2013, with kind permission of © VDI e.V. and Beuth-Verlag, Berlin, 2013, All rights reserved)
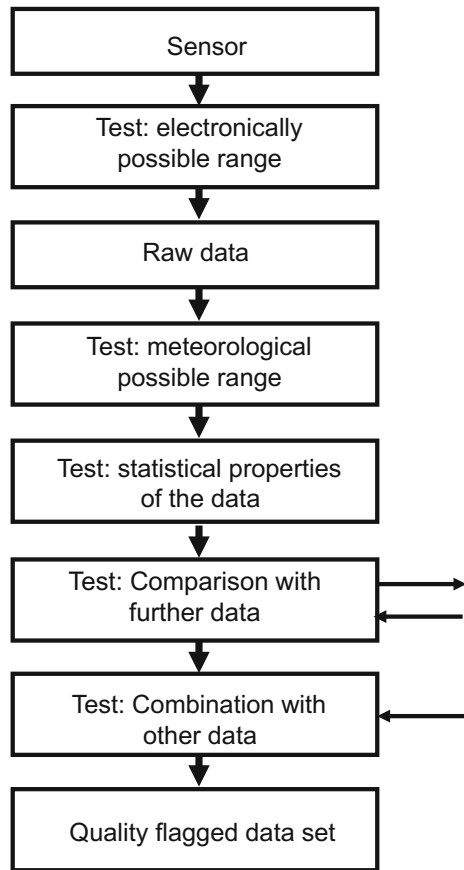

Table 6.16 Plausibility tests for wind velocity and direction (DeGaetano 1997)

Wind velocity	Wind direction
<0 ms^{-1}	
	<0° or >360°
<threshold velocity	for 1°–360°
>threshold velocity	for 0° (calm)
>60 ms^{-1} (height < 600 m a.s.l.)	

Measured values should be deleted if the data fall above or below the given thresholds

downwelling longwave radiation, the test is related to a black body (dome covered with water) and a grey body (clear sky with a radiation temperature of −55 °C):

$$0.7 \, \sigma \, T_G^4 \leq I \uparrow \, \leq \sigma \, T_G^4 \qquad (6.54)$$

For shortwave radiation the dependence on astronomical parameters and the transmission of the atmosphere is tested. For the reflected shortwave radiation the

test is made with the albedo (Table 1.1), where the albedo should only be calculated if the reflected radiation is >20–50 Wm^{-2}, otherwise large measurement errors occur. Values of the shortwave radiation at night, which differ from zero, should be set to zero and no offset correction should be applied.

Complicated micrometeorological measurements need a much higher quality control effort. For example, in the case of profile measurements comparisons with an approximation model can be used in the quality control and for assigning a quality criterion. Such comparisons can likely also provide information about possible internal boundary layers at the study site.

For many micrometeorological measurements, it is necessary to test if a fully turbulent regime is present. For eddy-covariance measurements, this can be done with a test on flux-variance similarities (Foken and Wichura 1996), as already shown in Sect. 4.2.5.

For large measurement programs, it is possible to compare different measurements. This can be in the simplest case the pure comparison of all wind and temperature data, where thresholds or altitude-dependent functions must be given. Also useful is the control of the energy balance, but the residual should be tested before selecting the measurement sites, the sensors, and the underlying surface. This should be taken into account by developing criteria (see Sect. 3.8), because the unclosed energy balance is specific for the measurement sites and not a quality criterion. Models, ranging from analytical up to meso-scale can be used for tests if the measured quantities are consistent with the model (Gandin 1988).

The quality control of meteorological measurements, especially of larger continuous measurement systems is still a developing question. Semi-automatic and fully automatic systems are only partly available. This is not only a question of software but also of research. Nevertheless, for available systems cases will be found where only experts are able to accurately separate meteorological effects from errors.

6.3.3 Intercomparison of Measurement Devices

Intercomparison experiments are an important requirement for the applications of sensors, because calibrations in wind tunnels and climate chambers have only a limited significance in the turbulent atmosphere. Such experiments also have high requirements on the terrain, which must be free of obstacles and allow an undisturbed installation of the sensors. The measurement heights should be chosen so that the near-surface gradients are small and do not have an influence on the measured results. The sensors for comparison should be in excellent condition and should have had a basic calibration.

Because in meteorology no absolute instruments exist for the comparisons, standards must be applied. These are devices, which were tested internationally over a long time and have shown constant results in previous comparisons. The sensor calibrations specification should be available.

For radiation measurements at the radiation centres, good standards are available. For turbulence measurements, this is a problem because wind tunnel calibrations of anemometers cannot simply be transferred to the turbulent flow. Nevertheless proven devices should be used, which have taken part in comparison experiments for at least 3–5 years.

The evaluations of comparisons are described with statistical numbers. One is the bias

$$b = \overline{(x_1 - x_2)} = \frac{1}{N} \sum_{i=1}^{N} (x_{1i} - x_{2i}), \tag{6.55}$$

where subscript 1 is the device to be compared and subscript 2 the standard (etalon). The comparability gives the differences due to the device and the medium:

$$c = \left[\frac{1}{N} \sum_{i=1}^{N} (x_{1i} - x_{2i})^2 \right]^{1/2} \tag{6.56}$$

The precision shows the systematic differences:

$$s = \left(c^2 - b^2 \right)^{1/2} \tag{6.57}$$

If the measurement accuracy and the influences of the surrounding medium for both devices are nearly equal, a mean regression line can be calculated, which can also be used for correction purposes. Note, if there is no real independent device available and for correlation coefficients <0.99, than two regression lines must be calculated and averaged (Schönwiese 2013; VDI 2013). This is identical with the orthogonal regression (Supplement 6.3), which is the easiest case with a uniform distribution of the errors of both measured parameters; otherwise more complicated methods should be applied (Dunn 2004).

The results of in situ comparison experiments are not comparable with laboratory measurements because the stochastic character of atmospheric turbulence and many uncontrolled influencing factors always create scatter even for equal sensor types. In all comparisons, the standard deviation of the vertical wind component has the best results. In contrast, comparisons of fluxes are significantly poorer, and the largest scatter occurs for the friction velocity. Reasons for this are the different spectra of the vertical and horizontal wind velocity, especially with respect to the frequency of the maximum of energy.

Supplement 6.3 Orthogonal regression

For comparison of the measured signals of two sensors with i measurement points and approximately the same error (Dunn 2004), i.e. no one device is free of errors, the orthogonal regression can be applied. For the determination of the regression line

$$\bar{y} = a\bar{x} + b \tag{S6.5}$$

the correlation coefficient is set to 1.0. With the mean value

$$\bar{m} = \frac{1}{N} \sum_{i=1}^{N} m_i \tag{S6.6}$$

and the variance of the measured data

$$\sigma(m)^2 = \frac{1}{N-1} \sum_{i=1}^{N} (m_i - \bar{m})^2 \tag{S6.7}$$

follows for the slope of the regression line

$$a = \frac{\sigma(y)}{\sigma(x)} \tag{S6.8}$$

and by application of a in Eq. (S6.5) the systematic difference (intercept) can be determined.

References

Albrecht F (1927) Thermometer zur Messung der wahren Temperatur. Meteorol Z. 24:420–424.

Andreas EL (1989) Two-wavelength method of measuring path-averaged turbulent surface heat fluxes. J Atm Oceanic Techn. 6:280–292.

Assmann R (1887) Das Aspirationspsychrometer, ein neuer Apparat zur Ermittlung der wahren Temperatur und Feuchtigkeit der Luft. Das Wetter. 4:245–286.

Assmann R (1888) Das Aspirationspsychrometer, ein neuer Apparat zur Ermittlung der wahren Temperatur und Feuchtigkeit der Luft. Das Wetter. 5:1–22.

Bartels J (1935) Zur Morphologie geophysikalischer Zeitfunktionen. Sitzungsberichte Preuß Akad Wiss. 30:504–522.

Bentley JP (2005) Principles of Measurement Systems. Pearson Prentice Hall, Harlow 528 pp.

Beyrich F, DeBruin HAR, Meijninger WML, Schipper JW and Lohse H (2002) Results from one-year continuous operation of a large aperture scintillometer over a heterogeneous land surface. Boundary-Layer Meteorol. 105:85–97.

Bovscheverov VM and Voronov VP (1960) Akustitscheskii fljuger (Acoustic rotor). Izv AN SSSR, ser Geofiz. 6:882–885.

Bowen AJ and Teunissen HW (1986) Correction factors for the directional response of Gill propeller anemometer. Boundary-Layer Meteorol. 37:407–413.

Braud J, Noilhan P, Bessemoulin P, Mascart P, Haverkamp R and Vauclin M (1993) Bare ground surface heat and water exchanges under dry conditions. Boundary-Layer Meteorol. 66:173–200.

Brock FV and Richardson SJ (2001) Meteorological Measurement Systems. Oxford University Press, New York, 290 pp.

Buck AL (1973) Development of an improved Lyman-alpha hygrometer. Atm Technol. 2:213–240.

de Vries DA (1963) Thermal Properties of Soils. In: van Wijk WR (ed.), Physics of the Plant Environment. North-Holland Publ. Co., Amsterdam, 210–235.

DeBruin HAR (2002) Introduction: Renaissance of scintillometry. Boundary-Layer Meteorol. 105:1–4.

DeBruin HAR, Meijninger WML, Smedman A-S and Magnusson M (2002) Displaced-beam small aperture scintillometer test. part I: The WINTEX data-set. Boundary-Layer Meteorol. 105:129–148.

DeFelice TP (1998) An introduction to meteorological instrumentation and measurement. Prentice Hall, Upper Saddle River, 229 pp.

DeGaetano AT (1997) A quality-control routine for hourly wind observations. J Atm Oceanic Techn. 14:308–317.

Denmead OT (2008) Approaches to measuring fluxes of methane and nitrous oxide between landscapes and the atmosphere. Plant Soil. 309:5–24.

DIN-EN (2009) Industrial platinum resistance thermometers and platinum temperature sensors (Industrielle Platin-Widerstandsthermometer und Platin Sensoren), IEC 60751:2008. Beuth-Verlag, Berlin, DIN-EN 60751, 28 pp.

Doetsch G (1985) Anleitung zum praktischen Gebrauch der Laplace-Transformation und der Z-Transformation. Oldenbourg, München, Wien, 256 pp.

Doorenbos J and Pruitt WO (1977) Guidelines for predicting crop water requirements. FAO Irrigation Drainage Pap. 24, 2nd ed.:145 pp.

Drinkov R (1972) A solution to the paired Gill-anemometer response function. J Climate Appl Meteorol. 11:76–80.

Dunn G (2004) Statistical Evaluation of Measurement Errors. Arnold, London, 216 pp.

Edwards GC, Neumann HH, den Hartog G, Thurtell GW and Kidd G (1994) Eddy correlation measurements of methane fluxes using a tunable diode laser at the Kinosheo Lake tower site during the Northern Wetlands Study (NOWES). J Geophys Res. 99 D1:1511–1518.

Elagina LG (1962) Optitscheskij pribor dlja izmerenija turbulentnych pulsacii vlaschnosti (Optical sensor for the measurement of turbulent humidity fluctuations). Izv AN SSSR, ser Geofiz. 12:1100–1107.

Emeis S (2010) Measurement Methods in Atmospheric Sciences. Borntraeger Science Publishers, Stuttgart, 257 pp.

Fiebrich CA and Crawford KL (2001) The impact of unique meteorological phenomena detected by the Oklahoma Mesonet and ARS Micronet on automatic quality control. Bull Amer Meteorol Soc. 82:2173–2187.

Foken T (1979) Temperaturmessung mit dünnen Platindrähten. Z Meteorol. 29:299–307.

Foken T, Kaiser H and Rettig W (1983) Propelleranemometer: Überblick und spezielle Entwicklungen am Meteorologischen Hauptobservatorium Potsdam. Veröff Meteorol Dienstes DDR. 24:48 pp.

Foken T, Dlugi R and Kramm G (1995) On the determination of dry deposition and emission of gaseous compounds at the biosphere-atmosphere interface. Meteorol Z. 4:91–118.

Foken T and Oncley SP (1995) Results of the workshop 'Instrumental and methodical problems of land surface flux measurements'. Bull Amer Meteorol Soc. 76:1191–1193.

Foken T and Wichura B (1996) Tools for quality assessment of surface-based flux measurements. Agrical Forest Meteorol. 78:83–105.

Foken T, Buck AL, Nye RA and Horn RD (1998) A Lyman-alpha hygrometer with variable path length. J Atm Oceanic Techn. 15:211–214.

Foken T and Falke H (2012) Technical note: Calibration device for the krypton hygrometer KH20. Atmos. Meas. Tech. 5:1861–1867.

Frankenberger E (1951) Untersuchungen über den Vertikalaustausch in den unteren Dekametern der Atmosphäre. Ann Meteorol. 4:358–374.

Fuchs M (1986) Heat flux. In: Klute A (ed.), Methods of Soil Analysis, Part 1: Physical and Mineralogical Methods, 2nd edn., vol 9. ASA and SSSA, Madison, WI, 957–968.

Gandin LS (1988) Complex quality control of meteorological observations. Monthly Weather Review. 116:1137–1156.

Gilgen H, Whitlock CH, Koch F, Müller G, Ohmura A, Steiger D and Wheeler R (1994) Technical plan for BSRN data management. World Radiation Monitoring Centre (WRMC), Technical Report. 1:56 pp.

Graf U (2004) Applied Laplace transforms and z-transforms for scientists and engineers. Birkhäuser, Basel, 500 pp.

Halldin S and Lindroth A (1992) Errors in net radiometry, comparison and evaluation of six radiometer designs. J Atm Oceanic Techn. 9:762–783.

Hanafusa T, Fujitana T, Kobori Y and Mitsuta Y (1982) A new type sonic anemometer-thermometer for field operation. Papers Meteorol Geophys. 33:1–19.

Hari P, Heliövaara K and Kulmala L (eds) (2013) Physical and Physiological Forest Ecology. Springer, Dordrecht, Heidelberg, New York, London, 534 pp.

Harrison GR (2015) Meteorological Measurements and Instrumentations. John Wiley and Sons, Chichester, 257 pp.

Haugen DA (1978) Effects of sampling rates and averaging periods on meteorological measurements. Fourth Symp Meteorol Observ Instr, Am Meteorol Soc:15–18.

Hayden KL, Anlauf KG, Hoff RM, Strapp JW, Bottenheim JW, Wiebe HA, Froude FA, Martin JB, Steyn DG and McKendry IG (1997) The vertical chemical and meteorological structure of the boundary layer in the Lower Fraser Valley during Pacific '93. Atmos Environm. 31:2089–2105.

Hebra AJ (2010) The Physics of Metrology. Springer, Wien, New York 383 pp.

Helmis CG, Sgouros G, Tombrou M, Schäfer K, Münkel C, Bossioli E and Dandou A (2012) A comparative study and evaluation of mixing-height estimation based on sodar-RASS, ceilometer data and numerical model simulations. Boundary-Layer Meteorol. 145:507–526.

Hill MK and Clifford SF (1978) Modified spectrum of atmospheric temperature fluctuations and its application to optical propagation. J Opt Soc Am. 68:892–899.

Hill R (1997) Algorithms for obtaining atmospheric surface-layer from scintillation measurements. J Atm Oceanic Techn. 14:456–467.

Hill RJ, Clifford SF and Lawrence RS (1980) Refractive index and absorption fluctuations in the infrared caused by temperature, humidity and pressure fluctuations. J Opt Soc Am. 70:1192–1205.

Horton R, Wieringa PJ and Nielsen DR (1983) Evaluation of methods for determining the apparent thermal diffusivity of soil near the surface. Soil Sci Soc Am J. 47:25–32.

Hübner J, Olesch J, Falke H, Meixner FX and Foken T (2014) A horizontal mobile measuring system for atmospheric quantities. Atmos Meas Techn. 7:2967–2980.

Huete A, Didan K, Miura T, Rodriguez EP, Gao X and Ferreira LG (2002) Overview of the radiometric and biophysical performance of the MODIS vegetation indices. Rem Sens Environm. 83:195–213.

Hupfer P and Kuttler W (eds) (2006) Witterung und Klima, begründet von Ernst Heyer. B. G. Teubner, Stuttgart, Leipzig, 554 pp.

ISO (1990) Solar energy - Specification and classification of instruments for measuring hemispherical solar and direct solar radiation, ISO 9060. Beuth-Verlag, Berlin, 21 pp.

ISO (1996) Acoustics - Attenuation of sound during propagation outdoors - Part 2: General method of calculation, ISO 9613–2. Beuth-Verlag, Berlin, 26 pp.

ISO (2002) Meteorology -Sonic anemometer/thermometer - Acceptance test method for mean wind measurements, ISO 16622. Beuth-Verlag, Berlin, 21 pp.

ISO (2007) Meteorology - Wind measurements - Part 1: Wind tunnel test methods for rotating anemometer performance. ISO 17713–1. Beuth-Verlag, Berlin, 17 pp.

Jacobs AFG and McNaughton KG (1994) The excess temperature of a rigid fast-response thermometer and its effects on measured heat fluxes. J Atm Oceanic Techn. 11:680–686.

Junghans (1967) Der Einfluß es Windes auf das Niederschlagsdargebot von Hängen. Archiv Forstw. 16:579–585.

Kaimal JC and Businger JA (1963) A continuous wave sonic anemometer-thermometer. J Climate Appl Meteorol. 2:156–164.

Kaimal JC and Gaynor JE (1991) Another look to sonic thermometry. Boundary-Layer Meteorol. 56:401–410.

Kaimal JC and Finnigan JJ (1994) Atmospheric Boundary Layer Flows: Their Structure and Measurement. Oxford University Press, New York, NY, 289 pp.

Kallistratova MA (1959) Eksperimentalnoje issledovanie rassejenija zvuka v turbulentnoj atmosfere (An experimental investigation in the scattering of sound in the turbulent atmosphere). Dokl AN SSSR. 125:69–72.

Kasten F (1985) Maintenance, calibration and comparison. Instrum Obs Methods Rep. 23 (WMO/TD 51):65–84.

Kleinschmidt E (ed) (1935) Handbuch der meteorologischen Instrumente und ihrer Auswertung. Springer, Berlin, 733 pp.

Kretschmer SI (1954) Metodika izmerenija mikropulsacii skorosti vetra i temperatura v atmosfere (A method to measure the fluctuations of the wind velocity and the temperature). Trudy geofiz inst AN SSSR. 24 (151):43–111.

Kretschmer SI and Karpovitsch JV (1973) Maloinercionnyj ultrafioletovyj vlagometer (Sensitive ultraviolet hygrometer). Izv AN SSSR, Fiz Atm Okeana. 9:642–645.

Kristensen L (1998) Cup anemometer behavior in turbulent environments. J Atm Oceanic Techn. 15:5–17.

Lai DYF, Roulet NT, Humphreys ER, Moore TR and Dalva M (2012) The effect of atmospheric turbulence and chamber deployment period on autochamber CO_2 and CH_4 flux measurements in an ombrotrophic peatland. Biogeosci. 9:3305–3322.

Latimer JR (1972) Radiation measurement, International Field Year of the Great Lakes, Techn. Manual Series No. 2, Information. Ottawa, 53 pp.

Leuning R and Judd MJ (1996) The relative merits of open- and closed path analysers for measurements of eddy fluxes. Global Change Biology. 2:241–254.

Liebethal C, Huwe B and Foken T (2005) Sensitivity analysis for two ground heat flux calculation approaches. Agrical Forest Meteorol. 132:253–262.

Liebethal C and Foken T (2006) On the use of two repeatedly heated sensors in the determination of physical soil parameters. Meteorol Z. 15:293–299.

Liebethal C and Foken T (2007) Evaluation of six parameterization approaches for the ground heat flux. Theor Appl Climat. 88:43–56.

Linacre ET (1994) Estimating U.S. Class-A pan evaporation from climate data. Water Internat. 19:5–14.

Martini L, Stark B and Hunsalz G (1973) Elektronisches Lyman-Alpha-Feuchtigkeitsmessgerät. Z Meteorol. 23:313–322.

Mauder M, Liebethal C, Göckede M, Leps J-P, Beyrich F and Foken T (2006) Processing and quality control of flux data during LITFASS-2003. Boundary-Layer Meteorol. 121:67–88.

Mayer J-C, Hens K, Rummel U, Meixner FX and Foken T (2009) Moving measurement platforms —specific challenges and corrections. Meteorol Z. 18:477–488.

McAllister LG, Pollard JR, Mahoney AR and Shaw PJR (1969) Acoustic sounding - A new approach to the study of atmospheric structure. Proc IEEE. 57:579–587.

Meijninger WML, Green AE, Hartogensis OK, Kohsiek W, Hoedjes JCB, Zuurbier RM and DeBruin HAR (2002) Determination of area-averaged water vapour fluxes with large aperture and radio wave scintillometers over a heterogeneous surface - Flevoland Field Experiment. Boundary-Layer Meteorol. 105:63–83.

Meijninger WML, Lüdi A, Beyrich F, Kohsiek W and DeBruin HAR (2006) Scintillometer-based turbulent surface fluxes of sensible and latent heat over heterogeneous a land surface - A contribution to LITFASS-2003. Boundary-Layer Meteorol. 121:89–110.

Mitsuta Y (1966) Sonic anemometer-thermometer for general use. J Meteor Soc Japan. Ser. II, 44:12–24.

Moene AF and van Dam JC (2014) Transport in the Atmosphere-Vegetation-Soil Continuum. Cambridge University Press, Cambridge, 436 pp.

Moncrieff JB, Massheder JM, DeBruin H, Elbers J, Friborg T, Heusinkveld B, Kabat P, Scott S, Søgaard H and Verhoef A (1997) A system to measure surface fluxes of momentum, sensible heat, water vapor and carbon dioxide. J Hydrol. 188–189:589-611.

Monson R and Baldocchi D (2014) Terrestrial Biosphere-Atmosphere Fluxes. Cambridge University Press, New York, XXI, 487 pp.

Monteith JL and Unsworth MH (2008) Principles of Environmental Physics, 3rd edition. Elsevier, Academic Press, Amsterdam, Boston, 418 pp.

Moore CJ (1986) Frequency response corrections for eddy correlation systems. Boundary-Layer Meteorol. 37:17–35.

Münkel C, Eresmaa N, Räsänen J and Karppinen A (2007) Retrieval of mixing height and dust concentration with lidar ceilometer. Boundary-Layer Meteorol. 124:117–128.

Neff WD and Coulter RL (1986) Acoustic remote sounding. In: Lenschow DH (ed.), Probing the Atmospheric Boundary Layer. American Meteorological Society, Boston, 201–236.

Ohmura A, Dutton EG, Forgan B, Fröhlich C, Gilgen H, Hegner H, Heimo A, König-Langlo G, McArthur B, Müller G, Philipona R, Pinker R, Whitlock CH, Dehne K and Wild M (1998) Baseline Surface Radiation Network (BSRN/WCRP): New precision radiometry for climate research. Bull Amer Meteorol Soc. 79:2115–2136.

Orlanski I (1975) A rational subdivision of scales for atmospheric processes. Bull. Am. Meteorol. Soc. 56:527–530.

Pattey E, Strachan IB, Desjardins RL, Edwards GC, Dow D and MacPherson IJ (2006) Application of a tunable diode laser to the measurement of CH_4 and N_2O fluxes from field to landscape scale using several micrometeorological techniques. Agrical Forest Meteorol. 136:222–236.

Philip JR (1961) The theory of heat flux meters. J Geophys Res. 66:571–579.

Philipona R, Fröhlich C and Betz C (1995) Characterization of pyrgeometers and the accuracy of atmospheric long-wave radiation measurements. Applied Optics. 34:1598–1605.

Philipona R, Dutton EG, Stoffel T, Michalsky J, Reda I, Stifter A, Wendung P, Wood N, Clough SA, Mlawer EJ, Anderson G, Revercomb HE and Shippert TR (2001) Atmospheric longwave irradiance uncertainty: Pyrgeometers compared to an absolute sky-scanning radiometer, atmospheric emitted radiance interferometer, and radiative transfer model calculations. J Geophys Res: Atmosph. 106:28129–28141.

Pihlatie MK, Christiansen JR, Aaltonen H, Korhonen JFJ, Nordbo A, Rasilo T, Benanti G, Giebels M, Helmy M, Sheehy J, Jones S, Juszczak R, Klefoth R, Lobo-do-Vale R, Rosa AP, Schreiber P, Serça D, Vicca S, Wolf B and Pumpanen J (2013) Comparison of static chambers to measure CH_4 emissions from soils. Agrical Forest Meteorol. 171–172:124–136.

Profos P and Pfeifer T (eds) (1997) Grundlagen der Meßtechnik. Oldenbourg, München, Wien, XIII, 367 pp.

Pumpanen J, Kolari P, Ilvesniemi H, Minkkinen K, Vesala T, Niinistö S, Lohila A, Larmola T, Morero M, Pihlatie M, Janssens I, Yuste JC, Grünzweig JM, Reth S, Subke J-A, Savage K, Kutsch W, Østreng G, Ziegler W, Anthoni P, Lindroth A and Hari P (2004) Comparison of different chamber techniques for measuring soil CO2 efflux. Agrical Forest Meteorol. 123:159–176.

Richardson SJ, Brock FV, Semmer SR and Jirak C (1999) Minimizing errors associated with multiplate radiation shields. J Atm Oceanic Techn. 16:1862–1872.

Richter D (1995) Ergebnisse methodischer Untersuchungen zur Korrektur des systematischen Meßfehlers des Hellmann-Niederschlagsmessers. Ber. d. Dt. Wetterdienstes. 194:93 pp.

Riederer M, Serafimovich A and Foken T (2014) Eddy covariance—chamber flux differences and its dependence on atmospheric conditions. Atmospheric Measurement Techniques. 7:1057–1064.

Rink J (1961) Thermistore und ihre Anwendung in der Meteorologie. Abh Meteorol Hydrol Dienstes DDR. 63:58 pp.

Rochette P, Ellert B, Gregorich EG, Desjardins RL, Pattey E, Lessard R and Johnson BG (1997) Description of a dynamic closed chamber for measuring soil respiration and its comparison with other techniques. Can J Soil Sci. 77:195–203.

Rochette P and Hutchinson GL (2005) Measurement ofsoil respiration in situ: Chamber techniques. In: Hatfield JL and Baker I (eds.), Micrometeorology in Agricultural Systems, vol 47. American Society of Agronomy, Madison, 247–286.

Sauer TJ, Harris AR, Ochsner TE and Horton R (2002) Errors in soil heat flux measurement: Effects of flux plate design and varying soil thermal properties. 25th Symp Agric & Forest Meteor:11–12.

Schönwiese C-D (2013) Praktische Statistik für Meteorologen und Geowissenschaftler. Borntraeger, Stuttgart, 319 pp.

Schrüfer E, Reindl L and Zagar B (2014) Elektrische Messtechnik. Fachbuchverlag im Carl Hanser Verlag, Leipzig, München, 445 pp.

Sentelhas PC and Folegatti MV (2003) Class A pan coefficients (Kp) to estimate daily reference evapotranspiration (ETo). Revista Brasilleira de Engenharia Agricola e Ambiental. 7:111–115.

Sevruk B (1981) Methodische Untersuchungen des systematischen Messfehlers der Hellmann-Regenmesser im Sommerhalbjahr in der Schweiz. Mitt. d. Versuchsanstalt f. Wasserb., Hydrol. u. Glaziol. 52:290 pp.

Shearman RJ (1992) Quality assurance in the observation area of the Meteorological Office. Meteorol Mag. 121:212–216.

Smajstrla AG, Zazueta FS, Clark GA and Pitts DJ (2000) Irrigation scheduling with evaporation pans. Univ of Florida, IFAS Ext Bul 254,9 pp.

Smith SR, Camp JP and Legler DM (1996) Handbook of Quality Control, Procedures and Methods for Surface Meteorology Data. Center for Ocean Atmospheric Prediction Studies, TOGA/COARE, Technical Report. 96–3:60 pp. [Available from Florida State University, Tallahassee, FL, 32306-33041].

Song C, Woodcock CE, Seto KC, Lenney MP and MacOmber SA (2001) Classification and change detection using Landsat TM data: when and how to correct atmospheric effects? Rem Sens Environm. 75:230–244.

Sonntag D (1966–1968) Hygrometrie. Akademie-Verlag, Berlin, 1086 pp.

Sonntag D, Scholz K and Schulze K (1989) The psychrometer equation for Assmann aspiration psychrometer for use in meteorological practice. Instrum Obs Methods Rep. 35 (WMO/TD No. 303):175–180.

Sonntag D (1994) Advancements in the field of hygrometry. Meteorol Z. 3:51–66.

Sturm P, Eugster W and Knohl A (2012) Eddy covariance measurements of CO_2 isotopologues with a quantum cascade laser absorption spectrometer. Agrical Forest Meteorol. 152:73–82.

Tatarski VI (1961) Wave Propagation in a Turbulent Medium. McGraw-Hill, New York, 285 pp.

Taubenheim J (1969) Statistische Auswertung geophysikalischer und meteorologischer Daten. Geest & Portig, Leipzig, 386 pp.

Thiermann V and Grassl H (1992) The measurement of turbulent surface layer fluxes by use of bichromatic scintillation. Boundary-Layer Meteorol. 58:367–391.

Tsvang LR (1960) Izmerenija tschastotnych spektrov temperaturnych pulsacij v prizemnom sloe atmosfery (Measurement of the spectra of the temperature fluctuations in the near surface layer of the atmosphere). Izv AN SSSR, ser Geofiz. 10:1252–1262.

van der Hegge Zijnen BG (1956) Modified correlation formulae for heat transfer by natural and by forced convection from horizontal cylinders. Appl Sci Res. A6:129–140.

van Loon WKP, Bastings HMH and Moors EJ (1998) Calibration of soil heat flux sensors. Agrical Forest Meteorol. 92:1–8.

VDI (2000) Umweltmeteorologie, Meteorologische Messungen für Fragen der Luftreinhaltung - Wind, VDI 3786 Blatt2. Beuth-Verlag, Berlin, VDI 3786, Blatt 2, 33 pp.

VDI (2006) Umweltmeteorologie - Meteorologische Messungen - Messstation, VDI 3786, Blatt 13. Beuth-Verlag, Berlin, 44 pp.

VDI (2013) Umweltmeteorologie - Meteorologische Messungen - Grundlagen (Environmental meteorology - Meteorological measurements - Basics), VDI 3786, Blatt 1. Beuth-Verlag, Berlin, 43 pp.

von Driest ER (1959) Convective heat transfer in gases. In: Lin CC (ed.), High speed aerodynamics and jet propulsion, Vol. V, Turbulent flow and heat transfer. Princeton University Press, Princeton, 339–427.

Vuerich E, Monesi C, Lanza LG, Stagi L and Lanzinger E (2009) WMO field intercomparison of rainfall intensity gauches. Instrum Obs Methods Rep. 99:1–290.

Wang K, Liu C, Zheng X, Pihlatie M, Li B, Haapanala S, Vesala T, Liu H, Wang Y, Liu G and Hu F (2013) Comparison between eddy covariance and automatic chamber techniques for measuring net ecosystem exchange of carbon dioxide in cotton and wheat fields. Biogeosci. 10:6865–6877.

Weitkamp C (2005) Lidar, Range-Resolved Optical Remote Sensing of the Atmosphere. Springer, New York, 456 pp.

Werle P, D'Amato F and Viciani S (2008) Tunable diode-laser spectroscopy: principles, performance, perspectives. In: Lackner M (ed.), Lasers in Chemistry - Probing Matter. Wiley-VCH, Weinheim, 255–275.

WMO (2008) Guide to meteorological instruments and methods of observation (updated 2010, 2012). WMO, Note. 8:7th edition.

Wyngaard JC and Clifford SF (1978) Estimating Momentum, Heat and Moisture Fluxes from Structure Parameters. J Atmos Sci. 35:1204–1211.

Xu L, Furtaw MD, Madsen RA, Garcia RL, Anderson DJ and McDermitt DK (2006) On maintaining pressure equilibrium between a soil CO2 flux chamber and the ambient air. J Geophys Res: Atmosph. 111:D08S10.

Chapter 7
Microclimatology

Microclimatology investigates mean states and permanent repeated phenomena on the micrometeorological scale. These are small-scale circulation systems such as mountain and valley winds, land-sea wind circulations, and katabatic winds. These phenomena are the subjects of many textbooks (Oke 1987; Stull 1988; Bailey et al. 1997; Hupfer and Kuttler 2005). Therefore, the following chapter does not provide a comprehensive overview, but rather discusses some typical microclimatological phenomena. These phenomena are present under special weather situations, and influence the small-scale climate in typical ways. Many of these local effects are described only in regional publications. The impressive wind system of the foehn is not described because it exists on the larger meteorological scale.

7.1 Climatological Scales

The scales of climate are not as strict and uniform as those of meteorology, as proposed by Orlanski (1975). The term microclimate is often applied to space scales up to 100 m as in micrometeorology. It follows that mesoclimate has an extension of up to 100 km which is about one class of scales lower in comparison to Orlanski's (1975) classes in meteorology (Hupfer 1991). In the small-scale range, terms such as urban climate, topo or area climate (Knoch 1949), ecoclimate, local climate, and others are usual. A comparison of different classifications is given in Table 7.1, where the classifications by Kraus (1983), formerly used in the Western part of Germany, and Hupfer (1989) are most likely comparable to the classifications by Orlanski (1975). The term microscale is often used for the much smaller scales. In what was formerly East Germany, the microscale classification applied to scales below 1 m (Böer 1959).

Figure 7.1 is an illustration of the various climate scales and the phenomena associated with them. Microclimate is mainly associated with processes in the

Table 7.1 Classifications of climatological scales (Hupfer 1991)

km	Orlanski (1975)	Böer (1959)	Kraus (1983)	Hupfer (1989)
10^4	makro-β	Large climate	Macro range	Global climate
10^3	meso-α	range	Synopt. range	Zonal climate
10^2	meso-β		Meso-	Landscape climate
10^1	meso-γ	Local climate	range	
10^0	mikro-α	range	Micro range	Plot climate
10^{-1}	mikro-β		Topo range	Small scale climate
10^{-2}	mikro-γ			
10^{-3}		Micro climate		Border layer climate
10^{-4}		range		

Fig. 7.1 The climate system in the macro, meso and micro scale (Hupfer 1996, adapted with kind permission of © Teubner Verlag Stuttgart, Leipzig 1996, All rights reserved)
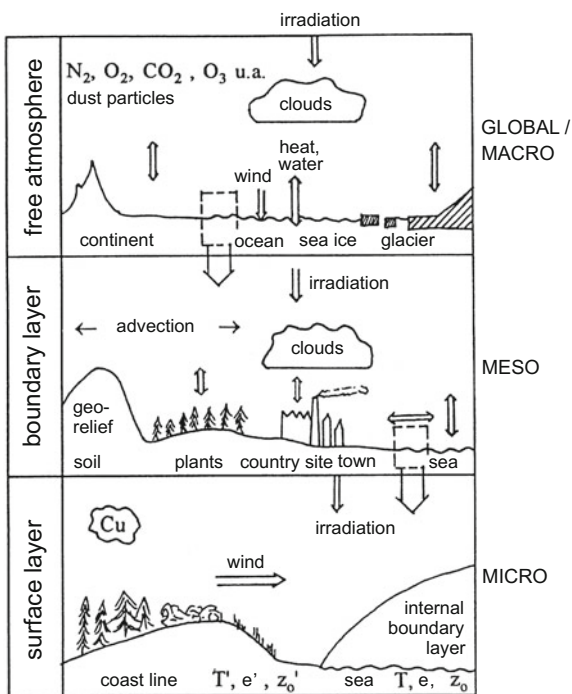
surface layer, e.g. energy and matter exchange, radiation processes close to the ground surface, effects of the underlying surface, etc. However, cumulus convection is not considered a part of the microclimate.

7.2 Generation of Local Climates

7.2.1 Small-Scale Changes of Climate Elements

Microclimatological effects often result in strikingly different phenomena if the climate elements have pronounced differences for certain weather situations or at certain time periods. Elements such as global and diffuse radiation in the absence of clouds show little climatological differences; however, differences can occur in mountainous regions. Exceptions may occur if long-duration local circulation systems are connected with clouds (see Sect. 7.3). For example, in the summer cumulus clouds will develop only over the land during a land-sea breeze. In the winter, the opposite effect occurs, i.e. clouds develop over the warmer sea.

Large-scale pressure fields cause wind speed and direction; however, the topography or obstacles near the measurement site also influence the winds, and these can lead to small-scale climate differences. Similar effects occur for precipitation where differences often cannot be clearly separated from measurement errors.

Air temperature and moisture in a uniform air mass and at the same altitude show very little differences, except for nights with high longwave up-welling radiation and cooling. Thus, the temperature minima near the ground may show remarkable differences (see Sect. 7.4). Similar results are found for the net radiation, which may be very variable on small scales due to the dependence on the albedo and the surface humidity.

Relevant climate elements in microclimatology are listed in Table 7.2. It is shown under which circumstances hardly any microclimatologically-caused differences occur.

7.2.2 Local Climate Types

Local climate types can be generated due to small-scale circulations (see Sect. 7.3), due to wind shadows, a changed radiation regime and vegetation (Bailey et al. 1997; Bendix 2004; Foken 2013; Barry and Blanken 2016). The smallest influences on the local climate are found in agricultural landscapes. However, if the terrain is sloped the radiation budget is already non-uniform. Beneficial *radiation climates* are often found along the slopes of river valleys, which are used for viticulture. Drainage of cold air from elevated regions above the vineyard must be averted. Walls or trails are used to block or channel the cold air down the slope, and also to

Table 7.2 Microclimatological relevant climate elements

Climate element	Range and reason of microclimatological differences	Hardly microclimatological differences
Global and diffuse radiation	Hardly available	Unlimited horizon, free of typical local clouds
Net radiation	Partly significant due to differences in albedo and surface temperature	Unlimited horizon and uniform underlying surface
Wind velocity and wind direction	Partly significant in complex terrain and in the case of obstacles	Large fetch over uniform surfaces and no obstacles
Temperature (general) and air humidity	Often small	Open location
Minimum of the temperature, temperature near the surface, temperature of the upper soil layers	Partly significant, especially in valleys and hollows (also in very small scales)	Open location
Precipitation	Partly significant but mostly in the range of the measurement error	Open location

prevent pooling of cold air in the valley that could affect the vineyards. Therefore, the lowest part of the slope is often used for frost-resistant fruit trees.

A very interesting climate type is the *forest climate*, as documented by the temperature observations in a forest shown in Fig. 3.3. The irradiation at day time heats up mainly the upper parts of the crown. Due to the stable stratification the cooler air from the night is still in the trunk space with a pleasant and often up to 5 degrees lower temperature. After sun set the top of the crown cools up by longwave up-welling radiation and the cooler air falls without a larger time lag into the trunk space. Nevertheless, the climate in the forest at night feels balmy in comparison to the surrounding of the forest, because the net longwave radiation in the trunk space is balanced. In the surrounding of the forest and on the top of the crown a larger cooling occurs.

The high heat capacity of water generates a special *lake climate*, causing the surroundings of water bodies to be warmer during cold nights. This effect is most common in autumn. The *climate of hollows* is often quite uncomfortable. During the night, cold air can pool in the hollow. Due to wind sheltering the evaporation is typically low and the hollow feels cool and moist. In contrary, during days with intensive irradiation the air in a hollow can be excessively hot. Similar effects also occur in gullies, but there cold air outflow is often possible.

Even in gardens a special *garden climate* (Häckel 1989) may persist. For instance, hedges act as a windbreak and emit longwave radiation in the evening often causing balmy conditions in their surroundings. However, downwind of the windbreak, in its wake, the evaporation is reduced and these areas are moister with

a tendency for growth of moss. Similar conditions prevail in rock gardens but in that case the high irradiation in the noon and afternoon hours is used to heat up the stones, which then act as a longwave heater at night. Windbreaks can increase this effect.

The **urban climate** has become a focus area (Kratzer 1956; Lietzke et al. 2015), also due to climate change research. Cold-air drainage (see Sect. 7.4) can have a strong effect on the urban climate. Because the buildings and streets within a city have high heat capacities, urban air cools more slowly at night than the surrounding rural areas leading to the formation of an *urban heat island*. If cold air is able to flow into a city, the heat island effect can be reduced. Green areas in cities are often very small and separated by buildings, and are therefore unable to produce enough cold air for the surrounding areas. Urban parks and grasslands should be larger than 200×200 m^2 and humid (Spronken-Smith and Oke 1999; Spronken-Smith et al. 2000).

Therefore, the facility and the protection of park areas inside towns have a high relevance. Open forms, like the English garden type, should be preferred. Also with architectonical action and the application of special building material the heating can be reduced.

Of increasing relevance are measurements in street canyons (e.g., Klein and Clark 2007). An overview of such studies is presented in Appendix A.5. The objectives of these studies include investigating the energy and matter exchange in cities, also for air quality management, the influence of the buildings and open areas, and the carbon dioxide balance of towns (Kotthaus and Grimmond 2012).

The number of modelling (Best and Grimmond 2014) and experimental (see Appendix A.5) studies has significantly increased over the last years. Advanced, state-of-the-art modelling techniques (Letzel 2015) and measurement methods are widely applied to identify problems and to support the planning process.

Besides the importance of cold-air drainage in urban climates, the properties of the heat island are relevant. To investigate both, special measurements are necessary, as described in Sect. 7.6, because classical climate maps cannot describe all relevant processes. For special bioclimatological investigations, Table 7.3 gives some suggestions for assessment criteria by the superposition of heat, pressure, and ventilation (Gerth 1986).

Table 7.3 Superposition of criteria for a bioclimatological assessment (Gerth 1986)

	High	Moderate	Low
Bioclimatological pressure			
Heat pressure	>25 days	All other combinations	≤ 25 days
Wind velocity	<2 m s^{-1}		≥ 2 m s^{-1}
Frequency of inversions	>30% a^{-1}		$\leq 30\%$ a^{-1}
Ventilation			
Wind velocity	≥ 2 ms^{-1}	All other combinations	<2 m s^{-1}

7.3   Microclimate Relevant Circulations

7.3.1   Land-Sea Wind Circulation

Land-sea wind circulations arise form weak background winds and large temperature differences between land and sea. The heating over the land generates low-pressure areas with rising air. For compensation, cold air from the sea forms a sea breeze. Above the sea, resides a high-pressure area with descending air, i.e. subsidence. The sea breeze front penetrates inland distances ranging from a few decametres up to kilometres, and causes remarkable temperature differences over small areas, as illustrated in Fig. 7.2. After the beginning of the land-sea wind circulation, the temperature at the beach may be unpleasantly cool, while a little distance inland pleasant temperatures are found. During the night, these relations are opposite but less developed.

7.3.2   Mountain-Valley Circulation

Cooling during the night caused by radiation is the reason that cold air from mountaintops and slopes descends under gravity into valleys and fills cold-air reservoirs. If drainage winds pass through narrow valleys, a considerable katabatic wind can be occur. The strongest katabatic wind are found in Antarctica (King and Turner 1997). On smaller scales, katabatic flows have a significant role (see. Sect. 7.4).

During the day, the valley and the slopes are heated faster than the mountaintops (low wind velocities, less air exchange), and warm air moves upward along the slopes. These flows slowly lift the inversion layer until the mixed layer is fully developed. This process is illustrated in Fig. 7.3 following the classical paper by Defant (1949). The dispersion of the inversion is also possible by convective events from the centre of the valley (Brötz et al. 2014).

Fig. 7.2 Temperature cycle at the beach of Zingst (Baltic Sea, broken line) and 200 m inland with offshore wind of 4–7 ms^{-1} over land on May 17, 1966 according to Nitzschke (1970, adapted with kind permission of © WILEY-VCH Verlag Weinheim 1970, All rights reserved)
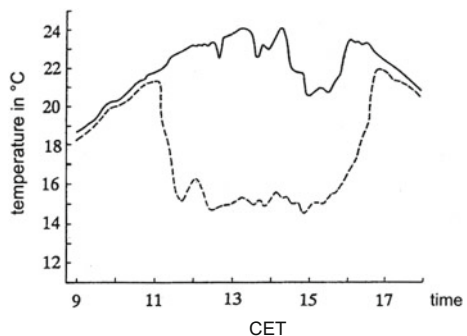
Fig. 7.3 Schematic view of the mountain-valley circulation (Adapted from Stull 1988, with kind permission of © Kluwer Academic Publisher B. V. Dordrecht 1988, All rights reserved)
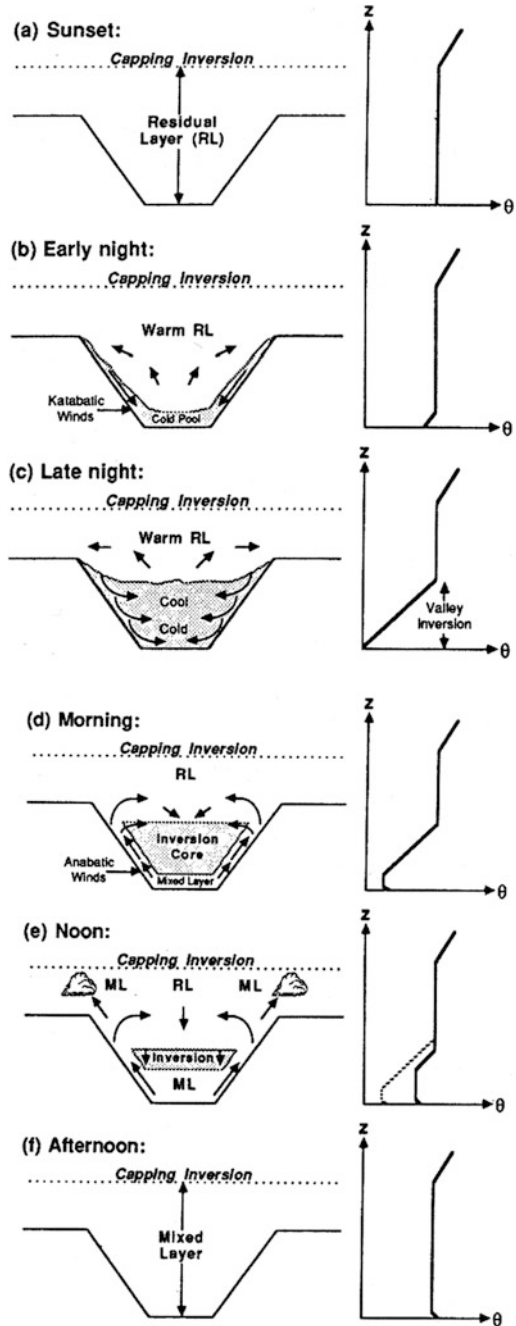
The strength of the katabatic wind can be determined from the temperature difference between the cold air flowing downslope and the surrounding area. Applying a local equilibrium between buoyancy and stress the velocity of the katabatic flow is (Stull 2000)

$$u_k = \left(\frac{g \cdot (T - T_k)}{T} \cdot \frac{h}{C_D} \cdot \sin \alpha \right)^{1/2} \tag{7.1}$$

h is the depth of the cold air layer, C_D is the drag coefficient, α is the angle of inclination of the slope, g is the acceleration due to gravity, T is the surrounding air temperature, and T_K is the temperature of the cold air layer. Also, Eq. (7.1) can be added as a buoyancy term into the Navier-Stokes equation Eq. (2.1).

7.4 Local Cold-Air Flows

Cold-air flows are the most common microclimatological phenomenon (VDI 2003). Source areas include, for example, open hilltops, forested slopes, and other inclined surface areas. The cold-air flow can be imagined as a flow of compact air parcels that can be interrupted or damped by obstacles. With a trained eye, the relevant cold-air flows can be localized according to the form of the landscape and the vegetation. This assessment can be made using a classification. Steps of the classification are detailed in Tables 7.4 and 7.5. The verifications can be made with well-aimed measurements (see Sect. 7.6). At very high risk, are cold air nights with strong longwave radiation due to cloudless skies. This is especially the case following synoptically-caused cold air advection (e.g. Three Saints' Days, a European weather phenomenon occurring in May). Two useful preventive measures are sprinkling with water so that more energy is necessary for the freezing of the water droplets, and fogging with smoke so that the cooling by long-wave radiation is above the plant canopy.

An impressive example of a small-scale cold-air flow is shown in Fig. 7.4. At the morning of May 04, 2011 a very significant late frost event occurred in Germany under clear sky after the inflow of fresh cold air. At a meadow slope with 200 m length and 40 m height difference temperatures measured at 5 cm above the surface at the bottom of the valley and the top of the slope differed by 6 K. At a

Table 7.4 Classification of the frost risk (cloudiness < 2/8, wind velocity < 3 ms^{-1}) according to Schumann (personal communication)

Risk class	Indication	Comparison to normal conditions
1	Favored	+1 to +5 K
2	Normal condition	−1 to +1 K
3	Weak to moderate frost risk	−2 to −4 K
4	High to very high frost risk	−5 to −8 K

Table 7.5 Risk class according to the profile of the terrain according to Schumann (personal communication)

Relief form	Cold air inflow, production	Cold air drainage	Risk class[a]
Closed basin	Existing	–	3
Ground of the valley, low slope	Existing	Weak	3
Ground of the valley, moderate slope	Existing	Moderate	3
Plates, Δh > 10 m	–	–	2
Slope, low inclination (1–3°)	–	Moderate	2
Slope, high inclination (>15°)	–	Very good	1
Hills h > 50 m, inclination > 10°	–	Very good	1

[a]marshy soil +1

nearby hill that was only 175 m above the bottom of the valley ground frost was weak and the temperature at 2 m height was above 0 °C, while in the valley the temperature was – 5 °C. Interestingly, the temperature in the valley increased at 03:30 local time, while the next higher measurement point had the lowest temperature, which can be explained by the formation of ground fog. Fog formation and breakup also caused temperature variations in the following hours. Such local cold air hazards can be easily detected by visual inspection.

Cold-air generation in valleys augmented by cold-air drainage can lead to radiation fog if the air is cooled below its dew point. After the generation of the fog, the strongest cooling by radiation occurs at the top of the fog. Because of this, the coldest temperatures are no longer found in the valley but along the slopes above the fog, as shown in the example above. The reduced longwave radiation from the ground causes a lifting of the fog, and in the low radiation season this is the reason for daylong low stratus within closed valleys or basins.

A special form of the fog is sea smoke, a cumulus-like cloud of some meters in thickness. This is generated by cold air flowing over warmer water. Because this convective effect can happen only for water-air temperature differences greater than 10 K (Tiesel and Foken 1987), sea fog occurs by advection of cold air most often in late spring, when small lakes are already warm, or in autumn and early winter over large lakes or the oceans.

7.5   Land Use Changes and Local Climate

Land use changes play nowadays an important role, because they significantly influence the local climate but may also affect the whole climate system in the case of changes over large areas (Cotton and Pielke Sr 2008; Mölders 2012). In this chapter examples of typical changes are shown. However, estimating the effect of
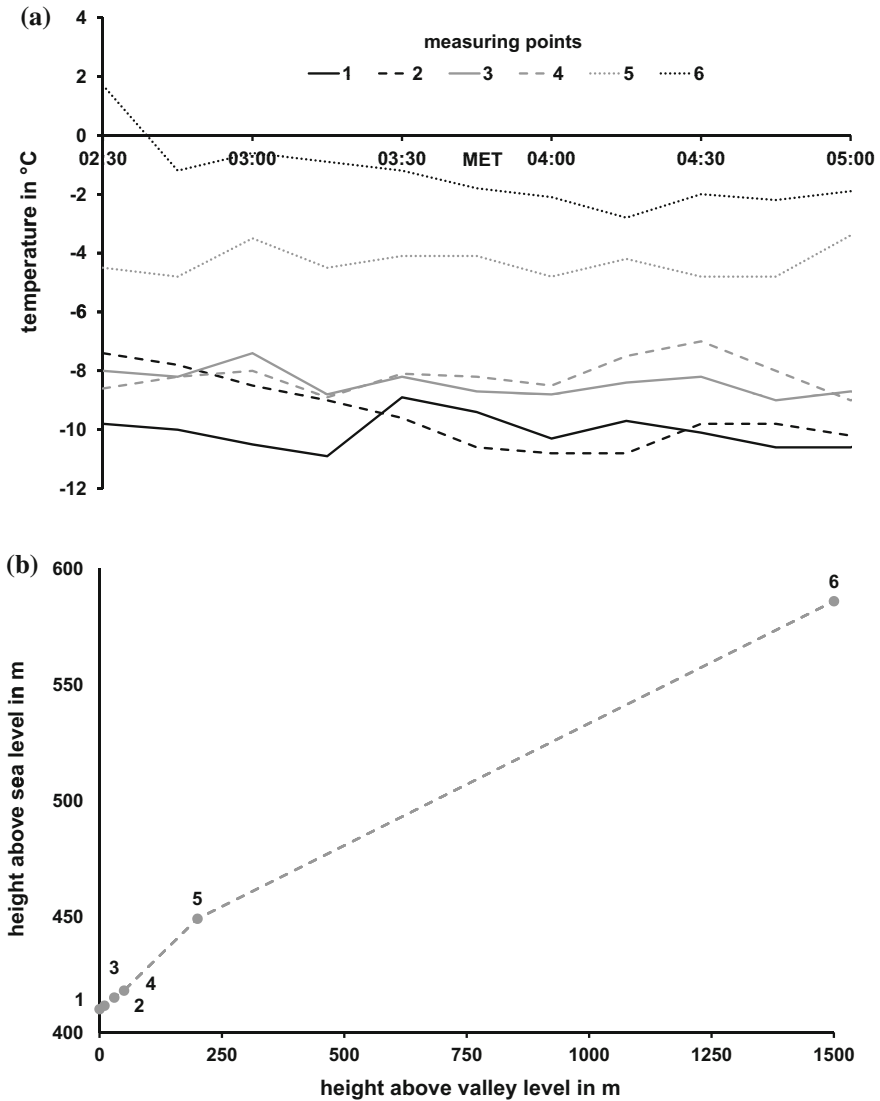
Fig. 7.4 Temperature **a** measured at 5 cm above the surface in the morning of May 04, 2011 near Frankenhaag (region Bayreuth, Germany) at 5 measurement points distributed along a slope as illustrated in the schematic height profile **b.** The sites were at the bottom of the valley (*1*), above a meadow (*2–4*), at a forest edge (*5*), and on the top of a nearby hill (*6*). Sun rise was at 04:45 MET. The data were collected during experiments with students of the University of Bayreuth

typical land use changes is not always simple, because the relationships are largely non-linear. Estimating the effects of roughness changes is most simple, while for albedo changes the relationships are extremely complex. Figure 7.5 illustrates the complexity of this question.
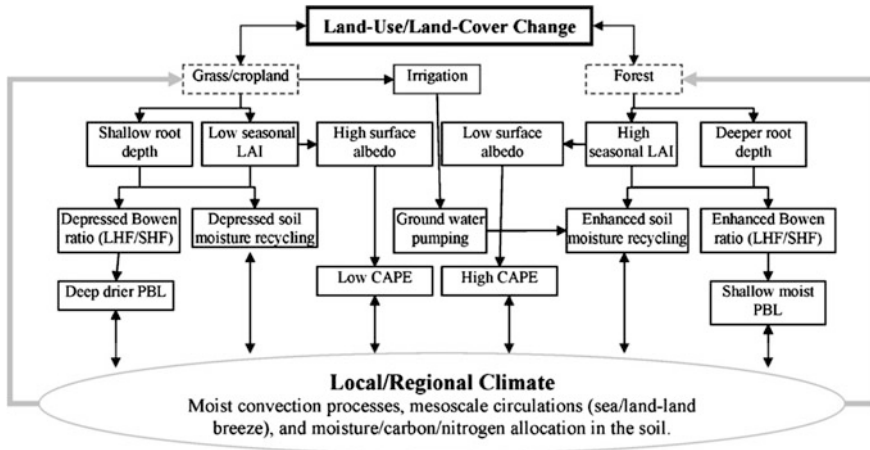
Fig. 7.5 Schematic illustration of the influence of land use and land cover changes on the local and regional climate (Adapted from Pielke Sr et al. 2007, with kind permission of © Elsevier AG Oxford 2004, All rights reserved)

7.5.1 Changes of Surface Roughness

Changes of the surface roughness are very common, e.g. due to deforestation, housing development, soil sealing. The implications can be easily estimated with Eq. (2.87), i.e. a reduction of the roughness length is related to an increase of the wind velocity. Given the proportionality of wind and friction velocity and of the roughness heights for momentum and scalars it also follows according to Eq. (2.90) that the fluxes of scalars increase. Because evaporation needs a lot of energy, which can be provided e.g. by a downward sensible heat flux (oasis effect), and the wind velocity may be high in the case of neutral stratification, an increase of the evaporation is possible. High wind velocities and a dehydration of the soil are the basis for erosion. This is very relevant in areas with fine-grained soil, like sand or loess. In areas with high wind velocities, like Great Britain or Northern Germany, the erosion potential was reduced by windbreaks (hedges or stone walls) already in ancient times. It is interesting that the typical distances are of the order of 100 m, which agrees well with the wind reduction zone due to internal boundary layer development (see Sect 3.2).

On the other hand, reduction of the wind velocity also occurs due to urban sprawl. However, the sensible heat flux often does not drastically decline, because the lower wind velocities and the shortwave down-welling radiation promote stronger heating of the surface and subsequently also an increase in air temperatures. Because the largest roughness elements dominate the roughness of an area, large wind farms reduce the wind velocity. This is of particular relevance for off-shore wind farms, where the effect is very large due to the low roughness of the ocean (Witha et al. 2014). Consequently, wind turbines are installed on the ocean

and on mountain hills like pearl necklaces, perpendicular to the mean wind direction. Above forests, the applicability of the relationship between wind velocity and roughness is limited due to the generation of an mixing layer (see Sect 3.5.3).

7.5.2 Changes of the Evaporation

In some parts of the World, actions to reduce the evaporation are already in use. A successful strategy has been to increase the surface roughness by using wind breaks, such as hedges and stonewalls, or groups of trees, such as savannahs and orchards, in more open landscapes which, in these cases, suppresses the evaporation from the soil or grass. Such measures will gain in importance due to climate change.

Very critical are the reduction of the evapotranspiration due to deforestation mainly in tropical regions but also due to the wide-spread urban sprawl and related sealing of large areas. The related environmental impacts on the water balance of the Earth are significant and the proportion of arid areas continues to rise. The preservation of natural forests with high carbon uptake and resistance to extreme weather events has a special significance (Herbst et al. 2015).

But also the extraction of water in arid areas is important. Thereby dew is a source for plants and animals which should not be underestimated. Open areas provide favourable conditions for dew formation as air quickly cools down in the case of low wind velocities and longwave up-welling radiation. This is e.g. the case in open savannah areas where dew formation in the morning is an important source of water for ground vegetation and animals. The increasing areas of scrublands counteract this effect. In a closed scrubland the top of the scrubs cools and the cold air sinks down, but the dew point temperature will not be reached at the surface. Therefore, fire-clearing is often applied.

7.5.3 Change of the Albedo

Changes of the albedo are discussed controversially. Often it is assumed that an increase of the albedo increases the reflected shortwave radiation which reduces the shortwave radiation balance (Davin and de Noblet-Ducoudré 2010). It is then argued that the energy loss caused by the higher reflection of shortwave radiation results in decreasing sensible heat fluxes and thus a cooling effect.

By comparison of Tables 1.2 and 1.4 with albedo and soil heat capacity data, respectively, it is obvious that an increase in albedo comes along with a brighter and dryer surface and thus also a lower heat capacity. It is true that the reflected shortwave radiation increases, but due to the lower heat capacity of the soil less energy is stored. Furthermore, since heat conductance also is low the ground heat

flux is reduced. Therefore, a very thin top layer of the soil strongly heats up causing the sensible heat fluxes and longwave upwelling radiation to rise. Furthermore, the erosion potential increases. The problem is very complex and expert studies often must rely on models, in which land-surface processes and atmospheric interactions are well parameterized.

Changes of the albedo have the most prominent effects in Arctic and Antarctic regions. Due to the melting of the sea ice the change can be, in the extreme case, from 95 to 5% and substantial amounts of energy can be stored in the water of the ocean. This increases the evaporation, which is much higher than the sublimation from the ice, with implications on cloudiness and precipitation patterns. Additionally, the deposition of dust and soot due to the increasing commercial utilisation of these areas and the thawing of ice surfaces are reasons for significant changes of the albedo. Also, on land areas the snowmelt suddenly changes the energy distribution (Westermann et al. 2009). Changes of the albedo in polar regions and the deforestation of the tropical rain forests have the strongest influence on the earth's climate.

7.5.4 Degradation

The degradation of the vegetation cover of soils if of great concern, particularly in sensitive and slowly growing ecosystems like alpine meadows, but also in areas with agricultural depletion or areas which will be drier due to climate change. Reasons are overgrazing, erosion, landslides, dehydration, degradation due to small rodents and similar factors. The effects can be of complex nature including a release of carbon dioxide from the exposed soil, the increase of the sensible heat flux over bare soils with a change of the Bowen ratio and the albedo. By the change from the plant covered to the non-plant covered surface there is a change from evapotranspiration to evaporation. Due to the missing regulation of the plants the water evaporates earlier on the day with earlier cloud generation and precipitation (Babel et al. 2014). Analogue to albedo changes, only careful modeling studies and validation experiments can provide insight about the complex and non-linear mechanisms.

7.6   Microclimatological Measurements

Microclimatological measurements have a high relevance for consulting activities (see Sect. 8.2.5). They are necessary for urban and health-spa climate assessments. Also, many applications are found in agriculture, for example assessing frost risk in orchards and vineyards. Engineers with different degrees of experience often make

these assessments. Assessments made using single situations are not sufficient for a generalization. It is important to find those processes that are relevant to the observations. Therefore, the special conditions of the near-surface layer discussed in Chap. 3 must be taken into account. Predominantly, only relevant state parameters are mapped out, e.g. cold-air flows or the heating of city centres. Typically, simple measurements (temperature, see Sect. 7.4; smoke experiments) are used which do not provide data for important parameters such as the volume flow. There are only a few approaches where atmospheric stability and turbulent fluxes are considered. These are important parameters that must be compared for instance in assessing deposition potential.

Microclimatological measurements cannot be done independently from climatologically measurements. This means that climatologically measurements must be made first. This requires the selection of a relevant basic climate station with measurements over many years and made by meteorological services. Furthermore, measurements in the area of investigation over 1–2 years are necessary to transfer the climatological data to this area. Such station can be a small automatic weather station, which should be placed at relevant points according to the classification of the landscape. The real microclimatological measurements are made with moving instrument packages such as cars, vans etc. or intensive field campaigns. Therefore, it is necessary that a weather situation must be chosen during which the phenomena being investigated are clearly seen. For cold-air risk investigations, clear nights after cold air advection are necessary. During these mobile measurements, the vehicles stop at the relevant measurement stations to correct the temporal trends. Mobile measurements can be supported by thermal pictures from aircraft. These are not alternatives to mobile measurements because of the missing wind information, which is important for the dynamics of the processes. Otherwise, there is a risk that single measurements can be over interpreted, which are absolutely different for other wind conditions. For visualizations, lasers and recently also fibre optic systems can be applied, while the latter method offers a direct temperature measurement (Zeeman et al. 2015).

Vertical soundings of the atmospheric boundary layer with balloons or indirect measurement techniques (sodar, lidar, passive remote sensing techniques in the infrared or microwave spectrum) may be useful. The aim is to study the local development of inversion layers and therefore the dilution of emitted air pollutions and depth of the exchange volume.

In heavily built up areas, radiation measurements are also necessary, e.g. the measurements of the reflected shortwave radiation or the longwave emitted radiation close to buildings. Because of climate change, these effects have an increasing relevance during hot summer days. In the last few years, the contribution of turbulent fluxes has not only been better understood, but also measured in many urban experiments. Appendix A.5 gives an overview about such experiments in the last years. Special problems are the determination of the zero-plane displacement height (see Sect. 3.1.2) and of the exact footprint (see Sect. 3.4.3, Leclerc and Foken 2014).

References

Babel W, Biermann T, Coners H, Falge E, Seeber E, Ingrisch J, Schleuß PM, Gerken T, Leonbacher J, Leipold T, Willinghöfer S, Schützenmeister K, Shibistova O, Becker L, Hafner S, Spielvogel S, Li X, Xu X, Sun Y, Zhang L, Yang Y, Ma Y, Wesche K, Graf HF, Leuschner C, Guggenberger G, Kuzyakov Y, Miehe G and Foken T (2014) Pasture degradation modifies the water and carbon cycles of the Tibetan highlands. Biogeosci. 11:6633-6656.

Bailey WG, Oke TR and Rouse WR (eds) (1997) The Surface Climate of Canada. Mc Gill-Queen's University Press, Montreal, Kingston, 369 pp.

Barry R and Blanken P (2016) Microclimate and Local Climate. Cambridge University Press, Cambridge, 316 pp.

Bendix J (2004) Geländeklimatologie. Borntraeger, Berlin, Stuttgart, 282 pp.

Best MJ and Grimmond CSB (2014) Key conclusions of the first international urban land surface model comparison project. Bull Amer Meteorol Soc. 96:805–819.

Böer W (1959) Zum Begriff des Lokalklimas. Z Meteorol. 13:5–11.

Brötz B, Eigenmann R, Dörnbrack A, Foken T and Wirth V (2014) Early-morning flow transition in a valley in low-mountain terrain. Boundary-Layer Meteorol. 152:45–63.

Cotton WR and Pielke Sr RA (2008) Human Impacts on Weather and Climate. Cambridge University Press, Cambridge, 320 pp.

Davin EL and de Noblet-Ducoudré N (2010) Climatic impact of global-scale deforestation: Radiative versus nonradiative processes. J Climate. 23:97–112.

Defant F (1949) Zur Theorie der Hangwinde, nebst Bemerkungen zur Theorie der Berg- und Talwinde. Archiv Meteorol Geophys Bioklim, Ser. A. 1:421–450.

Foken T (2013) Energieaustausch an der Erdoberfläche. Edition am Gutenbergplatz, Leipzig, 99 pp.

Gerth W-P (1986) Klimatische Wechselwirkungen in der Raumplanung bei Nutzungsänderungen. Ber Dt Wetterdienstes. 171:69 pp.

Häckel H (1989) Das Gartenklima. Ulmer, Stuttgart, 128 pp.

Herbst M, Mund M, Tamrakar R and Knohl A (2015) Differences in carbon uptake and water use between a managed and an unmanaged beech forest in central Germany. For Ecol Managem. 355:101–108.

Hupfer P (1989) Klima im mesoräumigen Bereich. Abh Meteorol Dienstes DDR. 141:181–192.

Hupfer P (ed) (1991) Das Klimasystem der Erde. Akademie-Verlag, Berlin, 464 pp.

Hupfer P (1996) Unsere Umwelt: Das Klima. B. G. Teubner, Stuttgart, Leipzig, 335 pp.

Hupfer P and Kuttler W (eds) (2005) Witterung und Klima, begründet von Ernst Heyer. B. G. Teubner, Stuttgart, Leipzig, 554 pp.

King JC and Turner J (1997) Antarctic Meteorology and Climatology. Cambridge University Press, Cambridge, 409 pp.

Klein P and Clark JV (2007) Flow variability in a North American downtown street canyon. J Appl Meteorol Climatol. 46:851–877.

Knoch K (1949) Die Geländeklimatologie, ein wichtiger Zweig der angewandten Klimatologie. Ber Dtsch Landesk. 7:115–123.

Kotthaus S and Grimmond CSB (2012) Identification of micro-scale anthropogenic CO_2, heat and moisture sources—Processing eddy covariance fluxes for a dense urban environment. Atmos Environm. 57:301–316.

Kratzer (1956) Das Stadtklima. Vieweg, Braunschweig, 184 pp.

Kraus H (1983) Meso- und mikro-skalige Klimasysteme. Ann Meteorol. 20:4–7.

Leclerc MY and Foken T (2014) Footprints in Micrometeorology and Ecology. Springer, Heidelberg, New York, Dordrecht, London, XIX, 239 pp.

Letzel MO (2015) Urban large-eddy simulation (LES), Advanced computational fluid dynamics for urban climatic maps. In: Ng E and Ren C (eds.), The Urban Climatic Map: A Methodology for Sustainable Urban Planning. Routledge, 421–428.

Lietzke B, Vogt R, Young DT and Grimmond CSB (2015) Physical fluxes in urban environment. In: Chrysoulakis Net al (eds.), Understanding Urban Metabolism. Routledge, Abingdon, New York, 29–44.

Mölders N (2012) Land-Use and Land-Cover Changes, Impact on climate and air quality. Springer, Dordrecht, Heidelberg, London, New York, 189 pp.

Nitzschke A (1970) Zum Verhalten der Lufttemperatur in der Kontaktzone zwischen Land und Meer bei Zingst. Veröff Geophys Inst Univ Leipzig. XIX:339–445.

Oke TR (1987) Boundary Layer Climates. Methuen, New York, 435 pp.

Orlanski I (1975) A rational subdivision of scales for atmospheric processes. Bull. Am. Meteorol. Soc. 56:527–530.

Pielke Sr RA, Adegoke JO, Chase TN, Marshall CH, Matsui T and Niyogi D (2007) A new paradigm for assessing the role of agriculture in the climate system and in climate change. Agrical Forest Meteorol. 142:234–254.

Spronken-Smith RA and Oke TR (1999) Scale modelling of nocturnal cooling in urban parks. Boundary-Layer Meteorol. 93:287–312.

Spronken-Smith RA, Oke TR and Lowry WP (2000) Advection and the surface energy balance across an irrigated urban park. Int J Climatol. 20:1033–1047.

Stull RB (1988) An Introduction to Boundary Layer Meteorology. Kluwer Acad. Publ., Dordrecht, Boston, London, 666 pp.

Stull RB (2000) Meteorology for Scientists and Engineers. Brooks/ Cole, Pacific Grove, 502 pp.

Tiesel R and Foken T (1987) Zur Entstehung des Seerauchs an der Ostseeküste vor Warnemünde. Z Meteorol. 37:173–176.

VDI (2003) Umweltmeteorologie, Lokale Kaltluft, VDI 3787, Blatt 5. Beuth-Verlag, Berlin, 86 pp.

Westermann S, Lüers J, Langer M, Piel K and Boike J (2009) The annual surface energy budget of a high-arctic permafrost site on Svalbard, Norway. The Cryosph. 3:245–263.

Witha B, Steinfeld G, Dörenkämper M and Heinemann D (2014) Large-eddy simulation of multiple wakes in offshore wind farms. J Phys: Conf Ser. 555: 012108.

Zeeman M, Selker J and Thomas C (2015) Near-surface motion in the nocturnal, stable boundary layer observed with fibre-optic distributed temperature sensing. Boundary-Layer Meteorol. 154:189–205.

Chapter 8
Applied Meteorology

In the previous chapters, the basics of applied meteorology as defined in Sect. 1.1 were presented. In this chapter, some examples of applications are presented which are important for practical work. Certainly, all countries have their own standards and other rules for expert reports, methods, and software programs; thus, in this chapter we can give only some hints that are not greatly different from the German regulations, which are also available in English and given in Appendix A.8.

8.1 Examples of Applied Meteorological Applications

8.1.1 Distribution of Air Pollution

The simplest models for the distribution of air pollution are Gaussian models. A more precise calculation needs a more sophisticated boundary layer model as described in the literature (Blackadar 1997; Arya 1999). Of micrometeorological relevance, is the determination of the stratification, and so measurements in the surface layer are necessary. The following air pollution situations which depend on wind velocity and stratification are typical and can be observed, (Blackadar 1997; Kraus 2004):

- For high wind velocities the turbulent eddies are small and the plume of pollutants in the atmosphere expands quickly. Note that for wind velocities above 6 ms^{-1}, nearly always neutral stratification can be assumed.
- If the size of the turbulent eddies approximately equals the width of the plume, then serpentine forms of sideways and up-and-down movements of the plume occur. This is typical for low wind speed and sunny conditions and is referred to as *looping*.
- For smaller eddies, instead of looping the plume shape is conical, and is referred to as *coning*.

Pasquill class	Description	σ_φ
A	Extreme unstable	25
B	Unstable	20
C	Light unstable	15
D	Neutral	10
E	Light stable	5
F	Stable	2.5

- An almost completely horizontal distribution of the plume exists for only low movements of air and on clear nights. This condition is referred to as *fanning*. In the case of an inversion layer and neutral or slightly unstable stratification near the surface, as in the morning hours, the plume can come in contact with the ground surface. This condition is referred to as *fumigation*.

The estimation of the stratification is often made using stability classes. These classes are based on meteorological observations or on the stability-dependent fluctuation of the wind direction, where the fluctuations of the wind component perpendicular to the mean wind direction σ_v are relevant. Note that for averaging of wind directions, the jump between 360 and 0° must be taken into account. If the wind direction fluctuation parameters are not observed, then a parameterization with the mixed layer z_i, the roughness parameter z_0, and integrated stability function $\psi(z/L)$, dependent on the Obukhov-length L, are possible (Blackadar 1997):

$$\sigma_\varphi \approx \frac{\sigma_v}{\overline{u}} = \frac{\kappa(12 - 0.5\,z_i/L)^{1/3}}{\ln(z/z_0) - \psi(z/L)} \tag{8.1}$$

With this and Table 8.1, the stability classes according to Pasquill (1961) can be determined. Note that in complex terrain the standard deviation of the wind direction is greater than that over flat terrain and a more unstable stratification is predicted. In the case of available direct measurements of the stratification, these should have priority.

An estimation of the stratification is also possible with the wind speed, the radiation, and the cloudiness (Table 8.2). The comparison of different stability classes is of special interest because the Pasquill classes are not used in all countries. In Germany, for example, the classes according to Klug-Manier (Klug 1969; Manier 1975; VDI 2015) are used. A comparison including the Obukhov length is given in Table 8.3. With the methods to measure the energy exchange given in Chap. 4 or the models given in Chap. 5, the necessary stratification for dispersion models can be determined.

The dispersion of air pollutions can be described with probability density functions (Blackadar 1997; Arya 1999):

Table 8.2 Determination of the Pasquill stability class from meteorological parameters (Blackadar 1997, adapted with kind permission of © Springer, Berlin, Heidelberg 1997, All rights reserved)

Surface wind ms^{-1}	Irradiation at day			Cloudiness at night	
	Strong clouds: 0/8–2/8	Moderate clouds: 3/8–5/8	Low clouds: 6/8–8/8	Thin clouds or ≥ 4/8	≤ 3/8
<2	A	A–B	B		
2	A–B	B	C	E	F
4	B	B–C	C	D	E
6	C	C–D	D	D	D
>6	C	D	D	D	D

Table 8.3 Comparison of different stability classes for rough or heterogeneous surfaces

	Klug/Manier	Pasquill	Obukhov length L	z/L for $z = 10$ m
Very unstable	V	A	−30	−0.33
Unstable	IV	B	−100	−0.1
Neutral to light unstable	III/2	C	−300	−0.033
Neutral to light stable	III/1	D (neutral)	5000	0.002
Stable	II	E (light stable)	250	0.04
Very stable	I	F (stable)	60	0.17

$$\int_{-\infty}^{\infty} F(x)\, dx = 1 \qquad (8.2)$$

For a three dimensional distribution follows:

$$\int_{-\infty}^{\infty} \int_{-\infty}^{\infty} \int_{-\infty}^{\infty} F(x)\, G(y)\, H(z)\, dx\, dy\, dz \qquad (8.3)$$

For a point source with constant emission rate $Q\, dt$ and constant horizontal wind velocity the distribution density function is:

$$F(x) = \frac{1}{\bar{u}\, dt} \qquad (8.4)$$

For the transverse horizontal and vertical distributions, the Gaussian distribution functions are used:

$$G(y) = \frac{1}{\sqrt{2\pi}\,\sigma_v} \exp\left(-\frac{y^2}{2\,\sigma_v}\right) \qquad (8.5)$$

$$H(z) = \frac{1}{\sqrt{2\pi}\,\sigma_w} \exp\left(-\frac{z^2}{2\,\sigma_w}\right) \qquad (8.6)$$

The concentration distribution can be also calculated with Fick's diffusion law:

$$\frac{\partial \chi}{\partial t} + \overline{u}\,\frac{\partial \chi}{\partial x} = \frac{\partial}{\partial x}\left(K_x\,\frac{\partial \chi}{\partial x}\right) + \frac{\partial}{\partial y}\left(K_y\,\frac{\partial \chi}{\partial y}\right) + \frac{\partial}{\partial z}\left(K_z\,\frac{\partial \chi}{\partial z}\right) \qquad (8.7)$$

The parameterization of the diffusion coefficients is made with error functions (see also Eq. 3.1):

$$\sigma_{u_x}^2 = 2K_x t \quad \sigma_{u_y}^2 = 2K_y\,t \quad \sigma_{u_z}^2 = 2K_z\,t \qquad (8.8)$$

The concentration distribution for constant source strength and horizontal wind speed in x-direction is given by:

$$\chi(x, y, z) = \frac{Q}{2\,\pi\,\overline{u}\,\sigma_{u_y}\,\sigma_{u_z}} \exp\left(-\frac{y^2}{2\,\sigma_{u_y}} - \frac{z^2}{2\,\sigma_{u_z}}\right) \qquad (8.9)$$

In the case of no meteorological data, the standard deviations of the wind components can be parameterized with micrometeorological approaches as described in Sect. 2.4.

Presently, a number of dispersion models are available. One widely distributed model is that developed by Gryning et al. (1983), which is the basis for the footprint model by Schmid (1997). Differences of various models are the parameterization of the wind components and the applications of three-dimensional wind fields in flat and complex terrain. Recent and more sophisticated models use numerical boundary layer approaches with parameterizations of the profiles of the turbulent wind components rather than the Gaussian distribution functions.

8.1.2   Meteorological Conditions of Wind Energy Use

In the beginning of wind energy use, meteorology was especially important in the investigations of the operational requirements and efficiency. The reason for this is that the capacity of wind power stations depends on the cube of the wind speed, u. Thus, slightly higher wind speeds make a significantly higher wind power capacity (F: area covered over by the rotor, ρ: air density):

$$P = \frac{\rho}{2} F u^3 \qquad (8.10)$$

A first and early comprehensive study to the meteorological aspects of wind energy use was presented by the World Meteorological Organization (WMO 1981). In that study, the remarkable influence of the surface roughness and internal boundary layers were mainly discussed (see Sects. 3.1 and 3.2).

Significant benefits for the meteorological support of wind energy were made with the European Wind Atlas (Troen and Lundtang Peterson 1989). The basis for expert reports on the capacity of wind power stations is the Weibull frequency distribution, where the skewness of the wind velocity distribution is well presented for $k < 3.6$. Using this distribution function, the power density can be determined:

$$P = A^3 \, F_P(k) \qquad (8.11)$$

The Weibull parameters A and k and the distribution $F_P(k)$ are tabulated for wind direction classes for all relevant meteorological stations. The basic idea of the wind atlas is to correct long-term climate measurements of meteorological reference stations regarding local influences, and to determine Weibull distributions that are free of these influences for these reference stations. For an expert review of a new location of a wind power station, the nearest reference station is used and the Weibull distribution will be corrected by the local influences of the site. From this, the possible wind power capacity of the new station can be estimated.

Some of the correction methods used are of general interest (compare also Sect. 3.3). One method is the determination of the surface roughness, which is dependent on the distribution of obstacles. For a uniform distribution of obstacles it follows

$$z_0 = 0.5 \frac{h \, S}{A_H}, \qquad (8.12)$$

where h is obstacle height, S is the area of the cross section of the obstacle in wind direction, A_H is the mean horizontal area where $A_H \gg S$. Over the ocean, the Charnock-equation Eq. (2.61) is used, and over land only four roughness classes are applied (sand/water, agricultural area with an open image, agricultural area with a complex image, and built-up areas/suburban areas). For the averaging of the roughness parameter, a special area averaging method was developed (Table 3.2). The method used for the determination of the wind shadow behind an obstacle was already discussed in Sect. 3.3. Furthermore, the wind atlas includes a current model, which also can calculate the increase of the wind speed over hills. In Europe and other regions, the European Wind Atlas together with the application software is presently applied in expert reviews. The determination of the wind energy potential over a large area is made with meso-scale models (Mengelkamp 1999). Many models are designed for flat lands, and are of limited use for mountain regions. In mountain regions, the very complex turbulence and flow structures

cause a high mechanical pressure on the wind power station, and the operation is not always optimal relative to the turbulence spectra. The influence of a hetero-geneous landscape can also be estimated with footprint models (Foken 2013).

The increasing use of wind energy production in hilly regions, large wind parks, and off-shore requires further meteorological research and a specific recommen-dation. Increasingly for off-shore applications Large-Eddy-Simulations are applied (Witha et al. 2014).

8.1.3   Sound Propagation in the Atmosphere

The propagation of sound in the atmosphere is an important issue because of increasing noise pollution for example by vehicle traffic on roads and aircraft. The noise is very disturbing during the night with stable stratification; however, these periods are not regulated by laws and are also insufficiently investigated from the scientific point of view.

The sound velocity can be determined in the dry atmosphere with the Laplace-equation

$$
\begin{aligned}
c_{tr} &= \sqrt{\gamma_{tr} p / \rho}, \\
\gamma_{tr} &= c_p / c_v,
\end{aligned}
\tag{8.13}
$$

where p is the air pressure. From the application of the ideal gas equation, which requires that the sound pressure $p_s \ll p$ and the frequency of the free molecule movement $f_s \ll 10^5$ kHz, and $\mu_d = 28.97$ kg kmol^{-1}, follows:

$$
c_d = \sqrt{\gamma_d R_L T / \mu_d}
\tag{8.14}
$$

For moist air:

$$
c_m = \sqrt{\gamma_d \frac{R_L T}{\mu_d} \left(1 + 0.28 \frac{e}{p}\right)}
\tag{8.15}
$$

The sound velocity of moist air can also be determined as an additional term in the sound velocity for dry air:

$$
\begin{aligned}
c_m &= c_d \sqrt{1 + 0.28 \frac{e}{p}} \\
c_m &= c_d \left(1 + 0.14 \frac{e}{p}\right) \qquad \text{for} \qquad t < 30\,^{\circ}\text{C}, e/p < 4\%
\end{aligned}
\tag{8.16}
$$
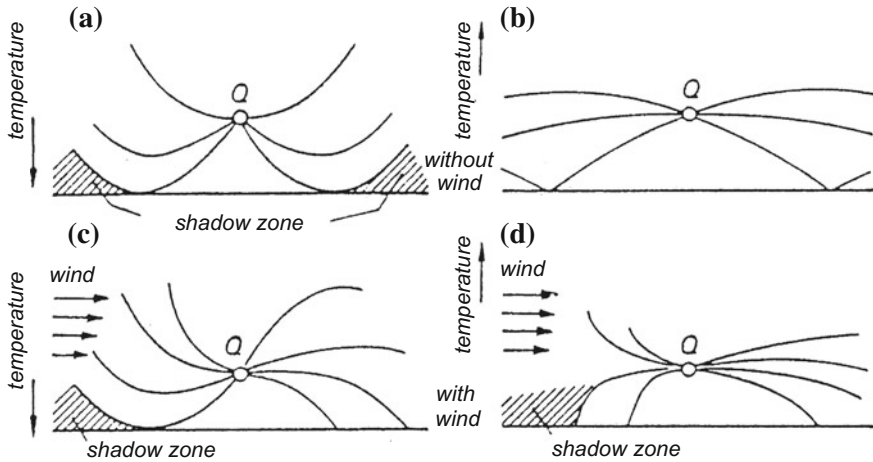
Fig. 8.1 Sound propagation close to the surface (VDI 1988, published with kind permission of ©
VDI e.V. and Beuth-Verlag Berlin 1988, All rights reserved)

Due to the strong vertical gradients of wind and temperature near the ground
surface, there are gradients of the sound velocity, which can cause deflections of
sound either to or from the surface

$$\frac{dc}{dz} = 0.6\frac{dT}{dz} + \cos\varphi\,\frac{du}{dz}, \tag{8.17}$$

where φ: angle of the sound direction to the vertical direction.

Consequently, sound deflection to the ground is connected with an increase of
the sound velocity with the height. This happens when the temperature increases
with height (inversion), and the deflection is stronger downwind of the sound
source than upwind. The opposite case occurs for unstable stratification, where the
sound deflection is upward and increases more upwind of the sound source than
downwind. Downwind of the sound source, shadow zones are found near the
ground surface. The situations are illustrated in Fig. 8.1.

The international standards (DIN-ISO 1999) combine the meteorological influ-
ences on sound velocity into a mean measure, which represents neutral and slightly
unstable stratification. But the sound propagation in the stable case is complex,
especially when the sound is deflected to the ground and the atmosphere is divided
into many thin layers. Sound can follow these layers without significant damping.
Increasing traffic-generated sound is connected with increasing noisiness especially
at night. This connection is not adequately reflected in laws and assessment pro-
cedures. Micrometeorologist can help solve such problems, but the ability to
describe stable stratification conditions is limited (see Sect. 3.7).

8.1.4   Human Biometeorology

Human biometeorology describes the specific influence of weather and climate on people (Tromp 1963; Hentschel 1982). The effects are classified based on effective mechanisms: The *thermo effect* mechanism includes temperature, humidity, wind velocity, shortwave, and long-wave radiation. The *actinic effect* mechanism includes the visible and ultraviolet radiation with a direct biological effectiveness (no heating). The *air hygienic* effect mechanism includes solid, liquid, and gaseous natural and anthropogenic air pollution. Furthermore noise, wind, and smells affect humans.

Fanger (1972) developed a Predicted Mean Vote (*PMV*) to combine the effects of these mechanisms on humans as an empirical heat balance equation. This is a very complex empirical function, which includes the internal heat production, the heat isolation by clothing, the air temperature, the water vapor pressure, the radiation temperature of the surface, and the wind velocity:

$$
\begin{aligned}
PMV = {} & \left[0.028 + 0.303 \, \exp\left(-0.036 \frac{M}{A_{Du}} \right) \right] \cdot \\
& \left[\frac{H}{A_{Du}} - Q_{Ed} - Q_{Esw} - Q_{Ea} - Q_{Ha} - Q_H - I \uparrow \right]
\end{aligned}
\tag{8.18}
$$

For the determination of the *PMV*, the internal heat production per unit area is related to the unit area, H/A_{Du}, in Wm^{-2}, where $H = M + W$ is the sum of the total energy turnover (metabolic value M), and W is the mechanical energy. From these values, the energy loss by the diffusion of water vapour through the skin Q_{Ed}, the evaporation of sweat Q_{Esw}, the latent Q_{Ea} and the sensible heat loss Q_{Ha} by respiration, the convective heat loss Q_H, and the longwave radiation loss $I\uparrow$ are subtracted. The equations are bulk equations similar to Eqs. (4.1)–(4.3) and the Stefan-Boltzmann equation Eq. (1.4), but the coefficients used are not comparable. The normalization of the equation is made in such a way that *PMV* values of ±0.5 are related to comfort conditions. The range from 0 to -3.5 is related to increasing cold stress, and from 0 to 3.5 to increasing heat stress. In the USA, a similar index (referred to as heat index) was developed (Steadman 1979a, b).

In Germany, the model for the *PMV* calculation is called Klimamichel (a word meaning the plane honest German) model (Höppe 1984, 1992; Jendritzky et al. 1990) which is shown schematically in Fig. 8.2. The calculations are based on a uniform man or woman. Therefore single values have no great significance. But frequency distributions give information about the heat stress in different regions. A transformation of the *PMV* index into a simple value for the heat stress on a human is the physiological equivalent temperature (*PET*, Höppe 1999) given in degrees centigrade. A comparison of both parameters is given in Table 8.4. These values also include related feeling classes and stress factors. With the *PET* index, urban climatologically and climatologically classifications of larger areas can be described (Matzarakis et al. 1999).
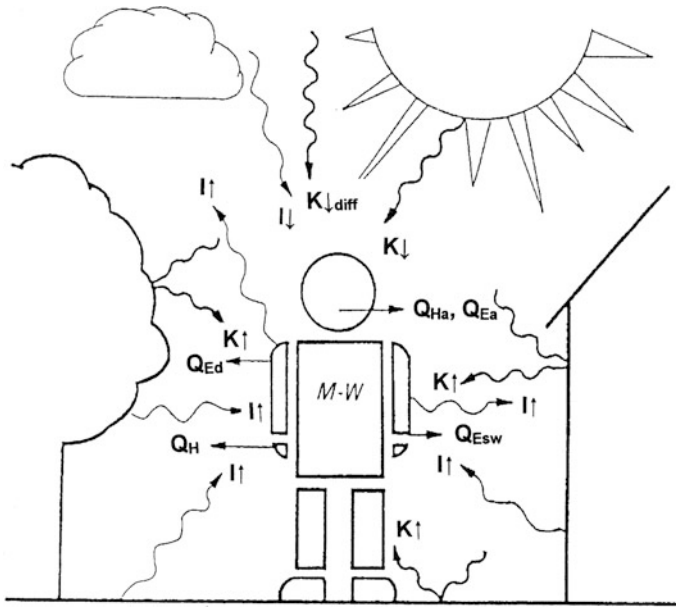
Fig. 8.2 Illustration of the *PMV* determination with the Klimamichel model (Adapted from Jendritzky et al. 1990, with kind permission of © Akademie für Raumforschung und Landschaftsplanung, Hannover, All rights reserved)

The significance of an integrated assessment of public health impacts in a changing climate was recognized in the last 15 years and on an international level the Universal Thermal Climate Index (*UTCI*) was developed (Jendritzky et al. 2012). This index is better adapted to the thermoregulation of the people and based on a model by Fiala et al. (2001) with several updates and the clothing model by Havenith et al. (2012). From Table 8.4 it is obvious that due to the thermal self-regulation of the human body the comfortable range is quite large from 9 to 26 °C. Above this temperature the thermal stress increases quite fast. For cold temperatures the stress has a significant larger range than in previous indices.

For the feeling of the stress due to the weather, which can also be different because of microclimatological effects, the cooling effect of the wind velocity (wind chill) and the level of sultriness (mugginess) are very meaningful parameters. The wind chill temperature is a hypothetic temperature for which under calm conditions the skin passes the same amount of heat as for a given temperature and wind velocity. Recently, the wind chill temperature has been repeatedly modified (Osczevski 2000; Tikusis and Osczevski 2002, 2003; Osczevski and Bluestein 2005), and the American Meteorological Service currently uses the following expression:

Table 8.4 Comparison table of the Predicted Mean Vote (*PMV*) and the physiological equivalent temperature (*PET*) and related feelings and stress effects (Matzarakis and Mayer 1997) and the Universal Thermal Climate Index (*UTCI*) with the related stress classification (Bröde et al. 2013)

PMV	PET in °C	Thermal feeling	Physiological pressure class	UTCI In °C	Physiological pressure class
				−55	
					Extreme cold stress
				−40	
		Very cold			Very strong cold stress
−3.5	4			−27	
		Cold	Strong cold stress		Strong cold stress
−2.5	8			−13	
		Cool	Moderate cold stress		Moderate cold stress
−1.5	13			0	
		Slightly cool	Light cold stress		Light cold stress
−0.5	18			9	
		Comfortable	No heat pressure		No heat pressure
0.5	23			26	
		Slightly warm	Light heat pressure		Moderate heat pressure
1.5	29			32	
		Warm	Moderate heat pressure		Strong heat pressure
2.5	35			38	
		Hot	Strong heat pressure		Very strong heat pressure
3.5	41			46	
		Very hot	Extreme heat pressure		Extreme heat pressure
				55	

Fig. 8.3 Determination of the level of sultriness according to Hentschel (1982) in the modification by Hupfer (1996), adapted with kind permission of © Teubner Verlag Stuttgart, Leipzig 1996, All rights reserved
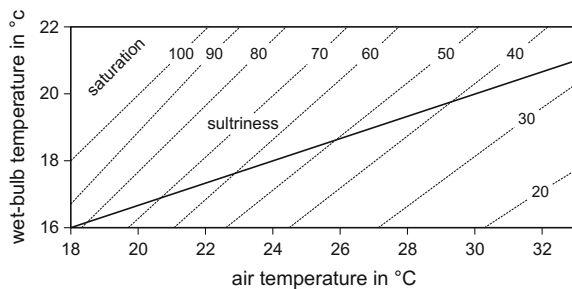
$$t_{Wind-Chill} = 13.12 + 0.6215t - 11.37u^{0,16} + 0.3965\, t\, u^{0,16}$$
$$t \text{ in } °C, u \text{ in } km\,h^{-1}$$

(8.19)

The sultriness depends on the air temperature and the atmospheric moisture. In Fig. 8.3, the level of sultriness is dependent on the wet bulb temperature measured with an aspirated psychrometer or it may be shown as a function of relative

humidity. In a similar way, a sultriness index was defined as part of the index developed by Steadman (1979a), which was later on called heat index.

8.2 Perspectives of the Applied Meteorology

It should be noted that the methods used in applied meteorology are often phenomenological or work with simple parameterizations. This may be in contrast to detailed theoretical explanations found in this book. This can be explained by the engineering work in applied meteorology, which uses simple analytical relations. In air pollution and wind energy investigations, in addition to simple standards numerical models are more often applied. The international tendency is to replace the description of state variables with the description of processes. Modern flux measurement methods and sensors as described in Chaps. 4 and 6 are increasingly being applied. The limiting application conditions of the methods in areas with obstacles and in complex terrain have been overcome with a quality assessment of the data and a combination of in-situ and wind tunnel measurements.

This book should be a basis for increasing the theoretical and experimental levels of applied meteorology. In this period of climate change, it is important to make qualitative statements, but it is even more important to make quantitative statements. Therefore basic knowledge is necessary.

References

Arya SP (1999) Air Pollution Meteorology and Dispersion. Oxford University Press, New York, Oxford, 310 pp.

Blackadar AK (1997) Turbulence and Diffusion in the Atmosphere. Springer, Berlin, Heidelberg, 185 pp.

Bröde P, Blazejczyk K, Fiala D, Havenith G, Holmér I, Jendritzky G, Kuklane K and Kampmann B (2013) The Universal Thermal Climate Index UTCI compared to ergonomics standards for assessing the thermal environment. Ind Health. 51:16–24.

DIN-ISO (1999) Dämpfung des Schalls bei der Ausbreitung im Freien, Teil 2, Allgemeine Berechnungsverfahren DIN ISO, 9613-2. Beuth-Verlag, Berlin, 26 pp.

Fanger PO (1972) Thermal comfort: Analysis and applications in environmental engineering. McGraw Hill, New York, 244 pp.

Fiala D, Lomas KJ and Stohrer M (2001) Computer prediction of human thermoregulatory and temperature responses to a wide range of environmental conditions. Int J Biometeorol. 45:143–159.

Foken T (2013) Application of footprint models for wind turbine locations. Meteorol Z. 22:111–115.

Gryning S-E, van Ulden AP and Larsen S (1983) Dispersions from a ground level source investigated by a K model. Quart J Roy Meteorol Soc. 109:355–364.

Havenith G, Fiala D, Błazejczyk K, Richards M, Bröde P, Holmér I, Rintamaki H, Benshabat Y and Jendritzky G (2012) The UTCI-clothing model. Int J Biometeorol. 56:461–470.

Hentschel G (1982) Das Bioklima des Menschen. Verlag Volk und Gesundheit, Berlin, 192 pp.

Höppe P (1984) Die Energiebilanz des Menschen. Wiss. Mitt. Meteorol. Inst. Uni. München. 49:173 pp.

Höppe P (1992) Ein neues Verfahren zur Bestimmung der mittleren Strahlungstemperatur im Freien. Wetter und Leben. 44:147–151.

Höppe P (1999) The physiological equivalent temperature—a universal index for biometeorological assessment of the thermal environment. Int J Biometeorol. 43:71–75.

Hupfer P (1996) Unsere Umwelt: Das Klima. B. G. Teubner, Stuttgart, Leipzig, 335 pp.

Jendritzky G, Metz G, Schirmer H and Schmidt-Kessen W (1990) Methodik zur raumbezogenen Bewertung der thermischen Komponente im Bioklima des Menschen. Beitr Akad Raumforschung Landschaftsplanung. 114:80 S.

Jendritzky G, de Dear R and Havenith G (2012) UTCI—Why another thermal index? Int J Biometeorol. 56:421–428.

Klug W (1969) Ein Verfahren zur Bestimmung der Ausbreitungsbedingungen aus synoptischen Beobachtungen. Staub - Reinhaltung der Luft. 29:143–147.

Kraus H (2004) Die Atmosphäre der Erde. Springer, Berlin, Heidelberg, 422 pp.

Manier G (1975) Vergleich zwischen Ausbreitungsklassen und Temperaturgradient. Meteorol Rundschau. 28:6–11.

Matzarakis A and Mayer H (1997) Heat stress in Greece. Int J Biometeorol. 41:34–39.

Matzarakis A, Mayer H and Iziomon M (1999) Applications of a universal thermal index: physiological equivalent temperature. Int J Biometeorol. 43:76–84.

Mengelkamp H-T (1999) Wind climate simulation over complex terrain and wind turbine energy output estimation. Theor Appl Climat. 63:129–139.

Osczevski R and Bluestein M (2005) The new wind chill equivalent temperature chart. Bull Amer Meteorol Soc. 86:1453–1458.

Osczevski RJ (2000) Windward cooling: An overlooked factor in the calculation of wind chill. Bull Amer Meteorol Soc. 81:2975–2978.

Pasquill F (1961) Estimation of the dispersion of windborne material. Meteorol Mag. 90:33–49.

Schmid HP (1997) Experimental design for flux measurements: matching scales of observations and fluxes. Agrical Forest Meteorol. 87:179–200.

Steadman RG (1979a) The Assessment of Sultriness. Part I: A Temperature-Humidity Index Based on Human Physiology and Clothing Science. J Appl Meteorol. 18:861–873.

Steadman RG (1979b) The Assessment of Sultriness. Part II: Effects of Wind, Extra Radiation and Barometric Pressure on Apparent Temperature. J Appl Meteorol. 18:874–885.

Tikusis P and Osczevski RJ (2002) Dynamic model of facial cooling. J Appl Meteorol. 41:1241–1246.

Tikusis P and Osczevski RJ (2003) Facial cooling during cold air exposure. Bull Amer Meteorol Soc. 84:927–933.

Troen I and Lundtang Peterson E (1989) European Wind Atlas. Risø National Laboratory, Roskilde, 656 pp.

Tromp SW (1963) Medical Biometeorology. Elsevier, Amsterdam, XXVII, 991 pp.

VDI (1988) Schallausbreitung im Freien, VDI 2714. Beuth-Verlag, Berlin, 18 pp.

VDI (2015) Umweltmeteorologie: Atmosphärische Ausbreitungsmodelle, Bestimmung der Ausbreitungsklasse nach Klug/Manier, VDI 3782, Blatt 6. Beuth-Verlag, Berlin, 8 pp.

Witha B, Steinfeld G and Heinemann D (2014) High-resolution offshore wake simulations with the LES model PALM. In: Hölling M et al (eds.), Wind Energy—Impact of Turbulence. Springer, Berlin Heidelberg, 175–181.

WMO (1981) Meteorological aspects of the utilization of wind as an energy source. WMO, Techn Note. 175:180 pp.

Appendix

A.1 Further Monographs

In the following, monographs are listed, which are recommended for a further study. The selection is limited to micrometeorological and measurement technique textbooks.

Further Micrometeorological Literature

Arya, SP (1999) Air pollution meteorology and dispersion. Oxford University Press, New York, Oxford, 310 pp.

Arya, SP (2001) Introduction to micrometeorology. Academic Press, San Diego, 415 pp.

Bailey, WG, Oke, TR, Rouse, WR (eds) (1997) The surface climate of Canada. Mc Gill-Queen's University Press, Montreal, Kingston, 369 pp.

Barry R and Blanken P (2016) Microclimate and local climate. Cambridge University Press, Cambridge, 379 pp.

Bendix, J (2004) Geländeklimatologie. Borntraeger, Berlin, Stuttgart, 282 pp.

Bird RB, Stewart WE and Lightfoot EN (2007) Transport phenomena. John Wiley & Sons, Inc., New York, 905 pp.

Blackadar, AK (1997) Turbulence and diffusion in the atmosphere. Springer, Berlin, Heidelberg, 185 pp.

Campbell GS and Norman JM (2013) Introduction to environmental biophysics. Springer, New York, 312 pp.

Garratt, JR (1992) The atmospheric boundary layer. Cambridge University Press, Cambridge, 316 pp.

Geiger R, Aron RH and Todhunter P (2009) The Climate near the ground. Rowman & Littlefield, Lanham, XVIII, 623 pp.

Hari P, Heliövaara K and Kulmala L (eds) (2013) Physical and physiological forest ecology. Springer, Dordrecht, Heidelberg, New York, London, 534 pp.

Hatfield JL and Baker JM (eds) (2005) Micrometeorology in agricultural systems. American Society of Agronomy, Madison, 584 pp.

Jones HG (2013) Plants and microclimate. Cambridge Univ. Press, Cambridge, 423 pp.

Kaimal, JC, Finnigan, JJ (1994) Atmospheric boundary layer flows: Their structure and measurement. Oxford University Press, New York, NY, 289 pp.

Kantha, LH, Clayson, CA (2000) Small scale processes in geophysical fluid flows. Academic Press, San Diego, 883 pp.

Kraus H (2008) Grundlagen der Grenzschichtmeteorologie. Springer, Berlin, Heidelberg, 211 pp.

Leclerc MY and Foken T (2014) Footprints in micrometeorology and ecology. Springer, Heidelberg, New York, Dordrecht, London, 239 pp.

Lee, X, Massman, WJ, Law, B (Editors) (2004) Handbook of micrometeorology: A guide for surface flux measurement and analysis. Kluwer, Dordrecht, 250 pp.

Moene AF and van Dam JC (2014) Transport in the atmosphere-vegetation-soil continuum. Cambridge University Press, Cambridge, 436 pp.

Mölders N (2012) Land-use and land-cover changes, Impact on climate and air quality. Springer, Dordrecht, Heidelberg, London, New York, 189 pp.

Mölders N and Kramm G (2014) Lectures in meteorology. Springer, Cham Heidelberg New York Dordrecht London 591 pp.

Monson R and Baldocchi D (2014) Terrestrial biosphere-atmosphere fluxes. Cambridge University Press, New York, 487 pp.

Monteith JL and Unsworth MH (2008) Principles of environmental physics, 3rd edition. Elsevier, Academic Press, Amsterdam, Boston, 418 pp.

Oke, TR (1987) Boundary layer climates. Methuen, New York, 435 pp.

Salby ML (2012) Physics of the atmosphere and climate. Cambridge University Press, Cambridge, 666 pp.

Stull, RB (1988) An Introduction to boundary layer meteorology. Kluwer Acad. Publ., Dordrecht, Boston, London, 666 pp.

Stull R (2015) Practical meteorology: An algebra-based survey of atmospheric science. © Author, CC Attribution 4.0 License, ISBN 978-0-88865-176-1, Vancouver, 924 pp.

Venditti JG, Best JL, Church M and Hardy RJ (2013) Coherent flow structures at Earth's surface. John Wiley & Sons, Ltd., Chichester, 387 pp.

Vilà-Guerau de Arellano J, Van Heerwaarden CC, van Stratum BJH and van den Dries K (2015) Atmospheric boundary layer. Cambridge University Press, Cambridge, 265 pp.

Wyngaard JC (2010) Turbulence in the atmosphere. Cambridge University Press, Cambridge, 393 pp.

Further Measurement Technique Literature

Aubinet M, Vesala T u. Papale D (eds.) (2012) Eddy covariance: A practical guide to measurement and Data Analysis. Springer, Dordrecht, Heidelberg, London, New York, 438 pp.

Bentley, JP (2005) Principles of measurement systems. Pearson Prentice Hall, Harlow, 528 pp.

Brock, FV, Richardson, SJ (2001) Meteorological measurement systems. Oxford University Press, New York, 290 pp.

DeFelice, TP (1998) An introduction to meteorological Instrumentation and measurement. Prentice Hall, Upper Saddle River, 229 pp.

Dobson, F, Hasse, L, Davis, R (Editors) (1980) Air-sea interaction, Instruments and methods. Plenum Press, New York, 679 pp.

Emeis S (2010) Measurement methods in atmospheric sciences. Borntraeger Science Publishers, Stuttgart, 257 pp.

Hebra AJ (2010) The physics of metrology. Springer, Wien, New York 383 pp.

Harrison GR (2015) Meteorological measurements and instrumentations. John Wiley and Sons, Chichester, 257 pp.

Kaimal, JC, Finnigan, JJ (1994) Atmospheric boundary layer flows: Their structure and measurement. Oxford University Press, New York, NY, 289 pp.

Strangeways I (2003) Measuring the natural environment. 2nd ed. Cambridge University Press, Cambridge, 534 pp.

A.2 Use of SI-Units

The following table includes important SI-units used in the book. The basic units
are **bold** highlighted.

Name	SI-unit	Unit	Calculation
Length	**Meter**	**m**	
Time	**Second**	**s**	
Velocity		$m\ s^{-1}$	$1\ km\ h^{-1} = (1/3.6)\ m\ s^{-1}$
Acceleration		$m\ s^{-2}$	
Mass	**Kilogram**	**kg**	
Density		$kg\ m^{-3}$	
Impulse		$kg\ m\ s^{-1}$	$1\ kg\ m\ s^{-1} = 1\ N\ s$
Force	Newton	N	$1\ N = 1\ kg\ m\ s^{-2}$
Pressure, friction	Pascal	Pa	$1\ Pa = 1\ N\ m^{-2}$ $1\ Pa = 1\ kg\ m^{-1}\ s^{-2}$
Air pressure	Hektopascal	hPa	$1\ hPa = 100\ Pa$
Work, energy	Joule	J	$1\ J = 1\ N\ m = 1\ W\ s$ $1\ J = 1\ kg\ m^2\ s^{-2}$
Power	Watt	W	$1\ W = 1\ J\ s^{-1} = 1\ N\ m\ s^{-1}$ $1\ W = 1\ kg\ m^2\ s^{-3}$
Energy flux density		$W\ m^{-2}$	$1\ W\ m^{-2} = 1\ kg\ s^{-3}$
Temperature	**Kelvin**	**K**	
Celsius-temperature		°C	$0\ °C = 273.15\ K$
Temperature difference		K	

A.3 Constants and Important Parameters

Even though the accuracy of meteorological measurements is at most only 3–5
significant digits, the following physical constants are given with errors expressed
in ppm, because sometimes in the literature different values are reported.

The values listed are taken from the 1986 calculations of Cohen and Taylor
(1986) and the international temperature scale ITS-90 as given by Sonntag (1990).

Constant	Symbol	Value	Error
Standard values			
Standard air pressure	p_0	1013.25 hPa	
Standard temperature	T_0	273.15 K = 0 °C	
Temperature of the triple point of water		273.16 K	
	g	$9.80665\ m\ s^{-2}$	

<div align="right">(continued)</div>

(continued)

Constant	Symbol	Value	Error
Standard acceleration due to gravity at latitude 45°			
General constants			
Velocity of the light in vacuum	c	299 792 458 m s^{-1}	Exact
Planck's constant	h	6.626 0755(40) 10^{-34} J s	0.60
Physical-chemical constants			
Avogadro number	N_A	6.022 1367(36) 10^{23} mol^{-1}	0.59
Atom mass ^{12}C/12	m_u	1.660 5402(10) 10^{-27} kg	0.59
Universal gas constant	R	8.314 510(70) J mol^{-1} K^{-1}	8.4
Boltzmann constant R/N$_A$	k	1.380 658(12) J K^{-1}	8.4
Molar volume (ideal gas)	RT_0/p_0	22.414 10(19) l mol^{-1}	8.4
Stefan-Boltzmann constant	σ_{SB}	5.670 51(19) 10^{-8} W m^{-2} K^{-4}	34
Wien's constant	$\lambda_{max}T$	2.897 756(24) 10^{-3} m K	8.4
Thermo-dynamical constants			
Molar mass of dry air	M_L	0.028 9645(5) kg mol^{-1}	17
Molar mass of water vapor	M_W	0.018 01528(50) kg mol^{-1}	27
Ratio M$_W$/M$_L$	γ	0.62198(2)	33
Gas constant of dry air	R_L	287.058 6(55) J kg^{-1} K^{-1}	19
Gas constant of water vapor	R_W	461.525 (13) J kg^{-1} K^{-1}	29

The following quantities are valid for 1013.25 hPa and 15 °C, if no other remark is given (Stull 1988):

Quantity	Symbol	Value	Remark
Air			
Specific heat of dry air at constant pressure	$(c_p)_L$	1004.67 J kg^{-1} K^{-1}	(1)
Specific heat of moist air at constant pressure	c_p	$= c_{pL} (1 + 0.84\ q)$, q in kg kg^{-1}	
Specific heat of dry air at constant volume	$(c_v)_L$	718 J kg^{-1} K^{-1}	(1)
Ratio of the specific heats	$(c_p/c_v)_L$	$= 7/5 = 1.4$	(1)

(continued)

(continued)

Quantity	Symbol	Value	Remark
Ratio of the gas constant and the specific heat for dry air	$(R_L/c_p)_L$	$= 2/7 = 0.286$	(1)
Density	ρ_L ρ_{L0}	1.225 kg m^{-3} 1.2923 kg m^{-3} · 0 °C	(1)
Kinematic molecular viscosity	υ	1.461 10^{-5} m^2 s^{-1}	
Molecular thermal conductivity	υ_T	2.06 10^{-5} m^2 s^{-1}	
Molecular Prandtl number	Pr	0.7092	
Dynamic molecular viscosity	$\mu = \rho_L/\upsilon$	1.789 10^{-5} kg m^{-1} s	
Molecular thermal diffusivity	$a_T =$ $\upsilon_T \cdot \rho_L \cdot c_{pL}$	2.53 10^{-2} W m^{-1} K^{-1}	
Psychrometric constant (water)		6.53 10^{-4} (1 + 0.000944 t') p K^{-1}	(2)
Psychrometric constant (ice)		5,75 10^{-4}p K^{-1}	(2)
Water and water vapor			
Specific heat of water vapor at constant pressure	$(c_p)_W$	1846 J kg^{-1} K^{-1}	
Specific heat of water vapor at constant volume	$(c_v)_W$	1389 J kg^{-1} K^{-1}	
Ratio of the specific heats	$(c_p/c_v)_W$	$= 4/3 = 1.333$	
Ratio of the gas constant and the specific heat	$(R_L/c_p)_W$	$= 1/4 = 0.25$	
Density of water	ρ_W	999.84 kg m^{-3} (0 °C, 1000 hPa)	(3)
Latent heat of vaporization	λ	$(2.501 - 0.00237$ t$)$ 10^6 J kg^{-1}	
Other quantities			
Coriolis parameter	f	1.458 10^{-4} sin φ s^{-1}	(1)
Solar constant	S	energy units: -1361 W m^{-2} kinematic units: -1.119 K m s^{-1}	(4)
Constant gravity acceleration	g_0	9.81 m s^{-2}	(5)

(1) identical data in Landolt-Börnstein (Fischer 1988) according to WMO recommendations

(2) Sonntag (1990)

(3) Wagner and Pruß (2002)

(4) Kopp and Lean (2011)

(5) Hantel (2013)

Temperature dependent quantities (Fischer 1988)

Temperature	Specific heat capacity in 10^3 J kg^{-1} K^{-1}		Latent heat in 10^6 J kg^{-1}		
	Ice	Water	Vaporization	Fusion	Sublimation
−20	1.959	4.35	2.5494	0.2889	2.8387

Temperature	Specific heat capacity in 10^3 J kg^{-1} K^{-1}		Latent heat in 10^6 J kg^{-1}		
	Ice	Water	Vaporization	Fusion	Sublimation
−10	2.031	4.27	2.5247	0.3119	2.8366
0	2.106	4.2178	2.50084	0.3337	2.8345
5		4.2023	2.4891		
10		4.1923	2.4774		
15		4.1680	2.4656		
20		4.1818	2.4535		
25		4.1797	2.4418		
30		4.1785	2.4300		
35		4.1780	2.4183		
40		4.1785	2.4062		

A.4 Further Equations

Calculation of Astronomical Quantities

In some applications, it is often necessary to determine the solar inclination angle as a function of time. The following approximations for some of these calculations must be applied in several steps:

To determine the declination of the sun, δ, the latitude of the sun, φ_s, must first be calculated (Sonntag 1989; VDI 2015)

$$\varphi_S = x - 77.51° + 1.92° \cdot \sin x$$
$$x = 0.9856° \cdot DOY - 2.72° \tag{A.1}$$

where *DOY* is the day of the year where the 1st of January has the number 1.

The declination is given by:

$$\sin \delta = 0.3978 \sin \varphi_S \tag{A.2}$$

To determine the position of the sun, the hour angle ω

$$\omega = (LTST - 12\text{h}) \cdot 15° \qquad \text{in } ° \tag{A.3}$$

must be calculated which gives the angular difference between δ and the zenith of the sun (Liou 1992), thereby *LTST* is the local true solar time. It is necessary to

apply the equation of time Z (Hughes et al. 1989), which gives the difference between the local true and the mean solar time (x see Eq. A.1).

$$Z = -7.66 \sin x - 9.87 \sin(2x + 24.99° + 3.83° \sin x) \quad \text{in min} \tag{A.4}$$

The time distance to culmination of the sun, t_H, for Central European Time ($\lambda = 15°$) is given by

$$t_H = \left\{ t - \left[12 + Z + \frac{(15 - \lambda)4}{60} \right] \right\} 3600, \tag{A.5}$$

where t: time in hours, and λ is longitude.

With the latitude φ in radians of a location, the angle of inclination of the sun can be determined for any time:

$$\sin \gamma = \sin \delta \cdot \sin \varphi + \cos \delta \cdot \cos \varphi \cdot \cos \omega \tag{A.6}$$

To determine the incoming extraterrestrial radiation at the upper border of the atmosphere from the solar constant the variability of the distance between the sun and the Earth must be taken into account

$$K \downarrow_{extraterr.} = S \left(\frac{r_0}{r} \right)^2 \sin \varphi, \tag{A.7}$$

where r_0 is the mean distance of the Earth from the Sun (149 597 870.66 km) and r is the actual distance. The ratio of both can be determined according to Hartmann (1994) as a Fourier series

$$\left(\frac{r_0}{r} \right)^2 = \sum_{n=0}^{2} a_n \cos(n\, \theta_d) + b_n \sin(n\, \theta_d) \tag{A.8}$$

with

$$\theta_d = \frac{2\pi\, DOY}{265} \tag{A.9}$$

where in the case of a leap year the denominator is 266. The coefficients for Eq. (A.8) are given in the following table:

n	a_n	b_n
0	1.000110	
1	0.034221	0.001280
2	0.000719	0.000077

Universal Functions

Even though the universal function formulated by Businger et al. (1971) and later modified by Högström (1988) are widely used, knowledge of other universal functions may be quite useful for different research activities. The following table is based on works of Dyer (1974), Yaglom (1977), Foken (1990), and Andreas (2002). The values the von-Kármán constant, κ, used in the formulations are given. The notation, 0.40*, indicates that the original function was re-calculated by Högström (1988) using $\kappa = 0.40$.

Reference	κ	Universal function for momentum exchange
Swinbank (1964)	–	$\frac{z}{L}\left(1 - e^{z/L}\right)^{-1} \quad z/L < 0$
Swinbank (1968)	0.40	$0.613(-z/L)^{-0.2} \quad -0.1 \geq z/L \geq -2$
Tschalikov (1968)	0.40	$1 + 7.74\,z/L \quad z/L > 0.04$
Zilitinkevich and Tschalikov (1968)	0.434	$1 + 1.45\,z/L \quad -0.15 < z/L < 0$ $0.41(-z/L)^{-1/3} \quad -1.2 < z/L < -0.15$ $1 + 9.9\,z/L \quad 0 < z/L$
	0.40*	$1 + 1.38\,z/L \quad -0.15 < z/L < 0$ $0.42(-z/L)^{-1/3} \quad -1.2 < z/L < -0.15$ $1 + 9.4\,z/L \quad 0 < z/L$
Webb (1970)	–	$1 + 4.5\,z/L \quad z/L < -0.03$
Dyer and Hicks (1970)	0.41	$(1 - 16\,z/L)^{-1/4} \quad -1 < z/L < 0$
Businger et al. (1971)	0.35	$(1 - 15\,z/L)^{-1/4} \quad -2 < z/L < 0$ $1 + 4.7\,z/L \quad 0 < z/L < 1$
	0.40*	$(1 - 19,3\,z/L)^{-1/4} \quad -2 < z/L < 0$ $1 + 6\,z/L \quad 0 < z/L < 1$
Dyer (1974)	0.41	$(1 - 16\,z/L)^{-1/4} \quad -1 < z/L < 0$ $1 + 5\,z/L \quad 0 < z/L$
	0.40*	$(1 - 15.2\,z/L)^{-1/4} \quad -1 < z/L < 0$ $1 + 4.8\,z/L \quad 0 < z/L$
Skeib (1980), see also: Foken and Skeib (1983) and Foken (1990)	0.40 0.40*	$1 \quad -0.0625 < z/L < 0.125$ $\left(\dfrac{z/L}{-0.0625}\right)^{-1/4} \quad -2 < z/L < -0.0625$ $\dfrac{z/L}{0.125} \quad 0.125 < z/L < 2$
Gavrilov and Petrov (1981)	0.40	$(1 - 8\,z/L)^{-1/3} \quad z/L < 0$ $1 + 5\,z/L \quad 0 < z/L$
Dyer and Bradley (1982)	0.40 0.40*	$(1 - 28\,z/L)^{-1/4} \quad z/L < 0$

(continued)

Reference	κ	Universal function for momentum exchange
Beljaars and Holtslag (1991)	0.40	$1 + z/L + \frac{2}{3}z/L(6 - 0.35z/L) \cdot e^{-0.35}z/L \quad 0 < z/L$
King et al. (1996)	0.40	$1 + 5.7\,z/L \leq 12 \quad 0 < z/L$
Handorf et al. (1999)	0.40	$1 + 5\,z/L \quad 0 < z/L < 0.6$ $4 \qquad 0.6 < z/L$

Reference	κ	Universal function for the exchange of sensible heat, $Pr_\mathrm{t} = 1$
Swinbank (1968)	0.40	$0.227\,(-z/L)^{-0.44} \quad -0.1 \geq z/L \geq -2$
Tschalikov (1968)	0.40	$1 + 5.17\,z/L \quad z/L > 0.04$
Zilitinkevich and Tschalikov (1968)	0.434	$1 + 1.45\,z/L \quad -0.15 < z/L < 0$ $0.41\,(-z/L)^{-1/3} \quad -1.2 < z/L < -0.15$ $1 + 9.9\,z/L \quad 0 < z/L$
	0.40*	$0.95 + 1.31\,z/L \quad -0.15 < z/L < 0$ $0.40\,(-z/L)^{-1/3} \quad -1.2 < z/L < -0.15$ $0.95 + 8.9\,z/L \quad 0 < z/L$
Webb (1970)	–	$1 + 4.5\,z/L \quad z/L < -0.03$
Dyer and Hicks (1970)	0.41	$(1 - 16\,z/L)^{-1/2} \quad -1 < z/L < 0$
Businger et al. (1971)	0.35	$0.74(1 - 9\,z/L)^{-1/2} \quad -2 < z/L < 0$ $0.74 + 4.7\,z/L \quad 0 < z/L < 1$
	0.40*	$0.95(1 - 11.6\,z/L)^{-1/2} \quad -2 < z/L < 0$ $0.95 + 7.8\,z/L \quad 0 < z/L < 1$
Dyer (1974)	0.41	$(1 - 16\,z/L)^{-1/2} \quad -1 < z/L < 0$ $1 + 5\,z/L \quad 0 < z/L$
	0.40*	$0.95(1 - 15.2\,z/L)^{-1/2} \quad -1 < z/L < 0$ $0.95 + 4.5\,z/L \qquad 0 < z/L$
Skeib (1980), see also: Foken and Skeib (1983) and Foken (1990)	0.40	$1 \qquad -0.0625 < z/L < 0.125$ $\left(\frac{z/L}{-0.0625}\right)^{-1/2} \quad -2 < z/L < -0.0625$ $\left(\frac{z/L}{0.125}\right)^{2} \qquad 0.125 < z/L < 2$
	0.40*	$0.95 \qquad -0.0625 < z/L < 0.125$ $0.95\left(\frac{z/L}{-0.0625}\right)^{-1/2} \quad -2 < z/L < -0.0625$ $0.95\left(\frac{z/L}{0.125}\right)^{2} \qquad 0.125 < z/L < 2$
Gavrilov and Petrov (1981)	0.40	$0.65\left[(1 - 35\,z/L)^{-1/2} + \dfrac{0.25}{1 + 8\,(z/L)^2}\right] \quad z/L < 0$ $0.9 + 6\,z/L \quad 0 < z/L$

(continued)

Reference	κ	Universal function for the exchange of sensible heat, $Pr_t = 1$
Dyer and Bradley (1982)	0.40 0.40*	$(1 - 14\,z/L)^{-1/2} \quad z/L < 0$
Beljaars and Holtslag (1991)	0.40	$1 + z/L\left(1 + \frac{2}{3}z/L\right)^{1/2} + \frac{2}{3}z/L(6 - 0.35z/L)\,\mathrm{e}^{-0.35z/L}$ $0 < z/L$
King et al. (1996)	0.40	$0.95 + 4.99\,z/L \le 12 \quad 0 < z/L$
Handorf et al. (1999)	0.40	$1 + 5\,z/L \quad 0 < z/L < 0.6$ $4 \qquad\;\; 0.6 < z/L$

Reference	κ	Universal function for the energy dissipation
Wyngaard and Coté (1971)	0.35	$\left[1 + 0.5\lvert z/L\rvert^{2/3}\right]^{3/2} \quad z/L < 0$ $\left[1 + 2.5(z/L)^{3/5}\right]^{3/2} \quad z/L > 0$
Högström (1990)		$1.24\left[1 - 19(z/L)^{-1/4} - \frac{z}{L}\right] \quad z/L < 0$ $1.24 + 4.7z/L \qquad\qquad\;\; z/L > 0$
Thiermann and Graßl (1992)		$(1 - 3z/L)^{-1} - z/L \qquad z/L < 0$ $\left[1 + 4z/L + 16(z/L)^2\right]^{-1/2} \quad z/L > 0$
Kaimal and Finnigan (1994)		$\left[1 + 0.5\lvert z/L\rvert^{2/3}\right]^{3/2} \quad z/L < 0$ $1 + 5z/L \qquad\qquad\;\; z/L > 0$
Frenzen and Vogel (2001)		$0.85\left[(1 - 16z/L)^{-2/3} - z/L\right] \qquad z/L < 0$ $0.85 + 4.26z/L + 2.58 \cdot (z/L)^2 \quad z/L > 0$
Hartogensis and DeBruin (2005)		$0.8 + 2.5 \cdot z/L \quad z/L > 0$

Reference	κ	Universal function for the temperature structure function parameter
Wyngaard et al. (1971), Wyngaard (1973)	0.35	$4.9(1 - 7z/L)^{-2/3} \qquad z/L < 0$ $4.9\left[1 + 2.4(z/L)^{2/3}\right] \quad z/L > 0$
	0.40**	$4.9(1 - 6.1z/L)^{-2/3} \qquad z/L < 0$ $4.9\left[1 + 2.2(z/L)^{2/3}\right] \quad z/L > 0$
Foken and Kretschmer (1990)	0.40	$(0.95/\kappa)^2(1 - 11.6\,z/L)^{-1/2} \quad -2 < z/L < 0$ $0.95/\kappa^2(0.95 + 7.8\,z/L) \qquad\;\; 0 < z/L < 1$

(continued)

Reference	κ	Universal function for the temperature structure function parameter
Thiermann and Graßl (1992)		$6.34\left[1 - 7z/L + 75(z/L)^2\right]^{-1/3}$ $z/L < 0$ $6.34\left[1 - 7z/L + 20(z/L)^2\right]^{1/3}$ $z/L > 0$
Kaimal and Finnigan (1994)		$5(1 + 6.4|z/L|)^{-2/3}$ $z/L < 0$ $4(1 + 3z/L)$ $z/L < 0$
Hartogensis and DeBruin (2005)		$4.7\left[1 + 1.6(z/L)^{2/3}\right]$ $z/L > 0$
Li et al. (2012)		$6.7(1 - 14.9z/L)^{-2/3}$ $z/L < 0$ $4.5\left[1 + 1.3(z/L)^{2/3}\right]$ $z/L > 0$
Maronga (2013)		$6.1(1 - 7.6z/L)^{-2/3}$ $z/L < 0$
Braam et al. (2014)		$4.4(1 - 10.2z/L)^{-2/3}$ $-76 < z/L < -0.0075$

Integral Turbulence Characteristics in the Surface Layer

Reference	σ_u/u_*	σ_v/u_*	Stratification
Lumley and Panofsky (1964), Panofsky and Dutton (1984)	2.45	1.9	Neutral, unstable
McBean (1971)	2.2	1.9	Unstable
Beljaars et al. (1983)	2.0	1.75	Unstable
Sorbjan (1986)	2.3		Stable
Sorbjan (1987)	2.6		
Foken et al. (1991)	2.7 $4.15(z/L)^{1/8}$		$-0.032 < z/L < 0$ $z/L < -0.032$
Thomas and Foken (2002)	$0.44\ln\left(\frac{1 m f}{u_*}\right) + 3.1$		$-0.2 < z/L < 0.4$

Reference	σ_w/u_*	σ_T/T_*	Stratification
Lumley and Panofsky (1964), Panofsky and Dutton ((1984)	1.45		Neutral, unstable
McBean (1971)	1.4	1.6	Unstable
Panofsky et al. (1977)	$1.3(1 - 2z/L)^{1/3}$		Unstable
Caughey u. Readings (1975)		$(z/L)^{-1/3}$	Unstable
Hicks (1981)	$1.25(1 - 2z/L)^{1/3}$	$0.95(z/L)^{-1/3}$	Unstable

(continued)

(continued)

Reference	σ_w/u_*	σ_T/T_*	Stratification
Caughey and Readings (1975)		$(z/L)^{-1/3}$	Unstable
Beljaars et al. (1983)		$0.95(z/L)^{-1/3}$	Unstable
Sorbjan (1986)	1.6	2.4	Stable
Sorbjan (1987)	1.5	3.5	Stable
Foken et al. (1991)	1.3 $2.0(z/L)^{1/8}$		$-0.032 < z/L < 0$ $z/L < -0.032$
Foken et al. (1991; 1997)		$1.4(z/L)^{-1/4}$ $0.5(z/L)^{-1/2}$ $(z/L)^{-1/4}$ $(z/L)^{-1/3}$	$0.02 < z/L < 1$ $-0.062 < z/L < 0.02$ $-1 < z/L < -0.062$ $z/L < -1$
Thomas and Foken (2002)	$0.21 \ln\left(\frac{1\,m \cdot f}{u_*}\right) + 6.3$		$-0.2 < z/L < 0.4$

A.5 Overall View of Experiments for the Investigation of the Surface Layer

The following table lists the important micrometeorological experiments which gave special consideration of the surface layer (McBean et al. 1979; Foken 1990; Garratt and Hicks 1990; Foken 2006); in this table ITCE means *International Turbulence Comparison Experiment*.

Experiment	Location, time	Reference
O'Neill	O'Neill, USA, 1953	Lettau (1957)
Kerang	Kerang, Australien, 1962	Swinbank and Dyer (1968)
Hay	Hay, Australien, 1964	
Hanford	Hanford, USA, 1965	Businger et al. (1969)
Wangara	Hay, Australia, 1967	Hess et al. (1981)
KANSAS 1968	Kansas, USA, 1968	Izumi (1971)
ITCE-1968	Vancouver, Canada, 1968	Miyake et al. (1971)
ITCE-1970	Tsimlyansk, Russia, 1970	Tsvang et al. (1973)
Koorin	Koorin, Australia, 1974	Garratt (1980)
ITCE-1976	Conargo, Australia, 1976	Dyer et al. (1982)
ITCE-1961	Tsimlyansk, Russia,	Tsvang et al. (1985)
Lövsta	Lövsta, Sweden, 1986	Högström (1990)
HATS	California, USA, 2000	Horst et al. (2004)
CHATS	California, USA, 2007	Patton et al. (2011)

Experiments Over Heterogeneous Landscapes

In the last 30 years, many micrometeorological experiments were conducted over heterogeneous landscapes and also included boundary layer processes and air chemical measurements (Mengelkamp et al. 2006, added).

Experiment	Location, time	Reference
HAPEX-MOBILHY	France 1986	André et al. (1990)
FIFE	Kansas, 1987–1989	Sellers et al. (1988)
KUREX-88	Kursk, Russia 1988	Tsvang et al. (1991)
HAPEX-SAHEL	Niger, 1990–1992	Goutorbe et al. (1994)
SANA	Eisdorf, Melpitz, Germany, 1991	Seiler (1996)
EFEDA	Spain 1990–1991	Bolle et al. (1993)
BOREAS	Canada, 1993–1996	Sellers et al. (1997)
SHEBA	Arctic 1998	Uttal et al. (2002)
LITFASS-98	Lindenberg, Germany, 1998	Beyrich et al. (2002)
CASES-99	Kansas, USA 1999	Poulos et al. (2002)
EBEX-2000	near Fresno CA, USA, 2000	Oncley et al. (2007)
LITFASS-2003	Lindenberg, Germany, 2003	Beyrich and Mengelkamp (2006)
COPS	Black Forest, Germany, 2007	Wulfmeyer et al. (2011)
BLLAST	Southern France, 2011	Lothon et al. (2014)
MATERHORN	Utah, USA, 2012	Fernando et al. (2015)

Experiments in the Urban Boundary Layer

The table is limited to experiments with flux measuring technique, for further experiments see Grimmond (2006)

Experiment	Location, time	Reference
	Chicago, USA 1995	Grimmond et al. (2002)
	Copenhagen, Denmark since 2000	Soegaard and Møller-Jensen (2003)
	Edinburgh, Scotland 2000	Nemitz et al. (2002)
ESCOMPTE	Marseille, France 2001	Grimmond et al. (2004), Salmond et al. (2005)
BUBBLE	Basel, Switzerland 2001–2002	Rotach et al. (2005),Vogt et al. (2006)
JU2003	Oklahoma City, USA 2003	Klein and Clark (2007), Nelson et al. (2011)

(continued)

Experiment	Location, time	Reference
	Helsinki, Finland 2005–2006	Vesala et al. (2008)
	London, England 2008–2011	Kotthaus and Grimmond (2012)
	Oberhausen, Germany 2010–2011	Goldbach and Kuttler (2013)

Other Experiments Referred to in the Text

The following table gives some information about further experiments mentioned in this book.

Experiment	Location, time	Reference
Greenland	Greenland, summer 1991	Ohmura (1992)
FINTUREX	Neumayer station, Antarktica, Jan.–Febr. 1994	Foken (1996), Handorf et al. (1999)
LINEX-96/2	Lindenberg, Germany, June 1996	Foken et al. (1997)
LINEX-97/1	Lindenberg, Germany, June 1997	Foken (1998)
WALDATEM-2003	Waldstein, Germany, May–July 2003	Thomas and Foken (2007)
EGER	Waldstein, Germany 2007, 2008, 2011	Foken et al. (2012b)

A.6 Meteorological Measurements Stations

In Sect. 6.2, different types of meteorological measurements stations were defined (Table 6.1). The measured parameters of these stations (VDI 2006) are given in the following table, where X indicates necessary parameters and o indicates desirable additional parameters. The measured parameters include air temperature (t_a), air moisture (f_a), wind velocity (u), wind direction (dd), precipitation (R_N), global radiation (G), net radiation (Q_{s*}), air pressure (p), state of the weather (ww), surface temperature (t_{IR}), photosynthetic active radiation (PAR), soil temperature (t_b), soil moisture (f_b), soil heat flux (Q_G), sensible heat flux (Q_H), latent heat flux (Q_E), deposition (Q_c), shear stress (τ).

The most important parameters are:

Type of the station	t_a	f_a	u	dd	R_N	G	Q_{S*}	p	ww
Agrometeorological	X	X	X	X	X	X	o	o	
Micrometeorological	X	X	X	X	X	o		o	o
Micrometeorological with turbulence measurements	X	X	X	X	X	o	X	o	

(continued)

(continued)

Type of the station	t_a	f_a	u	dd	R_N	G	Q_{S*}	p	ww
Air pollution	o	o	X	X		X	o	o	o
Pollutant concentrations	X	X	X	X	X	X			
Disposal site	X	X	X	X	X	o	X		
Noise measurements	X		X	X					
Traffic measurements		X	X	X					o
Hydrological	o	o	o		X		o		
Forest climate	X	X	X	X	X	X	o		
Nowcasting	X	X	X	X	X	o		o	X
Hobby	X	X	o	o				o	

Additional parameters measured at selected stations are:

Type of station	t_{IR}	PAR	t_b	f_b	Q_G	Q_H	Q_E	Q_c	τ
Agrometeorological		o	X	X	o				
Micrometeorological									
Micrometeorological with turbulence measurements					o	X	X	o	X
Air pollution									o
Pollutant concentration									
Disposal site									
Noise measurements									
Traffic measurements	o		o						
Hydrological									
Forest climate		o	o	o					
Nowcasting									
Hobby									

A.7 Available Eddy-Covariance Software

Overview of software packages used for eddy-covariance measurements (Mauder et al. 2008; Foken et al. 2012a, updated).

Software	TK3	Alteddy	ECPack[a]	EddySoft	EdiRE[a]	eth-flux[a]	R-packages	Eddypro[b]
Software	University of Bayreuth, KIT Garmisch-Partenkirchen	Alterra. Wageningen	University of Wageningen	Max-Planck-Institute Jena	University of Edinburgh	Swiss Federal Institute of Technology Zurich	NCAR/EOL	LiCor (Univ. Tuscia)
Devices	CSAT3, USA-1,HS, R2,R3,ATI-K,NUW, Young: 6262,7000, 7200, 7500,7700, KH20, EC 150, ADC OP-2, Aerodyn, Los Gatos	R2,R3,WMPro, HS, CSAT3, USA-1, Young, ATI-K; 6262,7500, 7000,7200, KH20, TGA100A, Los Gatos DLT100	R2,R3,CSAT3 KDTR90/TR617500, KH20, Lyman-α	CSAT3,USA-1,R2, R3,HS,Windmaster, Young; 6262,7000, 7200, 7500, ADC OP-2	many	CSAT3,R2,R3,HS; 6262,7000,7500, FM-100, MonitorLabs, Scintrex LMA3, Los Gatos FMA and FGGA, Aerodyne QCL	CSAT3, KH20,7000, 7500, EC 150 standard, other sensors possible	R2,R3, WMPro; CSAT3, USA-1, 6262,7500, 700s 7550 (7200/7700)
Data preparation	Test plausibility, spikes; block average; time lag (const/auto)	Test plausibility, spikes; block average; time lag (const/auto)	Test plausibility, spikes; detrending (linear); time lag (const.)	Test plausibility, spikes; block average, optional detrending; time lag (const/auto)	Test plausibility, spikes; optional detrending (linear/filter); block average; Time lag (const/auto)	Test plausibility, spikes; block average, optional detrending; time lag (const/auto)	Spikes; block average; time lag	Test plausibility, spikes; block average; optional detrending time lag (const/auto, moisture dependent)
Coordinate rotation	Planar fit/2D rotation; head-correction	2D rotation/planar fit	Planar fit/2D/3D rotation	Planar fit/2D/3D rotation	Planar fit/2D/3D rotation	2D/3D rotation	Planar fit, 2D rotation	Planar fit/2D/3D rotation, van Dijk et al. (2004); Nakai et al. (2006); Nakai and Shimoyama (2012)
Buoyancy flux → sensible heat flux	Schotanus et al. (1983), Liu et al. (2001)	Schotanus et al. (1983), Liu et al. (2001)	Schotanus et al. (1983)	Schotanus et al. (1983), Liu et al. (2001)	Schotanus et al. (1983), Liu et al. (2001)	–	Schotanus et al. (1983)	van Dijk et al. (2004)
Oxygen correction for KH20	Tanner et al. (1993)	Tanner et al. (1993), van Dijk et al. (2003)	Tanner et al. (1993),van Dijk et al. (2003)	–	–	–	van Dijk et al. (2003)	–
High frequency loss correction	Moore (1986)	Moore (1986), Leuning and King (1992)	Moore (1986)	Eugster and Senn (1995)	Moore (1986), Eugster and Senn (1995)	Eugster and Senn (1995)	Horst and Lenschow (2009)	Moncrieff et al. (1997)

(continued)

(continued)

Software	TK3	Alleddy	ECPack[a]	EddySoft	EdiRE[a]	eth-flux[a]	R-packages	Eddypro[b]
WPL Density correction	Webb et al. (1980)	Leuning and King (1992), Burba et al. (1980)	Webb et al. (1980)	Webb et al. (1980)	Webb et al. (1980)	Webb et al. (1980)	Webb et al. (1980)	Webb et al. (1980), Burba et al. (1980), Ibrom et al. (2007) for closed-path
Iteration of all corrections	Yes	One time	Yes	–	Yes	–	Equations solved simultaneously, Oncley et al. (2007)	Partly
Constants	$\lambda(T)$; $cp(c_{p,dry},q)$; $\rho(T,p)$	$\lambda(T)$; c_p = const.; $\rho(T,p)$	$\lambda(T)$; c_p = const.; $\rho(T,p)$	$\lambda(T)$; c_p = const.; $\rho(T,p)$	$\lambda(T)$; $cp(c_{p,dry},q)$; $\rho(T,p)$	$\lambda(T)$; c_p = const.; $\rho(T,p)$	$\lambda(T)$; $c_{p,dry}$ and $c_{p,water}$; $\rho(T,p)$	$\lambda(T)$; $cp(c_{p,dry},q)$; $\rho(T,p)$
Quality control	Test steady state, integral turbulence characteristics: Foken and Wichura (1996)	Test steady state, integral turbulence characteristics: Foken et al. (2004)	Statistical error: van Dijk et al. (2004)	Test steady state, integral turbulence characteristics: Foken and Wichura (1996)	Test steady state, integral turbulence characteristics: Foken and Wichura (1996), Vickers and Mahrt (1997)	Test steady state, integral turbulence characteristics: Foken and Wichura (1996)	Reference signal from neuronal network	Test steady state, integral turbulence characteristics: Foken et al. (2004)
Footprint	Kormann and Meixner (2001)	Dyer (1974), van Ulden and Holtslag (1985), Schuepp et al. (1990)		Schuepp et al. (1990)				Kljun et al. (2004), Kormann and Meixner (2001), Hsieh et al. (2000)

[a] No addition/correction of Foken et al. (2012a)
[b] The program package has more methods of data calculation

A.8 Glossary

Advection: Transport of properties of the air (momentum, temperature, water vapor, etc.) by the wind. As a rule, horizontal transport is understood. Because of advection, air properties change in both horizontal coordinates, and the conditions are no longer homogeneous. Vertical advection is the vertical movement air due to mass continuity rather than buoyancy, *i.e.* convection.

Atmospheric window: Frequency range of electromagnetic waves, which pass through the atmosphere down to the ground with little absorption. Within this frequency range, remote sensing methods of the surface properties can be applied. The most important atmospheric windows are in the visible range from 0.3 to 0.9 μm, in the IR-range from 8 to 13 μm, and in the microwave range for wave lengths greater than 1 mm for surface wetness.

Bolometer: A device for measuring radiant energy by using thermally-sensitive electric sensors (thermocouple, thermistor, platinum wire).

Calm: State of the atmosphere with no discernible air motion. The calm-threshold is the threshold speed of cup anemometers, which is about $0.3 \mathrm{~ms}^{-1}$. A wind direction cannot be determined under these circumstances.

CET: Abbreviation of Central European Time. It is the mean local time at 15° longitudes, and differs from UTC by 1 hour.

Clausius-Clapeyron equation: Clapeyron 1834 established and Clausius 1850 gave the reasons for the equations for the temperature dependence of equilibrium water-vapour pressure at saturation. Because of the equation's strong exponential dependence on temperature, the amount of water vapour in the atmosphere increases significantly with temperatures, and the atmosphere can therefore store more latent heat at higher temperatures.

Climate element: Meteorological and other parameters that characterize (individually or in combinations) different climate types. These are state variables and fluxes.

Coherence: In generally, coherence is a constant phase relation between two waves. Coherent structures in atmospheric turbulence research are velocity, temperature, and other structures, which are significantly larger and longer-lived than the smallest local eddies (*e.g.* squall lines, convective cells).

Coriolis force: Fictitious force in a rotating coordinate system, and named after the mathematician Coriolis (1792–1843). It is a force normal to the velocity vector causing a deflection to the right in the Northern hemisphere and to the left in the Southern hemisphere.

Coriolis parameter: Twice the value of the angular velocity of the Earth for a certain location of the latitude φ: $f = 2\,\Omega \sin \varphi$. At the equator $f = 0$, on the Northern hemisphere positive and on the Southern hemisphere negative.

Dissipation: Conversion of kinetic energy by work against the viscous stresses. Under turbulent conditions, it is the conversion of the kinetic energy of the smallest eddies into heat.

Element, meteorological: *see* climate element

Entrainment: Exchange process at the top of the atmospheric boundary layer, and is due to the actions of eddies that are smaller than those in the mixed layer.

Fetch: Windward distance from a measurements point to a change of the surface properties or an obstacle; extent of a measurements field for micrometeorological research.

Froude number: Dimensionless ratio of the inertia force to the gravity force $Fr = V^2 L^{-1} g^{-1}$ where V is a characteristic velocity and L is a characteristic length. For flow over hills, L is the characteristic distance between hills or obstacles. In these cases, the external Froude number with the Brunt-Väisälä frequency N is used, see Eq. (3.35): $Fr = V N^{-1} L^{-1}$.

Gas constant: Proportionality factor of the equation of state for ideal gases, and is expressed in mol. In meteorology, the gas constant is expressed in mass units, and a special gas constant for dry air is used. In moist air, the temperature in the equation of state must be replaced by the virtual temperature (see below).

Gravity waves: Gravity waves are generated at the interface of two atmospheric layers under stable stratification caused by buoyancy and gravity forces.

Hysteresis: The change between two states that depends on the way the change occurs, for example, the characteristics of a moisture sensor are different for wetting and drying.

Inversion: An air layer where the temperature increases with the altitude instead of the usual decrease. Inversions are of two types; surface inversion due to long-wave radiation from the ground, and elevated or free inversions *e.g.* at the top of the atmospheric boundary layer.

Kelvin-Helmholtz instability: A dynamic instability caused by strong wind shear resulting in breaking waves or billow clouds (Sc, Ac lent). Typically, these occur at inversions or above hills. They also can occur over obstacles and forests.

Leaf area density: The vertical probability density function of the leaf area.

Leaf area index: Ratio of the leaf area (upper side) within a vertical cylinder to the bottom area of the cylinder.

Low-level jet: Vertical band of strong winds in the lower part of the atmospheric boundary layer. For stable stratification, the low-level jet develops at the upper border of the nocturnal surface inversion. Typical heights are 100–300 m, and sometimes lower.

LTST: Abbreviation for Local True Solar Time. It is the time related to the meridian of all points on the same longitude. The local true solar time is the solar time measured from the daily lower culmination of the sun and changes with the time equation, which is the difference between the real and the mean solar time. The time equation is positive if the local true solar time earlier culminates than the mean solar time (sun day). It changes between –14 min 24 s (approx. middle of February) and +16 min 21 s (approx. beginning of November). For an approximation relation see A4.

Matrix potential: A measure of the absorption and capillary forces of the solid soil matrix on the soil water. Its absolute value is called tension.

Mixed layer: A layer of strong vertical mixing due to convection resulting in vertically-uniform values of potential temperature and wind speed but decreasing values of moisture. It is often capped by an inversion layer (see above).

MST: Abbreviation for Mean Solar Time. Time related to the meridian of the location and for all locations of the same longitude. The mean solar time is the solar time measured from the lower culmination of the sun. It is calculated by addition of 4 minutes to the universal time (UT) for each degree of longitude in eastward direction.

Parameterization: Representation of complicated relations in models by more simple combinations of parameters, which are often only valid under certain circumstances.

Rossby similarity: In the free atmosphere, the Rossby number is the ratio of the inertial force to the Coriolis force. In the atmospheric boundary layer, the roughness Rossby number is the ratio of the friction velocity to the Coriolis parameter, $Ro = u_* / (f\,z_0)$. The friction Rossby number is an assessment of the ageostrophic component of the wind.

Stability of the stratification: The static stability separates turbulent and laminar flow conditions depending on the gradient of the potential temperature (see below). If the potential temperature decreases with height, then the stratification is unstable, but if it increases with height, then the stratification is stable. Due to the effects of vertical wind sheer, the statically-stable range is turbulent up to the critical Richardson number.

Temperature, potential: The temperature of a dry air parcel that is moved adiabatically to a pressure of 1000 hPa, see Eq. (2.22).

Temperature, virtual: The temperature of a dry air parcel if it had the same density as a moist air parcel. The virtual temperature is slightly higher than the temperature of moist air, see Eq. (2.14).

Transmission: Permeability of the atmosphere for radiation. The radiation can be reduced *e.g.* by gases, aerosols, particles, and water droplets.

UTC: Abbreviation for Universal Time Coordinated, a time scale based on the international atomic time by setting the zero point to the zero meridian (Greenwich Meridian), with the mean solar day as a basic unit. It is the basis for political and scientific time.

Wind, geostrophic: Wind above the atmospheric boundary layer where pressure gradient force and Coriolis force (see above) are in equilibrium.

A.9 Micrometeorological Standards Used in Germany

In Germany, Austria, and Switzerland meteorological measurements techniques and some applied meteorological methods are standardized. Some of these standards were incorporated in the international ISO standards. Because these standards are available in English, only the most important standards are given. The relevant standards appear in volume 1B of the "VDI/DIN Handbook on Keeping the Air Clean" (Queitsch 2002, update 2017):

VDI/DIN	Sheet	Content
3781	2, 4	Atmospheric diffusion of pollutants
3782	1, 3, 5–7	Environmental meteorology—Atmospheric dispersion models
3783	1, 2, 4–6, 8–10, 12–14, 16, 18–21	Dispersion of pollutants in the atmosphere; dispersion of emissions by accidental releases
3784	1, 2	Environmental meteorology; cooling towers
3785	1, 2	Urban climate, Mobile measurements systems
3786	1–9, 11–14, 16–18, 20	Environmental meteorology—Meteorological measurements
3787	1, 2, 5, 9,10	Environmental meteorology—Climate and air pollution
3788	1	Environmental meteorology—Dispersion of odorants
3789		Environmental meteorology—Interactions between atmosphere and surfaces
3790	1–3	Environmental meteorology—Emissions of gases
3945	1, 3, 5	Environmental meteorology—Atmospheric dispersion models
4320	1–3	Measurement of atmospheric depositions

Because of a lack in the literature on meteorological measurements systems, the VDI/DIN 3786 (Sheets 1–20) and the relevant ISO standards may be of interest to a wide readership:

VDI/DIN, ISO	Issued	Title
ISO 16622	09/2002	Meteorology—Sonic anemometers/thermometers—Acceptance test methods for mean wind measurements
ISO 17713-1	05/2007	Meteorology—Wind measurements—Part 1: Wind tunnel test methods for rotating anemometer performance
ISO/DIS 17714	07/2007	Meteorology—Air temperature measurements—Test methods for comparing the performance of thermometer shields/screens and defining important characteristics
ISO 28902-1	01/2012	Air quality—Environmental meteorology—Part 1: Ground-based remote sensing of visual range by lidar
ISO/DIS 28902-2	11/2016	Air quality—Environmental meteorology—Part 2: Ground-based remote sensing of wind by heterodyne pulsed Doppler lidar
VDI 3786 Sheet 1	03/2013	Environmental meteorology—Meteorological measurements Fundamentals
VDI 3786 Sheet 2	12/2000 new: 2017	Environmental meteorology—Meteorological measurements concerning questions of air pollution—Wind

(continued)

VDI/DIN, ISO	Issued	Title
VDI 3786 Sheet 3	10/2012	Environmental meteorology—Meteorological measurements —Air temperature
VDI 3786 Sheet 4	06/2013	Environmental meteorology—Meteorological measurements —Air humidity
VDI 3786 Sheet 5	10/2015	Environmental meteorology—Meteorological measurements —Radiation
VDI 3786 Sheet 6	10/1983 new: 2017	Meteorological measurements of air pollution—turbidity of ground—level atmosphere standard visibility
VDI 3786 Sheet 7	10/2012	Environmental meteorology—Meteorological measurements —Precipitation
VDI 3786 Sheet 8	09/2015	Environmental meteorology—Meteorological measurements —Aerological measurements
VDI 3786 Sheet 9	10/2007	Environmental Meteorology—Meteorological measurements —Visual weather observations
VDI 3786 Sheet 10		Retracted
VDI 3786 Sheet 11	07/2015	Environmental meteorology—Ground-based remote sensing of the wind vector and the vertical structure of the boundary layer—Doppler sodar
VDI 3786 Sheet 12	10/2008 new: 2017	Environmental meteorology—Meteorological measurements —Turbulence measurements with sonic anemometers
VDI 3786 Sheet 13	08/2006 new: 2018	Environmental meteorology—Meteorological measurements —Measuring station
VDI 3786 Sheet 14	12/2001	Environmental meteorology—Ground-based remote sensing of the wind vector—Doppler wind LIDAR
VDI 3786 Sheet 15		Replaced by ISO 28902-1
VDI 3786 Sheet 16	07/2010	Environmental meteorology—Meteorological measurements —Atmospheric pressure
VDI 3786 Sheet 17	02/2007	Environmental meteorology—Ground-based remote sensing of the wind vector—Wind profiler radar
VDI 3786 Sheet 18	05/2010	Environmental meteorology—Ground-based remote sensing of temperature—Radio-acoustic sounding systems (RASS)
VDI 3786 Sheet 19	10/2016 (draft)	Environmental meteorology - Ground-based remote sensing of meteorological parameters - Particle backscatter lidar
VDI 3786 Sheet 20	09/2014	Environmental meteorology—Ground-based remote sensing of precipitation—Weather radar

References

André J-C, Bougeault P and Goutorbe J-P (1990) Regional estimates of heat and evaporation fluxes over non-homogeneous terrain, Examples from the HAPEX-MOBILHY programme. Boundary-Layer Meteorol. 50:77–108.

Andreas EL (2002) Parametrizing scalar transfer over snow and ice: A review. J Hydrometeorol. 3:417–432.

Beljaars ACM, Schotanus P and Nieuwstadt FTM (1983) Surface layer similarity under nonuniform fetch conditions. J Climate Appl Meteorol. 22:1800–1810.

Beljaars ACM and Holtslag AAM (1991) Flux parametrization over land surfaces for atmospheric models. J Appl Meteorol. 30:327–341.

Beyrich F, Herzog H-J and Neisser J (2002) The LITFASS project of DWD and the LITFASS-98 Experiment: The project strategy and the experimental setup. Theor Appl Climat. 73:3–18.

Beyrich F and Mengelkamp H-T (2006) Evaporation over a heterogeneous land surface: EVA_GRIPS and the LITFASS-2003 experiment - an overview. Boundary-Layer Meteorol. 121:5–32.

Bolle H-J, André J-C, Arrie JL, Barth HK, Bessemoulin P, A. B, DeBruin HAR, Cruces J, Dugdale G, Engman ET, Evans DL, Fantechi R, Fiedler F, Van de Griend A, Imeson AC, Jochum A, Kabat P, Kratsch P, Lagouarde J-P, Langer I, Llamas R, Lopes-Baeza E, Melia Muralles J, Muniosguren LS, Nerry F, Noilhan J, Oliver HR, Roth R, Saatchi SS, Sanchez Diaz J, De Santa Olalla M, Shutleworth WJ, Sogaard H, Stricker H, Thornes J, Vauclin M and Wickland D (1993) EFEDA: European field experiment in a desertification-threatened area. Ann Geophys. 11:173–189.

Braam M, Moene A, Beyrich F and Holtslag AM (2014) Similarity relations for C_T^2 in the unstable atmospheric surface layer: Dependence on regression approach, observation height and stability range. Boundary-Layer Meteorol. 153:63–87.

Businger JA, Miyake M, Inoue E, Mitsuta Y and Hanafusa T (1969) Sonic anemometer comparison and measurements in the atmospheric surface layer. J Meteor Soc Japan. 47:1–12.

Businger JA, Wyngaard JC, Izumi Y and Bradley EF (1971) Flux-profile relationships in the atmospheric surface layer. J Atmos Sci. 28:181–189.

Caughey SL and Readings CJ (1975) Turbulent fluctuations in convective conditions. Quart J Roy Meteorol Soc. 101:537–542.

Cohen ER and Taylor BN (1986) The 1986 adjustment of the fundamental physical constants. International Council of Scientific Unions (ICSU), Committee on Data for Science and Technology (CODATA). CODATA-Bull. No. 63:36 pp.

Dyer AJ and Hicks BB (1970) Flux-gradient relationships in the constant flux layer. Quart J Roy Meteorol Soc. 96:715–721.

Dyer AJ (1974) A review of flux-profile-relationships. Boundary-Layer Meteorol. 7:363–372.

Dyer AJ, Garratt JR, Francey RJ, McIlroy IC, Bacon NE, Hyson P, Bradley EF, Denmead DT, Tsvang LR, Volkov JA, Kaprov BM, Elagina LG, Sahashi K, Monji N, Hanafusa T, Tsukamoto O, Frenzen P, Hicks BB, Wesely M, Miyake M and Shaw WJ (1982) An international turbulence comparison experiment (ITCE 1976). Boundary-Layer Meteorol. 24:181–209.

Dyer AJ and Bradley EF (1982) An alternative analysis of flux-gradient relationships at the 1976 ITCE. Boundary-Layer Meteorol. 22:3–19.

Eugster W and Senn W (1995) A cospectral correction for measurement of turbulent NO_2 flux. Boundary-Layer Meteorol. 74:321–340.

Fernando HJS, Pardyjak ER, Di Sabatino S, Chow FK, De Wekker SFJ, Hoch SW, Hacker J, Pace JC, Pratt T, Pu Z, Steenburgh WJ, Whiteman CD, Wang Y, Zajic D, Balsley B, Dimitrova R, Emmitt GD, Higgins CW, Hunt JCR, Knievel JC, Lawrence D, Liu Y, Nadeau DF, Kit E, Blomquist BW, Conry P, Coppersmith RS, Creegan E, Felton M, Grachev A, Gunawardena N, Hang C, Hocut CM, Huynh G, Jeglum ME, Jensen D, Kulandaivelu V, Lehner M, Leo LS, Liberzon D, Massey JD, McEnerney K, Pal S, Price T, Sghiatti M, Silver Z, Thompson M, Zhang H and Zsedrovits T (2015) The MATERHORN: Unraveling the intricacies of mountain weather. Bull Amer Meteorol Soc. 96:1945–1967.

Fischer G (ed) (1988) Landolt-Börnstein: Numerical Data and Functional Relationships in Science and Technology,Group V: Geophysics and space research, Volume 4: Meteorology, Subvolume b: Physical and chemical properties of the air. Springer, Berlin, Heidelberg, 570 pp.

Foken T and Skeib G (1983) Profile measurements in the atmospheric near-surface layer and the use of suitable universal functions for the determination of the turbulent energy exchange. Boundary-Layer Meteorol. 25:55–62.

Foken T and Kretschmer D (1990) Stability dependence of the temperature structure parameter. Boundary-Layer Meteorol. 53:185–189.

Foken T (1990) Turbulenter Energieaustausch zwischen Atmosphäre und Unterlage - Methoden, meßtechnische Realisierung sowie ihre Grenzen und Anwendungsmöglichkeiten. Ber Dt Wetterdienstes. 180:287 pp.

Foken T, Skeib G and Richter SH (1991) Dependence of the integral turbulence characteristics on the stability of stratification and their use for Doppler-Sodar measurements. Z Meteorol. 41:311–315.

Foken T (1996) Turbulenzexperiment zur Untersuchung stabiler Schichtungen. Ber Polarforschung. 188:74–78.

Foken T and Wichura B (1996) Tools for quality assessment of surface-based flux measurements. Agrical Forest Meteorol. 78:83–105.

Foken T, Jegede OO, Weisensee U, Richter SH, Handorf D, Görsdorf U, Vogel G, Schubert U, Kirzel H-J and Thiermann V (1997) Results of the LINEX-96/2 Experiment. Dt Wetterdienst, Forsch. Entwicklung, Arbeitsergebnisse. 48:75 pp.

Foken T (1998) Ergebnisse des LINEX-97/1 Experimentes. Dt Wetterdienst, Forsch. Entwicklung, Arbeitsergebnisse. 53:38 pp.

Foken T, Göckede M, Mauder M, Mahrt L, Amiro BD and Munger JW (2004) Post-field data quality control. In: Lee Xet al (eds.), Handbook of Micrometeorology: A Guide for Surface Flux Measurement and Analysis. Kluwer, Dordrecht, 181–208.

Foken T (2006) 50 years of the Monin-Obukhov similarity theory. Boundary-Layer Meteorol. 119:431–447.

Foken T, Leuning R, Oncley SP, Mauder M and Aubinet M (2012a) Corrections and data quality In: Aubinet Met al (eds.), Eddy Covariance: A Practical Guide to Measurement and Data Analysis. Springer, Dordrecht, Heidelberg, London, New York, 85–131.

Foken T, Meixner FX, Falge E, Zetzsch C, Serafimovich A, Bargsten A, Behrendt T, Biermann T, Breuninger C, Dix S, Gerken T, Hunner M, Lehmann-Pape L, Hens K, Jocher G, Kesselmeier J, Lüers J, Mayer JC, Moravek A, Plake D, Riederer M, Rütz F, Scheibe M,

Siebicke L, Sörgel M, Staudt K, Trebs I, Tsokankunku A, Welling M, Wolff V and Zhu Z (2012b) Coupling processes and exchange of energy and reactive and non-reactive trace gases at a forest site – results of the EGER experiment. Atmos Chem Phys. 12:1923–1950.

Frenzen P and Vogel CA (2001) Further studies of atmospheric turbulence in layers near the surface: Scaling the TKE budget above the roughness sublayer. Boundary-Layer Meteorol. 99:173–458.

Garratt JR (1980) Surface influence upon vertical profiles in the atmospheric near surface layer. Quart J Roy Meteorol Soc. 106:803–819.

Garratt JR and Hicks BB (1990) Micrometeorological and PBL experiments in Australia. Boundary-Layer Meteorol. 50:11–32.

Gavrilov AS and Petrov JS (1981) Ocenka totschnosti opredelenija turbulentnych potokov po standartnym gidrometeorologitscheskim izmerenijam nad morem. Meteorol Gidrol:52–59.

Goldbach A and Kuttler W (2013) Quantification of turbulent heat fluxes for adaptation strategies within urban planning. Int J Climatol. 33:143–159.

Goutorbe JP, Lebel T, Tinga A, Bessemoulin P, Brouwer J, Dolman H, Engman ET, Gash JGC, Hoepffner M, Kabat P, Kerr YH, Monteny B, Prince SD, Said F, Sellers P and Wallace J (1994) HAPEX-SAHEL: A large scale study of land atmosphere interactions in the semi-arid tropics. Ann Geophys. 12:53–64.

Grimmond CSB, King TS, Cropley FD, Nowak DJ and Souch C (2002) Local-scale fluxes of carbon dioxide in urban environments: methodological challenges and results from Chicago. Environm Pollution. 116, Supplement 1:S243-S254.

Grimmond CSB, Salmond JA, Oke TR, Offerle B and Lemonsu A (2004) Flux and turbulence measurements at a densely built-up site in Marseille: Heat, mass (water and carbon dioxide), and momentum. J Geophys Res: Atmosph. 109:D24101.

Grimmond CSB (2006) Progress in measuring and observing the urban atmosphere. Theor Appl Climat. 84:3–22.

Handorf D, Foken T and Kottmeier C (1999) The stable atmospheric boundary layer over an Antarctic ice sheet. Boundary-Layer Meteorol. 91:165–186.

Hantel M (2013) Einführung Theoretische Meteorologie. Springer Spektrum, Berlin,Heidelberg, 430 pp.

Hartmann DL (1994) Global Physical Climatology. Academic Press, San Diego, New York, 408 pp.

Hartogensis OK and DeBruin HAR (2005) Monin-Obukhov similarity functions of the structure parameter of temperature and turbulent kinetic energy dissipation in the stable boundary layer. Boundary-Layer Meteorol. 116:253–276.

Hess GD, Hicks BB and Yamada T (1981) The impact of the Wangara experiment. Boundary-Layer Meteorol. 20:135–174.

Hicks BB (1981) An examination of the turbulence statistics in the surface boundary layer. Boundary-Layer Meteorol. 21:389–402.

Högström U (1988) Non-dimensional wind and temperature profiles in the atmospheric surface layer: A re-evaluation. Boundary-Layer Meteorol. 42:55–78.

Högström U (1990) Analysis of turbulence structure in the surface layer with a modified similarity formulation for near neutral conditions. J Atmos Sci. 47:1949–1972.

Horst TW, Kleissl J, Lenschow DH, Meneveau C, Moeng CH, Parlange MB, Sullivan PP and Weil JC (2004) HATS: Field observations to obtain spatially filtered turbulence fields from crosswind arrays of sonic anemometers in the atmospheric surface layer. J Atmos Sci. 61:1566–1581.

Horst TW and Lenschow DH (2009) Attenuation of scalar fluxes measured with spatially-displaced sensors. Boundary-Layer Meteorol. 130:275–300.

Hsieh C-I, Katul G and Chi T-W (2000) An approximate analytical model for footprint estimation of scalar fluxes in thermally stratified atmospheric flows. Adv Water Res. 23:765–772.

Hughes DW, Yallop BD and Hohenkerk CY (1989) The equation of time. Monthly Notice Roy Astron Soc. 238:1529–1535.

Ibrom A, Dellwik E, Larsen SE and Pilegaard K (2007) On the use of the Webb–Pearman–Leuning theory for closed-path eddy correlation measurements. Tellus. B 59:937–946.

Izumi Y (1971) Kansas 1968 field program data report. Air Force Cambridge Research Laboratory, Bedford, MA, 79 pp.

Kaimal JC and Finnigan JJ (1994) Atmospheric Boundary Layer Flows: Their Structure and Measurement. Oxford University Press, New York, NY, 289 pp.

King JC, Anderson PS, Smith MC and Mobbs SD (1996) The surface energy and mass balance at Halley, Antarctica during winter. J Geophys Res. 101(D14):19119–19128.

Klein P and Clark JV (2007) Flow variability in a North American downtown street canyon. J Appl Meteorol Climatol. 46:851–877.

Kljun N, Calanca P, Rotach M and Schmid HP (2004) A simple parameterization for flux footprint predictions. Boundary-Layer Meteorol. 112:503–523.

Kopp G and Lean JL (2011) A new, lower value of total solar irradiance: Evidence and climate significance. Geophys Res Letters. 38:L01706.

Kormann R and Meixner FX (2001) An analytical footprint model for non-neutral stratification. Boundary-Layer Meteorol. 99:207–224.

Kotthaus S and Grimmond CSB (2012) Identification of micro-scale anthropogenic CO_2, heat and moisture sources – Processing eddy covariance fluxes for a dense urban environment. Atmos Environm. 57:301–316.

Lettau HH and Davidson B (eds) (1957) Exploring the Atmosphere's First Mile. Pergamon Press, London, New York, 376 pp.

Leuning R and King KM (1992) Comparison of eddy-covariance measurements of CO_2 fluxes by open- and closed-path CO_2 analysers. Boundary-Layer Meteorol. 59:297–311.

Li D, Bou-Zeid E and De Bruin HR (2012) Monin–Obukhov similarity functions for the structure parameters of temperature and humidity. Boundary-Layer Meteorol. 145:45–67.

Liou KN (1992) Radiation and Cloud Processes in the Atmosphere. Oxford University Press, Oxford, 487 pp.

Liu H, Peters G and Foken T (2001) New equations for sonic temperature variance and buoyancy heat flux with an omnidirectional sonic anemometer. Boundary-Layer Meteorol. 100:459–468.

Lothon M, Lohou F, Pino D, Couvreux F, Pardyjak ER, Reuder J, Vilà-Guerau de Arellano J, Durand P, Hartogensis O, Legain D, Augustin P, Gioli B, Lenschow DH, Faloona I, Yagüe C, Alexander DC, Angevine WM, Bargain E, Barrié J, Bazile E, Bezombes Y, Blay-Carreras E, van de Boer A, Boichard JL, Bourdon A, Butet A, Campistron B, de Coster O, Cuxart J, Dabas A, Darbieu C, Deboudt K, Delbarre H, Derrien S, Flament P, Fourmentin M, Garai A, Gibert F, Graf A, Groebner J, Guichard F, Jiménez MA, Jonassen M, van den Kroonenberg A, Magliulo V, Martin S, Martinez D, Mastrorillo L, Moene AF, Molinos F, Moulin E, Pietersen HP, Piguet B, Pique E, Román-Cascón C, Rufin-Soler C, Saïd F, Sastre-Marugán M, Seity Y, Steeneveld GJ, Toscano P, Traullé O, Tzanos D, Wacker S, Wildmann N and Zaldei A (2014) The BLLAST field experiment: Boundary-Layer Late Afternoon and Sunset Turbulence. Atmos Chem Phys. 14:10931–10960.

Lumley JL and Panofsky HA (1964) The structure of atmospheric turbulence. Interscience Publishers, New Yotk, 239 pp.

Maronga B (2013) Monin–Obukhov similarity functions for the structure parameters of temperature and humidity in the unstable surface layer: Results from high-resolution large-eddy simulations. J Atmos Sci. 71:716–733.

Mauder M, Foken T, Clement R, Elbers J, Eugster W, Grünwald T, Heusinkveld B and Kolle O (2008) Quality control of CarboEurope flux data - Part 2: Inter-comparison of eddy-covariance software. Biogeoscience. 5:451–462.

McBean GA (1971) The variation of the statistics of wind, temperature and humidity fluctuations with stability. Boundary-Layer Meteorol. 1:438–457.

McBean GA, Bernhardt K, Bodin S, Litynska Z, van Ulden AP and Wyngaard JC (1979) The planetary boundary layer. WMO, Note. 530:201 pp.

Mengelkamp H-T, Beyrich F, Heinemann G, Ament F, Bange J, Berger FH, Bösenberg J, Foken T, Hennemuth B, Heret C, Huneke S, Johnsen K-P, Kerschgens M, Kohsiek W, Leps J-P, Liebethal C, Lohse H, Mauder M, Meijninger WML, Raasch S, Simmer C, Spieß T, Tittebrand A, Uhlenbrook S and Zittel P (2006) Evaporation over a heterogeneous land surface: The EVA_GRIPS project. Bull Amer Meteorol Soc. 87:775–786.

Miyake M, Stewart RW, Burling RW, Tsvang LR, Kaprov BM and Kuznecov OA (1971) Comparison of acoustic instruments in an atmospheric flow over water. Boundary-Layer Meteorol. 2:228–245.

Moncrieff JB, Massheder JM, DeBruin H, Elbers J, Friborg T, Heusinkveld B, Kabat P, Scott S, Søgaard H and Verhoef A (1997) A system to measure surface fluxes of momentum, sensible heat, water vapor and carbon dioxide. J Hydrol. 188–189:589–611.

Moore CJ (1986) Frequency response corrections for eddy correlation systems. Boundary-Layer Meteorol. 37:17–35.

Nakai T, van der Molen MK, Gash JHC and Kodama Y (2006) Correction of sonic anemometer angle of attack errors. Agrical Forest Meteorol. 136:19–30.

Nakai T and Shimoyama K (2012) Ultrasonic anemometer angle of attack errors under turbulent conditions. Agrical Forest Meteorol. 162–163:14–26.

Nelson MA, Pardyjak ER and Klein P (2011) Momentum and Turbulent Kinetic Energy Budgets Within the Park Avenue Street Canyon During the Joint Urban 2003 Field Campaign. Boundary-Layer Meteorol. 140:143–162.

Nemitz E, Hargreaves KJ, McDonald AG, Dorsey JR and Fowler D (2002) Micrometeorological measurements of the urban heat budget and CO_2 emissions on a city scale. Environm Sci Techn. 36:3139–3146.

Ohmura A, Steffen K, Blatter H, Greuell W, Rotach M, Stober M, Konzelmann T, Forrer J, Abe-Ouchi A, Steiger D and Neiderbäumer G (1992) Greenland Expedition, Progress Report No. 2, April 1991 to Oktober 1992. Swiss Federal Institute of Techology, Zürich, 94 pp.

Oncley SP, Foken T, Vogt R, Kohsiek W, DeBruin HAR, Bernhofer C, Christen A, van Gorsel E, Grantz D, Feigenwinter C, Lehner I, Liebethal C, Liu H, Mauder M, Pitacco A, Ribeiro L and Weidinger T (2007) The energy balance experiment EBEX-2000, Part I: Overview and energy balance. Boundary-Layer Meteorol. 123:1–28.

Panofsky HA, Tennekes H, Lenschow DH and Wyngaard JC (1977) The characteristics of turbulent velocity components in the surface layer under convective conditions. Boundary-Layer Meteorol. 11:355–361.

Panofsky HA and Dutton JA (1984) Atmospheric Turbulence - Models and Methods for Engineering Applications. John Wiley and Sons, New York, 397 pp.

Patton EG, Horst TW, Sullivan PP, Lenschow DH, Oncley SP, Brown WOJ, Burns SP, Guenther AB, Held A, Karl T, Mayor SD, Rizzo LV, Spuler SM, Sun J, Turnipseed AA, Allwine EJ, Edburg SL, Lamb BK, Avissar R, Calhoun RJ, Kleissl J, Massman WJ, Paw U KT and Weil JC (2011) The canopy horizontal array turbulence study. Bull Amer Meteorol Soc. 92:593–611.

Poulos GS, Blumen W, Fritts DC, Lundquist JK, Sun J, Burns SP, Nappo C, Banta R, Newsom R, Cuxart J, Terradellas E, Balsley B and Jensen M (2002) CASES-99: A comprehensive investigation of the stable nocturnal boundary layer. Bull Amer Meteorol Soc. 83:55–581.

Queitsch P (2002) TA Luft, Technische Anleitung zur Reinhaltung der Luft; Systematische Einführung mit Text der TA Luft 2002. Bundesanzeiger-Verl.-Ges., Bonn, 180 pp.

Rotach M, Vogt R, Bernhofer C, Batchvarova E, Christen A, Clappier A, Feddersen B, Gryning SE, Martucci G, Mayer H, Mitev V, Oke TR, Parlow E, Richner H, Roth M, Roulet Y-A, Ruffieux D, Salmond JA, Schatzmann M and Voogt JA (2005) BUBBLE - an urban boundary layer meteorology project. Theor Appl Climat. 81:231–261.

Salmond JA, Oke TR, Grimmond CSB, Roberts S and Offerle B (2005) Venting of heat and carbon dioxide from urban canyons at night. J Appl Meteorol. 44:1180–1194.

Schotanus P, Nieuwstadt FTM and DeBruin HAR (1983) Temperature measurement with a sonic anemometer and its application to heat and moisture fluctuations. Boundary-Layer Meteorol. 26:81–93.

Schuepp PH, Leclerc MY, MacPherson JI and Desjardins RL (1990) Footprint prediction of scalar fluxes from analytical solutions of the diffusion equation. Boundary-Layer Meteorol. 50:355–373.

Seiler W (1996) Results from the integrated research programme SANA, Phase I. Meteorol Z. 5:179–278.

Sellers PJ, Hall FG, Asrar G, Strebel DE and Murphy RE (1988) The first ISLSCP field experiment (FIFE). Bull Amer Meteorol Soc. 69:22–27.

Sellers PJ, Hall FG, Kelly RD, Black A, Baldocchi D, Berry J, Ryan M, Ranson KJ, Crill PM, Lettenmaier DP, Margolis H, Cihlar J, Newcomer J, Fitzjarrald D, Jarvis PG, Gower ST, Halliwell D, Williams D, Goodison B, Wickland DE and Guertin FE (1997) BOREAS in 1997: Experiment overview, scientific results, and future directions. J Geophys Res. 102:28 731–28 769.

Skeib G (1980) Zur Definition universeller Funktionen für die Gradienten von Windgeschwindigkeit und Temperatur in der bodennahen Luftschicht. Z Meteorol. 30:23–32.

Soegaard H and Møller-Jensen L (2003) Towards a spatial CO_2 budget of a metropolitan region based on textural image classification and flux measurements. Rem Sens Environm. 87:283–294.

Sonntag D (1989) Formeln verschiedenen Genauigkeitsgrades zur Berechnung der Sonnenkoordinaten. Abh Meteorol Dienstes DDR. 143:104 pp.

Sonntag D (1990) Important new values of the physical constants of 1986, vapour pressure formulations based on the ITC-90, and psychrometer formulae. Z Meteorol. 40:340–344.

Sorbjan Z (1986) Characteristics in the stable-continuous boundary layer. Boundary-Layer Meteorol. 35:257–275.

Sorbjan Z (1987) An examination of local similarity theory in the stably stratified boundary layer. Boundary-Layer Meteorol. 38:63–71.

Stull RB (1988) An Introduction to Boundary Layer Meteorology. Kluwer Acad. Publ., Dordrecht, Boston, London, 666 pp.

Swinbank WC (1964) The exponential wind profile. Quart J Roy Meteorol Soc. 90:119–135.

Swinbank WC and Dyer AJ (1968) An experimental study on mircrometeorology. Quart J Roy Meteorol Soc. 93:494–500.

Swinbank WC (1968) A comparison between prediction of the dimensional analysis for the constant-flux layer and observations in unstable conditions. Quart J Roy Meteorol Soc. 94:460–467.

Tanner BD, Swiatek E and Greene JP (1993) Density fluctuations and use of the krypton hygrometer in surface flux measurements. In: Allen RG (ed.), Management of Irrigation and Drainage Systems: Integrated Perspectives. American Society of Civil Engineers, New York, NY, 945–952.

Thiermann V and Grassl H (1992) The measurement of turbulent surface layer fluxes by use of bichromatic scintillation. Boundary-Layer Meteorol. 58:367–391.

Thomas C and Foken T (2002) Re-evaluation of integral turbulence characteristics and their parameterisations. 15th Conference on Turbulence and Boundary Layers, Wageningen, NL, 15–19 July 2002 2002. Am. Meteorol. Soc., pp. 129–132.

Thomas C and Foken T (2007) Organised motion in a tall spruce canopy: Temporal scales, structure spacing and terrain effects. Boundary-Layer Meteorol. 122:123–147.

Tschalikov DV (1968) O profilja vetra i temperatury v prizemnom sloe atmosfery pri ustojtschivoj stratifikacii (About the wind and temperature profile in the surface layer for stable stratification). Trudy GGO. 207:170–173.

Tsvang LR, Kaprov BM, Zubkovskij SL, Dyer AJ, Hicks BB, Miyake M, Stewart RW and McDonald JW (1973) Comparison of turbulence measurements by different instuments; Tsimlyansk field experiment 1970. Boundary-Layer Meteorol. 3:499–521.

Tsvang LR, Zubkovskij SL, Kader BA, Kallistratova MA, Foken T, Gerstmann W, Przandka Z, Pretel J, Zelený J and Keder J (1985) International turbulence comparison experiment (ITCE-81). Boundary-Layer Meteorol. 31:325–348.

Tsvang LR, Fedorov MM, Kader BA, Zubkovskii SL, Foken T, Richter SH and Zelený J (1991) Turbulent exchange over a surface with chessboard-type inhomogeneities. Boundary-Layer Meteorol. 55:141–160.

Uttal T, Curry JA, Mcphee MG, Perovich DK, Moritz RE, Maslanik JA, Guest PS, Stern HL, Moore JA, Turenne R, Heiberg A, Serreze MC, Wylie DP, Persson OG, Paulson CA, Halle C, Morison JH, Wheeler PA, Makshtas A, Welch H, Shupe MD, Intrieri JM, Stamnes K, Lindsey RW, Pinkel R, Pegau WS, Stanton TP and Grenfeld TC (2002) Surface heat budget of the Arctic ocean. Bull Amer Meteorol Soc. 83:255–275.

van Dijk A, Kohsiek W and DeBruin HAR (2003) Oxygen sensitivity of krypton and Lyman-alpha hygrometers. J Atm Oceanic Techn. 20:143–151.

van Dijk A, Kohsiek W and DeBruin HAR (2004) The principles of surface flux physics: theory, practice and description of the ECPACK library. University of Wageningen, Wageningen, 98 pp.

van Ulden AP and Holtslag AAM (1985) Estimation of atmospheric boundary layer parameters for diffusion applications. J Climate Appl Meteorol. 24:1196–1207.

VDI (2006) Umweltmeteorologie - Meteorologische Messungen - Messstation, VDI 3786, Blatt 13. Beuth-Verlag, Berlin, 44 pp.

VDI (2015) Umweltmeteorologie: Wechselwirkungen zwischen Atmosphäre und Oberflächen, Berechnung der spektralen kurz- und der langwelligen Strahlung, VDI 3789 (Draft). Beuth-Verlag, Berlin, 95 pp.

Vesala T, Järvi L, Launiainen S, Sogachev A, Rannik Ü, Mammarella I, Siivola E, Keronen P, Rinne J, Riikonen ANU and Nikinmaa E (2008) Surface–atmosphere interactions over complex urban terrain in Helsinki, Finland. Tellus B. 60:188–199.

Vickers D and Mahrt L (1997) Quality control and flux sampling problems for tower and aircraft data. J Atm Oceanic Techn. 14:512–526.

Vogt R, Christen A, Rotach MW, Roth M and Satyanarayana ANV (2006) Temporal dynamics of CO_2 fluxes and profiles over a Central European city. Theor Appl Climat. 84:117–126.

Wagner W and Pruß A (2002) The IAPWS Formulation 1995 for the Thermodynamic Properties of Ordinary Water Substance for General and Scientific Use. Journal of Physical and Chemical Reference Data. 31:387–535.

Webb EK (1970) Profile relationships: the log-linear range, and extension to strong stability. Quart J Roy Meteorol Soc. 96:67–90.

Webb EK, Pearman GI and Leuning R (1980) Correction of the flux measurements for density effects due to heat and water vapour transfer. Quart J Roy Meteorol Soc. 106:85–100.

Wulfmeyer V, Behrendt A, Kottmeier C, Corsmeier U, Barthlott C, Craig G, Hagen M, Althausen D, Aoshima F, Arpagaus M, Bauer HS, Bennett L, Blyth A, Brandau C, Champollion C, Crewell S, Dick G, Di Girolamo P, Dorninger M, Dufournet Y, Eigenmann R, Engelmann R, Flamant C, Foken T, Gorgas T, Grzeschik M, Handwerker J, Hauck C, Höller H, Junkermann W, Kalthoff N, Kiemle C, Klink S, König M, Krauß L, Long CN, Madonna F, Mobbs S, Neininger B, Pal S, Peters G, Pigeon G, Richard E, Rotach M, Russchenberg H, Schwitalla T, Smith V, Steinacker R, Trentmann J, Turner DD, van Baelen J, Vogt S, Volkert H, T. W, Wernli H, Wieser A and Wirth M (2011) The convective and orographically induced precipitation study (COPS): The scientific strategy, the field phase, and research highlights. Quart J Roy Meteorol Soc. 137:3–30.

Wyngaard JC, Izumi Y and Collins SA (1971) Behavior of the refractive-index-structure parameter near the ground. J Opt Soc Am. 61:1646–1650.

Wyngaard JC and Coté OR (1971) The budgets of turbulent kinetic energy and temperature variance in the atmospheric surface layer. J Atmos Sci. 28:190–201.

Wyngaard JC (1973) On surface layer turbulence. In: Haugen DH (ed.), Workshop on Micrometeorology. Am. Meteorol. Soc., Boston, 101–149.

Yaglom AM (1977) Comments on wind and temperature flux-profile relationships. Boundary-Layer Meteorol. 11:89–102.

Zilitinkevich SS and Tschalikov DV (1968) Opredelenie universalnych profilej skorosti vetra i temperatury v prizemnom sloe atmosfery (Determination of universal profiles of wind velocity and temperature in the surface layer of the atmosphere). Izv AN SSSR, Fiz Atm Okeana. 4:294–302.

Index